
Brittle Petrofabrics in the Central Bavarian Forest (SE Germany)

**Tectonic Evolution, Geomorphological Effects, and
Hydrogeologic Implications**

Matthias Zeitlhöfler



München 2007

Brittle Petrofabrics in the Central Bavarian Forest (SE Germany):
Tectonic Evolution, Geomorphological Effects, and Hydrogeologic
Implications

Dissertation

an der Fakultät für Geowissenschaften
der Ludwig-Maximilians-Universität München

vorgelegt von

Matthias Zeitlhöfler

München im Juni 2007

1. Gutachter: Prof. Dr. Bernd Lammerer, LMU München
2. Gutachter: Prof. Dr. Jelle Z. de Boer (Wesleyan University, Middletown, CT/USA)

Tag der mündlichen Prüfung: 18. Dezember 2007

Für Ruth

“Wer einmal im Bayerischen Wald von dieser jenseitigen Landschaft
angeschaut wurde, versteht, daß sich die Wahrnehmung ändern kann.
In der Einsamkeit des Bayerischen Waldes werden die Menschen zu Sehern.”

Bruno Jonas

List of figures and tables	IV
Acknowledgements	IX
Abstract	X
1 Introduction	1
1.1 Statement of the problem/ project outline	2
1.2 The study area	3
1.2.1 Regional geology	5
1.2.2 Structural geologic/ tectonic overview	14
1.2.3 Hydro(geo)logic and climatic overview	24
1.3 Previous work at the interface of brittle tectonics and hydrogeology	28
1.4 Terminology	37
1.4.1 Geologic terms	38
1.4.2 Hydrogeologic and technical terms	39
1.5 Methodology	40
1.5.1 Structural geology	40
1.5.1.1 Field Methods	40
1.5.1.2 Database construction and statistical analysis of field data	43
1.5.2 Photogeology and geostatistics	45
1.5.2.1 Aerial photography	45
1.5.2.2 INSAR Digital Elevation Model (DEM)	46
1.5.2.3 GIS-based analyses of remotely sensed structural data	47
1.5.3 Hydrogeology	48
1.5.3.1 Processing of data provided by companies and government institutions	48
1.5.3.2 Hydrogeologic modeling	49
2 Structural geology	50
2.1 Inventory of bedrock outcrops	50
2.2 Types of brittle tectonic features	53
2.2.1 Fractures parallel to the metamorphic foliation	53
2.2.1.1 Orientations and spatial distribution	55
2.2.1.2 Physical properties	57
2.2.2 Fractures intersecting the metamorphic foliation	64
2.2.2.1 Orientations and spatial distribution	65
2.2.2.2 Physical properties	66
2.2.3 Steep fractures in unfoliated rocks	73
2.2.3.1 Orientations and spatial distribution	73
2.2.3.2 Physical properties	75
2.2.4 Unroofing joints	82
2.2.4.1 Orientations and spatial distribution	82

2.2.4.2	Physical properties	85
2.3	Regionally characteristic fracture types based on orientation	89
2.3.1	Steeply inclined NW-SE striking fractures	90
2.3.2	Steeply inclined NNE-SSW to NE-SW striking fractures	92
2.3.3	Steeply inclined ENE-WSW to E-W striking fractures	94
2.3.4	Moderately NNE dipping fractures	96
2.4	Tectonic classification of brittle structures	98
2.4.1	Joints	98
2.4.1.1	Orientations and spatial distribution	98
2.4.1.1	Tectonic significance	100
2.4.2	Faults	102
2.4.2.1	Orientations and spatial distribution	102
2.4.2.2	Tectonic significance	104
2.4.3	Kinematic indicators	105
2.4.3.1	Geometric relationships between fractures and fracture systems	106
2.4.3.2	Slickensides	109
2.4.3.3	Offsets	116
2.4.3.4	Brittle fault rocks	119
2.5	Brittle tectonic history of the study area	121
3	Photogeologic analyses and geostatistics	127
3.1	Lineament analyses using an interferometric RADAR (INSAR) Digital Elevation Model	127
3.1.1	Results	129
3.1.1.1	General observations	129
3.1.1.2	Structural analysis and tectonic interpretation of the DEM	137
3.1.2	Difficulties with the interpretation of the DEM data	140
3.2	Lineament and fracture trace analyses using aerial photography	142
3.2.1	Results	142
3.2.2	Difficulties with the interpretation of photolineaments	148
3.3	Orientations of intrusives	150
3.4	Groundtruthing of remotely sensed structure data and domain overlap analysis	155
4	Hydrogeology	165
4.1	Data inventory	165
4.1.1	Drillers' logs and borehole geophysics	167
4.1.1.1	Drillers' logs	168
4.1.1.2	Pumping tests and flowmeter logs	169
4.1.1.3	Geophysics: Gamma ray, caliper, temperature, and salinity logs	177
4.1.2	Surface geophysics	181
4.2	Synoptic analysis of basement structure and hydrogeology	185
4.2.1	Spatial distribution of well yields	185

4.2.2	Correlation of well yields with geologic and structural entities	188
4.3	Case studies	194
4.3.1	Hydrogeologic properties of selected outcrops	194
4.3.1.1	Qualitative hydrogeologic observations in selected outcrops	195
4.3.1.2	Scanline surveys	198
4.3.1.3	Fracture networks in selected sampling stations	201
4.3.1.4	FracMan 3D discrete fracture and flow models of selected locations	206
4.3.2	Integration of the results from various prospecting approaches in the Bad Kötzing geothermal drilling project	212
5	Discussion and conclusion	215
5.1	Discussion	215
5.1.1	Results from structural geologic work	215
5.1.2	Results from remote sensing	220
5.1.3	Results from hydrogeologic analyses	223
5.2	Synopsis, conclusion and outlook	227
6	References	231

Appendices

Appendix A – Outcrop descriptions	A-1
Appendix B – Lithologic descriptions of drillers' logs	B-1
Appendix C – K-means analysis of fracture data	C-1
1 Conceptual model	C-1
2 Algorithm	C-2
3 Adjustments of the online procedure to the data clustering	C-3
3.1 Metrics	C-3
3.2 Derivation	C-3
3.3. Further problem-specific modifications	C-4
3.3.1 Vector doubling	C-4
3.3.2 Centroid doubling	C-5
3.3.3 Interpretation	C-5
4 Program procedure	C-6
5 References	C-8
Appendix D – FracMan/ MAFIC discrete fracture and flow modeling	D-1
1 Introduction	D-1
2 Model generation and basic assumptions	D-4
2.1 Parameters and boundary conditions in FracWorks	D-4
2.2 Parameters and boundary conditions in PAWorks	D-7
3 Model protocols	D-8
4 References	D-11
Appendix E – Geophysical logs	E-1
Appendix F – Cumulative stereographic plots and rose diagrams	F-1
1 Rose diagrams of steeply inclined fractures	F-1
2 Miscellaneous stereographic plots	F-3
Appendix G – Fracture characterization forms	G-1
Appendix H – Maps	H-1
Appendix I – Attribution of regionally important rock types to lithogroups	I-1

List of figures and tables

Section 1 – Introduction

- Figure 1-1 Topographic map of the study area.
 Figure 1-2 Geologic map 1:500,000 of the study area. Source: GLA (1996).
 Figure 1-3 Map of the Bohemian Massif and its subdivisions. Source: Stettner (1992).
 Figure 1-4 Geologic map 1:100,000 of the study area. Source: Troll (1964).
 Figure 1-5 Orogenic periods in the Moldanubian, Bohemian, and Saxothuringian terranes. Source: Stettner (1992).
 Figure 1-6 Paleogeographic reconstruction of the circum-Atlantic continents for the Lower Ordovician through Devonian times. Source: Tait et al. (1996).
 Figure 1-7 Tectonic map of the study area. Source: GLA (1996).
 Figure 1-8 Fracture roughness profiles obtained in twelve sampling stations.
 Figure 1-9 Representative fracture profiles for six roughness classes.

Section 2 – Structural Geology

- Figure 2-1 Map of fracture sampling stations in the study area.
 Figure 2-2 Photograph of fractures parallel to the metamorphic foliation.
 Figure 2-3 Chart of relative abundances of fractures parallel to the metamorphic foliation in various lithogroups.
 Figure 2-4 Cumulative equal-area plot of fractures parallel to the metamorphic foliation in the study area.
 Figure 2-5 Chart of roughness and planarity of fractures intersecting and paralleling the foliation.
 Figure 2-6 Schematic representation of fracture roughness and planarity in metamorphic bedrock exposures.
 Figure 2-7 Histogram depicting the trace length distribution of fractures parallel to the foliation.
 Figure 2-8 Scatter plot of fracture apertures in relation to trace lengths of fractures parallel to the foliation.
 Figure 2-9 Photograph and schematic representation of densely fractured zones in bedrock outcrops.
 Figure 2-10 Photograph of mineralized fracture planes on a metamorphic hand sample.
 Figure 2-11 Photograph of fractures intersecting the metamorphic foliation.
 Figure 2-12 Cumulative equal-area plot of fractures intersecting the metamorphic foliation in the study area.
 Figure 2-13 Histogram depicting the trace length distribution of fractures intersecting the foliation.
 Figure 2-14 Scatter plot of fracture apertures in relation to trace length of fractures intersecting the foliation.
 Figure 2-15 Mean spacings of fracture sets intersecting the foliation in relation to average trace lengths.
 Figure 2-16 Orientations of fractures intersecting the metamorphic foliation containing infillings.
 Figure 2-17 Scatter plot depicting the relationship between the trace lengths and widths of associated breccia seams of fractures intersecting the foliation.
 Figure 2-18 Photographs of fractures in unfoliated rocks.
 Figure 2-19 Cumulative equal-area plot of fractures in unfoliated rocks in the study area.
 Figure 2-20 Cumulative equal-area plot of fractures in igneous and hydrothermal rocks in the study area.
 Figure 2-21 Chart of roughness and planarity of fractures in igneous and hydrothermal rocks.
 Figure 2-22 Histogram depicting the trace length distribution of steeply inclined fractures in unfoliated rocks.
 Figure 2-23 Scatter plot of fracture apertures in relation to trace lengths of steeply inclined fractures in unfoliated rocks.
 Figure 2-24 Mean spacings of fracture sets in unfoliated rocks in relation to average trace lengths.
 Figure 2-25 Equal area plots depicting the orientations of variously mineralized fracture planes in unfoliated rocks.
 Figure 2-26 Equal area plot depicting orientations of fractures in unfoliated rocks associated with infillings.

- Figure 2-27 Scatter plot depicting the relationship between the trace lengths and widths of associated breccia seams of fractures in unfoliated rocks.
- Figure 2-28 Photograph of unroofing joints in a granitic location (7043-02).
- Figure 2-29 Equal area plot depicting the orientations of unroofing joints in unfoliated rocks.
- Figure 2-30 Chart depicting relative abundances of unroofing joints in various lithogroups.
- Figure 2-31 Cumulative frequency diagrams relating the presence of unroofing joints in weakly foliated lithologies to the inclinations of the foliation planes.
- Figure 2-32 Chart of roughness and planarity of unroofing joints.
- Figure 2-33 Conceptual model of the unroofing process. Source: Zeithöfler (2003).
- Figure 2-34 Histogram depicting the trace length distribution of unroofing joints.
- Figure 2-35 Scatter plot of fracture apertures in relation to trace lengths of unroofing joints.
- Figure 2-36 Diagram depicting the depth-dependency of unroofing joint spacings along three vertical profiles.
- Figure 2-37 Chart of roughness and planarity of steeply inclined NW-SE striking fractures.
- Figure 2-38 Histogram depicting the trace length distribution of steeply inclined NW-SE striking fractures.
- Figure 2-39 Scatter plot of fracture apertures in relation to trace lengths of steeply inclined NW-SE striking fractures.
- Figure 2-40 Chart of roughness and planarity of steeply inclined NNE-SSW to NE-SW striking fractures.
- Figure 2-41 Histogram depicting the trace length distribution of steeply inclined NNE-SSW to NE-SW striking fractures.
- Figure 2-42 Scatter plot of fracture apertures in relation to trace lengths of steeply inclined NNE-SSW to NE-SW striking fractures.
- Figure 2-43 Chart of roughness and planarity of steeply inclined ENE-WSW to E-W striking fractures.
- Figure 2-44 Histogram depicting the trace length distribution of steeply inclined ENE-WSW to E-W striking fractures.
- Figure 2-45 Scatter plot of fracture apertures in relation to trace lengths of steeply inclined ENE-WSW to E-W striking fractures.
- Figure 2-46 Chart of roughness and planarity of moderately NNE dipping fractures.
- Figure 2-47 Histogram depicting the trace length distribution of moderately NNE dipping fractures.
- Figure 2-48 Scatter plot of fracture apertures in relation to trace lengths of moderately NNE dipping fractures.
- Figure 2-49 Cumulative equal area plot depicting the orientations of joints in the study area.
- Figure 2-50 Cumulative equal area plots of faults in the study area.
- Figure 2-51 Conceptual 2-D model of the orientations of principal stresses, faults, and joints based on the Anderson theory of faulting.
- Figure 2-52 Photograph of a gently inclined brecciated fault in a poorly foliated rock (location 6943-14).
- Figure 2-53 Equal area plots of fractures associated with Riedel shear fractures.
- Figure 2-54 Equal area plots of fractures with conjugate relationships.
- Figure 2-55 Photograph of a slickensided fracture plane (location 7043-02).
- Figure 2-56 Cumulative equal area plots of slickensides recorded in the study area.
- Figure 2-57 Cumulative equal area plots of slickensides suggesting normal and reverse displacement recorded in the study area.
- Figure 2-58 Equal area plots of slickensides suggesting normal displacement due to uplift and NE-SW and NW-SE extension, respectively.
- Figure 2-59 Equal area plots of slickensides suggesting reverse displacement due to uplift and (W)NW-(E)SE and N-S extension, respectively.
- Figure 2-60 Cumulative equal area plots of slickensides suggesting strike-slip displacement recorded in the study area.
- Figure 2-61 Equal area plots of slickensides suggesting dextral strike-slip displacement due to NE-SW and N(N)W-S(S)E compression, respectively.
- Figure 2-62 Equal area plots of slickensides suggesting sinistral strike-slip displacement due to N(N)E-S(S)W and N(N)W-S(S)E compression, respectively.
- Figure 2-63 Equal area plots of slickensides suggesting both sinistral and dextral strike-slip displacement due to N(N)E-S(S)W and N(N)W-S(S)E compression, respectively.
- Figure 2-64 Equal area plots of slickensided faults with and without hydrothermal precipitates on their planes.

Figure 2-65	Distributions of the rakes of slickenlines on mineralized and unmineralized fault planes.
Figure 2-66	Equal area plots depicting offsets along fault planes in the study area.
Figure 2-67	Cumulative equal area plot of fractures in the study area associated with brittle fault rocks.
Figure 2-68	Scatter plots depicting the strikes and dips of fractures associated with brittle fault rocks in relation to the widths of fault rock seams.
Table 2-1	Classification scheme for bedrock outcrops regarding their quality for data acquisition.
Table 2-2	Distribution of roughness coefficients for cross fractures with different orientations.
Table 2-3	Mean spacings of fracture sets intersecting the metamorphic foliation with respect to their orientations.
Table 2-4	Mean spacings of steeply inclined fracture sets in unfoliated rocks with respect to their orientations.
Table 2-5	Dominant mean strike directions of subvertical joints as measures in various outcrops.
Table 2-6	Sampling stations with suborthogonal fracture sets.
Table 2-7	Sampling stations, in which faults were measured, classified according to their associated lithogroups.
Table 2-8	Brittle tectonic paleostress fields active in the study area based on data from this study. No chronological order implied.
Table 2-9	Sequence of brittle tectonic events since the Mesozoic as compiled from data of this study and Bergerat and Geyssant (1983).

Section 3 - Photogeologic analyses and geostatistics

Figure 3-1	Three-dimensional visualization of the ERS-DEM of the central Bavarian Forest.
Figure 3-2	2-D view of the ERS-DEM both as image depicting only altitude data and as raster showing pixel exposition (aspect).
Figure 3-3	Composite ERS-DEM raster depicting both pixel altitude and aspect.
Figure 3-4	Image of a composite ERS-DEM raster showing and example for one iteration of the lineament analysis.
Figure 3-5	Cumulative rose diagrams of DEM lineament orientations both normalized to abundances and cumulative lengths per 10° strike increment.
Figure 3-6	Lineament density map depicting both the densities of DEM lineaments and their intersections in the study area.
Figure 3-7	Maps of DEM lineaments in the study area separated according to prominent orientations.
Figure 3-8	Conceptual model and lineament map interpreting the tectonic evolution of the lineament pattern.
Figure 3-9	Rose diagram depicting DEM lineament orientations used for the tectonic interpretation of the lineament pattern.
Figure 3-10	Conceptual model of the tectonic evolution of the lineament pattern based on Riedel-type shear and extensional processes.
Figure 3-11	Subset of the ERS-DEM exposing an apparent semi-radial/dendritic drainage pattern.
Figure 3-12	Cumulative rose diagrams of photolineament orientations both normalized to abundances and cumulative lengths per 10° strike increment.
Figure 3-13	Lineament density map depicting both the densities of photolineaments and their intersections in the study area.
Figure 3-14	Maps of photolineaments in the study area separated according to prominent orientations.
Figure 3-15	Map showing both ERS-DEM- and photolineaments in the study area.
Figure 3-16	Rose diagrams depicting the orientations of elongation axes of all igneous and hydrothermal intrusions in the study area both normalized to abundances and lengths per 10° strike increment. Database: 1:25,000 scale geologic maps of the study area.
Figure 3-17	Rose diagrams depicting the orientations of elongation axes of quartz dikes and veins in the study area both normalized to abundances and lengths per 10° strike increment. Database: 1:25,000 scale geologic maps of the study area.

Figure 3-18	Rose diagrams depicting the orientations of elongation axes of pegmatite dikes and veins in the study area both normalized to abundances and lengths per 10° strike increment. Database: 1:25,000 scale geologic maps of the study area.
Figure 3-19	Rose diagrams depicting the orientations of elongation axes of quartz-mica-diorite dikes and veins in the study area both normalized to abundances and lengths per 10° strike increment. Database: 1:25,000 scale geologic maps of the study area.
Figure 3-20	Rose diagrams depicting the orientations of elongation axes of coarse-grained granite dikes and veins in the study area both normalized to abundances and lengths per 10° strike increment. Database: 1:25,000 scale geologic maps of the study area.
Figure 3-21	Rose diagrams depicting the orientations of elongation axes of medium-grained granite dikes and veins in the study area both normalized to abundances and lengths per 10° strike increment. Database: 1:25,000 scale geologic maps of the study area.
Figure 3-22	Rose diagrams depicting the orientations of elongation axes of fine-grained granite dikes and veins in the study area both normalized to abundances and lengths per 10° strike increment. Database: 1:25,000 scale geologic maps of the study area.
Figure 3-23	Scatter and equal area plots depicting the prominent strikes of steeply inclined fractures in the study area.
Figure 3-24	Distribution maps of DEM- and photolineaments in relation to fracture strikes in sampling stations. Orientations are separated based on regional prominent fracture strikes.
Figure 3-25	Contour maps of the distribution of lineament and fracture orientations per $\pm 10^\circ$ segment about prominent fracture orientations.
Figure 3-26	Synoptic comparison of photo- and ERS-DEM lineaments with ground truth.
Table 3-1	Numbers and cumulative lengths of DEM lineaments per 10° strike increment.
Table 3-2	DEM lineament distribution per 10° strike increment with regard to various statistical parameters.
Table 3-3	Numbers and cumulative lengths of photolineaments per 10° strike increment.
Table 3-4	Photolineament distribution per 10° strike increment with regard to various statistical parameters.
Table 3-5	Distances of sampling stations to lineaments with corresponding strikes.

Section 4 – Hydrogeology

Figure 4-1	Map depicting the distribution of bedrock wells in the study area and its vicinity.
Figure 4-2	Schematic profile of the subsurface in the study area as determined from drillers' logs and outcrop profiles.
Figure 4-3	Yield distribution over borehole length as determined from flowmeter measurements.
Figure 4-4	Comparison of total well yields with depth intervals from which at least 75 % or 100 %, or the total yield is obtained.
Figure 4-5	Pie diagram depicting the percentages of individual lithologies hosting primary influxes into boreholes.
Figure 4-6	Schematic profiles of flowmeter and drillers' logs displaying the stratigraphy and the locations of groundwater bearing zones.
Figure 4-7	Outline map of the study area depicting the location of the surface geophysical survey.
Figure 4-8	Profiles of the geoelectric tomography conducted by German Geo Services. Image source: Richert (2006a).
Figure 4-9	Map depicting the exact locations of the tomography profiles and the strikes of the low-resistivity zones.
Figure 4-10	Map depicting the distribution of well yields in the study area.
Figure 4-11	Diagram relating well yields to associated lithogroups.
Figure 4-12	Cumulative frequency diagram of well yields classified according to lithogroups.
Figure 4-13	Diagrams showing the correlations of well yields with the distances of a well to the closest DEM- and photolineaments.
Figure 4-14	Photographs and schematic profiles depicting visible groundwater flow in bedrock outcrops. Location: 6943-01.
Figure 4-15	Schematic model of the subsurface in granitic lithologies with low densities of steeply inclined fractures.

Figure 4-16	Photographs of plants growing out of fractures in locations 7043-02 and 6943-13.
Figure 4-17	Cumulative equal area plots of fracture measurements made in selected sampling stations using the subjective and objective approach.
Figure 4-18	FracWorks fracture network model for sampling station 6943-01.
Figure 4-19	FracWorks fracture network model for sampling station 7044-02.
Figure 4-20	FracWorks fracture network model for sampling station 6944-18.
Figure 4-21	FracWorks fracture network model for sampling station 7044-04.
Figure 4-22	FracWorks fracture network model for sampling station 6943-13.
Figure 4-23	Conceptual scheme showing the components of the PAWorks flow model.
Figure 4-24	PAWorks flow model for one representative path. Location: 6943-01
Figure 4-25	Two PAWorks flow models for one representative path. Location: 7044-02
Figure 4-26	Two PAWorks flow models for one representative path. Location: 6944-18
Figure 4-27	PAWorks flow model for one representative path. Location: 7044-04
Figure 4-28	PAWorks flow model for one representative path. Location: 6943-13
Figure 4-29	Equal area plot depicting fracture orientations measured in the vicinity of the Bad Kötztzing geophysical survey site.
Figure 4-30	Rose diagram depicting DEM lineament orientations mapped in the vicinity of the Bad Kötztzing geophysical survey site and the assumed trend of the faults identified in the geoelectric profiles.
Figure 4-31	Map of the Bad Kötztzing geophysical survey site depicting the distribution of mapped DEM lineaments.
Table 4-1	Inventory of communal drinking water wells in the study area and its vicinity.
Table 4-2	Inventory of geophysical surveys performed on boreholes in the study area and its vicinity.
Table 4-3	Legend to figure 4-6.
Table 4-4	Lithologic interpretation of resistivity ranges for the Bad Kötztzing geoelectric tomography. Source: Richert (2006a).
Table 4-5	List of scanline surveys performed in the study area.
Table 4-6	List of mean values of fracture orientations and metadata obtained from K-means clustering of scanline measurements in three sampling stations.
Table 4-7	Fracture set parameters employed in the model of sampling station 6943-01.
Table 4-8	Fracture set parameters employed in the model of sampling station 7044-02.
Table 4-9	Fracture set parameters employed in the model of sampling station 6944-18.
Table 4-10	Fracture set parameters employed in the model of sampling station 7044-04.
Table 4-11	Fracture set parameters employed in the model of sampling station 6943-13.

Acknowledgements

A large number of persons, companies and institutions significantly contributed to this study in various ways. I extend my deepest gratitude to all of them. Golder Associates Inc. provided me with a license of the FracMan/MAFIC software free of charge, the Deutsches Luft- und Raumfahrtzentrum (DLR) supplied a free digital elevation model, and the Bayerisches Landesamt für Umwelt (LfU) contributed digital geological maps, aerial imagery, hydrogeological data, as well as access to a large amount of additional information on various subjects in the fields of geology and hydrogeology. In particular I would like to thank the following LfU members: Dr. Hans Rohrmüller, Dr. Gerold Diepolder, Dr. Ulrich Teipl, Dr. Ernst Kroemer, Sven Blumenstein, Andreas Graf, Katharina Beger, Gabi Raum, and Elena Galádí-Enriquez. In addition, the LfU contracted me in the spring of 2006 to finance the completion of this dissertation. The state of Bavaria granted a two-year stipend to fund a significant part of this study. The city administration of Bad Kötzing provided funds to perform the geoelectric tomography in the Dampfbachtal. German Geo Services and Fontus Logging Services shared their results of several geophysical surveys in the study area. I am especially grateful for Peter Richert's valuable advice in the interpretation of these datasets.

I would also like to thank Lilian Chavez-Kus for all the fruitful discussions and the large amount of literature on the subject, as well as Ulrich Schwenk for countless hours of debating and programming the K-Means algorithm and for the solution of innumerable computer-related problems. I am deeply indebted to Dr. Klaus Dieter Raum of the SVB Prösl for his generous support and his willingness to discuss every detail of my work. My deepest gratitude goes out to my former advisor and mentor Prof. Dr. Jelle Z. de Boer of Wesleyan University. He introduced me to the field of geology, inspired my work and has accompanied and supported my career ever since I started it in his structural geology class. I would also like to extend my appreciation and thanks to my advisor for this dissertation, Prof. Dr. Bernd Lammerer, who introduced me to the Department of Earth and Environmental Sciences of the Ludwig-Maximilians-Universität München, secured funds to finance my dissertation, generously shared his vast knowledge of structural geology (especially during all those wonderful field trips in the Alps, on the island of Elba, and in Morocco), and has benevolently accompanied my career over the past three years.

Finally I would like to thank my parents for their loving support – both financial and immaterial –, as well as my wife Ruth, who helped and encouraged me wherever she could. Beyond being a wonderful companion she has been both my field assistant and editor of this dissertation.

Abstract

Brittle tectonic structures in the Central Bavarian Forest were studied in order to determine their influence on the geomorphology and the hydrogeological characteristics of the subsurface. Three different approaches were employed: field work, remote sensing, and numerical modeling of fractured aquifers using preexisting hydrologic data.

Field investigations unveiled the presence of several steeply inclined joint systems predominantly oriented NW-SE, \pm N-S, NE-SW, and \pm E-W. These fractures occur throughout the study area in varying abundances. Spatially distinct fracture domains could not be established. However, two types of tectonic discontinuities specific to the two major lithologies in the study area were identified. Well-layered metamorphic rocks contain a set of gently to steeply inclined fractures parallel to the foliation, while igneous rocks are frequently intersected by uplift-related unroofing joints.

Kinematic indicators suggest a polyphase deformation history beginning in the late Permian and reaching its main stage during the Tertiary. Several phases of fracturing and hydrothermal healing created the brittle petrofabrics of the region until the present-day patterns had been largely established.

The analysis of remote sensing data, i.e. a digital elevation model and aerial imagery, showed a good correlation between the dominant directions of topographic lineaments and the strikes of major fracture systems. At least one fracture set is oriented subparallel to a nearby lineament in any given locality. The geomorphologic patterns in the Bavarian Forest can thus be used to estimate the orientations of the predominant fracture sets in regions where sparse outcrops do not allow direct measurements of the bedrock structure.

Data from hydrogeological investigations at well drilling sites was processed and compared to well productivity in various lithologies and structural positions of the respective sites. The small number of data points suggests relatively high well yields in strongly folded and migmatitic rocks as well as in layered metamorphic lithologies, while igneous rocks turned out to host the least productive wells. The database was too small for an unambiguous correlation of a site's proximity to a topographic lineament and its productivity. Only a vague correlation between lineaments mapped on aerial imagery and well yield could be established statistically.

Several individual fracture sampling stations were selected for the simulation of local fracture networks and numerical groundwater flow modeling. Fracture data obtained in various bedrock outcrops was classified according to cluster orientations by the application of a K-means sorting algorithm specifically developed for this study. In these models fractures parallel to the metamorphic foliation turned out to be the most effective pathways for water in gneissic lithologies. Comparisons to tracer test results from preexisting studies corroborate this finding. In the models for igneous rocks a large portion of the flow is accommodated by subhorizontal unroofing joints. Channeling effects were detected, especially along their intersections with steeply inclined fractures. Infiltration occurs along the steeply inclined discontinuities. Observations made in the large granite quarries of the southern study area support these results. Thus, while a large part of the groundwater flow seems to occur preferentially along specific types of fractures, the entire network of discontinuities is needed for infiltration and groundwater storage. Therefore, flow in these lithologies has to be understood as highly anisotropic and heterogeneous, which does not allow the application of conventional hydrogeologic models and concepts originally devised for fluid migration in porous aquifers.

The relationships between the orientations of fractures, topographic features, and groundwater pathways presented in this study provide a degree of predictability which will be useful for future hydrogeologic analyses in the subsurface of the Central Bavarian Forest.

1. Introduction

The availability of clean drinking water is rapidly becoming a major issue in many parts of the world. Although southeastern Germany is not a region one would immediately link to this problem there are more and more indications that usable water is not an unlimited and ubiquitous resource, even in this relatively humid area. The combination of increasing industrialization and ongoing touristical development of the once thinly populated Bavarian Forest (Bayerischer Wald) with the contamination of surface waters and near-surface aquifers, mainly due to industrial and agricultural activities, makes it necessary to tap new sources of drinking water. The extremely hot and dry summer of 2003 showed once more the urgency of this issue. Since springs and shallow wells in low-yield fractured rock and saprolite aquifers are extremely susceptible to variations in precipitation many private and communal springs encountered massive drops in their yields (Sprenger et al., 2005). Several towns in the central and eastern Bavarian Forest had to fear a water shortage, and as a result several communal administrations such as Bayerisch Eisenstein, Böbrach, etc. started drilling projects to supplement their public water supplies.

The current procedure in this part of Bavaria is to explore almost exclusively the Tertiary/Quaternary sediment blankets and the underlying zone of partially weathered bedrock ("grus", or saprolite zone) and to neglect the deeper fractured bedrock. Few wells penetrate more than 50 m and thus reach the unweathered subsurface. However, in other parts of Germany, such as the Black Forest, fractured crystalline bedrock was found to be an aquifer with significant potential for groundwater exploitation. Many aquifers in this region are even used commercially for the production of bottled mineral waters (Stober, 1995). Both private and public supply bedrock wells with relatively high yields have been drilled as deep as 300 meters into the crystalline basement of the northeastern USA over the last few decades (Drew et al., 1999; Franke et al., 1998; Hansen et al., 1999; Mabee, 1999; Mabee et al., 2002; Melvin et al., 1995; Williams, 2000). The successful use of deep groundwater in these areas poses the question if the exploration of bedrock aquifers below the grus zone is also a viable way to supply communities in the Bavarian Forest with drinking water.

Fractures present the only significant pathways for groundwater in crystalline bedrock, since the matrix of unfractured igneous and metamorphic rocks yields hydraulic conductivities of 10^{-10} to $<10^{-13}$ m/s. In contrast to these extremely low values fracture space can reach conductivities several orders of magnitude higher than the intact rock (Freeze and Cherry, 1979) and fracture zones comprising as little as four per cent of the total rock volume can account for 94% of the rock's transmissivity (Olsson et al., 1988). Even turbulent flow has been observed in bedrock fractures with large apertures (Hölting, 1996).

Fractures in crystalline rocks are the result of tectonic stresses acting on an area throughout its history of brittle deformation. They usually form in distinct systems (so-called brittle petrofabrics) with quantifiable physical parameters, some of which are hydraulically highly significant. Brittle petrofabrics are neither homogenous nor isotropic occurrences and therefore strongly influence groundwater migration patterns (Zeitlhöfler, 2003; Zeitlhöfler and Raum, 2005). Therefore, structural analyses have proven to be valuable predictive tools in hard rock hydrogeology, as will be shown in the following chapters.

1.1 Statement of the problem/ project outline

This study intends to provide a synoptic view of both structural geologic and hydrogeologic aspects in the study area. This interdisciplinary approach thus draws knowledge and techniques from both fields of research and tries to bridge the gap between the frequently opposing concepts and opinions of hydrologists and geologists.

One of the major problems that still exist is to find widely applicable concepts and models about groundwater flow and solute transport in fractured media. Not only are these models inherently restricted to certain geologic and hydrologic boundary conditions, they are also in many cases scale-dependent, and different approaches have to be taken in order to assess fluid migration on local, small-scale and large-scale regional levels. As in many scientific disciplines, a comprehensive understanding of all the factors and interrelations in the bedrock hydrologic system is unlikely to be ever achieved. Still, this dissertation intends to come a bit closer to the truth in some questions. Among these are:

- Are there distinct fracture populations with specific physical properties that exist on regional, sub-regional and local levels?
- What role do specific fracture sets play in the bedrock hydrologic system?
- Is the presence of certain fracture populations linked to geologic or topographic entities such as lithologic units, major structural units etc. and can these entities be utilized to allow the prediction of certain fracture sets present in a given area?
- How does scale influence the distribution of fracture sets?
- How can the vertical distribution of fractures be characterized, and what is the maximum depth below the topographic surface to which groundwater can be extracted in sufficient quantities?

In order to design a conceptual model elucidating part of the “hydrogeologic mystery” of fractured rock aquifers this study has been designed as an analysis of brittle tectonic

features and their geologic history, the results of which are then applied to the solution of certain hydrologic problems. Accordingly, this work is based on three major approaches and resulting datasets: classical structural geologic field work in natural and artificial bedrock outcrops, remote sensing of airborne and satellite visual and active microwave imagery, and the geostatistical analysis of hydrologic datasets such as well pumping tests and geophysical logs. While the deciphering of the area's tectonic structure can mainly be achieved by field work and the processing of remotely sensed data the hydrogeologic research has to be carried out in collaboration with corporate and government institutions, since the acquisition of hydrologic data is a both labor and cost intensive enterprise. The following chronological outline will thus show which parts of this project are the results of the author's own research and which rely on "outside" help and data.

For a thorough understanding of a region's structural geology numerous field days of data sampling in quarries, abandoned mines, road cuts and natural outcrops are required. After a general reconnaissance in late 2003 this research was conducted in the field seasons of 2004 and 2005. To supplement the information gained from this work remotely sensed data was analyzed especially in order to characterize the geologic structure of regions in the study area where the bedrock is obscured by sedimentary blankets and zones of intense weathering. The analysis of these data sets, namely a digital elevation model provided by the German Center for Aeronautics and Space (Deutsches Luft- und Raumfahrtzentrum, DLR) as well both paper aerial imagery and digital orthophotos provided by the Bavarian state geological survey (Geologischer Dienst des Bayerischen Landesamtes für Umwelt) was carried out in the winter months of 2004/05.

Hydrologic datasets provided by the Bavarian state geological survey and several environmental consulting companies, as well as communal governments were analyzed in the fall and winter of 2005. The synoptic modeling of both the bedrock structure and fractured rock hydrology using primarily the FracMan/MAFIC suite and ArcGIS 8.3 was carried out in the winter of 2005/06.

1.2 The study area

The study area is located in the central Bavarian Forest, an intensely forested region in Eastern Bavaria, SE Germany. In its northern corner it is bordered by the Kaitersberg mountain ridge (1132m), in the West by the village of Kollnburg, in the South by the village of Bischofsmais, and in the East by the hamlet of Seebachschleife near Regenhütte. Thus, it forms a square with a side length of approximately 21 kilometers and covers an area of roughly 440 km² (figure 1-1).

Troll (1967c) subdivides the Bavarian Forest into the “Vorderer Bayerischer Wald” (Outer Bavarian Forest), the area S of the Bayerischer Pfahl (the Pfahl fault zone, or PFZ), and the “Hinterer Bayerischer Wald” (Inner Bavarian Forest) to the north of that lineament. This distinction is mainly based on lithologic and tectonic aspects of the region, but is now also the general terminology for the geographic as well as the socio-cultural structure of the area. The PFZ divides the study area in its southwestern part. Its geologic and tectonic significance will be detailed in the following sections.

The region’s morphology is that of a typical “Mittelgebirge”, a low mountain range with altitudes between 400 and 1450 meters above sea level. Crystalline basement rocks are frequently exposed, especially along ridges in higher elevations. Continuous weathering since the Tertiary (Priehäuser, 1968), the relatively humid present-day climate, the widespread forestation, and the general absence of regional glacial scouring during the Pleistocene –with a few exceptions in the glaciated summit areas- (Pfaffl, 1989) are the causes for the locally thick blankets of weathered material and quaternary deposits, as well as the intensely weathered and overgrown natural bedrock outcrops.

Although there are no areas with restricted access in the study area a continuous coverage with sampling locations is difficult to achieve. Due to the locally extensive blankets of Tertiary saprolite and Quaternary deposits the bedrock does not crop out in some areas, especially at the bottom of the large NW-SE trending valleys, where major faults are suspected (figures 1-2, 1-4, 1-5). Figure 2-1 shows the distribution of fracture sampling stations in the study area.

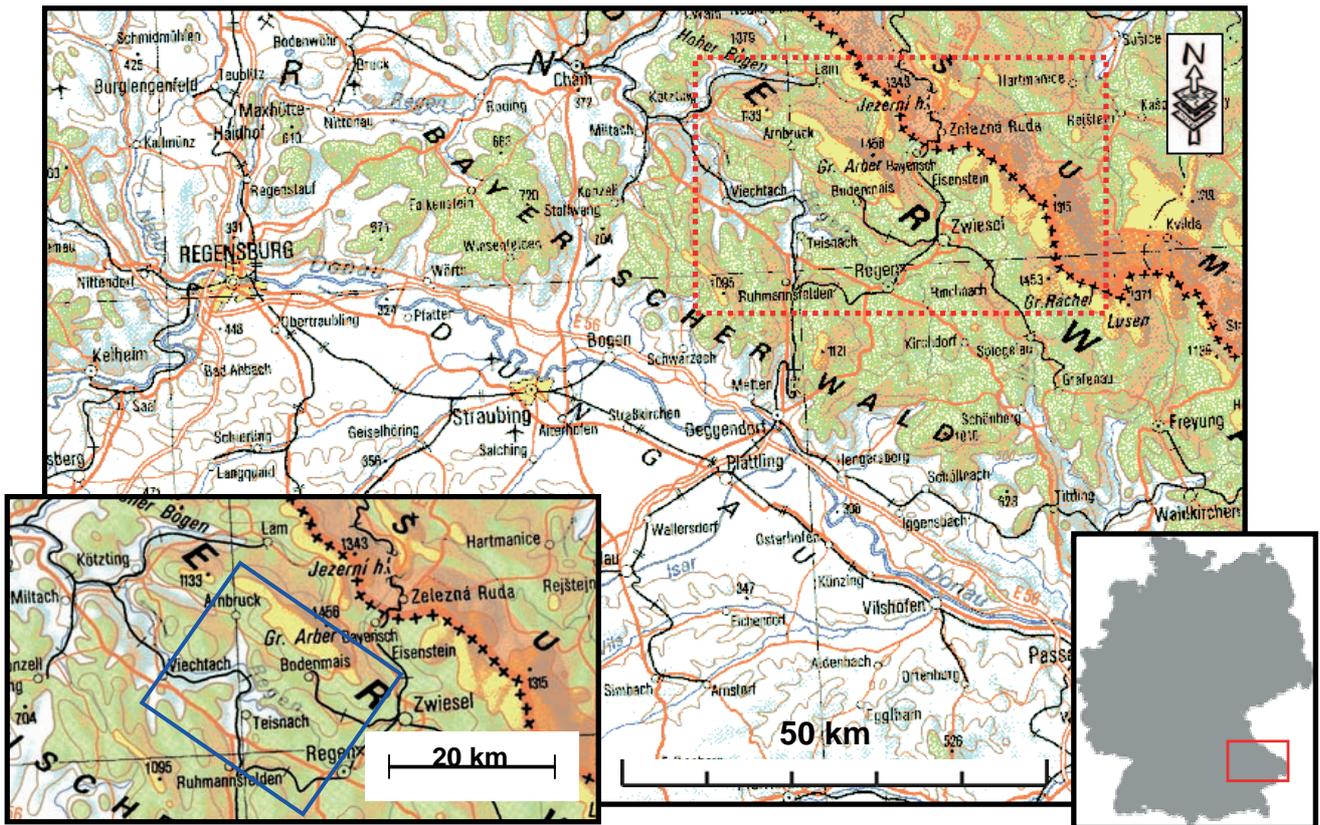


Figure 1-1: The study area. Right inset: location of main map within the Federal Republic of Germany. Left inset: Magnified view of the study area (blue rectangle); located in the red dashed rectangle on the main map.

1.2.1 Regional geology

The following section intends to give a brief synopsis of the regional geologic setting for this dissertation as well as a summary of the history of research in this field. Since a comprehensive treatment of all the aspects and local details of such a highly complex area as the eastern Bavarian crystalline basement is impossible to achieve at the scope of this dissertation only a summary of selected publications will be given.

While the history of geologic research already spans over 200 years, founded by the seminal works of Flurl (1792), Gümbel (1868) and Suess (1903), it took until the second half of the twentieth century to decipher at least part of the highly complex geology of the eastern Bavarian basement and to come up with today's widely accepted concepts and models. Especially the research by Fischer (1936; 1938; 1959; 1967a; 1967b; Fischer and Troll, 1973) contributed crucial insights to the recent understanding of various aspects of the area's geology, mineralogy and petrology.

The best introduction to the subject is given in the various articles compiled in the comments to Geologic Map of Bavaria 1:500 000 (Erläuterungen zur Geologischen Karte von Bayern 1:500 000; Freudenberger, 1996, fig. 1-2), which provides more or less the current state of knowledge. Among these are Bader (1996), Frank (1996), Jerz (1996) and Rohrmüller et. al. (1996a; 1996b). Similarly, comments to the local 1:25 000 scale geologic maps give valuable information as well. For the study area five such maps have been published to date, three of them with comments (List and Ott, 1982; Madel et al., 1968; Ott, 1983). For the Kötzing, Lam, and Bodenmais quadrangles (Nr. 6843, 6844, and 6944, respectively) Pfaffl (1990b; 1992; 1995) published geological and mineralogical descriptions.

Further important regional geologic studies include Bauberger (1969), Behr et. al. (1980), Fischer and Troll (1973), Stein (1988), and Troll (1967c; 1968; 1974), although many of them concentrate on the northern part of the Eastern Bavarian basement complex, especially the area around the continental deep drilling program (KTB) site (Bram and Hirschmann, 1992; Emmermann and Giese, 1989; Stettner, 1992). In addition, local researchers such as Georg Priehäuser (1930; 1937a; 1937b; 1938; 1951; 1952a; 1952b; 1955; 1956; 1958; 1961; 1963a; 1963b; 1966; 1968; 1971) and Fritz Pfaffl (1968; 1969; 1971; 1972a; 1972b; 1972c; 1973a; 1973b; 1973c; 1979a; 1979b; 1980; 1981a; 1981b; 1985a; 1985b; 1985c; 1985d; 1986; 1988a; 1988b; 1988c; 1989; 1990a; 1991; 1993; 1994; Pfaffl and Niggemann, 1967; Pfaffl and Niggemann, 1976; Pfaffl et al., 1976; Pfaffl and Troll, 1981; Pfaffl, 1982) contributed a plethora of valuable, though highly debated, research.



Figure 1-2: Geologic map of the study area. Inset: Legend depicting the common rock types in the study area (blue rectangle). Source: Geologische Karte von Bayern 1:500 000, GLA, 1996.

The information for the following synopsis has mainly been taken from Frank (1996), Jerz (1996), Rohrmüller et al. (1996a), and Stettner (1992). Other sources will be indicated in the text.

The crystalline basement rocks of the Bavarian Forest are part of the southwestern edge of the Bohemian Massif, which represents the eastern end of the European Variscan orogeny. It is mainly made up of late **Proterozoic** to early **Paleozoic** (Silurian) magmatic and sedimentary rocks –their sedimentation ages have not yet been defined with certainty-, which have undergone a number of deformational and metamorphic phases. In contrast to earlier opinions Stettner (1996) advocates a view which places the majority of sediments into the Early Cambrian thereby reducing the contribution of Proterozoic rocks. In the course of several ensuing periods they were intruded by younger igneous masses.

In eastern Bavaria this extensive basement is commonly subdivided into two major entities, the Saxothuringian, and the Moldanubian regions (Kossmat, 1927). The Moldanubian region is further classified into the Bohemikum and the Moldanubikum sensu stricto (the moldanubian terrane). Since the study area is located in the latter (fig. 1-3) the following discussion will focus on that region.

The moldanubian terrane is dominated by a monotonous succession of metamorphosed greywacke-pelitic protoliths (“Monotone Gruppe”) suggesting their sedimentation along a former passive continental margin and mainly consists of paragneisses interspersed with calc-silicate layers and lenses, as well as occasional mafic to felsic igneous rocks. In contrast to this rather uniform entity the “Bunte Gruppe” consists of

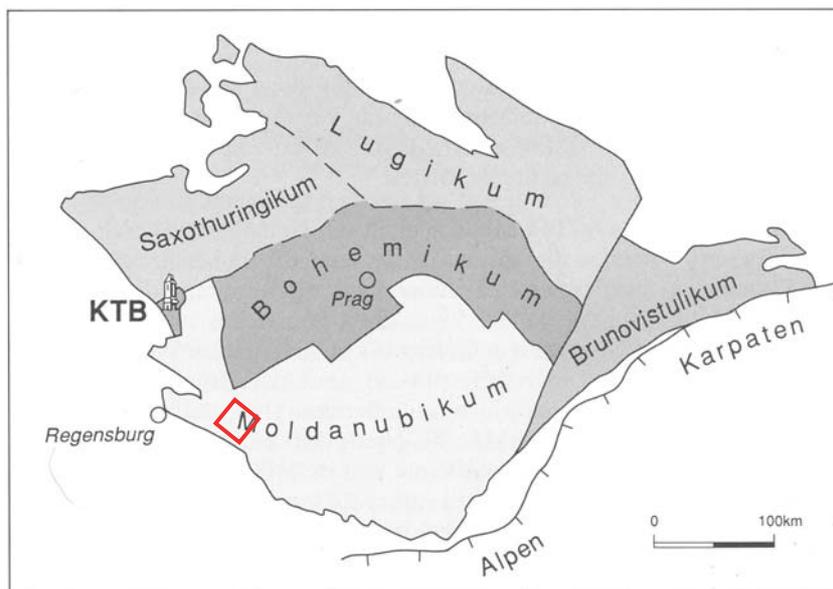


Figure 1-3: Subdivision of the Bohemian Massif according to Stettner (1992). KTB: Location of the Continental Deep Drilling Program site. Red rectangle: approximate location of the study area.

an assembly of paragneisses and amphibolites, marble, leucocratic gneisses and graphite layers, which have been interpreted as the remains of a volcano-sedimentary sequence of a possibly late Proterozoic to early Paleozoic age. The sulfide ore deposits of Lam and Bodenmais are attributed to volcanic-fumarolic activity of a yet

unknown age (Rohrmüller et al., 1996a), although Troll (1967a) links them to euxinic sediments metamorphosed at a maximum temperature of 730° C and a maximum pressure of 304 MPa (3000 atm), which corresponds to a depth of approximately 11km below the topographic surface. Geotectonically, the Bunte Gruppe has been associated with volcanism in continental rift zones, marginal seas, or small oceanic basins and is believed to be in a hanging position relative to the Monotone Gruppe.

The rocks in this terrane have endured several metamorphic events throughout the Paleozoic. The dominant process was a low pressure-high temperature event, which formed cordierite-K-feldspar- as well as garnet-cordierite-K-feldspar parageneses at pressures of 3-4 kbar and temperatures of 650-750°C. This main phase was most likely preceded by an older medium-pressure event, which has not been dated exactly but is assumed to be associated with the early Variscan or Caledonian orogenies. A more detailed summary of the terrane's tectonic evolution will be given in section 1.2.2.

The Pfahl fault zone separates two areas with different metamorphic grades. While high-grade paragneisses and local migmatites crop out north of the zone, partially molten migmatites, diatexites and anatexites, as well as completely homogenized granitoids dominate the area to its south. North of the PFZ the metamorphic grade increases from NE to SW. Thus, in the Künisches Gebirge just N of the study area mica schists associated with quartzites, metavolcanics, marbles, and graphite layers are the dominant lithology. Both Fischer (1965) and Vejnar (1965) as well as Stettner et al. (1997) interpret this unit as the early Paleozoic roof complex of the Moldanubian region. Towards the Rundinger Zone in the SW (fig. 1-5) the lithology grades into mica gneisses and cordierite-sillimanite-K-feldspar gneisses.

This old metasedimentary sequence was intruded by a series of Variscan plutons (radiometric dates revealed ages of 330 to 280 Ma, Stettner (1992)). According to Troll (1967b) the first magmatic bodies in the study area for this dissertation intruded in the form of massive NW-SE striking dikes of porphyric granite ("Kristallgranit I") followed by diorites and quartz-mica diorites oriented in the same direction. Medium to fine-grained granites represent the youngest igneous rocks with the exception of late-stage aplites and pegmatites, which conclude the period of variscan igneous intrusions. $^{87}\text{Sr}/^{86}\text{Sr}$ isotope ratios suggest that the granitic intrusions belong to the S-type (melts produced in lower crustal regions from formerly crustal rocks) while the dioritic bodies show I-type (mainly derived from mantle material) isotope ratios.

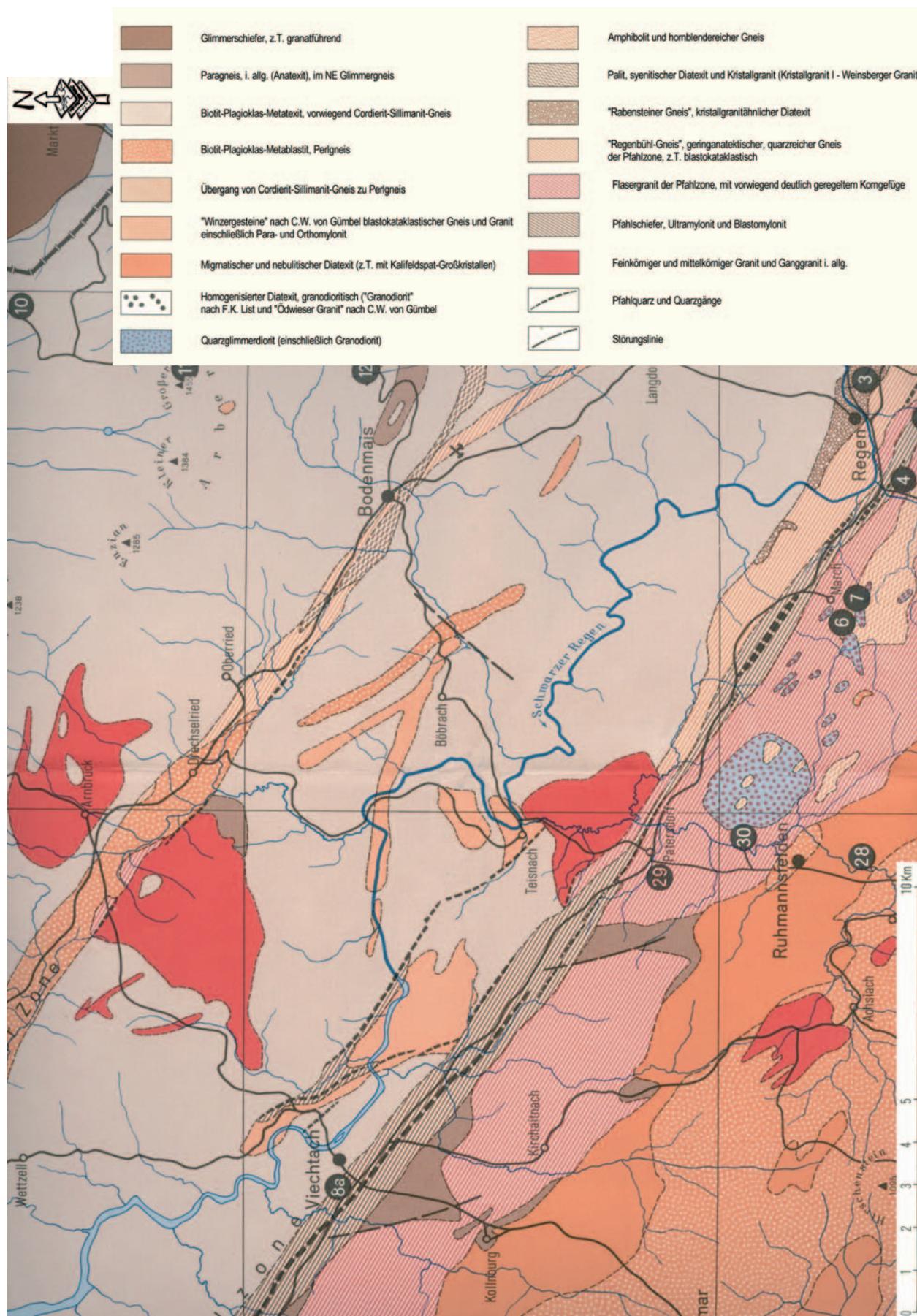


Figure 1-4: Geologic map 1:100,000 of the study area compiled by Troll (1964). Inset: Legend depicting the common rock types.

The Rundinger Zone and the Pfahl fault zone expose a special sequence of fault rocks. These NW-SE striking lineaments are associated with both high-temperature mylonites and greenschist-facies deformed rocks (proto-, ortho-, and ultramylonites with syntectonic quartz recrystallization, and to a minor extent microbreccia) as well as with cataclasites and lower-grade fault rocks. In addition, the PFZ encountered a late- and post-variscan hydrothermal phase (Horn et al., 1986), which silicified the fault and formed the now prominent walls of quartz cropping out in several locations along the lineament. The tectonic processes acting on these zones will be further described in section 1.2.2. Figure 1-4 gives a generalized impression of the distribution of the crystalline basement rocks in the study area.

While the literature provides little information on the **Mesozoic** rock record, the **Tertiary** in this region is characterized by intense bedrock weathering and denudation under (sub)tropical climate conditions, planation of the landscape, and the sculpting of most of today's relief due to brittle tectonic deformation and erosion. Since sedimentary blankets - with the exception of local quaternary infillings of valleys and surficial products of solifluction processes- are completely missing in the study area only in situ weathering material ("grus") covers the bedrock. In the study area's vicinity Tertiary sediments still crop out at the foot of the "Donaurandbruch" fault and in sedimentary bays interfingering with the crystalline basement at its southwestern edge (e.g. Hunderdorfer and Hengersberger Tertiärbucht) and in the sedimentary basin of the "Bodenwöhrer Senke" to the NW.

Priehäußer (1968) and Pfaffl (1989) describe the weathering processes and establish a time frame for the formation of the up to 70 meter thick grus blankets, which have been partly removed due to late Tertiary and Quaternary denudation. Grus blankets are an ubiquitous occurrence and have been observed to cover hills and ridges at altitudes of up to 1000 meters above sea level (Völkel, 1995). Priehäußer (1968) postulates that the weathering had been an ongoing process throughout the Tertiary until the Upper Miocene when the blankets reached their maximum thicknesses. The following colder climate of the Pliocene converted much of the lateritic, kaolinitized soils into cambisols.

Louis (1984) dedicates a short section on the development of the Regen river valley, but does not establish a connection between basement structure and relief formation. Moreover, he states, that especially the lower Regen valley formed completely independent of underlying geologic structures and attributes the NW-SE river valley between the towns of Regen and Viechtach solely to the trend of the Pfahl fault zone without acknowledging the very abrupt local deviations from the general direction. For the morphogenesis of the Upper Palatinate he postulates peneplanation until the Middle Miocene and contemporaneous to ensuing erosion of the river valleys, which in turn were partially filled and redirected by Late

Tertiary to Early Pleistocene gravel sediments. A similar approach is taken by Desiré-Marchand and Klein (1987). They describe the morphology of the Fichtelgebirge region, the Bohemian Forest, and the Bavarian Forest as a system of “Rumpftreppen” (peneplains arranged in steps of different altitude levels), which subdivide the regions in continuously distributed planes of equal altitude. This is achieved by solely denudative processes is not influenced by area’s tectonic structure. Kubiniok (1988) describes the *grus* units between the Danube river valley and the Inner Bavarian Forest as the root zone of a Tertiary tropoid weathering layer and maps out relictic peneplains and inselbergs for his study area. He also does not mention a relationship between relief and underlying basement structure.

In his morphogenetic description of the central Regen river valley Peterhoff (1986) begins to integrate the conventional model of peneplanation with regional tectonic aspects. Although he utilizes only the large Hercynian and Variscan lineaments for his explanation without recognizing the sub-regional and local tectonic structure he shows that the river generally follows the trends of major fault zones. Peterek (2001) describes the morphogenesis of a section of the northeastern Bavarian basement (the Fichtelgebirge mountains) and places the beginning of the formation of the present-day landscape in the Oligocene. In contrast to Louis’ (1984) view he postulates vertical crustal movements, erosion, and ensuing formation of river valleys as well as the partial removal of the older Tertiary saprolite as the dominant morphogenetic processes. He further establishes a close connection between the neotectonic evolution and relief development of that area (Peterek et al., 1996).

During the ***Pleistocene*** periglacial conditions predominated in the study area, although evidence for glaciations in higher elevations with end moraines at altitudes of 830 to 1025 meters above sea level has been reported (Jerz, 1995; Pfaffl, 1989; Priehäuser, 1930, 1963a; Raab, 1999). Lower elevations received an extensive coverage with firn blankets reaching down to approximately 400 meters above sea level at their lower end (Pfaffl, 1989; Priehäuser, 1963a). Especially Priehäuser (1955; 1961) describes glacial morphological formations such as cirques, moraines, outwash plains, bedrock outcrops exposed by glacial erosion, block fields, and cryoturbated soils. However, the “Firnegrundschutt”, a supposedly basal layer of compacted cryoturbated soil and debris beneath firn blankets postulated in his works (Priehäuser, 1930, 1951), was later dismissed and redefined as “Fließerde”, a gravitationally cryoturbated soil (discussion summarized in Völkel, 1995).

During cold periods permafrost penetrated the ground, while thawing in the active layer during the summer months loosened the uppermost 1 to 2 meters, which resulted in morphogenetic processes such as solifluction, freeze-thaw weathering, and the formation of

asymmetric valleys. On steep slopes along ridges and summit areas the Tertiary saprolite was locally completely removed, and the bedrock became exposed to periglacial weathering. Ice wedging in fractures produced blocky debris, which is now found in the block aprons below these exposures (Priehäüßer, 1961). The remaining grus layer faced downhill transport by solifluction processes during which the larger blocks frequently sunk into the surficial zone of the grusy matrix, thus forming deposits of several meters in thickness at the lower parts of hill slopes as well as in valleys (Jerz, 1996). A characteristic sign for this phenomenon are downhill bends of steeply dipping relictic gneissic foliations in the saprolite, whose uppermost parts became entrained in the transport and dragged with it (Priehäüßer, 1955). As a result of all these processes most of today's morphology of the study area was finally sculpted by the end of the Pleistocene.

Compared to the Pleistocene little research has been published on the **Holocene** geology of the study area. Most workers (Jerz, 1996; Pfaffl, 1989) dedicate only a short section in their publications on the Quaternary to this epoch. This most recent part of the area's geologic history is dominated by fluvial morphodynamic processes and anthropogenic reshaping of the landscape. Thus, small alluvial fans, terraces of gravel deposits in river valleys, peat in swamps produced by the aggradation of small glacial lakes, and organic soils represent the characteristic Holocene formations. Finally, anthropogenic deposits such as landfills, embankments etc. complete the sequence of geologic materials in the study area.

Rohrmüller et al. (1996a) summarize the geologic history of the Eastern Bavarian Basement the following:

Early Archaean	~ 3.8 Ga	Oldest magmatic event (zircon-date)
Precambrian	~ 2.5-2.6 Ga	Crystallization age of protoliths of the sedimentary rocks making up the moldanubian paragneisses
	~ 2.0-2.1 Ga	Magmatic events, granitic orthogneiss (granitic intrusion in southern Bohemia)
	~ 1.4 Ga	Magmatic events (felsic orthogneiss: Dobra-Gneiss)
	~ 1.0-1.1 Ga	Magmatic events, mafic and ?felsic melts (intrusion and extrusion)
Late Precambrian		Clastic sediments of shallow water coastal areas or open shelves
	~ 600 Ma	Crystallization age of the protoliths of the sedimentary rocks making up the Saxothuringian and Moldanubian paragneisses Cadomian orogeny, no unambiguous geochronological evidence for this event in Bavaria
Ordovician		Orogeny, regional metamorphism and anatexis, formation of Palites
Silurian		Subduction – closure of an ocean; sedimentation, microfossiliferous mica schists in the "Künisches Gebirge" (among other locations)
Carboniferous		Late Variscan orogeny including a low-pressure high-temperature metamorphism; nappe thrusting; HPLT metamorphism (formation of granulite; relictic kyanite)

	Termination of the regional HTLP metamorphism in the Moldanubian and Saxothuringian terranes; intrusion of gabbroid to dioritic and granitic melts; local mylonitization and diaphoresis as well as blastomylonitization; crustal cooling below 350-300°C and uplift;
Permian	Main phase of Saxothuringian and Moldanubian granite intrusion From Westfalian or Stefanian formation of "permo-carboniferous", postvariscan molasses; clastic sediments and alluvial fans in a structured relief ("Rotliegendtröge"), crustal extension
Triassic	Subsidence of the "Süddeutsche Großscholle" and of parts of the bordering Bohemian Massif (regional crustal extension) Reactivation of NW-SE fault zones, differential uplift of crustal blocks; formation of quartz mineralization in the Pfahl fault zone due to "rift-and-wrench-tectonics" (crustal extension with strike-slip component)
Cretaceous	Formation of peneplains and erosion of covering strata in locations of exposed basement rocks, compressional tectonic regime Upper Cretaceous transgression in areas of present-day exposed basement; uplift of the western edge of the Bohemian Massif in several phases; differential block tectonics (= crustal uplift and erosion)
Tertiary	Begin of the sedimentation in the Eger-Graben, local thrusting of basement rocks over upper Cretaceous sediments, formation of extensive erosional planes Formation of present-day relief, post-miocene uplift of gravel planes
Quaternary	Differential block tectonics with uplift rates of several tens of meters; further sculpting of the present-day relief, solifluction in periglacial areas Recent stress field: NNW-SSE compression; micro-earthquakes in the vicinity of the Eger-Graben

1.2.2 Structural geologic/ tectonic overview

The revolutionary concept of plate tectonics, which completely changed the perception of the Earth's structure, necessitated a revision of the traditional models explaining the structural evolution of the eastern Bavarian basement complexes. Rohrmüller et al. (1996b) provide a list of publications about the different approaches. In the 1980s, mobilistic - plate-tectonic models slowly became favored over the traditional fixistic concepts of crustal evolution (Rohrmüller et al., 1996a). However, this new knowledge did not lead to one single theory but resulted in a large variety of divergent opinions and models.

Throughout the 650 Ma lasting deformational history of the study area covered by various authors at least four major orogenies can be singled out from the rock record. Rohrmüller et al. (1996b) list the following ductile deformation events (only aspects relevant for the tectonic history of the study area are included here):

Cadomian orogeny	Cadomian metamorphism only detected in the zone of Tepla-Domazlice, not in the Moldanubian terrane s. str.
Caledonian orogeny	Ordovician and Silurian orogenies; only confirmed by radiometric dates; Formation of "moldanubian" rocks in the Bavarian Forest
Acadian (= early Variscan) orogeny	Nappe displacement, collision of the Moldanubian and Bohemian terranes; medium pressure/high temperature metamorphism
Sudetic (= Variscan) orogeny	Collision of Laurentia/Baltica with Gondwana, nappe movements, extensional structures in the Moldanubian terrane and at the interface with the Bohemian terrane (amphibolite to greenschist facies mylonitization); until 320 Ma: low pressure/high temperature metamorphism, then cooling below 350-300°C and regional uplift; late to postdeformational intrusion of granites and diorites (340 to 280 Ma); late Variscan mylonitization, formation of blastomylonites, and retrograde metamorphism in large fault zones (e.g. the Pfahl fault zone); final stage of the ductile deformation of the Eastern Bavarian basement

Stettner (1992) provides a more detailed picture and identifies seven individual orogenic phases for the Moldanubian terrane (figure 1-5). For the Moldanubian terrane tectonic transport directions as well as the continental plate configuration at the time of their collisions have rarely been the focus of research. Most publications concentrate on the orientation of different fold generations or petrologic-mineralogical aspects of the orogenies (Behr et al., 1980; Rohrmüller et al., 1996b). In contrast, the Bohemian crustal units such as the Zone Erbsdorf-Vohenstrauß, the Münchberger Masse, and the Gabbro-Amphibolitmasse Neukirchen b. Hl. Blut, as well as the Bohemikum-Moldanubikum-Saxothuringikum interfaces have received much more attention regarding the plate-tectonic framework (Duyster et al., 1995; Rohrmüller et al., 1996b; Stein, 1988; Stettner, 1992; Stettner, 1996).

Tait et al. (1996) establish a regional plate-tectonic and paleogeographic model for the Paleozoic (fig. 1-6). Based on this publication, a brief synopsis of the plate constellations throughout this period will be given before summarizing the available regional details. According to the aforementioned authors this time period was characterized by a 150 Ma lasting phase of collision and continental accretion, which eventually culminated in the Late Paleozoic assembly of the supercontinent Pangea. During the Early Ordovician the major continental units were Gondwana comprising the later African and South American plates, located about the South Pole, Laurentia –the largest part of present-day North America– situated in equatorial latitudes, and Baltica –today's Scandinavian region– between 30° and 60°S. While Laurentia remained geographically fairly stable in the early stages of this period Baltica and the Avalonian and Armorican platelets started drifting northward. The Bohemian Massif, together with the Iberian and Armorican Massifs, constitutes part of the Armorican microplate, which was attached to the northern margin of Africa at that time.

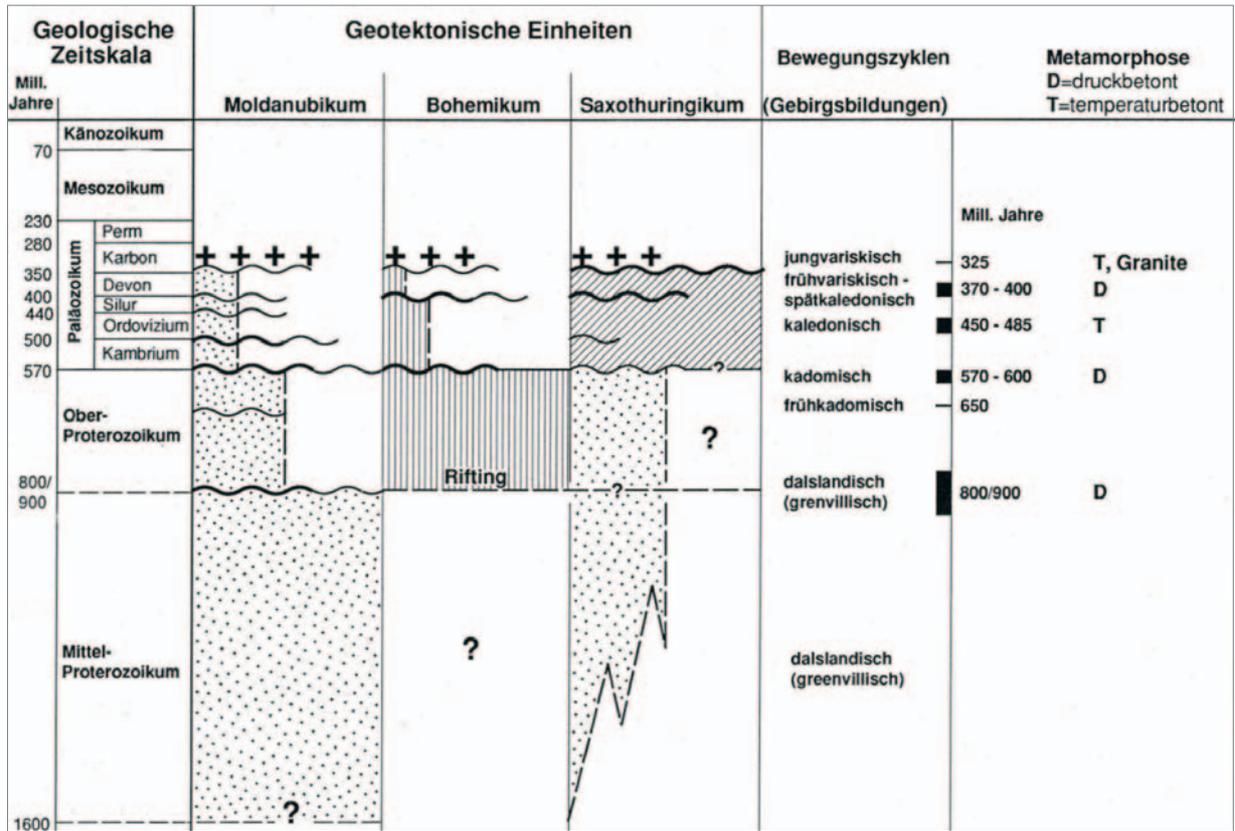


Figure 1-5: Orogenic periods in the Moldanubian, Bohemian, and Saxothuringian terranes. Wavy lines: orogenic phases; crosses: Upper Carboniferous granite intrusions. Source: Stettner (1992).

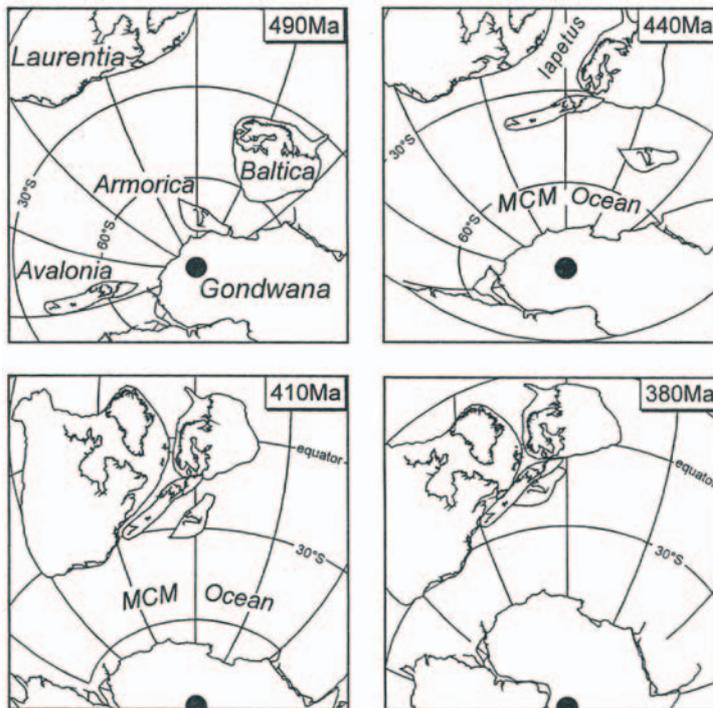


Figure 1-6: Paleogeographic reconstructions of the circum Atlantic continents for the Lower Ordovician through Devonian times, using paleomagnetic data taken from various authors. MCM Ocean: Massif Central-Moldanubian Ocean. Compiled by Tait et al. (1996).

By the late Ordovician Ashgillian age Armorica had rifted from northern Gondwana and followed Baltica and Avalonia on their drift towards Laurentia, although Van der Voo (1988) places this separation in the Devonian. He presents biogeographical arguments to corroborate an association between the two areas until the mid-Paleozoic. Thus, Gondwana would have drifted northwards along with the intervening microplates. However, Van der Voo (1983) also postulates Late Cambrian rifting and a separate drifting history of Armorica. Tait et al. (1996) point

out the controversial drift history of Gondwana, so the relationship between the two plates has to remain unresolved at this point. Until the Late Silurian/Early Devonian this drifting process entailed the successive closure of the Iapetus, Tornquist and Rheic oceans between Baltica and Laurentia, Baltica and Avalonia, and Avalonia and Armorica, respectively. By the Late Silurian the Bohemian Massif was adjacent to the southern edge of Baltica/Avalonia. During the Middle to Late Devonian an extensional period caused the partial re-opening of the Rheic Ocean, thereby bringing about the formation of the Rhenohercynian Basin in western Germany. Van der Voo (1988) places divergent plate motions between Laurentia and Gondwana in the same time period. Paleomagnetic data further suggest a counter-clockwise rotation of about 150° of the Bohemian Massif excluding the Saxothuringian terrane at some time between the Early Devonian and Late Carboniferous. This rotation is believed to have resulted in the collision between the Tepla-Barrandian and Saxothuringian terranes around 380-370 Ma. The final accretion of Pangea during the Late Carboniferous and Permian, which led to the present-day configuration of Variscan Europe, marks the latest Paleozoic tectonic event. During that time Laurentia and Gondwana collided in the equatorial region thereby compressing the intervening microplates between them and Baltica.

Comparing the paleomagnetic record and the resulting paleogeography to the tectonic timetable provided by Stettner (1992, fig. 1-6) reveals some interesting parallels between the rock record and the plate configuration at certain times during the Paleozoic. While the pre-Devonian plate configurations do not indicate major continent collisions, the late Caledonian (fig. 1-6) orogeny falls well within the timeframe of the collision between the microplates, Laurentia, and Baltica. According to Van der Voo (1988) an involvement of Gondwana is possible as well. Earlier orogenic events might thus be due to intraplate deformation within Armorica. Only Van der Voo (1983) shows a marginal entrainment of the western part of Armorica in the Late Ordovician/Early Silurian Taconic (in Europe Caledonian; see fig. 1-6) orogeny.

Regional petrographic and radiometric data from the Bohemian Massif, however, suggest a much more complex deformational history. For the Moldanubian terrane Rohrmüller et al. (1996b) point out a polyphase ductile deformation history characterized by several metamorphic events. Relictic garnet and kyanite suggest an older (Acadian/Caledonian) regional metamorphism. Connected to this event is the formation of anatexites in the Outer Bavarian Forest. The Variscan orogeny represents the dominant HTLP event dated at 330-320 Ma for the Moldanubian terrane. Remnants of the oldest foliation are present only in the internal structures of minerals such as garnet. The relative formation ages of later foliations and (semi-)ductile folds cannot be determined uniformly throughout the Moldanubian, since NW-SE trending folds refold NE-SW trending ones in

northern Upper Palatinate, NNE trending ones re-fold NW trending ones in the area of Waldmünchen, and NW trending ones re-fold NE trending ones in the Künisches Gebirge.

For the northern part of the Moldanubian region Stein (1988) reports five distinct ductile deformational phases. He attributes the D_1 to D_3 phases with their generally NE striking features to the final stage of the convergence of Laurentia and Gondwana. During this convergence the intervening mosaic of smaller terranes (older crustal segments) encountered several NW-SE directed collision events. In the course of these events an S directed subduction occurred, during which the Saxothuringian region was overridden by the Moldanubian. Thereby, the Moldanubian region acted as a wedge causing indentation structures similar to today's Himalayan arc. The D_1 generation is characterized by an s_1 metamorphic layering caused by compositional changes (leucosomes and melanosomes) on a mm to cm scale. Due to a later multi-phase deformation the original orientation of this fabric cannot be reconstructed. F_1 intrafolial monoclinial flow folding on a cm scale is associated with this phase. As with the layering, the original trends of fold axes remain unknown. D_2 is characterized by a symmetrical isoclinal F_2 flow folding with amplitudes from several cm to several dm. The frequently flat-lying axial planes are oriented subparallel to the s_1 layering. The folds strike NE-SW, verging both NW and SE. During this phase a penetrative s_2 fabric, marked by preferentially oriented biotite, formed. In contrast to the rather small-scale D_1 and D_2 features the F_3 fold generation formed syn- and antiformal structures several kilometers in size and thus is reflected in the regional morphology. It comprises open upright folds with rhombic symmetry. Related to the regional structures smaller parasitic flow folds were observed in outcrops. The F_3 generation was formed homoclinal to the F_2 and thus trends also NE-SW. A syn-deformational s_3 foliation developed, whose presence is dependent on the local lithology.

Similar to D_3 , D_4 deformation also shows upright open folds with amplitudes on a km scale associated with outcrop-scale parasitic folds. However, the folds are concentric with a uniform layer thickness on limbs and hinges and trend in (N)NW-(S)SE directions. A foliation did not develop during this phase. The D_5 generation is characterized by recumbent, both N-S and E-W trending, fracture folds with subhorizontal schistosity. Amplitudes range from centimeters to meters. Stein (1988) attributes this change in axial trends to a new NE-SW compressive regime, which also influences the later (semi-)brittle dextral shear system along NW-SE trending regional faults (D_6 phase). He interprets this stress field as the final stage of the Moldanubian indentation.

This now leads to the (post-)variscan semibrittle and brittle deformation of the Moldanubian terrane, the consequences of which largely dominate the topic of this

dissertation. Early tectonic activity in this period was mainly concentrated along the large semibrittle fault zones, such as the PFZ, the Rundinger Zone, or –further to the Southwest– the border fault complex of the Donaurandbruch, but occurred as rather localized mylonitic entities as well (fig. 1-7). Behr et al. (1980) summarize the semibrittle deformation history of the area and subdivide it into an older high temperature (>600°C) and a younger low temperature (<275-300°C) mylonitization event. The older one was placed in the Ordovician to Devonian and is assumed to have been caused by SW directed thrusting. Both the Rundinger Zone and the “Perlgneis” units South of the PFZ are seen as enormous thrust sheets, while the PFZ had not yet developed by this time. A later regional metamorphic event (“anatexis II”) formed the “Perlgneis” proper, which is characterized by metablastic plagioclase “pearls”. In zones, which were affected by a later mylonitization the old “mylonite I” fabrics had been widely obliterated. The second phase of LT mylonitization (mylonite II) produced the PFZ during the Upper Devonian to Upper Carboniferous due to the tilting and ensuing rotation of the block of the Outer Bavarian Forest. This process resulted in normal motion along the PFZ and the Donaurandbruch fault. The resulting rocks are subdivided into two groups: low-grade mylonites, which provide the protoliths for the more widespread second subgroup, the very-low-grade mylonites, characterized by chlorite + albite (+ epidote) (+ amphibole) parageneses. The late very-low-grade mylonitization was an ongoing process throughout the final stages of regional tilting. The sense of slip for the mylonite II generation was determined from lattice-preferred-orientations of quartz and cordierite to be mainly vertical for the “Pfahlschiefer” mylonites in the vicinity of the PFZ, and horizontal for the cataclastic deformation of augengneisses.

Cetin (1986) objects to this presentation and only describes high-grade mylonites for the central Bavarian Forest. He rejects the notion of the “Perlgneis” being a lower-crust mylonite and groups the remaining units into an older generation of statically recrystallized (e.g. in the Rundinger Zone) and a younger generation of dynamically recrystallized mylonites (ubiquitously distributed South of the PFZ, within the PFZ, and the Rundinger Zone). While he could not determine slip directions for the older group, he postulates NW directed low-angle normal motion along the NW-SE to E-S striking mylonitic foliation for the younger type.

Masch and Cetin (1991) modify the model presented by Behr et al. (1980) by enlarging the regional extent of the HT mylonitization event and by rejecting the assumption that either the Rundinger Zone or the “Perlgneis” areas of the Outer Bavarian Forest were active during the phase of LT mylonitization.

At this point it has to be noted, however, that most of the shear sense interpretations discussed above heavily rely on the analysis of quartz crystallographic fabric asymmetries, which Simpson and Schmid (1983) report to possibly produce equivocal results if not interpreted in connection with other shear sense indicators such as asymmetric augen or pressure shadow structures, or composite planar fabrics. Those more reliable indicators were considered –possibly due to a lack thereof- only to a minor extent.

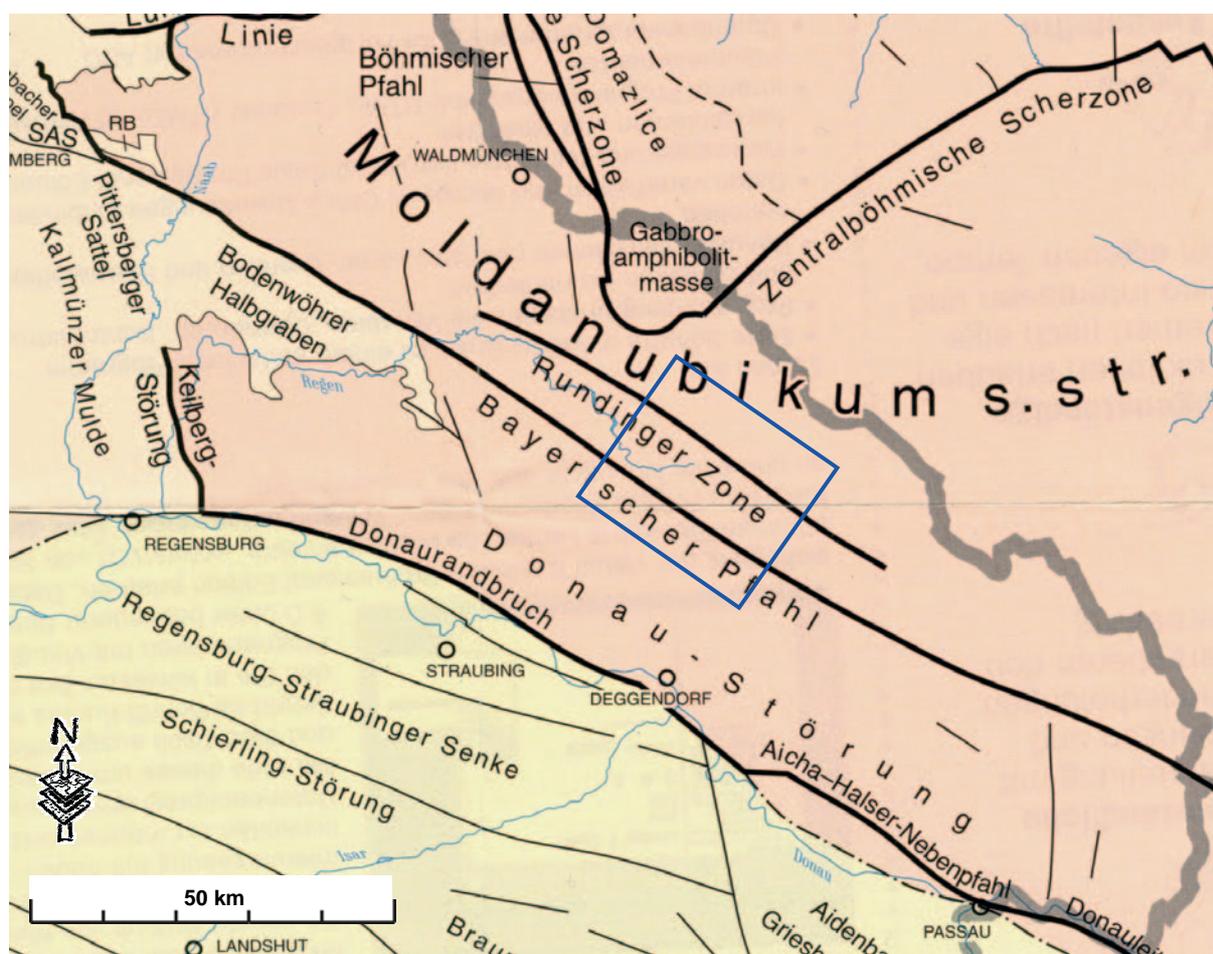


Figure 1-7: Tectonic map of the study area (blue rectangle). Source: Geologische Karte von Bayern GLA, 1996, Beilage 8.

The period between the Upper Carboniferous and the Upper Permian marks the onset of semi-brittle deformation in the Eastern Bavarian basement. The purely brittle tectonic history of the study area has been widely neglected by researchers, compared to the plethora of publications on ductile and semi-brittle tectonics. The different phases are commonly summarized as only one brittle deformational event (Rohrmüller et al., 1996b; Stein, 1988). In order to obtain more detailed information on this aspect one also has to browse publications dealing with the Mesozoic and Tertiary terranes surrounding the Bohemian Massif, which are underlain by the crystalline basement as well (Freudenberger, 1996; Unger, 1996). Research conducted by Bergerat and Geysant (Bergerat, 1981-1982; Bergerat and Geysant, 1982, 1983) focused on deciphering the complex brittle tectonic

history of Eastern Bavaria and integrated their findings into the continent-scale movements of the Eurasian and African plates since the early Tertiary.

Both Hofmann (1962) and Behr et al. (1980) report on the earliest brittle tectonic events along the Pfahl fault zone. Hofmann (1962) was the first to recognize that the PFZ is not merely one single quartz-filled fault, but a complex en échelon array (“Fiederspaltensystem”) of small (tens of meters in length) silicified extensional joints. According to his interpretation they are the result of a weak –possibly Sudetian- NW-SE oriented compression followed by an Upper Permian main-stage hydrothermal event. Steiner (1969) dismissed this notion of small individual quartz veins and proposed a two-stage model of initial quartz mineralization of the PFZ and ensuing break-up of a once continuous quartz vein by NNW-SSE oriented strike-slip faults. He in turn was disagreed with by Bültemann and Hofmann (1986), who claimed that he misinterpreted the age relationships between the main stage fault activity of the PFZ and the much younger hydrothermal activity. The angular relationships between the general strike of the PFZ and the en echelon veins were initially assumed to be conjugate with dextral displacement along the main faults and sinistral shear along the quartz veins. This view was modified by Gromes (1980), who identified the quartz veins as purely extensional features while the PFZ and tributary faults (especially the “Dietersdorfer Nebenpfahl) were assumed to represent the main dextral strike-slip fault associated with synthetic Riedel-type shears, respectively. Accordingly, NNE-SSW striking structures produce the sinistral antithetic shears. A similar model is proposed for the analysis of DEM lineaments in section 3.1.1.2. Rohrmüller et al. (1996b) relate the post-variscan deformation of the PFZ to Permo-Triassic rift-and-wrench tectonics.

From the analysis of fluid inclusions in the Pfahl quartzes Behr et al. (1980) deduce four SiO₂ precipitation events at temperatures of 200 to 250°C, which translate into an early-stage overburden thickness of 5 to 6 km and a late-stage (Upper Permian) thickness of 3-5 km. They estimate a total of 1300 to 6000 km³ of hydrothermal fluids to be necessary to form the bulk amount of the Pfahl quartzes. The quartzes of the older precipitation events had been cataclastically deformed, and intense seismic activity is assumed for the entire period of quartz mineralization. This is evidenced by the presence of pseudotachylites, ultramylonites and fault breccia in the rock record. For the polycyclic silicification event Behr et al. (1980) propose a “seismic pumping” mechanism described by Sibson et al. (1975). This model involves initial extensional fracturing above a doming focal region, which is the result of a volume increase of hydrothermal fluids. This fracturing leads to an effective porosity enhancement and the migration of the fluids. The emplacement of the hydrothermal solutions causes elevated pore pressures and reduced friction, which eventually results in failure, and thus, seismic activity. After the earthquake collapsing structures again increase the pore

pressure and thus squeeze the fluid into higher crustal levels. Another model for the explanation of the polyphase silicification of a fault zone, which, however, has not been considered by researchers in the Bavarian Forest so far, was postulated by Altamura (2003) for the Lantern Hill Fault in SE Connecticut (NE USA). It focuses on the strengthening of a rock during the sealing of open fractures by mineral precipitation from hydrothermal fluids. Once all fractures from a previous phase of fracturing are sealed strain can accumulate in the rock until it is released by ensuing brittle failure. Repeated cycles of fracturing and annealing produce an intricate pattern of cross-cutting fractures and shear zones.

While repeated cycles of faulting and silicification characterize the first brittle tectonic events in the study area the largest part of the brittle deformation has occurred since the late Mesozoic. Both Freudenberger (1996) and Unger (1996) describe the tectonic evolution of the geological entities surrounding the Bohemian Massif, thereby providing useful insights into the brittle deformation history of the crystalline basement as well. In his tectonic description of the Bavarian part of the epicontinental basin of Southern Germany Freudenberger (1996) establishes a relationship between the reactivation of Hercynian structural elements and the north-south oriented compressional tectonics of the alpine orogeny, which reactivated the old fault systems with a right-lateral shear sense. For the area of the Donaurandbruch fault zone he lists predominant NW-SE, NNE-SSW, and NNW-SSE trending brittle structures. In NE Bavaria he establishes an age relationship between the older NNW-SSE and the younger NW-SE faults.

Unger (1996) provides a timeline of tectonic events in the molasse basin to the South of the Bohemian Massif for the Cenozoic. The Molasse Basin is underlain by the southwestern extension of the crystalline basement, which has been displaced along the Donaurandbruch fault with a maximum throw of 1300 meters. Hercynian trending fault lines under the sedimentary blanket, such as the "Landshut-Neuöttinger Abbruch", have been geophysically identified. They have been deformed in a manner similar to the Bohemian Massif. Thus, the deformation history of this geotectonic unit is - to a certain extent - characteristic for the exposed crystalline basement to the North as well. Unger (1996) postulates a period of tectonic unrest between the Late Jurassic/Early Cretaceous and the Egerian during which the throw along the main fault lines and antithetic (N-dipping) structures had been increased. The regional tectonic context of this phase was a W to SW directed drift of the Bohemian Massif, which caused older lineaments, such as the Donaurandbruch and the Keilberg faults, to bend. Simultaneously, NNW-SSE oriented transform fractures began to open. After the Upper Oligocene end of this period the area remained relatively stable until the Middle Miocene. During this time the Bohemian Massif underwent an en bloc uplift independent of the N-directed stress exerted by the alpine orogeny. The transition from the

Middle to the Upper Miocene marks the last major phase of tectonic activity, which again increased the displacement along the main fault lines and was accompanied by a further subsidence of the alpine molasse basin.

A detailed picture of Tertiary brittle tectonics in Eastern Bavaria is provided by Bergerat and Geyssant (1983). From the rock record they derive a timeline subdivided into five individual stress fields, all related to the collision between the European and African continental plates: 1) N-S compression, 2) E-W extension, 3) NE-SW compression, 4) E-W compression, 5) N-S extension. After a Cretaceous to Eocene phase of regional arching (N-S extension) due to the early-stage Austro-Alpine and Carpathian orogenies, for which no field evidence was found by the authors, the first N-S compressive regime results from the advancing orogenic front of the central and eastern Alps. It manifests itself through right-lateral strike-slip displacement along the large NW-SE striking lineaments in Eastern Bavaria and reverse motion along E-W striking faults in the Franconian Jura. During the Upper Eocene the suture between Africa and Europe is strong enough to entrain the European plate into the general eastward motion of the African continent. This E-W extensional phase produces large regional structures, such as the Rhinegraben rift valley, in regions closer to the continental margins. In the Bohemian Massif it reactivates the Pfahl and Franconian Line fault zones with a normal sense of displacement. Moreover, the Cretaceous Bodenwöhr half-graben encountered further subsidence due to the eastwards attenuated extension. The transition from the Oligocene to the Miocene marks the end of the subduction process in the Carpathians to the East, thereby changing the stress regime from E-W extension to NE-SW compression. The ridge-push exerted by the ongoing opening of the Atlantic Ocean further adds to the NE-SW crustal shortening in the germano-czech triangle. The effect on the structures in Eastern Bavaria was a widespread reverse motion along the major fault lines (PFZ and Franconian Line) as well as minor hercynian striking lineaments. N-S to NNE-SSW striking faults in the Jurassic rocks to the West of the Franconian Line were active as dextral strike-slip faults, while E-W trending structures acted as conjugate faults with sinistral displacement. An ensuing clock-wise rotation of the maximum normal stress shifts the compression to E-W. It reactivated preexisting structures such as northwest-southeasterly striking faults (sinistral strike-slip), NE-SW striking faults (dextral strike-slip), and NNW-SSE striking faults (reverse motion). The last brittle tectonic phase derived from the rock record manifests itself in a localized Aquitanian to Helvetian N-S extension in northern Bohemia. It created subsiding grabens accompanied by alkaline volcanism as well as a number of ENE-WSW to WNW-ESE striking normal faults along a line roughly between the cities of Nürnberg and Amberg. The period since the Miocene is again characterized by renewed convergent plate movements of Europe and Africa. Seismic and in situ stress measurements suggest a recent NNW-SSE compressive stress field. This contemporary stress field is corroborated by

the World Stress Map database (Reinecker et al., 2004), which yields subhorizontal NW-SE to N-S directed compressive stresses.

1.2.3 Hydro(geo)logic and climatic overview

In a regional context, the region of the Bavarian Forest, in which the study area is located, is part of the major catchment of the Danube River and is draining its runoff over the tributary of the Regen River. The segment of the Regen River catchment containing the study area comprises 1001.89 km². In this region an average annual precipitation of approximately 1000 mm is reached. Annual mean temperatures range from 7 to 8 °C at lower elevations to 4 °C in the highlands of the Arber region. The average surficial runoff measured at the Teisnach stream gauge amounts to 22.2 l/s*km² (Bayerisches Amt für Wasserwirtschaft, 1998).

The rate of groundwater recharge in the Bavarian Forest National Park was quantified by Thums (1993) who calculated an average of 11 l/s*km². For smaller catchment areas of local springs Raum (2002) reports recharge rates of 5 to 10 l/s*km². Seiler and Müller (1995) mention lower rates of 70 mm/a (i.e. 2.22 l/s*km²) for regions with predominantly granitic lithologies and 60 mm/a (i.e. 1.90 l/s*km²) for regions with predominantly metamorphic lithologies. Wells in this region are commonly associated with yields ranging in the 0.5 to 5 l/s segment described by Krásný (2002) as potentially serving "... for local water supply (small communities, plants, etc.)".

For the Bavarian Forest and other German low mountain ranges several models of the stratigraphy of the hydraulically significant depth interval have been proposed by various workers (Altermann and Rabitzsch, 1977; Bader and Weinelt, 1975; Bronstert and Plate, 1996; Priehäuser, 1952b, 1963b; Priehäuser, 1971; Saker and Jordan, 1977; Seiler and Müller, 1995). Most of them agree on a general classification into three parts with different subdivisions introduced by the different studies. From top to bottom the three major units of the aquifer comprise a quaternary overburden, a zone of partially to completely decomposed bedrock (grus or "Zersatz"), and unweathered fractured bedrock. In their conceptual model of hard rock aquifers in France and India Lachassagne et al. (2001) structure the subsurface somewhat differently. Leaving out the quaternary overburden they begin at the top with a layer of sandy to clayey "alterites" representing the "Zersatz" horizon reported by the abovementioned authors. It can reach thicknesses of zero to tens of meters and is followed at depth by a "weathered-fissured zone", which can also extend vertically over several tens of meters. In granitic lithologies densely spaced subhorizontal unroofing joints predominate in this horizon while in metamorphic rocks fractures parallel to the foliation prevail, which are

assumed to form in response to a alteration-related volume increase of mica. This zone is also supposed to be associated with increased transmissivities. The bottom part of this model is formed by the unweathered crystalline basement, which is assumed to be highly transmissive along major fault and fracture zones.

The Quaternary overburden consists both of Pleistocene deposits including block fields, solifluction and outwash sediments, as well as occasional till in higher elevations, and Holocene sediments such as fluvial deposits and soils. A comprehensive classification of quaternary deposits in German low mountain ranges of the former German Democratic Republic is given by Altermann and Rabitzsch (1977). In parts of the Bavarian Forest the deposits can reach thicknesses of up to ten meters, however in most cases they are significantly less extensive (Bader and Weinelt, 1975). Priehäuser (1952b; 1963b) attributes only a limited hydrogeologic significance to these strata. According to him, block fields mainly accommodate interflow and do not possess any storage capacity. He only mentions special types of solidified earth flow deposits (“Firneisgrundscht”¹) as water-bearing strata. In contrast, Raum (2002) characterizes the overburden – depending on individual grain size distributions – as porous aquifers or aquitards with both laterally and vertically highly variable hydraulic properties. However, due to their shallow nature these deposits only possess a limited filtering capacity with respect to contaminants. Thus, water obtained from these strata is frequently inadequate for use as drinking water, especially in the vicinity of settlements and agricultural sites.

The unit underlying the quaternary deposits is of a very heterogeneous nature with respect to its hydrogeological properties and thus also controversially discussed. It is made up of partially to completely weathered bedrock (grus) interspersed with residual blocks of bedrock, which become larger and more densely spaced with decreasing distance to the unweathered basement. Priehäuser (1952b; 1963b; 1968) and Raum (2002) provide schematic profiles of this unit, which can reach thicknesses of several tens of meters. Especially the latter and Priehäuser (1968) subdivide this unit further. According to these workers the actual “grus” - a layer in which the bedrock loses its coherence and disintegrates into a quasi-unconsolidated matrix with a sandy texture interspersed with residual blocks - is overlain by strata, which underwent advanced chemical alteration during the subtropical climate periods of the Tertiary. From top to bottom the profile of these overlying strata includes a zone of Pliocene brown clayey soil beneath the Pleistocene cover, followed by a

¹ This term, suggesting a formation under a firn field (similar to a subglacial basal moraine), is no longer in use, because the old interpretation is now rejected. The actual processes leading to this type of deposit are not yet fully understood. Also, the “Firneisgrundscht” is no longer believed to store significant amounts of groundwater. Dr. Johann Rohrmüller (Geologischer Dienst – LfU Bayern). Personal communication, April 2007.

brick-red sandy and clayey horizon of decomposed bedrock. This horizon is separated from a yellowish-white kaolinic unit by a thin layer of hard blackish Fe-Mn precipitates. This unit is underlain by the abovementioned *grus*. With increasing depth the *grus* layer grades into the unweathered bedrock. Priehäußer (1968) inserts a zone of small-scale fracturing (“Zone der Kleinzerklüftung”) above the unaltered bedrock. Raum (2002) applies the term “zone of loosening” (“Auflockerungszone”) to steeply inclined slopes where gravitative processes lead to a further loosening of the topmost parts of the bedrock and to an increased opening of fractures subparallel to the strike of the slope.

While several authors (Bender, 2001; Breuer, 1998; Priehäußer, 1952b; Priehäußer, 1971) interpret this layer as a porous aquifer yielding significant amounts of groundwater tracer tests performed by Raum (2002) showed that this is frequently not the case. According to these tests relict fracture systems, frequently filled and thus stabilized with fractured quartzitic mineral precipitates, represent the dominant flow paths and therefore introduce hydraulic anisotropies in the presumed porous aquifer. With respect to the hydraulic conductivity of the *grus* units (leaving aside the secondary porosities) Raum (2002) quotes values of 5 to $6 \cdot 10^{-6}$ m/s. Karrenberg (1981) reports conductivities of $5 \cdot 10^{-7}$ to $4 \cdot 10^{-6}$ m/s. According to Freeze and Cherry (1979) these numbers lie in the order of magnitude of values for silt or silty sand deposits and correspond to those of fractured igneous and metamorphic rocks. Stober (1995) quotes transmissivities of $1.9 \cdot 10^{-4}$ to $3.6 \cdot 10^{-4}$ m²/s for heavily weathered granites in the Black Forest (SW Germany). Krásný (1999) lists transmissivity values for hard rock aquifers in Southern Bohemia (western Czech Republic). For intensely weathered gneiss he reports transmissivities of 25 to 150 m²/d (corresponds to $2.89 \cdot 10^{-4}$ m²/s to $1.74 \cdot 10^{-3}$ m²/s).

The underlying unweathered bedrock in the Bavarian Forest has not yet received a lot of attention, much in contrast to other crystalline basement regions in Germany, such as the Black Forest or the former German Democratic Republic. In the latter Hähne and Franke (1983) established a schematic model of a fractured bedrock aquifer and characterized its components. Until recently, this part of the subsurface was widely seen as an aquiclude in the Bavarian Forest (Bayerisches Amt für Wasserwirtschaft, 1998; Breuer, 1998). The contributors to the “Wasserwirtschaftlicher Rahmenplan Naab – Regen” (Bayerisches Amt für Wasserwirtschaft, 1998) only acknowledge fractured granitic lithologies as potential aquifers. According to them, metamorphic rocks do not possess significant storage capacities for groundwater. Thus, most studies so far have focused on the *grus* and weathering zone. Nonetheless, Priehäußer (1952b; 1963b) recognizes fractures in the bedrock, recharging from the overlying *grus*, as important contributors of groundwater in wells. He also mentions

a highly productive well (12 l/s) in the vicinity of Rabenstein (Bavarian Forest), which obtains most of its yield from a fractured paragneiss (Priehäußer, 1971).

Only recently did the fractured basement in this part of Germany attract more attention of researchers. However, most of their studies deal with the crystalline basement in the neighboring Czech Republic. Nonetheless, their findings can be applied to the Bavarian Forest as well, because both regions belong more or less to the same geologic entity. Havlík and Krásný (1998) calculated regional transmissivity values for the crystalline basement of the Bohemian Massif and came up with a background transmissivity of slightly more than 10 m²/d (equals about 1.2·10⁻⁴ m²/s). Superimposed on this background they identified several regional positive anomalies, which coincide with Tertiary fault zones. These anomalies are associated with transmissivity values about one order of magnitude above the background. With respect to the regional distribution of lithologic units (i.e. metamorphic and igneous) they could not establish any correlation. On a local scale they report very heterogeneous transmissivity values, for which they have no final explanation. However, they assume the different fracturing behavior of various lithologies, borehole design and location, as well as the local characteristics of the quaternary overburden to play a major role in the local heterogeneity of transmissivity. Masakova and Kobr (1998) reached similar conclusions in that they did not find a connection between well yields and lithology in the crystalline basement complexes of the Czech Republic. They relate groundwater discharge both to the “upper disintegrating zones” and to deep-seated fracture zones. Weise et al. (1998) report minimum fluid velocities of 50 m/d in deep-seated fault zones of NE Upper Palatinate. Based on hydrochemical analyses Dorsch et al. (1998) recognize groundwater contributions to surficial springs from deep-reaching fault zones.

Several authors report conductivities and transmissivities for various lithologies in the crystalline basement of the Bohemian Massif. Stober (1995) quotes studies which obtained conductivity values of 2.9·10⁻¹² m/s for gneisses in the KTB location (Windischeschenbach, Germany) and 3.0·10⁻⁷ m/s for the Falkenberg granite (Upper Palatinate, Germany). However, these values were obtained from drill cores and mainly represent the hydraulic properties of the rock matrix, thus grossly underestimating the rocks' bulk porosity stemming mostly from fractures (Stober, 1995, 2007b). For the Czech part of the Bohemian Massif Krásný reports transmissivity values of 0.3 to 180 m²/d (3.4·10⁻⁶ to 2.1·10⁻³ m²/s) for gneisses and migmatites, 0.25 to 25 m²/d (3.0·10⁻⁶ to 2.9·10⁻⁴ m²/s) for granites, 0.6 to 45 m²/d (6.9·10⁻⁶ to 5.2·10⁻⁴ m²/s) for orthogneisses, and 1.0 to 25 m²/d (1.2·10⁻⁵ to 2.9·10⁻⁴ m²/s) for granite veins. He attributes the large variations in these values to scaling effects due to heterogeneities introduced by brittle structures of various sizes. Increasing the size of the area of observation decreases the variability of the transmissivity values.

In conclusion it can be stated that the subsurface in the Bavarian Forest is a hydrogeologically very complex system, which is not yet fully understood. Especially on local scales large heterogeneities exist, which strongly complicate predictions with regard to the availability of drinking water in a given location. While the fractured bedrock has been neglected for a long time more and more recent drilling projects try to extract water from this part of the subsurface. Due to partly similar bulk transmissivities of unweathered fractured bedrock and the “Zersatz” zone (see above) these projects seem to be promising enterprises, some of which already proved to be successful (this study). However, because flow in the unweathered basement is entirely restricted to discrete zones, which have to be intersected by a borehole, the results of individual drilling projects can be highly variable. The aim of this study is to gain a better understanding of these discrete flow zones and therefore augment the probability of obtaining highly productive bedrock wells.

1.3 Previous work at the interface of brittle tectonics and hydrogeology

With respect to research integrating tectonics and hydrogeology the Bavarian Forest must still widely be seen as terra incognita. Nonetheless, a plethora of studies in the field of hard rock hydrogeology exists for other regions of Germany and the world. In the following a brief overview of a selection of the available literature shall be given.

While many standard text books on hydrogeology (e.g. Freeze and Cherry, 1979; Hölting and Coldewey, 2005) pay only little attention to fractured rock aquifers both special publications on the subject (e.g. Gelhar, 1993; Ingebritsen and Sanford, 1998; Karrenberg, 1981; Kolditz, 1997; Stober, 1986, 1995), conference publications (Annau et al., 1998; Seiler and Wohnlich, 2001a, b) and workshop readers (e.g. Kemmis and Kelleher, 2002; Stober, 2007a) as well as text books on engineering geology (e.g. Prinz and Strauß, 2006) give valuable introductions to various aspects in this field.

The bulk of the studies on specific aspects of hard rock hydrogeology can be grouped into three major fields: Theoretical and laboratory studies, research performed in field test sites, and regional studies. In the following a selection of publications will be briefly presented for each of these fields.

Theoretical and laboratory studies mainly focus on two aspects, namely fracture network characterization and fluid dynamics under controlled conditions. Concerning the former the earliest theoretical publications deal with methods of obtaining unbiased field data of fracture networks. Among the first was Terzaghi (1965) who introduced various methods of visualizing joint data and discussed various sources of bias in the sampling process. The

sampling techniques have been refined ever since. One of the latest methodological publications comes from Mauldon et al. (2001), who propose the use of circular scanlines and sampling windows, which widely eliminate sampling bias, instead of the traditional linear scanlines.

This type of research became increasingly important in the development of stochastic discrete fracture models, which try to mimic natural fracture networks as accurately as possible. A comprehensive theoretical introduction to this subject is given by Dershowitz and Einstein (1988) who discuss joint parameters important to the generation of stochastic networks and present various generation models. Black (1994) presents an update of these models and at the same time establishes a relationship between the numerical models and in situ packer tests, for which he shows type curves characteristic for various fractured aquifers. Advances in computer technology allowed the calculation of dual-porosity models, which integrate matrix porosity and fracture networks. Dershowitz and Miller (1995) discuss their application in fractured porous media. In order to enhance the performance of these models their constituting parameters were examined more closely. For instance, Power and Durham (1997) analyzed the topography of fracture planes and found that the surfaces of both natural and artificial extensional fractures had fractal characteristics with fractal dimensions of 2.25 and 2.45. Similar results were obtained for shear fractures, although they are associated with an anisotropic roughness due to slip. Keller et al. (1995) performed an X-Ray computer tomography on variable aperture fractures in small drill cores in order to calculate their transmissivities. The calculations underestimated the transmissivities with respect to the measured values. Cheema and Islam (1994) determined hydraulic anisotropies with a 2D analogue model based on the parameters fracture size and orientation. The experimentally obtained conductivity values agreed well with field measurements.

Because discrete fracture models require both significant data input and computation capacities several attempts were made to apply continuum models to larger-scale hard rock aquifers. Glass et al. (1995) developed a conceptual model applying characteristics of small-scale fracture networks to regional rock masses. Numerical 2D modeling performed by Zhang and Sanderson (1999) pursued the same goal by upscaling two-dimensional conductivity tensors determined from small-scale fracture networks. They concluded that the upscaling yields valid results for both constant and variable aperture fracture networks, although small sample sizes tend to overemphasize the magnitudes of the conductivity tensors. Bonnet et al. (2001) discuss various scaling methods in general and identify power laws and fractal geometries as the best descriptive tools for fracture network characterization. Several publications examine the possibility of a determination of a representative elementary volume (REV) from discrete fracture networks. Ji et al. (2004)

simulated 2D fracture networks and integrated various parameters of discrete elements, such as fracture density and aperture variability, to establish the REV of a given rock mass. They related the size of the REV to the correlation length (i.e. the mean distance of fractures belonging to the same cluster). However, in fractured media with large aperture variations they recommend the use of discrete fracture models. Similar limitations of the REV approach were found by Blum et al. (2007), who examined the parameters fracture orientation, length and density. Fracture density turned out to be the limiting factor in the determination of an REV. Low-density networks with densities of less than 13.1 m^{-1} could only be modeled with the discrete fracture approach. For fracture networks with higher densities REVs could be calculated. A different approach to determine bulk characteristics of fractured rock masses was taken by Boadu (1997). He calculated seismic attributes of fractured rocks, such as instantaneous amplitude, frequency and bandwidth and derived bulk characteristics of a fracture network.

The examination of fluid dynamics, the second prominent aspect of theoretical and laboratory studies, commonly focuses on flow within a single discrete fracture or simple fracture networks. An exception is made by Papadopoulos (1967) who was among the first to develop flow equations in anisotropic aquifers. In doing so he characterized flow through a fracture network of an infinite anisotropic aquifer, in which a well is pumped at a constant rate. Parney and Smith (1995) simulated flow in two-dimensional orthogonal fracture sets and found out that only a small percentage of the fracture network is effectively utilized for flow. They also correlated the lengths of flow paths with the flow velocities within specific fractures. However, the longest paths did not correspond to the highest velocities. A “velocity optimization mechanism” creates a restricted range of fracture lengths associated with high velocities. Vesely and MIs (1998) simulated flow in a hypothetical 1000 m long vertical fracture with variable aperture and showed flow channeling by the distribution of hydraulic head. Leven et al. (2001) experimented with a sandstone block with a size of 1 m^3 as an analogue model for dual porosity flow. Considering the entire flow region fracture flow predominated over matrix flow. However, under certain conditions, especially when flow was induced normal to the trends of brittle structures, matrix flow became significant. Probst et al. (2001) discussed in theory various aspects of flow in hard rock aquifers and concluded in their conceptual model of regional groundwater flow that continuum models are not suitable to describe flow in fractured media.

For engineering and groundwater prospecting applications, however, research performed in test sites, such as the Hvaler test area in Norway, the Grimsel rock laboratory in Switzerland, or the Yucca Mountain site in Nevada/ USA, often yields more useful and applicable information than the theoretical studies. The test sites have been installed for a

multitude of purposes, the most important of which are the investigation of radionuclide transport in potential hazardous waste repositories and the examination of possible groundwater extraction from various fractured aquifers. In the following a selection of literature will be presented.

Gustafson and Krásný (1994) give a general introduction to hydrogeological properties of fractured rocks and cite results from various test sites, mostly in Scandinavia. In the Great Basin desert of the southwestern USA the U.S. Department of Energy is planning a permanent repository for high-level radioactive waste. Together with the nearby Pahute Mesa nuclear test site (the area where the U.S. government exploded 85 nuclear devices) this region has undergone almost five decades of hydraulic investigation (Geldon, 2004). In the Yucca Mountain test site Barton et al. (1993) developed a methodology to characterize bedrock fractures with respect to various physical properties such as fracture trace length, orientation, connectivity, aperture, roughness, shear offset, density, and mineralization. Additionally, they found that joints tend to form densely spaced swarms, three to five meters wide and spaced at 150 to 200 meters. Also, they determined “tectonic” fractures to possess rougher surfaces than extensional cooling joints in the examined tuff. Ferrill et al. (1999) characterized faults and joints of the Yucca Mountain site with respect to the recent tectonic stress field and found out that fractures ideally oriented for slip or dilation in the current stress regime are the most transmissive structures. In contrast, discontinuities perpendicular to the maximum compressive stress tend to be closed and thus are less transmissive. Similar results come from Barton et al. (1995) who report findings from the Cajon Pass scientific drill hole (California, USA), the Long Valley exploratory well (California, USA), and the Yucca Mountain test site according to which critically stressed faults (i.e. those on the verge of failure) are the most transmissive ones. Geldon (2004) summarizes 14 years of hydraulic testing at Yucca Mountain, which lead to the conclusion that transmissive zones in the subsurface of this area are not bound by lithologic or stratigraphic contacts but only by brittle tectonic structures. According to him, the most important parameters for fracture transmissivity are fracture length, spacing, and connectivity. At Yucca Mountain, the prominent fracture systems align with regional faults, which act both as conduits and as barriers, depending on their physical properties and on the way they offset transmissive zones.

Studies related to research for radioactive waste storage also come from the Swiss Grimsel rock laboratory, established by NAGRA, the Swiss national commission for the storage of radioactive wastes. For example, Schild et al. (2001) examined the microcrack networks of drill cores obtained from metagranitoid rocks of the site to determine the matrix diffusion of nuclear contaminants into these networks. They found enhanced transmissivities

parallel to the metamorphic foliation. The microcrack network was in general oriented parallel to the macroscopic fracture sets. In addition, they determined the matrix transmissivity of the studied rock type to be $1.0 \cdot 10^{-12}$ while transmissivities in large faults could be as high as $3.0 \cdot 10^{-6}$ to $5.0 \cdot 10^{-5}$. Also new techniques and research materials are tested at the Grimsel site. For instance, Einsiedl et al. (2001) injected a new fluorescent tracer in rocks of the location. Research intended to be applied to nuclear waste storage projects was also carried out by Cacas et al. (1990) in the Fanay-Augères experiment site in central France. These workers sampled the fracture network and performed hydraulic as well as tracer tests in horizontal and inclined boreholes drilled in a tunnel of an active uranium mine. With these data sets they established a discrete fracture model and determined various hydraulic parameters of the site.

Several other test sites, most of them significantly smaller and less well funded, are designed to explore groundwater flow for the use in water supplies. In the Lawrence Berkeley Laboratory Fracture Hydrology Field Site Mabee and Hardcastle (1997) performed a fracture domain analysis developed by Mabee et al. (1994) with data obtained from outcrop and borehole televiewer measurements and correlated their findings with results from hydraulic tests. They identified a zone of laumontite-filled fractures as a flow barrier. Also, their fracture domain analysis gave a spatial distribution of various fracture sets, which allowed the prediction of specifically oriented fractures in the subsurface based on outcrop measurements. Thus, these workers recommend the recording of fracture locations in addition to strike and dip measurements.

A water supply tunnel construction site, on average 70 meters below the topographic surface, in eastern Massachusetts (USA) is the location of various surface, subsurface, and remote sensing studies. Williams (2000) sampled fracture data from 21 surface outcrops and a 9 km section of this tunnel and performed a fracture domain analysis. She found that fracture mineralizations are more abundant in the subsurface than in surficial outcrops and that both fracture trace lengths and spacings increase significantly with increasing depth. She also found a considerably stronger correlation between fracture density and increased groundwater flow than between rock type and flow. At the same site Mabee et al. (2002) tried to correlate topographic lineaments obtained from black and white, infrared, and SLAR aerial imagery with groundwater inflows in the tunnel, however with only limited success. They concluded that lineaments can be utilized for the identification of high-flow zones, but they should be analyzed in combination with other datasets, such as information about type and thickness of the overburden, bedrock type and the proximity to surface water bodies.

Regarding the applicability of lineament studies Banks et al. (1994) report similar results from the Hvaler study site in southeastern Norway. They stated that topographic and geophysical anomalies do not guarantee the identification of highly transmissive zones. Moreover, depending on their physical properties, fracture zones with significantly reduced transmissivities could be identified as well. They also mention a limited significance of geological research with respect to groundwater prospecting and call drilling for water in fractured bedrock largely a “game of chance”. In order to still enhance hard rock well productivities they recommend focusing on borehole design and the use of artificial enhancement techniques such as hydraulic fracturing. They also advise caution in the prediction of well yields and suggest that the probability of drilling a successful well rather than its productivity should be quantified.

Another study from southern Norway is reported by Skernjaa and Jørgensen (1994). They used azimuthal resistivity surveys to determine the orientations of fracture sets in the subsurface. The authors identified fracture orientation, density, aperture, trace length, and connectivity as parameters governing the results of the survey. In some cases the long axis of the resistivity ellipse lay between two dominant fracture sets, which was attributed to the resultant most conductive path combining the properties of the two sets. They also mention one drawback of the approach, which is the ambiguity stemming from similar electrical conductivities of water-bearing and clay-filled fractures. While the former represent the desired structures for groundwater exploration the latter may act as flow barriers.

Azimuthal resistivity surveys are also popular among researchers of the U.S. Geological Survey (USGS). Hansen et al. (1999) conducted a multi-approach study in igneous rocks at the Eastern Surplus Superfund Site in Meddybemps, Maine (USA), where groundwater contamination with volatile organic compounds (VOCs) was detected. The researchers employed surface and borehole geophysics, in particular azimuthal resistivity, acoustic borehole televiewer, and directional borehole radar surveys, to characterize the fracture network and to determine the potential extent of the contaminant plume. The resistivity data identified a high electrical conductivity in the NE-SW direction, while the other surveys found steeply inclined NNE-SSW and ENE-WSW to E-W trending fracture sets as well as a set of gently inclined discontinuities. Thus, the conductive zone identified by the resistivity measurements lies between two prominent fracture sets, similar to the findings by Skernjaa and Jørgensen (1994). Flowmeter data obtained in this site suggested groundwater inflow from all identified fracture populations.

A site in Durham, Connecticut (USA) contaminated with organic halides was also examined by the USGS with a variety of methods such as acoustic borehole televiewer log,

borehole geophysics, outcrop measurements, and azimuthal resistivity surveys. The subsurface in this location consists of Mesozoic basin-fill sediments and Quaternary lodgment till. Among their most important findings was that the drilling of bedrock wells alters the natural flow system by connecting previously unconnected fractures. Fracture flow influenced by natural and induced hydraulic gradients is the dominant transport process, while contaminant retardation occurs mainly by matrix diffusion.

In the crystalline basement of northeastern Connecticut (USA), which shows several similarities to the Bavarian Forest, Emery and Cook (1984) investigated the recharge from the overburden to a fractured bedrock aquifer. They stress the importance of the overburden to the underlying bedrock flow system, which derives 80 to 100 % of its recharge from surficial materials, and suggest that the two units be treated as one semi-unconfined aquifer complex. The authors also state that “hydrogeologists and engineers investigating the placement or migration of waste materials should never assume that bedrock is impermeable, and that the bedrock/ overburden interface will act as a natural hydraulic boundary.” Stasko and Tarka (2001) made similar observations in an abandoned mine in southwestern Poland. They also stress the significant contribution of the overburden to the groundwater flow in the fractured bedrock.

Several workers examined scaling effects of fracture networks and their hydraulic properties on various scales. Guimerà et al. (1995) report increasing hydraulic conductivities with increasing scale of observation at a granitic site in Spain. However, they suspect a sampling bias towards exaggerated conductivities at larger scales due to the siting of the pumping wells in highly productive zones in this particular test site. Nieto-Samaniego et al. (2005) analyzed the scaling behavior of fractures along a fault in granitic lithologies in Baja California (Mexico). After performing a fractal analysis of the fracture network at different scales they report a self-similar behavior as well as an upper limit of fracture density at a given scale.

Various other studies have been carried out at test sites all over the world dealing with a multitude of different aspects. Himmelsbach et al. (1999; 1992; 1994) performed a variety of hydraulic tests at sites in the southern Black Forest (Germany) to determine matrix and fracture porosities as well as mean fracture apertures in pristine granitic rocks and their faulted equivalents and in ore dikes to investigate transport processes in fissured rock aquifers. In the same locations Himmelsbach (1993) used natural and fluorescent tracers to determine transport characteristics and groundwater residence times in various parts of a granitic hard rock aquifer. Piscopo (2001) compared fracture measurements obtained from bedrock outcrops to pumping test data at two sampling sites in southern Italy and concluded

that outcrop fracture data can be utilized to determine both the heterogeneity and the hydraulic anisotropy of a fissured rock aquifer. Only the problematic extrapolation of the findings into greater depths limits the applicability of this approach due to the overestimation of fracture apertures at depth. Wang et al. (2001) investigated a road construction site at the Arizona state route 260 (USA) with respect to the long-term availability of construction water. For this purpose they created a discrete fracture model based on acoustic televiewer data and pumping test results, which they used to predict the water level decline in the construction well field over the duration of the road construction project. In a sealed-off section of a sandstone quarry in southwestern Germany (site layout described by Bäuml et al. (1998)) Thüringer et al. (2001) combined the results of gas tracer tests with a discrete fracture model to determine flow and matrix diffusion in a double-porosity medium. Findings from a deep drilling project in the crystalline Ötztal-Stubai complex are reported by Kriegl et al. (2001). According to this study water-bearing zones with fracture porosities of up to 25 % were found at depths of 904 and 1835 m below the surface. From this data average aquifer porosities and transmissivities of 6.6 % and $1.20 \cdot 10^{-5} \text{ m}^2/\text{s}$ were determined. The geothermal well constructed in this project finally yielded 4.5 l/s of 47° C warm water for a thermal spa.

Finally, a number of regional studies is reported by various authors. Drew et al. (1999) performed a U.S. quadrangle-sized exploratory variography of well yields of the Pinardville quadrangle (Maine, USA) and correlated their findings with several lithologic and structural geologic aspects of the area. They established a direct relationship between rock types and the properties of fracture patterns and found that zones of high and low well yields aligned with regional tectonic structures and lithologies.

Mabee et al. (1994) examined a 44 km² island off the coast of Maine (USA) with respect to topographic lineaments and proposed a new method of reducing the noise in lineament data, which includes various sampling trials, reproducibility tests, and a “domain overlap analysis”. In addition, they found that wells situated within 30 meters of lineaments filtered with this new approach were significantly more productive than wells at greater distances of such lineaments. For the same study area Mabee (1999) identified a set of factors predominantly influencing the transmissivities in 35 domestic bedrock wells. In decreasing order of importance he lists bedrock type, topographic setting (i.e. the location of a given well e.g. in an upland valley, on a ridge, etc.), proximity to fracture-correlated lineaments, and structural position (i.e. the location of a well e.g. in the hinge or the flank of a regional fold). The influence of other aspects, such as type and thickness of the overburden, the proximity to surface water bodies, and the water table depth turned out to be statistically insignificant. He further mentions that usually a combination of several factors, rather than a single one, is responsible for the productivity of a bedrock well: He also states that “a set of

factors in one geologic setting does not necessarily have the same significance when applied to wells in a different geologic setting.” In the crystalline basement of Great Bay, New Hampshire (USA) Degnan and Clark (2002) carried out an analysis of topographic lineaments over an approximately 390 km² region and found a good correlation between dominant fracture systems and neighboring lineaments. A lineament study performed in the Mesozoic formations of the Kinzig Basin (part of the Main river catchment, Germany) by Anbazhagan et al. (2001) suggested correlations between the proximity of topographic lineaments with well data, such as specific yields, transmissivities and static water levels. They also suspect the intersections of major lineaments to be the most promising sites for highly productive wells.

In the Norfolk Chalk (England) Toynton (1983) compared transmissivity anisotropies with fracture patterns obtained from bedrock outcrops and found good correlations between the two datasets. He mentions that “a comparison of fracture orientations with point and areal transmissivity ellipsoids shows not only that the anisotropic nature of the aquifer is a direct result of the fracturing but also that this behaviour can be predicted by studying the fracture pattern and vice versa.” Anisotropic flow conditions were also postulated for a study region in southern Portugal by Tröger et al. (2001). Their results show a relationship between fracture conductivity and the in situ stress field. Similar to Barton et al. (1995) and Ferrill et al. (1999) they found highly conductive fracture sets at specific angles to the maximum compressive stress (σ_1). These fractures were all critically stressed and oriented at 0 to 30° with respect to σ_1 . However, in contrast to the findings by Ferrill et al. (1999) purely extensional joints parallel to σ_1 were not associated with elevated transmissivities.

Fracture transmissivity data for almost 500 faults in the crystalline massifs of the central Swiss Alps compiled by Loew (2001) showed that only 1 to 10 per cent of the all fractures make significant contributions to the groundwater flux. Based on these findings he mentions that REVs cannot always be determined in this region due to the high variability of the transmissivity on various scales.

Stibitz (1998) created a map of potential groundwater resources in the Austrian part of the Bohemian Massif, which is based on borehole data, lineament analyses, and the analyses of landforms. Similar to Mabee (1999) he identified a set of factors predominantly influencing well yields. For his study area he determined lithology, topographic location (classified as high plains above 700 m a.s.l., low lands below 700 m, and other areas), and distance to neighboring lineaments to be the most influential factors for well productivity. Mira and Chambel (2001) related well yields to lithology in a study region in southern Portugal and found that highly productive wells were predominantly located in gneisses, migmatites,

gabbros, and amphibolitic gneisses, while little to unproductive wells were found mainly in granitic and dioritic lithologies as well as in orthogneisses, amphibolites, schists, and greywackes. However, they do not provide explanations for their in part contradictory results. Neither do they consider structural aspects for the distribution of well productivities. For the Czech part of the Bohemian Massif Masakova and Kobr (1998) determined the lithology in which a well is located to be insignificant for its productivity. Similar to Emery and Cook (1984) they stress the importance of the overburden to the overall performance of a hard rock aquifer and characterize the groundwater of this area as rather variable with respect to mineralization, composition, and temperature.

Finally, fluorescent tracer tests carried out in the “Zersatz” zone of various locations in the Bavarian Forest and Upper Palatinate by Raum (2002) showed that even the topmost parts of the subsurface are still controlled by a remnant fracture network. Flow paths determined in this study frequently deviated significantly from the direction of the hydraulic gradient and aligned with locally prominent joint sets and topographic lineaments. These important findings show that disintegrating bedrock cannot simply be modeled as porous aquifer, but that groundwater flow is still largely controlled by brittle petrofabrics in this medium. If at all, a double porosity situation may be assumed, in which the grusy matrix predominantly serves for storage. (Fast) flow, however, is preferentially accommodated by the remnant fracture systems. Only in the special case of reworked sandy granitic grus predominantly porous aquifer conditions may exist. Thus, the entire depth interval of the subsurface used for groundwater exploitation in the study area must be regarded as a heterogeneous and anisotropic aquifer.

1.4 Terminology

In order to ensure an unambiguous communication of this study's findings several geologic and hydrogeologic terms are specified in the following. Terms annotated with an asterisk are defined based on the American Geological Institute's *Glossary of Geology* (Neuendorf et al., 2005); text in brackets are comments by the author.

1.4.1 Geologic terms

cataclasite*	A fine-grained, cohesive cataclastic rock, normally lacking a penetrative foliation or microfabric. A cataclasite forms by pervasive fracturing, milling, crushing, and grinding by brittle deformation typically under conditions of elevated pressure, sufficient to keep the material from losing coherence and becoming a gouge. [In contrast to common practice this term is not applied to uncohesive fault rocks such as gouge and breccia.]
densely fractured / brecciated zone	A discontinuity in a rock mass along which shear displacement has initiated without discernable offset. The result is a zone of high fracture density grading into brecciation (cf. fig. 2-9 in section 2).
discontinuity*	A surface separating two unrelated groups of rocks; e.g. a fault or unconformity [used for all types of fractures, i.e. faults and joints].
fault*	A discrete surface or zone of discrete surfaces separating two rock masses across which one mass has slid past the other.
fracture*	A general term for any surface within a material across which there is no cohesion, e.g. a crack. Fracture includes cracks, joints, and faults.
fracture trace	The surficial expression of a fracture on a two-dimensional surface. (a) Structural geology: the line of intersection of a fracture with the surface of a bedrock outcrop. (b) Photogeology: topographic expression of an underlying fault/ fracture zone with lengths of commonly less than one kilometer. Fracture traces longer than 1 km are called lineaments.
grus*	A silicious sand resulting from weathering and granular disintegration of a parent rock, usually granite. [In the study area the grus overburden can consist of significant amounts of clayey weathering products. Thus, it is used synonymously with the term "saprolite" or the German "Zersatz" and is not subdivided any further for the purpose of this study.]
joint*	A planar fracture, crack, or parting in a rock, without shear displacement; the surface is usually decorated with a plumose structure. Often occurs with parallel joints to form part of a joint set.
lineament*	A linear topographic feature of regional extent that is believed to reflect crustal structure. Examples are fault lines, aligned volcanoes, and straight stream courses. [In this study used for structures longer than 1 km.]
lithogroup	A term introduced by Stone (2002). It is used for groups of rock types with similar physical properties in order to categorize lithologies for hydrogeologic purposes.
petrofabric*	The complete spatial and geometrical configuration of all those components that make up a deformed rock. It covers all terms such as texture, structure, and preferred orientation, and so is an all-encompassing term that describes the shapes and characters of individual parts of a rock mass and the manner in which these parts are distributed and oriented in space. [The term is synonymous with the German word "Gefüge".]
saprolite*	A soft, earthy, clay-rich, thoroughly decomposed rock, formed in place by chemical weathering of igneous, sedimentary, and metamorphic rocks. It often forms a layer or cover as much as 100 m in thickness, esp. in humid and tropical or subtropical climates; the color is commonly some shade of red or brown, but it may be white or gray. Saprolite is

characterized by preservation of structures that were present in the unweathered rock. [In this study it is synonymous with the term “grus”.]

scanline A survey line (i.e. a measuring tape) set up along a portion of a bedrock exposure. All fracture traces in reach of this line are recorded with respect to various physical parameters. Because the location of a fracture’s intersection with the scanline is recorded this information can be used for the calculation of fracture intensity.

1.4.2 Hydrogeologic and technical terms

cluster ID	Identification number attributed to a fracture based on its orientation during the K-means cluster analysis.
depth to casing	Depth of the lower end of the cased depth interval in a borehole.
fracture aperture	Average distance of separation across a fracture normal to its walls.
fracture density	Number of fractures of a specific fracture set per distance interval; equals the reciprocal of fracture spacing.
fracture intensity	Generally synonymous to fracture density. Special case: in FracWorks fracture intensity is the mean fracture area per unit volume of a rock mass.
fracture metadata	Physical properties of a fracture besides its orientation, e.g. fracture size, aperture, etc.
fracture planarity	Measure of the degree to which a fracture plane deviates from a flat surface. In this study the continuum from entirely planar to curved/undulatory was classified into five groups.
fracture spacing	Distance between two fractures belonging to the same fracture set normal to their planes; equals the reciprocal of fracture density.
fracture trace length	Distance along which the intersection of a fracture with the surface of a bedrock exposure can be observed.
fracture roughness/asperity	A measure defining the size and distribution of irregularities on a fracture surface. A high roughness decreases the effective aperture of a fracture. On the other hand, a high roughness prevents a fracture from completely closing in response to an applied tectonic stress. Thus, the hydraulically effective aperture of a rough fracture can be maintained over a large range of different stress regimes. In this study this parameter was grouped into six classes from very smooth to very rough.
groundwater influx	Point or depth interval where significant amounts of groundwater enter a well. In hard rock aquifers usually associated with fracture or fault zones. Used synonymously with the term “point of groundwater discharge”.
K-means clustering	A hierarchical cluster analysis to determine fracture sets based on the orientations of individual fractures of a dataset. For the clustering an initial number of clusters has to be specified to which individual fractures are attributed based on the distances of their poles in a stereographic projection.
point of groundwater discharge	Point where significant amounts of groundwater enter a well. In hard rock aquifers usually associated with fracture or fault zones. Used synonymously with the term “groundwater influx”.

primary porosity*	The porosity that developed during the final stages of sedimentation or that was present within sedimentary particles at the time of deposition. [Primary porosity is virtually absent in igneous and metamorphic rocks.]
secondary porosity*	The porosity developed in a rock after its deposition or emplacement, through such processes as solution or fracturing. [Secondary is the dominant hydraulic effective porosity in igneous and metamorphic rocks.]
variography / variogram*	A measure of spatial continuity that contains the information necessary for geostatistical estimation. A variogram is analogous to an autocorrelation function in time series analysis. Variograms may be anisotropic, i.e. may change in different directions.
well cuttings*	Rock chips cut by a bit in the process of well drilling, and removed from the hole in the drilling mud in rotary drilling or by the bailer in cable-tool drilling. Well cuttings collected at closely spaced intervals provide a record of the strata penetrated.

1.5 Methodology

In this section the methods used in this dissertation will be presented. While standard geologic and hydrologic techniques will only be mentioned briefly, special attention will be paid to detailing the rather unconventional approaches as well as the processing of data gained by them. Especially the geostatistical treatment of field data and the hydrogeological modeling with commercial software programs will be focused on, since the knowledge of their functioning is crucial to the interpretation of their results. For the statistical analysis of fracture data a sorting algorithm was programmed. Its function, along with further technical details on the hydrogeologic modeling will be discussed separately in appendices C and D.

1.5.1 Structural geology

1.5.1.1 Field methods

The examination of structural geologic features in the study area was conducted using standard field techniques described by Compton (1985) and van der Pluijm and Marshak (1997). Although this study focuses on brittle deformation, ductile and semi-ductile phenomena, such as outcrop-scale folds, rotated porphyroblasts, etc. were occasionally recorded to complement the brittle structural analysis. Fracture data were collected in the field in order to characterize six basic parameters: orientation, size (planar or trace length), density (spacing), kinematic indicators (slickenlines, conjugate relationships, etc.) mineralizations, and infillings (breccia, gouge). In addition fracture roughness, planarity, and aperture were measured in selected outcrops.

Fracture orientations were measured with a Brunton Pocket Transit corrected for 1.5° eastern declination using the right-hand rule. Alternatively, dip azimuths and angles (“Freiberger” method) were recorded together with the rake of lineations found on fracture planes, depending on the type of transit used for the measurements.

Since many outcrops were small and scattered, data of fracture orientations were collected in most locations using a modified version of the “subjective” approach explained by Spencer and Kozak (1974). With this method the observer records orientation measurements with respect to what he considers to be representative fracture patterns. In contrast to their approach more than one measurement of fractures within a single representative population were taken and mean values were calculated for each of them from a contoured density stereographic plot. The number of subjective measurements commonly totalled around 80 to 120 measurements per sampling location; in very small outcrops at least 50 data points were taken.

The “objective”, or “scanline” approach was only used in selected locations where the setup of an at least 15 meter long continuous scanline was practicable. For the scanlines a modified set up devised by Walsh and Clark (2000) and Williams (2000) was applied. Wherever possible the scanlines were randomly placed to eliminate sampling bias. Then, every fracture within 50 centimeters of the scanline (a measuring tape) with a trace length of more than 20 centimeters was recorded with regard to its orientation and the physical properties listed below. In addition, its distance from the scanline origin was measured for a fracture density analysis. As to the reliability of data obtained with the two methods reasonably good agreement of the data sets was found. Williams (2000) performed a statistical comparison of fracture data measured with the objective and subjective approaches in various outcrops and came to advocate the latter because it “takes approximately half the time of a scanline survey, gives generally the same results, and urges the geologist to spend time understanding the relationships between fracture sets in the outcrop.”

Physical properties of individual fractures, such as fracture size (or in case only fracture traces could be examined in vertical exposures, trace length), plane roughness, aperture, type of infillings/mineralizations, kinematic indicators, connectivity, and density/spacing were recorded according to methods described by Barton et al. (1993) and Williams (2000). For the data collection along scanlines standardized fracture characterization forms were used (see Appendix G), similar to those compiled by Williams (2000).

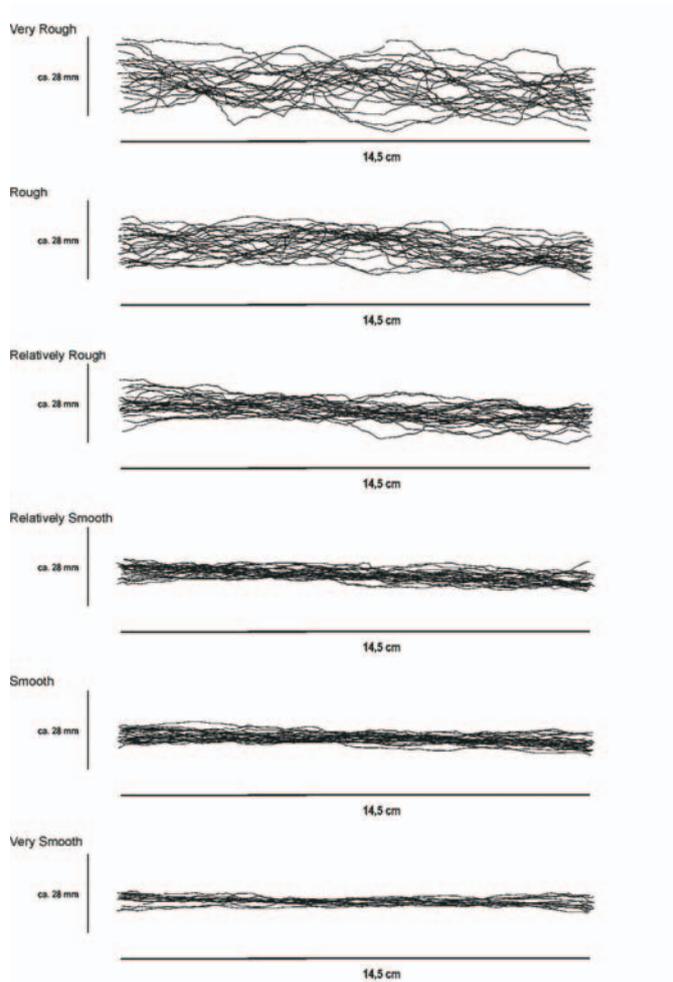


Figure 1-8: Roughness profiles obtained in twelve sampling stations. $n_{total} = 131$.

Fracture plane roughness was measured with a Vogel profile gauge with an effective length of 15 cm and a horizontal resolution of 0.8 mm. In selected outcrops reference profiles were taken for every one of the six roughness classes (very smooth to very rough). Figure 1-8 displays the results of the reference profile gauge measurements. Representative profiles were created from the measured profiles (fig. 1-9). These profiles were used for the comparison with fracture planes in the field, which were then classified accordingly. A similar approach was taken by Barton and Choubey (1977), who developed classification scheme consisting of ten classes. The situation in the outcrops for this study led to the establishment of six classes; a higher resolution could not be achieved in the field.

Roughness	Representative Profile	Amplitude (mm)
Very Rough		16.73
Rough		12.15
Relatively Rough		8.54
Relatively Smooth		5.96
Smooth		4.01
Very Smooth		3.58

Figure 1-9: Representative profiles for the six roughness classes. Amplitudes denote the mean values of individual roughness classes.

Fracture apertures between 1 and 15 millimeters were measured with a Vogel taper gauge (resolution 0,1mm); larger ones were measured with a standard DIN 862 caliper (resolution 1mm). It has been acknowledged by a variety of authors (e.g. Karrenberg, 1981) that the measurements of fractures intersecting surficial bedrock outcrops do not necessarily represent their actual aperture in the rock mass due to strain release effects in the vicinity of the free

surface. Thus, aperture measurements are most likely biased towards exaggerated values. However, the measurements made for the purpose of this study are not intended to derive

bulk secondary porosities in the rock mass but to highlight trends among the heterogeneously oriented fracture sets. Thus, assuming that strain release effects equally affect all fracture sets present in a given sampling location, the mean measured aperture of one set relative to that of another set was used to estimate potentially preferred flow directions of groundwater.

1.5.1.2 Database construction and statistical analysis of field data

The measurements collected in the field were plotted and contoured on equal-area diagrams using both StereoNett 2.46 and GEORient 9.2 software. Contours were calculated in StereoNett using the cosine sum method for smoothing and were expressed in multiples of random distribution (mrd). This contouring algorithm calculates the average density of poles for the entire stereographic net and expresses the contour intervals as integer multiples of that average (for more detailed information refer to the StereoNett Help File). Where available, kinematic indicators were added to the StereoNett database and paleostress configurations were calculated. This analysis was performed both for individual outcrops and in cumulative plots on a regional scale. For every sampling station a field report was compiled (appendix A). It contains a cumulative contoured stereographic plot of all fractures measured in a particular location as well as tabulated values of mean orientations of the dominant populations and their concentration on the plot as a measure for the variability of fracture orientations within a single population. Furthermore, additional plots of features of interest, such as slickensided planes or fractures with particular geometric relationships to each other were included. Short texts describing general observations in the respective sampling stations complete the field reports.

In addition to the plotting of fracture orientations in StereoNett and GEORient the data was also entered in Microsoft Excel for the further analysis of fracture properties in combination with their orientations. For this purpose both spreadsheets containing measurements taken in individual outcrops and spreadsheets with cumulative regional-scale data were compiled. This database was established to (1) define fracture classes possessing specific physical properties with respect to their orientations and to (2) obtain mean values for the stochastic generation of discrete fracture networks in the FracMan software. This classification was achieved by both the visual examination of stereographic plots and the statistical cluster analysis of tabulated fracture data. Since the hand-picking of individual fractures from stereographic plots for further processing has proven to be a rather tedious enterprise a multivariate statistical approach has been devised for the automated

classification of the raw data. This approach comprises a K-means cluster analysis² of fracture orientations attributing individual fractures to a pre-defined number of cluster centers (i.e. mean fracture orientations for each population)³. Once classified and attributed with cluster ID numbers these fractures could be sorted and filtered in MS Excel for the further analysis of their physical properties. For this purpose a MS VisualBasic for Applications macro was written, which performs the K-means analysis of fracture data and attributes the cluster ID numbers to fracture orientations in a MS Excel spreadsheet.

The sorted fracture data was separated with respect to the specific clusters and mean values of fracture metadata such as size, aperture, density etc. were calculated. In datasets containing measurements from scanline surveys fracture densities were calculated based on their distance from the scanline origin. Additionally, they were corrected for the angular relationships between fracture orientation and scanline trend in order to eliminate the sampling bias described by various authors (Terzaghi, 1965; Weiss, 1989; Witthüser and Himmelsbach, 1998). Since the distance between fractures of a specific set is commonly measured normal to their fracture planes their spacing along the trace of the scanline does not represent their real density. These values have to be corrected for both scanline trend and fracture dip. This was achieved by employing the following equations:

$$d_s = \sin \alpha \cdot d_m \text{ and} \quad \text{eq. 1-1}$$

$$d = \sin \beta \cdot d_s, \quad \text{eq. 1-2}$$

where d_s is the fracture distance corrected for the angle between the fracture strike and the trend of the scanline, α is the angle between fracture strike and scanline trend, d_m is the fracture spacing measured along the scanline, d is the real fracture spacing, and β is the dip of the fracture.

Thereupon, the results of the abovementioned processing were interpreted during the structural geologic (section 2), photogeologic (section 3), and hydrogeologic (section 4) analyses and utilized for the generation of stochastic discrete fracture models (more detailed information in appendices C and D).

² Developed as a MS Excel Macro in collaboration with Ulrich Schwenk (OptWare GmbH, Regensburg/ Germany)

³ A detailed documentation of the program code is provided in appendix C

1.5.2 Photogeology and geostatistics

For both local and regional-scale fracture-trace and lineament analyses several remote-sensing techniques have been employed, each with regard to the size of the area of interest. For small-scale (local) interpretations of remotely-sensed data aerial black and white photographs on a scale of 1:24,000 were chosen. Larger-scale analyses were performed on a satellite-based INSAR Digital Elevation Model approximately 56 by 45 kilometers in size.

Structural data extracted from both types of imagery were further processed in ArcGIS 8.3, ArcView 3.1, Microsoft Excel 2000 and GEORient 9.2.

1.5.2.1 Aerial photography

Aerial imagery was provided by the Bavarian state geological survey in the form of black and white photographs on a 1:24,000 scale. The data was acquired in the summer/fall of 1963 using an airborne metric camera with a focal length of 152,51 mm at a nominal altitude of 4170 meters. Almost all images were taken vertically except for several flight lines of low oblique pictures along the Czech border on the Lam, Bayerisch Eisenstein, and Zwiesel quadrangles (map sheet numbers 6844, 6845, and 6945, respectively). The images were analyzed in stereoscopic pairs using a Stereo Aids Geoscope Mirror stereoscope with 1.2x magnifying lenses. Fracture traces were drawn on transparencies laid over one picture of the stereo pair and digitized on georeferenced digital orthophotographs in ArcGIS 8.3 for further processing (see chapter 1.4.2.3). For the structural geologic interpretation of the imagery standard text book methods were applied (Gold and Parizek, 1999; Gupta, 2003; Jensen, 2000).

The following linear features were considered for the interpretation of fracture traces:

- linear segments of streambeds
- linear segments of major valleys
- elongated topographic depressions
- any other linear feature clearly not related to anthropogenic activity/ structures (e.g. roads, power lines, embankments, channels, etc.) or noise due to the data acquisition process (e.g. shadows).

1.5.2.2 INSAR Digital Elevation Model (DEM)

The INSAR DEM used for the analyses was created from C-Band ($\nu = 5,3$ GHz, $\lambda = 5,6$ cm) RADAR imagery taken by the ERS-1 and ERS-2 satellites operated by the European Space Agency (ESA). ERS-1 had been active from 1991 to 1999, ERS-2 has been active since 1995. Both satellites follow sun-synchronous orbits at a nominal altitude of 785 km. The azimuth resolution along their 102,5 km wide track is 30 m, their range resolution is 26 m. The digital elevation model was derived from a multiple-pass interferometry with a recurrence rate of 35 days (Jensen, 2000).

The DEM used for the lineament analyses presented here possesses a horizontal resolution of 25 m and a vertical resolution of 1 m. The data was projected in the German Grid Zone 4 (Gauß-Krüger grid). The corner coordinates were 4548170 E 5457360 N (northwestern corner) and 4603890 E 5411790 N (southeastern corner).

In order to better visualize the structural features of the study area the DEM was transformed into an aspect raster with the ArcGIS Spatial Analyst and reclassified into eight aspect classes. These classes group the exposition of every pixel in the raster into 45° bins (N to NE, NE to E, E to SE, and so on). A higher resolution of the aspect classes neither enhanced nor deteriorated the analysis of the image.

For the lineament analysis several polyline shapefiles were created on which linear topographic features of the aspect raster were traced. First, lineaments were identified on a full view of the raster image (the scale was approximately 1:390,000). Then the image was viewed on a 1:200,000 and 1:100,000 scale for the identification of smaller lineaments. The scale was not reduced further, since the relatively coarse resolution of the raster (25 meter pixels) did not warrant unambiguous linear structures. For smaller-scale fracture trace analyses aerial imagery was used (see chapter 1.4.2.1). A total of seven iterations of this process were performed to ensure a higher confidence of the numbers, lengths and orientations of the lineaments identified.

In order to eliminate sampling noise the data from the seven analysis runs were merged into one shapefile. All lineaments that did not appear at least three times in the merged file and did not strike within roughly $\pm 10^\circ$ of each other (this was determined only by visual inspection) were determined to be not reproducible and therefore removed from the dataset. The shapefiles were then used for further data analysis in ArcView 3.1 and GEOrient 9.2 (see chapter 1.5.2.3).

1.5.2.3 GIS-based analyses of remotely sensed structural data

The shapefiles created by the processes described in chapters 1.5.2.1 and 1.5.2.2 were imported into ArcView 3.1, since the Lineament Analysis Tool downloaded from the ESRI script database (Kim, 2004)⁴ could not be used in ArcGIS 8.3 due to a change in the programming language of the software.

The shapefiles containing the lineaments and fracture traces of each separate analysis run were interpreted with the Lineament Analysis Tool with regard to the following parameters:

- Lineament/ fracture trace length
- Orientation
- Number of intersections with other lineaments/fracture traces

The lineament/fracture trace orientations were grouped into 10° bins in a half circle, ranging from W over N to E (the bins ranged from -90° to 90°). The lineament statistics were output as dBase (.dbf) files and imported into Microsoft Excel for further processing. The data was regrouped into spreadsheets and prepared for plotting with regard to their orientations, numbers and lengths. Since a total of seven analysis runs exists mean and median values as well as the standard deviations were calculated for the whole dataset and visualized in several diagrams. Subsets of the regional dataset containing the study area *sensu stricto* were clipped and analyzed separately.

Lineament and fracture trace data were further exported as ASCII text files for processing in GEOrient 9.2. With this software lineament strike rose diagrams were created and normalized the cumulative lengths and counts of lineaments/fracture traces contained in each 10° bin. Finally the remotely sensed data was compared to the fracture data collected in the field. For this purpose, the strikes of fracture planes with dips greater than 50° measured in the field were plotted in rose diagrams in GEOrient 9.2.

In addition to the Lineament Analysis Tool (Kim, 2004) the Point & Polyline Tools for ArcView 3.x (Alsleben, 2001) were utilized to add lengths as well as start and end coordinates of the lineaments/fracture traces to the shapefiles. This allowed calculating the strike azimuth for each individual lineament/fracture trace in MS Excel and adding this information to the shapefile. With the help of these values groups of lineaments/fracture traces associated with specific strikes were mapped. The same tools provide a means to locate lineament/fracture trace intersections, which were mapped as described by Gupta

⁴ <http://arcscripts.esri.com>

(2003). From both the lineament/fracture trace and the intersection maps density distributions were calculated with the ArcGIS 8.3 Spatial Analyst (ESRI, 2002) and depicted for the study area with a one-standard deviation contour interval.

The results of each of the remote sensing analyses were compared with each other and with the ground truth data by conducting a domain overlap analysis (Mabee et al., 1994). For this approach fracture data from sampling stations distributed over the study area were laid over the modified lineament and fracture trace maps. Then the spatial distributions of fracture trends were compared with similarly trending coincident lineaments and fracture traces.

In order to achieve the correlation of fracture and lineament orientations the dominant strike directions were determined from the regional fracture dataset by the creation of a fracture frequency diagram. To this end fractures with inclinations of less than 50° were removed from the database, because mainly steep to subvertical fractures are presumed effective in the formation of topographic lineaments. After the dominant fracture orientations were identified sampling stations associated with one or more of these orientations were mapped and their fracture record compared to the trends of neighboring lineaments. In case the lineaments surrounding a sampling station were oriented similar to a prominent fracture strike present in this station the lineament was determined to be fracture-correlated.

The results of the domain overlap analysis are displayed as lineament density maps, on which correlated sampling stations are mapped. Additionally, the regional fracture and lineament data was plotted in rose diagrams to show larger-scale correlations.

1.5.3 Hydrogeology

Since hydrogeologic field investigations could not be conducted in the course of this study for cost and time reasons existing data compiled by hydrogeological consulting and geophysical survey companies as well as government institutions had to be resorted to. The sources of the specific datasets are mentioned in the sections in which they are discussed.

1.5.3.1 Processing of data provided by companies and government institutions

Data compilations provided by commercial and government institutions include various types of conventional and geophysical well logs and, in one case, surface geophysical information. The well logs can be referred to in appendices B and E. For several well sites in the study area only general information on well yields without further details

could be obtained. Especially information on yields of relatively old boreholes drilled in the 1960s and 1970s deviates significantly from present-day production rates. Yield data from more recent wells also tends to overestimate actual production rates for drinking water supplies. The reason for this possibly lies in the relatively short durations of the pumping tests, during which skin effects often prevail. Thus, the tests were frequently aborted before the true production rates could be determined. As a result, several wells are operated at rates below those established by the pumping tests. In sites where this was the case these yields were replaced by estimates made by the supervising engineering geologist who determined the effective rates under normal operation conditions.

Unfortunately, the well data was too sparse and unevenly distributed to conduct geostatistical analyses. Thus, the regionalization of well data was restricted to the calculation of mean values of various parameters and their comparison with several geological, tectonic, and hydrogeological aspects. More details on the specific approaches taken in the analyses of well data are presented in the respective subchapters of section 4.

1.5.3.2 Hydrogeologic modeling

The hydrogeological modeling conducted in this study consists of a three-step process and was performed with a K-means sorting algorithm developed specifically for this study and the FracMan/ MAFIC modeling suite provided by Golder Associates Inc. (Seattle, Washington – USA).

During the first step fracture sampling stations suitable for hydrogeological modeling were selected based on the availability and amount of fracture data. This data was processed with the K-means sorting algorithm such that fracture clusters with specific orientations could be established. For these clusters mean values of fracture metadata, such as size, aperture, intensity, etc. were calculated for their further processing.

In the second step stochastic fracture networks of these sampling stations were generated in the FracWorks module of the FracMan/ MAFIC suite based on mean values of specific physical characteristics of calculated fracture clusters. In the third step the networks were attributed with a number of hydrogeological boundary conditions (cf. section 4.3.1.4 and appendix D) and then used for flow simulations.

Further information on the modeling process can be obtained from appendices C and D as well as from sections 4.3.1.3 and 4.3.1.4.

1.6 References

- Bayerisches Amt für Wasserwirtschaft (ed.), 1998, Wasserwirtschaftlicher Rahmenplan Naab-Regen, v. München, 240 p.
- Alsleben, S., 2001, Point & Polyline Tools for ArcView 3.x, v. 1.1
- Altamura, R.J., 2003, Tectonics of the Lantern Hill Fault Zone, Southeastern Connecticut: Evidence for the Embryonic Opening of the Atlantic Ocean., *in* LeTourneau, P. M., Paul E. Olson, ed., The Great Rift Valleys of Pangea in Eastern North America. Volume 1. Tectonics, Structure, and Volcanism., Volume 1: New York, Columbia University Press.
- Altermann, M., and Rabitzsch, K., 1977, Zur Gliederung und Dokumentation der wichtigsten Lockersedimente der Mittelgebirge: Zeitschrift für angewandte Geologie, v. 23, p. 130-139.
- Anbazhagan, S., Aschenbrenner, F., and Knoblich, K., 2001, Comparison of aquifer parameters with lineaments derived from remotely sensed data in Kinzig basin, Germany, *in* Seiler, K. P., and Wohnlich, S., eds., New approaches characterizing groundwater flow, Volume 2: Lisse, A.A. Balkema Publishers, p. 883-886.
- Annau, R., Bender, S., and Wohnlich, S., 1998, Hard rock hydrogeology of the Bohemian Massif. 3rd international workshop. Windischeschenbach, Germany, October 1998: Munich, Ludwig-Maximilians-Universität München, 184 p.
- Bader, K., 1996, Analyse des geologischen Untergrundes mit Hilfe der Geophysik, Erläuterungen zur Geologischen Karte 1:500.000: München, Bayerisches Geologisches Landesamt, p. 280-287.
- Bader, K., and Weinelt, W., 1975, Geologisch-geophysikalische Untersuchungen für die geplante Trinkwassertalsperre Frauenau (Bayerischer Wald): Geologica Bavarica, v. 74, p. 179-192.
- Banks, D., Rohr-Torp, E., and Skarphagen, H., 1994, Groundwater resources in hard rock: experiences from the Hvaler Study, Northeastern Norway, Applied Hydrogeology, Volume 2: Hannover, Germany, Verlag Heinz Heise, p. 33-42.
- Barton, C.A., Zoback, M.D., and Moos, D., 1995, Fluid flow along potentially active faults in crystalline rock.: Geology, v. 23, p. 683-686.
- Barton, C.C., Larsen, E., Page, W.R., and Howard, T.M., 1993, Characterizing fractured rock for fluid-flow, geochemical, and paleostress modeling: Methods and preliminary results from Yucca Mountain, Nevada: Denver, Colorado, United States Geological Survey.
- Barton, N., and Choubey, V., 1977, The shear strength of rock joints in theory and practice: Rock Mechanics, v. 10, p. 1-54.
- Bauberger, W., 1969, Geologischer Strukturplan der Oberpfalz: Geologica Bavarica, v. 60, p. 45-51.
- Bäumle, R., Hötzl, H., Thüringer, C., and Witthüser, K., 1998, Rock test site for investigations of flow and transport processes in porous fractured media, *in* Annau, R., Bender, S., and Wohnlich, S., eds., Hard Rock Hydrogeology of the Bohemian Massif. 3rd International Workshop, Volume 8: Münchner Geologische Hefte, Reihe B: Windischeschenbach, Germany, p. 111-116.

- Behr, H.J., Engel, W., and Franke, W., 1980, Guide to excursion, Münchberger Gneismasse und Bayerischer Wald, April 12-15, 1980: Göttingen, Federal Republic of Germany, Geol.-Palaeontol. Inst. Mus., 100 p.
- Bender, S., 2001, Mixing processes of groundwater in the transitional zone of granites and moldanubian gneisses, *in* Seiler, K. P., and Wohnlich, S., eds., *New approaches characterizing groundwater flow*, Volume 2: Lisse, A.A. Balkema Publishers, p. 903-906.
- Bergerat, F., 1981-1982, Le couloir rhodanien au Paléogène: analyse de la fracturation et interprétation cinématique régionale: *Rev. Géol. dyn. et Géogr. phys.*, v. 23, p. 329-343.
- Bergerat, F., and Geysant, J., 1982, Tectonique cassante et champ de contraintes tertiaire en avant des Alpes orientales: le Jura souabe: *Geologische Rundschau*, v. 71, p. 537-548.
- , 1983, Fracturation tertiaire et evolution des contraintes en Baviere orientale; le Jura franconien et la foret bavaroise (R. F. A.): *Geologische Rundschau*, v. 72, p. 935-953.
- Black, J.H., 1994, Hydrogeology of fractured rocks - a question of uncertainty about geometry: *Applied Hydrogeology*, v. 3, p. 56-70.
- Blum, P., Mackay, R., Riley, M.S., and Knight, J.L., 2007, Hydraulische Modellierung und die Ermittlung des repräsentativen Elementarvolumens (REV) im Kluffgestein: *Grundwasser*, v. 12, p. 48-65.
- Boadu, F.K., 1997, Relating the Hydraulic Properties of a Fractured Rock Mass to Seismic Attributes: Theory and Numerical Experiments.: *Int. J. Rock Mech. Min. Sci.*, v. 34, p. 885-895.
- Bonnet, E., Bour, O., Odling, N.E., Davy, P., Main, I., Cowie, P., and Berkowitz, B., 2001, Scaling of fracture systems in geological media: *Reviews of Geophysics*, v. 39, p. 347-383.
- Bram, K., and Hirschmann, G., 1992, KTB-Report 92-3. Ergebnisse geowissenschaftlicher Umfelduntersuchungen: Hannover, Projektleitung Kontinentales Tiefbohrprogramm der Bundesrepublik Deutschland im Niedersächsischen Landesamt für Bodenforschung, p. 261.
- Breuer, B., 1998, Hydrogeological situation in the weathered zone near the continental deep drilling project (KTB), Upper Palatinate, Germany, *in* Annau, R., Bender, S., and Wohnlich, S., eds., *Hard Rock Hydrogeology in the Bohemian Massif*, Volume 8: *Münchner Geologische Hefte*, Reihe B: München, Ludwig-Maximilians-Universität München, p. 19-24.
- Bronstert, A., and Plate, E., 1996, Ein physikalisch begründetes hydrologisches Modell für Hänge und kleine Einzugsgebiete: *Wasserwirtschaft*, v. 86, p. 318-323.
- Bültemann, H.-W., and Hofmann, R., 1986, Die Mineralisation des Bayerischen Pfahls: *Geologisches Jahrbuch*, Reihe D, v. 83, p. 47.
- Cacas, M.C., Ledoux, E., de Marsily, G., Tillie, B., Barbreau, A., Durand, E., Feuga, B., and Peaudecerf, P., 1990, Modeling fracture flow with a stochastic discrete fracture network: Calibration and validation. 1. The flow model: *Water Resources Research*, v. 26, p. 479-489.
- Cetin, B., 1986, Petrographische und gefügekundliche Untersuchungen an duktilen Bewegungszonen des Bayerischen Waldes [PhD thesis]: München, Universität München.
- Cheema, T.J., and Islam, M.R., 1994, Experimental Determination of Hydraulic Anisotropy in Fractured Formations: *Bulletin of the Association of Engineering Geologists*, v. 31, p. 329-341.

- Compton, R.R., 1985, *Geology in the field*: New York, John Wiley & Sons, Inc., 398 p.
- Degnan, J.R., and Clark, S.F., 2002, Fracture-correlated lineaments at Great Bay, Southeastern New Hampshire: *Pembroke, New Hampshire*, U.S. Geological Survey, p. 14.
- Dershowitz, W., and Einstein, H.H., 1988, Characterizing rock joint geometry with joint system models: *Rock Mechanics and Rock Engineering*, v. 21, p. 21-51.
- Dershowitz, W., and Miller, I., 1995, Dual porosity fracture flow and transport: *Geophysical Research Letters*, v. 22, p. 1441-1444.
- Desire, M.J., and Klein, C., 1987, Fichtelgebirge, Bohmerwald, Bayerischer Wald; Contribution a l'etude du probleme des Piedmonttreppen, *in* Bremer, H., and Godard, A., eds., *Geomorphology of European massifs*, Volume 65: *Zeitschrift fuer Geomorphologie*. Supplementband: Berlin-Stuttgart, Federal Republic of Germany, Gebrueder Borntraeger, p. 101-138.
- Dorsch, K., Bender, S., and Wohnlich, S., 1998, The Influence of Granitic Intrusions on the Hydrochemistry in Gneiss Areas, *in* Annau, R., Bender, S. & Wohnlich, S., ed., *Hard Rock Hydrogeology of the Bohemian Massif*, Volume B-8: *Münchener Geologische Hefte, Reihe B*: Munich, Institut für Allgemeine und Angewandte Geologie, Ludwig-Maximilians Universität, München, p. 134-148.
- Drew, L.J., Karlinger, M.R., Armstrong, T.R., and Moore, R.B., 1999, Relations between Igneous and Metamorphic Rock Fracture Patterns and Groundwater Yield from Variography of Water-Well Yields - Pinardville Quadrangle, New Hampshire.: *Natural Resources Research*, v. 8, p. 137-152.
- Duyster, J., Kontny, A., de Wall, H., and Zulauf, G., 1995, Postvariszische Krustenstapelung am Westrand der Böhmisches Masse: *Geowissenschaften*, v. 13, p. 135-141.
- Einsiedl, F., Maloszewski, P., and Wohnlich, S., 2001, Tracer test in a fractured zone of NAGRA rock laboratory using a new fluorescent dye (PTA), *in* Seiler, K. P., and Wohnlich, S., eds., *New approaches characterizing groundwater flow*, Volume 1: Lisse, A.A. Balkema Publishers, p. 935-937.
- Emery, J.M., and Cook, G.W., 1984, A determination of the nature of recharge to a bedrock fracture system, Eastern Regional Ground Water Conference: Newton, Mass., (USA), The Association, p. 62-77.
- Emmermann, R., and Giese, P., 1989, KTB-Report 89-3. Beiträge zum 2. KTB-Kolloquium, Volume 89-3: Hannover, Projektleitung Kontinentales Tiefbohrprogramm der Bundesrepublik Deutschland im Niedersächsischen Landesamt für Bodenforschung, p. 477.
- ESRI, 2002, *ArcGis Spatial Analyst*, v. 8.3: Redlands, Ca. (USA)
- Ferrill, D.A., Winterle, J., Wittmeyer, G., Sims, D., Colton, S., and Armstrong., A., 1999, Stressed Rock Strains Groundwater at Yucca Mountain, Nevada.: *GSA Today*, v. 9, p. 1-8.
- Fischer, G., 1936, Das Dach des Moldanubikums in Schlesien, dem Bayrischen Wald und Mähren: *Jahrbuch der Preussischen Geologischen Landesanstalt*, v. 56, p. 733-741.
- , 1938, Geologischer Bau und Bodenschätze des Bayerischen Waldes: *Jahrbuch der Preussischen Geologischen Landesanstalt*, v. 58, p. 855-857.

-
- , 1959, Der Bau des Vorderen Bayerischen Waldes: Jahresberichte und Mitteilungen des Oberrheinischen Geologischen Vereines, v. 41, p. 1-21.
- , 1965, Über das Moldanubikum in Bayern: Zvásní Otisk Vestníku Ústředního Ústavu Geologického Rocnik, v. 40, p. 221-232.
- , 1967a, Kristallin des Bayerischen Waldes und der Oberpfalz: Fortschritte der Mineralogie, v. 45, p. 8-11.
- , 1967b, Über das Moldanubikum der bayerischen Oberpfalz und des Bayerischen Waldes, Zur Mineralogie und Geologie der Oberpfalz., Volume 16: Der Aufschluss, Sonderheft: Heidelberg, Federal Republic of Germany, Vereinigung der Freunde der Mineralogie und Geologie, p. 27-111.
- Fischer, G., and Troll, G., 1973, Bauplan und Gefügeentwicklung metamorpher und magmatischer Gesteine des Bayerischen Waldes, Petrographische Arbeiten über das Grundgebirge des Bayerischen Waldes., Volume 68: Geologica Bavarica: Munich, Federal Republic of Germany, Bayerisches Geologisches Landesamt, p. 7-44.
- Flurl, M., 1792, Beschreibung der Gebirge von Baiern und der oberen Pfalz: München, 642 p.
- Frank, H., 1996, Geologie Bayerns - ein Überblick, Erläuterungen zur Geologischen Karte von Bayern 1:500.000: München, Bayerisches Geologisches Landesamt, p. 1-15.
- Franke, O.L., Reilly, T.E., Pollock, D.W., and LaBaugh, J.W., 1998, Estimating Areas Contributing Recharge to Wells. Lessons from Previous Studies: Denver, Colorado, U.S. Geological Survey.
- Freeze, A.R., and Cherry, J.A., 1979, Groundwater: Englewood Cliffs, N.J., Prentice-Hall.
- Freudenberger, W., 1996, Tektonik, Deckgebirge nördlich der Donau, *in* Freudenberger, W., and Schwerd, K., eds., Erläuterungen zur Geologischen Karte von Bayern 1:500.000: München, Bayerisches Geologisches Landesamt, p. 259-265.
- Freudenberger, W., and Schwerd, K., 1996, Erläuterungen zur Geologischen Karte von Bayern 1:500 000: München, Bayerisches Geologisches Landesamt.
- Geldon, A.L., 2004, Hydraulic tests of Miocene volcanic rocks at Yucca Mountain and Pahute Mesa and Implications for groundwater flow in the Southwest Nevada Volcanic Field, Nevada and California: Boulder, CO, USA, The Geological Society of America, 93 p.
- Gelhar, L., 1993, Stochastic Subsurface Hydrology.: Englewood Cliffs, N.J., Prentice-Hall.
- GLA, 1996, Geologische Karte von Bayern 1:500000: München, Bayerisches Geologisches Landesamt.
- Glass, R.J., Nicholl, M.J., and Tidwell, V.C., 1995, Challenging models for flow in unsaturated, fractured rock through exploration of small scale processes.: Geophysical Research Letters, v. 22, p. 1457-1460.
- Gold, D.P., and Parizek, R., 1999, Fracture Trace and Lineament Analysis: Application to Ground Water Resources Characterization and Protection: Westerville, Ohio, National Ground Water Association.

- Gromes, N., 1980, Geologische und mikrothermometrische Untersuchungen zur Mineralisation des Bayerischen Pfahls [Diplom Thesis thesis]: Göttingen, University of Göttingen.
- Guimerà, J., Vives, L., and Carrera, J., 1995, A discussion of scale effects on hydraulic conductivity at a granitic site (El Berrocal, Spain): *Geophysical Research Letters*, v. 22, p. 1449-1452.
- Gümbel, C.W., 1868, *Geognostische Beschreibung des Ostbayerischen Grenzgebirges oder des Bayerischen und Oberpfälzer Waldgebirges*: Gotha, Justus Perthes, 968 p.
- Gupta, R.P., 2003, *Remote Sensing Geology*: Berlin, Springer-Verlag, 655 p.
- Gustafson, G., and Krásný, J., 1994, Crystalline rock aquifers: their occurrence, use and importance: *Applied Hydrogeology*, v. 2/94, p. 64-75.
- Hähne, R., and Franke, V., 1983, Bestimmung anisotroper Gebirgsdurchlässigkeiten in situ im grundwasserfreien Festgestein: *Z. angew. Geol.*, v. 29, p. 219-226.
- Hansen, B.P., Stone, J.R., and John, W.L.J., 1999, Characteristics of Fractures in Crystalline Bedrock Determined by Surface and Borehole Geophysical Surveys, Eastern Surplus Superfund Site, Meddybemps, Maine: Northborough, Massachusetts, U.S. Geological Survey.
- Havlík, M., and Krasny, J., 1998, Transmissivity distribution in southern part of the Bohemian Massif: Regional trends and local anomalies, *in* Annau, R., Bender, S., and Wohnlich, S., eds., *Hard Rock Hydrogeology of the Bohemian Massif. 3rd International Workshop, Volume 8: Münchner Geologische Hefte, Reihe B: Windischeschenbach, Germany*, p. 11-18.
- Himmelsbach, T., 1993, Untersuchungen zum Wasser- und Stofftransportverhalten von Störungszonen im Grundgebirge (Albtalgranit, Südschwarzwald): Karlsruhe, 14+238 p.
- , 1999, Dipoltests zur Untersuchung des Stofftransportes in Kluftgrundwasserleitern: *Steir. Beitr. z. Hydrogeologie*, v. 42, p. 131-150.
- Himmelsbach, T., Hötzl, H., Käss, W., Leibundgut, C., Maloszewski, P., Meyer, T., Moser, H., Rajner, V., Rank, D., Stichler, W., Trimborn, P., and Veulliet, E., 1992, Fractured rock - test site Lindau/Southern Black Forest (Germany), Transport phenomena in different aquifers (Investigations 1987-1992), Volume 43: *Steir. Beitr. z. Hydrogeologie*: Graz, ATH, p. 159-228.
- Himmelsbach, T., Hötzl, H., and Malozewski, P., 1994, Forced gradient tracer tests in a highly permeable fault zone: *Applied Hydrogeology*, p. 40-47.
- Hofmann, R., 1962, Die Tektonik des Bayerischen Pfahls: *Geologische Rundschau*, v. 52, p. 332-346.
- Höltling, B., 1996, *Hydrogeologie*: Stuttgart, Enke, 441 p.
- Höltling, B., and Coldewey, W.G., 2005, *Hydrogeologie. Einführung in die Allgemeine und Angewandte Hydrogeologie*: München, Spektrum Akademischer Verlag, 326 p.
- Ingebritsen, S.E., and Sanford, W.E., 1998, *Groundwater in Geologic Processes.*: Cambridge, Cambridge University Press.
- Jensen, J.R., 2000, *Remote sensing of the environment: an earth resource perspective*: Upper Saddle River, NJ, Prentice-Hall, Inc., 544 p.

- Jerz, H., 1995, Bayern, *in* Benda, L., ed., *Das Quartär Deutschlands*: Berlin-Stuttgart, Borntraeger, p. 296-326.
- , 1996, *Gesteinsfolge des Quartärs, Erläuterungen zur Geologischen Karte von Bayern 1:500.000*: München, Bayerisches Geologisches Landesamt, p. 236-251.
- Ji, S.-H., Lee, K.-K., and Park, Y.-C., 2004, Effects of the correlation length on the hydraulic parameters of a fracture network: *Transport in Porous Media*, v. 55, p. 153-168.
- Karrenberg, H., 1981, *Hydrogeologie der nichtverkarstungsfähigen Festgesteine*: Wien, Springer Verlag, 385 p.
- Keller, A.A., Roberts, P.V., and Kitanidis, P., K., 1995, Prediction of single phase transport parameters in a variable aperture fracture: *Geophysical Research Letters*, v. 22, p. 1425-1428.
- Kemmis, T., and Kelleher, D., 2002, *Improving hydrogeologic analysis of fractured bedrock systems*: Sheboygan, Wisconsin (USA), Midwest GeoSciences Group.
- Kim, G.-B., ESRI ArcScript Database, 2004, *Lineament Analysis Tool*: Redlands, CA (USA)
- Kolditz, O., 1997, *Strömung, Stoff- und Wärmetransport im Kluftgestein*: Berlin-Stuttgart, Borntraeger, 663 p.
- Kossmat, F., 1927, *Gliederung des varistischen Gebirgsbaues*: Abh. Sächs. Geol. L.-Anst., v. 1, p. 39.
- Krásný, J., 1999, *Hard-rock hydrogeology in the Czech Republic*: *Hydrogéologie*, v. 2, p. 25-38.
- , 2002, *Quantitative hardrock hydrogeology in a regional scale*: *Bulletin of the Geological Survey of Norway*, v. 439, p. 7-14.
- Kriegl, C., Vasváry, V., and Goldbrunner, J., 2001, Deep drilling Längenfeld Thermal 2 - first hydrogeological results from a deviated well in metamorphic rocks of the Austroalpine Ötztal-Stubai crystalline complex, Tyrol, *in* Seiler, K. P., and Wohnlich, S., eds., *New approaches characterizing groundwater flow*, Volume 2: Lisse, A.A. Balkema, p. 995-999.
- Kubiniok, J., 1988, *Kristallinvergrusung an Beispielen aus Südostaustralien und Deutschen Mittelgebirgen*: Köln, 178 p.
- Lachassagne, P., Golaz, C., Thiery, D., Ahmed, C., Maréchal, J., Touchard, F., and Wyns, R., 2001, A methodology for the mathematical modelling of hard-rock aquifers at catchment scale, based on the geological structure and the hydrogeological functioning of the aquifer, *in* Seiler, K. P., and Wohnlich, S., eds., *New approaches characterizing groundwater flow*, Volume 1: Lisse, A.A. Balkema Publishers, p. 367-370.
- Leven, C., McDermott, C.I., Teutsch, G., and Sauter, M., 2001, New methods for the investigation of fractured porous media, *in* Seiler, K. P., and Wohnlich, S., eds., *New approaches characterizing groundwater flow*, Volume 2: Lisse, A.A. Balkema Publishers, p. 1007-1011.
- List, F.K., and Ott, W.-D., 1982, *Geologische Karte von Bayern 1:25 000. Erläuterungen zum Blatt Nr. 7043 Ruhmannsfelden*: München, Bayerisches Geologisches Landesamt, 55 p.
- Loew, S., 2001, *Natural groundwater pathways and models for regional groundwater flow in crystalline rocks*, *in* Seiler, K. P., and Wohnlich, S., eds., *New approaches characterizing groundwater flow*, Volume 2: Lisse, A.A. Balkema Publishers, p. 1013-1318.

- Louis, H., 1984, Zur Reliefentwicklung der Oberpfalz, *in* Louis, H., ed., Zur Reliefentwicklung der Oberpfalz: Berlin-Stuttgart, Borntraeger, p. 1-66.
- Mabee, S.B., 1999, Factors influencing Well Productivity in Glaciated Metamorphic Rocks.: Ground Water, v. 37, p. 88-97.
- Mabee, S.B., Curry, P.J., and Hardcastle, K.C., 2002, Correlation of lineaments to ground water inflows in a bedrock tunnel: Ground Water, v. 40, p. 37-43.
- Mabee, S.B., and Hardcastle, K.C., 1997, Analyzing Outcrop-Scale Fracture Features to Supplement Investigations of Bedrock Aquifers: Hydrogeology Journal, v. 5, p. 21-36.
- Mabee, S.B., Hardcastle, K.C., and Wise, D.U., 1994, A Method of Collecting and Analyzing Lineaments for Regional-Scale Fractured-Bedrock Aquifer Studies: Ground Water, v. 32, p. 884-894.
- Madel, J., Propach, G., Reich, H., Brunnacker, K., Vidal, H., Ziehr, H., and Teuscher, E.O., 1968, Erläuterungen zur Geologischen Karte von Bayern 1:25.000, Blatt Nr. 6945 Zwiesel: München, Bayerisches Geologisches Landesamt, 88 p.
- Masakova, I., and Kobr, M., 1998, Fracture aquifer well-log analysis for hard rock evaluation, *in* Annau, R., Bender, S., and Wohnlich, S., eds., Hard Rock Hydrogeology of the Bohemian Massif. 3rd International Workshop: Münchner Geologische Hefte, Reihe B: Windischeschenbach, Germany, p. 157-164.
- Masch, L., and Cetin, B., 1991, Deformationsmechanismen in ausgewählten Hochtemperatur-Mylonitzonen im Moldanubikum des Bayerischen Waldes: Geologica Bavarica, v. 96, p. 7-27.
- Mauldon, M., Dunne, W.M., and Rohrbaugh, M.B., Jr., 2001, Circular scanlines and circular windows: new tools for characterizing the geometry of fracture traces: Journal of Structural Geology, v. 23, p. 247-258.
- Melvin, R.L., Stone, J.R., Craft, P.A., Lane, J.W.J., and Davies, B.S.r., 1995, Geohydrology of the Durham Center Area, Durham Connecticut: Hartford, CT, U.S. Geological Survey.
- Mira, F., and Chambel, A., 2001, Productivity of hard rock aquifers in Alentejo region, South Portugal, *in* Seiler, K. P., and Wohnlich, S., eds., New approaches characterizing flow, Volume 2: Lisse, A.A. Balkema, p. 1035-1039.
- Neuendorf, K.K.E., Mehl, J.P., Jr., and Jackson, J.A., 2005, Glossary of Geology: Alexandria, Va., USA, American Geological Institute, 779 p.
- Nieto-Samaniego, A.F., Alaniz-Alvarez, S.A., Tolson, G., Oleschko, K., Korvin, G., Xu, S.S., and Pérez-Venzor, J.A., 2005, Spatial distribution, scaling and self-similar behavior of fracture arrays in the Los Planes Fault, Baja California Sur, Mexico: Pure and Applied Geophysics, v. 162, p. 805-826.
- Olsson, O., Black, J.H., Gale, J.E., and Holmes, D.C., 1988, Site Characterization and Validation: Stockholm, Sweden, Swedish Geological Company.
- Ott, W.-D., 1983, Geologische Karte von Bayern 1: 25 000. Erläuterungen zum Blatt Nr. 6943 Viechtach: München, Bayerisches Geologisches Landesamt, 71 p.

- Papadopoulos, I.S., 1967, Nonsteady flow to a well in an infinite anisotropic aquifer., Hydrology of fractured rocks., Volume 1: Dubrovnic, Yugoslavia, Int. Ass. Sci. Hydrol., p. 21-31.
- Parney, R., and Smith, L., 1995, Fluid Velocity and path length in fractured media.: Geophysical Research Letters, v. 22, p. 1437-1440.
- Peterek, A., 2001, Zur geomorphologischen und morphotektonischen Entwicklung des Fichtelgebirges und seines unmittelbaren Raumes: Geol. Bl. NO-Bayern, v. 51, p. 37-106.
- Peterek, A., Schröder, B., and Nollau, G., 1996, Neogene Tektonik und Reliefentwicklung des nördlichen KTB-Umfeldes (Fichtelgebirge und Steinwald): Geologica Bavarica, v. 101, p. 7-25.
- Peterhoff, F., 1986, Morphologische Untersuchungen zur Talgeschichte des mittleren Regens [PhD thesis]: Regensburg, Universität Regensburg.
- Pfaffl, F., 1968, Ueber Andalusit von der Bloetz im Bayerischen Wald: Der Aufschluss, Sonderheft, v. 19, p. 237-239.
- , 1969, Allanit (Orthit) von Tittling (Bayerischer Wald): Der Aufschluss, Sonderheft, v. 20, p. 26-28.
- , 1971, Schriftgranit aus dem Bayerischen Wald: Der Aufschluss, Sonderheft, v. 22, p. 83-84.
- , 1972a, Die Rauchquarze von Saldenburg im Bayerischen Wald: Der Aufschluss, Sonderheft, v. 23, p. 386-388.
- , 1972b, Klufthmineralien aus Bischofsmais im Bayerischen Wald: Der Aufschluss, Sonderheft, v. 23, p. 338-339.
- , 1972c, Verbreitung und Mineralfuehrung der Pegmatite bei Bodenmais: Geologische Blaetter fuer Nordost-Bayern und Angrenzende Gebiete, v. 22, p. 43-55.
- , 1973a, Die Pegmatit- und Kontaktlagerstaette Stanzen bei Eck im Bayerischen Wald: Der Aufschluss, Sonderheft, v. 24, p. 236-240.
- , 1973b, Faserkiesel aus dem Bayerischen Wald (Beitrag zur Morphologie des ostbayerischen Moldanubikums): Geologische Blaetter fuer Nordost-Bayern und Angrenzende Gebiete, v. 23, p. 123-128.
- , 1973c, Neuer Meta-Autunit-Fund vom Huehnerkobel: Der Aufschluss, Sonderheft, v. 24, p. 372.
- , 1979a, Die Mineralien des Huehnerkobel-Pegmatits bei Zwiesel (Bayerischer Wald): Der Aufschluss, v. 30, p. 93-99.
- , 1979b, Klufthmineralien aus dem Bayerischen Wald: Lapis (Muenchen), v. 4, p. 28-29.
- , 1980, Erstmaligner Fund von "Wuerfelquarzen" im Kristallin des Bayerischen Waldes: Geologische Blaetter fuer Nordost-Bayern und Angrenzende Gebiete, v. 30, p. 43-47.
- , 1981a, Die Mineralien des Bayerischen Waldes: Grafenau, Federal Republic of Germany, Morsak, 100 p.

-
- , 1981b, Pseudokubische Quarzkristalle ("Wuerfelquarze") aus dem Kristallin des Bayerischen Waldes, in Anonymous, ed., Referate der Vortraege auf der 59. Jahrestagung der Deutschen Mineralogischen Gesellschaft und der Tagung der Oesterreichischen Mineralogischen Gesellschaft, Volume 59; 1: Fortschritte der Mineralogie, Beiheft: Stuttgart, Federal Republic of Germany, E. Schweizerbart'sche Verlagsbuchhandlung, p. 154.

 - , 1985a, Beryllvorkommen im Bayerischen Wald: Der Bayerische Wald, v. 8, p. 115-117.

 - , 1985b, Vivianit vom Silberberg bei Bodenmais (Bayerischer Wald): Der Bayerische Wald, v. 10, p. 182-183.

 - , 1985c, Zur Geologie der Loessvorkommen im Bayerischen Wald; Teil 2: Der Bayerische Wald, v. 9, p. 134-155.

 - , 1985d, Zur Geologie der Loess-Vorkommen im Bayerischen Wald; Teil 1: Der Bayerische Wald, v. 8, p. 120-130.

 - , 1986, Glazialmorphologische Untersuchungen an den Lachen im Arbergebiet, Bayerischer Wald: Geologische Blaetter fuer Nordost-Bayern und Angrenzende Gebiete, v. 36, p. 269-278.

 - , 1988a, Die Mineralien der Kalksilikatfelse und Pegmatite von Lichtenthal bei Zwiesel/ Bayerischer Wald: Geologische Blaetter fuer Nordost-Bayern und Angrenzende Gebiete, v. 38, p. 93-96.

 - , 1988b, Die Titanmineralparagenese von Steinerleinbach bei Waldkirchen (Bayerischer Wald): Geologische Blaetter fuer Nordost-Bayern und Angrenzende Gebiete, v. 38, p. 97-106.

 - , 1988c, Glazialmorphologische Untersuchungen am Bachel-Nordkar und am Grossen Arbersee im Bayerischen Wald: Geologische Blaetter fuer Nordost-Bayern und Angrenzende Gebiete, v. 38, p. 7-26.

 - , 1989, Der Bayerische Wald im Tertiär und Quartär: Geologische Blätter für Nordost-Bayern und Angrenzende Gebiete, v. 39, p. 1-38.

 - , 1990a, Der Mineralien der Sulfiderz-Lagerstaette Silberberg bei Bodenmais, Bayerischer Wald: Mineralien-Welt, v. 1, p. 49-55.

 - , 1990b, Zur Geologie und Mineralogie des Blattes Bodenmais 1:25000 (Nr. 6944) im Bayerischen Wald: Geologische Blaetter fuer Nordost-Bayern und Angrenzende Gebiete, v. 40, p. 123-172.

 - , 1991, Die Klufftmineralien vom Granitsteinbruch am Teufelstisch, Bischofsmais (Bayrischer Wald): Mineralien-Welt, v. 2, p. 42-44.

 - , 1992, Zur Geologie und Mineralogie des Blattes Kötztling 1:25000 (Nr. 6843) im Bayerischen Wald: Geologische Blätter für Nordost-Bayern und Angrenzende Gebiete, v. 42, p. 167-204.

 - , 1993, Kritische Anmerkungen zum Toteishuegel-Problem im Bayerischen Wald: Geologische Blaetter fuer Nordost-Bayern und Angrenzende Gebiete, v. 43, p. 341-348.

 - , 1994, Idiomorphe Quarzkristalle in Porphyren des Hauzenberger Granitmassivs (Suedlicher Bayerischer Wald): Geologische Blaetter fuer Nordost-Bayern und Angrenzende Gebiete, v. 44, p. 109-112.

 - , 1995, Zur Geologie und Mineralogie des Blattes Lam 1:25.000 (Nr. 6844) im Bayerischen Wald: Geologische Blätter für Nordost-Bayern und Angrenzende Gebiete, v. 45, p. 103-151.

- Pfaffl, F., and Niggemann, M., 1967, Tracht und Habitus von Turmalinkristallen aus einigen Pegmatiten des Bayerischen Waldes: Der Aufschluss, v. 18, p. 171-178.
- , 1976, Rechts- und Links-Quarze aus einer Granitkluff bei Bischofsmais im Bayerischen Wald: Der Aufschluss, v. 27, p. 161-162.
- Pfaffl, F., Puhm, G., and Puhm, H., 1976, Ueber Mineralisationen in den Gneisen bei Hochbruck und Schoenberg im Bayerischen Wald: Der Aufschluss, v. 27, p. 347-351.
- Pfaffl, F., and Troll, G., 1981, Zur Geschichte der geologischen und mineralogischen Erforschung des Bayerischen Waldes, *in* Troll, G., ed., Mineralvorkommen im oestlichen Bayerischen Wald; Bildung, Inhalt und Bergbaugeschichte, Volume 31: Der Aufschluss, Sonderheft: Heidelberg, Federal Republic of Germany, Vereinigung der Freunde der Mineralogie und Geologie, p. 9-13.
- Pfaffl, F.A., 1982, Erstfund im Bayerischen Wald; Wuerfelquarz vom Teufelstisch: Mineralien Magazine, v. 6, p. 456-459.
- Piscopo, V., 2001, Fracturing degree of outcropping rocks compared to pumping test results in two aquifers of Southern Italy, *in* Seiler, K. P., and Wohnlich, S., eds., New approaches characterizing groundwater flow, Volume 2: Lisse, A.A. Balkema Publishers, p. 1041-1046.
- Power, W.L., and Durham, W.B., 1997, Topography of natural and artificial fractures in granitic rocks: Implications for studies of rock friction and fluid migration: *Int. J. Rock Mech. Min. Sci.*, v. 34, p. 979-989.
- Priehäuser, G., 1930, Die Eiszeit im Bayerischen Wald: *Abh. geol. Landesunters. Bayer. Oberbergamt*, v. 2, p. 46.
- , 1937a, Ablagerungen unter Gletscher- und Firneis und Fliesserdebildungen im Bayr. Wald.
- , 1937b, Fossile Roterde im Bayrischen Wald, vorläufige Mitteilung.
- , 1938, Eiszeitliche Toteisbildungen im Bayerischen Wald: *Zs. Gletscherkunde*, v. 26, p. 97-111.
- , 1951, Der Nachweis der Eiszeitwirkungen im Bayer. Wald mit Hilfe von Schuttausbildungen: *Geologische Blätter für Nordost-Bayern und angrenzende Gebiete*, v. 1, p. 81-91.
- , 1952a, Roterdevorkommen im Bayerischen Wald: *Geologische Blätter für Nordost-Bayern und angrenzende Gebiete*, v. 2, p. 81-89.
- , 1952b, Über die natürliche Speicherung von Wasser im Bayerischen Wald: *Landw. Jb. f. Bayern*, v. 29, p. 449-484.
- , 1955, Störungen im Zersatz kristalliner Gesteine unter eiszeitlichen Schuttdecken im Bayrischen Wald: *Geologische Blätter für Nordost-Bayern und angrenzende Gebiete*, v. 5, p. 97-109.
- , 1956, Der Klimaablauf der Späteiszeit im Bayerischen Wald: *Geologische Blätter für Nordost-Bayern und angrenzende Gebiete*, v. 6, p. 55-66.
- , 1958, Über den Aufbau und die Oberflächenformen der Ablagerungen aus dem Firneis der letzten Kaltzeit (Endwürm) im Bayerischen Wald: *Geologische Blätter für Nordost-Bayern und angrenzende Gebiete*, v. 8, p. 152-157.

-
- , 1961, Felsfreistellungen, Blockmeere, Blockströme und Blockstreuungen im Bayer. Wald: Geologische Blätter für Nordost-Bayern und angrenzende Gebiete, v. 11, p. 123-132.
- , 1963a, Altpleistozäne Eiszeitspuren im Bayerischen Wald: Geologische Blätter für Nordost-Bayern und angrenzende Gebiete, v. 13, p. 163-177.
- , 1963b, Über die Sicherung des Landschaftswasserhaushaltes im Bayerischen Wald: Landw. Jb. f. Bayern, v. 40, p. 334-353.
- , 1966, Beitrag zur Frage der Entstehung von Lockerbraunerde im Bayerischen Wald auf pleistozäner Bodenunterlage: Geologische Blätter für Nordost-Bayern und angrenzende Gebiete, v. 16, p. 183-191.
- , 1968, Über die Verwitterung kristalliner Gesteine zu Zersatz von der Oberfläche aus; Beispiele aus dem Bayerischen Wald: Geologische Blätter für Nordost-Bayern und angrenzende Gebiete, v. 18, p. 162-172.
- , 1971, Über Trinkwasservorräte im Zersatz kristalliner Gesteine im Bayerischen Wald: Geologische Blätter fuer Nordost-Bayern und angrenzende Gebiete, v. 21, p. 127-135.
- Prinz, H., and Strauß, R., 2006, Abriss der Ingenieurgeologie: München, Spektrum Akademischer Verlag, 671 p.
- Probst, M., Schöpfer, C., and Zipfel, K., 2001, Analysing regional groundwater flow in fractured aquifers using a conceptual model, *in* Seiler, K. P., and Wohnlich, S., eds., *New approaches characterizing groundwater flow*, Volume 2: Lisse, A.A. Balkema, p. 1047-1049.
- Raab, T., 1999, Würmzeitliche Vergletscherung des Bayerischen Waldes im Arbergebiet: Regensburg, Institut für Geographie an der Universität Regensburg, 327 p.
- Raum, K.-D., 2002, Markierungstechnische, bruchtektonisch-gefügekundliche und fotogeologische Untersuchungen zur Ermittlung der Grundwasserfließverhältnisse in der Verwitterungszone kristalliner Gesteine in Quellgebieten des Oberpfälzer/Bayerischen Waldes (Ost-Bayern/Deutschland) [PhD Dissertation thesis]: Erlangen, Friedrich-Alexander Universität Erlangen-Nürnberg.
- Reinecker, J., Heidbach, O., Tingay, M., Connolly, P., and Müller, B., 2004, The 2004 release of the World Stress Map, The World Stress Map Project, Retrieved: 23.06.2004 from
- Rohrmüller, J., Mielke, H., and Gebauer, D., 1996a, Gesteinsfolge des Grundgebirges nördlich der Donau und im Molasseuntergrund, Erläuterungen zur Geologischen Karte von Bayern 1:500.000: München, Bayerisches Geologisches Landesamt, p. 16-54.
- , 1996b, Tektonik, Grundgebirge, Erläuterungen zur Geologischen Karte von Bayern 1:500.000: München, Bayerisches Geologisches Landesamt, p. 252-259.
- Saker, R., and Jordan, H., 1977, Zu hydrologischen Eigenschaften der Verwitterungszonen erzgebirgischer Gneise: Z. angew. Geol., v. 23, p. 606-611.
- Schild, M., Braun, R., Siegesmund, S., and Vollbrecht, A., 2001, Modellierung lokaler hydraulischer Wegsamkeiten und ihre Bedeutung für die Endlagerung in Kristallingesteinen: Zeitschrift der Deutschen Geologischen Gesellschaft, v. 152, p. 577-591.

- Seiler, K.P., and Müller, K., 1995, Grundwasserneubildung und Grundwasserumsatzräume im Kristallin des Bayerischen Waldes: Deutsche Gewässerkundliche Mitteilungen, v. 39, H. 6, p. 194-199.
- Seiler, K.P., and Wohnlich, S., 2001a, New approaches characterizing groundwater flow, Proceedings of the XXXI International Association of Hydrogeologists Congress, Volume 1: Munich, A.A. Balkema Publishers, Lisse, p. 1-688.
- , 2001b, New approaches characterizing groundwater flow, Proceedings of the XXXI International Association of Hydrogeologists Congress, Volume 2: Munich, A.A. Balkema Publishers, Lisse, p. 691-1328.
- Sibson, R.H., McMoore, J., and Rankin, R.H., 1975, Seismic pumping - a hydrothermal fluid transport mechanism: Journal of the Geologic Society of London, v. 131, p. 653-659.
- Simpson, C., and Schmid, S.M., 1983, An evaluation of criteria to deduce the sense of movement in sheared rocks: Geological Society of America Bulletin, v. 94, p. 1281-1288.
- Skernjaa, L., and Jørgensen, N.O., 1994, Evaluation of local fracture systems by azimuthal resistivity surveys: Examples from South Norway: Applied Hydrogeology, v. 2, p. 19-26.
- Spencer, E.W., and Kozak, S.J., 1974, Determination of Regional Fracture Patterns in Precambrian Rocks - a Comparison of Techniques, in Hogson, R. A., S.P. Gay, J.Y. Benjamins, ed., First International Conference on New Basement Tectonics: Salt Lake City, Utah, Utah Geological Association.
- Sprenger, W., Bittersohl, J., Willy, H., Aschauer, K., Schöttl, C., and Irmgard, H., 2005, Grund- und Bodenwasser, Wasserwirtschaftlicher Bericht - Niedrigwasserperiode 2003, Volume 2/05: Informationsberichte des Bayerischen Landesamtes für Wasserwirtschaft: München, Bayerisches Landesamt für Wasserwirtschaft, p. 27-70.
- Stásko, S., and Tarka, R., 2001, Ground water flow in fractured hard rock based on field data from the Sudety Mts., SW Poland, in Seiler, K. P., and Wohnlich, S., eds., New approaches characterizing groundwater flow, Volume 2: Lisse, A.A. Balkema, p. 1069-1072.
- Stein, E., 1988, Die strukturgeologische Entwicklung im Übergangsbereich Saxothuringikum/Moldanubikum in NE-Bayern, in Schwerd, K., ed., Strukturgeologie, Lagerstätten-Typisierung und Metallogenese im Übergangsbereich Saxothuringikum-Moldanubikum in Nordostbayern, Volume 92: Geologica Bavarica: München, Bayerisches Geologisches Landesamt, p. 150.
- Steiner, L., 1969, Scherflächenpaare in Oberbau und Unterbau: Geotekt. Forsch., v. 33, p. 62.
- Stettner, G., 1992, Geologie im Umfeld der Kontinentalen Tiefbohrung Oberpfalz - Einführung und Exkursionen: München, Bayerisches Geologisches Landesamt, 240 p.
- , 1996, Zu den geotektonischen Beziehungen von Saxothuringikum, Moldanubikum und Bohemikum im Umfeld der Tiefbohrung Oberpfalz: Geologica Bavarica, v. 101, p. 181-209.
- Stettner, G., Rohrmüller, J., and Hirschmann, G., 1997, Bayerischer Wald / Oberpfälzer Wald (14), Stratigraphie von Deutschland II: Ordovizium, Kambrium, Vendium, Riphäikum, Teil I: Thüringen, Sachsen, Ostbayern: Courier Forschungsinstitut Senckenberg 200, Frankfurt am Main, Senckenbergische Naturforschende Gesellschaft, p. 373-399.

- Stibitz, M., 1998, Investigation of groundwater potential in the crystalline of the Bohemian Massif in Austria. - Methodical framework, *in* Annau, R., Bender, S., and Wohnlich, S., eds., *Hard Rock Hydrogeology of the Bohemian Massif. 3rd International Workshop, Volume 8: Münchner Geologische Hefte, Reihe B: Windischeschenbach, Germany*, p. 123-128.
- Stober, I., 1986, Strömungsverhalten in Festgesteinsaquiferen mit Hilfe von Pump- und Injektionsversuchen: *Geologisches Jahrbuch*, v. C 42, p. 204.
- , 1995, Die Wasserführung des kristallinen Grundgebirges: Stuttgart, Ferdinand Enke Verlag, 191 p.
- , 2007a, Fortbildungsveranstaltung Hydrogeologie der Festgesteine: Freiburg, FH-DGG.
- , 2007b, Hydrologie der Festgesteine. Einführung, Allgemeines, *in* Stober, I., ed., Fortbildungsveranstaltung Hydrogeologie der Festgesteine: Freiburg.
- Stone, J.R., 2002, Characterization of bedrock aquifers in Connecticut: (1) Geologic mapping and analysis., Geological Society of America Northeastern Section, Annual Meeting: Springfield, Massachusetts, Geological Society of America, p. A-23.
- Suess, F.E., 1903, Bau und Bild der Böhmisches Masse, Bau und Bild Österreichs, Volume L: Wien, p. 1-322.
- Tait, J.A., Bachtatse, V., Soffel, H.C., and Franke, W., 1996, Paleomagnetic constraints on the evolution of the European Variscan Foldbelt: *Geologica Bavarica*, v. 101, p. 221-232.
- Terzaghi, R.D., 1965, Sources of error in joint surveys: *Géotechnique*, v. 15, p. 287-304.
- Thums, S., 1993, Niederschlags- und Abflussauswertung der 10jährigen Meßreihe 1980-1989 für das Einzugsgebiet der Großen Ohe im Nationalpark Bayerischer Wald in Anlehnung an die Auswerteempfehlung des Deutschen IHP/OHP - Nationalkomitees, 196 p.
- Thüringer, C., Bäuml, R., and Hötzl, H., 2001, Evaluation of hydraulic parameters in fissured rocks by gas tracing, *in* Seiler, K. P., and Wohnlich, S., eds., *New Approaches Characterizing Groundwater Flow, Volume 2: Lisse, A.A. Balkema Publishers*, p. 1073-1077.
- Toynton, R., 1983, The relation between fracture patterns and hydraulic anisotropy in the Norfolk Chalk, England.: *The Quarterly Journal of Engineering Geology*, v. 16, p. 169-185.
- Tröger, U., Dussel, M., Moeck, I., and Schandelmeier, H., 2001, A new approach to the reconnaissance of groundwater flow in hard rocks: Hydrotectonic, *in* Seiler, K. P., and Wohnlich, S., eds., *New approaches characterizing groundwater flow, Volume 2: Lisse, A.A. Balkema Publishers*, p. 1079-1083.
- Troll, G., 1964, Geologische Übersichtskarte des Bayerischen Waldes: München, Bayerisches Geologisches Landesamt.
- , 1967a, Bau und Bildungsgeschichte des Bayerischen Waldes, *in* Troll, G., ed., *Führer zu geologisch-petrographischen Exkursionen im Bayerischen Wald. Teil I: Aufschlüsse im Mittel- und Ostteil, Volume 58: Geologica Bavarica: München, Bayerisches Geologisches Landesamt*, p. 15-21.
- , 1967b, Die blastokataklastischen Kristallingesteine der Stallwanger Furche, Bayerischer Wald, *in* Troll, G., ed., *Führer zu geologisch-petrographischen Exkursionen im Bayerischen Wald. Teil*

- I: Aufschlüsse im Mittel- und Ostteil, Volume 58: München, Bayerisches Geologisches Landesamt, p. 22-33.
- , 1967c, Führer zu geologisch-petrographischen Exkursionen im Bayerischen Wald; Teil I, Aufschlüsse im Mittel- und Ostteil: München, Bayerisches Geologisches Landesamt, 188 p.
- , 1968, Führer zu geologisch-petrographischen Exkursionen im Bayerischen Wald; Teil II, Aufschlüsse im Westteil: Regensburger Wald: München, Bayerisches Geologisches Landesamt, 188 p.
- , 1974, Igneous and metamorphic rocks in the southern Bavarian Forest, Excursion Guidebook; Excursion B 8., Volume 52; 1: Fortschritte der Mineralogie: Stuttgart, Federal Republic of Germany, Deutsche Mineralogische Gesellschaft, p. 167-194.
- Unger, H.J., 1996, Tektonik, Molassebecken, *in* Schwerd, K., ed., Erläuterungen zur Geologischen Karte von Bayern 1:500.000: München, Bayerisches Geologisches Landesamt.
- van der Pluijm, B., and Marshak, S., 1997, Earth Structure: An Introduction to Structural Geology and Tectonics, WCB/McGraw-Hill, 495 p.
- Van der Voo, R., 1983, A plate-tectonics model for the Paleozoic assembly of Pangea based on paleomagnetic data., *in* R.D Hatcher, H. W., I. Zietz, ed., Contributions to the Tectonics and Geophysics of Mountain Chains: Boulder, Colorado, Geological Society of America, p. 19-23.
- , 1988, Paleozoic paleogeography of North America, Gondwana, and intervening displaced terranes: Comparisons of paleomagnetism with paleoclimatology and biogeographical patterns: Geological Society of America Bulletin, v. 100, p. 311-324.
- Vejnar, Z., 1965, Bemerkungen zur lithostratigraphischen Beziehung zwischen dem mittelböhmischen Algonkium und dem Moldanubikum: N. Jb. Geol. Paläont. Mh., p. 102-111.
- Vesely, M., and Mls, J., 1998, Groundwater flow in a long fracture with variable aperture, *in* Annau, R., Bender, S., and Wohnlich, S., eds., Hard Rock Hydrogeology of the Bohemian Massif. 3rd International Workshop, Volume 8: Münchner Geologische Hefte, Reihe B: Windischeschenbach, Germany, Ludwig-Maximilians-Universität München, p. 129-134.
- Völkel, J., 1995, Periglaziale Deckschichten und Böden im Bayerischen Wald und seinen Randgebieten: Z. Geomorphol., v. Suppl. Bd. N.F. 96, p. 1-301.
- Walsh, G., J., and Clark, S.F., 2000, Contrasting Methods of Fracture Trend Characterization in Crystalline Metamorphic and Igneous Rocks of the Windham Quadrangle, New Hampshire: Northeast Geology and Environmental Sciences, v. 22, p. 109-120.
- Wang, M., Kulatilake, P.H.S.W., Panda, B.B., and Rucker, M.L., 2001, Groundwater resources evaluation case study via discrete fracture flow modeling: Engineering Geology, v. 62, p. 267-291.
- Weise, S.M., Bräuer, K., Strauch, G., Kämpf, H., Koch, U., and Tesar, J., 1998, Seismically induced release of deep-seated fluids as tracer of fast transport up to surface in fractured rocks of the Bohemian Massif, *in* Annau, R., Bender, S., and Wohnlich, S., eds., Hard Rock Hydrogeology of the Bohemian Massif. 3rd International Workshop, Volume 8: Münchner Geologische Hefte, Reihe B: Windischeschenbach, Germany, p. 183-184.

-
- Weiss, E.G., 1989, Über die Notwendigkeit einer Korrektur bei kluftstatistischen Aufnahmen, die Berechnung des mittleren Kluftabstandes und die Darstellung des Zerklüftungsgrades: Z. dt. geol. Ges., v. 140, p. 193-200.
- Williams, K.W., 2000, Surface and subsurface fracture characterization and the occurrence and characterization of subsurface flow along a cross-strike transect in eastern Massachusetts. [Master's thesis]: Amherst, Massachusetts, University of Massachusetts.
- Witthüser, K., and Himmelsbach, T., 1998, Erhebungsmethoden von Kluftparametern für eine stochastische Kluftnetzgenerierung: Grundwasser, v. 3, p. 103-109.
- Zeithöfler, M., 2003, Bedrock Structure in Southeastern Connecticut: Hydrologic Implications. [Master's thesis]: Middletown, CT, Wesleyan University.
- Zeithöfler, M., and Raum, K.D., 2005, Relationships between brittle tectonic structure and groundwater migration patterns in fractured rock aquifers of the Central Bavarian Forest, SE Germany, in Löffler, S.-B., ed., GeoErlangen 2005. System Earth - Biosphere Coupling. Regional Geology of Central Europe - International Conference and Annual Meeting Geologische Vereinigung (GV), Deutsche Gesellschaft für Geowissenschaften (DGG), Volume 39: Schriftenreihe der Deutschen Gesellschaft für Geowissenschaften: Erlangen, Deutsche Gesellschaft für Geowissenschaften, p. 423-424.
- Zhang, X., and Sanderson, D.J., 1999, Scale up of two-dimensional conductivity tensor for heterogeneous fracture networks: Engineering Geology, v. 53, p. 83-99.

2 Structural Geology

2.1 Inventory of bedrock outcrops

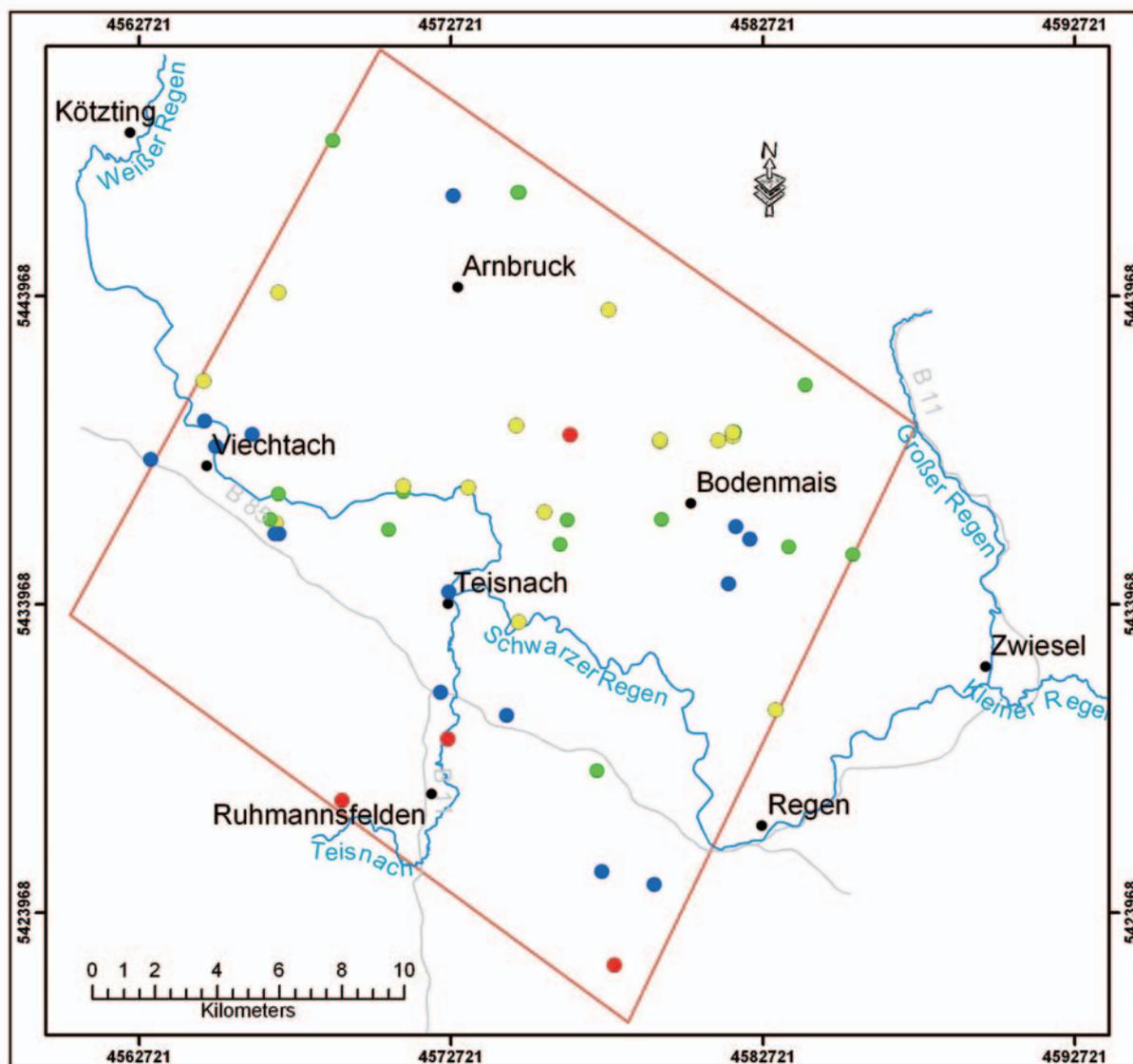


Figure 2-1: Fracture data sampling stations (dots) in the study area (red square). Color of dots depicts the quality of the bedrock exposures. Red: very good, Blue: good, Green: poor, Yellow: very poor (for explanation see table 2-1).

For both the structural and the hydrogeologic analyses in the following chapters a total of 49 bedrock outcrops spread over the study area has been selected. Figure 2-1 shows both their spatial distribution and their relative quality (the key to the quality classes is given in table 2-1). Due to the very heterogeneous presence of bedrock exposures in this region the coverage is not entirely continuous. Especially the southwestern section of the study area consists of wide valleys and rolling hills enveloped by thick blankets of autochthonous weathering materials and sedimentary infillings. Other areas, such as the southern part, are well exposed due to the intensive quarrying of the large Permo-Carboniferous granitic intrusions and quartz veins of the Pfahl fault zone during the 19th and 20th centuries. Many of

the smaller pits and quarries, which were abandoned usually more than thirty years ago, have been rapidly reclaimed by nature and are today completely overgrown and/or filled with water. The still active or only recently abandoned sites in this area provide the best structural data for deciphering the brittle tectonic history of the region. In this group the large quarries of Prünst near Ruhmannsfelden, Teufelstisch near Bischofsmais, and the smaller site of the Zeithof quarry near Achslach range among the most important ones. The northern part of the study area is in general better exposed, since the bedrock crops out naturally along the Kaitersberg-Arber range and in the deep ravines cutting into the landscape of the Inner Bavarian Forest. However, these outcrops, especially along the ridges, are frequently of a poor quality due to their longtime exposure to the elements. As a result, plant growth, intensive weathering (especially along fracture planes), and possible gravitational shifting of individual outcrop blocks render these sites less suitable for both structural and hydrogeologic investigations. A few road cuts and small quarries exist as well, which give a somewhat better insight into the geology of the metamorphic domains in the northern part of the study area. There, the Haberbühl quarry near Unterried, the road cuts along the road Bodenmais-Langdorf (ST 2132), and the abandoned quarry near Eck should be mentioned as the most informative. The exposures around Viechtach in the northwestern part of the study area (especially those near Rugenmühle in the Regen river valley) provide important clues for the kinematic analysis of the brittle structures in this study.

The “good” and “very good” outcrops displayed in figure 2-1 yield the most important information on the brittle structures of the region and its tectonic development. The many locations classified as “poor” or “very poor” usually provide only data on fracture orientations, sizes and spacings. Kinematic indicators are very rare in these outcrops. However, for lack of better exposures these have been included into the dataset in order to receive a more continuous regional coverage.

Quality Class	Description
1 (Very good)	All planes look fresh, only minimal coverage with lichen etc. Structures on fracture planes are well recognizable
2 (Good)	Planes look generally fresh, some oxidation/mineral coverage from surficial runoff present, moderate coverage with moss, lichen, and other plants
3 (Poor)	Most planes are weathered and/or strongly mineralized/dirty from surficial runoff, extensive coverage with moss, lichen, and other plants
4 (Very poor)	Heavily weathered outcrop. Grusy appearance of entire exposure, fractures are gaping due to gravitational shifting, most edges are rounded (woolsack-weathering). Fracture planes are dirty and heavily mineralized from surficial runoff; moss, lichen etc. cover almost every surface of the outcrop.

Table 2-1: Classification scheme for bedrock outcrops regarding their quality for data acquisition.

The following sections will in part deal with the relationship between fractures and the rock type they occur in. Since lithologic units are very diverse in the study area and not always continuous across the borders of individual map quadrangles it proved helpful to group these units into categories of rocks with similar properties with respect to brittle behavior. Stone (2002) calls these categories "lithogroups". However, these lithogroups, originally designed for southern New England/USA, cannot be used in other regions without modifications taking into account local and regional phenomena. Thus, the lithogroups in the case of this study area were classified as follows: (1) Granitic rocks: These rocks contain both pure granites and granitic gneisses, which are generally poorly foliated and of a very massive appearance. (2) Layered metamorphic rocks: This group contains all metamorphic rocks with a well-developed gneissic foliation. Fractures parallel to this layering are abundant. (3) Strongly folded and migmatitic rocks: Rocks in this category in part possess a gneissic foliation, but it has frequently been rendered useless as planes of weakness for fracturing. Tight folding or anatectic processes have altered or destroyed the layering. (4) Hydrothermal and pneumatolytic rocks: This group contains veins and dikes of quartz (e.g. the infillings of the Pfahl fault zone) and pegmatite. These rocks are generally highly fractured and are extensive in only one direction without large widths. Therefore, these outcrops frequently lack three-dimensional control and also often inherit the fracture patterns of the adjacent country rocks. A total of 8 outcrops (16.3 %) are located in lithogroup 1, 13 (26.5 %) in lithogroup 2, 23 (46.9 %) in lithogroup 3, and 5 (10.2 %) in lithogroup 4. Respectively, the individual lithogroups cover 19.17 %, 45.05 %, 13.09 %, and 0.10 % of the entire study area, amounting to a total of 78.22 %. The remaining 21.78 per cent are mapped as surficial deposits, water bodies, or anthropogenic structures.

The attribution of initial lithologic units to a specific lithogroup was achieved by the examination of outcrops in sampling stations or by the interpretations of unit descriptions in the comments to the respective geologic maps. Unfortunately, many geologic units and their exact descriptions are not consistent across the borders of individual map quadrangles, so a certain amount of ambiguity concerning the allocation of certain units could not be eliminated. Furthermore, due to the fact that several generations of geologists have compiled the geologic maps of the study area some conceptual problems arose. For instance, many of the units formerly interpreted as magmatic, such as the "Paragranodiorit", the "Ödwieser Granit", etc. are now classified as highly homogenized migmatites. Notwithstanding their new interpretations these high-grade migmatites were attributed to the granitic lithogroup, since due to their textural similarities to granites they are expected to behave more like granitic than metamorphic rocks in response to brittle deformation. Appendix I holds a table listing the most frequently occurring rock types and their allocated lithogroup.

2.2 Types of brittle tectonic features

The brittle tectonic structures encountered in the study area can be classified according to various genetic and functional aspects. Generally, any discontinuity in a rock, be it a simple joint, a fault, or a fractured bedding or foliation plane, is called a fracture. The following sections will describe the fractures measured throughout the study area in terms of their genetic origin, their function in the brittle tectonic regime, and their geometric relationships to each other.

For the lithologies present in the study area a distinction into four major fracture classes has proven useful. These classes are further subdivided with respect to their kinematic significance during the tectonic evolution of the region. The four classes comprise fractures parallel to the tectonic grain, i.e. the metamorphic foliation, fractures cutting across the grain, steeply dipping fractures in unfoliated rocks, and subhorizontal unroofing joints. The former two are mainly made up of moderately to steeply inclined discontinuities in metamorphic lithologies while the latter two are predominantly found in igneous and hydrothermal rocks. All fractures are related in some way to the tectonic history of the study area. Thus, fractures grouped according to the four classes can either be purely extensional features, or faults caused by the relative displacement of adjacent rock blocks. Furthermore, fractures that originated as extensional joints could have been reactivated as faults by a later tectonic regime.

2.2.1 Fractures parallel to the metamorphic foliation

The metamorphic regions of the study area are characterized by a relatively uniformly oriented gneissic foliation. This planar fabric is for the most part made up of phyllosilicates such as muscovite and biotite, which act as planes of weakness producing anisotropic conditions in the rock. Such fabrics frequently cause the rock to fracture parallel to their planes, even if the principal stresses would have initiated fractures with somewhat different orientations. In many places of the study area this foliation has been destroyed by the partial homogenization of the rocks during high-grade metamorphic events. In other locations the foliation has been strongly folded and sometimes even re-folded, thus leading to ductile petrofabrics, which could no longer be reactivated during brittle deformation. In these cases the presence of foliation parallel fractures is highly heterogeneous. While most sampling stations located in foliated rocks, such as gneisses, mylonites, and partially homogenized metamorphics, show foliation parallel fracturing to some degree its importance with respect to other joint families in an outcrop varies.

Figure 2-2 depicts an outcrop where the fractured foliation dominates the brittle structures. Since the foliation here has undergone only minor folding and is therefore fairly planar, partings parallel to the fabric could easily develop. In this case the joints are densely spaced but can rarely be traced over more than one meter. Other locations show large foliation parallel faults several meters in length while still others, although foliated but folded, possess hardly any fractures along the planar fabric.



Figure 2-2: Fractures parallel to the gneissic foliation. Small exposure E of Schareben. Inset: White dashed lines highlight some of the fractures. Leatherman tool for scale.

2.2.1.1 Orientations and spatial distribution

Relating the occurrence of fractures parallel to the gneissic foliation to the lithology in which they were found the “granitic rocks” and “hydrothermal rocks” lithogroups can be neglected, since they are not associated with any appreciable foliations. In figure 2-3 all sampling locations belonging to the layered metamorphic and folded/migmatitic groups are plotted. However, an examination based solely on the abundance of fractures represented in the contoured stereographic diagrams can be misleading, since most outcrops did not allow standardized scanline surveys. Therefore, over- or undersampling bias with respect to the fracture families present in any given location is likely. Moreover, taking merely the number of fractures into consideration does not do justice to other important, but often hard to quantify parameters such as fracture size and spacing, roughness, planarity, brecciation along planes, and other aspects significant for both structural and especially hydrogeologic analyses. In order to include these aspects and to eliminate sampling bias as far as possible a ranking of fracture sets based on the visual examination of the outcrop was performed in every location.

For the diagrams in figure 2-3 fractures parallel to the foliation were determined to be dominant if they constitute the most or second most abundant fracture set compared to the total number of measurements made in an outcrop (fig. 2-3a) or were ranked the most or second most important set as a result of the visual inspection in the field (fig. 2-3b). Both plots show a clear trend, which attributes a diminished importance of foliation parallel fractures to outcrops belonging to the “strongly folded and migmatitic rocks” lithogroup. Figure 2-3a shows an approximately 30 per cent drop between the two groups, being less than the difference in figure 2-3b, which lies closer to 40 per cent. This shows that the apparently most abundant fracture population in an outcrop is not necessarily the dominant one, and therefore highlights the likelihood of a distorted representation of brittle structures – especially for hydrogeologic purposes- in case only the absolute number of fractures measured per sampling location is taken into consideration.

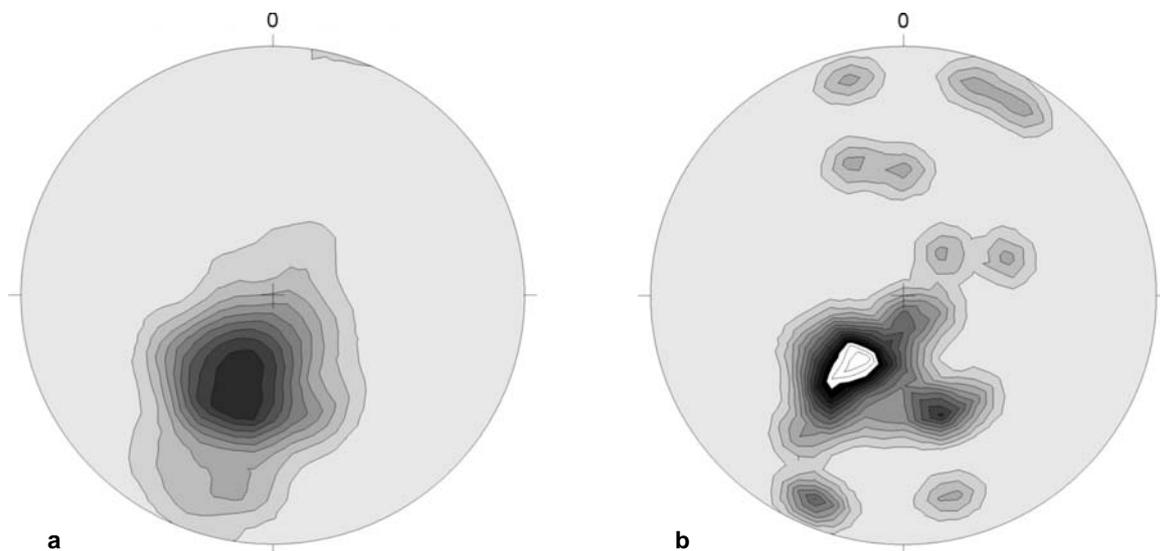
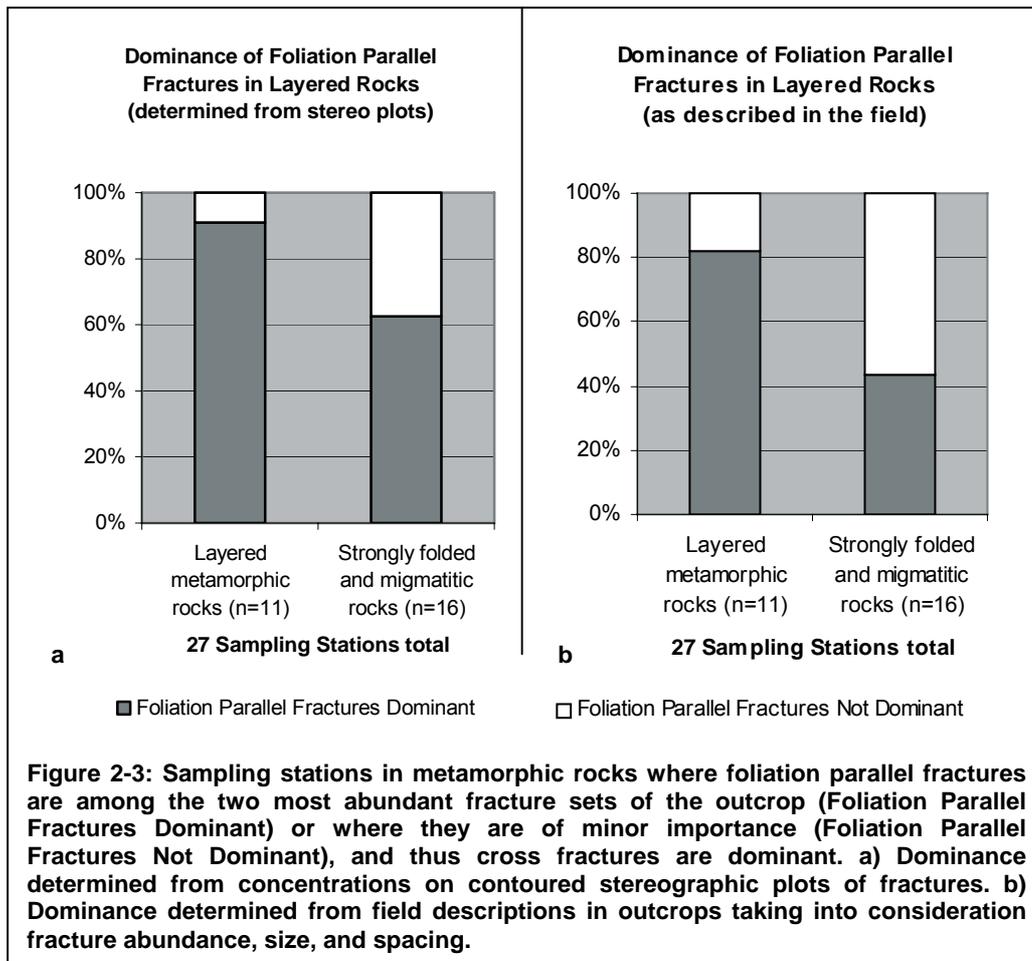
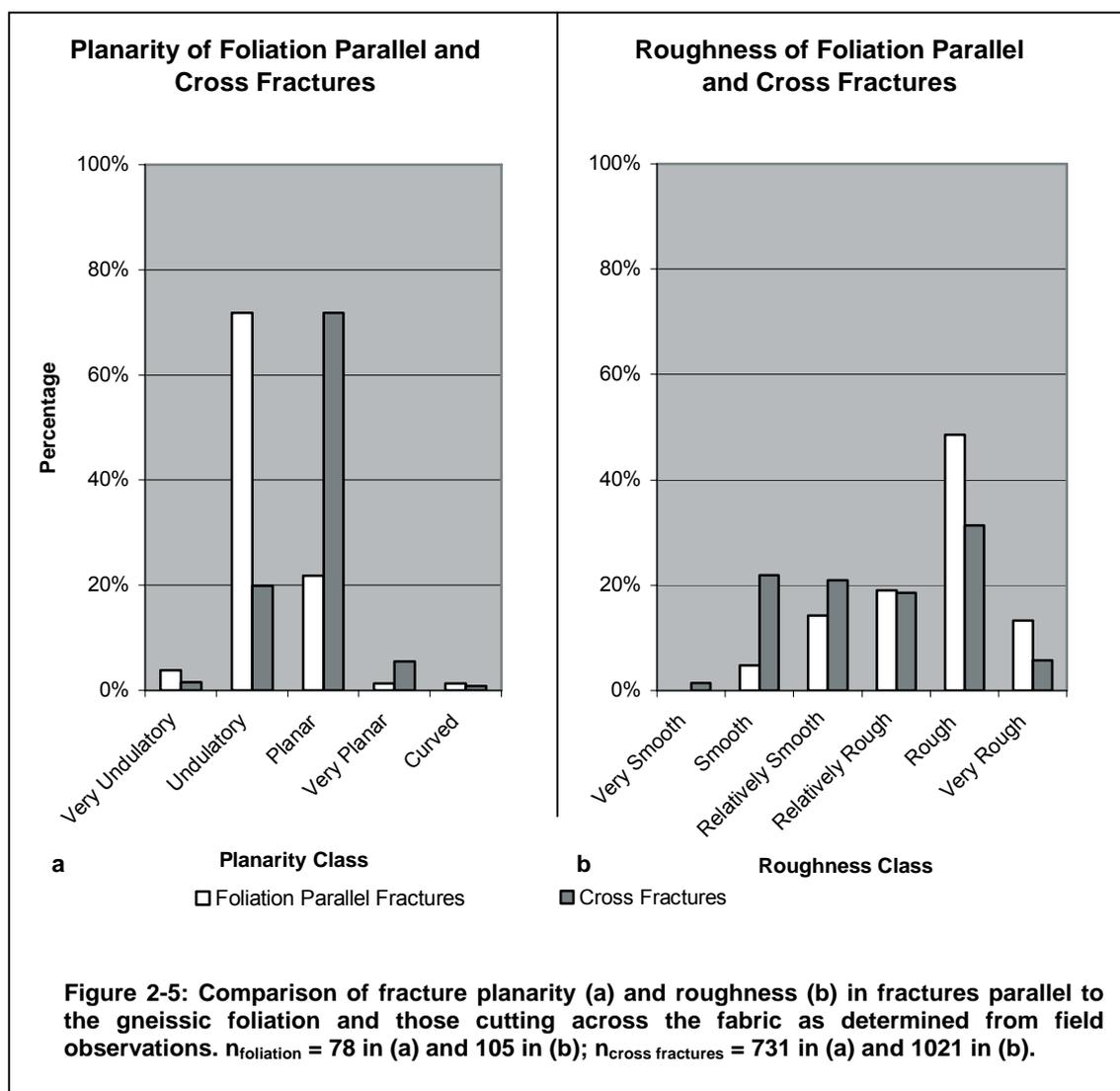


Figure 2-4: (a) Equal area plot of all fractures parallel to the gneissic foliation measured in the study area. $n = 574$. (b) Equal area plot of mean foliation parallel fractures determined from contoured plots of fracture orientations in individual sampling locations. $n = 32$, contours represent integer multiples of random distribution (mrd).

Figure 2-4 shows the orientations of fractures parallel to the foliation. While plot 2-3a summarizes all the individual discontinuities sampled in the study area plot 2-3b depicts a cumulative representation of the average orientations in every sampling station. Local orientations of the foliation are mapped in appendix H. The distribution shows relatively uniform fracture strikes, but an elongation of the contours in the dip direction, similarly to a WNW-ESE trending asymmetric fold with a NNE vergence, which has been reported by Rohrmüller et al. (1996) for the nearby Künisches Gebirge.

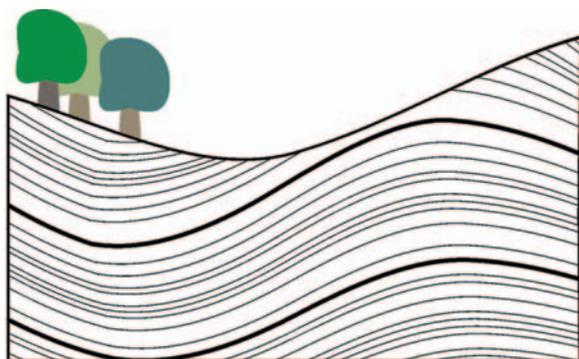
2.2.1.2 Physical Properties

Fractures parallel to the gneissic foliation can have resulted from a variety of different tectonic deformation mechanisms. Thus, foliation parallel joints as well as faults exist all over the study area. Depending on the type and intensity of deformation, as well as the orientation of the planar fabric the physical properties such as fracture size, planarity and roughness are developed in different ways. The attempt to produce a detailed and comprehensive

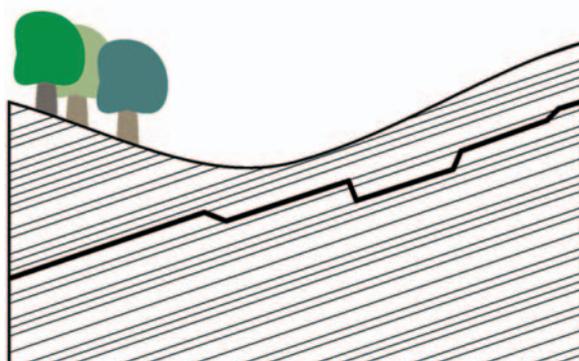


characterization of foliation parallel fractures valid for the entire study area and beyond is difficult to achieve due to their occurrence in different lithologies and different tectonic contexts. Nonetheless, general tendencies with respect to certain fracture characteristics can be discerned for this set of discontinuities.

The examination of two hydrologically very important parameters – fracture **planarity** and **roughness** - on a regional scale unveils clear trends if foliation parallel and cross cutting fractures are compared (fig. 2-5). Fracture planarity is a property, which obviously developed differently in the two types of discontinuities. While the majority of cross cutting fractures possesses rather straight planes the ones parallel to the fabric are predominantly undulatory. This property results from two factors observed in the field. In locations where the foliation is weakly folded on a decimeter to meter scale the fractures frequently follow the folded planes of weakness thus producing undulatory fractures. However, the fractures start to cut across the fabric in case the folding becomes too tight, i.e. if it occurs with wavelengths on a centimeter scale. In other cases the discontinuities tend to “jump” between individual foliation planes thus producing a stepped appearance. This type of foliation parallel fracturing is intermediate between foliation parallel and cross cutting fracturing, since the fissures



a



b

Figure 2-6: Schematic representation of outcrops in layered metamorphic rocks. (a) Fractures following the folded foliation. (b) Fractures alternating between individual foliation planes. Thin black lines: metamorphic foliation; bold black lines: fractures.

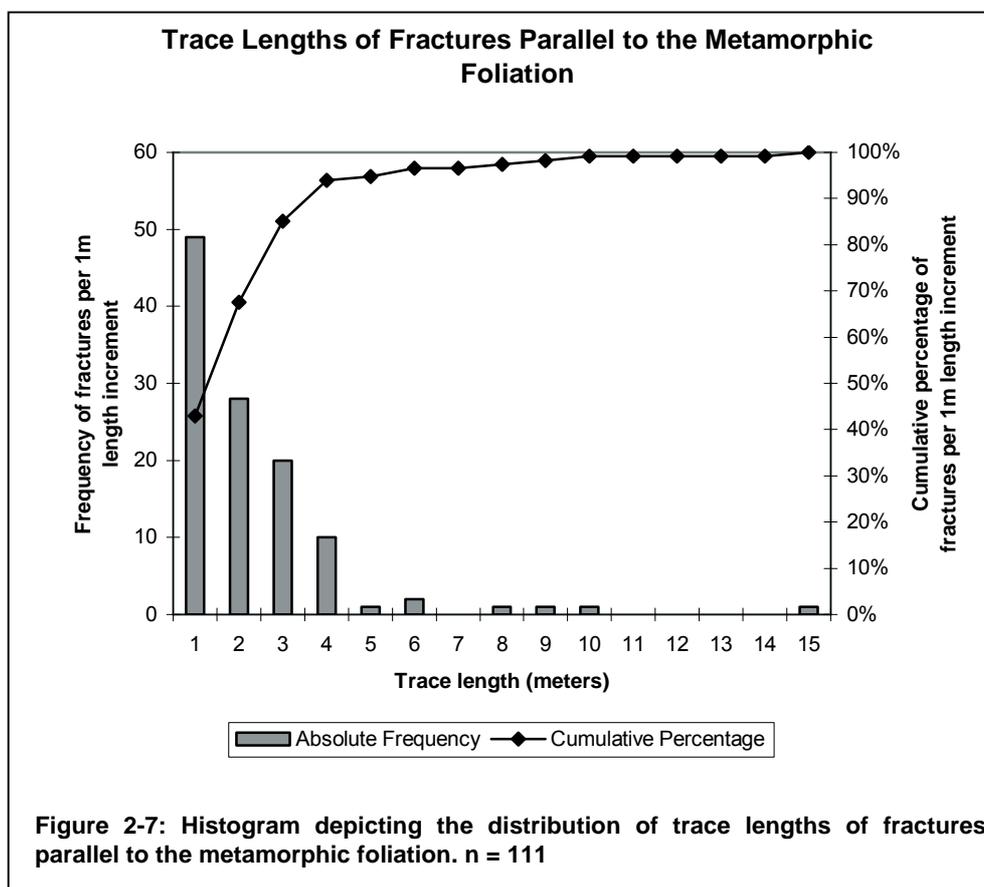
producing the “steps” actually intersect the fabric. However, since the superordinate discontinuities containing these steps in general follow to the foliation planes they are included in the group of foliation parallel fractures. They are frequently associated with rocks with a discontinuous metamorphic fabric or places where weakly developed small-scale folding is present. Figure 2-6 gives a schematic impression of these phenomena.

As can be inferred from figure 2-5b fracture roughness exhibits a tendency to be higher on planes of fractures parallel to the fabric, although the difference to the asperity of cross fractures is not as striking as in the comparison of planarity. For this phenomenon, observations in the field yield an explanation similar to the one for the development of the planarity of foliation parallel fractures, however

on a much smaller scale. If examined closely it becomes obvious that the fracture planes also contain millimeter-scale steps resulting from the utilization of various adjacent foliation planes (similar to fig. 2-6b) thus producing an uneven fracture surface.

Other reasons for the increased asperity of fracture planes are of a tectonic nature. For instance, plumose structures created by jointing or rough surfaces resulting from brecciation during fault motion enhance fracture roughness. However, these structures are not unique to discontinuities parallel to the metamorphic fabric and therefore cannot be used as parameters to distinguish between foliation parallel and cross cutting fractures.

On a regional scale, the **trace lengths** of foliation parallel fractures are extremely variable, ranging from less than 20 centimeters (the lower cutoff for this parameter) to more than 15 meters, in which case they are usually not traceable over a longer distance, but are assumed to continue further into the rock mass (fig. 2-7). Of all fractured foliation planes for which trace lengths were measured ($n=111$) the mean was computed to be 1.94 meters with a 95% confidence of ± 0.40 meters. This suggests that the majority of fractures traces approximately between 1.5 and 2.5 meters. However, these statistical values are based on a relatively small sample and do not have much practical meaning for the description of fracture sizes, especially since the scale of trace lengths can vary over about two orders of

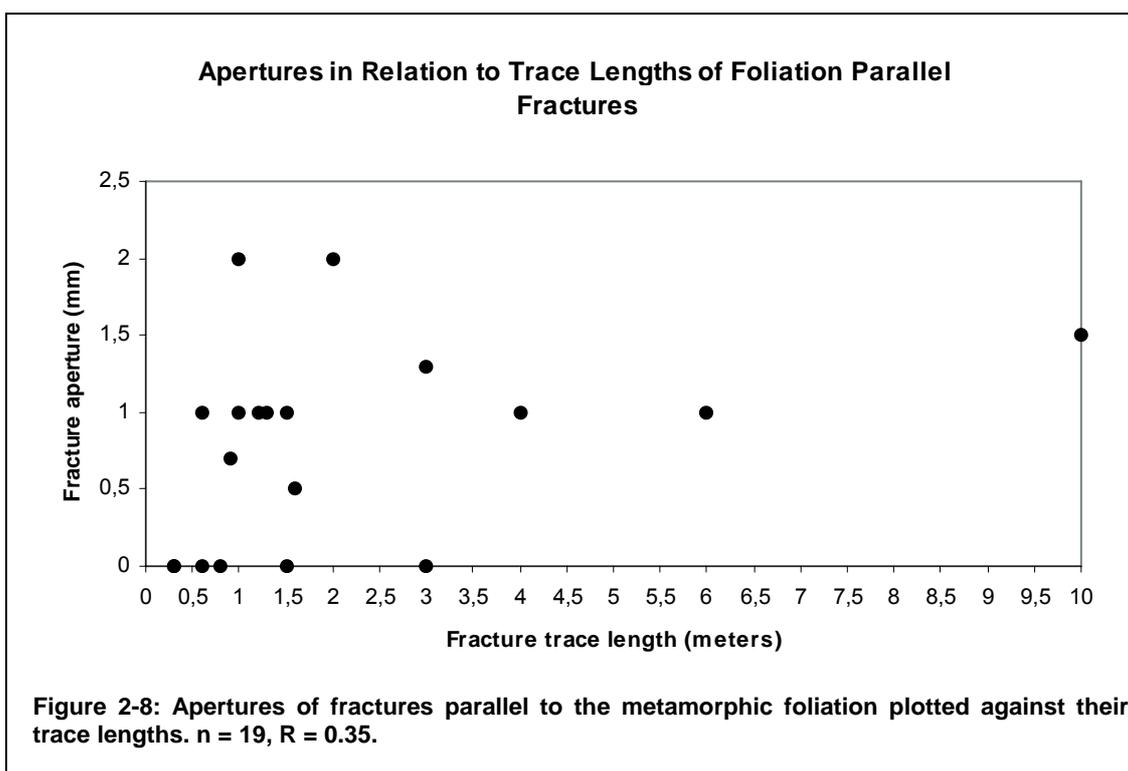


magnitude within one single outcrop. Moreover, in locations where the measured fractures were selected subjectively fractures with traces close to the mean value are the most conspicuous.

Also, steeply inclined fractures tracing more than 2 meters are frequently out of reach for exact measurement. Thus, lengths of large fractures frequently had to be estimated. Sampling bias is therefore likely. A scaling effect was observed in several locations, which expresses itself in a tendency of large fractures to form densely fractured zones rather than single planes. Especially discontinuities tracing more than approximately five meters are frequently associated with a zone of relatively short fractures, which are spaced at only a few centimeters. Figure 2-9 depicts an example for this hardly quantifiable observation.

Another factor being directly related to the parameters above is fracture **aperture**. At the same time it is an aspect almost impossible to quantify with field measurements in bedrock outcrops because of strain release effects in the rock close to where the exposure surfaces. Thus, aperture measurements obtained with devices such as taper gauges are inevitably biased towards exaggerated values. Further complications involve the geometric properties of bedrock outcrops, which frequently preclude the use of measuring devices, the high aperture variability within one single fracture due to the asperity of its planes, and the presence of breccia. However, since alternative methods to obtain aperture values, such as hydraulic testing, may yield questionable results as well (Cheema and Islam, 1994), the aperture measurements taken in the exposures are included in the analysis. According to Barton et al. (1993) it has to be recognized that the results cannot be treated as absolute quantities, but as general trends, which are still of value, since “an imperfect measure of aperture is preferable to no measure” (25). Only 25 aperture measurements could be obtained from fractures parallel to the metamorphic foliation due to the problems mentioned above, which are represented in the chart in figure 2-8. The mean and median values of the entire sample are 0.79 mm and 1 mm, respectively with a minimum of 0 mm and a maximum of 2 mm. Larger apertures were frequently observed, but were attributed to intense weathering or the gravitational shifting of sections of a bedrock exposure. Also, brecciated fractures, which frequently reach widths of more than ten centimeters are not included. As can be inferred from fig. 2-8 most values range between 0 and 1 mm¹, and only a very weak positive correlation –possibly in part due to the low number of datapoints and the sampling difficulties- between aperture and fracture trace length can be discerned.

¹ The resolution of the taper gauge used for the aperture measurements is 0,1mm, starting at approximately 0.5 to 0.6mm.



Fracture spacing, in combination with trace length, represents an indicator for the hydraulic connectivity of a fracture network. For the sampling stations in the metamorphic lithologies the spacings were usually recorded as rounded mean values of a few measurements representing the entire exposure, because in most places the outcrops were too small and/or discontinuous to obtain meaningful scanline measurements. Of the 30 metamorphic outcrops displaying a macroscopically visible foliation a total of 20 could be used to measure or estimate the spacings of foliation parallel fractures.

An undifferentiated examination of this parameter leads to the conclusion that the spacings in this group are highly irregular and impossible to quantify. However, if further classified, the distribution turns out to be more uniform. This classification is related to the trace length of fractures and to the type and degree of their deformation. Accordingly, spacings are grouped into those of short fractures, longer fractures, and discrete densely fractured zones. In this context short fractures are defined as having trace lengths on a centimeter to decimeter scale, while longer fractures usually trace more than one meter. Densely fractured zones are a special case, since each of them consists of a large number of closely spaced small fractures, but at the same time can be seen as a single discontinuity spaced at a certain distance to the next one, depending on the scale of observation (fig. 2-9). Almost all of these zones are traceable over several meters; some even cut the entire extent

of an outcrop. In the field they were frequently interpreted as very young faults having developed at shallow crustal depths.

Mean spacings of short fractures parallel to the foliation in the metamorphic exposures included in this analysis ($n_{\text{Outcrops}} = 8$) range from 0.02 to 0.38 meters with an average value of 0.17 m. Larger fractures (> 1 m trace length) are on average spaced at 1.02 m with a minimum of 0.45 m and a maximum of 2 m ($n_{\text{Outcrops}} = 9$). Average spacings of densely fractured zones (see fig. 2-9) range from 1.25 to 2.5 meters with a mean value of 1.95 m ($n_{\text{Outcrops}} = 6$), although in some cases they were highly irregular. The fracture density within those zones is very high with spacings of commonly less than 0.1 m, sometimes even less than 0.01 m. The higher the density, the shorter and more interconnected the fractures become, which leads to the point where the fracturing grades into brecciation. Thus, these zones were frequently called “densely fractured/brecciated zones” in the field notes.

From these values it can be inferred that – at least in a very general way – fracture spacing is proportional to trace length, since there is a continuous increase in spacing from short to long fractures to densely fractured zones.

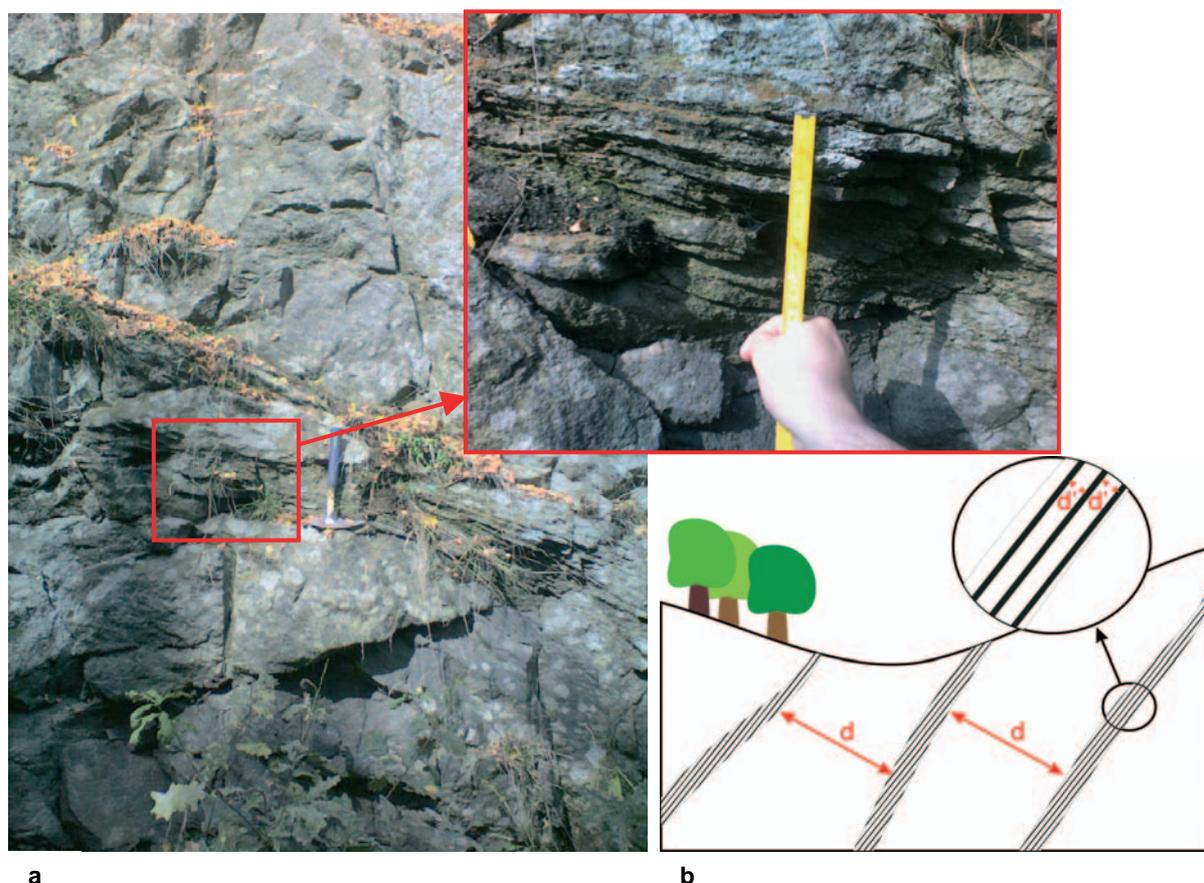


Figure 2-9: Spacings of densely fractured zones. (a) Photograph of a densely fractured zone. Location: Viechtach, Alterberg (6943-14). (b) Schematic representation of densely fractured zones. d = spacing of zones; d' = spacings of fractures within a single zone.

Mineralizations on fractures parallel to the metamorphic foliation were recorded in only very small numbers. Apart from the observation that fractures belonging to other sets are more intensely mineralized, the high degree of weathering in the metamorphic exposures and the frequent brecciation of fracture planes due to shearing obscure potential



Figure 2-10: Sample of a fracture plane parallel to the metamorphic foliation within quartzo-feldspathic and graphitic mineralizations. Red line indicates trend of slickenlines. Sample taken from location 6944-13 (Unterried quarry).

mineralizations. Where present, the minerals consist of a mix of leachates from ore deposits (especially in the Bodenmais area), such as hematite or limonite, or -probably hydrothermal-quartzo-feldspathic precipitates. A special case is the Rundinger Zone where extensive graphite covers were encountered on foliation parallel fault planes (fig. 2-10).

Phases of hydrothermal fracture healing must have predated the latest stages of brittle deformation along fractures parallel to the foliation, because almost all mineralized discontinuities have been reopened by relatively young brittle tectonics. The only significant exception constitute rocks in the vicinity of ore bodies (e.g. in the Barbarastollen of the Silberberg mine near Bodenmais) where dissolution and reprecipitation of metalliferous minerals is still an ongoing process.

Infillings in fractures parallel to the foliation occur in several outcrops of the metamorphic lithologic domain and may influence the hydraulic behavior of discontinuities. However, compared to the total number of measurements of foliation parallel fractures their frequency is relatively low ($n_{\text{clearly brecciated fractures}} = 22$). This is in part due to the fact that many brecciated fractures cannot be clearly identified as being parallel to the foliation because of their brecciation. Also, brecciation is usually associated with larger fractures, which are less numerous in this fracture type than in the sets cutting across the foliation (compare figs. 2-7 and 2-13). Nonetheless they exist and constitute the majority of foliation parallel fractures with large trace lengths. The infillings mainly consist of fault breccia and gouge, which can both increase and decrease the permeability of a fracture, depending on their physical properties. While fault breccia can greatly enhance the permeability, the more fine-grained, clayey fault gouge can even act as an aquiclude (Freeze and Cherry, 1979). For the vadose zone in the grusy upper layer of the metamorphic rocks in the Bavarian Forest Raum (2002) found out that clayey fracture infillings may completely change groundwater migration

patterns, depending on the moisture content in the ground. Dry gouge may still allow water to flow through a fracture, but the increased moisture introduced by the ongoing flow soon causes clay minerals to swell and clog the conduit. For the more deep-seated aquifers this process is significant as well, since it can strongly influence the infiltration behavior of the topmost hydraulic layer, which is important for the recharge of the underlying reservoirs.

In the study area foliation parallel fractures frequently contain a mix of infillings with different grain sizes ranging from the clay/silt-sized fraction to up to fist-sized blocks. The dominant form of infillings, however, is approximately 2 to 5 cm in diameter and frequently elongated in one direction (in many cases parallel to the orientation of the fracture plane). Additionally, the breccia are mostly associated with the densely fractured zones described above. These zones are usually 5 to 20 cm wide, but can reach widths of up to 40 cm. Along planes of this fracture type only noncohesive breccia and gouge was found. Compacted or cemented breccia sheets were not observed. Trace lengths of brecciated fractures are rather long, ranging from 1.5 to 15 meters with an average length of 7.0 m. Several of these fractures were associated with moisture or even dripping water. Soil and plants, such as various types of grass and moss but also little trees, were found in a number of such discontinuities thus indicating the presence and flow of water in these fissures.

2.2.2 Fractures intersecting the metamorphic foliation

In the metamorphic regions of the study area there are also discontinuities, which formed independently of preexisting mineral fabrics. In this context they are called “fractures cutting across the metamorphic foliation”, or simply “cross fractures”. These fractures are of a purely tectonic origin and are not influenced by preexisting planes of weakness. Thus, phenomena such as partial melting or tight folding of the host rock have generally no effect on the presence and orientation of these types of discontinuities. This group of fractures comprises extensional joints, such as the ones visible in fig. 2-11, as well as major faults. They are an ubiquitous occurrence throughout the metamorphic lithologic domains, no matter if a set of foliation parallel fractures has developed or not. In fact, there are several locations where a clear distinction between foliation parallel and cross cutting fractures could not be made, because in some cases fractures at very small acute angles to the metamorphic fabric exist. Also, in places where the foliation is only weakly developed, strongly folded, or partially destroyed by later thermal events fractures frequently follow the fabric where it is present and suitable as planes of weakness, but become cross-cutting as soon as the foliation can no longer be used for fracturing.

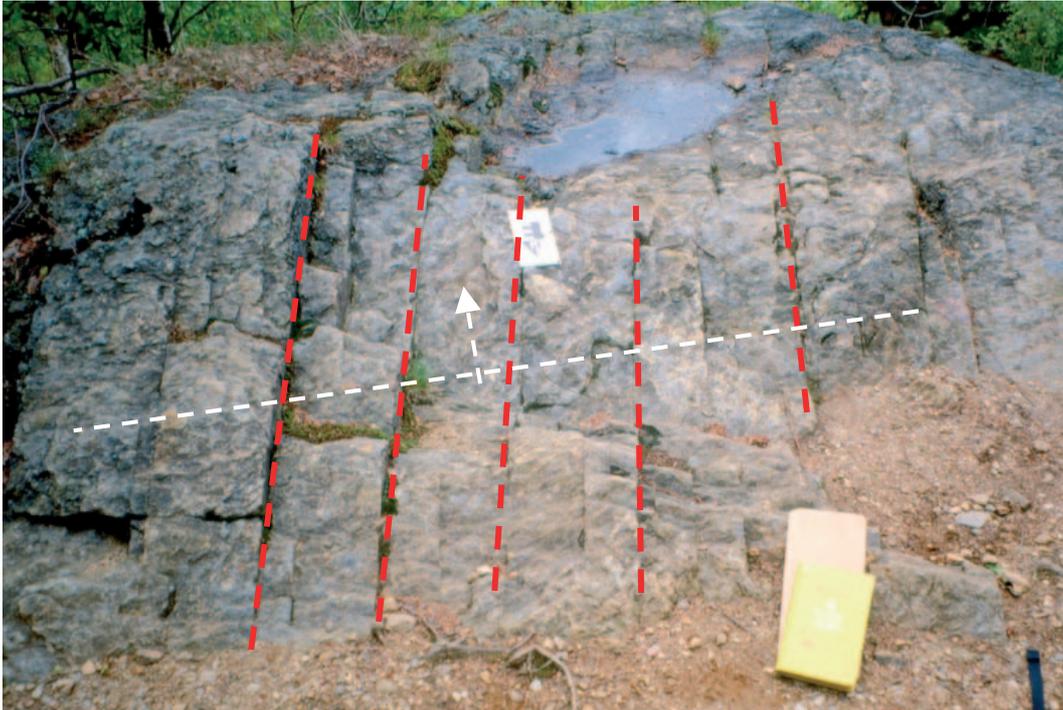


Figure 2-11: Fractures cutting across the metamorphic foliation (several of the larger ones highlighted by red dashed lines) White dashed line and arrow depict approximate strike and dip direction of the foliation. Field book for scale. Location: Silberberg/Gottesgab (6944-04).

2.2.2.1 Orientations and spatial distribution

Concerning the spatial distribution of cross fractures, some information has already been given in the preceding subchapter (2.2.1.1) on foliation parallel fractures. As figure 2-3 displays, the cross fractures' dominance relative to that of fractures parallel to the tectonic grain (i.e. cross fractures are the principal fracture sets in locations where foliation parallel fractures are not dominant) varies with respect to the lithogroup in which the specific sampling stations are encountered. Thus, cross fractures are rather dominant in strongly folded and migmatitic rocks while they are of reduced importance in the layered metamorphic lithologies. In contrast to the foliation parallel fractures the cross fractures are an ubiquitous occurrence all over the metamorphic regions of the study area, since their purely "tectonic" origin does not necessitate preexisting planes of weakness. Looking at the absolute numbers of measurements taken of foliation parallel and cross fractures a large difference becomes obvious ($n_{\text{foliation parallel fractures}} = 574$; $n_{\text{cross fractures}} = 2333$). This dominance of cross fractures is in part due to the fact that they consist of not only one, but several different sets of fractures with distinct orientations, which have formed in response to the various stress fields that have acted on the area during its brittle tectonic history. Another reason for the relatively low number of measured foliation parallel fractures is the high metamorphic grade of many rocks in the study area, which frequently destroyed macroscopically visible foliations. Examples for

these rock types are the Körnelgneis or the diatexites in the vicinity of the granitic intrusions in the southern part of the study area.

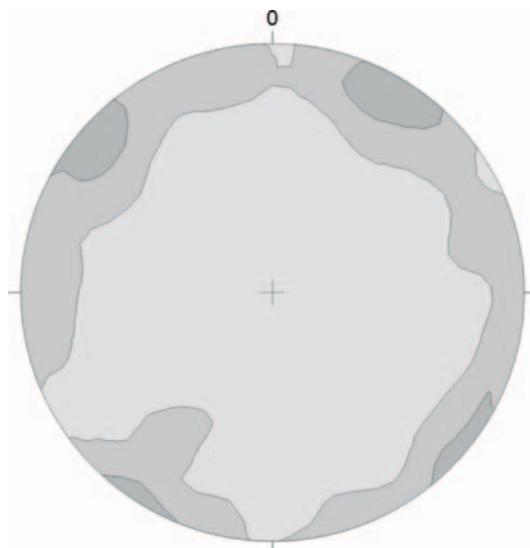


Figure 2-12: Equal area plot of all fractures cutting across the gneissic foliation measured in the study area. $n = 2333$, contours represent integer mrd.

The examination of the plot in figure 2-12 yields two prominent strike directions of cross fractures, one of which follows the general trend of the foliation parallel discontinuities (fig. 2-4) and of the large Hercynian structures. The other one strikes at right angles to the former, subparallel to the predominant orientations of fractures in the unfoliated lithogroups (fig. 2-19). The cross cutting planes are predominantly steeply inclined and do not possess the high variability in dip like the foliation. If plotted in smaller numbers gently dipping to subhorizontal planes become evident as well, but in the bulk sample they only play a subordinate role.

Cross cutting fractures exist both as purely extensional joints and as faults in all the metamorphic lithologies. A great number of them show evidence of multiple phases of brittle deformation. Their evolution is very likely to have proceeded contemporaneously with that of the foliation parallel discontinuities. A simultaneous tectonic activity along both types of fractures can be assumed, since many foliation parallel planes contain kinematic indicators suggesting stress fields similar to those which have acted on the cross cutting variety. A more detailed description of this phenomenon will be given in section 2.4.3.

2.2.2.2 Physical properties

Similar to subchapter 2.2.1.2 parameters such as planarity, roughness, size, aperture, mineralizations, and infillings will be described for the fractures intersecting the metamorphic fabric. Discontinuities of the cross cutting group also possess a certain degree of variability in their characteristics. However, general trends concerning their physical properties do exist.

Regarding **planarity** and **roughness** of cross fractures figure 2-5 shows that this type of discontinuity tends to form rather straight and smooth planes as opposed to the more rough and undulatory foliation parallel fractures. Since they form independent of a metamorphic fabric they are not forced to follow preexisting undulating planes of weakness

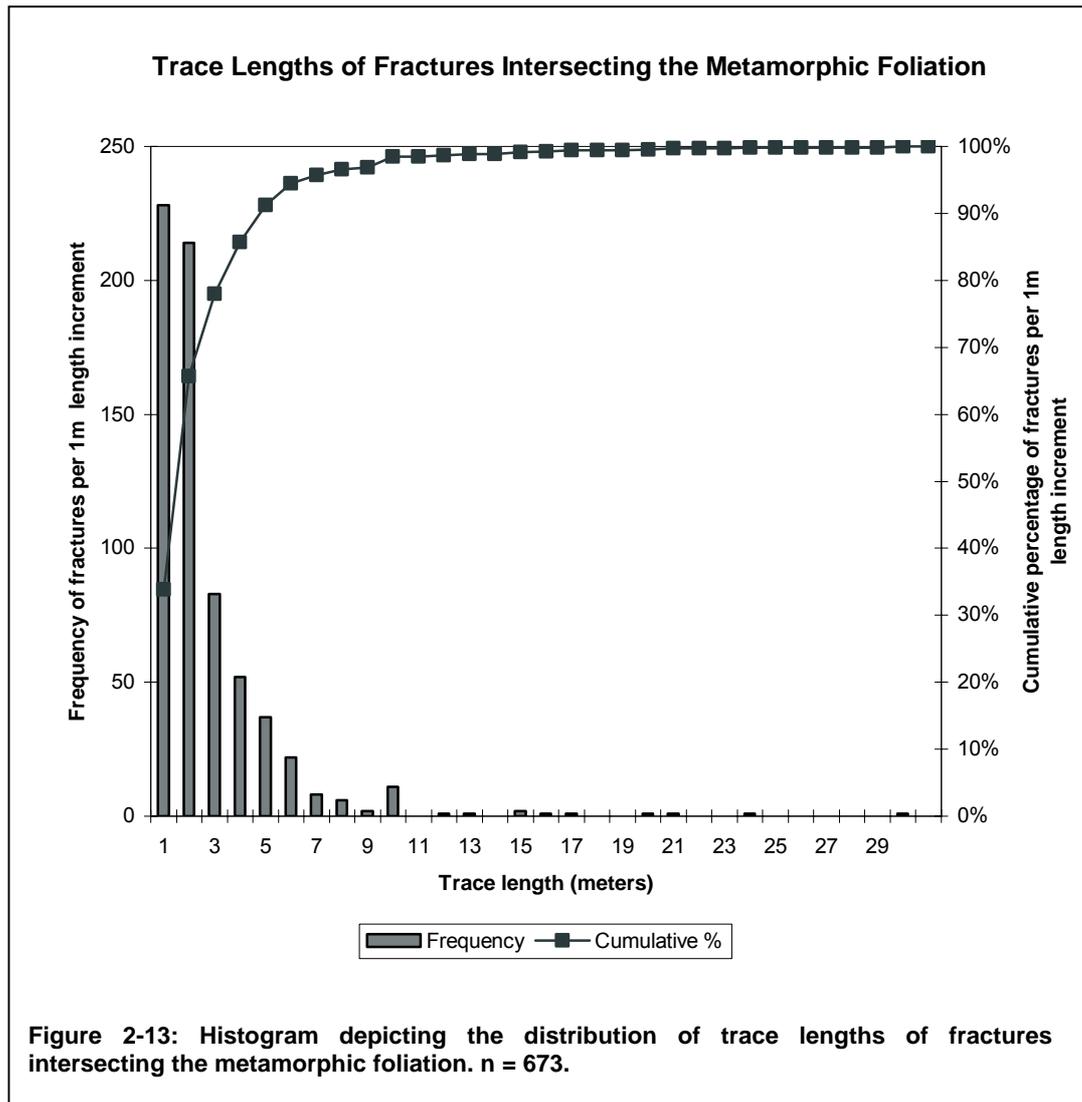
or to alternate between such planes, as schematically represented in figure 2-6. However, several factors can increase the roughness of a cross fracture, the most important of which being brittle shearing associated with brecciation along the fracture plane. Thus, purely extensional joints frequently tend to be smoother than brecciated faults, although the formation of slickensides, i.e. displacement without brecciation, often tends to polish fault planes. Differential weathering is another process increasing the asperity of a fracture plane, especially in rocks at shallow depths. It partially removes mineral coatings of fracture planes, frequently giving them a “patchy” appearance of mineralizations and uncoated bedrock. In addition, differential weathering in layered rocks frequently removes the easy to erode phyllosilicates and causes the more resistant felsic layers to stick out, thereby enhancing the overall asperity of the fracture plane.

In order to highlight variations of cross fracture asperities with respect to their orientations the dataset was subdivided into three major groups: steeply dipping fractures striking N-S to ENE-WSW, steeply dipping fractures striking WNW-ESE to NNW-SSW, and moderately to gently dipping fractures (dip angles $<40^\circ$). Table 2-2 lists the results of this classification:

Roughness Coefficient	Steeply dipping, northeasterly (NE $\pm 30^\circ$) striking fractures	Steeply dipping, northwesterly (NW $\pm 30^\circ$) striking fractures	Moderately to gently dipping fractures
1 (very smooth)	2,04%	0,62%	0,00%
2 (smooth)	27,11%	16,67%	8,93%
3 (relatively smooth)	22,45%	24,07%	7,14%
4 (relatively rough)	14,29%	22,84%	12,50%
5 (rough)	29,74%	28,40%	55,36%
6 (very rough)	4,37%	7,41%	16,07%

Table 2-2: Distribution of roughness coefficients for cross fractures with different orientations.

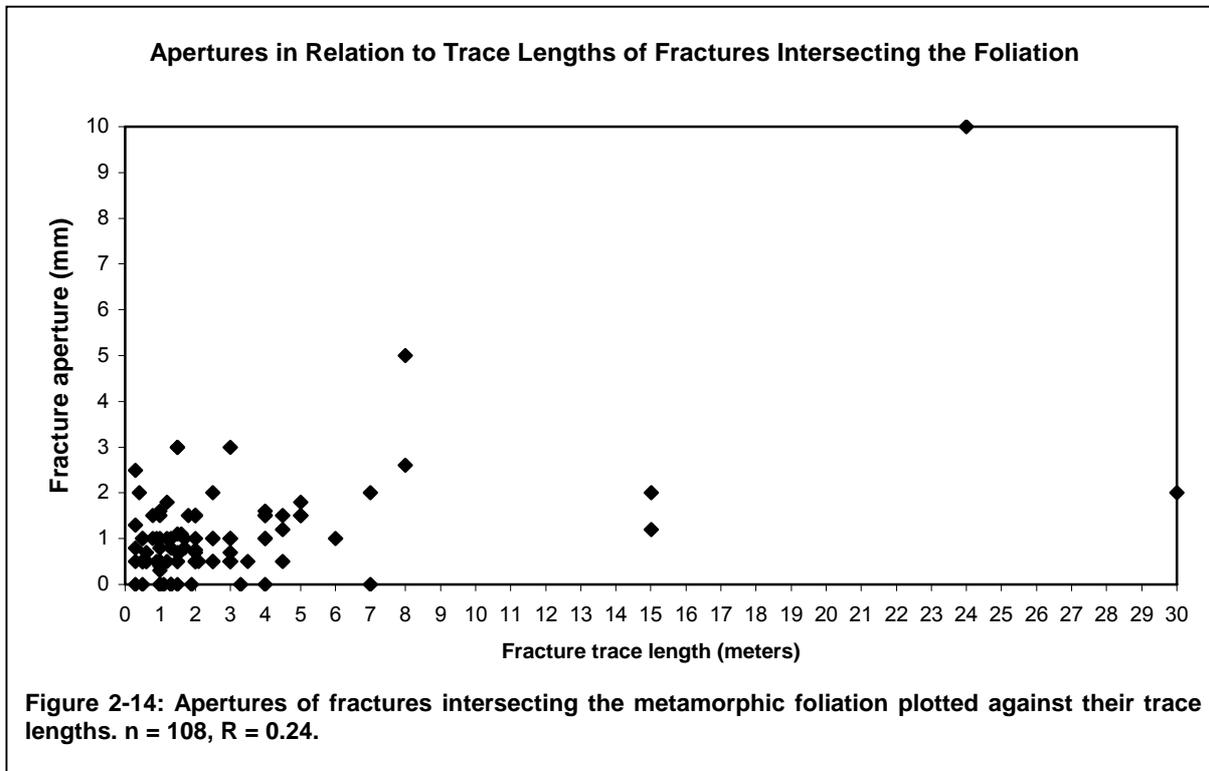
Comparing the roughness coefficients of the different fracture groups several trends become evident. Both steeply dipping sets show a comparatively large percentage of relatively smooth and smooth fractures although the dataset is dominated by rough fractures. The steeply dipping, northeasterly striking discontinuities expose a rather bimodal distribution with peaks at the roughness classes 2 and 5 while the northwesterly trending ones show a certain degree of clustering in classes 3, 4, and 5. Much in contrast to the steeply dipping populations the majority of the moderately to gently inclined cross fractures display a very pronounced peak in class 5 (rough planes) surrounded by minor concentrations in classes 4 and 6. Gently dipping discontinuities possessing smooth surfaces represent the exception.



Compared to the length distribution of foliation parallel fractures the **trace lengths** of fractures intersecting the fabric tend to be somewhat longer on average (mean = 2.50 m) falling within ± 0.21 meters of the mean at the 95% confidence level. In addition, the range of values (minimum length = 0,1 m, maximum length = ca. 30 m) is about twice that of the foliation parallel fractures. Of course, the restrictions concerning the statistical validity of the measurements and the possible sampling effects mentioned in the section on the trace lengths of foliation parallel fractures apply to the cross fractures as well. The tendency of large fractures to form zones of breccia and smaller fractures rather than one continuous fissure also exists in this group of discontinuities. However, relatively smooth-walled individual long fractures (tracing several meters) with no signs of brecciation are a common occurrence, much in contrast to fractures parallel to the fabric.

Apertures of cross fractures range from 0 to 10 millimeters, averaging at 0.98 mm. The median value lies at 0.7 mm. Two measurements greatly exceeded values of 10

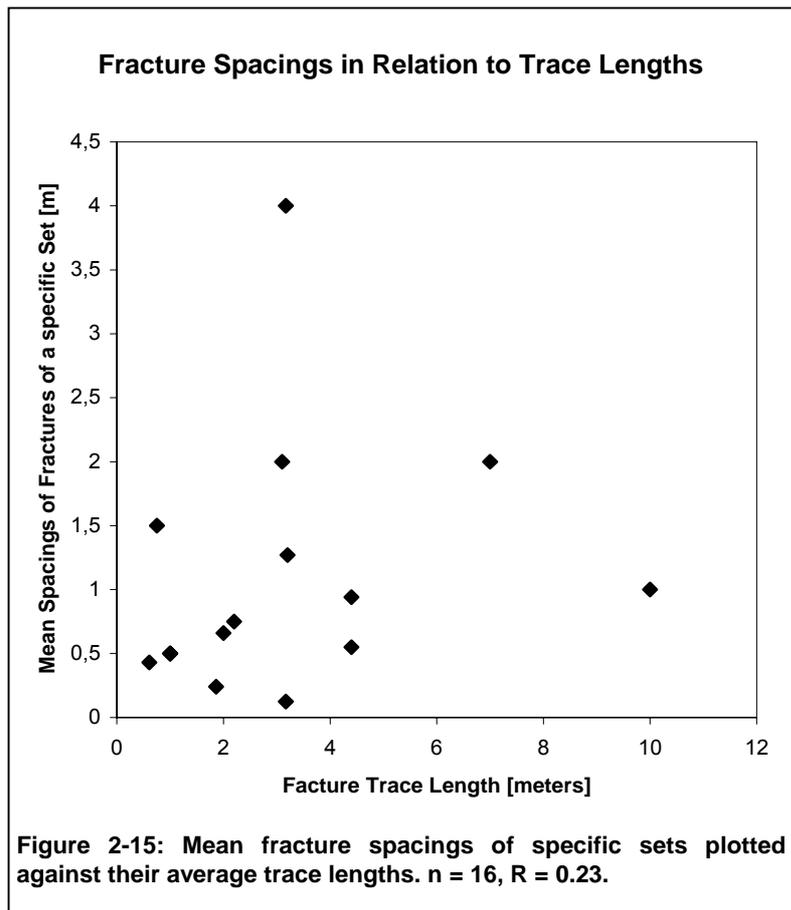
millimeters and were discarded from the sample, since gravitational or weathering effects could not be ruled out with certainty. Figure 2-14 shows a weak positive correlation between fracture aperture and trace length, similar to fig. 2-8 for the fractures parallel to the foliation.



The mean **spacings** of cross fractures in the particular sampling stations show – similar to those of the foliation parallel fractures - highly irregular values if looked at the bulk dataset. Thus, the data was subdivided into groups with specific orientations and specific types of fractures (single fractures, fractures within swarms, and densely fractured/brecciated zones, table 2-3). Single fractures are those not associated with any brecciation or fracture swarms. Their mean trace lengths usually reach more than two meters, so they were not further categorized into short and long fractures. Fracture swarms are spatially limited zones in an outcrop where a high density of fractures with similar orientations exists. As opposed to densely fractured/brecciated zones these swarms comprise relatively large (meter-sized) distinct fractures (mostly joints) without any brecciation. Densely fractured/brecciated zones look in principle the same as those parallel to the metamorphic foliation (fig. 2-9). In these zones distinct fractures are difficult to identify because of their close spacings and short trace lengths, which frequently cause a brecciated appearance of the entire zone.

Orientation of Fracture Sets		Mean Spacings of single fractures [m]	Mean Spacings within fracture swarms [m]	Mean Spacings of densely fractured/brecciated zones [m]
Steeply dipping / subvertical	N-S	0,90	0,75	
	NNE-SSW	0,44	0,09	
	NE-SW	0,85	0,13	2,75
	ENE-WSW	0,75	0,18	3,50
	WNW-ESE	1,29	0,30	2,83
	NW-SE	0,52	0,10	1,00
Gently dipping / Subhorizontal		0,94		0,94

Table 2-3: Mean spacings of fracture sets with respect to their orientations and the three subgroups (spacings of single fractures, within fracture swarms, and of densely fractured/brecciated zones).



Comparing the three fracture types in table 2-3 with respect to their orientations several general tendencies can be observed, the most obvious of which are the relatively uniform spacings within each fracture type. Mean spacings of single fractures average at 0.93 meters (median: 0.75 m, minimum: 0.125 m, maximum: 5.00 m), of fractures within swarms at 0.21 m (median: 0.125 m, minimum: 0.08 m, maximum: 0.75 m), and of densely fractured/brecciated zones at 2.60 m (median: 2.50 m, minimum:

0.94 m, maximum: 4.50 m). In contrast, fractures within each orientation group (i.e. with the same strike, but across the fracture types) do not show any correlation. For example, the orientation group with the largest spacings of densely fractured/brecciated zones (the steeply dipping ENE-WSW trending one) possesses an intermediate value for individual fractures and a low value for the fractures within swarms. Thus, the spacing of a specific fracture type

does not allow any conclusions regarding the spacings of all fractures with the same orientation in a sampling station.

Figure 2-15 shows an extremely weak correlation between fracture spacing and trace length, i.e. longer fractures tend to be spaced at greater distances than shorter ones. However, it has to be kept in mind that the number of datapoints is very low and the data on spacings is derived from mean values obtained from semiquantitative acquisition methods.

Mineralizations on cross cutting fracture planes were recorded focusing on the following minerals: quartz, feldspar, graphite, epidote, chlorite, hematite, and precipitates of leached-out metalliferous ores. Only about 10 per cent of all cross fractures measured were found to contain mineral coatings on their planes. The actual percentage is likely to be higher, but, as it is also the case with foliation parallel fractures, weathering and overgrowth with lichen and moss frequently obscure large portions of a fracture plane. Graphite mineralizations were only recorded in one sampling station (6944-13), where the vast majority of mineralized planes paralleled the local foliation. Only three cross fractures with graphite coatings exist in the dataset. In contrast, other mineralizations could be found throughout the entire metamorphic part of the study area. Quartz and feldspar (or in many cases most likely a macroscopically not distinguishable mix thereof), as well as hematite, epidote and chlorite occur on all major sets of cross cutting fractures, thus suggesting that mineralized solutions permeated the rocks after all major fracture systems had been established. Currently open fissures, sometimes associated with the formation of plumose structures on mineralized surfaces, in turn indicate the reactivation of formerly healed fractures. Precipitates from leached ore deposits are less ubiquitously distributed and concentrate mainly in the Bodenmais/Silberberg area, although they were also found in other places, especially in the vicinity of meta- to anatectic rocks. These mineralizations also do not seem to be restricted to specific fracture orientations, but occur on all major sets.

Infillings of cross fractures consist mostly of unconsolidated fault breccia and gouge, ranging in grain size from the clay to the gravel fraction with a general dominance of coarser-grained material. In many fractures a mélange of fine-grained gouge and coarser-grained breccia can be observed. Fissures with purely clay- or silt-sized infillings are rare, while exclusively gravel-sized ones are a widespread occurrence. Plotting the discontinuities containing infillings on the stereographic net shows a predominance of NW-SE striking fractures while only a few strike NE-SW (fig. 2-16). Separating the dataset with respect to the grain size of the infillings reveals that fractures containing fine-grained material trend almost exclusively NW-SE while the ones filled with coarser-grained breccia exist in all concentrations depicted in figure 2-16.

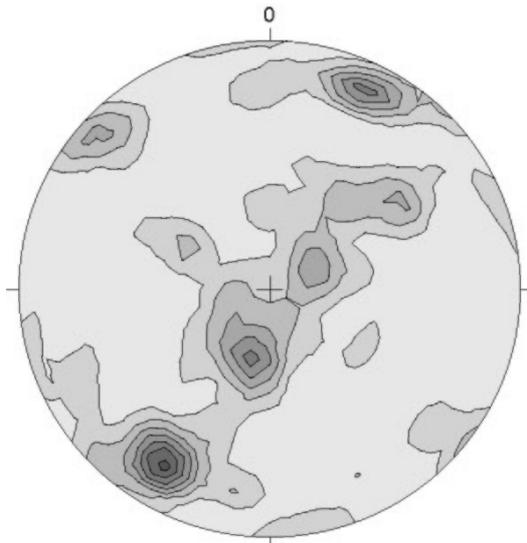
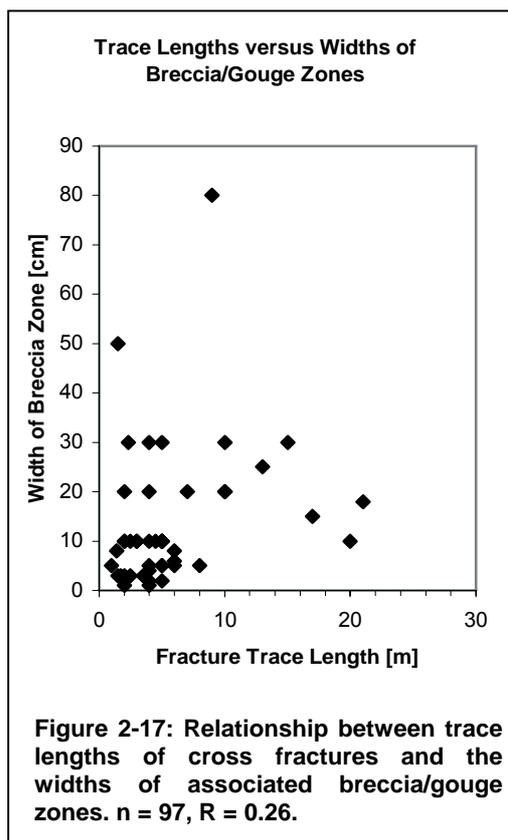


Figure 2-16: Orientations of fractures intersecting the metamorphic foliation containing infillings. $n = 95$, contours represent integer mrd.



In terms of trace length cross fractures with infillings belong to the relatively large ones, ranging from 0.5 to over 20 meters with an average length of 4.98 m. The widths of the breccia/gouge seams within the fractures are highly variable (ranging from 0.01 to 0.80 m) and only marginally depend on the trace length of the fractures they are associated with. However, a very weak tendency of long fissures to develop wider breccia seams than short ones can be observed when plotted against each other (fig. 2-17). Several outliers, especially those with large widths of breccia/gouge zones and short trace lengths, exist in the dataset. These are most likely the result of difficulties in measuring the exact trace lengths of partially obscured fractures extending far beyond the exposed rock surface of an outcrop.

Infillings not originated from tectonic deformation exist in the form of soil developed from weathered fault gouge and in the form of various kinds of plants, especially grass and moss, but also bushes and little trees. These types of infillings occur in fractures of all orientations.

About 10 per cent of the fissures containing infillings carry significant amounts of water, i.e. water is either dripping or even flowing out of the open fractures. Especially gently inclined and NW-SE striking fractures were found

to be water bearing. This agrees well with the observations made concerning the roughnesses of cross fractures with specific orientations (table 2-2), given that the assumption that rough fractures are more likely to carry water holds true.

2.2.3 Steep fractures in unfoliated rocks

In the study area several rock types possessing no foliation and therefore being without any preexisting planes of weakness exist. Thus, structural anisotropies are not present in these lithologies and brittle failure as well as the resulting orientations of fractures should be expected to be caused solely by an active stress field. Nonetheless, as will be shown in the next section, regional structural entities, formed during phases of metamorphism, such as the Pfahl fault zone, do have an effect on fracture orientations in the granitic and hydrothermal lithogroups as well. Figure 2-18 shows two examples for fractures in unfoliated rocks (a granite and a quartz exposure, respectively) proving that dominant orientations and high fracture densities are also common in these lithologies.



Figure 2-18: Fractures in unfoliated rocks. (a) Fractures in a medium-grained granite. Vertical extent of the image is approximately seven meters. Location: Steinbruch Prünst (6932-01), (b) Fractures in a quartz dike of the Pfahl zone. Folding rule (2m) for scale. Location: Quarzbruch Zuckenried (6944-17).

2.2.3.1 Orientations and spatial distribution

Thirteen sampling stations in the study area are located in unfoliated lithologies such as granite, quartz, and pegmatite. These rock types are predominantly found in the granitic plutons of the southern study area and in the hydrothermal precipitates permeating the Pfahl fault zone. In the northern part of the area these lithologies exist only in small dikes and

veins, or in smaller granitic intrusions such as the Arnbruck granite pluton, which, unfortunately, has not undergone extensive quarrying and is therefore poorly exposed.

The plot in figure 2-19 depicts a distribution of fracture orientations similar to that of the cross fractures in the metamorphic lithologies (fig. 2-12) with the exception that an additional N-S striking population and a cluster of subhorizontal fractures exist. Although included in fig. 2-19 the subhorizontal fractures will be discussed separately in one of the following sections. Most of these fractures were identified as unroofing joints in the exposures of igneous rocks. Since this type of discontinuities is profoundly different from the steeply inclined fractures in both orientation and physical properties its description is not included in the subchapter on fractures in unfoliated rocks. In contrast to unroofing joints, low angle fractures in metamorphic lithologies are mainly parallel to the foliation. Therefore, fractures parallel to the foliation are likely to have been reactivated during the uplift and unroofing process while new fractures formed in unfoliated rocks. The steeply inclined fractures striking in northwesterly directions are of a secondary importance compared to the northeasterly striking ones. This stands in contrast to the distribution of cross fractures in the metamorphic domains, where both sets show approximately equal abundances.

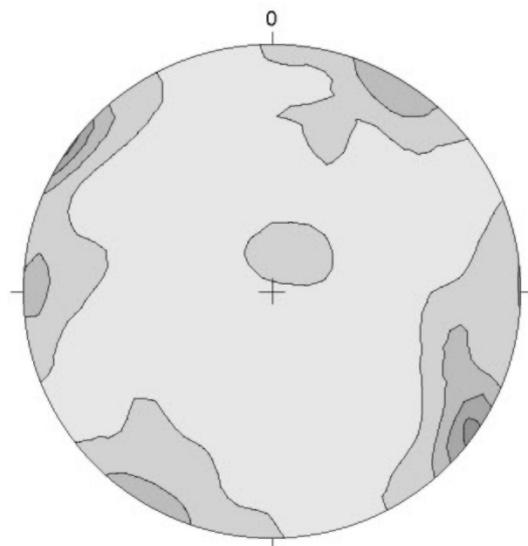
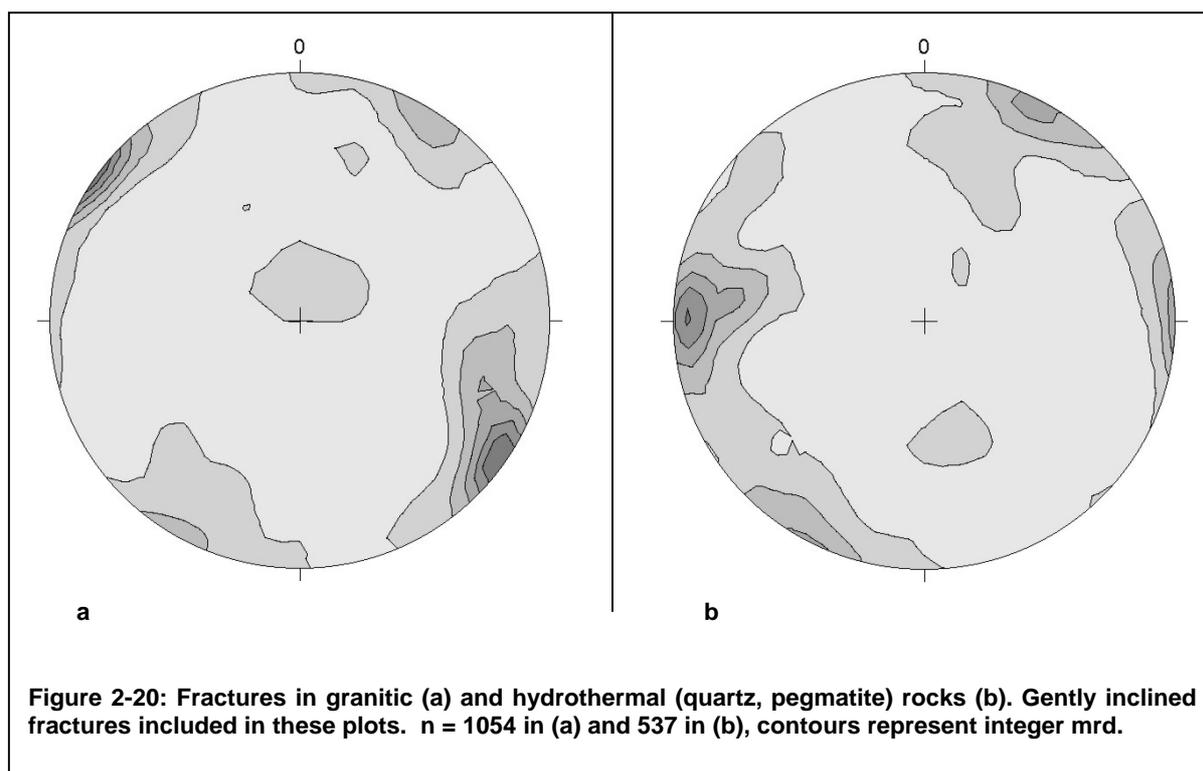


Figure 2-19: Equal area plot of all fractures in sampling stations located in the unfoliated lithologies of the study area. Gently dipping fractures included in this plot. $n = 1591$, contours represent integer mrd.

Separating the dataset into two groups representing the lithologies in which the fractures occur shows that the subvertical N-S striking concentration is restricted to the hydrothermal rock types while in the same lithogroup NE-SW striking fractures are relatively unimportant. The same is true for subhorizontal fractures, which are widely absent in the hydrothermal rocks. Instead, a small subset of moderately N dipping discontinuities is present in fig. 2-20b, thus oriented subparallel to the foliation in the metamorphic regions of the study area. Since the quartz and pegmatite bodies are predominantly embedded in metamorphic rocks as relatively small dikes and veins a continuation of foliation-parallel fractures from

adjacent gneisses into the hydrothermal rocks is a possible explanation for the presence of the N-dipping fracture population in this lithogroup. As a result of these observations it becomes evident that the directional similarities between steeply inclined fractures in granitic and metamorphic rocks are greater than between those in granitic and hydrothermal rocks.

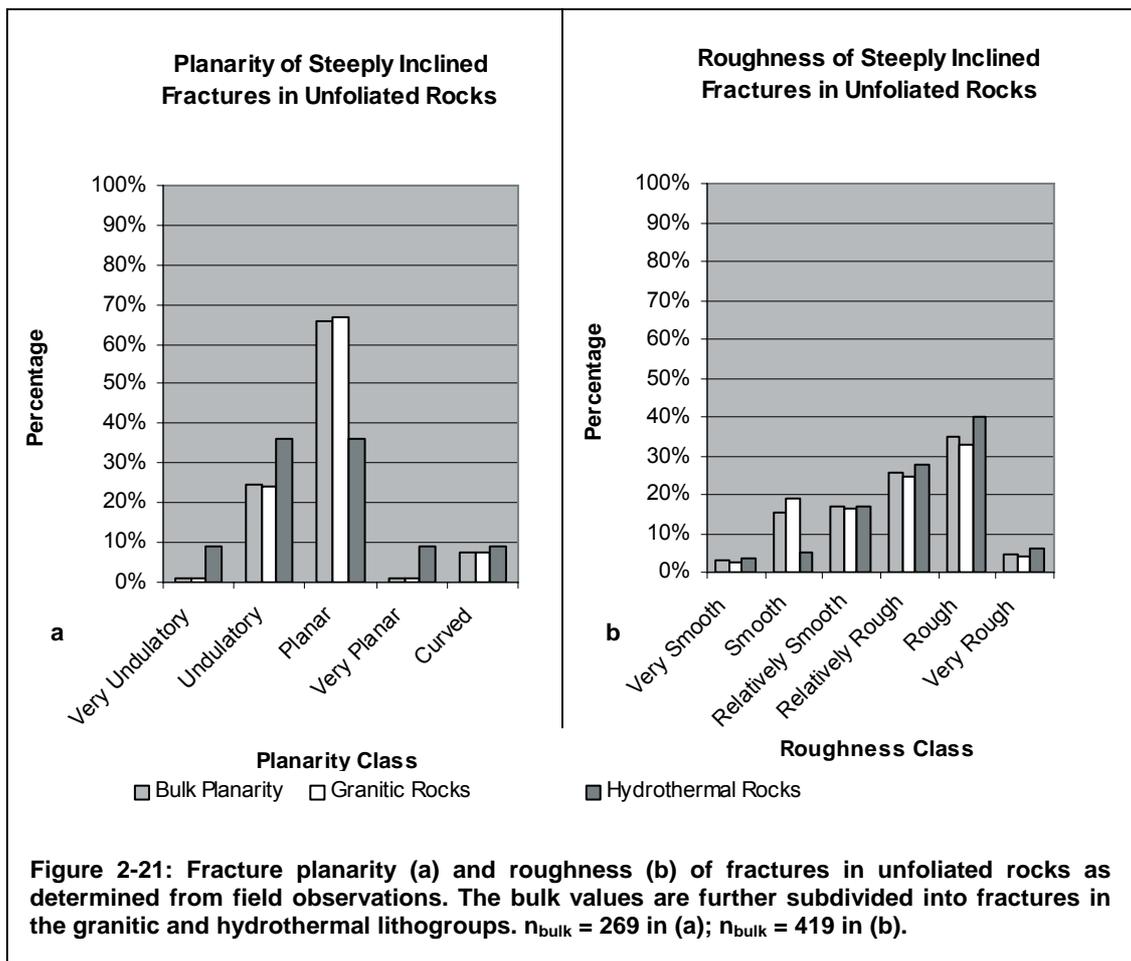


2.2.3.2 Physical properties

For the bulk dataset in granitic and hydrothermal rocks fracture **planarity** shows a clear predominance of planar discontinuities (fig. 2-21). When separated into fractures belonging to one or the other of the two unfoliated lithogroups the difference between granitic and hydrothermal rocks becomes evident. Granitic rocks show a striking tendency to develop planar fractures while hydrothermal lithologies equally produce both planar and undulatory ones. However, several fractures in hydrothermal rocks were classified as very planar as well as very undulatory, much in contrast to those in granitic rocks. Therefore, the planarity of fractures in hydrothermal rocks seems to be more heterogeneous than in granitic ones.

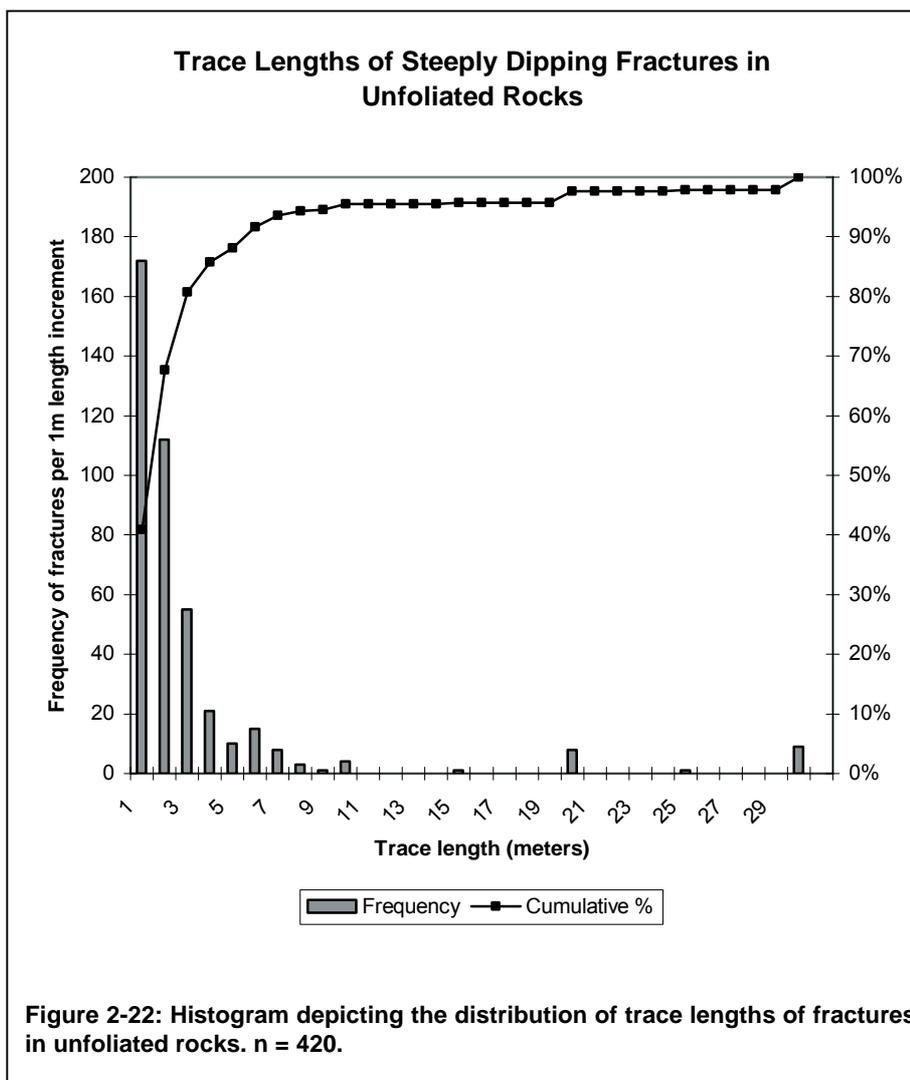
Another prominent feature is the presence of curved fractures, which are negligible in the foliated lithologies (fig. 2-5). The difference between them and undulatory fractures is that a curved fracture has no wavelike appearance (i.e. alternating dip azimuths) but a consistent curvature (i.e. a consistent dip azimuth, but changing dip angles). While undulatory fractures in metamorphic lithologies are frequently oriented subparallel to a foliation curved fractures in unfoliated rocks do not follow preexisting structures. Large-scale curved joints following the local topography were interpreted as unroofing joints (cf. 2.2.4). However, curved planes also occur in relatively short and steeply inclined fractures, which are in no way related to geomorphologic features. In the field, their formation during quarrying, when blasting and the

removal of large volumes of rock could have caused localized strain release, was seen as one possible explanation for their presence.



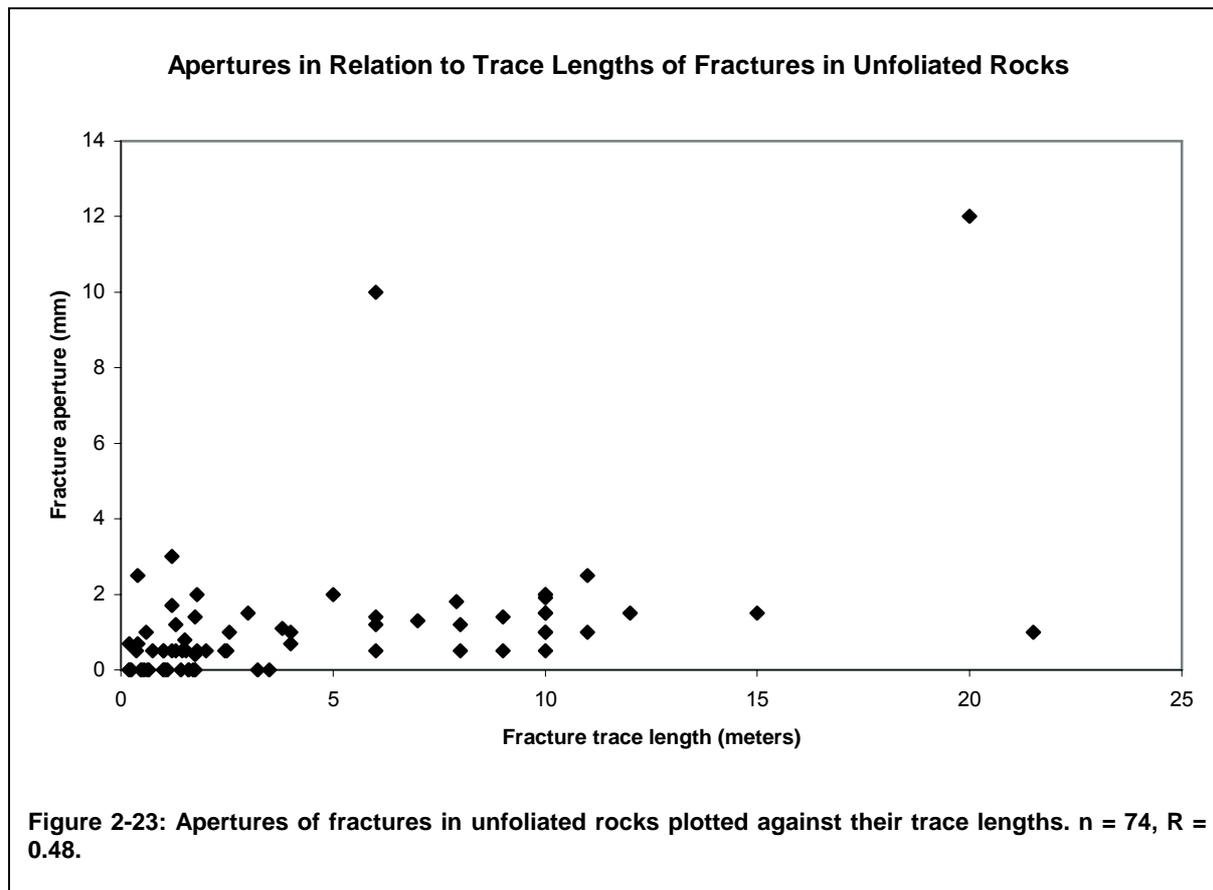
Fracture **roughness** shows similar trends for fractures in hydrothermal and granitic rocks except in the “smooth” class, where a relatively large number of fractures from the granitic lithogroup can be found, while those from the hydrothermal group are relatively few. Similar to discontinuities in metamorphic rocks the predominant roughness class is “rough”. Asperity on fractures in unfoliated rocks is especially enhanced along extensional joints where hackly and plumose structures heighten the relief of their walls. In addition, joints preferentially use the boundaries of the irregularly oriented mineral grains in granitic rocks thereby contributing to the roughness of these fractures. Fault planes can – similar to those in metamorphic lithologies – belong to any of the six roughness classes, depending on the type of deformation mechanism that acted on them. Fractures having encountered shear displacement that produced polished and slickensided surfaces are generally smooth-walled while those having undergone brecciation tend to have rougher planes. In some instances mineralizations on fracture planes, which either consist of macroscopically visible crystals or which do not continuously cover the plane (i.e. which have a “patchy” appearance”) also increase their asperity.

The distribution of **trace lengths** of fractures in unfoliated rocks (fig. 2-22) is similar to that of the cross fractures in metamorphic lithologies (fig. 2-13) with about 40% of the fractures being shorter than one meter and approximately 90% being shorter than five meters. The population ($n = 420$) ranges from a minimum of 0.2 m to a maximum of 30 m, averaging at 2.98 m. The variation at the 95% confidence level lies at ± 0.17 m. Possible sampling errors for trace length measurements have already been described in chapter 2.2.1.2. In contrast to cross fractures in metamorphic rocks the tendency of unbrecciated fractures in unfoliated rocks to be relatively short and of brecciated ones to belong to the largest discontinuities could not be observed in this sample. Both brecciated and unbrecciated fractures were found over the entire range of measured trace lengths.



Fracture **apertures** in this population reach from 0 to 12 millimeters with the average value lying at 1.09 mm and the median at 1 mm. The confidence interval at the 95% level is ± 0.30 mm. Thus, the values fall in the range of those obtained for fractures in metamorphic rocks. The problems concerning the accuracy of aperture measurements described in chapter 2.2.1.2 were also encountered in this population, although weathering effects are expected to have had a lesser influence, because most of the data in this sample was obtained from relatively young artificial exposures such as road cuts and quarries. On the other hand, strain release effects due to blasting are likely to weigh more heavily in the anthropogenic outcrops than in the natural ones. Similar to fractures in other lithologies figure

2-23 shows a low positive correlation ($R = 0.48$ for a linear regression curve) between fracture aperture and trace length for discontinuities in unfoliated rocks.

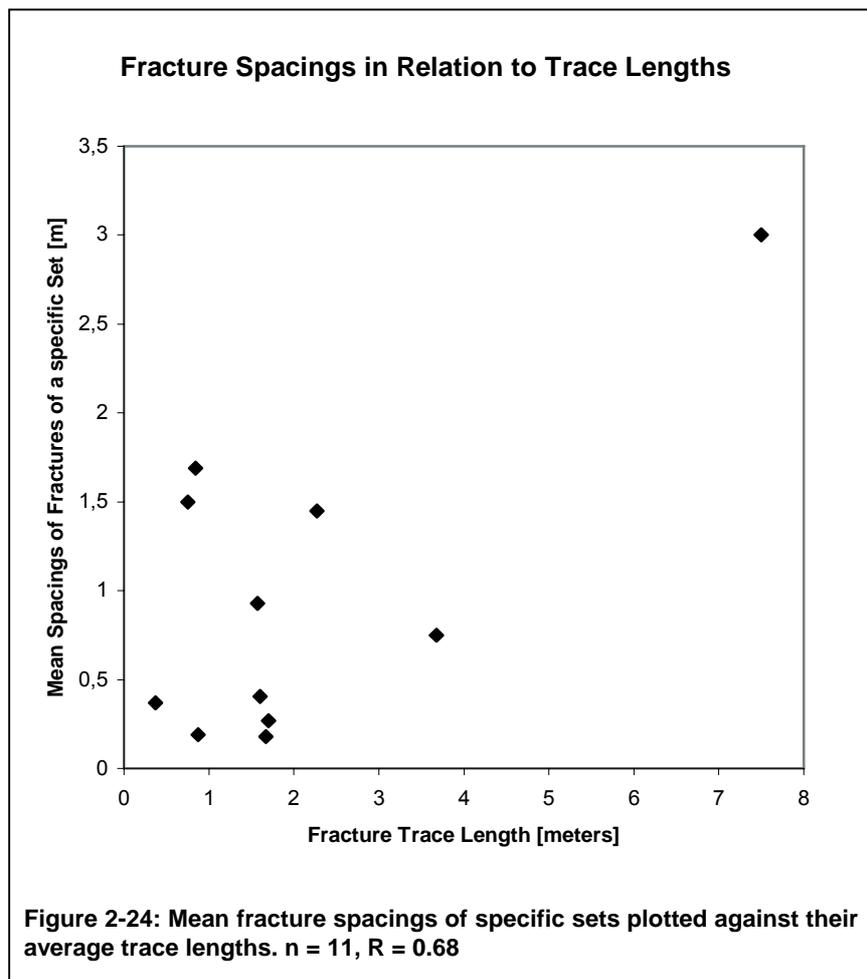


Due to the relatively low number of outcrops examined in granitic and hydrothermal rocks ($n = 13$) mean fracture **spacings** constitute only a small sample for this lithogroup. The dataset was separated into different classes based either on physical properties (long fractures, short fractures, or densely fractured/brecciated zones) or on the approximate orientations of fractures. Table 2-4 summarizes this classification. Similar to the trends in table 2-3 the spacings of densely fractured/brecciated zones tend to be among the largest in the sample while fractures shorter than one meter show a tendency to be rather closely spaced. Although their mean value lies fairly close to that of fractures longer than one meter their maximum mean spacing is only about half of that of the long fractures. The small sample size did not allow a subdivision of the orientation groups based on physical properties the way it was carried out for cross fractures in metamorphic rocks (table 2-3).

Fracture Population	Mean Spacing [m]	Minimum Spacing [m]	Maximum Spacing [m]
Short single fractures (<1 m trace)	0.94	0.19	1.69
Long single fractures (>1 m trace)	1.00	0.18	3.00
Densely fractured/brecciated zones	1.63	0.90	3.00
E-W trending fractures	0.34	0.27	0.41
NE-SW trending fractures	0.80	0.33	1.50
NNE-SSW trending fractures	1.62	0.37	3.00
N-S trending fractures	0.82	0.18	1.45
NW-SE trending fractures	0.91	0.30	1.50
WNW-ESE trending fractures	0.46	0.19	0.75

Table 2-4: Mean spacings of fracture sets with respect to their physical properties and orientations.

Thus, the values for the orientation groups in table 2-4 (lower section) do not provide very detailed information, since they represent fractures of all sizes and shapes. According to the tabulated values the closest spacings exist in the E-W trending fractures while the largest can be found in the NNE-SSW striking set. NE-SW, N-S, and NW-SE striking fractures exhibit relatively similar values. However, it has to be noted that some of these groups

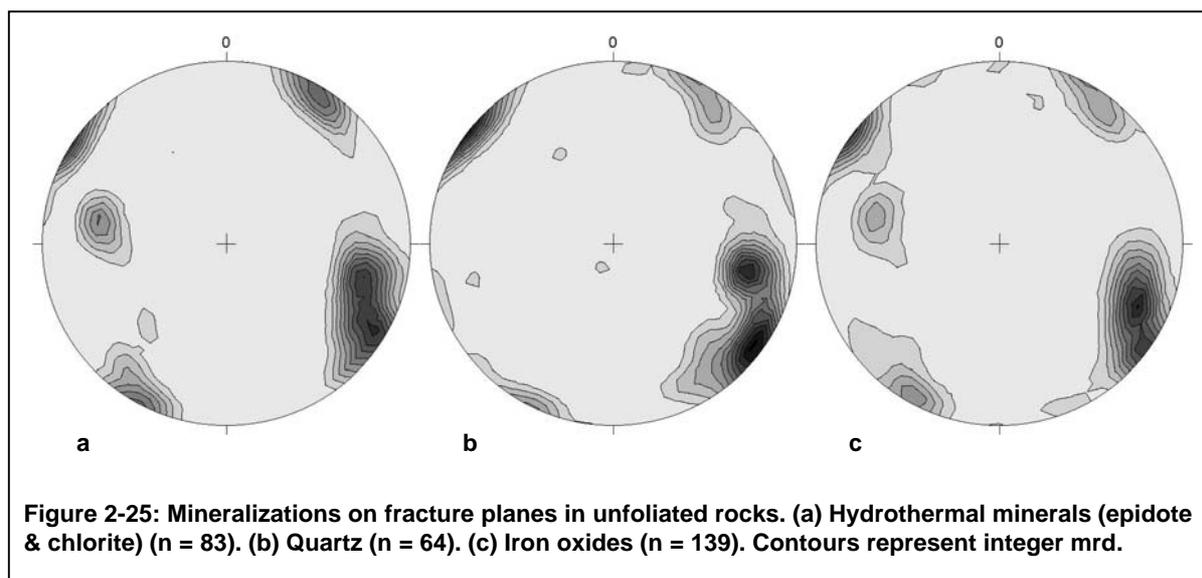


consist of less than three datapoints. Therefore the significance of these values should not be overestimated.

The plot in figure 2-24, however, unveils a relatively conspicuous positive correlation ($R = 0.68$ for a linear regression curve) between mean fracture spacing and mean trace length, thereby corroborating the less unambiguous findings made in the datasets of cross fractures in the metamorphic lithologies.

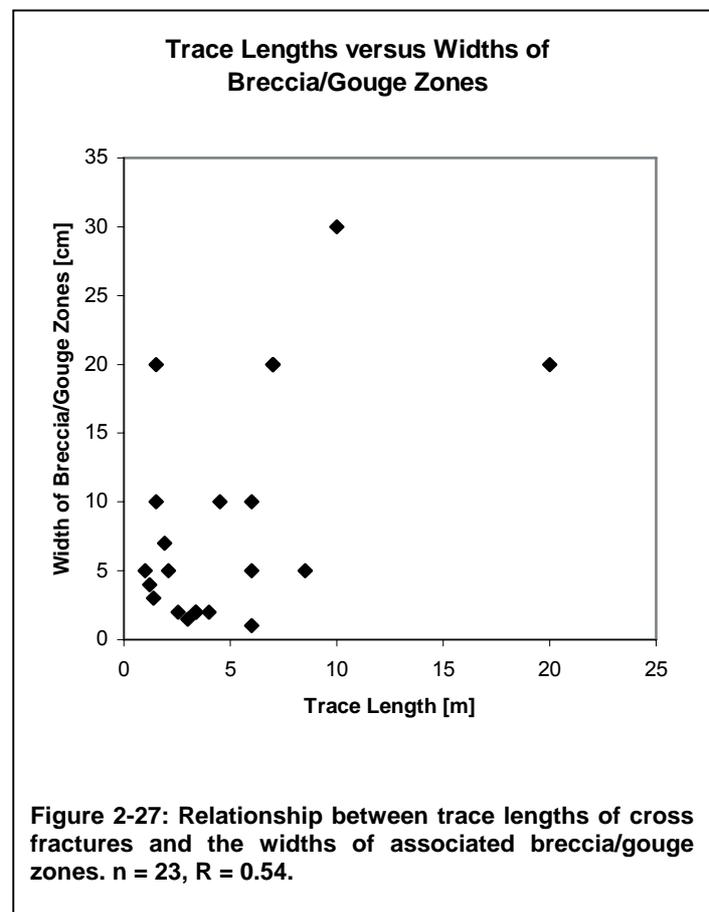
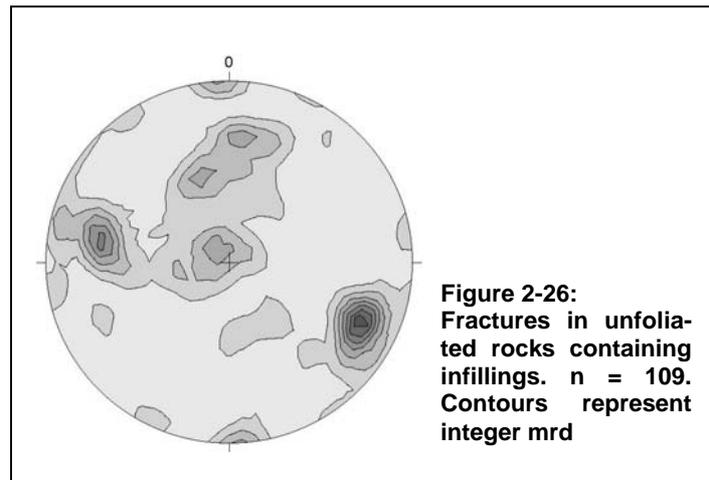
The types of **mineralizations** in unfoliated rocks are similar to those found in the metamorphic units. Thus, the dominant minerals either belong to the group of hydrothermal precipitates, such as epidote, chlorite, and quartz, or to the group of various iron and manganese oxides. Due to the good quality of outcrops in unfoliated lithologies many unweathered fracture planes could be examined and mineralizations could be plotted based on the orientations of the fractures they were encountered on. Figure 2-25 depicts the results of this analysis and shows essentially similar distributions of the various types of mineral coatings on all major fracture sets in this lithologic domain except the population of unroofing joints (cf. fig. 2-19). Only the diagram exhibiting the orientations of quartz-covered fractures (fig. 2-25b) lacks the moderately to steeply W to WNW plunging concentration of normals, which is due to the fact that fractures of this attitude were mainly measured in the quartz outcrops of the Pfahl fault zone where such mineralizations could not be discerned on a country rock consisting of up to 98 % SiO_2 .

Due to the ubiquity of mineralizations on fractures of all orientations it can be inferred that the latest precipitation of both hydrothermal and oxide minerals postdated the original formation of brittle tectonic structures in this area. Most of the previously hydrothermally healed fractures are now open again, thereby suggesting a later reactivation of these original structures. The reactivation occurred both in terms of the formation of joints and faults, evidenced by brecciated or slickensided mineralized fracture planes in the case of faults and by hackly/plumose structures on mineralized planes in the case of joints. Iron oxide stains and coatings on hydrothermal precipitates indicate that these oxides mineralized after the reopening of the fractures, possibly due to the relatively recent percolation of meteoric groundwaters.



Approximately 90 % of all inorganic fracture **infillings** were encountered in the form of various types of fault breccia, only about 10 per cent belong to the –silt to sand-sized- fraction of fault gouge. In the breccia fraction the vast majority (79 %) of fractures contain unconsolidated breccia not further specified regarding grain size. About 3 % contain noticeably large-grained (several centimeters in diameter), while 7 % possess conspicuously small-grained (up to ca. 1 cm in diameter) breccia. In several instances (ca. 11 %) the breccia exist as compacted sheets, which, in contrast to the unconsolidated variety, form cemented masses with much lower porosities.

Figure 2-26 depicts the orientations of fractures containing infillings. In part it resembles the cumulative plot of fractures in unfoliated lithologies (fig. 2-19) in that it shows NNE-SSW and east-westerly striking fracture populations. In contrast, however, clearly NW-SE striking discontinuities are virtually missing, while a relatively large number dips gently to moderately in southerly directions. These gently to moderately dipping fractures are also emphasized in the plot of infillings of cross fractures in metamorphic rocks (fig. 2-16) with respect to the total number of fractures in this lithologic unit (fig. 2-12). In the field they were interpreted as a population of low-angle faults unrelated to the unroofing process, but caused by relatively young thrusting or low-angle normal faulting. With regard to fracture orientations no difference exists between the types of unconsolidated infillings. Consolidated breccia sheets were only encountered in a small number of steeply dipping, NNE-SSW striking fractures.



Soil infillings were only observed in very few low-angle fractures (mostly unroofing joints), while steeply dipping ones are usually not associated with significant soil contents. Fractures containing organic infillings such as grass, moss, and other plants do not show any preferential orientations. Only about two per cent of the total dataset of fractures in unfoliated rocks contain organic infillings, which might be due to the relatively young age of many of the artificial outcrops where plants could only recently populate fractures in greater depths below the topographic surface.

Despite the small sample size ($n = 23$) a reasonably good positive correlation ($R = 0.54$) exists between the width of breccia and gouge infillings and the trace lengths of the associated fractures (fig. 2-27), thereby confirming the tendencies found for fractures in metamorphic lithologies (fig. 2-17). The reason for this more convincing result in the unfoliated rock types might lie in the larger extents of the bedrock exposures in this lithologic domain, which allows tracing fractures over longer distances and thus estimating the actual trace lengths more accurately.

2.2.4 Unroofing joints

Unroofing joints are brittle features frequently occurring during the uplift of a region. Strain release normal to the topographic surface causes them to produce planes generally curving parallel to the relief (Ahnert, 1999). Figure 2-28 shows such fractures in a granite quarry. In several cases gently dipping fractures are associated with brecciation. These could not be identified unequivocally as unroofing joints and were thus left out of this analysis. An uplift-related origin is possible, but then ensuing reactivation by shear would have had to occur. The tectonic significance of these fractures will be discussed in a later section.

2.2.4.1 Orientations and spatial distribution

Of a total of the 46 sampling stations taken into consideration 13 were associated with unroofing joints. Figure 2-29 shows that the majority of poles to the planes plunge about the subvertical. However, moderately inclined unroofing joints exist as well. In these cases fractures striking in northeast-southwesterly directions seem less abundant. A comparison of the fracture strikes with the regional topography shows that there are few topographic features striking in that same direction. Since unroofing joints tend to follow the curvature of the land surface the decreased abundance of NE-SW trending fractures is logical.

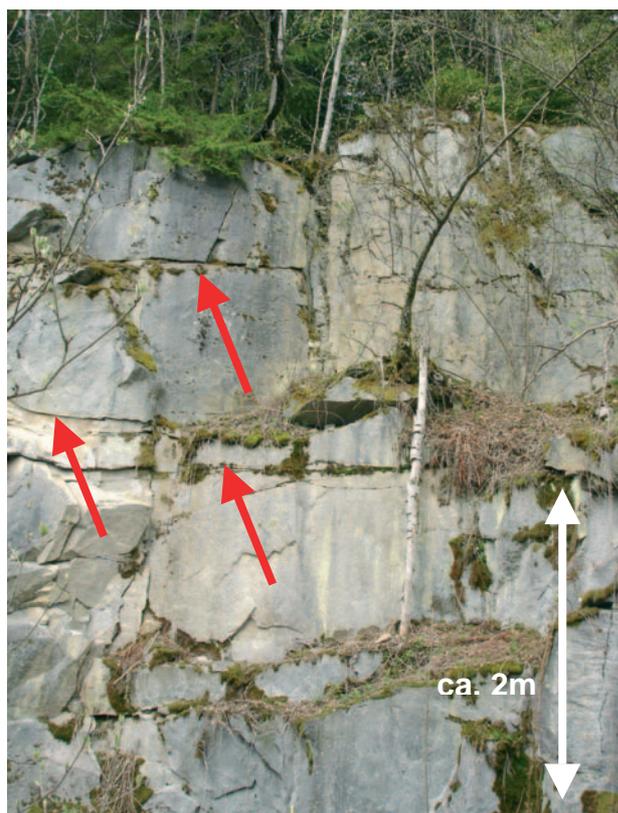


Figure 2-28: Unroofing joints (red arrows) in granite. Location: Steinbruch Zeitlhof (7043-02).

Figures 2-30 and 2-31 give an impression of the spatial distribution of the joints with respect to certain lithologic parameters. Determining the occurrence of unroofing joints with respect to lithogroups (fig. 2-30) shows that unfoliated granitic rocks possess a clear tendency to develop such fractures while others do not. In the case of hydrothermal rocks it has to be noted that they are mostly embedded in metamorphic country rocks as relatively small bodies. Consequently, as already mentioned in section 2.2.3.1, these units frequently adapt the fracture patterns of the surrounding units. Therefore, the absence of unroofing joints in the adjacent country rock may account for their absence the embedded hydrothermal or pneumatolytic body. Metamorphic lithologies do not

expose significant unroofing joints due to the fact that they frequently possess gently inclined foliation planes, which were suitable for reactivation during the unloading process. Thus, many of the low angle foliation parallel fractures described in section 2.2.1 are likely to have been active as unroofing joints. In contrast, the few locations with a more steeply inclined foliation are likely to possess a separate set of unroofing joints (fig. 2-31).

For this case figure 2-31 plots the frequency of locations with or without unroofing joints in relation to the dip of the gneissic foliation. Note that in order to increase the size of the sample outcrops of the group “Strongly folded and migmatitic rocks”, which contain sections with measurable foliation, are also included in the analysis. The comparison of figures 2-31 a and b highlights –given a certain degree of error due to the different sample sizes in the two plots- a tendency of locations possessing a steeply inclined foliation to develop unroofing joints while locations where the fabric dips less than about 50° do not. Especially the very conspicuous peak at 80° in fig. 2-31a, which does not exist in fig. 2-31b highlights this tendency.

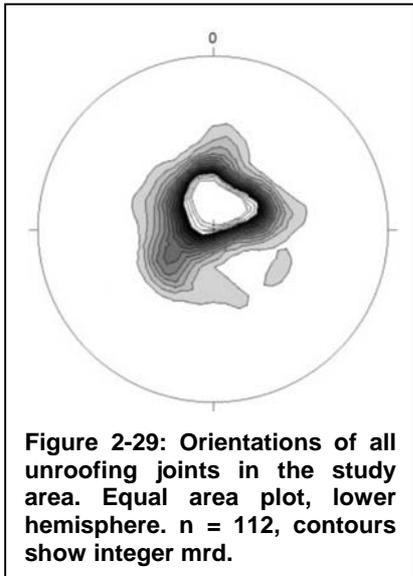


Figure 2-29: Orientations of all unroofing joints in the study area. Equal area plot, lower hemisphere. n = 112, contours show integer mrd.

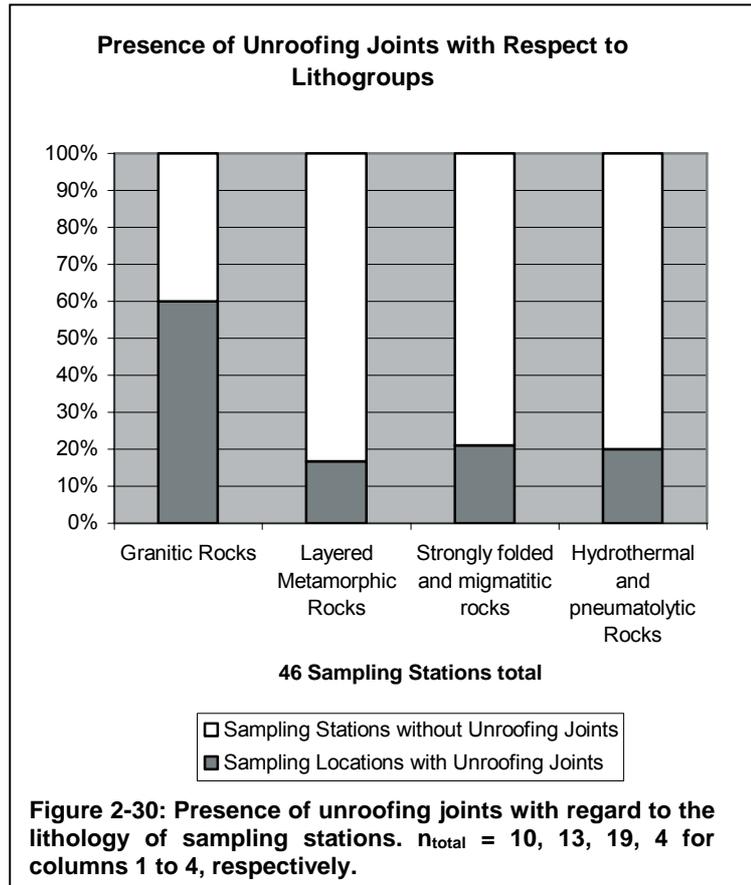


Figure 2-30: Presence of unroofing joints with regard to the lithology of sampling stations. n_{total} = 10, 13, 19, 4 for columns 1 to 4, respectively.

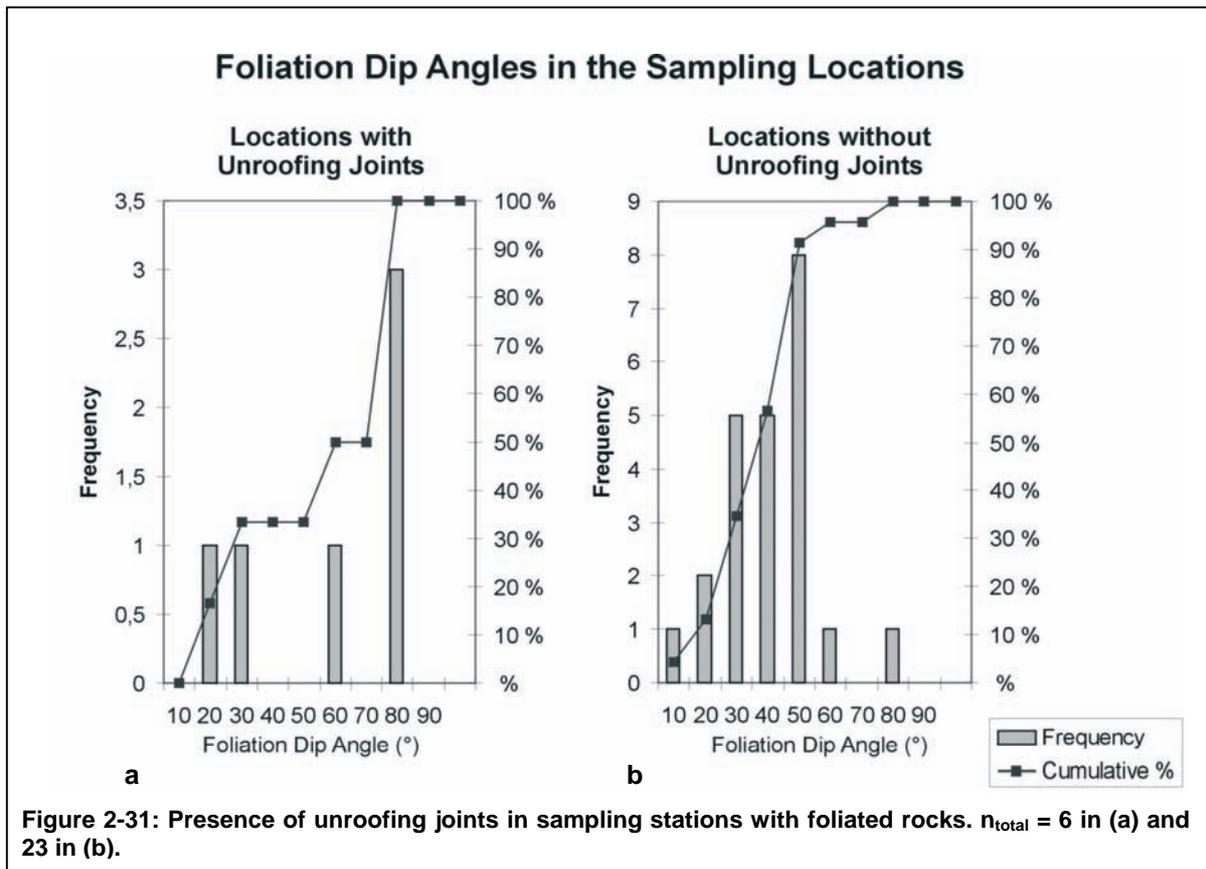
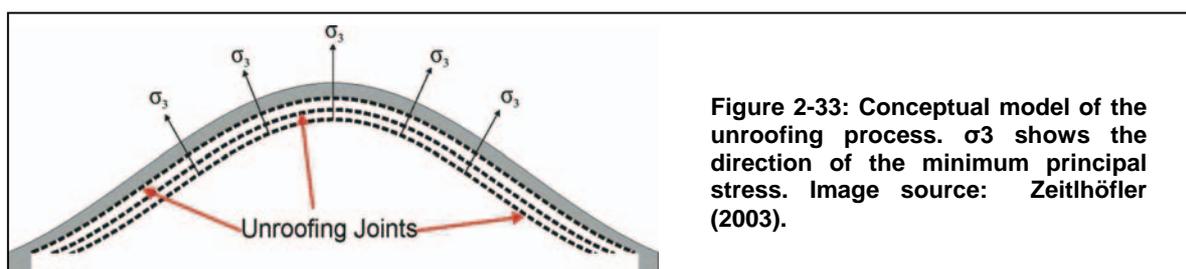
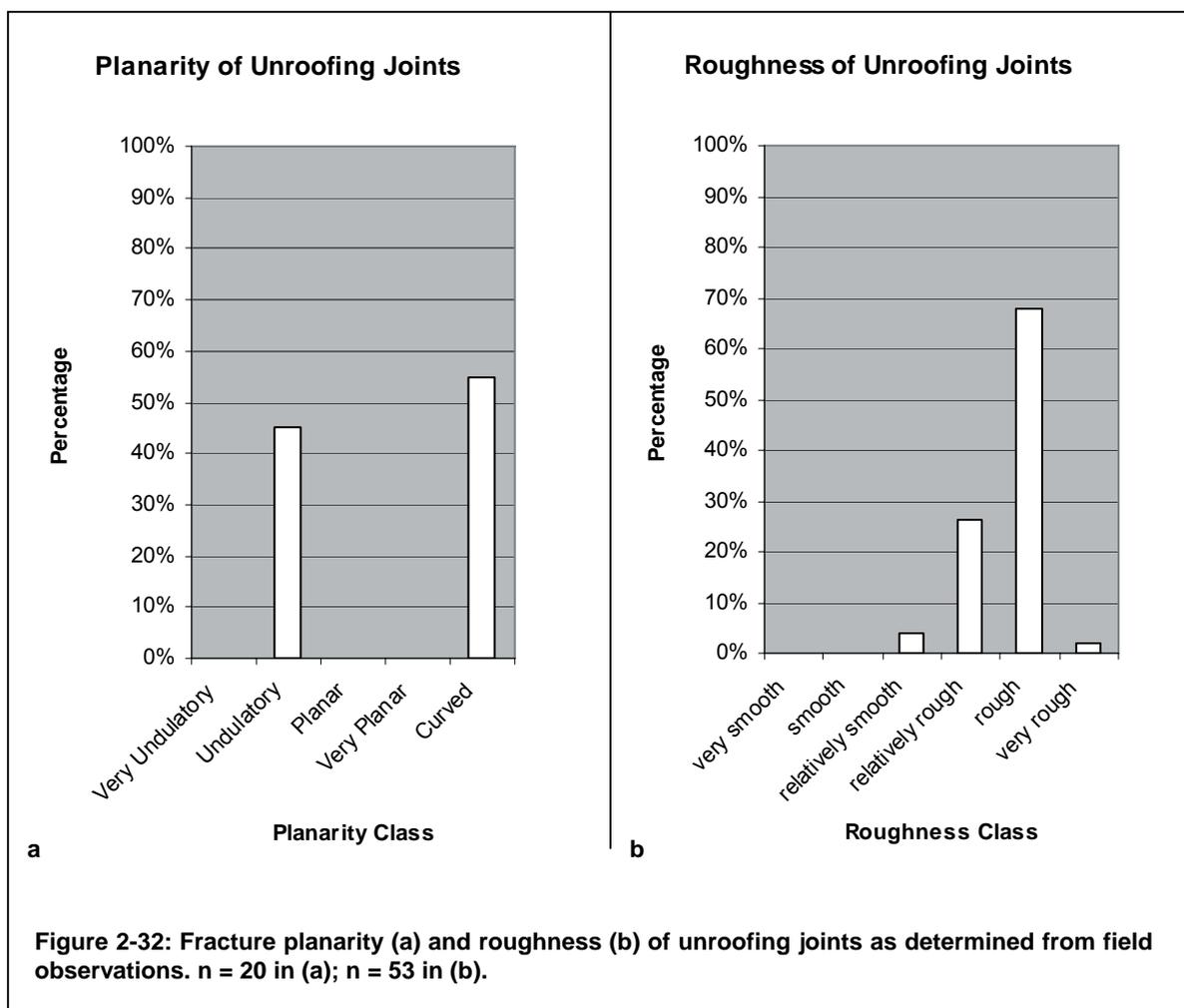


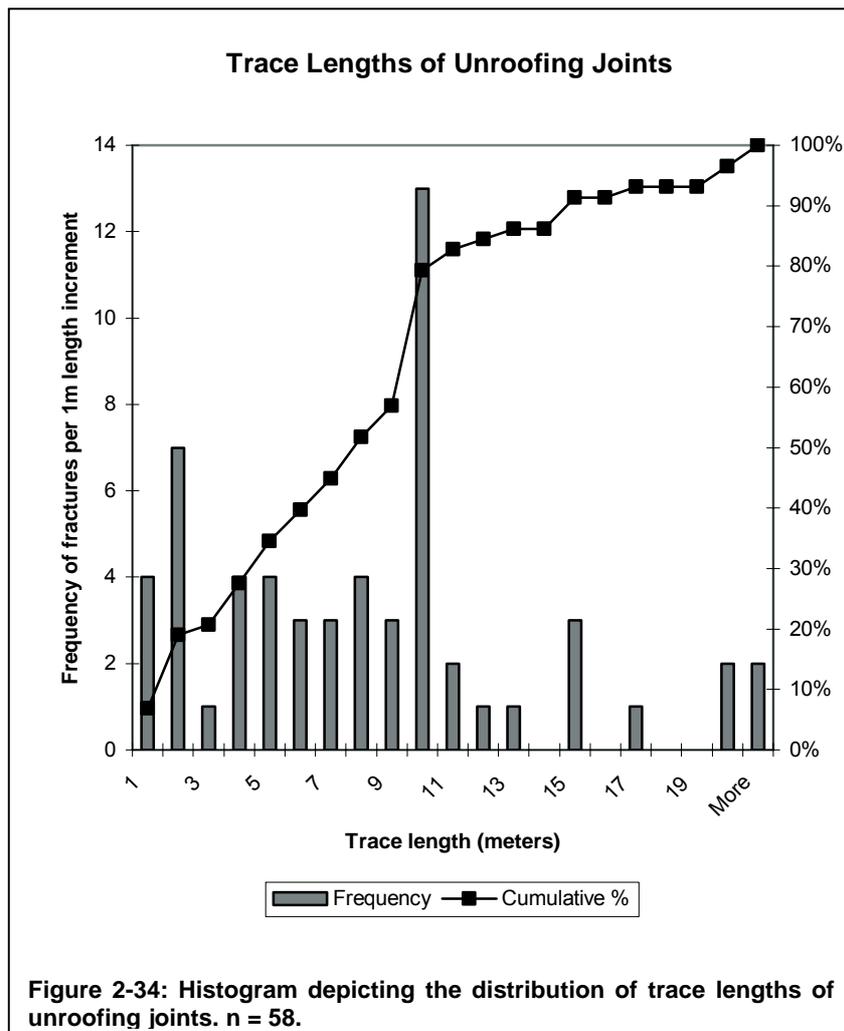
Figure 2-31: Presence of unroofing joints in sampling stations with foliated rocks. n_{total} = 6 in (a) and 23 in (b).

2.2.4.2 Physical properties

Figure 2-32 depicts the distribution of **planarity** and **roughness** of unroofing joints thereby unveiling very specific characteristics of this fracture type. Thus, unroofing joints tend to be either undulatory or curved (fig. 2-32a) and possess rather rough planes (fig. 2-32b). This type of discontinuity frequently parallels the topographic relief, which consists of rolling hills for the most part. The removal of overlying rock masses during the unroofing process produced a minimum principal stress normal to the topographic surface due to strain release, causing the rock to fail along planes at right angles to the minimum stress (fig. 2-33). Therefore, the curved nature of the joints is a direct result of the study area's morphology.



As for the distribution of roughness coefficients the extensional origin of the unroofing joints produces rather irregular fracture planes. The utilization of grain boundaries – already described in section 2.2.3.2 – is one likely reason for the relatively high roughness. Of course, hackly and plumose structures can also form along subhorizontal fractures and several unroofing joints expose brecciated fracture traces, thus suggesting a certain degree of later shear displacement. The cause of this displacement, be it tectonic or simply due to slight gravity-induced shifting during the uplift process, could not be discerned.

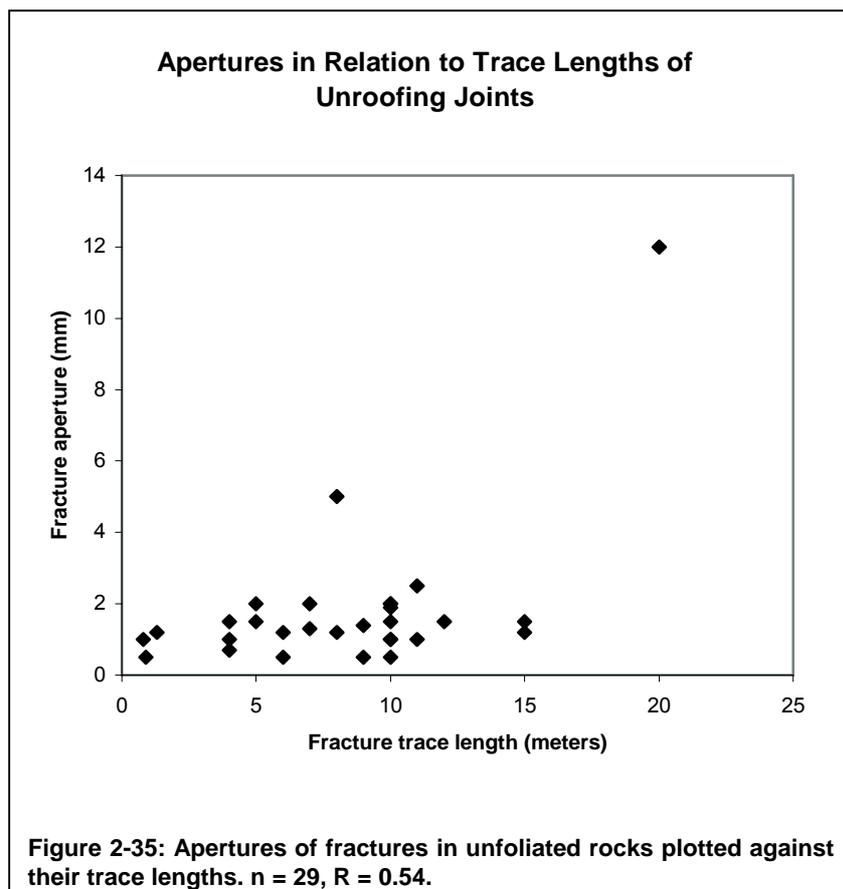


On average, **trace lengths** of unroofing joints are significantly longer than those of any other fracture group (fig. 2-34). This is in part due to sampling bias, since most outcrops are exposed over a much larger horizontal than vertical extent. Nonetheless, a relatively large number can be traced over more than ten meters and still continue beyond the visible part of bedrock exposures. The mean and median trace

lengths lie at 8.5 and 8 meters, respectively and fall within ± 0.58 m of the mean at the 95% confidence level. Several of the joints being part of the chart in fig. 2-34 could not be measured but had to be estimated with respect to their trace lengths, because of their large extent. The percentage of fractures subject to censoring effects and errors in the estimation of trace lengths is particularly high in this sample because of their large extent and their general horizontality, which frequently places them out of reach for accurate measurement. A number of unroofing joints, whose trace length was estimated, was recorded as being “longer than ten meters”, which, after attributing absolute values to the estimates (i.e. in these cases the minimum length of ten meters), were placed in the 10 m bin of the chart in fig. 2-34. This leads to an overrepresentation of fractures with this specific length and introduces a bias

towards the 10 m bin. In reality, the number of joints longer than ten meters should be somewhat higher in this sample.

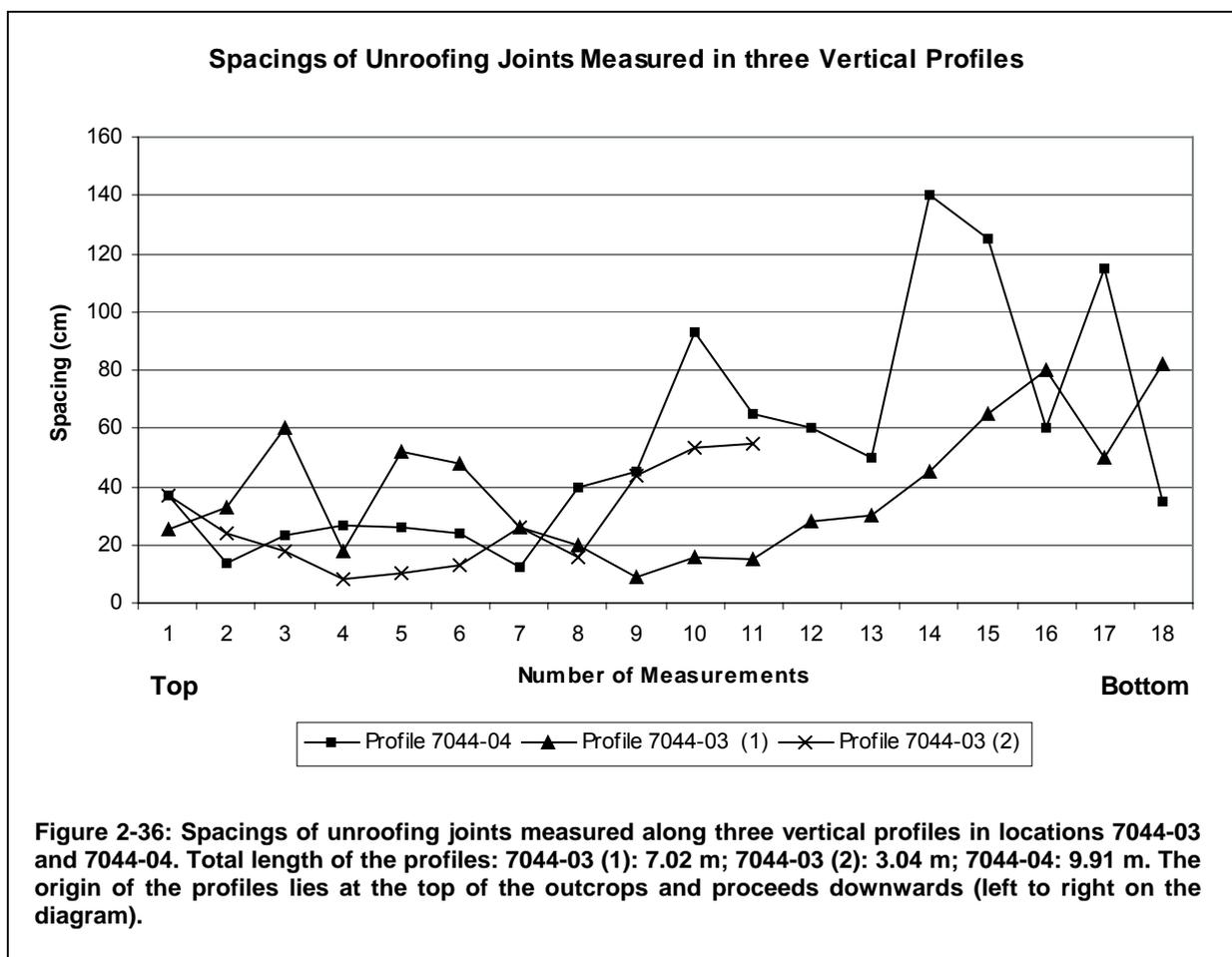
Fracture **apertures** in this population range from 0.5 to 12 millimeters with mean and median values of 1.8 and 1.3 mm, respectively. The confidence interval at the 95% level is 0.29 mm. Thus, apertures in unroofing joints are significantly higher than in other fracture sets. Moreover, no unroofing joint was recorded as having no visible aperture, much in contrast to the steeply dipping populations. In several cases much higher apertures than



those included in fig. 2-35 were observed, especially in the top parts of exposures. However, these were not measured, because of accessibility problems and significant weathering effects due to their proximity to the topographic surface.

Relating aperture to trace length (fig. 2-35) shows an even more pronounced mutual dependency between these two parameters than in the previous plots (figs. 2-8, 2-14, and 2-23).

As can be inferred from fig. 2-36 **spacings** of unroofing joints show a tendency to expand with increasing depth below the topographic surface. Therefore, significant mean values characteristic for this fracture type are difficult to derive from the dataset. Due to the relatively high average trace lengths of fractures and the general absence of closely spaced cm-scale fractures in this group the relationship between trace length and spacing is less pronounced and largely attenuated by depth-dependency effects. Trendlines computed for the three profiles yielded correlation coefficients $R = 0.56$ for profile 7044-03 (1), $R = 0.45$ for profile 7044-03 (2), and $R = 0.66$ for profile 7044-04. According to the chart spacings range from less than 0.2 to 1.4 meters with sometimes significant variations among adjacent values. The overall tendency, however, is a positive correlation between spacing and depth below the surface. Higher values (spacings larger than two meters) could be observed in vertically extensive outcrops. However, complete profiles could not be taken in these sites due to the restricted access as a result of the heights of these exposures. At a certain depth below the topographic surface a phasing out of unroofing joints can be expected at levels where the lithostatic pressure is high enough to prevent strain-release processes. These levels, however, were not reached in surficial bedrock exposures, the deepest of which possess vertical extents of approximately 50 to 60 meters.



Hydrothermal **mineralizations** on planes of unroofing joints were not recorded, thus indicating a very young formation age, which postdates the permeation of hydrothermal solutions evidenced by coatings on planes of the steeply inclined fracture sets. Only iron oxide stains created by recently flowing water were occasionally found.

As for fracture **infillings**, only a very small number of measured unroofing joints contain any. If present, they frequently consist of 20 to 30 cm wide gouge and breccia seams, thereby suggesting minor recent motion along their planes. The presence of sheared material along fractures declared as unroofing joints gives rise to the suspicion that some of fractures of this group could also have originated as low angle thrust faults, which were later reused for the unroofing process. Fig. 2-28 shows that unroofing joints are discontinuities preferentially used for plant growth. This is undoubtedly connected to the fact that over 15 per cent of all measured joints were observed to contain various amounts of water (ranging from flowing water to significantly moist infillings).

2.3 Regionally characteristic fracture types based on orientation

In order to obtain a regional distribution of characteristic fracture orientations the complete fracture dataset was initially filtered to remove subhorizontal fractures such as unroofing joints, which have been dealt with in the preceding section. Thus, only fractures, which initiated unrelated to unloading phenomena, are included in the further examinations. Then, a K-means cluster analysis of fracture orientations was performed, thereby indexing every datapoint with an ID-number attributing it to a cluster with a specific mean orientation. Based on this indexing further calculations with regard to the spatial distributions of dominant fracture types as well as their physical properties could be carried out. For more detailed descriptions on the K-means analysis procedure refer to the methodology section.

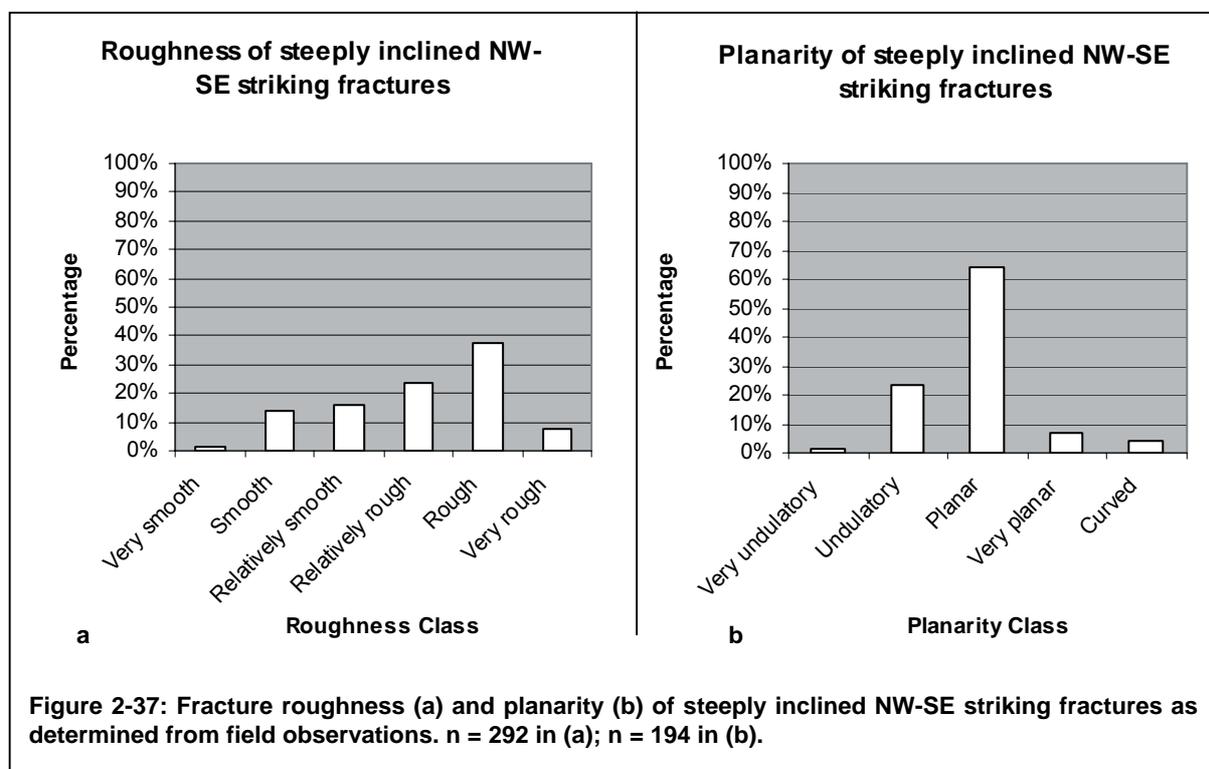
Upon visual examination of the filtered dataset in a contoured stereographic plot four major fracture concentrations could be identified. These concentrations strike NW-SE, NNE-SSW to NE-SW, and ENE-WSW to E-W, all steeply inclined to subvertical. The fourth concentration consists of fractures striking WNW-ESE and dipping moderately NNE. The physical properties of these populations will be detailed in the following subsections. In contrast to the genetic classifications in the preceding sections fracture characteristics in this analysis are solely based on their orientations.

Regarding the spatial distributions of fractures with specific orientations all four clusters turned out to be more or less evenly distributed over the entire study area irrespective of lithologic units. Only with respect to their proximity to similarly oriented

topographic lineaments (see domain overlap analysis in section 3) a certain degree of spatial clustering could be observed. Thus, the following subchapters will not focus on the spatial distributions of specific fracture clusters but on their physical properties, similar to the analyses of the genetic fracture types in the preceding sections.

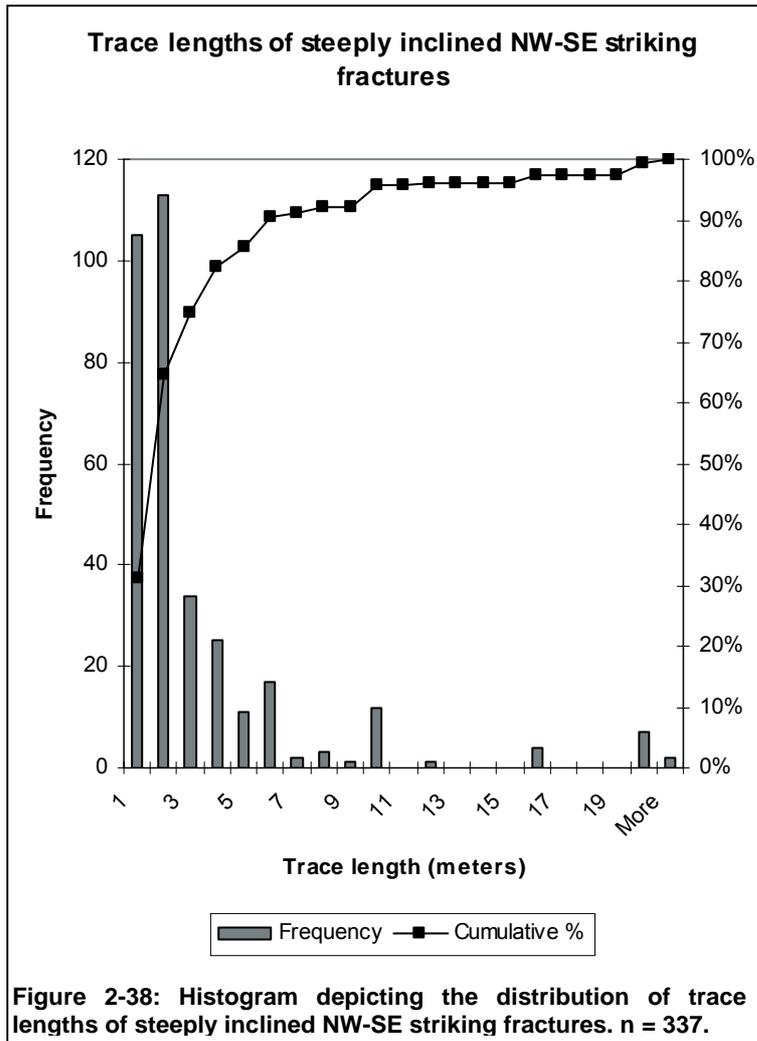
2.3.1 Steeply inclined NW-SE striking fractures

Steeply inclined NW-SE oriented fractures strike parallel to the regional metamorphic foliation, but are generally more steeply inclined. Thus, they represent a fracture population different from the reactivated foliation. With a total number of 1074 individual fractures they comprise approximately one fourth of the entire dataset. To begin with, their roughness and planarity distributions are displayed in fig. 2-37.



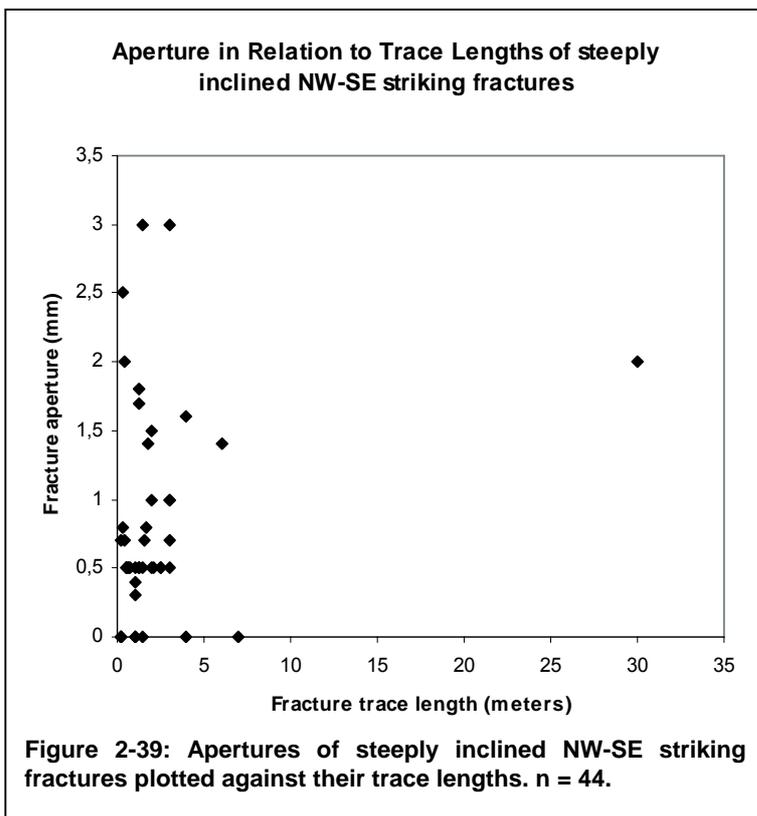
While the roughness distribution in this cluster shows a relatively wide spectrum there is a slight tendency to form relatively rough to rough fracture planes, which are predominantly of a straight character and only to a lesser degree undulatory.

Fracture trace lengths concentrate in the length segment < 5 meters with only few individual fractures extending over larger distances (fig. 2-38). The dominant trace length lies between 2 and 3 meters. With regard to fracture aperture a clear relationship to trace length does not become obvious due to the outlier at 30 m trace length in the plot. But even if this data point is neglected no correlation ($R = 0.01$) between the two parameters could be



established. Even relatively large fractures (up to 7 m) can be associated with no measurable aperture, while short ones often are significantly open.

Mineral precipitates on NW-SE striking fractures comprise hydrothermal mineralizations such as epidote and chlorite as well as quartzo-feldspathic minerals. Hematite staining is occasionally encountered. For only about 10 per cent of the fractures in this cluster mineralizations were recorded, which is in part due to the high degree of weathering in many bedrock exposures obscuring fracture plane coatings.



Approximately five per cent of the fractures are associated with major infillings such as up to 50 cm wide breccia seams. In a few cases fault gouge as well as concentrations of accessory fractures were observed. Thus, part of the fractures in this cluster originated from shear displacement at some point in the geologic record.

2.3.2 Steeply inclined NNE-SSW to NE-SW striking fractures

With a total number of 1339 individual fractures this cluster represents the most abundant population in the dataset. It strikes parallel to a prominent lineament direction (cf. section 3) and exists as a dominant fracture set in some of the largest sampling stations, which potentially introduced some bias in the distribution of relative abundances.

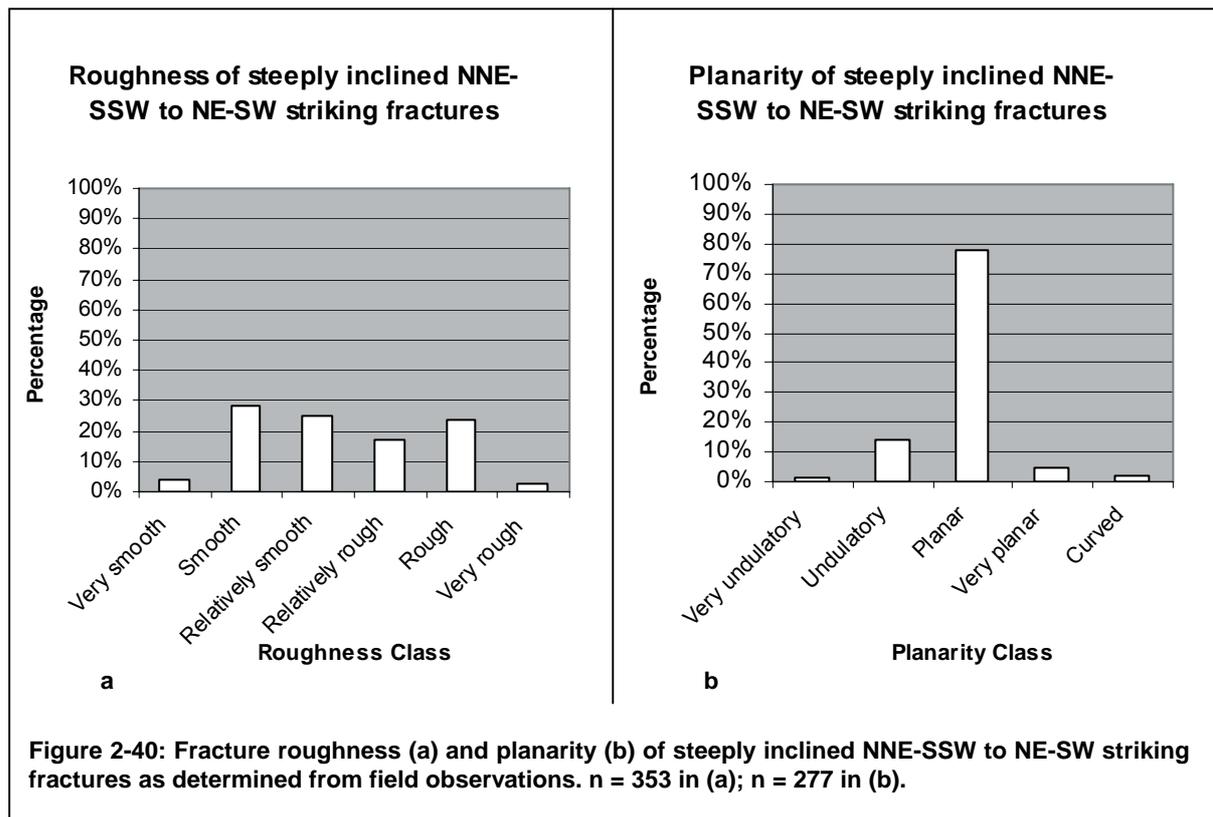
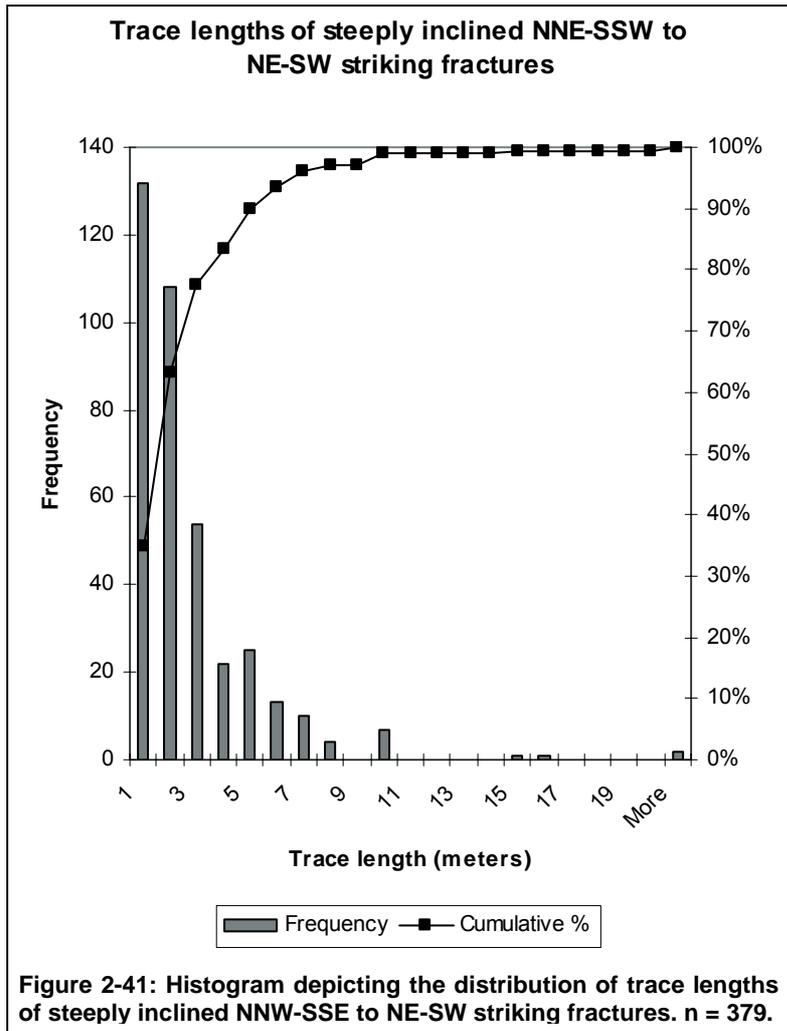
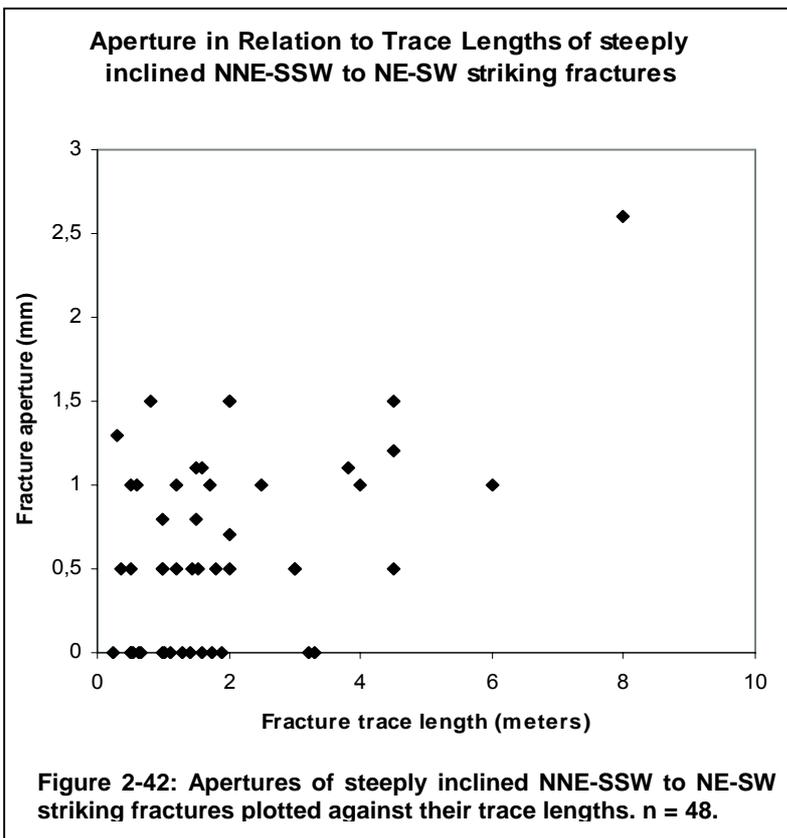


Figure 2-40 shows an even more uniform distribution of fracture roughness. However, in contrast to the steeply inclined NW-SE trending fractures the planes of this cluster expose a slight tendency to produce relatively smooth to smooth fractures. Fracture planarity is also similar to that of the preceding cluster. The vast majority of fractures possess straight planes, only a fraction of them is undulatory.

Fracture trace lengths (fig. 2-41) are dominated by values of less than four meters. The shortest lengths (< 1 m) are the most abundant ones, while fractures extending over more than 10 meters represent rare occasions. Relating fracture trace lengths to fracture aperture (fig. 2-42) yields a moderate correlation ($R = 0.50$) between these two parameters, i.e. larger fractures tend to be associated with larger apertures. However, high trace lengths do not guarantee open fractures as can be inferred from the range of discontinuities having zero aperture in plot 2-42.



For approximately 16 per cent of the data record in this cluster fracture mineralizations were observed. These include again hydrothermal precipitates such as quartz, epidote, chlorite, and feldspar as well as oxidation products from the infiltration of cold oxygenated water. The percentage of mineralized fractures is likely to be somewhat higher, but, as already mentioned, poor outcrop quality frequently prevented the examination of fresh fracture planes.

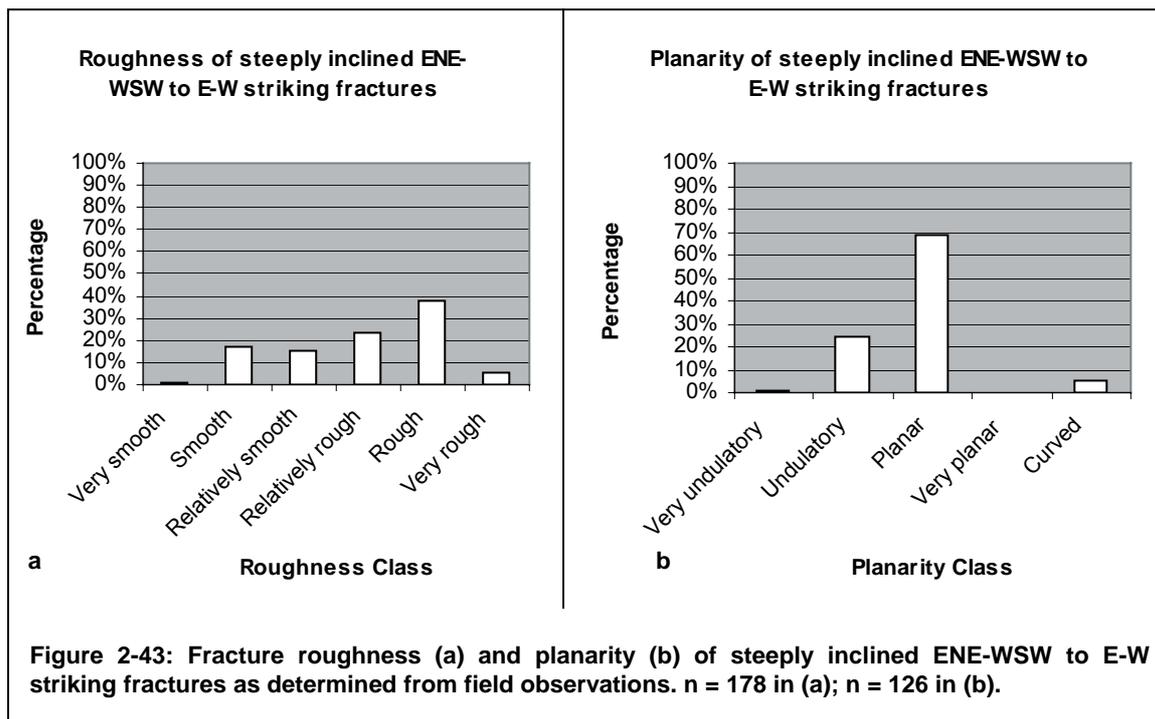


Less than four per cent of fractures in this cluster are associated with signs for shearing, such as fault breccia, gouge, or zones of high fracture density. The vast majority of these discontinuities is located in sampling station 6943-01, which neighbors a NE-SW trending lineament, and for which a NNE-SSW to NE-SW trending fault zone is assumed. Thus, fractures having originated as faults seem to be rather localized phenomena while the bulk of N(N)W-S(S)W striking

fractures may rather have initiated as extensional joints, which were later reactivated by shearing displacement accompanied by the formation of slickensides. The predominance of joints striking in this direction presented in section 2.4.1.1 supports this assumption.

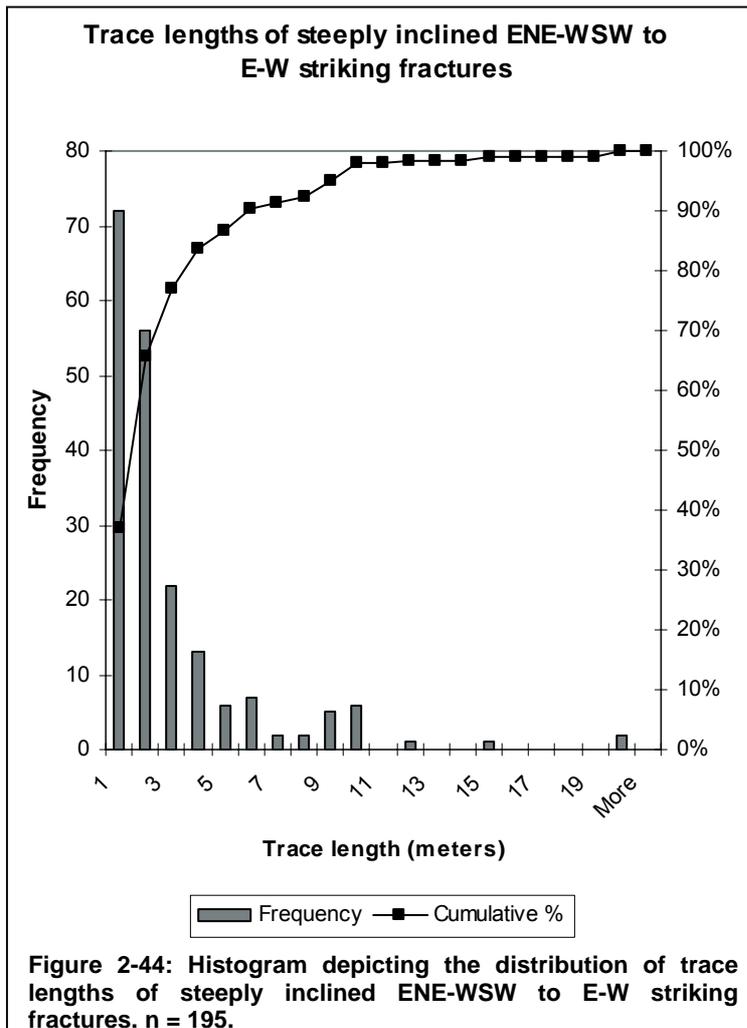
2.3.3 Steeply inclined ENE-WSW to E-W striking fractures

This cluster comprises the smallest number of fractures ($n = 831$) in this analysis. These discontinuities mainly exist as secondary sets in the sampling stations, although they occasionally have an effect on the geomorphology (cf. section 3.4).



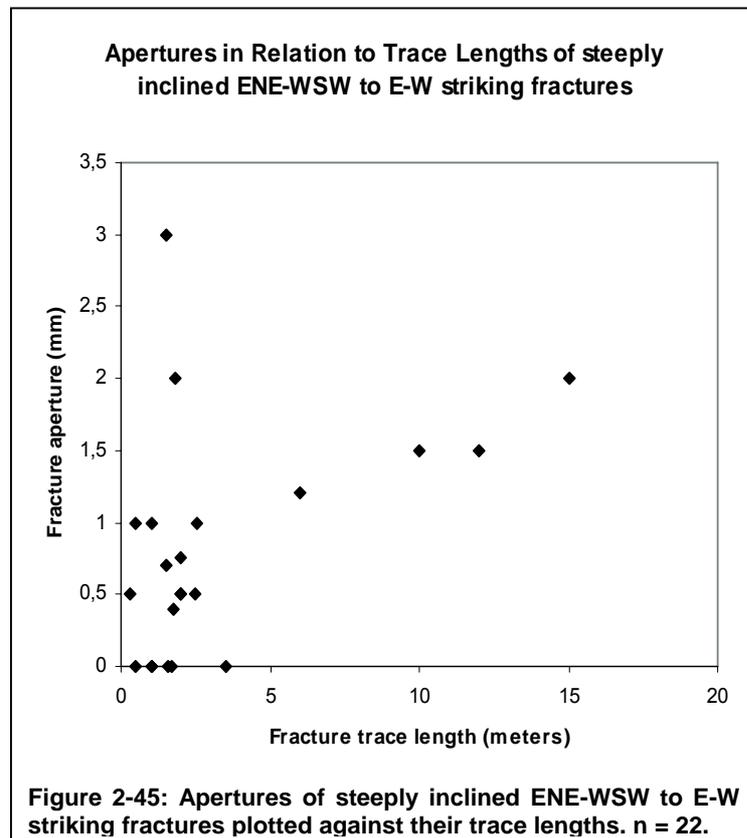
In terms of fracture roughness and planarity (fig. 2-43) they resemble the NW-SE striking population in that they expose a tendency towards rough and straight planes. However, about 60 per cent fall in the range of smooth to relatively rough fractures. Undulatory planes represent a minority.

Fracture trace lengths (fig. 2-44) are distributed similar to the preceding two clusters. The data record is dominated by discontinuities shorter than four meters with a prominent peak in the < 1 m bin. Fractures extending over more than ten meters are rare. With regard to the relationship between fracture trace length and aperture (fig. 2-45) a weak positive correlation ($R = 0.46$) exists between the two parameters. However, two outliers attributing high apertures to relatively short fractures introduce considerable scatter into the distribution. Ignoring them would lead to a high correlation with a high coefficient $R = 0.78$.



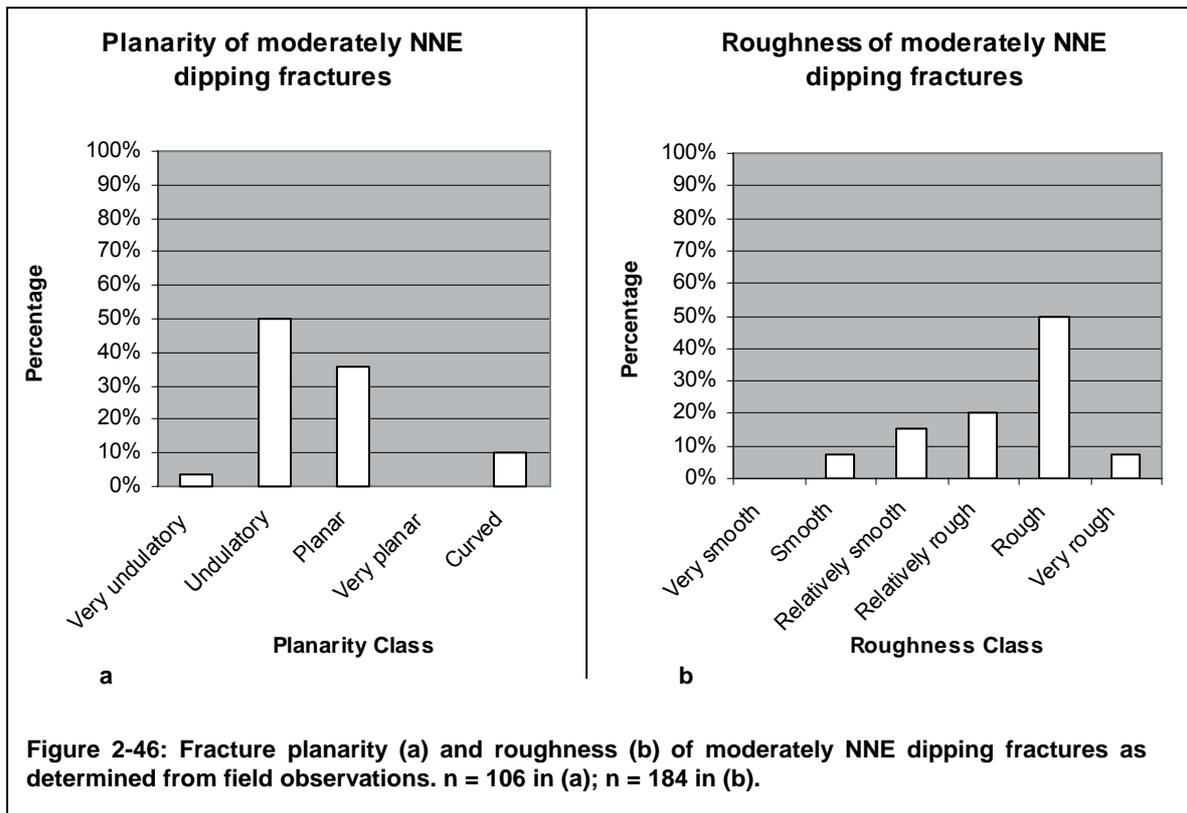
Mineralizations were recorded on approximately five per cent of the fractures in the cluster. While quartz precipitates are relatively abundant other hydrothermal minerals occur only scarcely. The dominant fracture mineralization is represented by iron oxide coatings.

Fracture infillings such as breccia and gouge as well as seams of high fracture densities were found on about six per cent of the fractures in this cluster. The widths of these breccia/fracture seams reach up to 0.8 m in one case. More commonly, the widths range from 5 to 20 cm. Fracture infillings in this cluster are more widely distributed over the various sampling stations than for example in the cluster of N(N)E-S(S)W striking fractures, in which infillings are concentrated in only a few locations. Thus, ENE-WSW to E-W directed discontinuities having originated in response to shear displacement seem to be a spatially widespread occurrence.



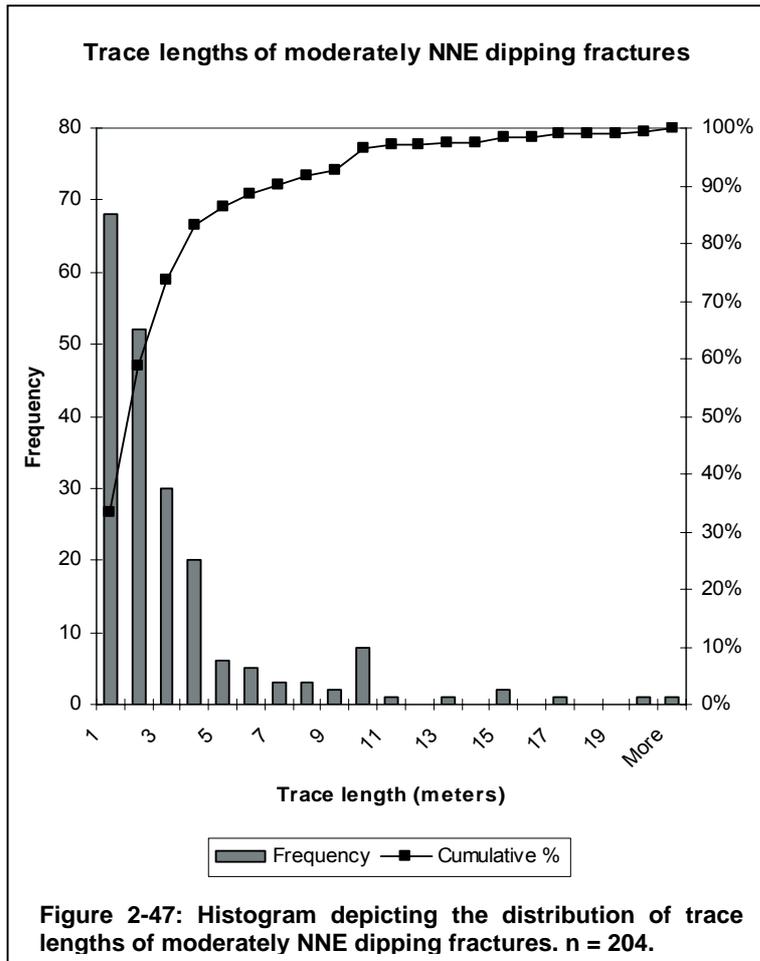
2.3.4 Moderately NNE dipping fractures

With a total number of 863 individual fractures this cluster is the second smallest in this analysis. It is the only one containing predominantly moderately inclined discontinuities. Approximately 40 per cent of the fracture record was identified to parallel a local metamorphic foliation. However, this fracture type is not restricted to metamorphic lithologies, although it does not play a major role in granitic rocks.



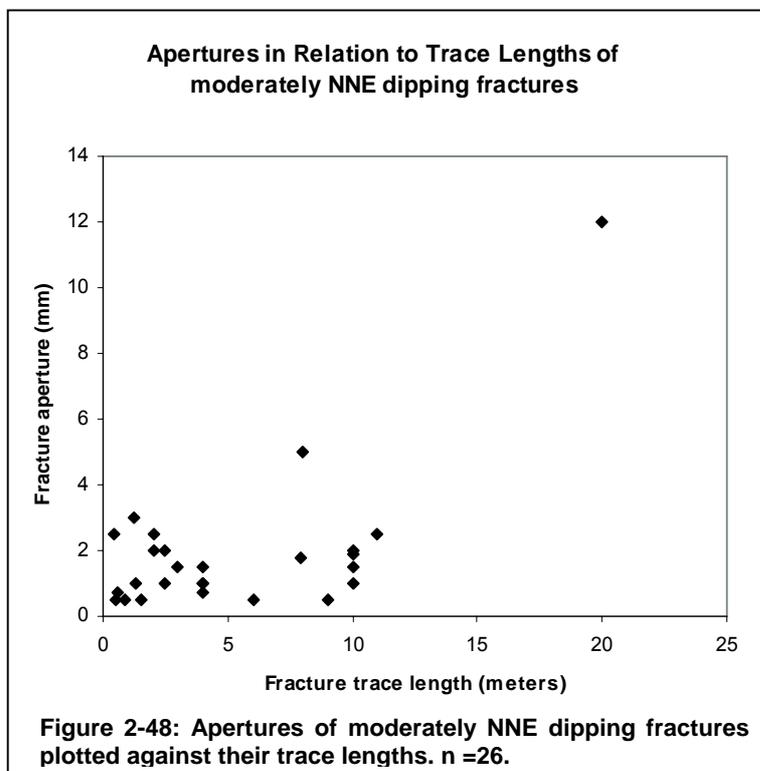
With respect to fracture roughness and planarity (fig. 2-46) this cluster shows characteristics completely different from those of the steeply inclined ones. Fractures show a clear proclivity towards rough planes. Only about a quarter of the data record is associated with smooth to relatively smooth planes. Also, the distribution of planarity is inverted with respect to the other clusters. Here, undulatory planes dominate. For fractures parallel to the metamorphic grain this phenomenon is explained in section 2.2.1.2.

The distribution of trace lengths in this cluster (fig. 2-47), however, resembles that of the others in that the bulk of the fractures trace less than four meters and discontinuities shorter than one meter dominate the record. Thus, the trace length distributions for both the genetic and the orientation-based fracture classes are exponential. The only exception can be found in the unroofing joints, which yield a rather heterogeneous distribution with a peak in the ten meter bin (cf. section 2.2.4.2).



The values of fracture apertures and trace lengths (fig. 2-48) correlate reasonably well ($R = 0.65$), so increasingly long fractures tend to be associated with increasingly large apertures, although, as in the other clusters, low apertures may also occur along relatively extensive fractures.

With the exception of quartz, hydrothermal mineral precipitates are comparatively rare in this cluster. Iron oxides are relatively more abundant. A special type of graphite mineralization belonging to this cluster was only found in one location (6944-13). There, it covers fracture planes parallel to the metamorphic foliation and is heavily slickensided. Fracture mineralizations make up less than five per cent of the bulk record in this cluster.



Fracture infillings mainly consist of 5 to 30 cm (in some rare cases up to 60 cm) wide breccia and gouge seams. More than seven per cent of the fractures in this cluster are associated with such infillings, which suggests that shear

displacement was more active in creating new fractures in this cluster than in the others.

2.4 Tectonic classification of brittle structures

After the previous classification, which was based on the physical properties of different fracture types and their occurrence in specific lithological environments the discontinuities will now be grouped according to their significance in various tectonic processes. This classification also bears a hydrogeological significance, since the tectonic processes acting upon a fracture strongly influence parameters such as aperture, trace length, or the presence of breccia and gouge seams, and hence has an impact on the permeability of such a structure.

2.4.1 Joints

Apart from unroofing joints (see section 2.2.4) only a relatively small number of fractures could be determined to have originated as purely extensional joints, which is largely due to the overprinting of indicators by a later reactivation of a significant part of those fractures. Indicators for a fracture's purely extensional origin are plumose or hackly structures such as described by van der Pluijm and Marshak (1997). It is very likely that the majority of – especially the smaller – discontinuities came to existence as tensile joints even though no physical evidence could be found on their planes.

Figure 2-49 depicts all fractures which are clearly extensional, i.e. which expose plumose or hackly structures on their planes, or which have been determined to be joints in the field due to an obvious lack of displacement. Many other fractures were determined to be extensional joints during the ensuing tectonic analysis simply for want of kinematic indicators or angular relationships to other fracture sets indicative of shear displacement. These can also by mistake include faults, along which tectonic markers or shear sense indicators are missing. However, this should be the case only very sporadically.

2.4.1.1 Orientations and spatial distribution

At first glance the fractures and concentrations in fig. 2-49 show angular relationships causing them to appear as orthogonal joint systems. Thus, NW-SE and NE-SW populations are dominant both in the plot depicting joints containing plumose structures (fig. 2-49a) and the one showing joints *sensu lato* (fig. 2-49b). However, this is only true for observations on a regional scale. Examining the joint sets on an outcrop scale unveils angular relationships very different from those of an orthogonal joint system. Table 2-5 lists the strike directions of the dominant joint sets depicted in fig. 2-49a classified with respect to the sampling locations in which they were measured.

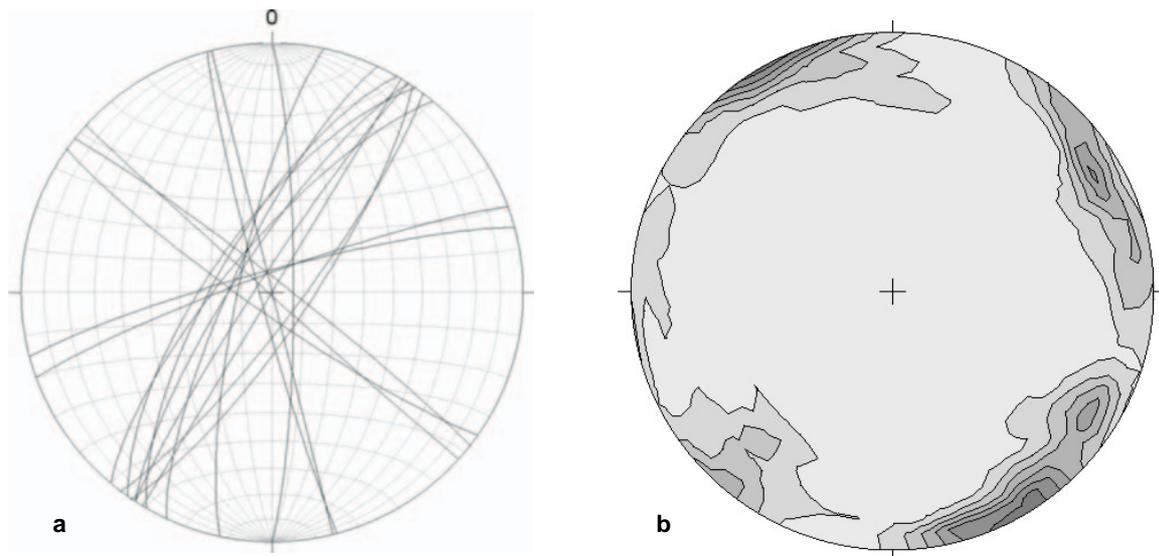


Figure 2-49: (a) Fracture planes exposing plumose or hackly structures. $n = 18$. (b) Data of (a) plus all fractures explicitly called “joint” in the field. $n = 76$, contours represent integer mrd.

The table shows that in most cases only one subvertical set of joints with plumose structures on their planes was found. Taking into account the complete fracture record of each of the sampling stations listed in table 2-5 (see appendix A) reveals orthogonal fracture sets (i.e. including fractures not explicitly classified as joints) only in locations 6843-04 and 7044-02.

Outcrop ID	Strike of joint set 1	Strike of joint set 2
6843-01	NW-SE	
6843-04	NE-SW	
6943-01	NE-SW to ENE-WSW	NW-SE
7043-02	NNW-SSE	
7044-02	NNE-SSW	WNW-ESE
7044-04	N-S to NNE-SSW	

Table 2-5: Dominant mean strike directions of subvertical joints (plotted in fig. 2-49a).

Applying the assumption that steeply dipping fractures which do not show any indication of fault motion originated as extensional joints to the entire fracture database, 14 of the total 49 sampling stations possess orthogonal fracture sets (allowing for a $\pm 10^\circ$ variation in strike). However, due to the fact that usually more than two steeply inclined fracture sets are present in a particular sampling station orthogonal relationships between two specific populations are sometimes only speculative. An observation made during the comparison of

cumulative fracture plots in appendix F is that orthogonal fracture sets seem to have a tendency to occur in unfoliated, weakly foliated, or strongly folded lithologies (table 2-6; description of lithogroups see section 2.1) where preexisting metamorphic fabrics have little or no influence on the formation of discontinuities. The tectonic significance of these orthogonal sets will be detailed in section 2.4.1.2.

Outcrop ID	Strike Set 1 (°)	Strike Set 2 (°)	Deviation from Orthogonal (°)	Comment	Lithogroup
6843-04	36	121	5	angle between foliation parallel and cross fractures	Granitic rocks
6844-02	290	11	9		Layered gneissic rocks
6943-05	124	218	4	angle between only minor concentrations	Strongly folded and migmatitic rocks
6943-08	47	297	10		Granitic rocks
6943-10	35	306	1		Strongly folded and migmatitic rocks
6943-13	9	106	8		Strongly folded and migmatitic rocks
6943-14	48	316	2		Strongly folded and migmatitic rocks
6944-04	287	203	6		Strongly folded and migmatitic rocks
6944-05	8	287	9		Strongly folded and migmatitic rocks
6944-06	306	43	7		Strongly folded and migmatitic rocks
6944-14	30	117	3		Layered gneissic rocks
6944-16	218	132	6		Strongly folded and migmatitic rocks
6944-18	45	125	10		Strongly folded and migmatitic rocks
7044-02	197	109	2		Strongly folded and migmatitic rocks

Table 2-6: Sampling stations with suborthogonal ($\pm 10^\circ$) fracture sets.

2.4.1.2 Tectonic significance

The tectonic significance of subvertical joints in general is the implication that stress fields exerting a subhorizontal extension on the study area must have existed during its brittle deformation history. According to general models (van der Pluijm and Marshak, 1997) the minimum principal stress (σ_3) lies normal to the joint plane while the maximum principal stress (σ_1) is oriented parallel to its plane. Consequently, subvertical joints formed in response to a horizontal or vertical compression. The direction of compression can usually be deduced from the joints' propagation directions, which in turn are indicated by the orientations of arrest lines and twist hackles. Unfortunately, in most cases the plumose structures detected in the study area were very faint, so clear propagation directions could not be obtained for the majority of joints. In addition, certain problems arose from the analysis of plumose structures. For one, joints exposing these structures on their planes could also have been created by blasting. Since most of them were found in granite quarries an anthropogenic origin must be considered. Thus, the tectonic origin of a fracture had to be

ensured, which was achieved by the exclusion of curved joint planes. These planes were assumed to have originated as a result of blasting and were interpreted as structures similar to the impact shatter cones described by Eisbacher (1991). Additionally, only joint planes containing hydrothermal minerals were examined, because hydrothermal alteration is a sure sign for a relatively old, and therefore non-anthropogenic, age of formation. Another complication for the analysis of plumose structures is that most of them belong to the curvy variety (van der Pluijm and Marshak, 1997), and only parts of a structure have been preserved in almost all cases. Thus, a clear propagation direction was very difficult to obtain. However, on a few fracture planes very vague propagation directions could be determined. There, the orientations of arrest lines and twist hackles suggest a subvertically oriented compressional stress suggesting that the joints formed during uplift.

Additionally, several other indicators suggest joint formation during regional uplift: (1) The presence of normal faults with strikes similar to those of the joints (see section 2.4.2.1) indicates a subvertical σ_1 with two more or less orthogonal σ_3 directions. Similar extension directions can also be obtained from fig. 2-49. Furthermore, several joints were later reactivated by dip-parallel shearing, which can only result from a subvertical σ_1 . (2) The presence of approximately orthogonal fracture sets in several sampling stations, which do not show any appreciable cross-cutting relationships or offsets, suggests a more or less contemporaneous formation due to an uplift-related σ_1 as well as a σ_2 and σ_3 of a relatively equal magnitude. This stress configuration can lead to a switch in the orientations of σ_2 and σ_3 , resulting in the formation of joints at right angles to each other. However, these orthogonal sets must have formed at times when the northward directed push from the alpine orogeny, which, despite its present-day distance of about 200 km, had an influence on the regional stress field. According to Bergerat and Geysant (1982; 1983) this push was comparatively minor such that σ_2 and σ_3 could have similar magnitudes.

Yet certain complications with regard to the orthogonal fracture sets in metamorphic regions can arise. The distribution of discontinuities in well-foliated rocks is frequently dominated by those parallel to the metamorphic foliation, which represent preexisting planes of weakness preferentially used for fracturing. Thus, extensional strain is predominantly accommodated by these planes, which are not necessarily oriented at right angles to the regional minimum principal stress. As a result, joint sets, which would otherwise form at right angles to each other due to the mechanisms described above, are oriented at various angles. In such cases outcrops are frequently dominated by a set of fractures parallel to the foliation, and one cutting across at high angles. Depending on the inclination of the foliation planes shearing motion can occur along the foliation parallel fractures, because only vertical joints can respond to subhorizontal extension without any displacement. Thus, instead of

orthogonal joint sets different combinations of joints and faults with varying angles with respect to each other can occur in metamorphic lithologies in response to an uplift-related vertical σ_1 .

2.4.2 Faults

In the study area 258 faults *sensu stricto* have been documented. These fractures clearly show signs of displacement along their planes. These signs comprise offsets of tectonic markers, slickensides, or the presence of fault rocks such as loose or compacted breccia seams. In the latter case, however, only fractures labeled as faults in the field notes are included in this dataset, which is presented in fig. 2-50a. Adding all fractures not labeled as faults in the field notes, but associated with breccia seams, which are very likely to have been caused by shearing motion (i.e. faults *sensu lato*), to the dataset of faults amounts to a total of 471 structures (fig. 2-50b).

2.4.2.1 Orientations and spatial distribution

The examination of the plots in fig. 2-50 yields similar orientations of both faults *sensu stricto* and *sensu lato*. Thus, the majority of fractures possess conspicuously steep inclinations, although fig. 2-50b also contains two gently inclined populations. The moderately to steeply SW dipping concentrations of poles in both plots trend subparallel to the metamorphic foliation planes. Approximately 84 (i.e. 5 out of 31 faults in fig. 2-50a) and 78 (i.e. 13 out of 59 faults in fig. 2-50b) per cent of the faults of this orientation were recorded in metamorphic lithologies.

The other dominant populations trend in northerly directions, NW-SE and NE-SW. Thus, they are in part subparallel to the joints plotted in fig. 2-49. Only the northerly strikes occur predominantly in the group of faults. About half of the outcrops (i.e. 7 out of 14) in which these strikes were recorded are situated in the vicinity of major topographic lineaments trending in similar directions. A connection between northerly striking faults and lithologic units could not be established. The NW-SE and NE-SW trending faults with their conspicuous subparallelism to the dominant joint sets will be discussed in the following section.

Lithogroup	Total Number of Outcrops	Outcrops with Faults sensu stricto	Outcrops with Faults sensu lato
1 Granitic rocks	8	8 (100 %)	8 (100 %)
2 Layered metamorphic rocks	12	8 (67 %)	11 (91 %)
3 Strongly folded and migmatitic rocks	21	12 (57 %)	17 (82 %)
4 Hydrothermal and pneumatolytic rocks	5	4 (80 %)	5 (100 %)

Table 2-7: Sampling stations, in which faults were measured, classified according to their associated lithogroups.

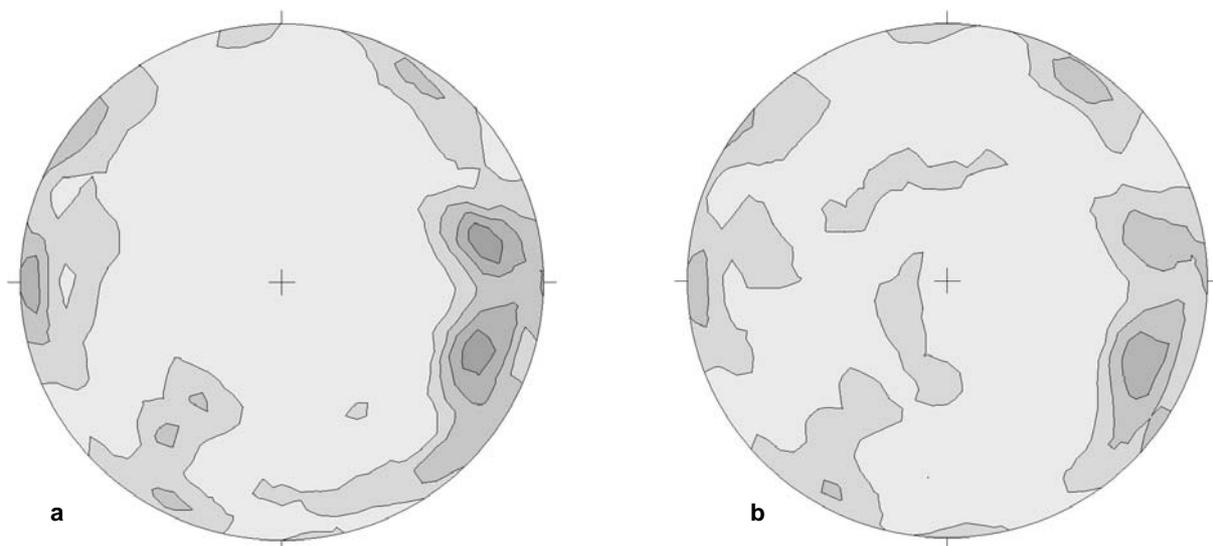


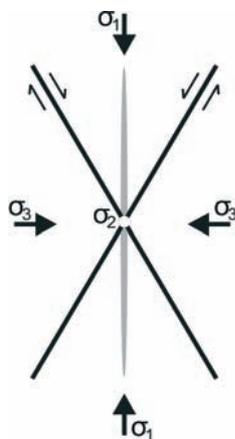
Figure 2-50: Cumulative Plots of faults in the study area. (a) Plot of planes explicitly called "fault" in the field. (b) Data from (a) plus all fractures associated with breccia and/or gouge suggesting fault motion. $n = 257$ in (a); $n = 470$ in (b), contours represent integer mrd.

Faults in general are relatively evenly distributed over the study area. Of a total of 49 sampling stations 32 possess faults sensu stricto and 41 faults sensu lato. Classified according to their occurrence in the particular lithogroups shows that all outcrops situated in granitic rocks contain faults s. str. while only about two thirds of the exposures located in strongly folded and migmatitic rocks do so (table 2-7). Layered metamorphic rocks show slightly higher values and hydrothermal/pneumatolytic rocks rank second. Faults s. l. are an ubiquitous feature existing in 80 to 100 % of the outcrops in a specific lithogroup.

2.4.2.2 Tectonic significance

Faults are the direct results of displacement between two rock blocks in response to deviatoric stresses. Thus, in case the direction of displacement is obvious, faults can identify paleo-stress fields. As will be detailed in the following sections several kinematic indicators such as slickenlines, offsets and the presence of fault rocks were used to elucidate the region's tectonic history.

A very striking property of many faults in the database is their extremely steep dip, even though a large number of them could be identified as dip-slip faults, which usually tend to be rather moderately inclined. Also, their orientations are very similar to those of the extensional joints. In one of the preceding sections the joints were related to uplift, in which probably also the dip-slip faults have their origin. In keeping with the predictions of the Mohr-Coulomb criterion (van der Pluijm and Marshak, 1997) and the Anderson theory of faulting (Marshak and Mitra, 1988) fig. 2-51 illustrates how the angular relationships between joints and faults in an uplift-regime should exist. In this model vertical joints form along with faults inclined at angles of approximately 60° . In the reality of this study area this is obviously not the case. Instead, since in a number of incidents slickensides and plumose structures were



found on the same fracture planes, it is suspected that shear reactivation followed joint formation. Thus, the joints acted as preexisting planes of weakness, which were easier to reuse for shear displacement than to create new faults. Also, since major offsets along fault planes have not been found the throw is expected to have been relatively minor.

Figure 2-51: Conceptual 2-D model of the orientations of principal stresses, faults, and joints based on the Anderson theory of faulting (Marshak and Mitra, 1988). σ_1 , σ_2 , and σ_3 represent principal stresses. Vertical gray tapered line represents a joint opening normal to σ_3 . σ_2 stands normal to this page. Diagonal black lines represent a conjugate set of faults. Half-arrows point in the direction of displacement.

A relatively small number of faults is moderately to gently inclined (fig. 2-50a) or even gently inclined to subhorizontal (fig. 2-50b). The subhorizontal fractures (inclined at up to 20°) were exclusively recorded in outcrops belonging to lithogroups 1 and 3 (i.e. granitic rocks and strongly folded/migmatitic rocks) and are characterized as faults by the presence of breccia seams. Offsets and slickensides are generally absent. Especially in the granites these discontinuities appear to be reactivated unroofing joints, where uplift initially created flat-lying extensional fractures, which were later reactivated by subhorizontal compression. For the fractures in the lithogroup of strongly folded/migmatitic rocks the interpretation becomes more difficult, because in these cases the fractures do not have the appearance



Figure 2-52: Gently inclined fault in a poorly foliated rock (Körneltgneis). Location: Viechtach/ Alterberg, 6943-14.

typical for unroofing joints. They rather exist as densely fractured and brecciated zones, which show no signs for having resulted from the reactivation of formerly extensional joints (fig. 2-52). In fig. 2-50b this group of NNE to E dipping faults is represented by the steeply to subvertically NNW to W plunging concentration. The strikes of these fractures are noticeably similar to those of the metamorphic foliation, even though a macroscopically detectable fabric – with the occasional exception of preferentially oriented porphyroblasts - is widely absent in these rocks. Nonetheless, the belt of moderately to steeply SW inclined poles in fig 2-50a definitely parallels the metamorphic foliation, even more so because many faults belonging to this concentration were actually recorded in well-layered rocks.

Thus, it can be assumed that the majority of faults in the study area came into existence by the reactivation of preexisting planes of weakness such as vertical joints, unroofing joints, or foliation planes. Still, occasional primary formations are possible.

2.4.3 Kinematic indicators

In the preceding section on faults in the study area an overview regarding their orientations and general properties was presented. Now, the kinematic aspects thereof shall be concentrated on. At this point it must be mentioned that clear and unambiguous kinematic indicators are extremely rare in this region. Outcrop-scale offsets and cross-cutting relationships usable for paleostress analyses are virtually absent and even if such features were found the magnitude of displacement indicated usually did not exceed a few decimeters. The reasons for this lie either in the frequent absence of tectonic markers in the mostly homogenized or plutonic rocks, or in very minute rates of displacement along individual faults, which only amount cumulatively to throws of greater magnitudes.

Thus, in order to decipher the tectonic history of the study area one primarily has to fall back on the interpretation of geometric relationships between fracture systems,

slickensides, and the distribution of brittle fault rocks. These are ubiquitous features in the study area, although not all outcrops could be used for their sampling. Especially the slickensides are dependent on the degree of weathering in a particular exposure and are thus restricted to relatively fresh outcrops, such as the granite quarries in the southern study area. In the gneissic regions they are usually more rare, most likely because intense weathering has frequently worn off the top part of the fault planes or obscured the slickenlines with seams of weathered material. Nonetheless, sufficient data could be collected to obtain an impression of the brittle tectonic mechanisms that have acted on the study area since the late Mesozoic.

2.4.3.1 Geometric relationships between fractures and fracture systems

Geometric relationships between fractures and fracture systems were mainly identified in the form of conjugate sets (Anderson, 1942) and Riedel-type shear fracture relationships (Eisbacher, 1991; van der Pluijm and Marshak, 1997).

Riedel shear fractures are subsidiary fractures significantly smaller than the main slip planes they are associated with. Ideally, they exist as conjugate pairs of syn- and antithetic fractures oriented at specific angles (usually less than 20° for synthetic, and about 70° to 80° for antithetic shears) to the main slip plane. In the field they are usually not recognizable as conjugate pairs but produce wedge-shaped breakouts on fault planes, of which the wedge points in the direction of displacement. The surfaces of the breakouts usually represent the planes of the synthetic shears and are usually too small to measure. Nonetheless, the shear sense can be determined qualitatively by their visual examination.

In the study area Riedel shears could only be determined on relatively fresh fault planes in predominantly granitic or highly homogenized metamorphic rocks. Highly weathered outcrops did not yield unambiguous information and thus were not examined with respect to Riedel-type shear sense indicators.

As can be seen in fig. 2-53 Riedel shear fractures are not unique to specific fracture sets. Only the very few datapoints for strike-slip faults (fig. 2-53a and b) seem to restrict this type of displacement to the \pm NE-SW direction. As a result, stress configurations similar to those obtained for slickensided strike-slip faults (i.e. subhorizontal \pm NE-SW and \pm NNW-SSE compression, respectively; see section 2.4.3.2) were obtained.

In contrast, the dip-slip faults do not show conspicuously regular patterns with respect to orientation. However, the dataset of normal faults (fig. 2-53c) contains dominant orientations similar to those of slickensided normal faults, i.e. NE-SW and NW-SE, (see section 2.4.3.2) as well as a group of N-S

striking fractures. The stress configurations estimated for the slickensided faults suggest an extensional regime with a subvertical maximum principal stress and extension in various subhorizontal directions. Similar conditions are also assumed for the faults containing subsidiary Riedel shear fractures. As will be detailed in the section on the study area's brittle tectonic history this stress configuration is attributed to ongoing regional uplift associated with crustal extension, which in turn is evidenced by the presence and orientations of the extensional joint systems discussed in section 2.4.1.

Regarding reverse faults (fig. 2-53d) there are also similarities between slickensided faults and those associated with Riedel shears. Accordingly, the dominant strikes are NE-SW and NW-SE. In cases where the displacement arrows in fig. 2-53d do not parallel the dip direction the Riedel shears occur along with slickenlines on the same fracture plane, which is usually not the case for the other types of faults presented in fig. 2-53. Whether or not these subsidiary fractures formed contemporaneously with the slip lineations could not be determined. However, in case they did not, the Riedel shears must have predated the slickenlines since they are features linked to initial fault propagation. Nonetheless, the slip directions of slickensides were included in this image, because they allow for better

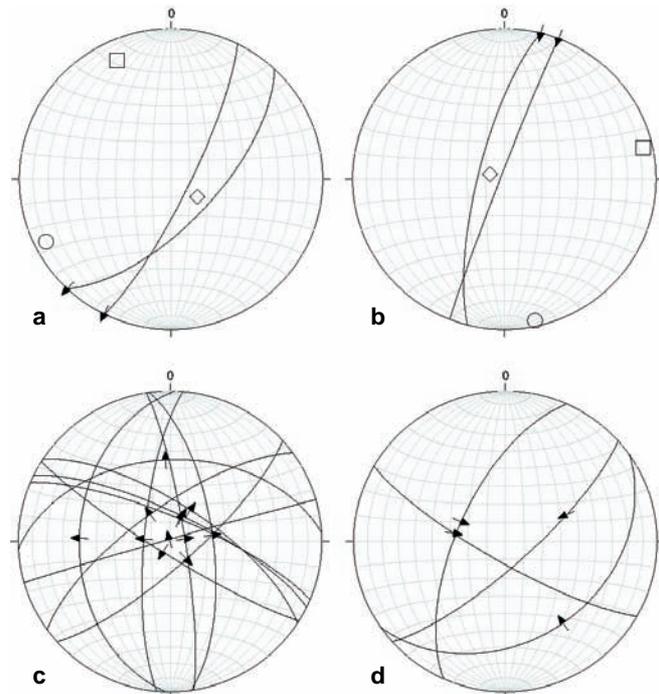


Figure 2-53: Fault planes associated with Riedel shear fractures. (a) Faults suggesting dextral strike-slip motion, (b) faults suggesting sinistral strike-slip motion, (c) faults suggesting normal motion, (d) faults suggesting reverse motion. In (a) and (b) paleostress configurations were calculated: $\circ = \sigma_1$, $\diamond = \sigma_2$, $\square = \sigma_3$. $n_{\text{faults}} = 2$ in (a) and (b); $n_{\text{faults}} = 12$ and for in (c) and (d), respectively.

constraints on the latest directions of displacement than the frequently ambiguous orientations of Riedel-type breakouts on fracture planes. The attempt to deduce meaningful stress configurations for this group of faults must remain dissatisfactory due to the small amount and large scatter of datapoints. At best, gently to moderately inclined maximum principal stresses oriented \pm NW-SE and \pm NE-SW could be envisaged. Similar directions of compression, however with subhorizontal σ_1 , were determined for slickensided strike-slip faults (section 2.4.3.2).

In the field conjugate relationships between individual fractures were noted in a total of 14 sampling stations in all lithogroups. Frequently, they consisted only of two or three fractures per outcrop, while in other locations an entire fracture set showed a conjugate relationship with another one. This is especially the case for the low-angle fractures conjugate to the foliation parallel fractures.

Figure 2-54 depicts cumulative representations of their angular relationships. The raw dataset of conjugate fractures was separated

into fracture sets with similar orientations. The resulting subgroups consist of moderately inclined \pm N-S striking sets (fig. 2-54a), moderately inclined \pm NW-SE striking sets (fig. 2-54b), gently inclined \pm NW-SE and \pm NNE-SSW striking sets (fig. 2-54c), and steeply inclined sets with varying strikes (fig. 2-54d). As assumed for the normal faults associated with Riedel shears an uplift regime in combination with various subhorizontal directions of extension is envisioned. Thus, according to the Anderson theory (fig. 2-51) E-W extension is attributed to

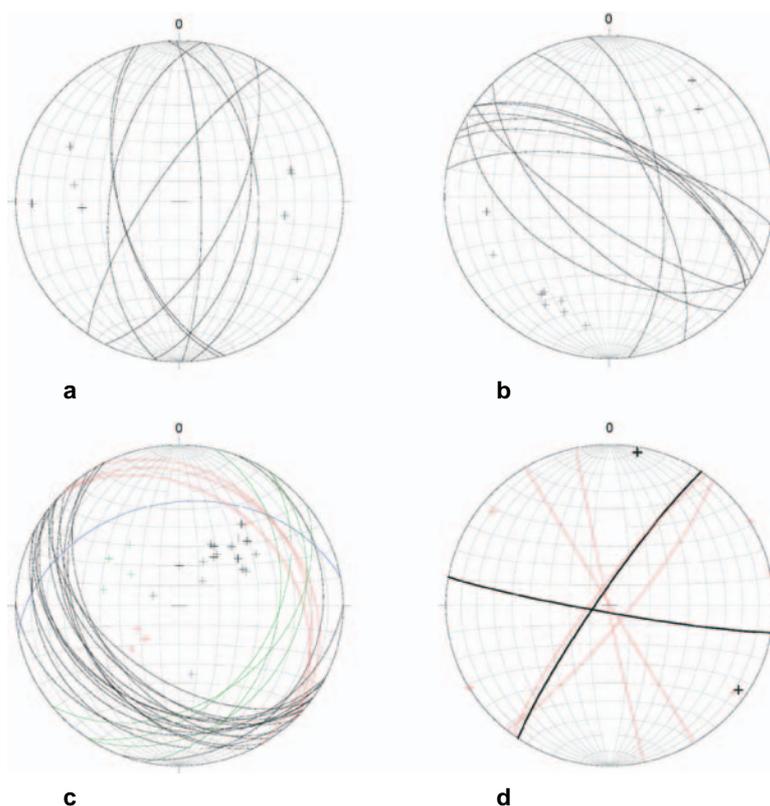


Figure 2-54: Conjugate fracture sets in the study area. (a) Fractures suggesting uplift and E-W extension. $n = 8$. (b) Fractures suggesting uplift and NE-SW extension. $n = 11$. (c) Fractures antithetic to those parallel to the metamorphic foliation, mainly suggesting subhorizontal NE-SW compression. Black planes are fractures conjugate to NE dipping foliation planes (red); green planes are fractures conjugate to NNW dipping foliation planes (blue). $n = 25$. (d) Conjugate fractures suggesting ENE-WSW compression (black planes) and NNE-SSW compression (red planes). $n = 6$. Black crosses represent poles to the planes.

the \pm N-S striking faults in fig. 2-54a, and NE-SW extension to the \pm NW-SE striking ones in fig. 2-54b.

The gently inclined conjugate sets presented in fig. 2-54c constitute a rather interesting phenomenon. Here, sets of fractures cutting across the metamorphic foliation are related to those parallel to the fabric. In these cases the foliation parallel fractures usually dip in northerly directions while the cross fractures are inclined towards SSE to SW. The presence of unconsolidated fault breccia along these sets was frequently observed in the field, although no appreciable displacement could be detected. It is assumed that this type of deformation is the result of a northerly directed subhorizontal compression activating the metamorphic fabric as planes of weakness and creating additional fracture sets at conjugate angles.

Figure 2-54d depicts a very small sample of steeply inclined fractures. In keeping with the Anderson theory these conjugate sets are the results of strike-slip displacement in response to two different compressional stress fields. One (red planes in fig. 2-53d) suggests NNE-SSW compression and WNW-ESE extension, the other (bold black lines) is attributed to ENE-WSW compression and NNW-SSE extension. However, due to the scarcity of datapoints these results will not be credited with much further attention in the tectonic analysis of the area unless other evidence leads to comparable findings.

In conclusion of the discussion of subsidiary fractures and fault geometries it has to be mentioned that the kinematic information they provided often was not entirely clear and thus must be seen as fairly unreliable indicators for the deformation mechanisms in the study area. Thus, the more indicative shear sense indicators such as slickenlines and offset features will be given more weight in case of doubt.

2.4.3.2 Slickensides

Although slickensided planes are ubiquitous features in the study area they are often difficult to recognize and even more difficult to use as kinematic indicators. Due to intense bedrock weathering, especially in the gneissic outcrops, fracture surfaces have been worn down and the topmost surface containing the slip lineations removed. By van der Pluijm and Marshak's (1997) definition slickensides comprise both simple striae or groove lineations, which do not necessitate mineral growth parallel to the slip direction, and fiber lineations, which form due to the precipitation of minerals (mostly quartz, epidote, and chlorite) elongated in the direction of displacement. Slickenlines occur mostly as groove lineations (fig. 2-55), but also fiber lineations formed during hydrothermal activity in the area. However,

their distinction is greatly complicated by the fact that fractures coated with hydrothermal minerals have been repeatedly reactivated. Therefore, lineations resembling, but not necessarily being, fiber lineations can be found on those mineralized planes. The mechanisms of slickenline formation are described by Marshak and Mitra (1988). Figure 2-55 shows an example for one of the few well-recognizable slip lineations. In the field, slickenlines were examined visually and by sliding a hand up and down the fracture surface in the shear direction to feel anisotropies on the fault planes, thereby following the instructions described by van der Pluijm and Marshak (1997). Figure 2-56 depicts the orientations of the entire inventory of lineations measured in the study area, of which merely a fraction could be used to determine the shear sense. Only these planes will be taken into consideration in the following. Generally, the slickenlines can be subdivided into two subgroups with respect to their orientations: (1) slickenlines with steep to subvertical rakes and (2) slickenlines with gentle to subhorizontal rakes. In both of these groups several different types of shear sense can be distinguished.



Figure 2-55: Slickensided fracture plane. Red line highlights the orientation of the slickenlines. Location: Steinbruch Zeitlhof, 7043-02.

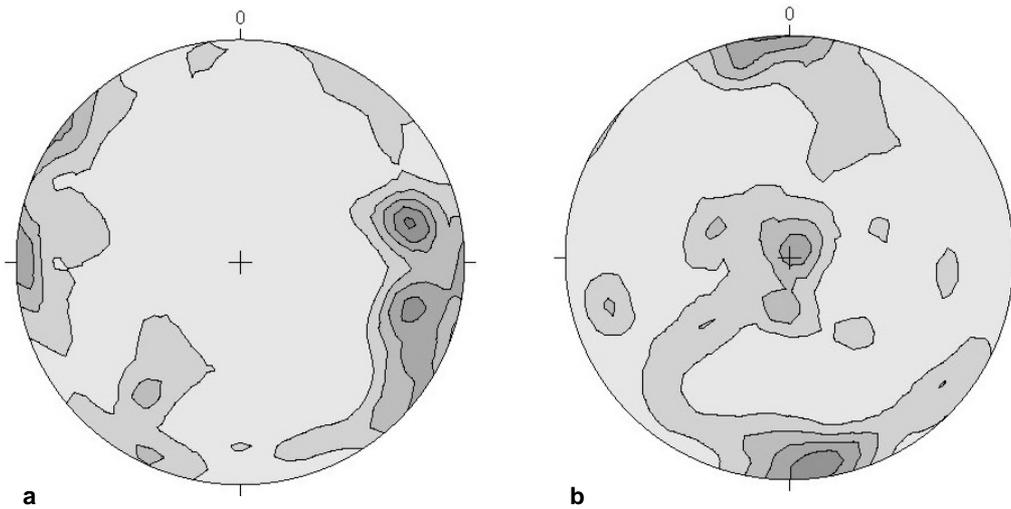


Figure 2-56: Cumulative plots of slickensides. (a) Orientations of slickensided fracture planes. (b) Orientations of slickenlines. In both plots $n = 246$, contours represent integer mrd.

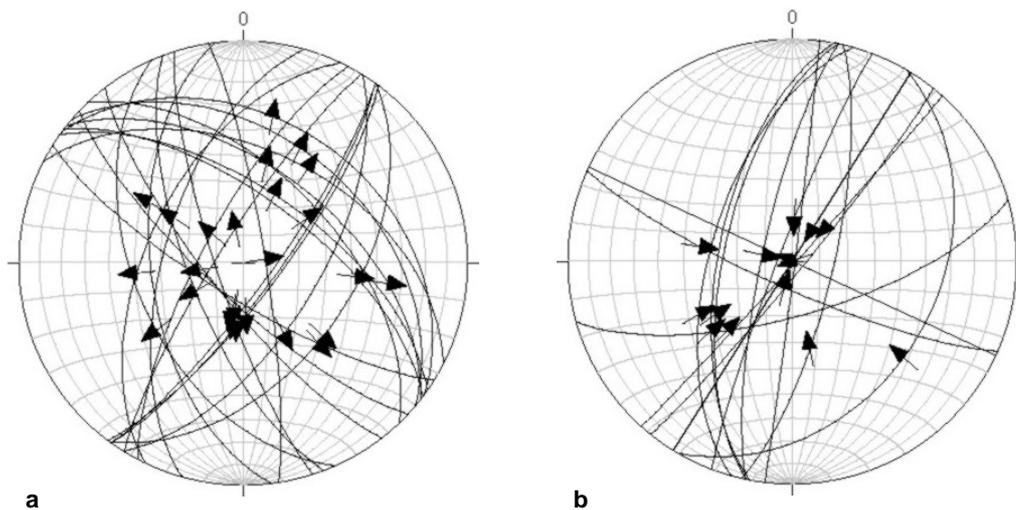


Figure 2-57: All slickensided fracture planes suggesting normal (a) and reverse (b) motion. Arrows depict slip directions on fracture planes. $n = 25$ for (a) and 15 for (b).

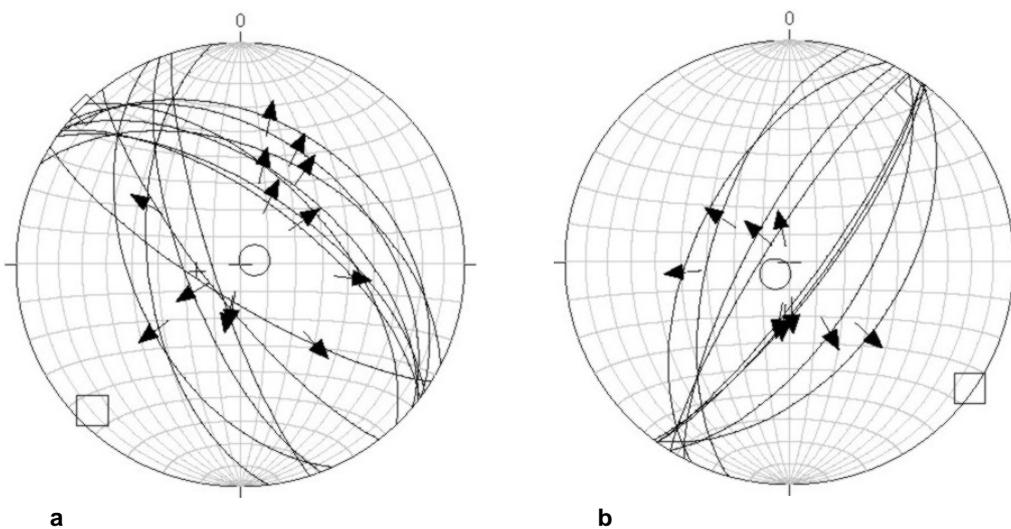


Figure 2-58: Slickensided fractures suggesting normal motion due to uplift with (a) NE-SW extension and (b) NW-SE extension. Arrows depict slip directions on fracture planes. $\circ = \sigma_1$ $\diamond = \sigma_2$ $\square = \sigma_3$. $n = 14$ for (a) and 9 for (b).

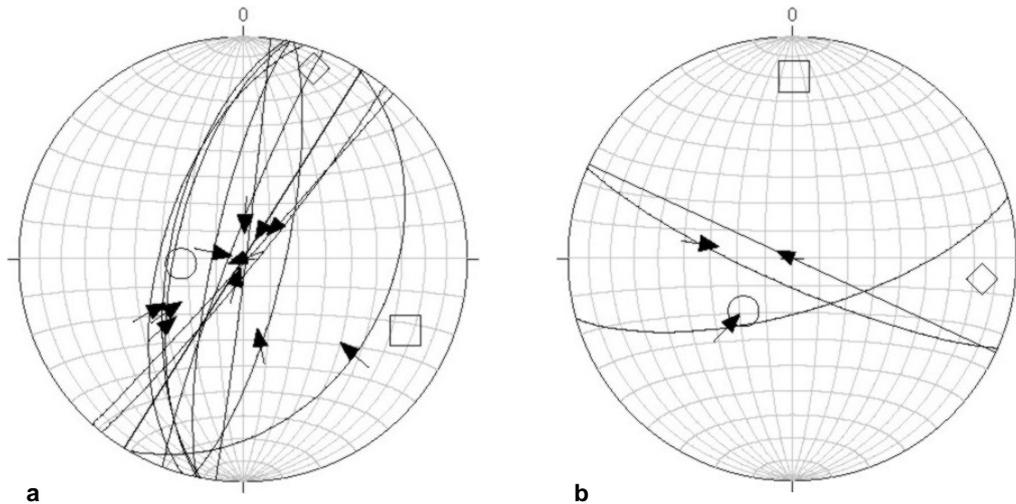


Figure 2-59: Slickensided fractures suggesting reverse motion related to uplift with (a) (W)NW-(E)SE extension and (b) N-S extension. Arrows depict slip directions on fracture planes. $\circ = \sigma_1$ $\diamond = \sigma_2$ $\square = \sigma_3$. $n = 25$ for (a) and 3 for (b).

The equal-area plots in figures 2-57, 2-58, and 2-59 show the orientations of fracture planes containing lineations with more or less dip-parallel rakes. Since normal as well as reverse motion are suggested by the slickenlines, and the orientations are rather variable in the cumulative plot (fig. 2-57), the dataset is further subdivided with respect to the strikes of specific fracture families. In doing so two generations of normal faults appear, one striking NW-SE, the other NE-SW. Both of them are due to a vertical σ_1 (fig. 2-58). The extensional σ_3 direction trends NE-SW in one, and NW-SE in the other case.

Similarly, the reverse faults can be subdivided into two groups, although the relatively low number of datapoints makes this distinction more difficult. The result is a NNE-SSW and a WNW-ESE trending population (fig. 2-59). The resulting stress configurations include a very steeply inclined σ_1 and WNW-ESE as well as N(NE)-S(SW) extension, respectively. Almost all reverse faults are steeply inclined to vertical. As a result, an unequivocal identification as reverse faults is often problematic, especially in cases where subvertical fractures show undulating traces. Nonetheless, the maximum normal stresses are close to vertical and thus similar to the ones computed for the normal faults.

The fractures containing strike-parallel trending slickenlines are plotted in figures 2-60, 2-61, and 2-62. The cumulative plots in figure 2-60 show the orientations of the entire inventory of dextral and sinistral strike-slip faults. While the dextral ones are more difficult to classify the sinistral faults expose a clear bimodal distribution. Nevertheless, for both the case of left-lateral and right-lateral faults two distinct major orientations can be determined. Figure 2-61 depicts the two subgroups of dextral faults. Compared to the sinistral ones they show a higher variability in their strikes such that no sharp limits exist in their distributions.

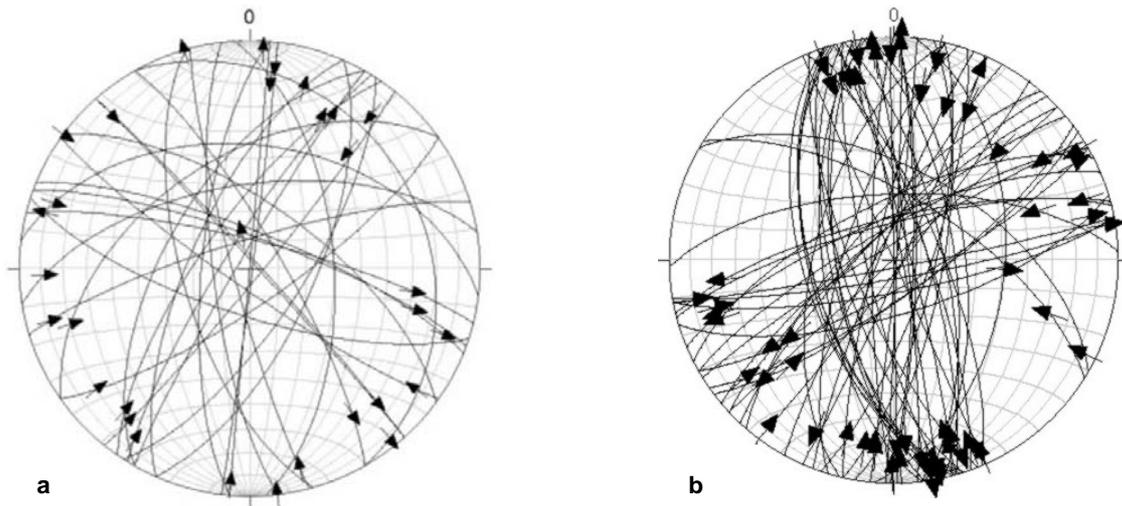


Figure 2-60: All slickensided fracture planes suggesting dextral (a) and sinistral (b) strike-slip motion. Arrows depict slip directions on fracture planes. $n = 32$ for (a) and 61 for (b).

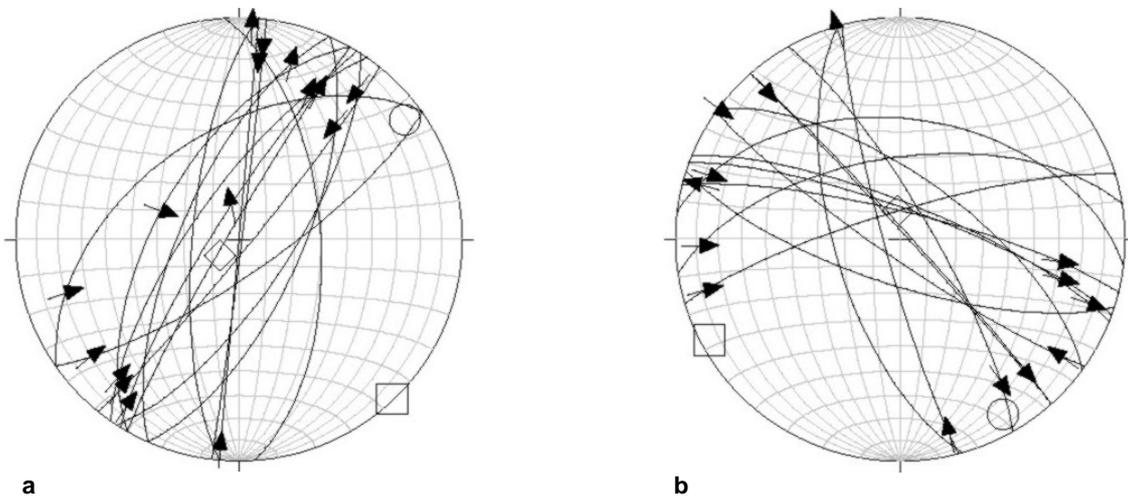


Figure 2-61: Slickensided fractures suggesting dextral strike-slip due to (a) NE-SW compression and (b) N(N)W-S(S)E compression. Arrows depict slip directions on fracture planes. $\circ = \sigma_1$ $\diamond = \sigma_2$ $\square = \sigma_3$. $n = 16$ for (a) and 14 for (b).

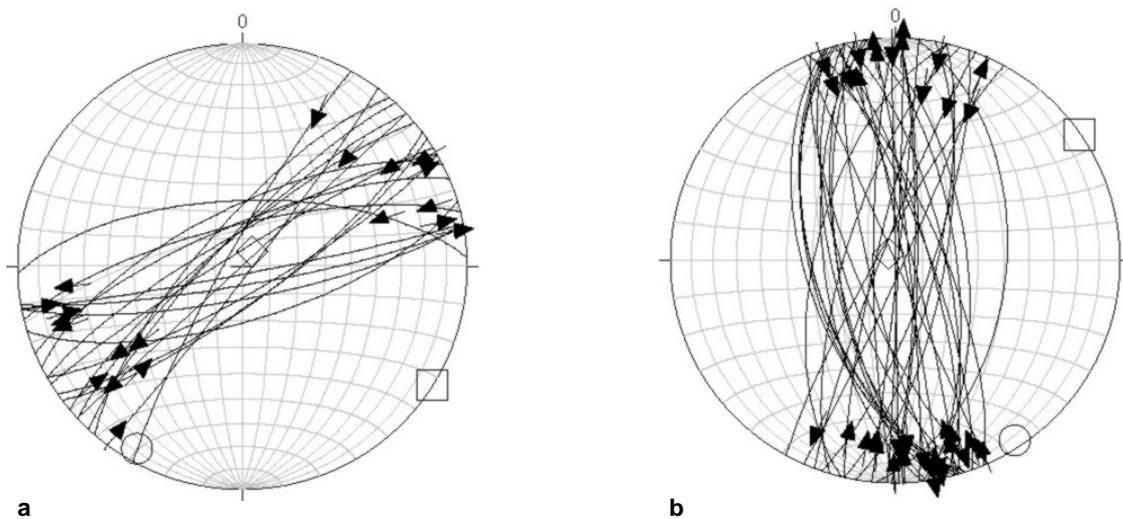


Figure 2-62: Slickensided fractures suggesting sinistral strike-slip due to (a) N(N)E-S(S)W compression and (b) N(N)W-S(S)E compression. Arrows depict slip directions on fracture planes. $\circ = \sigma_1$ $\diamond = \sigma_2$ $\square = \sigma_3$. $n = 21$ for (a) and 39 for (b).

The NNE-SSW trending population in fig. 2-61a suggests NE-SW compression and NW-SE extension while for the NW-SE striking group in fig. 2-61b N(N)W-S(S)E compression and (E)NE-(W)SW extension was calculated. The NE-SW to ENE-WSW trending sinistral strike-slip faults in fig. 2-62a are due to a N(N)E-S(S)W compressional stress field. In contrast, N(N)W-S(S)E compression was determined for the NNW-SSE to NNE-SSW striking population in fig. 2-62b.

A comparison of the stress configurations in figures 2-61 and 2-62 shows that – given a certain degree of variability - only two main compressional and extensional directions exist. These possibly acted simultaneously on one subgroup of each of the two families of right- and left-lateral faults. Thus, the N-S to NE-SW trending dextral faults were active during the same compressional stress field as the NE-SW to E-W trending sinistral faults. The same relationship exists for the \pm NW-SE trending dextral and \pm N-S trending sinistral ones. Figure 2-63 combines fractures with opposite slip directions belonging to one stress field or the other.

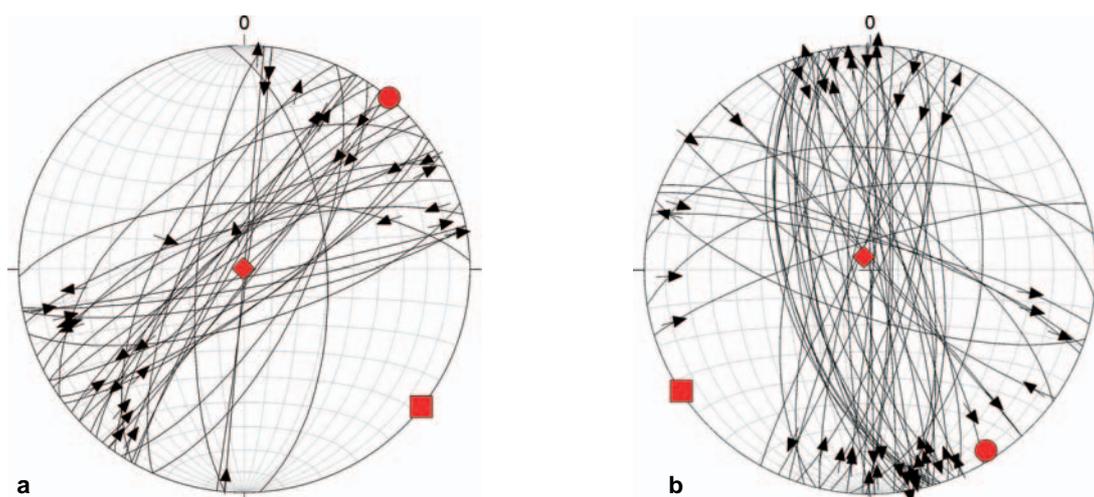


Figure 2-63: Slickensided fractures suggesting both sinistral and dextral strike-slip due to (a) N(N)E-S(S)W compression and (b) N(N)W-S(S)E compression. Arrows depict slip directions on fracture planes. $\circ = \sigma_1$ $\diamond = \sigma_2$ $\square = \sigma_3$. $n = 37$ for (a) and 53 for (b).

Another comparison potentially important for deciphering the brittle tectonic history of the study area is that between the orientations of mineralized slickensided faults and unmineralized slickensided faults (i.e. those bearing true groove lineations). However, this examination necessitates some restricting assumptions. Since the dataset covers a larger area it requires the entire study region to have been affected by hydrothermal activity. The ubiquity of quartz mineralizations of fracture planes as well as of quartz and pegmatite dikes validates this assumption, although the presence of other hydrothermal minerals, such as epidote, is concentrated in the vicinity of the large granitic plutons. Another assumption is

that all unmineralized fractures must have formed after the period of hydrothermal activity for which there is no evidence.

As already mentioned above, the distinction between slip fibers and simple groove lineations is often difficult on fracture planes bearing hydrothermal precipitates. However, this difference is important, because groove lineations may have postdated the hydrothermal activity, while slip fibers are most likely contemporaneous. Thus, only unmineralized slickensided fractures are certain to have formed after the precipitation of hydrothermal minerals. Figure 2-64 depicts this relationship. Here, it becomes evident that, while similar fracture orientations exist in both plots, the unmineralized faults are predominantly oriented N-S, while the mineralized ones trend more NNE-SSW and NW-SE. Although N-S trending mineralized faults exist they are of minor importance.

Thus, possible explanations are that either N-S faulting initiated during the final stages of hydrothermal activity and continued into later periods of deformation or that preexisting mineralized N-S joints became reactivated after the end of mineral precipitation. For the latter case the slickenlines on these fractures would be simple groove lineations. In any event, one phase of motion along N-S trending planes most likely postdated the hydrothermal activity.

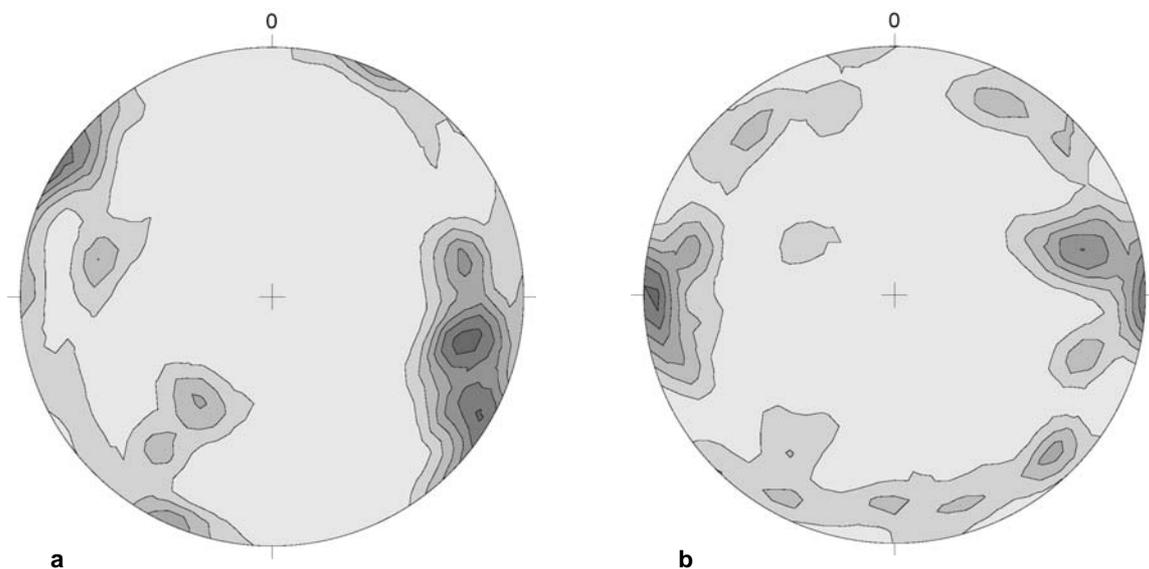
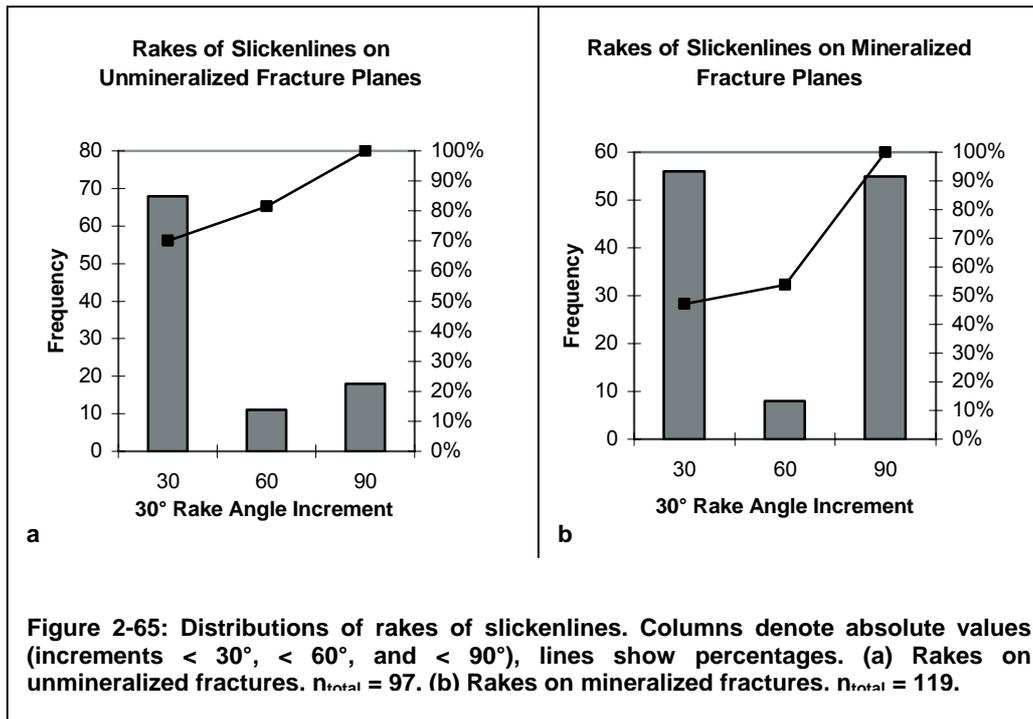


Figure 2-64: Slickensided faults in the study area. (a) Mineralized planes bearing slickenlines, $n = 100$. (b) Slickensided fractures not associated with mineral precipitates, $n = 91$. Contours represent integer mrd in both plots.

In order to shed somewhat more light on the question whether strike-slip or dip-slip motion was the first to occur on slickensided fracture planes the rakes of slip lineations recorded on mineralized and unmineralized fractures are plotted in fig. 2-65.



While rakes of all orientations can be found on both mineralized (fig. 2-65b) and unmineralized (fig. 2-65a) fracture planes a clear tendency of subvertical to steeply inclined rakes to occur preferentially on mineralized fracture planes becomes obvious. Thus, assuming that fractures carrying hydrothermal mineral coatings predate those which do not suggests that vertical fault motion is also older than the horizontal. Moreover, the distribution of rake orientations shows two peaks for the mineralized fractures, thus indicating that these discontinuities were active during both dip-slip and strike-slip displacement. Rakes of intermediate inclinations are rare in both plots, so oblique motion can be presumed to have been of minor importance.

However, the situation is complicated by the fact that the field records contain several fracture measurements with two or more lineations for which dip-slip motion was determined to be younger, because subvertical slickenlines were situated on top of subhorizontal ones. Additionally, figure 2-65a displays a number of steeply inclined to subvertical rakes, so one possible explanation is that several phases of strike-slip and dip-slip displacement followed each other with the dip-slip phases being among the first and the last to occur.

2.4.3.3 Offsets

Macroscopically visible offsets are rare occurrences in this study area. The predominant clues to detect shear displacement are slickensided fault planes and the presence of fault rocks which are thought to have come to existence during initial shearing along a newly formed fault. As for the presence of fault rocks without appreciable

displacement it is assumed that the stress most likely did not suffice in magnitude or duration to actually move the rock blocks past each other, but only created a “process zone of high crack density behind which there is coalescence into a through-going fault” (Snoke et al., 1998).

The offset features presented in fig. 2-66 are all the results of minor, centimeter- to decimeter-scale, displacements. Also, only the apparent displacement could be recorded in most cases, because the orientations of the offset features frequently could not be measured due to outcrop geometry. Taking this into consideration normal, reverse, and strike-slip offsets can be observed, however always as very isolated occurrences.

Figures 2-66a to 2-66e show faults along which normal motion was detected. The maximum amount of displacement recorded is 0.3 m. All normal faults are associated with a subvertical σ_1 and σ_3 trending subhorizontally in various directions. N-S extension was observed in two locations (fig. 2-66a and b), while NW-SE, NE-SW and E-W extension each was recorded once. Apparent normal motion due to actual strike-slip can only be ruled out for fig. 2-66a because of the angular relationship between offsetting and offset fracture. The offset features in fig. 2-66c and e could not be further specified. In fig. 2-66b and d apparent normal motion due to actual strike-slip is possible, because offset feature and offsetting fault are oriented at high angles to each other. Thus, (oblique) sinistral strike-slip is another potential sense of displacement. The resulting stress regimes would be \pm ENE-WSW compression and \pm NNW-SSE extension for fig. 2-66b, as well as NNW-SSE compression and ENE-WSW extension for fig. 2-66d.

Similarly, the apparent sinistral offset in fig. 2-66l could also be due to normal motion and ENE-WSW extension. However, due to the very steep dips of the fractures, which generally diminish the apparent effects, the actual displacement is indeed most likely sinistral strike-slip. Then, the resulting stress regimes are subhorizontal NW-SE compression and NE-SW extension in both fig. 2-66k and l. The amounts of displacement are 8 and 1 cm, respectively.

Several offsets were created by reverse motion along faults (figs. 2-66f to j), the majority of which were detected in location 6943-01. There, the offsets do not provide uniform directions. The directions of compression are oriented N-S, NE-SW, and ENE-WSW, all plunging gently. The comparison of all reverse offsets shows recurring \pm N-S and \pm NE-SW compression (figs. 2-66f and l, and 2-66g and j, respectively), although σ_1 is inclined at varying angles.

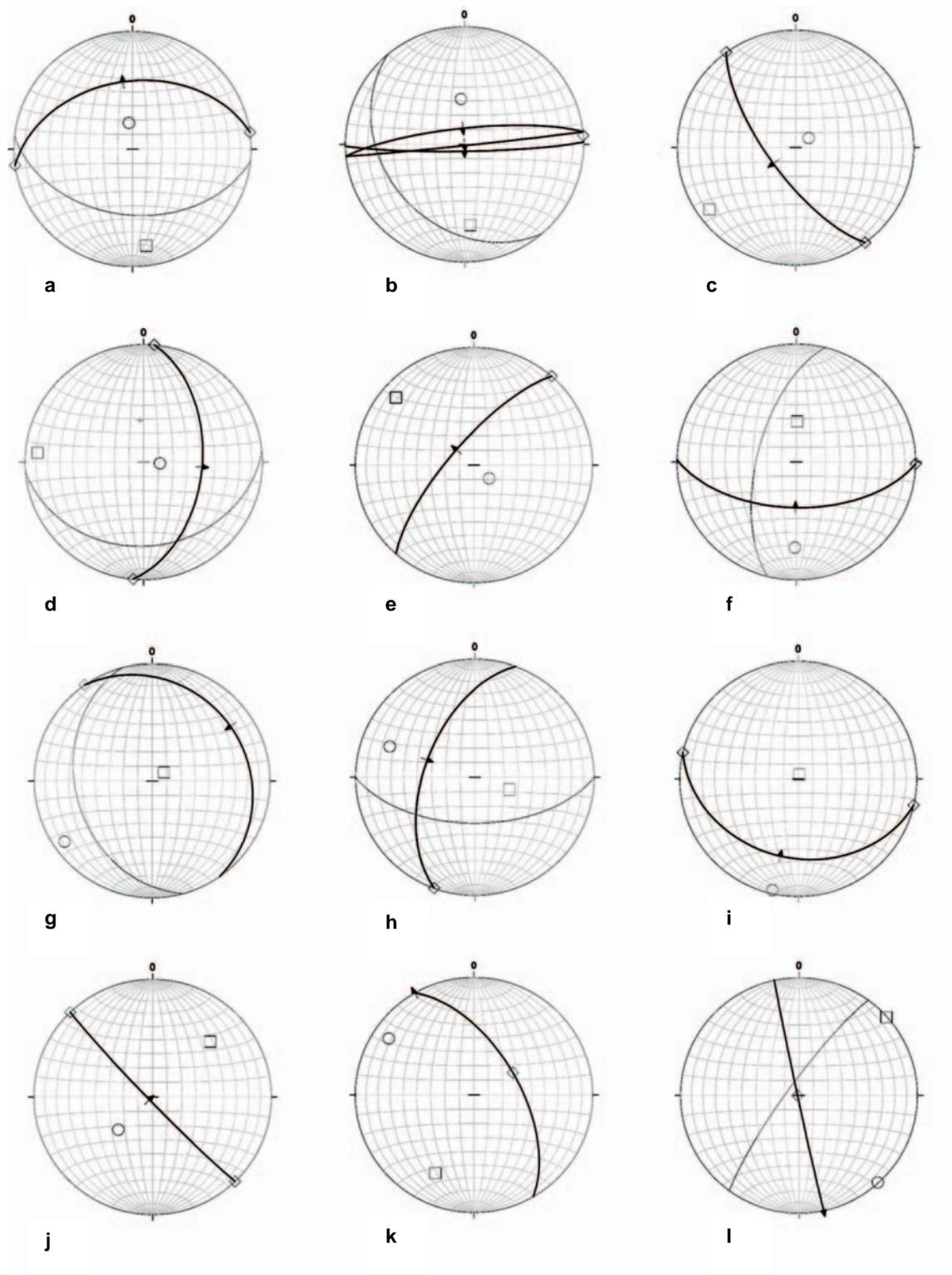


Figure 2-66: Offsets along fault planes in the study area. (a) to (e): Faults suggesting normal motion (sampling stations from (a) to (e): 6844-03, 6943-01, 6943-10, 6943-12, 6944-13). (f) to (j): Faults suggesting reverse motion (sampling stations: 6943-01 (f) to (h); 6943-13 (i) and 6943-14(j)). (k) and (l): Faults suggesting sinistral strike-slip (sampling stations: 6944-07 for (k) and 7043-02 for (l)). Bold lines represent faults offsetting features; thin lines represent features offset by the faults. Paleostress configurations were calculated for all plots. $\circ = \sigma_1$ $\diamond = \sigma_2$ $\square = \sigma_3$.

2.4.3.4 Brittle fault rocks

As already mentioned in the preceding section brittle fault rocks may already occur during initial fault formation when many small individual cracks coalesce into one major fault. Experience shows that there is a wide spectrum in the degree of fracturing in such a fault. At one end, a higher fracture density (usually with spacings of only a few centimeters or less) compared to that of the surrounding rocks is all that implies the presence of a shear zone. At the other, an up to 50 cm wide seam of brecciated rock or even completely ground up gouge along the trace of a fracture is a sure sign of displacement along it. Because of the frequent lack of unambiguous tectonic markers in most cases fault rocks are the only indicators for the fault character of a fracture. Although they cannot be used for a paleostress analysis without further kinematic indicators they still give an impression of the orientations of faults in the study area.

Brittle fault rocks were mostly found in the form of unconsolidated fault breccia and gouge. Compact breccia sheets, i.e. breccia cemented onto the fault plane, were found only in sampling station 6944-13, located in an outcrop of mylonitic/cataclastic rocks in the Rundinger Zone. The lack of cementation implies the formation of brecciated faults at relatively shallow crustal levels of up to a maximum of 4 km as described by Marshak and Mitra (1988), Snoke et al. (1998), and van der Pluijm and Marshak (1997).

Contemplating fig. 2-67 a predominance of subhorizontal to gently N(N)E and S(S)W dipping, as well as steeply inclined NE-SW striking faults becomes obvious. NW-SE striking faults are of minor importance. As for the gently inclined fracture sets, they show a distribution similar to that of the conjugate systems presented in fig. 2-54c. There, fractures parallel to the metamorphic foliation were determined to be in a conjugate relationship with gently SW dipping cross fractures. Similarly, several of the gently NE dipping fractures in fig. 2-67 were also identified as parallel to the fabric. The fact that brecciated faults are distributed in a way similar to a predominant conjugate system of fracture sets thus underscores the notion that these sets underwent fault motion and possibly formed contemporaneously at the same crustal level.

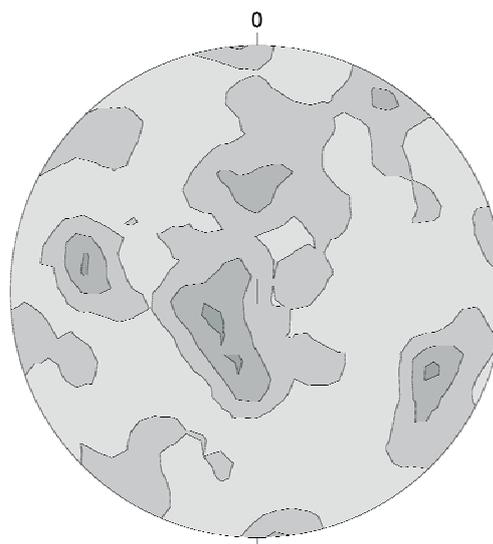
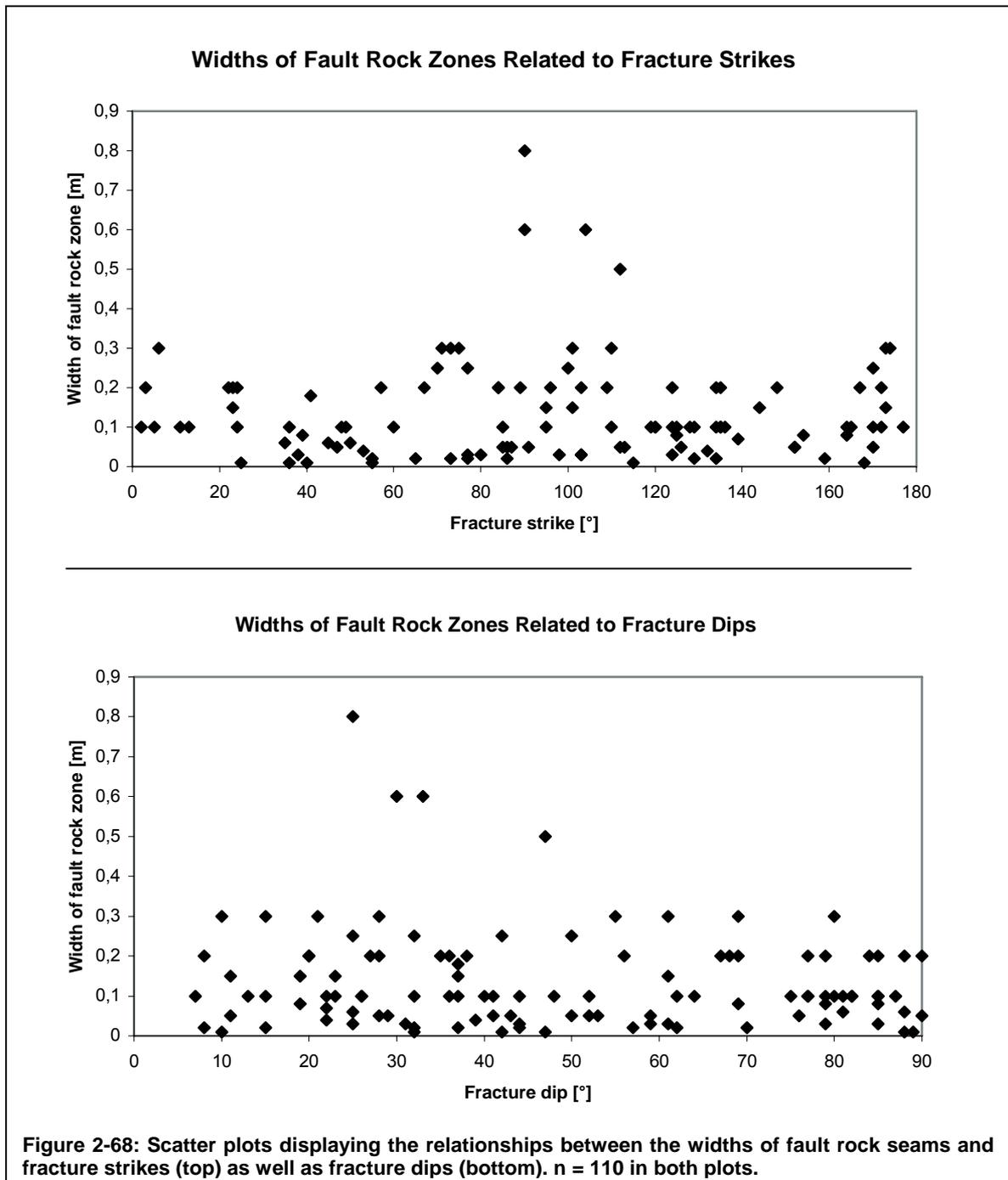


Figure 2-67: Orientations of fractures in the study area associated with fault rocks. $n = 191$. Contours represent integer mrd.



Brecciated moderately to steeply inclined N(N)E-S(S)W striking fractures can also be related to fault motion due to the fact that several slickensided planes oriented in similar ways, which suggest both normal and strike-slip displacement, were described in section 2.4.3.2. The contemporaneous formation of slickensided and brecciated faults, however, remains questionable, since the possibility exists that the slickenlines were created during the reactivation of preexisting joints. Therefore, the concurrence of fault formation (i.e. of brecciated faults) and reactivation of preexisting joints in response to one single stress field is another possible scenario. The same assumptions can be applied to the less important

NW-SE striking fractures. These concentrations also occur in the dataset of slickensided faults and thus enhance the likelihood that the brecciation along these fractures is indeed a reaction to shear displacement.

In order to obtain an idea about the directional distribution of faults associated with fault rock seams of varying widths these two parameters are plotted against each other in fig. 2-68. In the visualization of the strikes of the respective discontinuities (fig. 2-68, top) two major peaks rise above the otherwise relatively uniform dataset. Accordingly, ENE-WSW to WNW-ESE striking fractures possess the widest fault rock seams with values of up to 80 cm. A secondary peak exists in the group of \pm N-S striking discontinuities. The diagram representing the correlation with fracture dips (fig. 2-68, bottom) shows that there are several outliers around gentle to moderate inclinations among the otherwise also relatively uniformly distributed values.

Comparing these results to the general distribution of fault orientations (fig. 2-67) shows that the fractures associated with the widest fault rock seams coincide with the dominant concentrations and also align approximately with the regional strike of the metamorphic foliation (compare with fig. 2-4) as well as the conjugate set of cross fractures (compare with fig. 2-54c). Similarly, the scatter plot displaying the dip angles suggests that gently to moderately inclined foliation parallel faults and conjugate cross fractures underwent the most intense brecciation. This suggests that this type of deformation was the most active during relatively shallow-level N(N)E-S(S)W compression

2.5 Brittle tectonic history of the study area

The brittle tectonic history of the study area commenced at the time when the rocks exposed at today's topographic surface passed through the transitional regime between ductile and brittle deformation (ca. 300° - 400° C, (Eisbacher, 1991; Lowrie, 1997)) as a result of regional uplift. For the site of the Continental Drilling Program (KTB) in northern Upper Palatinate Stettner (1992) places this transition at the end of the Variscan orogeny, i.e. the Late Permian, when the P-T regime reached lower greenschist to zeolite facies conditions. According to him, the earliest brittle structures exist as granite, aplite and pegmatite dikes and veins possessing orientations similar to those of later fractures. Measurements of granite, pegmatite and aplite veins made in the course of this study (see section 3.3) corroborate this assumption. The analogy to the KTB site, located in the Bohemian terrane, is valid, because it was sutured to the Moldanubian terrane prior to 320 Ma (Coyle and Wagner, 1995) and thus has shared a common geologic evolution since then. However, some regional variations in uplift rates due to differential block tectonics have to be

taken into account. Fission track analyses performed by the same authors suggest that temperatures had dropped to approximately 300° C by the Late Permian (250 Ma), which they translate to an overburden of 10 to 11 km (assuming a present-day geothermal gradient of ca. 28° K/km). However, the overburden thickness most likely has to be estimated somewhat lower due to the presence of the cooling Variscan plutons, which surely contributed to elevated subsurface temperatures.

The preexisting planes of weakness, such as mylonitic and metamorphic fabrics, utilized by some of the younger brittle faults and joints most likely date from pre-Permian deformation events, for instance the – possibly Devonian to Carboniferous – mylonitization along the PFZ (Behr et al., 1980). The relationship between brittle and (semi-)ductile petrofabrics is evidenced by the ubiquity of fractures parallel to the metamorphic foliation.

Most authors agree on the Permo-Triassic onset of brittle tectonics in the Eastern Bavarian basement. Around the KTB-location, Stettner (1992) associates the initial formation of the majority of fracture systems with greenschist to lower zeolite facies conditions due to the presence of hydrothermal mineral precipitates such as quartz, epidote, chlorite etc. on fractures of various orientations. According to Colye and Wagner (1995) these conditions had prevailed from the Late Permian to the commencing Late Cretaceous when a new phase of relatively rapid uplift had lowered the temperature to approximately 100° C -the partial annealing zone temperature for apatite- by the very end of the Mesozoic. During this approximately 150 Ma lasting period a part of the joints and faults bearing mineral coatings and lineations has most likely formed.

The rakes of slickenlines discussed in section 2.4.3.2 suggest initial dip-slip displacement due to the fact that mineralized – and therefore presumably older – fractures are significantly more often associated with subvertical lineations than unmineralized ones. Nonetheless, lineations with subvertical rakes also occur to some extent on unmineralized discontinuities. This and the field observation that on several fractures subvertical slickenlines overlie subhorizontal ones lead to the conclusion that phases of dip-slip (i.e. regional uplift and extension) and phases of strike-slip (i.e. regional compression) alternated with dip-slip displacement being the last to be recorded by the formation of slickenlines.

However, slickensided faults associated with mineral precipitates possess orientations similar to those of unmineralized discontinuities, so it remains debatable whether the faults are primary structures or if they initially formed as joints and were reactivated in a later phase of deformation. Comparing the cumulative plots of dip-slip faults in figures 2-56 and 2-57 to the plot of purely extensional joints in fig. 2-49 similarities between the

orientations of faults and joints become evident. Slickensided fractures frequently dip very steeply to subvertically. In addition, plumose structures overprinted by slickenlines were observed on some planes. Thus, an origin as extensional joints followed by a later polyphase reactivation as strike-slip and/or dip-slip faults is likely for many of the slickensided planes. Unfortunately for this case, hydrothermal precipitation is possible over a wide range of temperatures, depending on the saturation of the fluids and the pressure exerted on them. Therefore, taking into account the average exhumation rates determined by Coyle and Wagner (1995) for the area S of the KTB location, hydrothermal activity must have been possible until the Neogene and thus cannot be used for the dating of presumed Tertiary mineralized faults. This renders the distinction between mineralized and unmineralized fractures rather ambiguous, because only a relatively short period of time can be ruled out to have been affected by hydrothermal activity. Thus, other explanations for the heterogeneously distributed rakes on mineralized and unmineralized fault planes in fig. 2-65 might be that the hydrothermal fluids did not circulate through the entire fracture network at times, or, as noted before, that fault motion reactivated previously created and mineralized joints.

As already mentioned in section 2.4.3.2 it is mostly difficult to distinguish whether slickenlines on mineralized fault planes are primary (i.e. slip fibers formed during initial fracture formation associated with hydrothermal activity) or secondary (i.e. groove lineations formed under “dry” conditions during the reactivation of joints) features. However, notwithstanding their obscure origin both mineralized extensional joints and slickensided dip-slip faults suggest regional uplift at some point during the period of hydrothermal activity while strike-slip faults are a sign for horizontal regional compression.

In order to decipher the sequence of events leading to the formation of the slickenline patterns described above previous work about the brittle tectonic evolution of areas bordering the Moldanubian Mass has to be consulted. Due to the scarcity of tectonic markers in the granite and gneiss lithologies a timeframe for the brittle deformation of the study area can be established only in relationship to the Mesozoic and Tertiary stratigraphy absent in the crystalline basement. Thus, one has to rely on the works of Bergerat and Geysant (1982; 1983), who compiled one of the very few both detailed and comprehensive brittle deformation histories of Eastern Bavaria, to chronologically arrange the phases evidenced by the field database.

In summary, the following table gives an impression of the stress fields determined in this study from kinematic indicators in the study area:

Stress field	Active structures	Kinematic indicators
NE-SW compression	ENE-WSW striking faults (sinistral strike-slip) N(NE)-S(SW) striking faults (dextral strike-slip) ± NW-SE striking faults (thrust & reverse)	Slickensides, Slickensides Conjugate sets
N(N)W-S(S)E compression	± N-S striking faults (sinistral strike-slip) ± NW-SW striking faults (dextral strike-slip)	Slickensides, Offsets Slickensides
N(NE)-S(SW) extension	subvertical ENE-WSW striking reverse faults ± E-W striking normal faults	Slickensides Offsets
NE-SW extension	NW-SE striking normal faults	Slickensides, Conjugate sets, Offset
E-W extension	N-S striking normal faults	Conjugate sets, Offset
NW-SE extension	NE-SW striking normal faults	Slickensides, Offset

Table 2-8: Brittle tectonic paleostress fields active in the study area based on data from this study. No chronological order implied.

Several of the abovementioned stress regimes deduced from the field data can be attributed to one of Bergerat and Geyssant's (1983) tectonic phases. The authors begin with a suspected Cretaceous N-E extensional phase, for which they did not find evidence in the Franconian Jurassic or the crystalline basement. This regime is associated with the opening of the Penninic Ocean in the South of the European plate. Only further to the West, in the Swabian Jura did this stress regime occur. It therefore is questionable if the N(NE)-S(SW) extensional stress field listed in table 2-8 belongs to this early tectonic stage, because the offsets evidencing N and S directed normal motion are associated with presumably younger breccia seams. Only the very few slickensided reverse faults could hint at this type of deformation. Although it is uncommon to attribute reverse motion to an extensional regime the plot in fig. 2-59a suggests a very steeply inclined σ_1 in combination with gently dipping extension. This is due to the frequently subvertical faults along which reverse displacement was detected. Since they usually undulate somewhat the sense of motion is difficult to determine, which can make them normal and reverse in different sections along their traces. Thus, crustal extension is a thinkable mechanism for their formation.

The first stress field derived from Bergerat and Geyssant's (1983) dataset is a horizontal N-S compression, attributed to the Upper Eocene indentation of the European plate by the advancing Alpine orogenic front. This indentation is bordered by the NNE-SSW striking Rhinegraben in the West and the NW-SE trending Elbe line in the East, thus forming the Germano-Czech triangle. The Hercynian structures in the Bavarian Forest, such as the Pfahl fault zone strike subparallel to the latter and therefore adopt their sense of displacement, i.e. dextral strike-slip. In the database to this study this type of deformation is manifested in the slickensided NW-SE striking (frequently foliation parallel) strike-slip faults

and the conjugate sinistral N-S trending strike-slip faults. The maximum compressional stress calculated from the orientations of these faults, however trends somewhat to the W of N, which is still within the limits of local variations also present in Bergerat and Geysant's records.

The authors report an ensuing Oligocene E-W to ENE-WSW directed extensional phase due to the E directed entrainment of Europe by Africa after the suture between these two plates had been established. This eastward motion caused the rifting along the Rhinegraben and subduction in the Carpathians. The region of the Bavarian Forest was therefore situated in a transitional regime between extension in the West and compression in the East. The net effect, however, was the mentioned E-W to ENE-WSW extension. The dataset for this study shows two types of structures, which may be attributed to this regime. Clear evidence for it comes in the form of N-S striking conjugate fault sets, Bergerat and Geysant observed a rotation of the extensional direction towards ENE-WSW in the vicinity of the large hercynian fault systems. Findings in this study corroborate this assumption, because slip lineations on preexisting NW-SE striking faults suggest normal motion. Yet the paleostress calculations for these faults indicate an even further rotation of the direction of extension to NE-SW.

At the Oligocene-Miocene interface the stress situation becomes inversed due to the stoppage of the Carpathian subduction and contemporaneous onset of the ridge push exerted by the opening Atlantic Ocean. According to the abovementioned authors this results in a NE-SW compressional regime. This tectonic phase is also reflected in the dataset for this study in the form of \pm ENE-WSW striking left-lateral and \pm N-S striking right-lateral strike-slip faults. Hereby, the displacement is evidenced solely by slickensides.

The latest deformational event described by Bergerat and Geysant (1983) is a N-S directed extension present only in Southern Franconia. It has been dated Aquitanian-Helvetian and attributed to subsiding graben structures accompanied by alkalic volcanism. The region of this study did not undergo this kind of deformation. Moreover, it is likely that the extension in the North translates to N-S compression in the Bavarian Forest, which is suspected to be the latest tectonic phase for the study area. The onset of this stage is proposed to be Early Miocene by Bergerat and Geysant when convergent plate movements between Africa and Europe resumed. The faulting associated with brecciation (section 2.4.3.4) along (N)NE dipping fractures parallel to the metamorphic foliation and the formation of conjugate (S)SW dipping cross fractures (section 2.4.3.1) is thought to be a result of this compression. These features are attributed to the youngest deformation for several reasons: According to Snoke et al. (1998) brecciation occurs at very shallow crustal levels of up to a

depth of 4 km. Considering the continuous uplift of the region since the Cretaceous the shallowest structures should also be the youngest. Also, fractures possessing breccia seams occasionally cut across older discontinuities and several offset features were found along these faults.

However, the recent stress fields at shallow depths determined by the World Stress Map (WSM) project for locations N and S of the study area (Reinecker et al., 2005, see appendix H) suggest a horizontal σ_1 trending slightly West rather than East of North. Unfortunately, no stress data is available for the Central Bavarian Forest per se, so local variations cannot be observed. Nonetheless, a certain degree of scatter exists in the WSM dataset, and a local variation from the regional stress field is conceivable due to the fact that faulted foliation planes presented preexisting planes of weakness somewhat misaligned with respect to the compressive stress.

In agreement with the findings of Bergerat and Geysant (1983) the following sequence of events can be deduced from the brittle tectonic data obtained for this study:

Period/Epoch/Age	Regional Tectonic Event	Characteristic Structures
Late Paleozoic/ Late Variscan orogeny	Initial semi-ductile deformation along large regional fault lines such as the Pfahl Fault zone, the Rundinger Zone, or the Donaurandbruch, most likely due to oblique dextral strike-slip	Mylonite seams along the large fault lines, in part intruded by Permo-Triassic hydrothermal precipitates
Mesozoic until Cretaceous	Regional uplift at different rates and crustal extension	Mineralized joints, few slickensided, \pm E-W striking dip-slip faults
Upper Eocene	Indentation of the European plate by the advancing Alpine orogenic front	Dextral strike-slip along NW-SE faults, sinistral strike-slip along \pm N-S faults
Oligocene	Eastward motion of the European plate and subduction in the Carpathians due to the pull of the sutured African plate, crustal E-W extension	Normal reactivation of NW-SE striking faults, N-S striking conjugate sets
Oligocene-Miocene	Ongoing eastward motion of the European Plate, but stoppage of the subduction in the Carpathians. Result: inversion of the stress field to a NE-SW compressional regime	Sinistral strike-slip along \pm ENE-WSW striking faults; dextral strike-slip along \pm N-S striking faults
Early Miocene until Recent	\pm N-S (in the study area rather \pm NNE-SSW) compression due to the further converging European and African plates	Foliation parallel brecciated thrust faults and antithetic cross faults

Table 2-9: Sequence of brittle tectonic events since the Mesozoic as compiled from data of this study and Bergerat and Geysant (1983).

2.6 References

- Ahnert, F., 1999, Einführung in die Geomorphologie: Stuttgart, Ulmer, 440 p.
- Anderson, E.M., 1942, The Dynamics of Faulting and Dyke Formation with Applications to Britain: Edinburgh, Oliver and Boyd, 191 p.
- Barton, C.C., Larsen, E., Page, W.R., and Howard, T.M., 1993, Characterizing fractured rock for fluid-flow, geochemical, and paleostress modeling: Methods and preliminary results from Yucca Mountain, Nevada: Denver, Colorado, United States Geological Survey.
- Behr, H.J., Engel, W., and Franke, W., 1980, Guide to excursion, Münchberger Gneismasse und Bayerischer Wald, April 12-15, 1980: Göttingen, Federal Republic of Germany, Geol.-Palaeontol. Inst. Mus., 100 p.
- Bergerat, F., and Geysant, J., 1982, Tectonique cassante et champ de contraintes tertiaire en avant des Alpes orientales: le Jura souabe: Geologische Rundschau, v. 71, p. 537-548.
- , 1983, Fracturation tertiaire et evolution des contraintes en Baviere orientale; le Jura franconien et la foret bavaroise (R. F. A.): Geologische Rundschau, v. 72, p. 935-953.
- Cheema, T.J., and Islam, M.R., 1994, Experimental Determination of Hydraulic Anisotropy in Fractured Formations: Bulletin of the Association of Engineering Geologists, v. 31, p. 329-341.
- Coyle, D.A., and Wagner, G.A., 1995, Spaltspuren - ein Beitrag zur postvarizischen Tektonik und Abtragung des KTB-Umfelds: Geowissenschaften, v. 13, p. 142-146.
- Eisbacher, G.H., 1991, Einführung in die Tektonik: Stuttgart, Enke, 310 p.
- Freeze, A.R., and Cherry, J.A., 1979, Groundwater: Englewood Cliffs, N.J., Prentice-Hall.
- Lowrie, W., 1997, Fundamentals of Geophysics: Cambridge, Cambridge University Press, 354 p.
- Marshak, S., and Mitra, G., 1988, Basic Methods of Structural Geology: Englewood Cliffs, N.J., Prentice-Hall Inc., 446 p.
- Raum, K.-D., 2002, Markierungstechnische, bruchtektonisch-gefügekundliche und fotogeologische Untersuchungen zur Ermittlung der Grundwasserfließverhältnisse in der Verwitterungszone kristalliner Gesteine in Quellgebieten des Oberpfälzer/Bayerischen Waldes (Ost-Bayern/Deutschland) [PhD Dissertation thesis]: Erlangen, Friedrich-Alexander Universität Erlangen-Nürnberg.
- Reinecker, J., Heidbach, O., Tingay, M., Sperner, B., and Müller, B., 2005, The 2005 release of the World Stress Map, Retrieved: 29.11.2006 from www.world-stress-map.org
- Rohrmüller, J., Mielke, H., and Gebauer, D., 1996, Tektonik, Grundgebirge, Erläuterungen zur Geologischen Karte von Bayern 1:500.000: München, Bayerisches Geologisches Landesamt, p. 252-259.
- Snoke, A.W., Tullis, J., and Todd, V.R., 1998, Fault-related rocks: a photographic atlas: Princeton, New Jersey, Princeton University Press, p. 617.

Stettner, G., 1992, Geologie im Umfeld der Kontinentalen Tiefbohrung Oberpfalz - Einführung und Exkursionen: München, Bayerisches Geologisches Landesamt, 240 p.

Stone, J.R., 2002, Characterization of bedrock aquifers in Connecticut: (1) Geologic mapping and analysis., Geological Society of America Northeastern Section, Annual Meeting: Springfield, Massachusetts, Geological Society of America, p. A-23.

van der Pluijm, B., and Marshak, S., 1997, Earth Structure: An Introduction to Structural Geology and Tectonics, WCB/McGraw-Hill, 495 p.

Zeitlhöfler, M., 2003, Bedrock Structure in Southeastern Connecticut: Hydrologic Implications. [Master's thesis]: Middletown, CT, Wesleyan University.

3 Photogeologic analyses and geostatistics

3.1 Lineament analyses using an interferometric RADAR (INSAR) Digital Elevation Model

The analysis of the digital elevation model created from RADAR data compiled by the European Remote Sensing Satellite (ERS-DEM, fig. 3-1) yielded valuable information on the regional basement structure of the central Bavarian Forest. As explained in the methodology (section 1.5.2.2) the altitude data (fig. 3-2a) was transformed into a raster image depicting the exposition of each pixel (“aspect-raster”) in order to enhance the visibility of linear features on the ERS-DEM raster (fig 3-2b). Figure 3-3 shows an image combining the ERS-DEM with the aspect raster. Note that the interpretations below all relate to the study area *sensu stricto*, not the entire extent of the DEM.

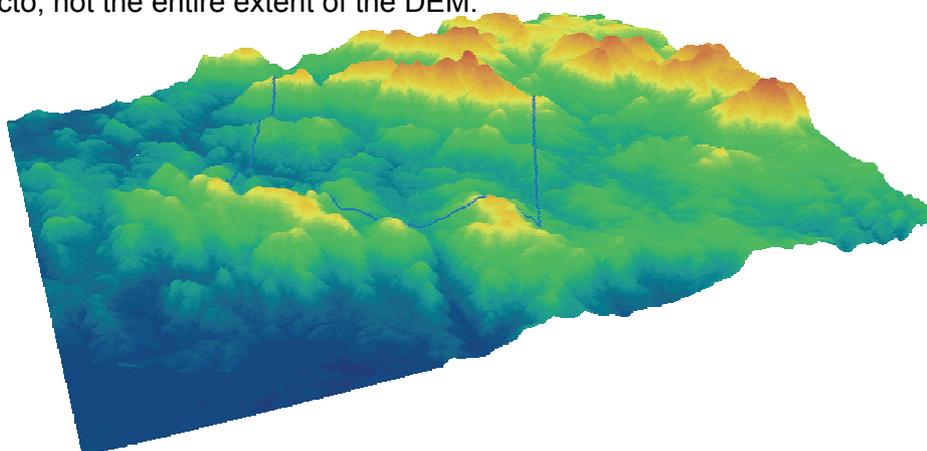
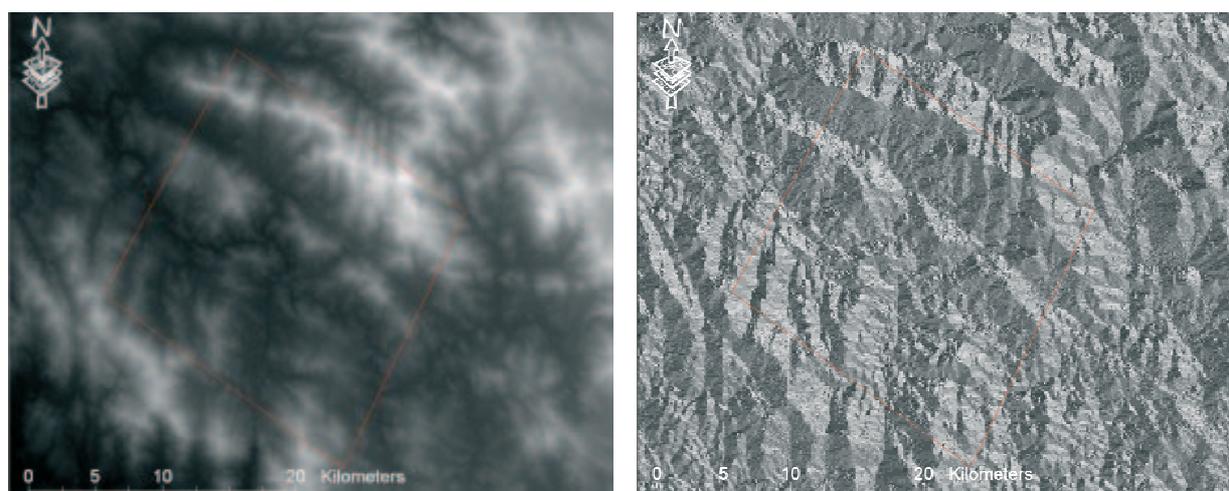


Figure 3-1: Three dimensional visualization of the ERS-DEM of the central Bavarian Forest. Image size is approximately 56 x 45 kilometers. Vertical exaggeration is 6.17979. Blue line depicts the boundaries of the study area *sensu stricto*.



a

b

Figure 3-2: (a) 2D view of the ERS-DEM. Grayscale depicts altitude above sea level. (b) 2D view of the ERS-DEM aspect raster. Grayscale depicts exposition of each pixel. Red square shows the study area *sensu stricto* in both images.

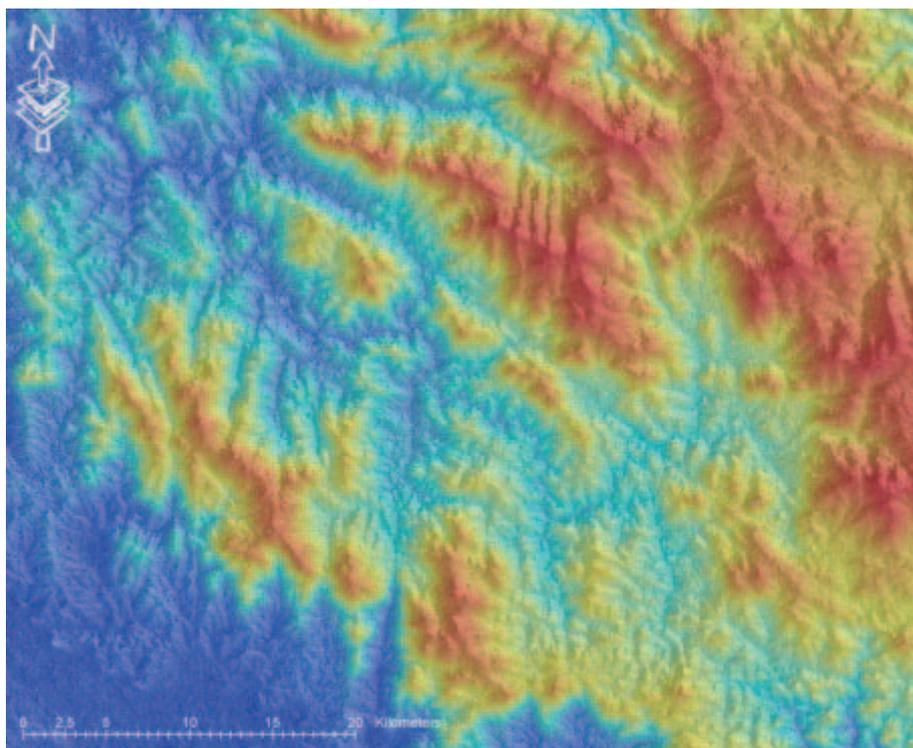


Figure 3-3: ERS-DEM image combined with the aspect raster. Elevation is depicted as blue-to-red-scale, aspect as semitransparent grayscale.

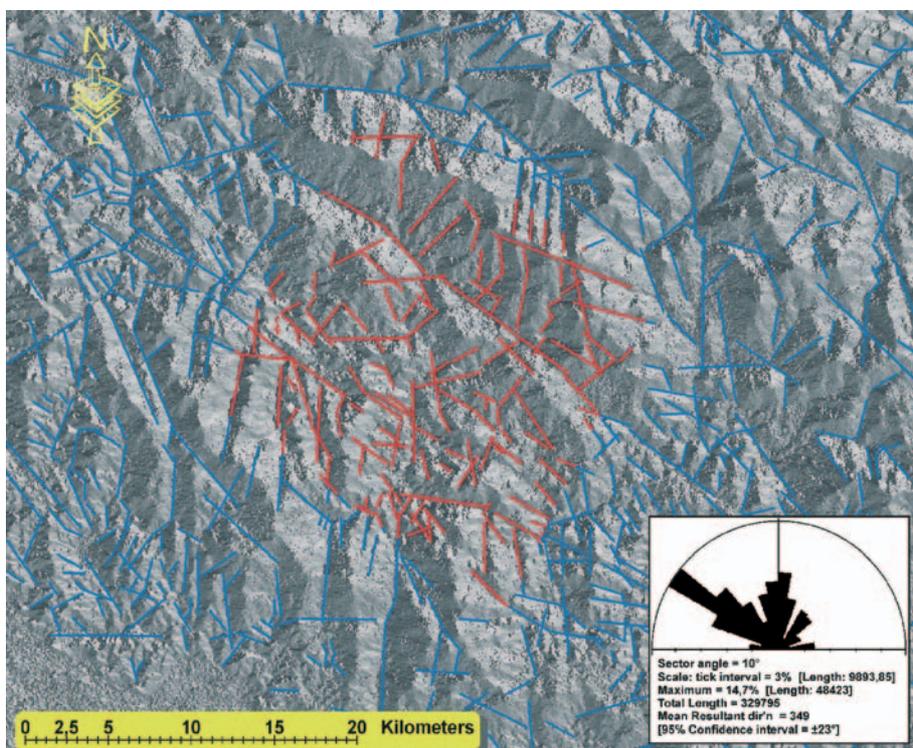


Figure 3-4: Example for one iteration of the lineament analysis. Blue lines: lineaments traced throughout the entire extent of the DEM; red lines: lineaments inside the study area sensu stricto. Inset: Rose diagram depicting length-normalized lineament orientations in the study area sensu stricto.

An example for one of a total of seven analysis runs is presented in figure 3-4. The resulting 234 lineaments for the study area *sensu stricto* are plotted length-normalized in the rose diagram on the inset. The numbers and diagrams described below relate to the cumulative results of all of the seven analysis runs.

Some authors differentiate between “fracture traces” and “lineaments”. According to Cheema and Islam (1994) a lineament is defined as “a fracture trace that is at least one mile long and may be expressed continuously or discontinuously for many miles.” On the other hand, fracture traces are by definition less than one mile (ca. 1.6 km) long. In this study these two terms are used widely synonymously. Only in specific cases “lineament” is used to describe a rather large linear feature as opposed to a rather localized “fracture trace”.

3.1.1 Results

3.1.1.1 General observations

From the visual inspection of figure 3-3 alone it becomes obvious that the study area possesses several predominant orientations of topographic features. The most striking among them are the very extensive and continuous NW-SE trending valleys together with the somewhat less prominent N-S trending lineaments. Although the N-S features are generally shorter and less continuous there is one large topographic low cutting through all of fig. 3-3 slightly left of the image’s center. Considering that locally very thick blankets of soil and weathered bedrock attenuate the topographic relief, the underlying structure still shows through and allows the localization of brittle deformed zones. As will be detailed in section 3.1.2 there are some drawbacks which demand caution in the interpretation of some of the information the DEM provides, but the following will show in a semi-quantitative way that the DEM is a valuable tool for the interpretation of the study area’s basement structure.

The seven consecutive analysis runs produced a total of 1714 linear features with lengths of one meter to 14.4 kilometers. After the elimination of the sampling noise (see 1.4.2.2) the number of lineaments in the study area *sensu stricto* was reduced to a total of 1430 linear features. The very short lineaments (shorter than approximately 100 meters) cannot have originated from the sampling process, since the pixel size is 25 meters and some distance is required to draw a lineament. These are artifacts from the clipping process (figure 3-4), during which some lineaments along the border of the study area *sensu stricto* have been cut off. After removing all lineaments with lengths shorter than 100m the final number reaches 1310 (fig. 3-5). For this number the mean and median lineament lengths are 1494 and 1262 meters, respectively, with a standard deviation (1σ) of 1223.14.

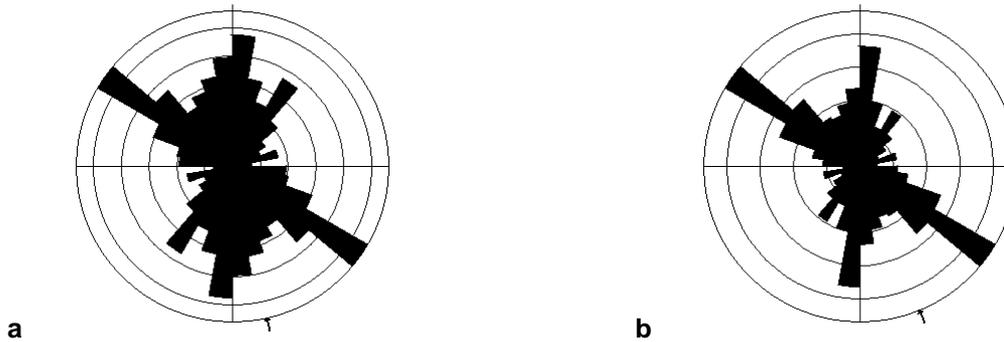


Figure 3-5: Cumulative lineament orientations mapped in the seven consecutive analysis runs. (a) Rose diagram depicting lineament strikes in the study area sensu stricto normalized to their absolute number per 10° strike bin. (b) Rose diagram depicting lineament strikes in the study area sensu stricto normalized to their cumulative length per 10° strike bin. Total cumulative length: 1957102 meters. n = 1310 in both plots. The data was plotted in the northern half-circle and then projected into the southern as a mirror-image in order to obtain a full-circle rose-diagram. The numeric values for each strike bin are listed in table 1. Data source: ERS-DEM Aspect Raster.

Orientation (°)	270-279	280-289	290-299	300-309	310-319	320-329	330-339	340-349	350-359
count	50	53	80	147	94	66	75	87	104
length (m)	64961	84468	151669	274785	154548	101077	95655	113412	138105
Orientation (°)	0-9	10-19	20-29	30-39	40-49	50-59	60-69	70-79	80-89
count	125	85	65	96	56	36	29	44	18
length (m)	213262	117841	74207	112962	74125	53230	36054	65932	30806

Table 3-1: Numbers and cumulative lengths of lineaments per 10° increment of orientation (counted clockwise on a half-circle from West to East). n (lineaments) total = 1310. Data Source: ERS-DEM Aspect Raster.

Orientation (°)	270-279	280-289	290-299	300-309	310-319	320-329	330-339	340-349	350-359
Min. Length (m)	159.6	113.2	128.9	108.8	102.7	132.1	104.9	135.9	121.9
Max. Length (m)	5197.7	4898.0	10082.7	14359.0	4919.0	4791.8	3623.2	5334.7	5489.0
Mean Length (m)	1362.8	1593.7	1895.9	1869.3	1644.2	1531.5	1275.3	1270.8	1328.0
Median Length (m)	1296.7	1223.0	1211.9	1437.7	1429.9	1350.6	1018.2	1149.9	1218.2
1σ	1010.8	1215.8	1949.4	1916.8	1112.3	983.1	857.8	857.6	934.4
Orientation (°)	0-9	10-19	20-29	30-39	40-49	50-59	60-69	70-79	80-89
Min. Length (m)	105.8	117.6	118.0	107.3	124.5	124.0	117.0	111.0	134.6
Max. Length (m)	4836.8	7181.6	2671.6	4069.5	5107.6	4447.4	4305.6	3596.2	3105.2
Mean Length (m)	1704.1	1386.4	1141.7	1176.7	1323.7	1478.6	1243.3	1498.4	1711.5
Median Length (m)	1555.0	1130.5	1081.2	1074.7	1208.5	1142.5	1071.5	1525.1	1712.5
1σ	1014.1	1313.3	666.4	793.4	1069.8	1087.8	996.5	860.7	868.1

Table 3-2: Lineament length distribution per 10° strike increment with regard to minimum, maximum, mean, and median length as well as the standard deviation (1σ) per 10° increment (tabulated clockwise from West to East). n (lineaments) total = 1310. Data Source: ERS-DEM Aspect Raster.

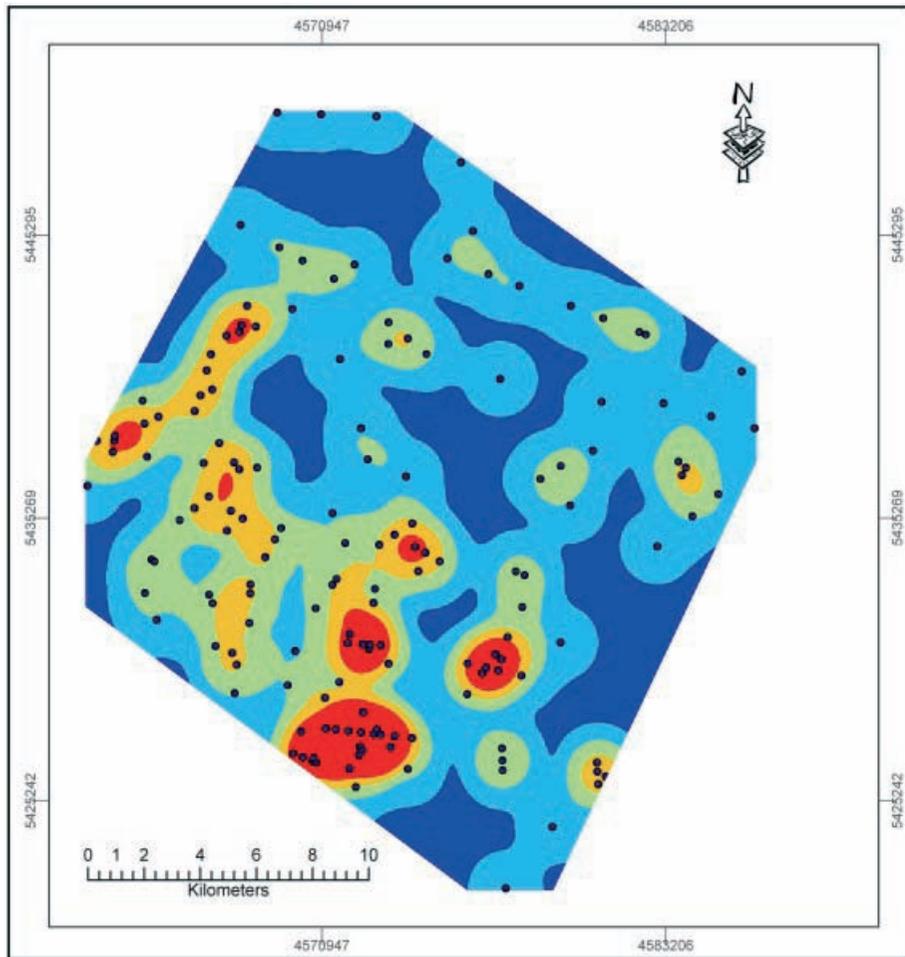
Both plots in figure 3-5 show three conspicuous peaks in the directional distribution of the lineaments. These are located in the 300°-309°, 0°-9°, and 30°-39° bins. A minor peak lies at 70°-79°. Although these bins possess the highest counts and cumulative lengths (table 3-1) the highest values of the other parameters, such as maximum, mean and median

length, (table 3-2) do not necessarily coincide with them. This has partially to do with the fact that very long lineaments could not always be traced with one single line due to their sometimes slightly curvilinear character, which could not be accounted for in the analyses. This breaking-up of otherwise continuous lines leads to somewhat lower maximum, mean, and median lengths per strike increment, so the distribution of these values is biased to a certain degree.

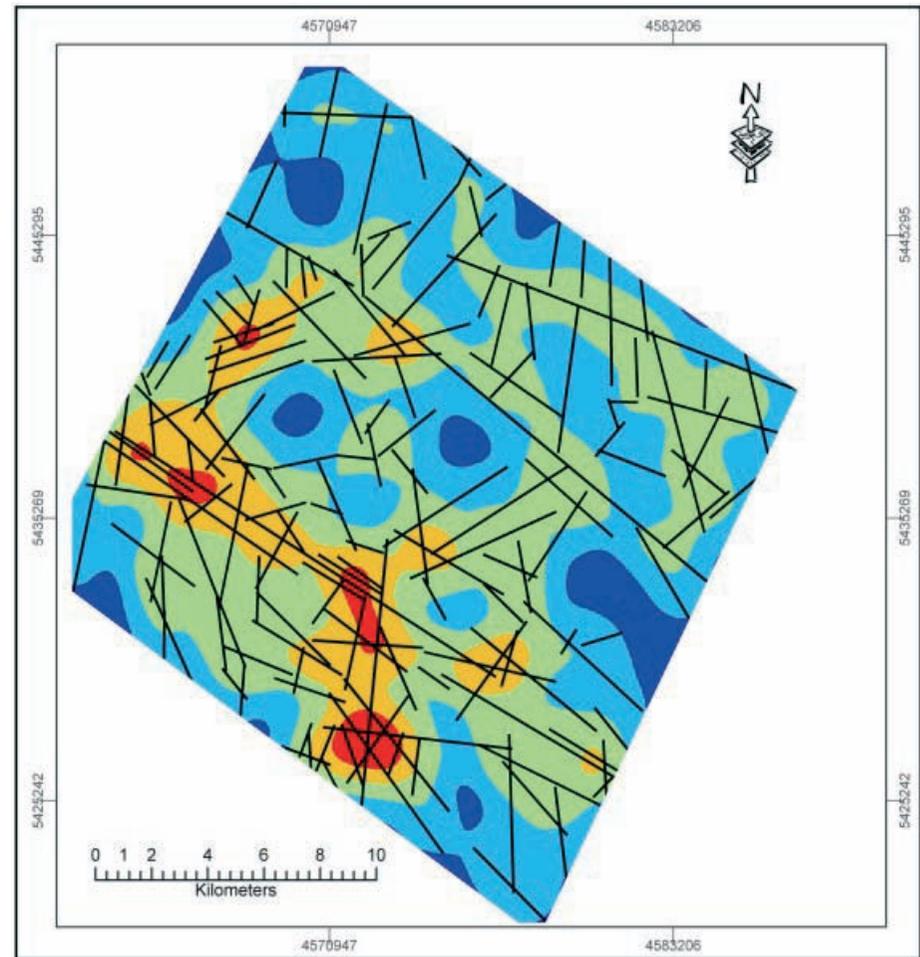
Figure 3-5a represents the directional distribution of lineaments normalized to their absolute number. As will be explained in section 3.3 this plot looks more similar to the rose diagram depicting the field data. The peaks in this plot are less pronounced, since the shorter lineaments, which do not belong to one of the major directions, are counted with the same weight as the longer ones. In order to reduce that noise, and to give a more real impression of the lineament distribution in the study area figure 3-5b depicts lineaments with regard to their lengths.

The length-normalized data shows that the NW-SE striking population (300° - 309° bin) is not only the most numerous but also possesses the highest cumulative length. A comparison with figure 3-3 corroborates this finding and at the same time shows the location of the major NW-SE lineaments. They coincide with the large valleys following the hercynian fault complexes such as the Bayerischer Pfahl or the Rundinger Zone (Rohrmüller et al., 1996a, b). In contrast to the laterally rather restricted N-S trending valleys they form deeply eroded swaths several hundreds of meters wide. From a statistical point of view the relatively large discrepancy between mean and median, as well as between minimum and maximum values for this strike segment (table 3-2) suggests a widely scattered distribution of lineament lengths while the majority is rather short relative to the mean value. This means that a relatively low number of very (several kilometers) long lineaments add up to this large cumulative length.

The second prominent population of lineaments falls into the 0° - 9° bin. Their absolute number and cumulative length being significantly smaller (table 3-1) than in the dominant population, their mean and median lineament lengths lie much closer to each other, and the range of minimum and maximum values (table 3-2) is only about half the range in the 300° - 309° segment. This indicates that the N-S lineaments are generally shorter, but relatively numerous. The comparison with figure 3-3 supports these findings. Only one large lineament cuts through the entire extent of the DEM, but had to be broken up into shorter segments to be traced accurately. Other lineaments seem to be concentrated in areas with higher elevation. However, this is likely to be biased by the fact that the lowlands (i.e. the large NW-



a



b

Figure 3-6: Lineament density map depicting the density of lineament intersections (points in fig. 6-a) and the density of lineaments (black lines; (b) below) in the study area derived from the ERS-DEM. Analysis parameters: Density type: Kernel; search radius: 2000m, output cell (pixel) size: 25m. The contour interval from low (blue) to high (red) densities is one standard deviation from the mean density.

SE valleys) do not possess sufficient relief to resolve the linear features. Also, the valleys frequently contain deeply weathered zones, in which streams can meander to a certain extent and thus blur the underlying structures.

The 30°-39° bin represents a minor, but still isolated peak. The relatively high count compared to the relatively low cumulative length (fig. 3-5, table 3-1) suggests that this strike segment consists of a relatively large number of shorter lineaments. The low values for maximum, mean, and median length lead to the same conclusion. The population is not very conspicuous in the DEM at the scale presented in figure 3-3. Only in magnified subsets do they become more obvious.

A virtually minuscule, but no less isolated peak exists in the 70°-79° bin. Although the maximum length is among the shortest in the entire sample its considerably high mean and median values (table 3-2) suggest a relatively low number of relatively long lineaments (between approximately 1500 and 3600 meters in length). As with the other minor peak, lineaments from this strike segment only show up sporadically in figure 3-3. This is partially due to their low number as well as to the large scale of the image, which only allows to clearly identify lineaments several kilometers in length.

Analyzing the spatial distribution of lineaments regions with different densities have been mapped out in the study area. For this purpose standard geostatistical methods (ESRI, 2002; Gupta, 2003) have been employed. In figure 3-6a it becomes evident that lineaments – or to be more accurate the intersections thereof- are more closely spaced in the southwestern than in the northeastern part of the map. A comparison of this image with figure 3-4 shows that the interface between the low- and high-density regions approximately coincides with the southernmost of the large NW-SE valleys (i.e. the lineament of the Pfahl fault zone). There is, however, one drawback to this visualization, since it depicts only the intersections, not the lineaments themselves. Thus, in case zones of densely spaced subparallel lineaments, which do not intersect, exist anywhere in the area of interest, they will not appear as regions of high lineament densities in this type of analysis.

In order to eliminate this potential source of error figure 3-6b depicts the actual density of lineaments per unit area. The densities in this visualization tend to be higher than in figure 3-6a, since in this case the lineaments do not have to intersect in order to be counted. However, the tendency to reach higher concentrations in the southwestern part of the study area (approximately SW of the Pfahl fault zone) shows in figure 3-6b as well.

In both images there are several regions of higher densities further to the North and Northeast. The belt of elevated concentrations along the NW border of the study area extends from Viechtach-Blossersberg in the SSW through Wiesing to Arnbruck in the NNE and thus connects the valleys of the Pfahl fault zone and the Rundinger Zone. In the northeastern part two belts of somewhat higher density – best visible in figure 3-6b - trend roughly NW-SE. The one closer to the NE border of the study area coincides with the ridge connecting the Ecker Sattel through the Mühlriegel and Hochstein with the Großer Arber. There, a WNW-ESE trending lineament cuts through the ridge at an acute angle. It is in proximity of several shorter N-S striking lineaments crossing both the northeastern and southwestern flanks of the ridge. The belt further away from the NE border of the study area follows the valley of the Rundinger Zone. There, one large NW-SE trending line intersects mainly with ENE-WSW and N-S striking lineaments.

A very conspicuous N-S trending concentration of both lineaments and lineament intersections occurs in the south-central part of the study area and reappears in several locations in the northern part. It is a section of the vast N-S striking entity separating the full-view DEM in roughly two halves (figure 3-3). In its entire length it extends from the Deggendorfer Bucht (near Zachenberg) in the South through the Ecker Sattel to the Czech border in the North.

Comparing these findings with the distribution of lithologies in the study area brings up an interesting agreement between topography and rock types. Although small-scale (1:25,000) geologic maps without any generalization show too much detail to produce an obvious connection between lithology and the distributions and densities of lineaments, regional-scale geologic units seem to correlate to a certain extent with these parameters. In the comment to the Bavarian State Geologic Map 1:500,000 (Rohrmüller et al., 1996a) a distinction is made between the higher-grade diatectic and anatectic rocks interspersed with abundant granites and diorites SW of the Pfahl zone and the relatively lower-grade cordierite-gneisses with significantly less igneous intrusions to the NE of it. Thus, an area with mainly unfoliated, near-granitic and granitic rocks tends to possess higher densities of lineaments than areas with predominantly gneissic lithologies. These rheological differences not only manifest themselves in the development of topography on a regional scale, but also in the different fracturing behavior of rocks on an outcrop scale (section 2.2).

In figure 3-7 the lineaments are separated and grouped into three major directions. As in figure 3-5 it becomes obvious that the predominant direction is NW-SE (fig. 3-7a). However, this population can be further subdivided into a group of relatively long lineaments

trending truly NW-SE and a group trending closer to NNW-SSE. A possible explanation for this phenomenon is presented in the following section. The linear structures in fig. 3-7a are concentrated in the areas of the Pfahl Fault Zone and the Rundinger Zone. Figure 3-7b depicts lineaments trending in north-southerly directions. They are generally shorter and more evenly distributed than the ones in fig. 3-7a. Only in the central part of the image (approximately located in the hills between the valley of the river Regen and the Zellertal) there is a NW-SE trending swath with a low lineament density. The lineaments in figure 3-7c are strikingly absent in areas of high densities in figs. 3-7a and b. On the other hand, they cluster in regions where lineaments of the other two groups are less abundant. Overall, they are generally the least numerous and seem to be widely absent within and south of the Pfahl Fault Zone. To a certain extent, it is possible that their presence has been veiled by lineaments of one of the other groups, especially in areas of high lineament densities, but similar distributions can also be observed in the analysis of the aerial imagery (fig. 3-14).

In summary, the topographic structures in the study area clearly follow a systematic pattern consisting of four dominant directions. While the major ones are very conspicuous in the full-view DEM (fig. 3-3), the minor ones appear only in magnified portions of the image and the rose diagrams (fig. 3-5). Nonetheless, the minor peaks are present in the fracture data set as well, in part even more strongly than the dominant ones in this analysis. The lineaments in the study area are not uniformly distributed. They tend to form clusters, which concentrate around the large NW-SE trending valleys. The highest densities of lineaments occur in the two large valleys of the Pfahl and the Rundinger Zone as well as SW of the Pfahl fault zone, an area which differs in rock type from the area NW of the Pfahl.

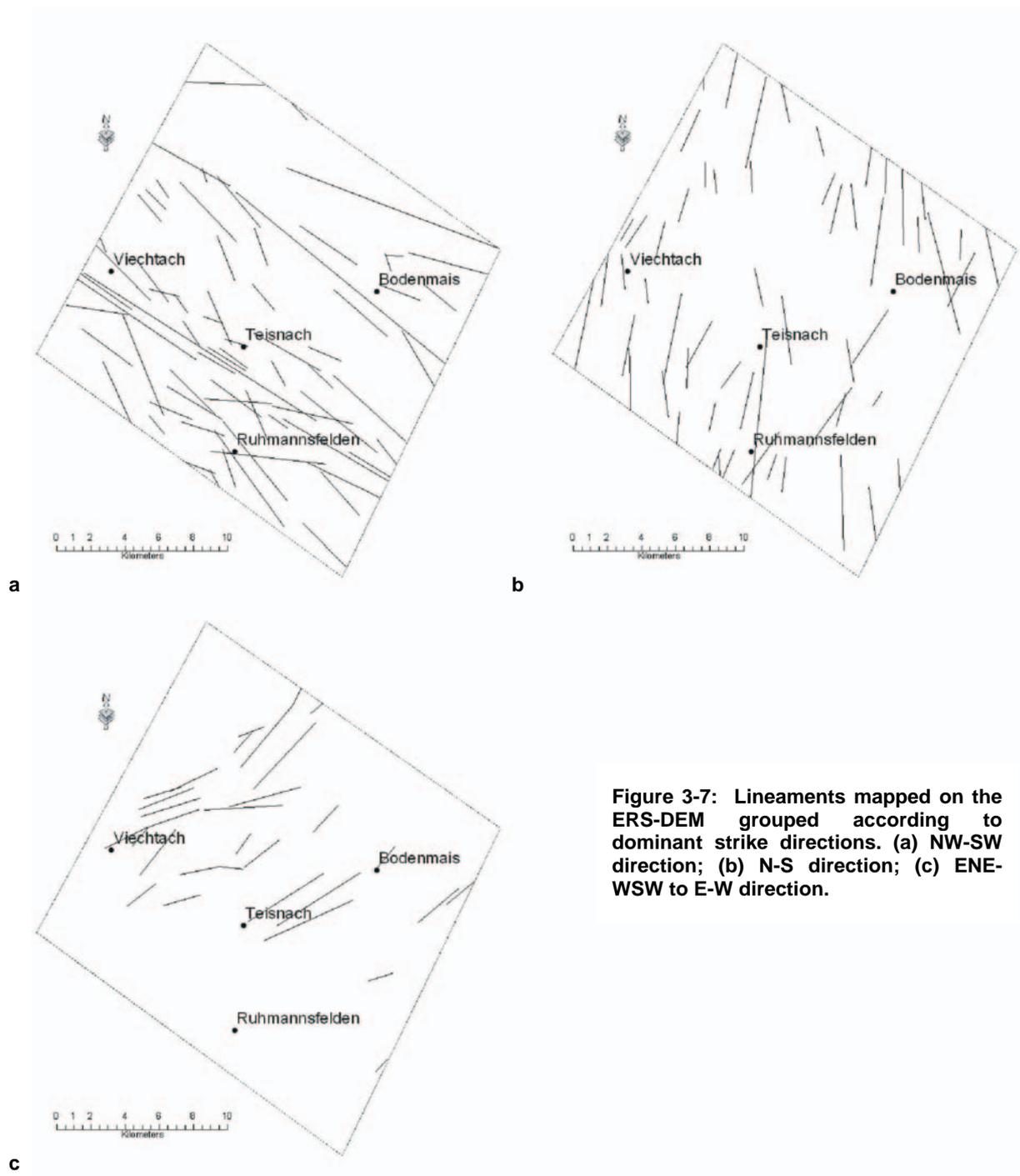


Figure 3-7: Lineaments mapped on the ERS-DEM grouped according to dominant strike directions. (a) NW-SW direction; (b) N-S direction; (c) ENE-WSW to E-W direction.

3.1.1.2 Structural analysis and tectonic interpretation of the DEM

For the structural analysis of the DEM its entire extent was used to obtain a better view of the regional tectonics. The multitude of possible lineament constellations allows for several structural interpretations of linear features, depending on the hypothetical functions the different lineament populations are assigned to.

Figure 3-8 shows one such possible constellation. In this interpretation only the large NW-SE and N-S to NNE-SSW trending lineaments are considered. Figure 3-5 identifies the 300°-309° bin as the dominant one in the NW-SE striking population. However, a certain degree of variability exists in the rose diagram, such that also the neighboring bins (especially 310°-319°; fig. 3-5a) still possess considerably high values. When comparing this with the actual DEM (figure 3-8) it becomes obvious that several large lineaments strike at an acute angle (clockwise) to the main NW-SE direction. On the micro- and mesoscopic scale such an array of fractures is known as an array of Riedel (R-) shears (van der Pluijm and Marshak, 1997) suggesting right-lateral strike-slip displacement. In this constellation the lineaments trending in north-southerly directions would act as antithetic (R'-) shears with the opposite (left-lateral) sense of displacement.

Dextral strike-slip motion is indeed the deformational mechanism several workers (Bergerat and Geysant, 1983; Hofmann, 1962) have proposed for different tectonic phases in the Pfahl fault zone. In this context the study conducted by Hofmann (1962) yields especially interesting results, since a close inspection of the map presented in his publication also suggests a Riedel-type deformational mechanism (although the author did not interpret his results that way). This tectonic phase was placed in the middle to late Permian, during which time hydrothermal activity produced the massive quartz deposits visible at the surface today. The hydrothermal fluids intruded syntectonically into an en-echelon array of extensional fractures, which indicates dextral strike-slip during a "rift-and-wrench" tectonic phase (Rohrmüller et al., 1996b). The stress regime Hofmann (1962) concluded resulted in a NW-SE directed maximum principal stress. However, this interpretation cannot account for the shear sense encountered at one of the accessory faults of the main Pfahl zone. This fault can be seen at the western border of the DEM (fig. 3-8; NNW-SSE trending dashed line). In this analysis of the DEM it was interpreted as a synthetic Riedel shear accessory to the main Pfahl fault (solid lines in fig. 3-8). Hofmann (1962) identified this lineament as the "Dietersdorfer Nebenpfahlsystem" and mapped it as an en-echelon array of silicified extensional fractures, which also suggested a dextral sense of displacement.

Since several such lineaments were detected in the DEM (fig. 3-8) a synthetic Riedel-relationship between the large hercynian fault zones and the lineaments trending slightly to their NNW is one possible interpretation of this dataset. The related stress field is assumed to be a NNW-SSW to N-S directed subhorizontal compression (figs. 3-8, 3-9). Unfortunately, there is little data on sinistral strike-slip motion along the lineaments trending in north-southerly directions, which would represent the antithetic shears in this model. However, this type of displacement has been detected in the field (this study; Bergerat and Geysant, 1983), but has been placed in the Upper Eocene (Bergerat and Geysant, 1983). Gromes (1980) devised a similar model of synthetic and antithetic Riedel-type shears for the Dietersdorfer Nebenpfahl based on the analysis of aerial imagery and field investigations.

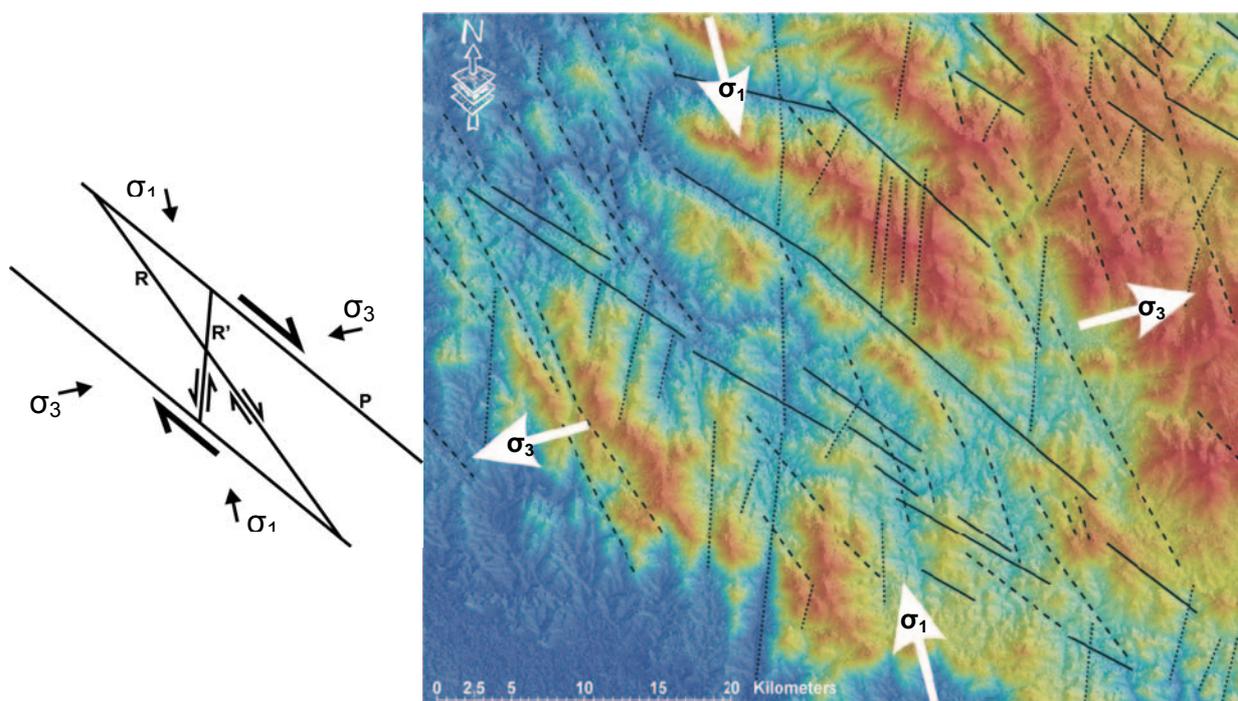


Figure 3-8: Structural interpretation of the Digital Elevation Model of the Study Area. Left: Riedel-type shear model. Right: DEM lineaments. Solid lines: main slip planes; dashed lines: synthetic (R-) Riedel shears; dotted lines: antithetic (R'-) Riedel shears. White arrows: maximum (σ_1) and minimum (σ_3) principal stresses resulting from the lineament geometry.

Figure 3-9 gives an impression of the cumulative orientations of the lineaments mapped in figure 3-8. It shows three dominant strike directions. The NW-SE and N-S trending populations form a 60° conjugate angle, the NNW-SSE trending one is interpreted to function as synthetic Riedel (R-) shears, although the angle between the NW-SE and the synthetic NNW-SSE lineaments seem rather large for a Riedel relationship.

This interpretation implies that the Late Permian deformational event produced a fault pattern, which, after several phases of brittle reactivation, is responsible for the geomorphological development of the central Bavarian Forest and its surroundings.

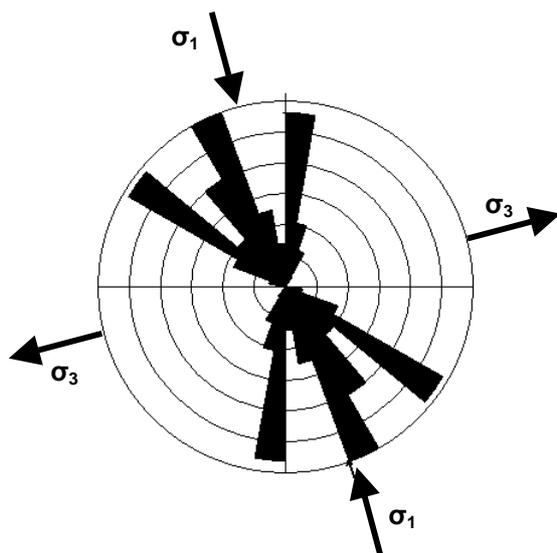


Figure 3-9: Rose diagram depicting the lineament orientations presented in fig. 6 (length-normalized). Black arrow shows maximum (σ_1) and minimum (σ_3) principal stresses resulting from the lineament geometry.

A somewhat different interpretation agrees better with the “rift- and wrench- tectonics” model for post-variscan uplift of the area mentioned by Rohrmüller et al. (1996b). This model proposes a transtensional mechanism including crustal extension due to regional uplift and strike-slip displacement. In this case the main NW-SE trending fault planes are still interpreted as strike-slip faults with right-lateral shear-sense. Also, the synthetic Riedel shear faults proposed in the previous interpretation fit in. However, the N-S trending lineaments would then have initiated as extensional fractures with no displacement in the beginning (figure 3-10). Both normal and strike-slip displacement along the N-S striking lineaments, which were detected in the field, would be due to a later reactivation. The appealing aspect of this interpretation is that an extensional tectonic regime allows for the rise of hydrothermal fluids providing the raw material for the ubiquitous quartz mineralizations on fracture planes of virtually all major populations. Rohrmüller et al. (1996b) placed this event at the

Permian/Triassic interface, the beginning of the brittle tectonic deformation of the area.

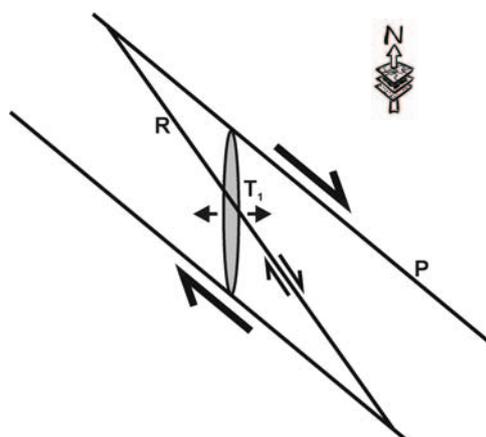


Figure 3-10: Structural Interpretation of the Digital Elevation Model of the Study Area (fig. 8). P: Main Slip planes; R: Synthetic Riedel (R-) shear planes; T₁: Extensional fractures.

Regardless which interpretation yields the most convincing arguments there is still a significant amount of uncertainty as to the exact origin of each set of lineaments and their relationships to each other. The DEM is only a momentary snapshot of the present-day morphology of the area and represents the cumulative result of a number of tectonic phases that have deformed the regional bedrock throughout its geologic history.

3.1.2 Difficulties with the interpretation of DEM data

During the interpretation of the ERS-DEM several difficulties arose. A major problem, which inherently exists in data covering such a large geographical extent has to do with scale and resolution. As mentioned in section 1.5.2 the model's resolution is 25 x 25 m, and its horizontal extent covers 45 x 56 km. For the detection of major structural entities such as the large Hercynian fault complexes large scales are needed, but at the same time the ability to identify local features is limited. Minor faults and fracture zones, which do not produce significant topographic relief do not show up in the DEM. Also, little relief frequently results in highly variable expositions of the topographic surface, very similar to the higher variability in the strikes of gently dipping fractures. Since the aspect raster depicts the exposition of every pixel a high variability in this parameter cannot lead to linear structures in the DEM. Thus, features with relatively low relief and fracture traces with lengths shorter than about 100 meters cannot be resolved at all.

Finding the exact location of faults and zones of dense fracturing poses another problem for the lineament analysis. Although especially the aspect raster appears to exactly locate lineaments, it only depicts the points of lowest elevation, i.e. the place where the general exposition of the pixels changes. These points, frequently appearing in a linear array, do not necessarily coincide with the exact trace of a lineament in a tectonic sense. This becomes especially evident when looking at the wide NW-SE striking valleys in the DEM (figure 3-3). These valleys generally measure several hundreds of meters in width and possess considerable sedimentary infillings, which makes the exact location of a major fault plane in the DEM virtually impossible. Comparing the seven individual analysis runs shows that individual lineaments rarely coincide exactly in all runs. Even minimal deviations in the DEM translate to several tens of meters in the field.

Another drawback in the lineament analysis lies in the genetic interpretation of the linear features. Since the Bavarian Forest is an area which has endured bedrock weathering, erosion and sedimentation since the Tertiary (Priehäuser, 1968) a thick blanket of semi- or unconsolidated material covers the pristine bedrock. This poses the question to what extent the development of the topographic relief can be attributed to the bedrock structure and how much of it is a result of erosional processes. This leads to two phenomena, which are both related to the tendency of surficial flow of water to follow the topographic gradient in easily erodable materials. Figure 3-11 shows an example of such a borderline case. Although most lineaments depicted here coincide with the dominant strikes of fractures and lineaments in

the study area their specific array in this location could as well be interpreted as a result of erosion of surficial materials with no connection to the underlying bedrock structure.

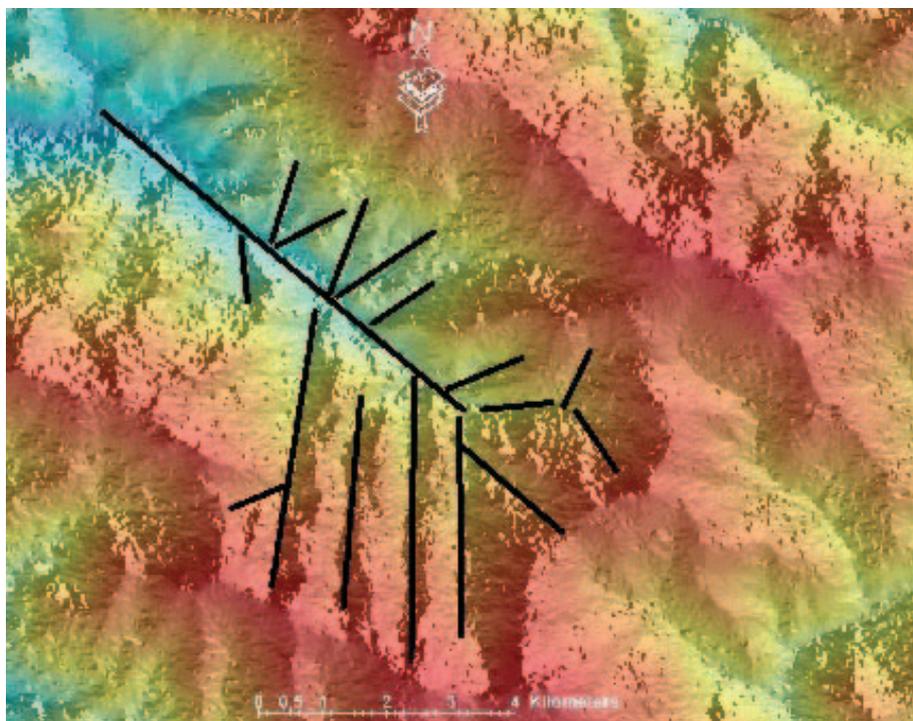


Figure 3-11: Subset of the ERS-DEM exposing an apparent semi-radial/dendritic drainage pattern. Black lines: linear features in the DEM.

A similar situation occurs in places where lineaments trend subnormal to the strike of prominent ridges. This could lead to the conclusion that erosion in these locations simply followed the topographic gradient. Since the major fracture systems in the Bavarian Forest predominantly trend NW-SE and NNE-SSW to NE-SW (see sections 2.3 and 3.4), i.e. subnormal to each other, both ridges and topographic gradient are often subparallel to the bedrock structure. In these cases a distinction between down-gradient erosion and erosion controlled by underlying fracture systems cannot be made with any certainty.

However, it has been observed in some locations that lineaments, which are seemingly due to the erosion of surficial materials cross a ridge and continue on its opposite flank. The same occurs across valleys. In these cases the likelihood is high that the lineaments are indeed structure-controlled, since it would be a coincidence if erosion formed matching channels on opposite flanks of ridges or valleys. On the scale of the entire DEM these two phenomena are of only minor influence on the overall interpretation of the data. Since lineaments related to them are mainly short and frequently oriented subparallel to the

dominant lineament strikes they do not introduce significant noise on this scale. Only for local observations these effects may become considerable.

Other difficulties arose during the structural and tectonic interpretation of the DEM. In order to establish a conclusive model several restrictive boundary conditions have to be assumed. Since a multitude of different lineament families were mapped out in the analyses only the ones with special geometric relationships to each other were selected in order to come up with a deformation model. However, the DEM only shows a momentary snapshot of the present bulk inventory of all lineaments and, unless cross-cutting relationships exist, no statement can be made regarding the relative ages and tectonic connections of individual populations. The result is a number of possible lineament constellations, which might fit specific tectonic models, but could also be only the cumulative product of several unconnected tectonic events rather than a single-phase deformation.

3.2 Lineament and fracture trace analyses using aerial photography

Aerial Photographs provided by the Bavarian Geological Survey were analyzed with regard to linear features, which were mapped and digitized from stereoscopically viewed image pairs. Fracture traces with lengths shorter than 10 meters were eliminated from the data set. The further analysis procedure was conducted similarly to the analysis of the ERS-DEM. In contrast to the DEM, the aerial imagery was examined only once due to the time-consuming nature of the procedure. However, the results yielded striking similarities between these two remotely sensed data sets, considering the completely different scales and data acquisition processes from which the data was obtained.

3.2.1 Results

The bulk lineament/fracture trace orientations derived from the analysis of the aerial imagery are presented in figure 3-12. Both the absolute number (fig. 3-12a) and the length-normalized (fig. 3-12b) plots show the same dominant NW-SE direction (300°-309° bin) as the one obtained in the DEM analysis. In contrast to the DEM data the rose diagrams here do not show several distinct minor peaks. In figure 3-12a, which depicts the absolute number of lineaments per 10° strike increment, the distribution of lineaments only shows minor variations with the exception of the 300°-309° direction. There is a conspicuous absence of lineaments striking truly E-W. Also, the minuscule ENE-WSW peak identified in the DEM does not occur in this data set. The slightly elevated lineament counts in fig. 3-12a occur in the 290°-299°, 320°-329°, 350°-359°, 0°-10° and 20°-29° strike bins.

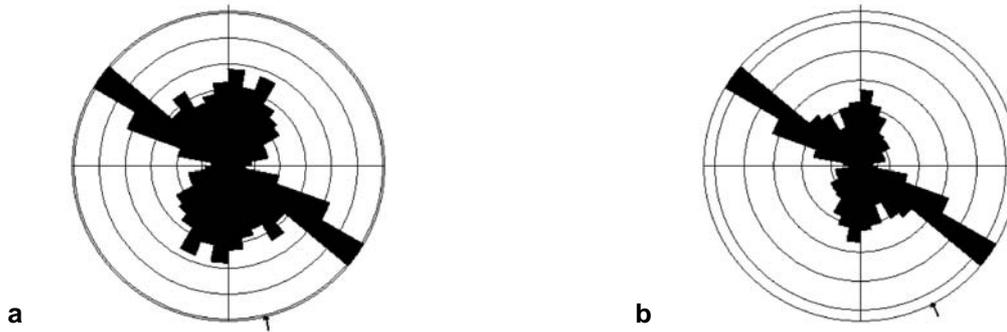


Figure 3-12: (a) Rose diagram depicting lineament / fracture trace strikes in the study area sensu stricto normalized to their absolute number per 10° strike bin. (b) Rose diagram depicting lineament strikes in the study area sensu stricto normalized to their cumulative length per 10° strike bin. Total cumulative length: 665362 meters. $n = 670$ in both plots. The data was plotted in the northern half-circle and then projected into the southern as a mirror-image in order to obtain a full-circle rose-diagram. The numeric values for each strike bin are listed in table 3. Data source: Aerial b/w Imagery.

The 290°-299° peak lies closely to the dominant NW-SE direction and is most likely not an individual population, but the tapering-off of the 300°-309° bin. In contrast to that, the 320°-329° peak is separated from the dominant direction by 10° and is interpreted as an isolated concentration. Although it does not appear in the analysis of the DEM (section 3.1.1.1, fig. 3-5) a similar peak (although offset by 10° to the North) occurs in the structural interpretation of the DEM in section 3.1.1.2, where it was suspected to be a population of synthetic Riedel shears related to dextral motion along the major NW-SE lineaments. The 350°-359° and 0°-9° increments are probably related, similar to the 290°-299° and 300°-309° bins and represent a group of lineaments striking in north-southerly directions. The same peak can be observed in figure 3-5 of section 3.1.1.1. The fourth isolated peak occurs in the 20°-29° strike bin. Interestingly, it is absent in the length-normalized plot (fig. 3-12b). The analysis of the DEM even shows a distinct low in this increment.

The length-normalized plot in figure 3-12b shows a rather bimodal distribution of lineament strikes. The two dominant peaks (300°-309° and 0°-9°) are consistent with the maxima occurring both in figure 3-12a and the analysis of the DEM. This discrepancy between the absolute and length-normalized values suggests that the lineaments/fracture traces that do not strike in one of the two major directions are relatively numerous but not very long. The numeric values in table 3-3 corroborate this result in that the lineament lengths vary 62% about the mean length (36965 meters per strike increment) while the absolute counts vary only 46% about the mean number (37.2 lineaments per strike increment), i.e. with regard to their orientations the absolute numbers of the lineaments are more evenly distributed than their lengths.

While table 3-3 lists the cumulative results for each strike increment the statistical parameters for individual fractures in each bin are tabulated in table 3-4. Considering individual values the mean and median lengths for the entire population of 670 lineaments/fracture traces are 993.1m and 780.4m, respectively, with a standard deviation (1σ) of 767.0.

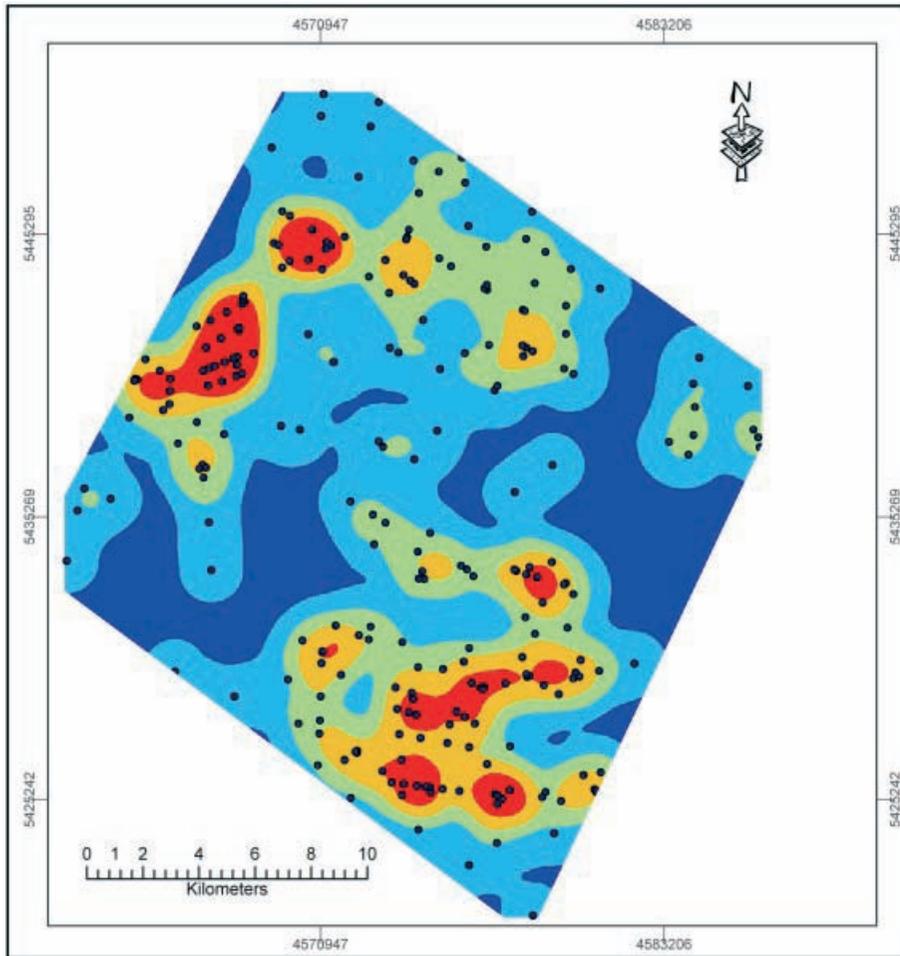
Some parameters in table 3-4 show clear trends and correlate well with others, such as the ones depicted in figure 3-12 or in table 3-3. Among these are the maximum length of a lineament in a particular bin and –to a certain extent- the standard deviation (1σ) of the length distribution. Both these parameters clearly show that their highest values coincide with the dominant lineament strike directions. Thus, the direction with the longest cumulative lineament length (table 3-3) also possesses the longest individual lineament as well as the highest variability in individual lengths. This is true for both the 300° - 309° and the 0° - 9° maxima. In contrast, the minimum, mean, and median lengths show trends less clearly or do not follow any at all. The minimum lengths show a weak tendency to correlate with the maximum length distribution, i.e. the bins with the longest lineaments also possess the shortest, which agrees with the distribution of the standard deviations of their lengths.

Orientation (°)	270-279	280-289	290-299	300-309	310-319	320-329	330-339	340-349	350-359
count	9	26	56	81	38	45	35	38	44
length (m)	11647	32889	64409	107022	45810	41436	28509	41265	44262
Orientation (°)	0-9	10-19	20-29	30-39	40-49	50-59	60-69	70-79	80-89
count	51	42	50	37	33	31	21	21	12
length (m)	52731	42640	36409	25591	23919	23452	17502	17477	8391

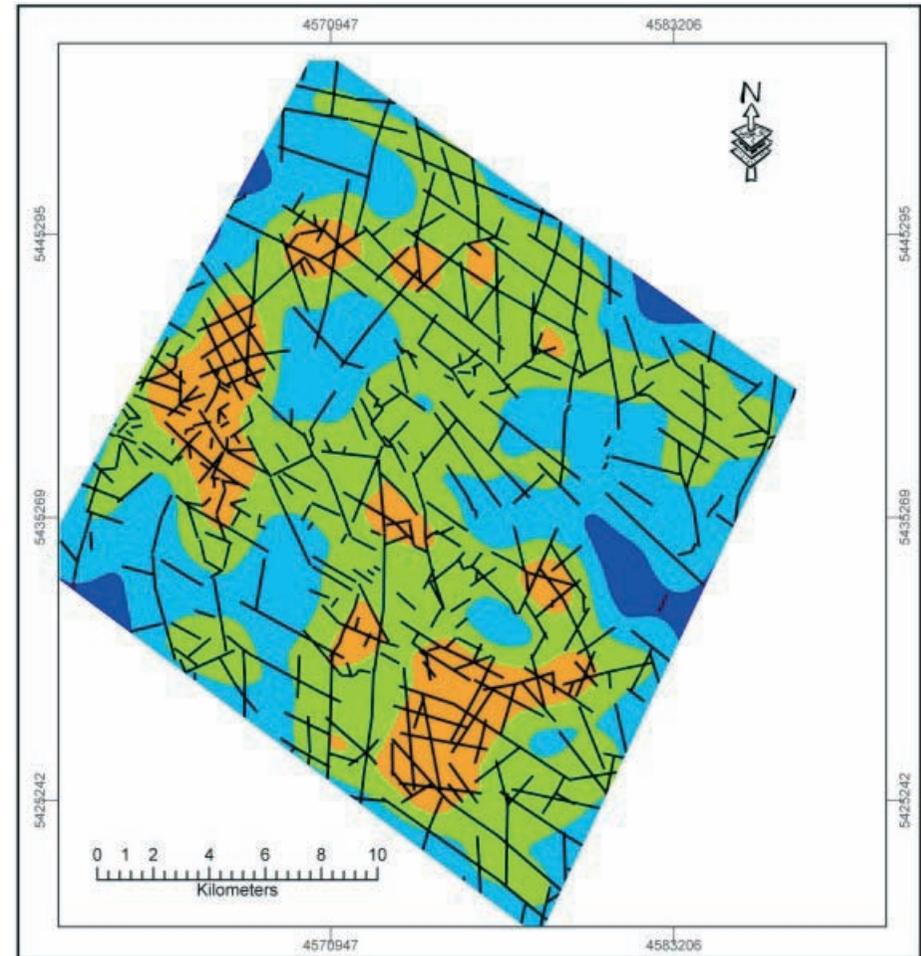
Table 3-3: Numbers and cumulative lengths of lineaments / fracture traces per 10° increment of orientation (counted clockwise on a half-circle from West to East). $n_{(\text{lineaments}) \text{ total}} = 670$. Data Source: Aerial b/w imagery.

Orientation (°)	270-279	280-289	290-299	300-309	310-319	320-329	330-339	340-349	350-359
Min. Length (m)	251,9	135,7	24,3	172,0	121,3	178,3	199,6	323,2	78,4
Max. Length (m)	2990,5	3467,9	4326,1	5036,4	4683,0	2959,9	2848,1	2442,2	2621,3
Mean Length (m)	1283,1	1256,5	1144,4	1326,2	1168,0	931,5	836,5	1101,5	978,3
Median Length (m)	1129,5	755,8	804,5	1019,1	785,7	785,0	727,3	1052,3	762,6
1σ	995,1	942,4	983,9	1044,1	967,1	605,2	490,7	559,5	647,1
Orientation (°)	0-9	10-19	20-29	30-39	40-49	50-59	60-69	70-79	80-89
Min. Length (m)	16,9	199,1	129,9	82,0	99,2	14,2	211,7	279,9	328,0
Max. Length (m)	4135,8	3844,4	2439,7	2779,0	2495,7	2103,9	1600,7	1615,9	1357,6
Mean Length (m)	1051,0	1008,2	726,7	731,3	695,2	772,0	821,7	825,9	735,9
Median Length (m)	873,8	842,1	628,2	603,8	485,6	569,0	775,5	740,7	739,0
1σ	868,9	790,2	438,0	532,4	546,2	491,8	381,4	397,7	358,0

Table 3-4: Lineament / fracture trace length distribution per 10° strike increment with regard to minimum, maximum, mean, and median length as well as the standard deviation (1σ) per 10° increment (tabulated clockwise from West to East). $n_{(\text{lineaments}) \text{ total}} = 670$. Data Source: Aerial b/w imagery.



a



b

Figure 3-13: Lineament / fracture trace density map depicting the density of lineament intersections (points in fig. 13-a) and the density of lineaments (black lines; (b) below) in the study area derived from aerial photographs. Analysis parameters: Density type: Kernel; search radius: 2000m, output cell (pixel) size: 25m. The contour interval from low (blue) to high (red) densities is one standard deviation from the mean density.

More information than from the tabulated values can be obtained from the lineament density maps in figure 3-13. As in the DEM analysis, standard methods described by Gupta (2003) were employed. The distribution of photolineament intersections is similar to that of the DEM lineaments (fig. 3-6). Thus, the highest densities occur in the southern part of the study area, south of the Pfahl zone as well as along its northwestern border approximately between Viechtach-Blossersberg and Arnbruck.

However, in contrast to the DEM lineament intersections the density of photolineament intersections varies more strongly, such that high-density areas are more pronounced in this analysis. In the southern part of the study area photolineament intersections are more densely distributed towards its southern corner; i.e. it does not cover the entire swath subparallel to the Pfahl zone. Thus, the high-density areas are located where the regional lineament cutting the entire field of view along a N-S line between the Deggendorfer Bucht and the Czech border (see DEM analysis in section 3.1.1.1 and fig. 3-3) enters the study area and intersects the Pfahl zone. Although this lineament's further trace towards North can only be guessed in figure 3-13a, figure 3-13b shows a continuous north-trending swath of elevated photolineament density approximately between Zachenberg and Arnbruck.

The intersections along the northwestern border are more highly concentrated with respect to their surroundings than in the DEM analysis. Another interesting difference exists in the zone of elevated density along the northeastern border of the study area. While the intersections of the DEM lineaments are more densely spaced towards the ridge between the Ecker Sattel and the Großer Arber the photolineament intersections are more concentrated in the valley to the SW of it, i.e. the Rundinger Zone, and the southwestern flank of the ridge, approximately between the villages of Arnbruck and Schönbach.

The distribution of the photolineaments per se (fig. 3-13b) exposes a pattern similar to the one in figure 3-13a. However, the density variations are not as significant as in the intersection density map (fig. 3-13a) or the lineament density map of the DEM analysis (fig. 3-6b). This is due to the fact that not all the lineaments intersect with others, and that they are more evenly distributed compared to the ones obtained from the DEM. Still, the common pattern can also be identified in this image. There are clear concentrations in the regions of high density identified above, such as the southern corner of the study area, along its northwestern corner, subparallel to the Rundinger Zone and the mountain ridge adjacent to the North of it, and along the large N-S trending lineament cutting through its center (to be seen most obviously in fig. 3-3). Figure 3-14 depicts individual lineaments separated

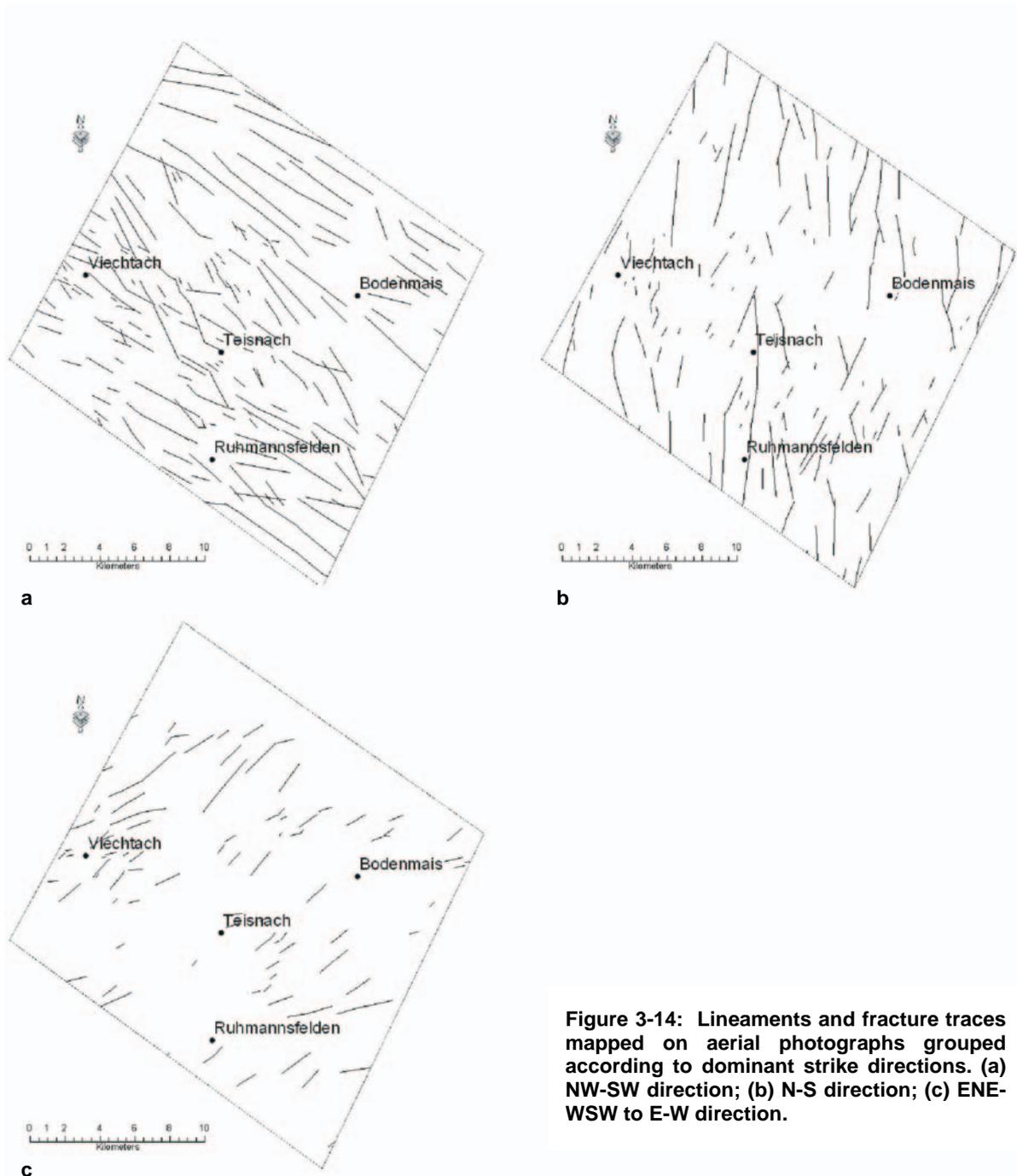


Figure 3-14: Lineaments and fracture traces mapped on aerial photographs grouped according to dominant strike directions. (a) NW-SW direction; (b) N-S direction; (c) ENE-WSW to E-W direction.

according to their dominant directions. The distributions are similar to those of the DEM lineaments. While the NW-SE and N-S lineaments (figs. 3-14a and b, respectively) are relatively uniformly distributed – the latter having only a significant absence in the area of the Rundinger Zone – the ENE-WSE striking ones (fig 3-14c) tend to cluster in the regions around Viechtach, the Rundinger Zone, and the southern part of the study area.

In general, the photolineaments are shorter and more abundant than the DEM lineaments, which is due to the different resolutions and scales of observation of the two

datasets. A direct comparison of the lineaments in figures 3-6 and 3-13, however, shows an impressive agreement between the two lineament analyses (figure 3-15).

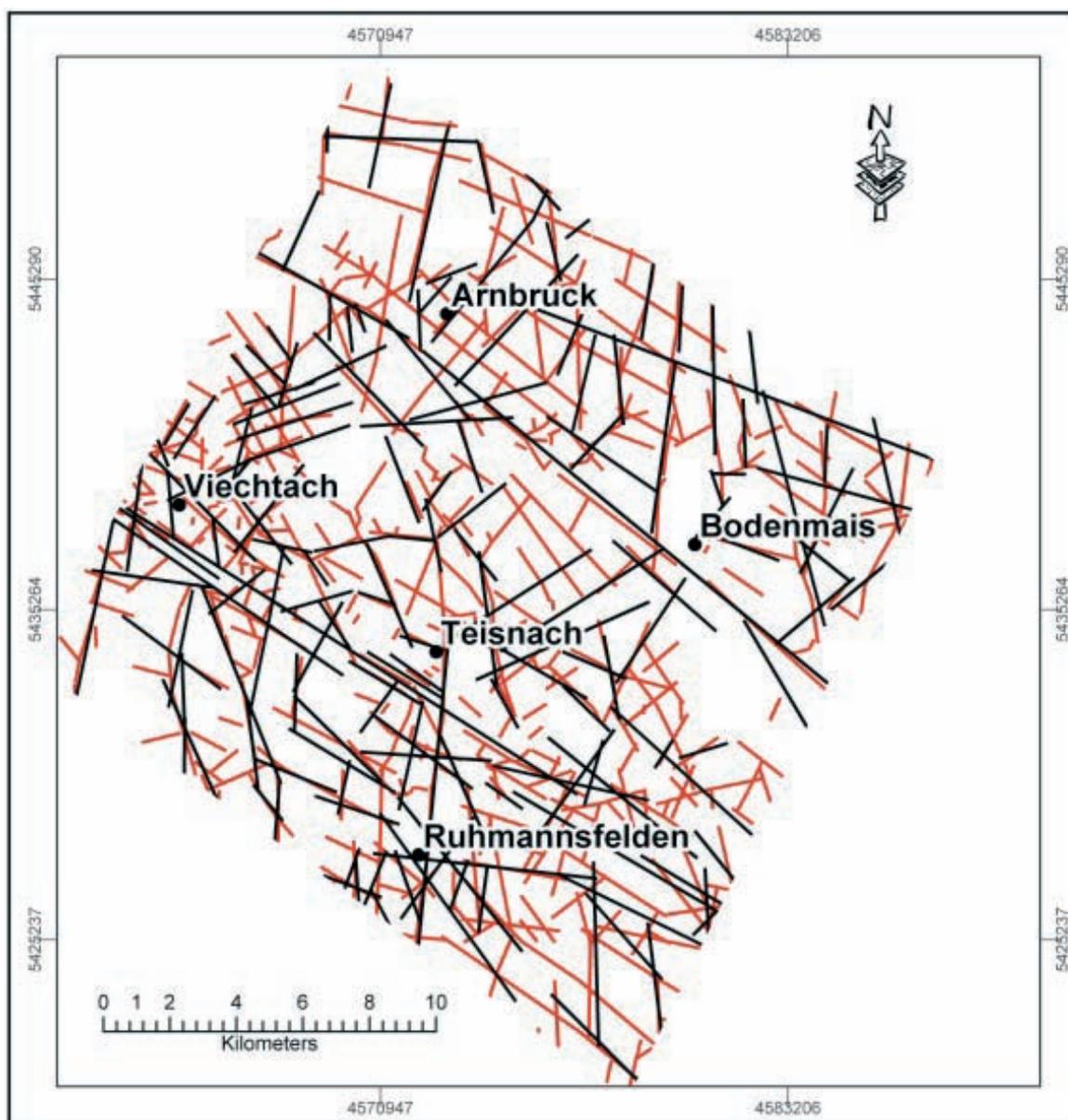


Figure 3-15: Map showing ERS-DEM lineaments (black lines) and photolineaments (red lines).

3.2.2 Difficulties with the interpretation of photolineaments

Apart from the common limitations of the interpretation of aerial imagery described by Gupta (2003) and Jensen (2000) several other problems emerged both with the images provided and the landscape they depict. Several image elements introduced the risk of misinterpretation. The greatest difficulties were posed by the presence of forested areas with little relief. There, minor changes in topography were frequently attenuated by the tree cover,

so local structures were occasionally difficult to identify. In addition, partially overgrown dirt roads associated with embankments frequently appear as linear structures in forests. The same problem applies to open agricultural land where extensive boundary ridges between individual lots of land could be mistaken for local geologic structures. Similar to the forested areas, wide valley bottoms frequently expose little relief, so faults following their trace could not be located exactly. Some misleading structures also emerged from the overlapping of images under the stereoscope. Slight variations in the brightness of the photographs, either due to the developing process or the aging of the images (most pictures were taken in the 1960s), sometimes caused effects which, in some cases, could influence their structural interpretation.

Another potential source of error lay in the digitizing of the data. As already mentioned in the methodology section lineaments were mapped on transparencies laid over one image of the stereoscopic pair. The lineaments on the transparencies were then digitized by visually locating their trace on digital orthophotographs on the computer screen. Due to the orthorectification process slight distortions with respect to the unrectified image pairs could emerge, which in some instances caused problems in the exact location of the lineaments. Also, placing lineaments in widely featureless forested areas took its toll on the accuracy of the placement in a few cases. However, since the orientations and lengths rather than the exact locations of the lineaments were focused on in the analyses minor deviations from their exact position can be neglected. Moreover, an accuracy similar to that of the DEM lineaments could be achieved in any event because of the relatively coarse resolution of the DEM, whose limitations were already described in section 3.1.2.

Only careful work during the entire analysis process and the repeated examination of ambiguous image pairs could ensure the highest possible accuracy and the elimination of the bulk of potential errors. Nonetheless, as will be shown in the domain overlap analysis below, the results of the different methods of data acquisition (interferometric satellite RADAR versus stereoscopic b/w aerial imagery) with their various scales of observation expose striking similarities, thereby adding further credibility to the interpretations of the remotely sensed data material. Additionally, the findings obtained from the lineament analyses will further be corroborated by their correlation with actual fracture patterns measured in the field.

3.3 Orientations of intrusives

Preferred orientations exist in an area not only in the form of topographic lineaments, fractures, and faults, but also in a number of other geologic entities such as lithologic contacts or the intrusions of magmatic or hydrothermal rocks. For the study area lithologic contacts are only ambiguous indicators of preferred orientations for several reasons. Most importantly, the classification of lithologic units in the central Bavarian Forest is still highly debated and not consistent beyond individual map quadrangles. Thus, the delineation of contacts, especially between metamorphic rock types, cannot be carried out satisfactorily until this debate has been resolved. Even if an agreement had been found, unambiguous mapping of the contacts is not likely to be achieved due to the extensive coverage of the bedrock by surficial materials.

However, hydrothermal and magmatic intrusions are valuable indicators for anisotropies in the rock record. These rock types are commonly easy to distinguish from the metamorphic country rock and extend over relatively small areas, which makes them easier to map. The seven geologic map quadrangles meanwhile available for the study area contain a multitude of different magmatic and hydrothermal dikes and veins the orientations of which were mapped separately for each rock type. Additionally, in cases where larger plutons show a distinctive elongation in one direction the long axes of these intrusions were mapped as well. The results were then plotted in the rose diagrams presented below according to the most abundant rock types present in the study area. Orientations of dikes, veins, and elongation axes were determined for the following rock types: quartz, pegmatite, and quartz-mica diorite, as well as coarse-, medium-, and fine-grained granite.

Figure 3-16 displays the cumulative orientations of all mapped intrusions. This representation makes it obvious that their vast majority trends in the Variscan NW-SE direction (fig. 3-16a). Similar to the lineament analyses also the cumulative lengths per 10° increment were plotted (fig. 3-16b). This shows a splitting of the prominent peak and a 20° counterclockwise rotation of the maximum. Also, a minor NE-SE striking population becomes evident. Comparing the cumulative distributions to the ones classified according to the respective lithologies shows which types of dikes contribute to which peaks in the cumulative plots in fig. 3-16a.

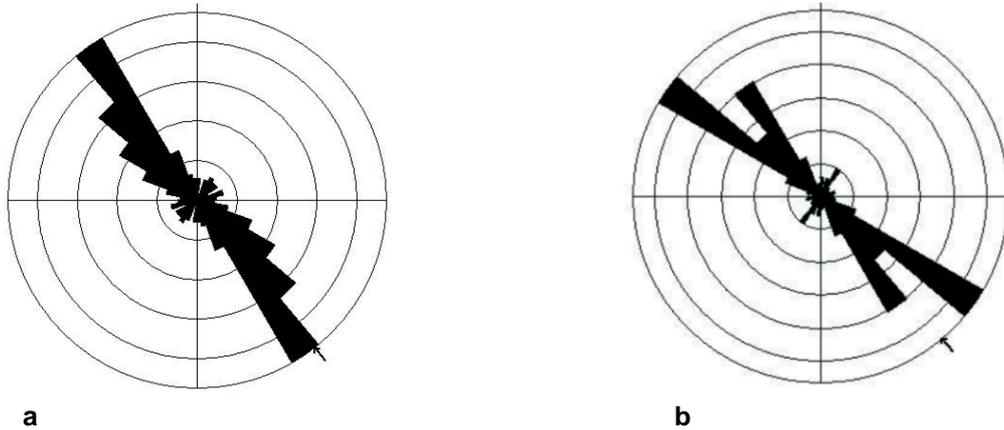


Figure 3-16: Trends of elongation axes of igneous and hydrothermal intrusives. (a) Number of all axes ($n = 329$) . (b) Cumulative lengths per 10° strike increment. Cumulative length is 91785 meters.

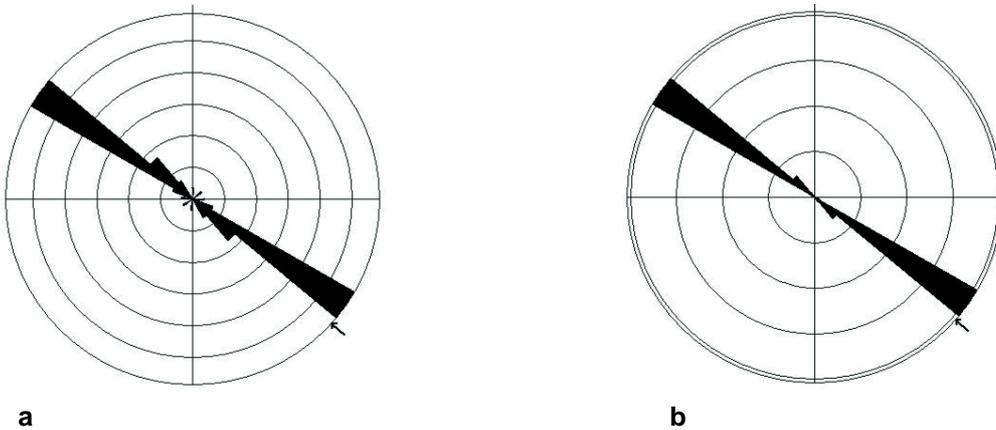


Figure 3-17: Trends of elongation axes of quartz dikes and veins. (a) Number of all axes ($n = 29$) . (b) Cumulative lengths per 10° strike increment. Cumulative length is 18003 meters.

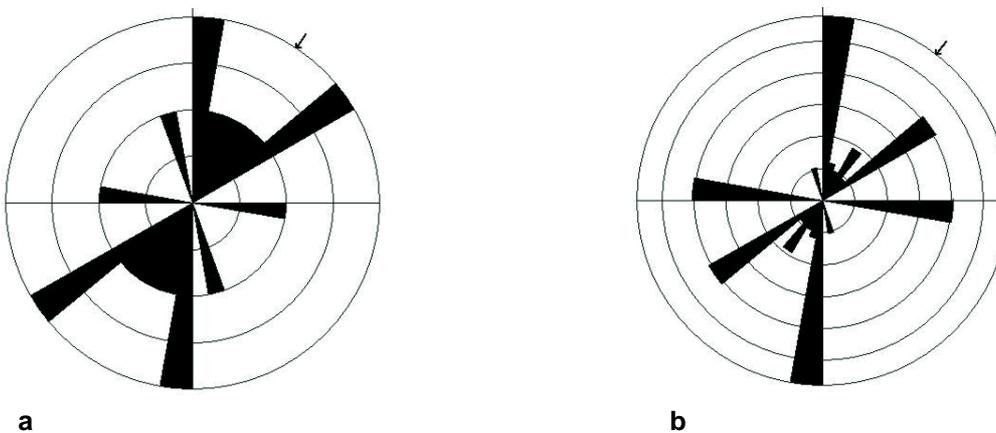


Figure 3-18: Trends of elongation axes of pegmatite dikes and veins. (a) Number of all axes ($n = 10$) . (b) Cumulative lengths per 10° strike increment. Cumulative length is 1352 meters.

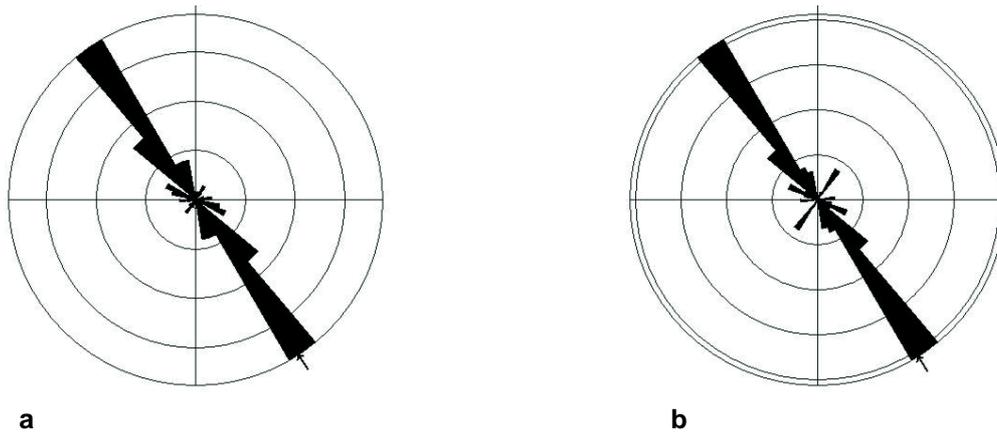


Figure 3-19: Trends of elongation axes of Quartz-Mica-Diorite dikes and veins. (a) Number of all axes ($n = 61$) . (b) Cumulative lengths per 10° strike increment. Cumulative length is 14210 meters.

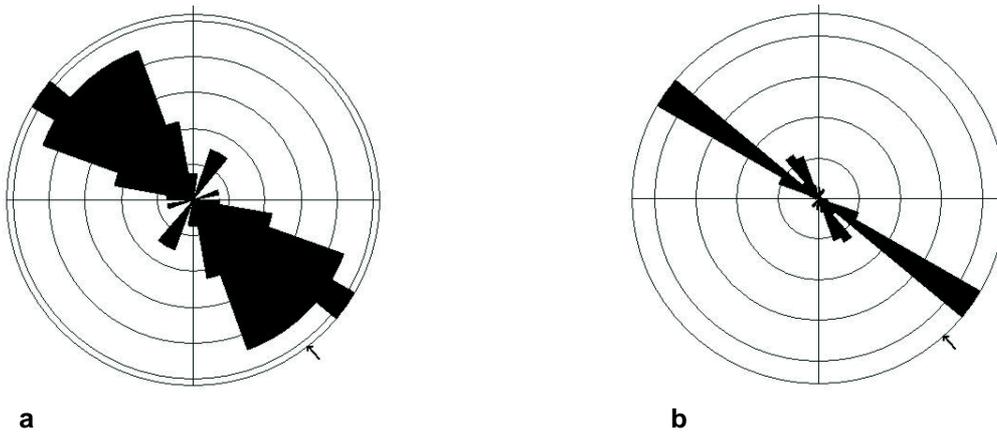


Figure 3-20: Trends of elongation axes of coarse-grained granite dikes and veins. (a) Number of all axes ($n = 45$) . (b) Cumulative lengths per 10° strike increment. Cumulative length is 15493 meters.

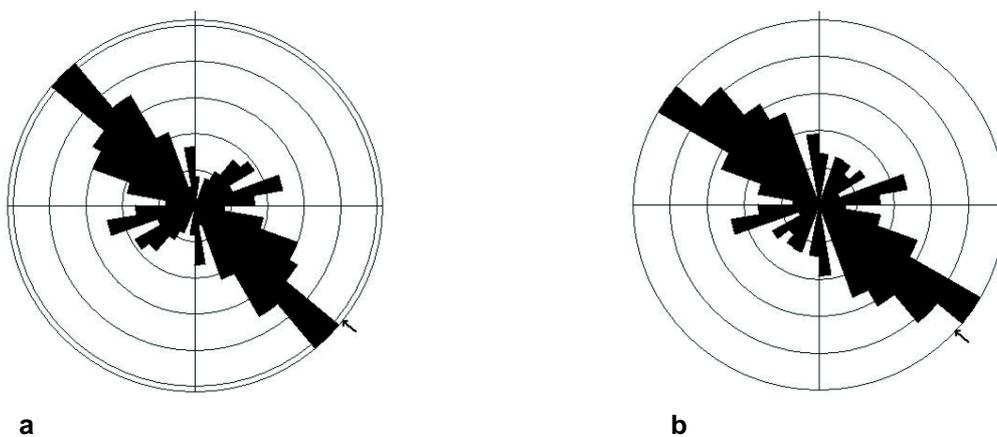


Figure 3-21: Trends of elongation axes of medium-grained granite dikes and veins. (a) Number of all axes ($n = 123$) . (b) Cumulative lengths per 10° strike increment. Cumulative length is 24198 meters.

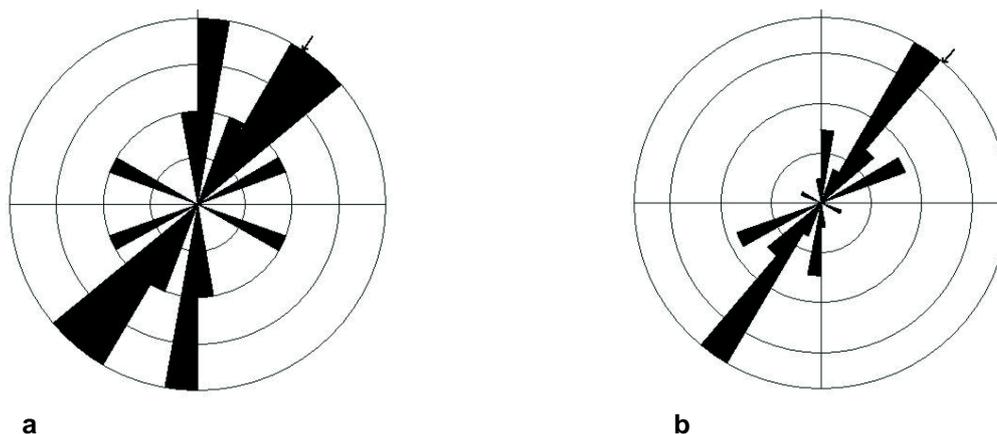


Figure 3-22: Trends of elongation axes of fine-grained granite dikes and veins. (a) Number of all axes (n = 10) . (b) Cumulative lengths per 10° strike increment. Cumulative length is 5203 meters.

The most uniform of all distributions can be found in the quartz dikes and veins (fig. 3-17). Their trends are exclusively NW-SE (in the 130° segment) and thus parallel the large Variscan fault lines. Indeed, a large part of the quartz dikes exists as fault mineralizations in the PFZ. Their cumulative length of approximately 18 km is distributed over only 29 individual entities, which makes them on average the longest individual intrusions (mean length lies at 621 m) in the study area. In contrast to the quartz dikes, the pegmatitic intrusions (fig. 3-18) represent the smallest sample of dikes with a total number of 10 and a cumulative length of approximately 1.35 km. Nonetheless, the scatter of directions is considerable. The distribution is dominated by a N-S striking peak, but NW-SE and E-W oriented dikes are present as well. Only the NW-SE direction prominent in most other plots is completely absent in the pegmatites.

The quartz-mica diorites (fig. 3-19) are again very consistently NW-SE oriented. However, the peak lies in the 150° segment and is thus rotated clockwise by 20° with respect to that of the quartz dikes. The scatter about the prominent peak is also somewhat higher than in the quartz distribution and a minor concentration trends NE-SW (best visible in fig. 3-19b). The cumulative length (ca. 14.2 km) of the quartz-mica diorite dikes is distributed over 61 individual entities, which makes their average length of 234 m relatively short.

Similar to the quartz and quartz-mica diorite dikes the coarse and medium-grained granite intrusions also mostly follow the NW-SE direction, however with a considerable amount of scatter and several subordinate peaks at various orientations. The majority of the coarse-grained granite dikes (fig. 3-20) trend in the direction of the quartzes (i.e. 120°), although a minor peak also exists in the 150° (i.e. that of the quartz-mica diorites) segment. A number of NE-SW striking dikes are visible in fig. 3-20a, which, however, do not appear in

the cumulative length plot (fig. 3-20b) and thus are only very short entities. The cumulative length of approximately 15.5 km distributed over 45 individual dikes produces an average length of 344 m. In contrast to the coarse-grained granites the medium-grained granite dikes (fig. 3-21) already show reasonably well-established N-S, NE-SW, and ENE-WSW peaks in addition to the prominent NW-SE direction, which also has its maximum in the 120° segment. At a cumulative length of 24.2 km the 123 individual dikes represent the most abundant population, which causes their average length to lie at 198 meters.

The distribution of fine-grained granite dikes (fig. 3-22) strongly resembles that of the pegmatites. For both these populations the absence, respectively the low number, of NW-SE striking dikes is characteristic. Instead, the distribution is dominated by the NE-SW direction. Subordinate peaks are oriented ENE-WSW, N-S, and, to a very small extent, NW-SE. Both the cumulative length and number of dikes are low, however, the average dike length of 520 m is the second highest in the entire record.

Several of the igneous and hydrothermal intrusions have been dated and thus can be used for establishing a sequence of tectonic events which produced the dikes. Both Ott (1983) and List and Ott (1982) quote the study by Gebauer (1977) and use his results to attribute ages to the igneous intrusions. According to these authors the coarse-grained granite was emplaced at 340-320 Ma followed by dioritic rocks (320-310 Ma) and by the bulk of medium- and fine-grained granites from 310 to 280 Ma. The quartz mineralization of the large Variscan fault complexes was placed into the Permo-Triassic by Rohrmüller et al. (1996b). Thus, when attributing the orientations of the respective lithologies to these ages the following development of tectonic structures can be derived (from old to young): NW-SE → ENE-WSW → NE-SW and N-S. The emplacement of the quartz dikes in the Permo-Triassic suggests a renewed activity of the NW-SE structures. No age information could be obtained for the pegmatites. They are assumed to be roughly contemporaneous with the quartz and to be related to the final stages of the granite emplacement. This assumption is corroborated by the similarity of the dike orientations of pegmatites and fine-grained granites. Note that this sequence is based on the predominance of the specific orientations. Some later directions are also present as very minor peaks in earlier distributions. Nonetheless, this chronological trend is obvious when comparing the plots of the respective lithologies in the order of radiometric dates.

The analysis of the orientations of igneous and hydrothermal intrusives shows that the prominent directions identified both in the fracture and the lineament record existed already at the time when the Variscan plutons were emplaced. Thus, the brittle tectonic

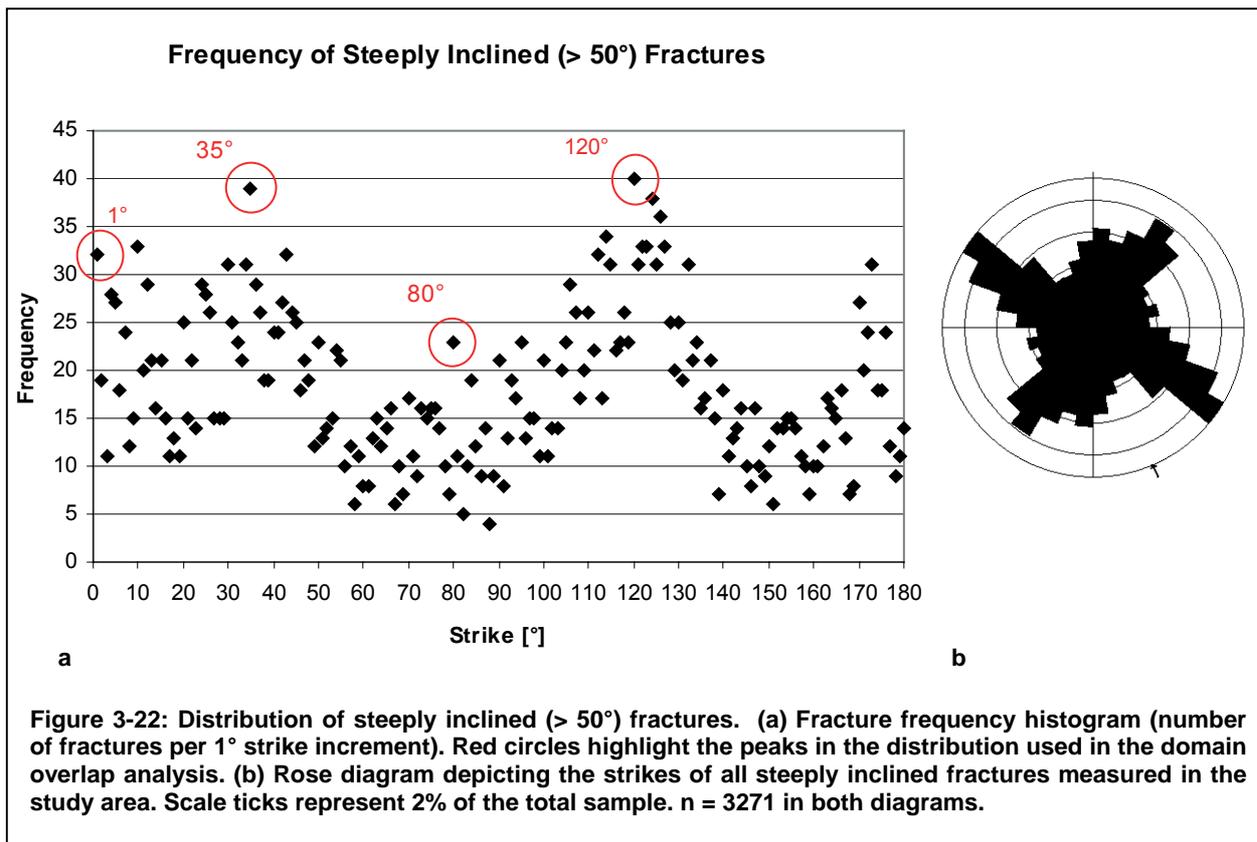
evolution largely reutilized petrofabrics established as early as the late Paleozoic when the rocks exposed at the surface today were still under semi-brittle conditions. This realization has even further-reaching implications, because if most of the study area's brittle tectonic evolution is based on the reactivation of old structures these preexisting planes of weakness may have caused local stress configurations deviating to a certain extent from the regional stress fields. Therefore, calculating the regional stress regime based on local observations may not yield exact results.

3.4 Groundtruthing of remotely sensed structure data and domain overlap analysis

After analyzing the orientations of topographic lineaments the question arises whether or not they correlate spatially with the orientations of bedrock fractures. To this end Mabee et al. (1994) devised a method called "domain overlap analysis", a modified version of which will be employed here. The basic aspects of this approach have already been presented in section 1.5.2.3.

The first step in the domain overlap analysis is the identification of prominent directions in the fracture dataset. Preceding this, the bedrock fracture database was filtered to eliminate fractures with inclinations of less than 50°. Figure 3-23 shows the distribution of the strikes of steeply inclined fractures measured in the study area. As can be inferred from the fracture frequency diagram (fig. 3-23a) four pronounced peaks can be isolated in this sample. Those peaks lie at 1°, 35°, 80°, and 120°, thereby representing the four prominent fracture orientations in the study area. Figure 3-23b shows the same distribution in a rose diagram. Fractures clustering around those peaks at angles of less than $\pm 10^\circ$ were attributed to those prominent orientations.

In agreement with those four orientation classes both the photolineament and the DEM lineament dataset was filtered, and the surviving lineaments were classified accordingly. The results of the combination of the filtered lineament maps and the fracture rose diagrams shown by sampling station can be regarded in fig. 3-24. Concerning the selection process of the fractures in this representation it has to be noted that only outcrops where fractures of a specific orientation were the most or second-most abundant in the sample. In some cases the second-most abundant fractures may appear only as minuscule peaks rising hardly above the background noise. Nonetheless, they represent fracture orientations present at these particular locations, which coincide with the strikes of the corresponding lineaments.



The maps in fig. 3-24 depict lineaments and fractures separated according to the four prominent orientations. Here, one drawback to this analysis becomes obvious. Due to the inhomogeneous distribution of sampling stations in the area as a result of the widespread blankets of surficial materials not every lineament can be associated with a bedrock outcrop. Thus, missing fracture data does not necessarily point to regions where there is no correlation between lineaments and fractures, but rather that the lack of bedrock exposures prevents a possible correlation. As a result, a derivation of well-delimited fracture domains *sensu* Mabee et al. (1994) could not be achieved. However, a local comparison of prominent fracture and lineament strike seems rather feasible. Another fact to ponder is the exclusion of minor fracture sets from this analysis (for clarity reasons only the two dominant fracture populations in each sampling station were included). Therefore, some sampling stations without a rose diagram in a particular map may in fact possess fractures of the respective orientation, but only to a very minor extent.

Despite all possible problems arising from sampling bias several observations can be made, both on a local and on a regional scale. The 1° , the 35° , and the 120° lineaments are relatively ubiquitous occurrences. Merely the 80° segment (fig. 3-24c) appears to be concentrated in the central part of the study area, although the relatively low number of lineaments in this group renders it difficult to identify clear concentrations.

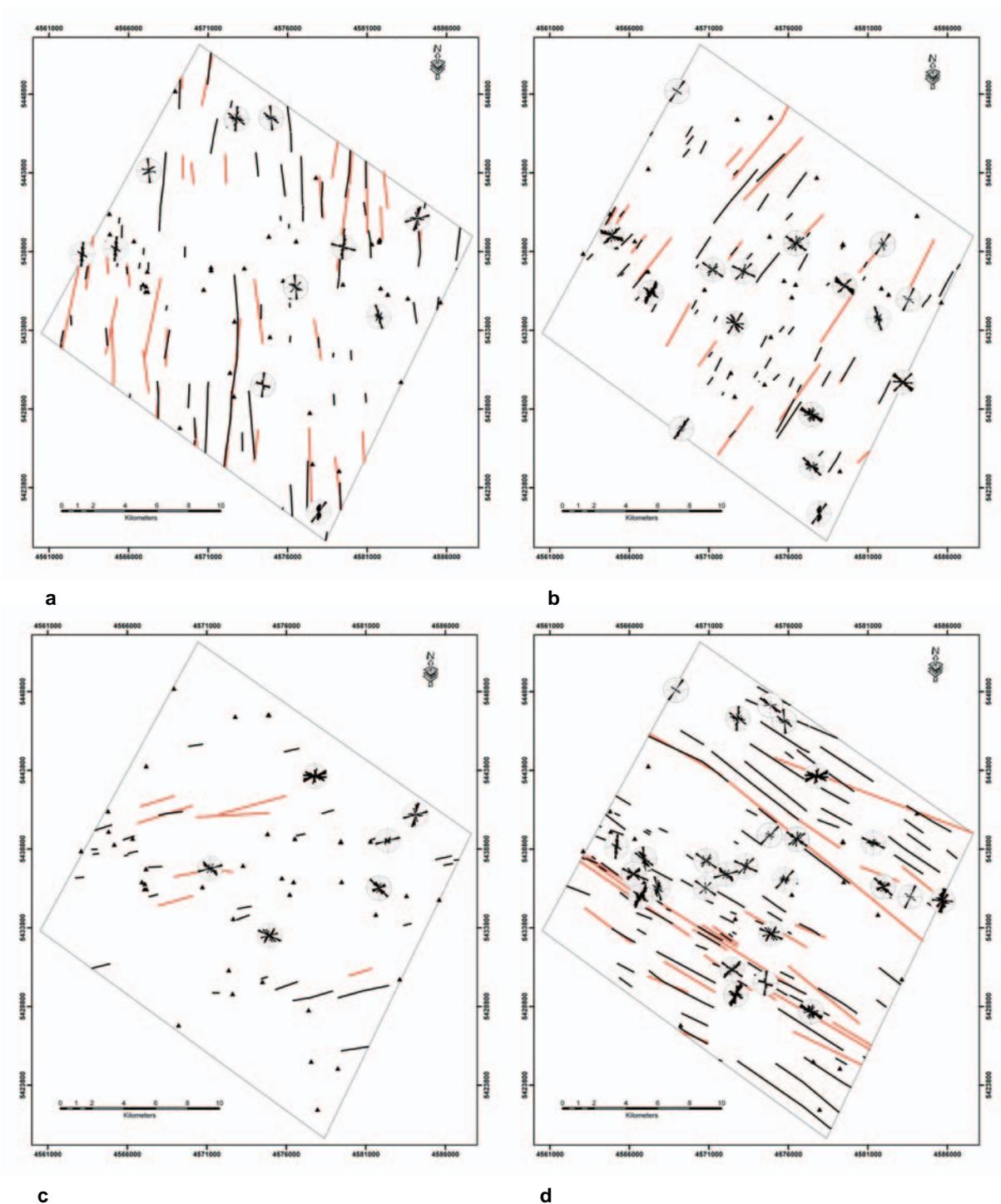


Figure 3-23: Comparison of lineament and fracture distributions separated by prominent trend. (a) $1^\circ \pm 10^\circ$; (b) $35^\circ \pm 10^\circ$; (c) $80^\circ \pm 10^\circ$; (d) $120^\circ \pm 10^\circ$. Black lines: lineaments mapped from aerial photographs. Red lines: lineaments mapped from the DEM. Rose diagrams depict sampling stations where the respective lineament orientation occurred in the fracture dataset.

Strike direction	Sampling stations: Distance to lineament						No Correlation	Total
	<100 m	<200 m	<300 m	<400 m	<500 m	Sub-total		
1° Segment	2	2	0	1	2	7	4	11
35° Segment	2	1	1	0	1	5	11	16
80° Segment	0	2	0	0	0	2	4	6
120° Segment	5	0	6	3	1	15	9	24

Table 3-5: Distances (< 500 m) of sampling stations to lineaments with corresponding strikes.

The most uniform distribution can be found in the 1° segment map (fig. 3-24a). The 35° segment map (fig. 3-24b) shows low concentrations in the W corner and along the NE edge. The 120° segment map (fig. 3-24c) displays a NW-SE trending swath of lower concentrations in the central part of the study area. Thus, domains encompassing areas with unique lineament orientations cannot be established in a meaningful way. However, the larger-scale examination of the Eastern Bavarian crystalline basement complexes indeed shows regional concentrations of lineaments with specific orientations (Zeithöfler, 2006b). These areas of increased concentrations commonly cover several 1:25,000 map quadrangles. Therefore, the study area for this dissertation with its coverage of approximately four quadrangles appears to be too small for the delineation of lineament domains. Similarly, prominent fracture orientations are also not distributed in recognizable patterns over the extent of the study area. Thus, the domain overlap analysis sensu Mabee et al. (1994) could not be carried out successfully in this study area.

Nonetheless, agreement between lineaments and fractures can be found on the local scale. To analyze these relationships the sampling stations were encircled with 500 meter radius buffer zones, which were subdivided into concentric 100 m wide rings. That way the distances between sampling stations, which possess dominant fracture sets falling into one of the four prominent strike directions, and lineaments with corresponding trends were determined. Table 3-5 lists the results of this analysis. As can be inferred from this list the majority of sampling stations (64 % and 63 %, respectively) possessing dominant fracture sets in the 1° and 120° segments is located within 500 meters of a corresponding lineament. After raising the buffer radius to 1000 m the proportion of sampling stations associated with lineaments of corresponding orientations increased to 71 % for the 120° segment. The increase had no effect on the 1° segment because the four sampling stations showing no correlation in the 500 m buffers are located in areas of an overall low lineament concentration.

For the 35° and 80° segments the percentages are rather low (31 % and 33 %, respectively) because of the relatively low concentrations of lineaments striking in these directions in the study area. Thus, the probability of sampling stations being located near such lineaments is significantly lower. However, the intermediate concentration of lineaments in the 35° segment caused the largest effect with the increase of the buffer radius to 1000 m. As a consequence, the percentage of sampling stations associated with corresponding lineaments rose to 75 per cent. Increasing the buffer for the 80° segment did not cause any change in the proportions at all because the concentration of lineaments and the density of sampling stations possessing fractures with this orientation is still too low to obtain significant overlap for this buffer radius.

Recapitulating the observations made in fig. 3-24 and table 3-5 it can be concluded that for the 1°, 35°, and 120° segments the majority of sampling stations shows local correlations between the strikes of lineaments and prominent fracture sets. For the 80° segment the densities of both lineaments and sampling stations with dominant fracture orientations are too low to show significant agreement between these two parameters.

Another way of displaying the relationships between fracture and lineament orientations is presented in fig. 3-25. In this case the four maps show the density of lineaments belonging to a specific strike segment per unit area. Additionally, the distributions of corresponding fracture sampling stations are laid over the contoured maps. Examining the density contours the photolineaments (blue contours) appear to be more widespread than the DEM lineaments (red), which is caused by the very different numbers of lineaments mapped on the aerial imagery and the DEM. Especially in figs. 3-25b and c the contour maps are truncated within the extent of the study area, which is due to the density search algorithm of the GIS program. Density maps can only be displayed as unrotated rectangles and areas with no lineament coverage are omitted in the search. As a result, only the region with a non-zero lineament count is displayed as a rectangle truncated by the extent of the study area.

As in fig. 3-24, lineament domains characteristic exclusively for specific subregions of the study area also do not appear in this representation. Irrespective of this drawback a certain degree of overlap between DEM lineaments, photolineaments and fracture orientations can be observed, especially in figs. 3-25a and d as well as to a lesser extent in figs. 3-25b and c. The 1° segment is strongly influenced by a number of long lineaments in the southern part of the study area, the most prominent of which extends from the southwestern edge into its center. Both the photo- and the DEM lineaments show high concentrations there. Although only one sampling station in the vicinity of this large lineament

meets the criteria established for the domain overlap, two more stations show fracture orientations falling only slightly out of the $1 \pm 10^\circ$ segment (fig. 3-26a).

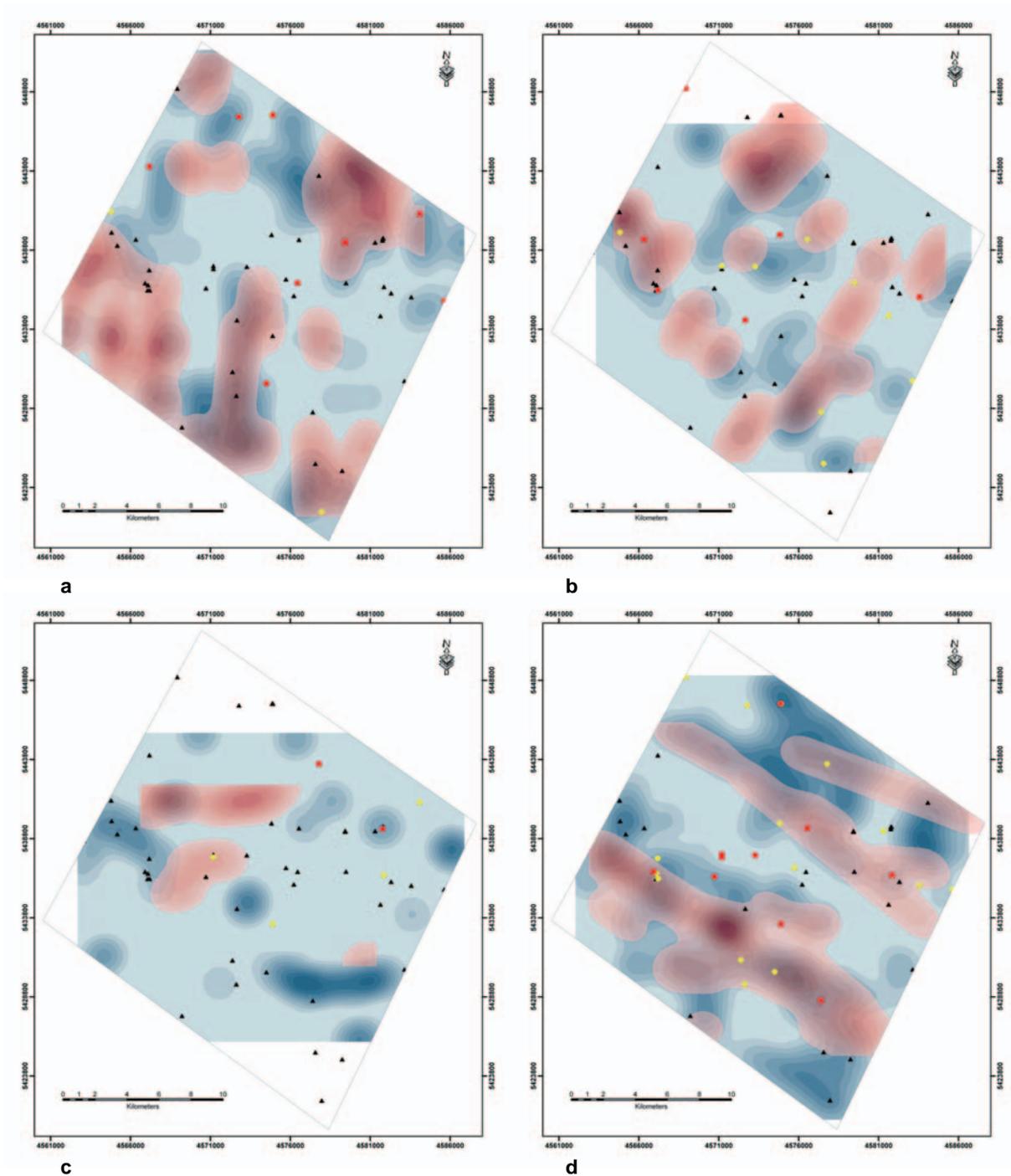


Figure 3-24: Contour maps of the distribution of lineament and fracture orientations per $\pm 10^\circ$ segment about prominent fracture orientations. (a) 1° peak; (b) 35° peak; (c) 80° peak; (d) 120° peak. Contours depict equal intervals of the lineament number in the search radius. Search radius: 2000 m; Output pixel size: 25 m. Unit area is 1 km^2 . Red contours: density distribution of lineaments mapped on the DEM. Blue contours: density distribution of lineaments mapped on the aerial photographs. Lowest-level contour of the DEM lineaments omitted for better visibility. Red dots show fracture sampling stations where the respective orientation is primary; yellow dots show those where the respective orientation is secondary in the fracture record. Black triangles represent uncorrelated sampling stations. White areas in the maps exist where the density of the respective lineaments is absolute zero.

Nonetheless, several outcrops along this prominent lineament do not seem to be dominated by fractures striking in its direction. The reason for that might lie in the fact that this lineament covers a region where all four strike segments show elevated densities. Particularly the concentrations on the 35° segment partially overlap with the 1° lineaments in this region. Thus, each of the four prominent strike directions may contribute to the fracture record of those sampling stations to a certain extent. Since only the two dominant fracture sets of each station, whose orientations represent mean values obtained from stereographic plots, were taken into consideration the ones parallel to the N-S lineament may have been outnumbered by fractures with different strikes and ignored in the designation of the two dominant sets. In the northern and northwestern parts of the study area several sampling stations coincide with elevated densities, especially of the photolineaments. Thus, an overlap between fractures and lineaments could be established fairly well for the 1° strike segment.

The distribution of elevated lineament densities in the 35° segment (fig. 3-25b) is even more patchy than in the previous one, which is both due to the relatively low number of features in this segment as well as their relatively short lengths. Only two approximately NE-SW trending zones located in the northwestern and southeastern thirds of the study area extend over larger areas. These zones overlap in part with regions of elevated densities of other lineament directions. Additionally, higher concentrations also follow the trace of the Pfahl fault zone (compare to fig. 3-25d). Regardless of their patchiness, the concentrations of DEM and photolineaments agree reasonably. Also, the distribution of sampling stations possessing corresponding fracture sets overlaps with the lineament concentrations in most instances. Only three outcrops are located at greater distances to zones of elevated lineament densities.

The lowest concentrations of all four prominent directions exist in the 80° segment. Only two major zones of elevated densities are present slightly N of the trace of the PFZ. The photolineaments only partially overlap with the DEM lineaments and only two out of six sampling stations containing the 80° direction as a prominent fracture set are located within an elevated concentration. However, several uncorrelated outcrops fall into regions of higher densities. Examining the strikes of steeply inclined fractures in these outcrops (see plots in appendix F) it becomes evident that in many instances these locations possess a minor (sometimes even minuscule) peak in the 80±10° segment. Albeit, the overprint by other prominent directions is commonly too heavy for these fractures to appear on the overlap map.

The highest concentrations of the entire dataset were found in the 120° segment (fig. 3-25d). The zones of elevated densities both follow the trends of the two major fault complexes (i.e. the PFZ and the Rundinger Zone) and coincide with their locations. Especially the DEM lineaments are strongly influenced by these two structures. The photolineaments show additional concentrations in the southernmost corner as well as along the northeastern edge of the study area. Thus, except for a relatively narrow NW-SE trending swath in the center of the map, lineaments belonging to the 120° segment could be called ubiquitous features. Also, the majority of sampling stations falling into the high-concentration regions contain this direction as a prominent fracture set. Even outside the elevated concentrations fractures of this orientation dominate the map and the overlap of high-density areas of other directions does not significantly influence their predominance. Thus, the Variscan NW-SE direction has the most widespread impact on the orientations of both fractures and lineaments in the study area. In addition to their quasi-ubiquitous occurrence this segment's lineament lengths are the longest measured in the analyses (see also fig. 3-24).

In order to visualize both regional and local interrelationships between fractures and lineaments figure 3-26a depicts a map containing the DEM and photolineaments as well as the mean strikes of the two dominant fracture sets in every sampling station in the study area. Figure 3-26b represents the cumulative orientations of all steeply inclined discontinuities measured in this project. Figures 3-26c and d plot the orientations of the DEM lineaments, while figs. 3-26e and f show the strikes of the photolineaments¹.

The lineament map gives an impression of the unfiltered distribution of fracture and lineament strikes, which provides in some instances a better view of the relationships between the three datasets. While the domain overlap analysis in figs. 3-24 and 3-25 imposes sharp cutoffs on the four predominant strike directions the representation below yields a continuous distribution of fracture and lineament orientations. That way, structures, which fall only slightly out of the $\pm 10^\circ$ segments, but still show reasonable agreement, can be visualized. The result shows in most cases good correlations between the general trends of one or even two fracture sets in a particular sampling station and the orientations of neighboring lineaments.

¹ The rose diagrams in fig. 3-26 are a compilation of the plots in figs. 3-5, 3-12, and 3-23.

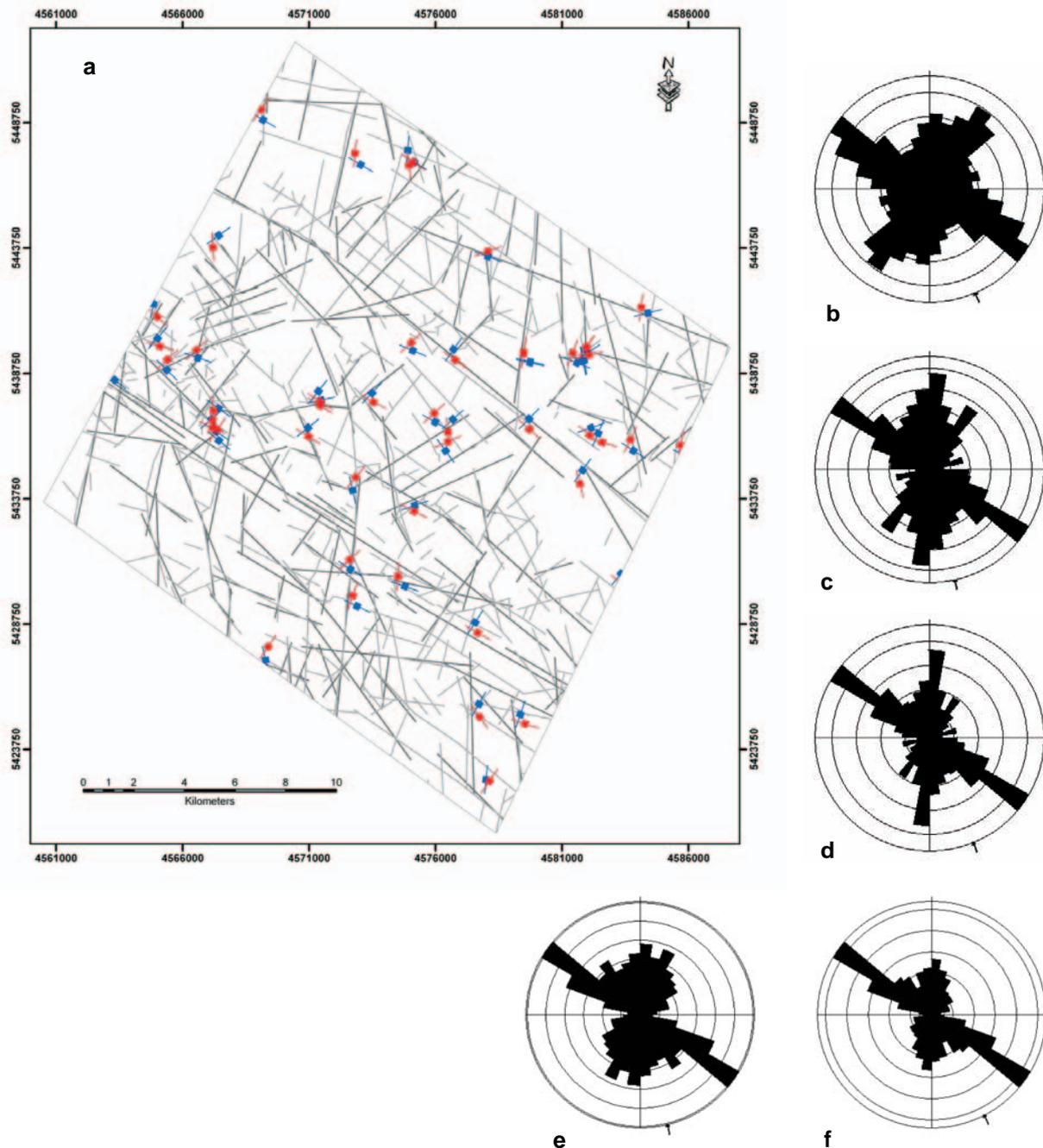


Figure 3-26: Synoptic comparison of photo- and ERS-DEM lineaments with ground truth. (a) Lineament map and fracture orientations at sampling stations. Light gray lines: photolineaments; dark gray lines: DEM lineaments, red symbols: strikes of first-order fracture sets, blue symbols: strikes of second-order fracture sets. (b) Rose diagram depicting strikes of all fractures with dips $\geq 50^\circ$ measured in outcrops in the study area. $n = 3271$. (c) Rose diagram depicting DEM lineament strikes in the study area sensu stricto normalized to their absolute number per 10° strike bin. $n = 1310$. (d) Rose diagram depicting DEM lineament strikes in the study area sensu stricto normalized to their cumulative length per 10° strike bin. Total cumulative length is 1957102 meters. (e) Rose diagram depicting photolineament strikes in the study area sensu stricto normalized to their absolute number per 10° strike bin. $n = 670$. (f). Rose diagram depicting photolineament strikes in the study area sensu stricto normalized to their cumulative length per 10° strike bin. Total cumulative length is 665362 meters. Database for (c) and (d): ERS Digital Elevation Model; database for (e) and (f): aerial b/w imagery.

The comparison of the cumulative plots also shows a generally good regional agreement between the three different datasets. First, it has to be noted that figs. 3-26c and e represent the numbers of lineaments per 10° strike segment while figs. 3-26d and f display the cumulative lengths of lineaments per 10° strike segment. In the following, only the latter will be discussed, because the length-normalized distributions reflect the actual situation better than the mere number of features without paying attention to their regional extent. Furthermore, the length-normalized plots expose less scatter and thus show better-defined peaks than the plots displaying absolute numbers.

With the exception of the distribution of photolineaments (fig. 3-26f) all four prominent strike directions determined from the fracture dataset for the domain overlap analysis are present in the rose diagrams. The photolineaments lack both the 35° (which, however, does exist in fig. 3-26e) and the 80° peak. In the DEM distribution all four peaks are well-recognizable, although their order in terms of their importance differs from the fracture data. While the ranking –in descending order- of the peaks in fig. 3-26c is 120°-35°-1°-80° the peaks in the lineament distributions rank 120°-1°-35°-(80°).

Combining the findings of the domain overlap analysis with the observations made in the examination of the cumulative distributions of fractures and lineaments in figs. 3-26b to f corroborates the notion that the entire extent of the study area is primarily dominated by the NW-SE trending structures, followed by the N-S striking ones. The NE-SW oriented population prominent in the fracture data is rather subordinate in the lineaments, thus suggesting that it did not play the same role in shaping the morphology of the study area as the NW-SE and N-S structures. The 80° segment shows clear, but very small peaks in the fracture and DEM lineament distributions. This causes the relatively distinct population in the cumulative rose diagrams to be of minor importance in terms of its spatial extent and predominance in specific regions in the study area.

In conclusion, a reasonably good correlation between remotely sensed structures and in situ measured fracture data could be established. Although clearly defined coincident fracture and lineament domains do not exist in the study area, local agreement between the orientations of lineaments and prominent fracture sets is a widespread phenomenon. Thus, remotely sensed structures represent valuable proxies for the distribution of fracture orientations at neighboring sampling stations in this region and thus also may prove useful in groundwater prospecting projects.

3.5**References**

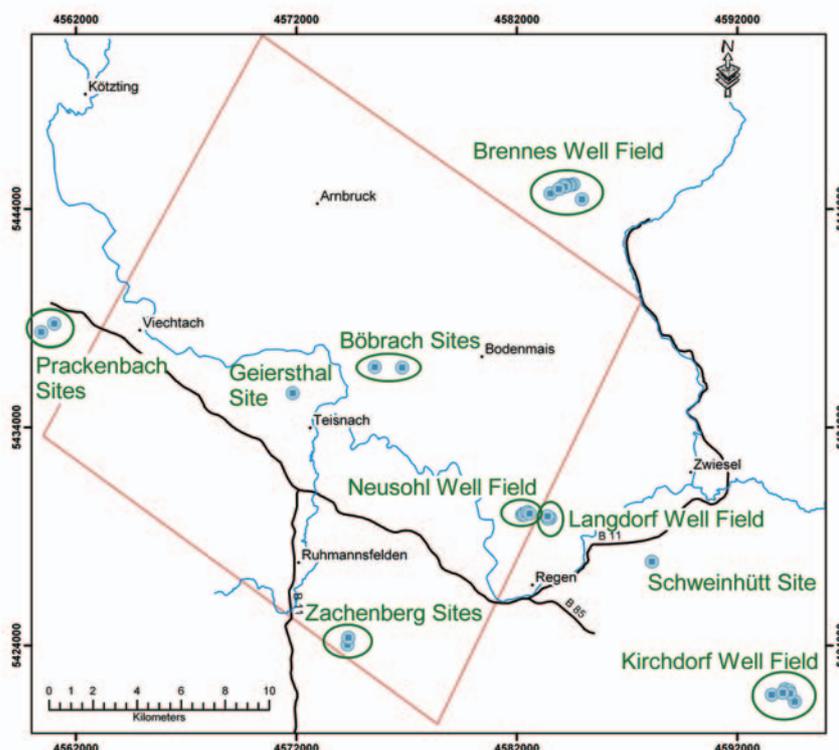
- Bergerat, F., and Geysant, J., 1983, Fracturation tertiaire et evolution des contraintes en Baviere orientale; le Jura franconien et la foret bavaroise (R. F. A.): *Geologische Rundschau*, v. 72, p. 935-953.
- Cheema, T.J., and Islam, M.R., 1994, Experimental Determination of Hydraulic Anisotropy in Fractured Formations: *Bulletin of the Association of Engineering Geologists*, v. 31, p. 329-341.
- ESRI, 2002, *ArcGis Spatial Analyst*, v. 8.3: Redlands, Ca. (USA)
- Gebauer, D., 1977, Die Entwicklungsgeschichte des Moldanubikums aufgrund radiometrischer Altersbestimmungen, *in* Bauberger, W., ed., *Geologische Karte von Bayern 1:25 000, Erläuterungen zum Blatt Nr. 7046 Spiegelau und zum Blatt Nr. 7047 Finsterau etc.*: München, Bayerisches Geologisches Landesamt, p. 12-18.
- Gromes, N., 1980, *Geologische und mikrothermometrische Untersuchungen zur Mineralisation des Bayerischen Pfahls* [Diplom Thesis thesis]: Göttingen, University of Göttingen.
- Gupta, R.P., 2003, *Remote Sensing Geology*: Berlin, Springer-Verlag, 655 p.
- Hofmann, R., 1962, Die Tektonik des Bayerischen Pfahls: *Geologische Rundschau*, v. 52, p. 332-346.
- Jensen, J.R., 2000, *Remote sensing of the environment: an earth resource perspective*: Upper Saddle River, NJ, Prentice-Hall, Inc., 544 p.
- List, F.K., and Ott, W.-D., 1982, *Geologische Karte von Bayern 1:25 000. Erläuterungen zum Blatt Nr. 7043 Ruhmannsfelden*: München, Bayerisches Geologisches Landesamt, 55 p.
- Mabee, S.B., Hardcastle, K.C., and Wise, D.U., 1994, A Method of Collecting and Analyzing Lineaments for Regional-Scale Fractured-Bedrock Aquifer Studies: *Ground Water*, v. 32, p. 884-894.
- Ott, W.-D., 1983, *Geologische Karte von Bayern 1: 25 000. Erläuterungen zum Blatt Nr. 6943 Viechtach*: München, Bayerisches Geologisches Landesamt, 71 p.
- Priehäuser, G., 1968, Über die Verwitterung kristalliner Gesteine zu Zersatz von der Oberfläche aus; Beispiele aus dem Bayerischen Wald: *Geologische Blätter für Nordost-Bayern und angrenzende Gebiete*, v. 18, p. 162-172.
- Rohrmüller, J., Mielke, H., and Gebauer, D., 1996a, Gesteinsfolge des Grundgebirges nördlich der Donau und im Molasseuntergrund, *Erläuterungen zur Geologischen Karte von Bayern 1:500.000*: München, Bayerisches Geologisches Landesamt, p. 16-54.
- , 1996b, *Tektonik, Grundgebirge, Erläuterungen zur Geologischen Karte von Bayern 1:500.000*: München, Bayerisches Geologisches Landesamt, p. 252-259.
- van der Pluijm, B., and Marshak, S., 1997, *Earth Structure: An Introduction to Structural Geology and Tectonics*, WCB/McGraw-Hill, 495 p.
- Zeitlhöfler, M., 2006, Bericht zur Lineamentanalyse auf Basis von SRTM-Satellitenhöhendaten für die Hydrogeologische Landesaufnahme im EU-Ziel-II-Gebiet im Auftrag des Bayerischen Landesamtes für Umwelt - Geologischer Dienst: Regensburg, p. 51.

4 Hydrogeology

After the geological and geomorphological analyses of the study area in the previous chapters the hydrogeological characteristics of this region shall be examined by means of various datasets. In the following, these datasets will be presented, analyzed and correlated with each other as well as with results from the preceding sections. Special attention will be paid to the spatial distributions and correlations of geologic and hydrologic features such as major fault zones and high-yield wells. However, it must be mentioned that an area-wide coverage with hydrogeologic data could not be achieved due to the scarcity of drilling projects at the time of completion of this study. In order to augment the amount of data results from drilling sites outside the study area were consulted. Due to the geologic, tectonic, and geomorphologic similarities between the study area and these drilling sites the incorporation of their data records is legitimate.

4.1 Data inventory

The inventory of hydrogeologic data in the study area can at best be characterized as fragmentary. Only recently did the Eastern Bavarian crystalline basement attract more attention of hydrogeologists due to dwindling resources of surficial and near-surface water supplies. Thus, the scientific collection and evaluation of borehole data obtained from drinking water wells is still in its beginning stage. Nonetheless, a certain amount of information could be obtained from various sources such as the Bavarian Geological Survey's BIS¹, geotechnical engineering



4-1: Distribution of bedrock wells in the study area and its vicinity.

¹ BIS is the acronym for “**B**oden**I**nformations**S**ystem”, a state database containing geological, hydrological, and geotechnical data compiled and maintained by the Bavarian Geological Survey (Bayerisches Landesamt für Umwelt – Geologischer Dienst, Lazarettstr. 67, 80636 München).

companies and communal institutions. In the following the different datasets will be presented and analyzed beginning with borehole data, i.e. results from pumping tests and downhole geophysics. Further on, findings from surface geophysical examinations will be discussed.

Well Name	Gauß-Krüger Coordinates		Altitude above SL [m]	Average Yield [l/s]	Depth to Casing Point [m]	Total Depth [m]	Date of Pumping Test
	E	N					
Brennes, Br. Arberalm*	4583515	5444710	1030	0,1	34,8	35	20000914
Bayerisch Eisenstein, Br. 1*	4561026	5438747	n/a	2**	65	65	n/a
Böbrach Br.1	4575558	5436765	n/a	1**	50	50	n/a
Böbrach Br.2	4576801	5436740	n/a	1**	40	40	n/a
Brennes, Arberbergbahn, Br. 1*	4584562	5445133	n/a	0,35	55	55	n/a
Brennes, Arberbergbahn, Br. 2*	4584438	5445099	n/a	2	40	40	n/a
Brennes, Arberbergbahn, Br. 3*	4584357	5445085	n/a	1	52	52	n/a
Brennes, Arberbergbahn, Br. 4*	4584209	5445083	n/a	1	49	49	n/a
Brennes, Arberbergbahn, Br. 5*	4584159	5445080	n/a	0,8	61	61	n/a
Brennes, Arberbergbahn, Br. 6*	4584123	5445092	n/a	0,8	71	72	n/a
Brennes, Arberbergbahn, Br. 7*	4584164	5445018	n/a	3	31	31	n/a
Brennes, Arberbergbahn, Br. 10*	4583894	5444909	n/a	0,8	41	42	n/a
Kirchdorf, Br. 1*	4594598	5421445	n/a	1**	50	50	n/a
Kirchdorf, Br. 2*	4594157	5422011	n/a	1,5**	50	50	n/a
Kirchdorf, Br. 3*	4594328	5421951	n/a	2**	51	51,3	n/a
Kirchdorf, Br. 4*	4594372	5421816	n/a	3,5**	51	51,4	n/a
Kirchdorf, Br. 5*	4594050	5421844	n/a	1**	47	49	n/a
n Kirchdorf, kommun. WV, Br.D*	4593550	5421760	810	1,5	50	50	n/a
n Geiersthal, kommun. WV, Tbr.	4571840	5435570	558,27	1,66	50	51,2	19950810
no Neusohl, WV Regen, TBr.1	4582240	5429990	587	5,49	39,7	40	19640331
no Neusohl, WV Regen, TBr.2	4582300	5430050	590	2,22	48	48	19640400
no Neusohl, WV Regen, TBr.3	4582340	5430010	590	7,32	45,5	45,5	19710000
no Neusohl, WV Regen, TBr.4	4582480	5430128	n/a	3,5*	55	56	n/a
no Neusohl, WV Regen, TBr.5	4582573	5430055	n/a	3,5*	55	56	n/a
Pilgramsberg, Br. 1*	n/a	n/a	n/a	1**	46	50	n/a
Pilgramsberg, Br. 2*	n/a	n/a	n/a	1**	45	48	n/a
Prackenbach, VB 1*	4540765	5432796	n/a	0,5**	n/a	40	n/a
Prackenbach, VB 2*	4560439	5438366	n/a	0,7**	n/a	40	n/a
s Langdorf, WV Regen, Br.2*	4583500	5429850	667,53	2,09	50	50	19580000
s Langdorf, WV Regen, Br.3*	4583400	5429820	668,99	1,95	39	39	19580000
s Langdorf, WV Regen, Br.4*	4583390	5429930	670,92	2,7	20	20	19580000
Schweinhütt, Br. 1*	4588116	5427852	n/a	2**	54	56	n/a
s Zachenberg, kommun. WV, Br.1	4574144	5424012	842	1,19	70	70,5	n/a
Zachenberg, Br. 2	4574360	5424376	n/a	0,3**	50	77	n/a

* Site located outside the study area sensu stricto (up to 15 km)

** Values estimated by the supervising engineering geologist, Dr. K.D. Raum (company: SVB Dr. Prösl, Velden/Vils, Germany)

Table 4-1: Inventory of communal drinking water wells in the study area and its vicinity. Sources: Bayerisches Landesamt für Umwelt, Geologischer Dienst and SVB Prösl (Velden/Vils, Germany).

Table 4-1 lists the current inventory of bedrock wells drilled for communal water supplies along with further information on parameters such as their locations, average yields, and depths. All these wells are classified as bedrock wells, although a number of them penetrate massive layers of grus before they reach unweathered material. Thus, in cases where the principal points of influx are situated in the saprolite it is debatable whether or not a well can technically be called “bedrock well”. Yet this technicality has little effect on the actual situation, because Raum (2002) found in the analysis of tracer tests that groundwater pathways commonly follow remanent tectonic structures also present in heavily weathered layers. According to his studies even springs tapping only the near-surface flow are influenced by flow along structural anisotropies. The outline map in fig. 4-1 gives an impression of the spatial distribution of the wells tabulated in table 4-1. Only ten wells of a total of 34 are located in the study area *sensu stricto*. Some of the remaining sites lie relatively close by, while a few are situated at distances of up to 15 km. The majority of bores cluster in the four major well fields, which yield a relatively high resolution on a local scale, but on the other hand leave large parts of the study area uncovered. Thus, well yield variographies *sensu* Drew et al. (1999) could not be performed due to the discontinuous coverage with data points.

The individual wells did not receive equal scientific attention. While some of the larger ones, such as several wells in the Neusohl, Kirchdorf, Böbrach and Bayerisch Eisenstein/Brennes fields were treated with borehole geophysical surveys, many of the small low-yield wells were only explored with short-term pumping tests. For a number of wells drilled decades ago only scarcely documented pumping tests exist, whose results at times differ strongly from the actual production rates at which these wells are pumped today. In these cases the yields determined from the pumping test were replaced with current values estimated or measured by the supervising engineering geologist. Thus, it has to be pointed out that the yields presented here are only approximate values used to highlight trends in the following analyses rather than to produce accurate results. This less reliable data will be utilized in the regional characterizations of well properties (section 4.2). For the local analyses only geophysically logged boreholes will be consulted.

4.1.1 Drillers’ logs and borehole geophysics

For the majority of the wells listed in table 4-1 there is little more information available than their locations, depths and yields. However, in some of the larger drilling projects, especially in the Neusohl and Kirchdorf well fields, several boreholes were surveyed with a variety of geophysical approaches. Table 4-2 provides an overview over the methods applied

to specific boreholes. The geophysical surveys were conducted by two logging companies: German Geo Services (Niederlindach/ Germany) and FONTUS Logging Services (Pleinfeld/ Germany). In addition, the associated drillers' logs, compiled from the examinations of well cuttings, shed light on the stratigraphy of those boreholes, which is important for the characterization of the points of groundwater discharge into the wells. As can be gathered from table 4-2 the standard repertoire of well logging in these projects consists of the measurements of water temperature, salinity (derived from electric conductivity), and flow under both idle and pumping conditions. Additional, more sporadically applied methods include measurements of magnetic susceptibility, borehole caliper and gamma radiation. While the data provided by FONTUS Logging Service include only the logs the data provided by German Geo Services consist of the logs and the survey reports (Richert, 2002a, b, 2004, 2005a, b; unpublished reports).

Object Name		Type of geophysical log					
Drillers' Logs	Geophysical Logs	Magnetic Susceptibility	Caliper	Gamma Ray	Temperature	Salinity	Flowmeter
no Neusohl, WV Regen, TBr.4**	Neusohl VB 1	n/a	n/a	n/a	available	available	available
no Neusohl, WV Regen, TBr.5**	Neusohl VB 2	n/a	n/a	n/a	available	available	available
Böbrach Br.1**	Böbrach B 1	n/a	n/a	available	available	available	available
Kirchdorf, Br. 1*	Kirchdorf VB 1	available	n/a	available	available	available	available
Kirchdorf, Br. 2*	Kirchdorf VB 6	n/a	n/a	n/a	available	available	available
Kirchdorf, Br. 3*	Kirchdorf VB 3	n/a	n/a	n/a	available	available	available
Kirchdorf, Br. 4*	Kirchdorf VB 4	n/a	n/a	n/a	available	available	available
Kirchdorf, Br. 5*	Kirchdorf VB 5	n/a	n/a	n/a	available	available	available
Schweinhütt, Br. 1**	Schweinhütt VB 4	n/a	n/a	available	available	available	available
Wiesenfelden, Br. 2 [†] **	Wiesenfelden B 1	n/a	n/a	available	available	available	available
Bayerisch Eisenstein, Br. 1*	Bayer. Eisenstein	n/a	available	n/a	available	available	available

[†] Site is located approximately 20 km W of the study area. Data included here due to the site's similarity to the study area
^{*} Geophysical survey conducted by FONTUS Logging Service, Pleinfeld/ Germany
^{**} Geophysical survey conducted by German Geo Services, Niederlindach/ Germany

Table 4-2: Inventory of geophysical surveys performed on boreholes in the study area and its vicinity.

In the following, especially the flowmeter logs in combination with the drillers' logs will be focused on, because these datasets turned out to yield the least ambiguous information as well as the highest degree of correlation with each other. Nonetheless, the remaining geophysical data records will be presented as well in order to complement the results derived from the former.

4.1.1.1 Drillers' logs

For a large part of the wells listed in table 4-1 drillers' logs containing the borehole stratigraphies are on file. However, due to the problem that those logs by themselves provide little information on the relationship between borehole stratigraphy and well productivity only

the logs of wells surveyed with geophysical approaches were examined in detail. Especially section 4.1.1.2 will focus on the comparison of these two parameters. The reports on the examination of well cuttings can be found in appendix B.

A typical borehole of a water supply well in the Eastern Bavarian crystalline basement consists of two distinct lithologic entities. The top part of most wells is made up of a layer of soil, surficial sediments such as earth flow deposits and, with increasing depth

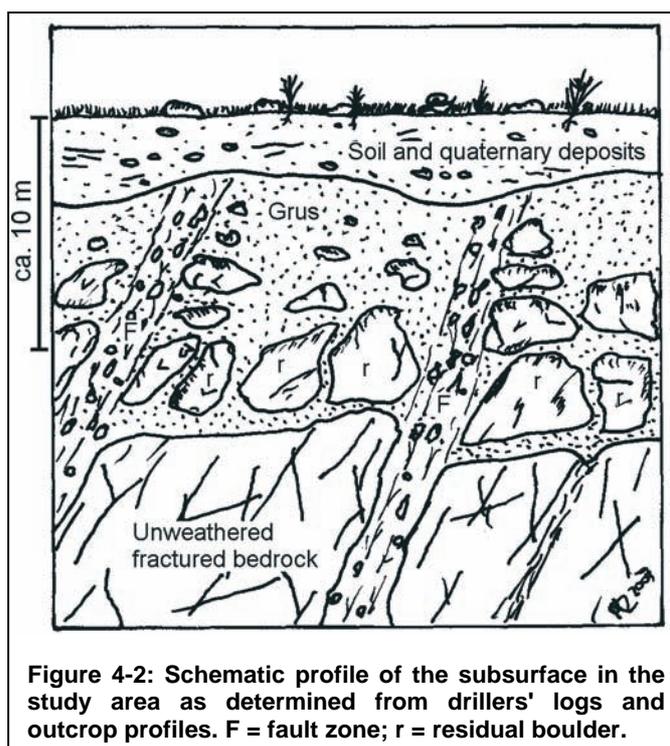


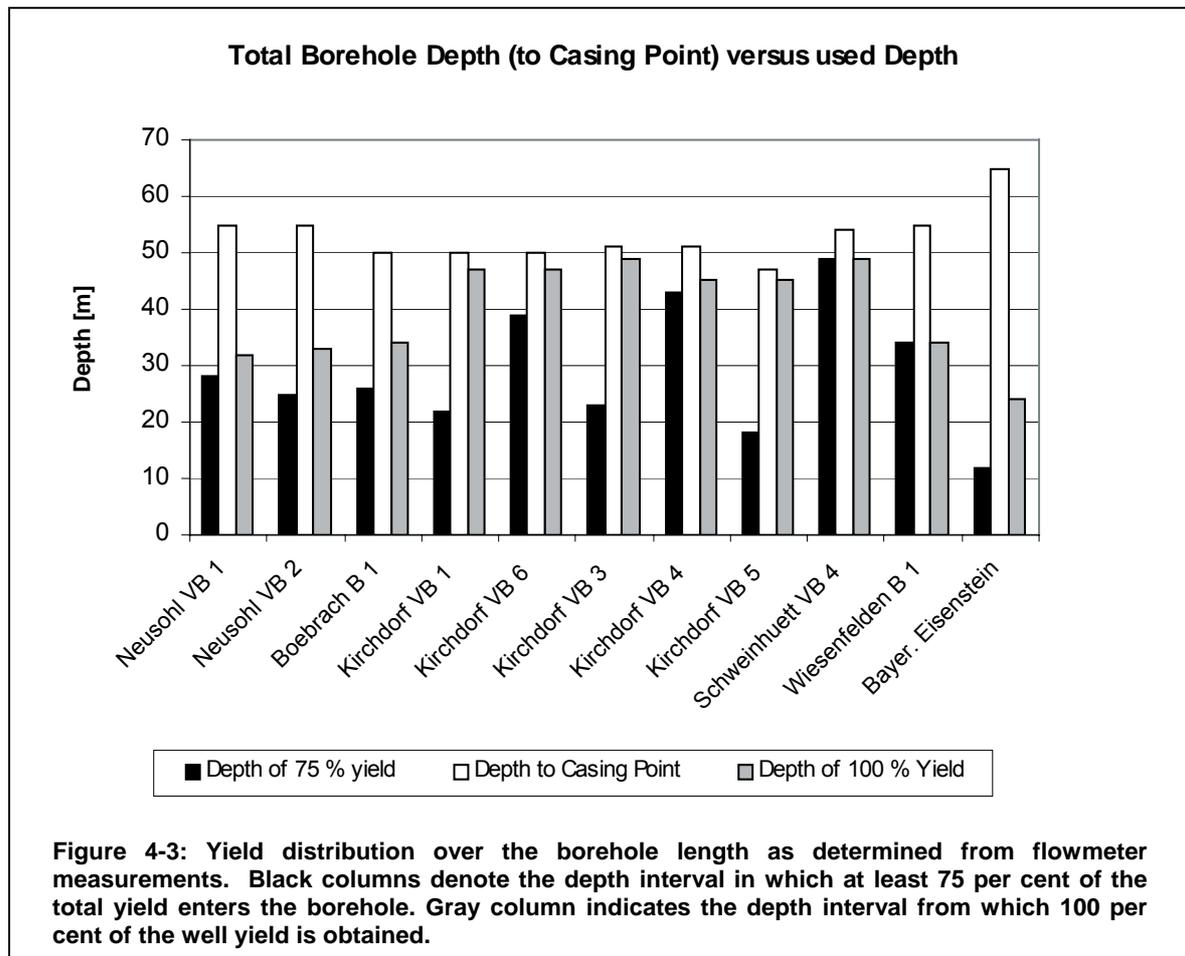
Figure 4-2: Schematic profile of the subsurface in the study area as determined from drillers' logs and outcrop profiles. F = fault zone; r = residual boulder.

below the topographic surface, of intensely weathered bedrock (grus), which has lost most of its coherence. Further down, this grus is gradually replaced by less weathered bedrock, frequently in the form of residual boulders interspersed with grus units. Especially along faults, which allow groundwater to percolate further into the subsurface, the grus zones can extend to deeper levels and therefore be juxtaposed with blocks of relatively unweathered and unfractured bedrock. Geologic structures, such as faults or folds can still be present in the grus layer, as long as no reworking has occurred. Moreover, Raum (2002) identified remanent silicified fractured fault zones in the grus as the prominent groundwater avenues in this material. Figure 4-2 provides a conceptual model of the subsurface as it is envisioned from the analysis of well cuttings and the visual inspection of large bedrock exposures. Along with further explanations the profiles used for this model will be presented –in a very simplistic way- in section 4.1.1.2 where they will be compared with the results from the flowmeter surveys.

4.1.1.2 Pumping tests and flowmeter logs

For the analysis of well productivity the flowmeter logs and pumping test results provided the most valuable information. Flowmeter surveys were conducted in all wells listed in table 4-2. Only the logs recorded during the pumping tests are presented here, because they represent best the behavior of wells under production conditions. Additionally, drillers' logs are available for each well, so groundwater influx into the borehole can be correlated with lithology.

To begin with, the distribution of individual points of discharge over the length of a borehole adding to its cumulative well yield will be focused on. Figure 4-3 displays the total and the effective depths of the surveyed wells. Both the depth interval producing 100 per cent and the interval contributing at least 75 per cent of the total yield are juxtaposed with the wells' depth to their casing points. From this figure it becomes obvious that the majority of wells do not utilize their entire depth for the production. Moreover, about two thirds of the wells produce at least 75 per cent of their total yield in the top half of the borehole. For 100 per cent of their yields about half of the wells utilize more than 80 per cent of their length. The remaining boreholes produce their total yield over 60 to 80 percent of their lengths. The only exception is the *Bayerisch Eisenstein* well, whose primary point of discharge contributing 90 % of the yield lies at 10 to 12 m below the surface while the only secondary point is located at 21 to 24 m, thus leaving the remaining parts of the overall 65 m deep hole obsolete.



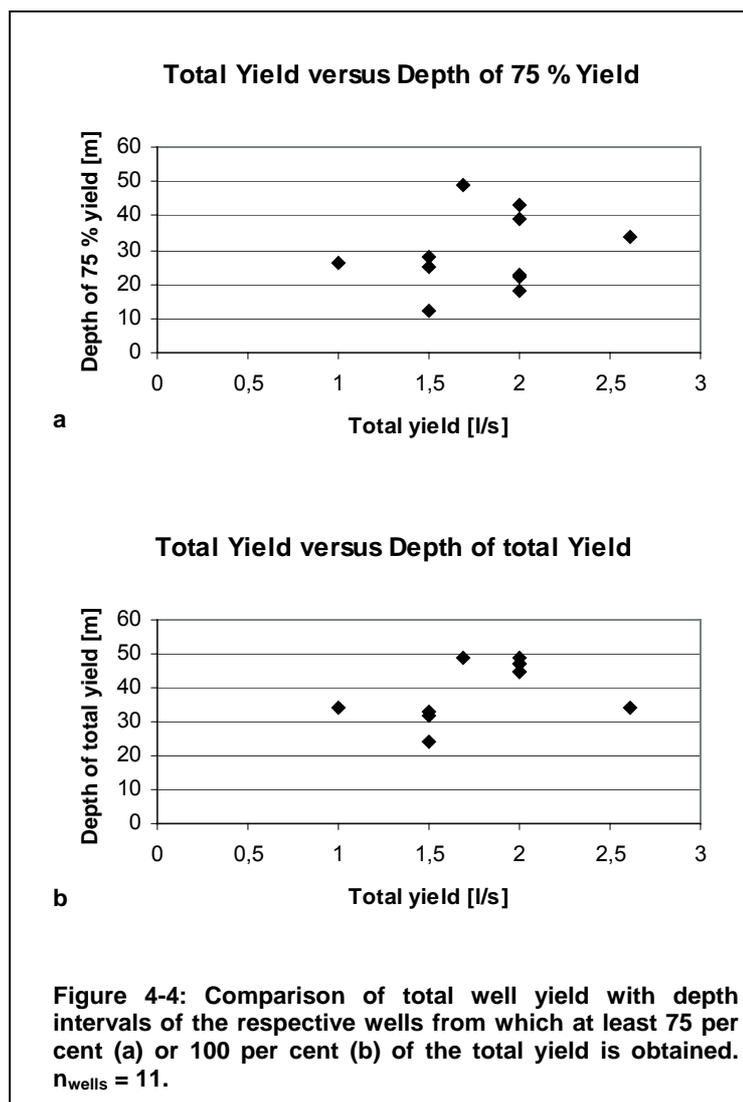
The distribution of effective depths in fig. 4-3 is very heterogeneous. Thus, it does not provide an absolute depth below which no further groundwater can be expected, at least not in the depth intervals presented here and the decision on how deep to drill seems to remain largely a game of chance. The two extremes highlighting this dilemma are the

abovementioned *Bayerisch Eisenstein* well and the *Schweinhütt VB 4* site. While for the former a large part of the invested financial assets were wasted in the design of a deep borehole, which essentially produces the bulk of its yield in the top fifth of the hole, the latter turned out to be a success with over 90 per cent of its extent used to extract groundwater.

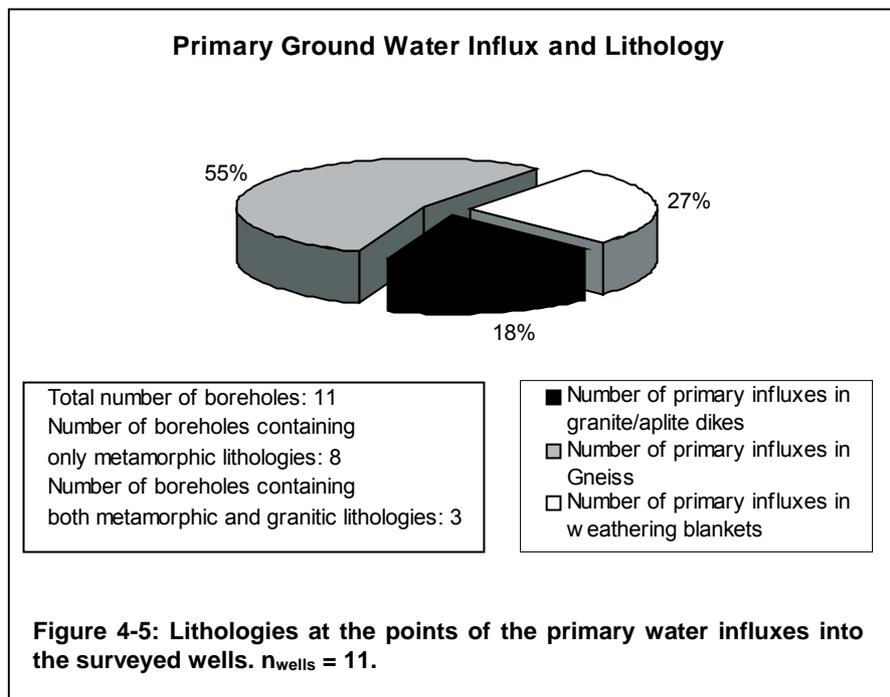
In contrast to the representation of relative well productivities in fig. 4-3 the plots in fig. 4-4 quantify the well yields with respect to their depths. For both the 75 and the 100 per cent levels there is a slight, though statistically insignificant, tendency for wells with larger effective depths to be associated with somewhat higher

productivities, especially when considering the total yield (fig. 4-4b). For the 75 per cent yield level (fig. 4-4a) there is more scatter in the distribution, thus indicating again that the water gain of a deeper well is restricted to a minor fraction of its total discharge. However, in highly productive wells the absolute value associated with this fraction can amount to a relatively large quantity of water.

As already mentioned all boreholes surveyed by flowmeter come with drillers' logs. Comparing the borehole stratigraphy with the locations of groundwater bearing zones allows the identification of the conductive lithologies in a particular well. The pie chart in fig. 4-5 shows that almost 75 % of the primary influxes are situated below the sedimentary or weathered overburden in the more or less pristine bedrock. Where present, highly fractured igneous intrusions into the metamorphic lithologies are preferentially used by the primary influxes. However, igneous rocks are recorded only in three borehole profiles. Wells situated



exclusively in igneous lithologies were not geophysically surveyed but are generally associated with relatively low yields (section 4.2.2). Minor influxes from the overburden only exist in boreholes, which intersect relatively thick layers of surficial materials. This is the case in four out of eleven wells. The relationships between borehole stratigraphy and zones of groundwater discharge can be observed in more detail in fig. 4-6. The profiles presented are simplified schematic representations of the interpretations of well cuttings obtained in one meter increments during the drilling process. Lithologic distinctions are made between layers of overburden, gneiss showing varying degrees of weathering and igneous intrusions associated with various degrees of fracturing. The zones of discharge are classified according to their relative contributions to the overall well yield (cf. table 4-1). Table 4-3 contains the detailed legend for the profiles in fig. 4-6.



Color	Unit
	Zones of groundwater influx into the borehole with decreasing significance from dark to light blue
	Sediment and/ or grus blanket
	Gneiss, significantly weathered
	Gneiss, moderately weathered to unweathered
	Igneous intrusion with highly fractured zones
	Igneous intrusion weakly fractured to unfractured

Table 4-3: Legend to fig. 4-6. Blue colors denote zones with varying intensity of discharge into the borehole in the flowmeter log. Remaining colors are attributed to lithologic units in the drillers' log.

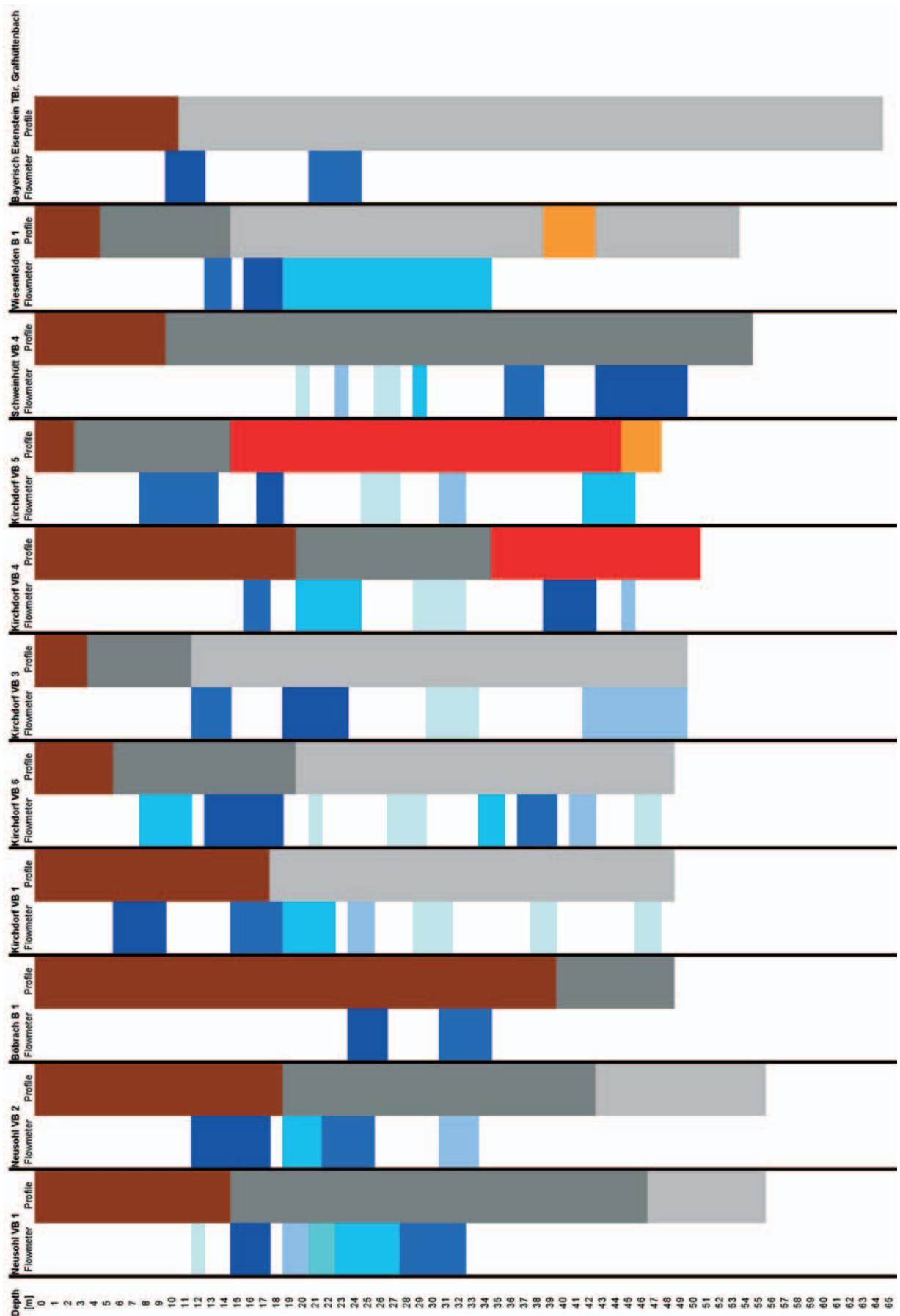


Figure 4-6: Schematic profiles of flowmeter (blue colors) and drillers' (brown, gray, and red colors) logs displaying the stratigraphy of the boreholes and the locations of groundwater bearing zones. Legend is detailed in table 4-3.

As can be inferred from fig. 4-6 the cumulative yields of the surveyed wells are commonly obtained from several conductive zones over the length of the boreholes. The relative contributions of the individual zones frequently vary over as much as one order of magnitude. For example, in well *Kirchdorf VB 3* the primary influx yields 1.36 l/s while the least productive influx contributes only 0.06 l/s. In the majority of cases the primary influx yields more than 50 per cent of a well's total yield, in some instances even up to 90 per cent. This highlights the importance of striking highly conductive zones in a hard rock well and at the same time explains why the well yields are so heterogeneous in this area. Comparing the vertical extents of primary and secondary zones of discharge show that the zones which contribute most to the cumulative yields are frequently relatively narrow compared to those contributing less (e.g. in wells *Wiesenfelden B 1* or *Kirchdorf VB 5*).

Pertaining to the lithologic units intersected by the boreholes it can be observed that all wells pierce a certain amount of overburden before they reach the bedrock, whose degree of weathering commonly decreases gradually with increasing depth below the surface. The overburden thickness varies from less than one meter to more than 35 m. A relationship between the overburden thickness and the location of a particular well (e.g. in a valley where the blanket might be expected to be thicker or on slopes where it might be thinner) could not be established based on this dataset. At a certain depth the grusy overburden grades into bedrock. This interface is not represented by a sharp transition but rather by a layer in which blocks of relatively unweathered gneiss are interspersed with weathered material. In this context weathering processes have to be understood as three-dimensional systems, which progress not only vertically but also laterally. This is especially the case where intensely fractured zones or faults in the bedrock allow water to percolate deeper into the bedrock and corrode it laterally. The result is commonly known as woolsack weathering, especially in granitic areas, although similar processes can also act in fractured metamorphic lithologies. It can be observed nicely in deep road cuts and quarries as well as along mountain ridges throughout the study area. Thus, when drilling into an old inactive fault where long-term weathering has decomposed the gneiss to grus the driller's log can indicate a thick layer of overburden while a hole a few meters away might pierce relatively fresh gneiss at the same depth.

It has already been mentioned that in most cases significant amounts of groundwater do not enter the well through the overburden but rather through fractures in the relatively fresh gneiss. Most profiles corroborate this notion. However, it also raises the question if large fault zones are always the best locations for drilling productive wells. As described above, heavy weathering in an old inactive fault can produce material similar to the surficial

grus, which can effectively cement and clog the pathways due to the production of easily swelling clay minerals. Banks (1994) described this effect for the Hvaler test site in SE Norway, while Dobner (1983) mentioned it without going into details in his appraisal of the hydrogeologic situation on the Viechtach map quadrangle. Raum (2002) discovered another effect during tracer tests on surficial springs. These springs, although situated in the grusy overburden, which frequently has been described as porous aquifer (Bender, 2001; Propach, 1968), turned out to be mainly fed through remanent fractures. For their conductivity their infillings play a significant role. While fractured quartz infillings proved to be highly conductive clayey weathering deposits effectively closed the conduits after percolating precipitation had wetted them. Transferring these findings to deeper-reaching fault zones the degree of weathering and the type of infilling decide over a fault's/ fracture zone's conductivity.

Examining the bedrock sections of the profiles in fig. 4-6 shows that groundwater enters the well through relatively narrow zones at various depths thus highlighting the aquifer's non-porous properties. Although in several boreholes the distinction between significantly and moderately weathered to unweathered gneiss is made it has to be understood as a very simplistic approximation to the actual situation. In reality, the degree of weathering in a borehole is a continuum of decreasing intensity with increasing depth, although local variations (described in the interpretations of the well cuttings) exist, but cannot be resolved in the profiles in fig. 4-6.

Regarding the hydraulic properties of the penetrated metamorphic and granitic lithologies the observations only lead to ambiguous results. Sites *Neusohl VB 1* and *VB 2*, as well as *Kirchdorf VB 5* and *VB 6* suggest that significant weathering of gneiss is conducive to well productivity, because major parts of their yields are derived from this layer. By contrast, wells *Kirchdorf VB 3*, *Bayerisch Eisenstein Br. 1* (which both are missing a layer of significantly weathered gneiss) and *Wiesenfelden B 1* draw the bulk of their yields from moderately weathered to unweathered gneiss. Several major points of influx are located at depths where lithologic changes occur. For instance, in wells *Neusohl VB 1* and *VB 2*, *Kirchdorf VB 1*, and *Bayerisch Eisenstein* zones of major discharge are situated at or near the interface between grusy material and bedrock. As already mentioned this interface cannot be envisioned as a sharp border, but as a very heterogeneous mixture of hard rock and weathering products, which seems to have created an environment allowing significant groundwater flow. However, not only such high lithologic contrasts as those between grus and gneiss produce increased conductivity. Depth intervals at which the well cuttings suggest a significant decrease in the intensity of weathering of the gneiss, the contact to a granitic intrusion, or a change in the degree of fracturing in granitic lithologies are also sites at or

above which groundwater preferentially enters a well. Examples for this phenomenon are wells *Kirchdorf VB 6* and *VB 5*, and *Wiesenfelden B 1*.

Boreholes intersecting igneous rocks tend to show increased groundwater influx in these lithologies, as can be observed in sites *Kirchdorf VB 4* and *VB 5*. The contributions of these individual influxes amount to over 50 per cent of the total yields in both wells. Thus, granitic intrusions seem to be associated with elevated transmissivities with respect to the metamorphic host rocks. However, this seems not to be the case where wells are drilled into purely igneous lithologies such as the extensive granitic plutons in the southern part of the study area where gneissic host rocks are absent. As can be seen in the regional analysis of well yields in section 4.2.2 massive granitic rocks turn out to be relatively low-yield aquifers. Thus, igneous rocks appear to be especially transmissive only in places where they occur as small-scale intrusions such as dikes and veins. There, rheological differences between host rock and intrusion can induce varying brittle behavior with respect to tectonic stresses and therefore cause differences in the intensity of fracturing. Raum (2002) observed this effect on small remanent quartz veins in a grusy matrix. Thus, as in the overburden rheological differences between grus and quartz veins caused the latter to fracture and become more transmissive – much in contrast to the more ductile grus - the rheological differences between gneiss and igneous intrusions may produce the same effect. Adding to their increased tendency to fail is also their –with respect to the extent of the host rocks- relatively thin and sheet-like form, because relative bed thickness is another criterion for a rock's proclivity to fracture (van der Pluijm and Marshak, 1997). Contacts between vein and host rock may serve as additional planes of weakness for fracturing and thus become avenues for flow.

In summary, several general aspects concerning the flowmeter surveys shall be pointed out. The most striking observation is that in the Eastern Bavarian crystalline basement the fractured bedrock commonly contributes more to the total yield of a well than the surficial sediments and weathering products. Secondly, the relative amounts of water entering a well through individual influxes underlie large variations. The bulk of the productivity of a well thus depends on a few single highly productive influxes. If they are missed in the drilling of the borehole the resulting well will show a significantly decreased productivity. Thirdly, lithologic interfaces tend to be associated with elevated yields. This is especially true for igneous dikes and veins. Where present, these intrusions can be expected to produce the bulk of a well's overall yield. Finally, in the analysis of the flowmeter and drillers' logs it has become evident that definitive predictions on the productivity of a prospected well cannot be made due to the multitude of parameters influencing the well

properties. Only the probability of drilling a productive well can be augmented with considering the abovementioned aspects. Also, caution has to be advised when pondering the absolute values of well yields determined by the flowmeter. Since the surveys were performed during short-term pumping tests they reflect the near-field transmissivity around the borehole very well. During production, however, the yield becomes dependent on the recharge rates, which frequently do not suffice to utilize the full potential transmissivity. Therefore, long-term production rates frequently tend to decrease over time by up to 80 per cent in some rare cases².

4.1.1.3 Geophysics: Gamma ray, caliper, temperature, and salinity logs

As stated in table 4-2 only salinity and temperature logs were recorded for all listed boreholes. Gamma ray and caliper were measured rather sporadically. The single magnetic susceptibility log recorded in well *Kirchdorf VB 1* will not be considered, because this method has no significance in groundwater prospecting. The logs referred to in this section can be found in appendix E.

The **gamma ray logs** recorded in wells *Böbrach VB 1*, *Kirchdorf VB 1*, *Schweinhütt VB 4*, and *Wiesenfelden B 1* generally did not yield many useful results for the identification of zones of high groundwater flow. This method is commonly used in sedimentary formations for the distinction of water-bearing strata, which frequently consist of sandy material. By contrast, low-conductivity layers are usually associated with material rich in clay, which contains elevated levels of the radioactive ⁴⁰K isotope. Thus, the higher the γ radiation the higher is the clay content of a layer, and the lower is its expected hydraulic conductivity (Denzel et al., 1995; Hölting and Coldewey, 2005; Prinz and Strauß, 2006). Higher concentrations of this isotope also exist in mica. Therefore, its application in metamorphic and igneous lithologies is rather improper for the distinction between conductive and non-conductive layers. Nonetheless, slight tendencies could be observed in the logs.

In well *Böbrach VB 1*, which penetrates the grus layer for most of its extent, the depth interval in which its two major influxes are situated is characterized by slightly depressed γ values. This indicates that the clay content of the grus at this level is slightly lower and therefore the conductivity somewhat higher.

In well *Kirchdorf VB 1* a prominent spike marks the transition from grus to bedrock, which, however was located about 2 m higher by the driller's log. Lithologic anomalies such

² Dr. K. D. Raum (SVB Präsl, Velden/ Vils, Germany). Personal communication, March 2007.

as elevated concentrations of clays or mica, or the presence of an igneous dike potentially containing high levels of radioactive isotopes, which might explain this peak, were not mentioned in the analysis of well cuttings. At the depth level of this grus-bedrock transition the second-most productive influx is situated. The dominant influx, however, cannot be correlated with anomalies in the γ ray log. Below the depth of 35 m the graph becomes very jagged. However, at these depth levels no lithologic variations are recorded in the driller's log. Thus, the reason for this might lie in background noise in combination with variations in the mica contents of the gneiss.

In well *Schweinhütt VB 4* a prominent spike of 238 API³ exists approximately at the interface between grus and bedrock, which in this case, however, is not associated with groundwater influx. Since the grus is mainly a weathering product of the underlying gneiss the presence of the grus-bedrock transition does not explain this anomaly. Moreover, γ radiation values of more than 200 API are rather uncommon for clays and mica (Richert, 2005b). Thus, the elevated radiation must stem from other sources, possibly an intruded igneous dike containing elevated levels of radioactive minerals. However, the driller's log does not mention a lithologic change at this level. The remaining part of the log shows mainly background noise, thus suggesting a relatively uniform stratigraphy of the borehole, which is corroborated by the driller's log. Generally, the bedrock exhibits elevated γ radiation levels with respect to the grus layer. A relationship between groundwater influx and gamma ray anomalies could not be identified at all.

The gamma ray log of well *Wiesenfelden B 1* shows a pattern similar to those of the other locations. The relatively thin grus layer with a thickness of four meters is characterized by relatively low gamma ray values. A sharp increase exists at the transition to the partially weathered bedrock, which, however, is not associated with groundwater inflow. The remaining log shows generally high API values of up to 275, thus suggesting again the presence of radioactive minerals other than clays and mica. Interestingly, the most prominent peak is located at a depth where the driller's log identifies a small aplite dike. Apart from this dike the gamma ray and the driller's logs do not correspond well. Moreover, some sections in which the well cuttings suggest a high content of biotite are associated with very low API values. Again, the hydraulic situation in the borehole is not reflected in the curve of the gamma ray log.

In summary it should be mentioned that the gamma ray logs generally do not provide much useful information with respect to groundwater prospecting in the Eastern Bavarian

³ API is the current standard unit for the measurement of gamma radiation in boreholes. It was established by the American Petroleum Institute.

crystalline basement. They merely allow to a certain extent the distinction between the grus layer and the bedrock, which, however, is more easily and more accurately achieved in the examination of well cuttings.

Unfortunately, only one **caliper log** exists in the entire data record. The reason for this is the provisional casing, which is installed during or immediately after the drilling to prevent the borehole from collapsing. Wells in this area face a relatively high risk of borehole collapse due to the thick and frequently unstable overburden blankets many of them penetrate. Only in well *Bayerisch Eisenstein Br. 1* the borehole was left open and a caliper log was compiled. This type of log surveys changes in the borehole diameter and is extremely helpful for the detection of borehole breakouts in hard rocks. These breakouts are commonly attributed to the presence of potentially water-bearing fracture zones (Hölting and Coldewey, 2005). In the surveyed well the top 11 meters show a very irregular caliper log curve, which corresponds to the depth interval in which the driller's log mentions surficial material. This unstable material breaks out easily when drilled and thus produces irregular borehole walls. According to the flowmeter measurements the dominant groundwater influx accounting for 90 per cent of the well's cumulative yield lies in this zone. Therefore, the caliper log cannot provide information on water-bearing breakouts due to the irregular nature of the borehole in this section. At depths of 22.5, 30, 31.5, 44, and 46.5 meters the otherwise flat curve shows singular caliper variations of up to 25 mm. The one at 22.5 m is associated with a peak in the flowmeter log (at ca. 23 - 25m). The other breakouts show no correlation with the flowmeter curve, thus suggesting that not every fracture zone is an active avenue for groundwater flow. However, a comment inserted in the associated temperature/ salinity log at this depth level suggests several small, though not quantifiable inflows. A very large breakout with a caliper variation of over 50 mm exists at the depth interval between 50 and 54 meters. Again, no inflow of groundwater was detected by the flowmeter at this level.

The **salinity and temperature logs**, which are usually analyzed in combination with each other, are mainly used to corroborate the results from the flowmeter tests. Because the flowmeter's propeller has a stimulus threshold very small fluxes often cannot be recognized. The temperature/ salinity logs help to identify such small fluxes, which, if a certain number of them are present, can amount to a significant portion of the cumulative well yield⁴. The ranges of temperature variations are generally less than 1°C. Groundwater temperatures usually lie between 6° and 9°C. Salinities commonly fall between 50 and 150 µS/cm. All salinity measurements are normalized to a temperature of 25°C (EU-standard EN 27888). With regard to the flowmeter logs the salinity and temperature logs frequently provide

⁴ Peter E. Richert (German Geo Services). Personal communication, February 2007

redundant information. Therefore, only logs complementing the flowmeter measurements will be presented here. This is the case in wells *Neusohl VB 1*, *Böbrach B 1*, *Wiesenfelden B 1*, and *Bayerisch Eisenstein Br. 1*.

In wells *Neusohl VB 1* and *Böbrach B 1* discrepancies between temperatures under idle and pumped conditions suggest minor influx of slightly warmer groundwater below the lowest zone of influx determined by flowmeter measurements. However, the amounts of discharge could not be quantified. On the other hand, several zones of major influx determined by the flowmeter did not cause any reaction in the temperature and the salinity logs of well *Neusohl VB 1*.

In well *Wiesenfelden B 1* the flowmeter and salinity/ temperature curves diverge somewhat. While the flowmeter shows significant inflow from 34 m upwards the salinity/ temperature curves exhibit a significant drop at about 40 m below the surface and then remain relatively constant. The temperature recovers to levels above this sharp drop approximately at the depth of the topmost influx (at ca. 12 m). However, surficial effects raising the water temperature also have to be taken into consideration. Therefore, due to the temperature/ salinity anomaly at 40 m minor influx below the maximum inflow depth determined by the flowmeter is possible, although not quantifiable, similar to the situation in *Böbrach* and *Neusohl*.

The salinity and – to a lesser extent - the temperature logs in well *Bayerisch Eisenstein Br. 1* show a prominent anomaly at the depth interval from 55 to 60 meters, which is not accounted for in the flowmeter log. Interestingly, this is approximately the depth where the caliper log shows an increase in borehole diameter of about 50 mm. As already mentioned in the description of the well's caliper log a side note in the temperature/ salinity log suggests individual points of minuscule inflow for the depth interval from 25 to 65 meters. However, while the caliper shows several irregularities over that increment the temperature and salinity exhibits a very uniform gradient.

In conclusion it has to be noted that the various geophysical approaches add little further information to that obtained from the flowmeter tests, which are regarded as the most valuable tool in the analysis of well productivity. The gamma ray logs merely show the transition between grus cover and bedrock, which, however, can as well be obtained from the examination of well cuttings. The temperature and salinity logs partially complement the findings of the flowmeter logs and occasionally identify additional points of groundwater influx. Yet this information is of little practical use because this influx cannot be quantified

and its contribution to the cumulative well yield remains questionable. The caliper log is potentially a powerful tool for the identification of fracture zones in the subsurface. Unfortunately, the limited availability of this kind of data precludes the general assessment of its value for well surveys in the study area.

4.1.2 Surface geophysics

Surface geophysical data acquisition is carried out extremely rarely in groundwater prospecting projects in the Eastern Bavarian basement complexes. Thus, only one such study can be presented here. The study location is situated approximately 7 km W of the NW corner of the study area. Nonetheless, the high quality of the results and the comprehensive examination (including fieldwork and remote sensing discussed in section 4.3) render it an extremely valuable source of information not to be ignored. This study was commissioned by the city council of Bad Kötzing and carried out by German Geo Services⁵ as part of the prospecting efforts for a

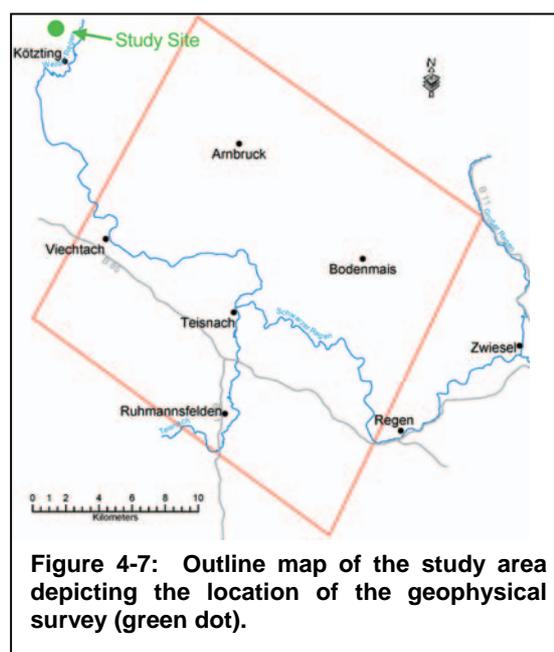


Figure 4-7: Outline map of the study area depicting the location of the geophysical survey (green dot).

geothermal well. For this purpose, true resistivity data was obtained from a multi-electrode geoelectric tomography. The electrode configuration was set up in a dipole-dipole array. The quantity to be measured was the true electric resistivity of the ground in Ohm*m. Further information on the technical setup, data acquisition and processing can be obtained from the project reports (Richert, 2006; Zeitlhöfler, 2006a). The study site is located in the Dampfbach valley⁶, a local NNW-SSE trending valley North of the town of Bad Kötzing, near the village of Zeltendorf (fig. 4-7). This valley was suspected to be underlain by a fault zone and therefore was chosen as a potential candidate for a thermal water drilling project. A previous study (Polivka, 1999) suggested that the valley holds the southern extension of the Marienbad fault zone, also known as the Western Bohemian shear zone (Rohrmüller et al., 1996). As will be detailed in the case study in section 4.3 no evidence was found to corroborate this assumption. Nonetheless, the following data will show that the valley has developed over a major fault zone, be it part of the Western Bohemian shear zone or not.

⁵ German Geo Services is a geophysical engineering company based in Niederlindach/ Germany

⁶ Although the German "Dampf" means "steam" the location name intends no historically documented allusion to geothermal activity in this area

Figure 4-8 depicts the results of the tomography. The two profiles with lengths of 790 and 560 meters, respectively, reach depths of up to 130 meters in their central parts. A total of 80 sampling points were installed along profile 1, 47 points along profile 2. The color scheme reflects the contoured measured resistivities. Their lithologic interpretation was devised as follows:

Resistivity (Ohm*m)	Lithologic interpretation
< 400	Layer of weathered material (clay-rich); sedimentary valley infilling
400 – 1100	Layer of weathered material (sandy, grusy); transition to unweathered gneiss
600 - 1600	Fracture/ fault zone
> 2000	Pristine gneiss

Table 4-4: Lithologic interpretation of resistivity ranges for the Bad Kötzing geoelectric tomography. Source: Richert (2006a).

The classification of the resistivity ranges in table 4-4 is based on the assumption that pristine bedrock is relatively non-conductive for electric currents and therefore possesses a high resistivity. On the contrary, water-saturated sediment or fractured rock is electrically more conductive and thus is associated with a relatively low resistivity. The resistivity of pure groundwater in this area lies at approximately 200 to 250 Ohm*m as determined from borehole geophysical analyses performed at water supply wells in the vicinity of the town of Regen, ca. 25 km SE of this location. The relatively similar lithologies around Bad Kötzing and Regen allow this comparison. Table 4-4 shows a certain degree of overlap in the resistivity ranges, which depends on the location of a specific measuring point in the profiles. For instance, a value of 1200 Ohm*m (colored pink in profile 2) collected close to the topographic surface is attributed to the surficial weathering layer while the same value found further down between blocks of solid gneiss is related to a fracture/ fault zone.

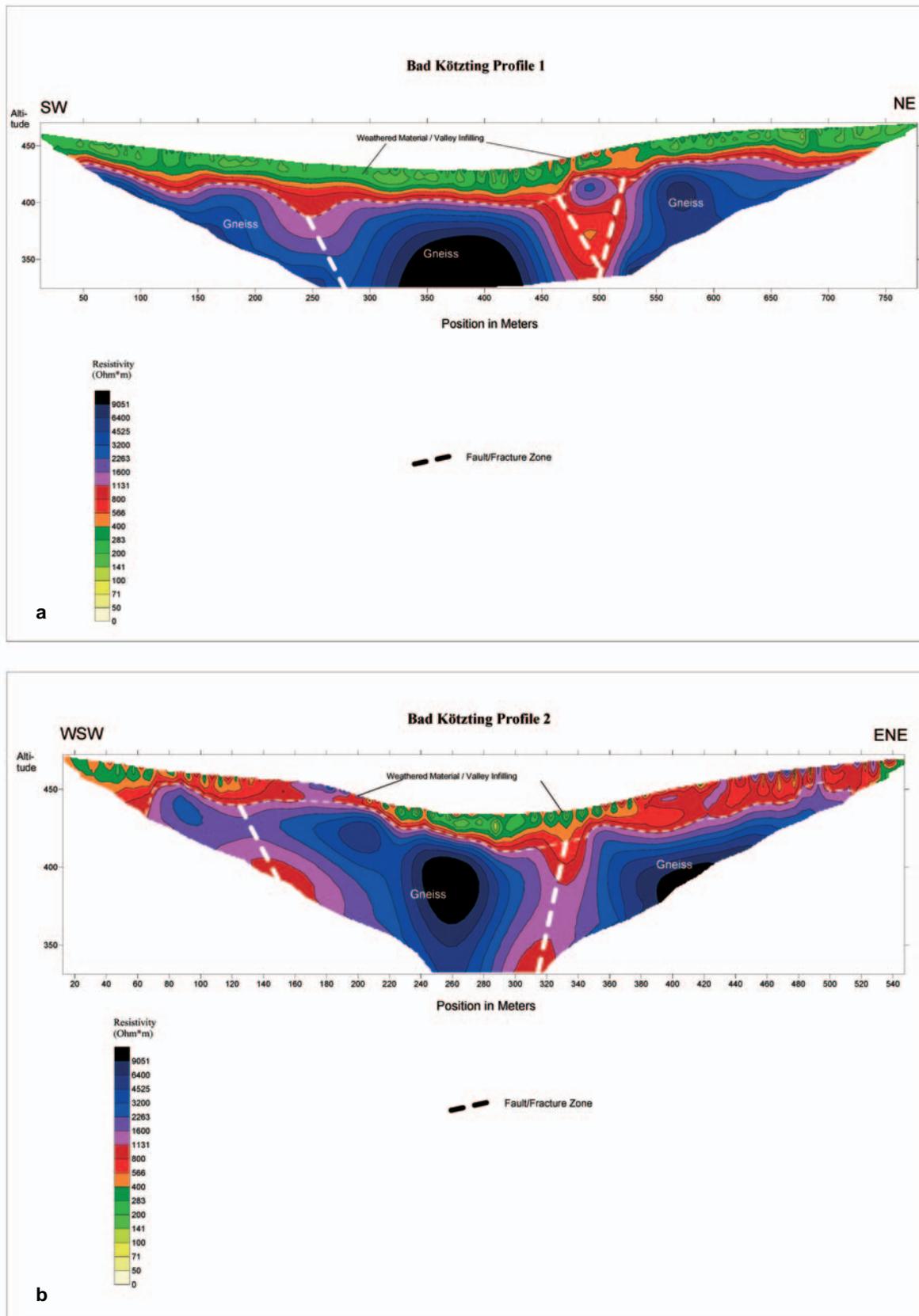


Figure 4-8: Profiles of the geoelectric tomography conducted by German Geo Services. Colors depict true resistivity. Image source: Richert (2006a).

The resistivity distribution in both profiles shows surficial layers with low values. In profile 1 an almost continuous low-resistivity layer with values ranging from 150 to 400 Ohm*m (green colors) can be seen. This profile transects a part of the valley where its width increases while its topographic relief decreases. Thus, a relatively thick and stable zone of weathering material with a comparatively high water content could develop. On the contrary, profile 2 is located in a part of the valley where its flanks become steeper and its bottom narrower. There, loose material is more readily removed from the flanks by erosion and gravitational processes, such that relatively unweathered bedrock reaches close to the surface around the valley shoulders. Low-resistivity layers are found mainly in its bottom, where sediment can accumulate ground water as well as surficial water supplied by the little stream flowing through the valley. In both profiles the resistivity generally increases with increasing depth below the topographic surface except for two steeply inclined zones in each transect. Both of these zones are situated in similar locations along the two profiles, possess similar inclinations, and thus can be connected by the assumed faults traces in fig. 4-9.

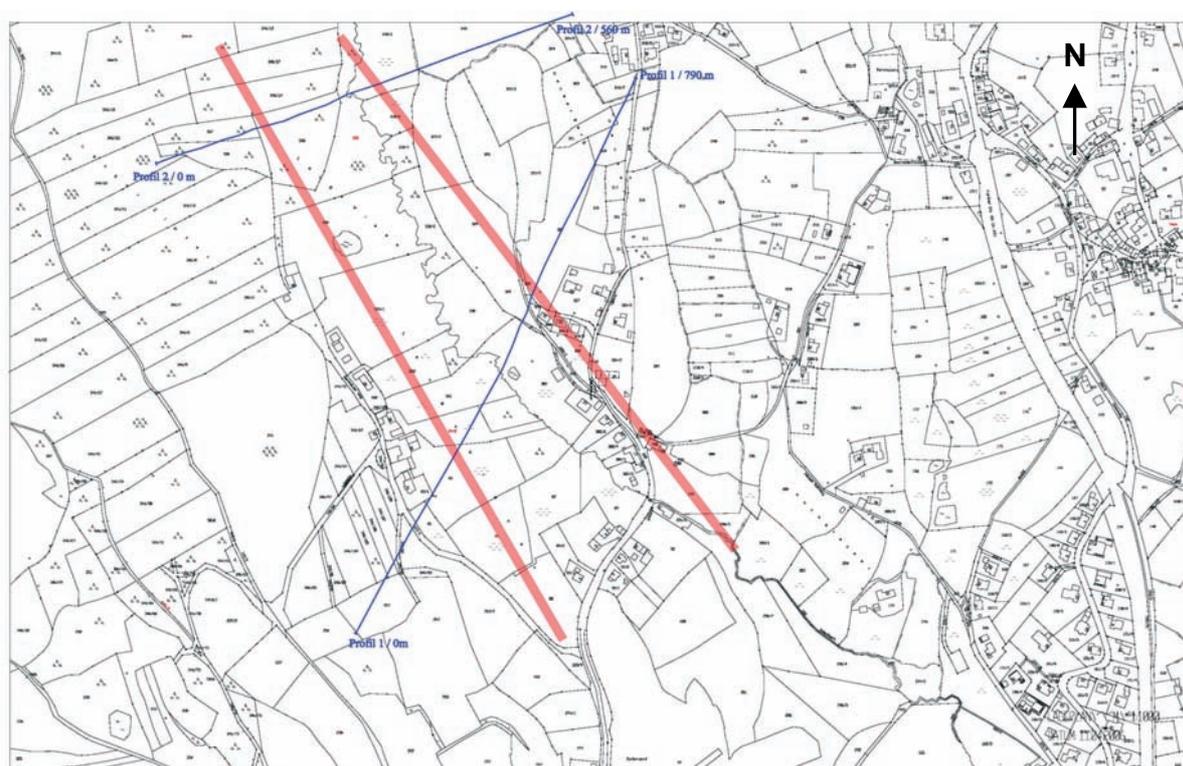


Figure 4-9: Exact locations of the tomography profiles (blue lines). Red lines connect the low resistivity zones in the two profiles and thus depict the strikes of the assumed faults. Scale is approximately 1:10,000.

The northeastern one of the two assumed fault traces shows a more pronounced low-resistivity zone in the two profiles. According to the geophysical interpretation (Richert, 2006) it dips at an angle of approximately 77° towards SW. The southwestern one appears less

conspicuously as a well-defined zone in the two profiles, although, especially in profile 2, low resistivity values clearly reach the lower limit of the transect. The interpreted dip of the fault lies at approximately 55° to the NE.

In the case study in section 4.3 the results from this geoelectric tomography will be integrated with data from remote sensing and fieldwork in the vicinity of the geophysical study site.

4.2 Synoptic analysis of basement structure and hydrogeology

In the following subchapters the findings from the preceding sections shall be integrated. This integration comprises both aspects from the remote sensing analyses and fieldwork as well as from well data obtained from the various sources of information. First, the spatial dimension of well productivity will be focused on. As will become evident, reliable results from this analysis are very difficult to procure due to the scarcity and inhomogeneous distribution of datapoints. In the ensuing subchapter structural and lithologic parameters will be compared to groundwater aspects. While the small database is still a complicating factor several general statements can be made. Due to the fact that these structural and geologic parameters comprise a spatial component certain inferences can also be made about the spatial distribution of well yields.

4.2.1 Spatial distribution of well yields

As already mentioned in the comments on the data inventory the spatial sketchiness of the data on well yields prevents regionally continuous analyses such as the well yield variographies presented by Drew et al. (1999) or Starn (2002). These workers used kriging algorithms on a large GIS database of well yields in order to highlight regions with specific average yields. Moreover, based on these variographies structural and geologic entities could be located in their study areas. To achieve meaningful results, however, a large number of datapoints spread out evenly over the entire study area is required. This is not (yet) the case in the Bavarian Forest, so analyses of this type have to be deferred until a sufficient density of documented wells has been reached.

Examining the mapped well yields in fig. 4-10 does not provide much information on regions where well yields are significantly higher than in others. However, it does show the high variability of yields, even on a local scale. This becomes evident in the Bayerisch Eisenstein/ Brennes, Neusohl, Langdorf, and Kirchdorf well fields (cf. fig. 4-1). In these

locations a relatively high number of wells was drilled in a comparatively small area. In numbers, the Bayerisch Eisenstein/ Brennes field comprises an area of approximately 1.1 km² with ten wells yielding from 0.1 to 3 l/s (average and median yields are 1.2 and 0.9 l/s, respectively). The Neusohl field covers 8 ha and possesses five wells with yields ranging from 2.22 to 7.32 l/s (although this maximum value is not reached at present-day production rates) with average and median yields of 5.01 and 5.49 l/s, respectively. The nearby Langdorf field comprises 2.9 ha with three wells yielding between 1.95 and 2.7 l/s (average and median yields are 2.25 and 2.09 l/s, respectively). In the Kirchdorf field six wells are spread out over an area of 0.5 km². The yields range from 1 to 3.5 l/s, averaging at 1.75 l/s, the median yield is 1.5 l/s.

These large local productivity variations suggest that increasing the number of wells on a groundwater production site increases the chance of obtaining higher well productivities. As mentioned previously the bulk of a well's yield is frequently derived from a few single highly productive influxes. Increasing the number of wells thus raises the likelihood to intersect them. By contrast, locations with only one or two wells, such as for example Böbrach or Geiersthal, show significantly lower average and median yields. Thus, the likelihood to miss highly productive zones in the subsurface seems to be higher than to hit them.

A complicating aspect, however, is the pressure to succeed in tapping new sources of groundwater for a communal administration and its financial capabilities⁷. While for instance the city administration of Regen put significant effort in developing a self-sufficient water supply the administration of Böbrach merely sought to complement its existing supply network. This has an effect on the prospecting and siting of wells. While the design of a new well field allows more freedom in the selection of an optimal drilling location the creation of small supporting wells is frequently subject to less favorable boundary conditions, such as a preexisting infrastructure, which has to be reused for cost reasons. In the latter case this often leads to the selection of a rather suboptimal well location and correspondingly lower yields. This effect can be observed when comparing the Neusohl and Langdorf well fields, where hydrogeologic necessities could be met better than in the Böbrach well sites where infrastructure and cost considerations prevailed.

⁷ Dr. K. D. Raum (SVB Präsl, Velden/ Vils, Germany). Personal communication, March 2007.

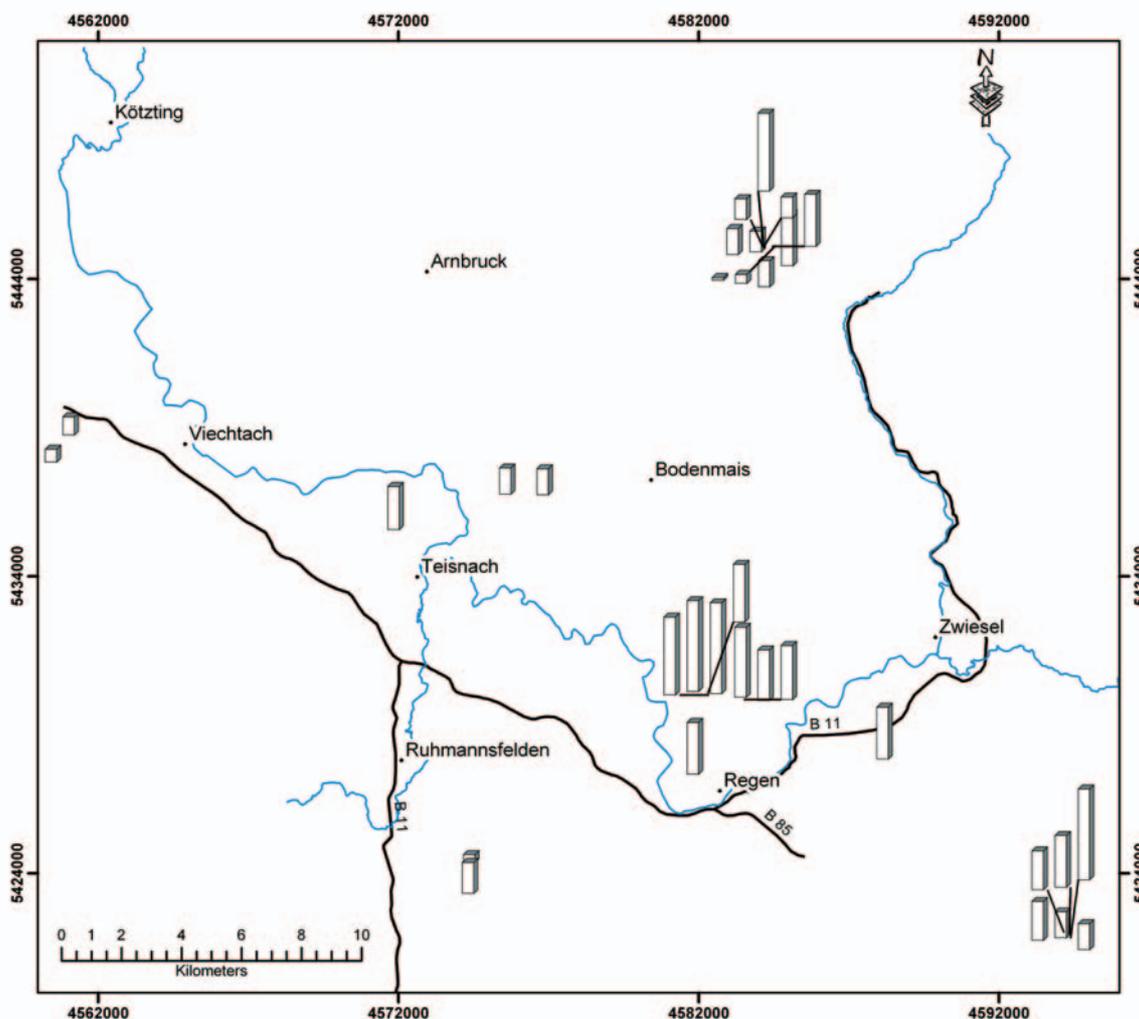


Figure 4-10: Distribution of well yields in the study area. Column height is proportional to well yield. Lowest value is 0.3 l/s, highest value is 3.5 l/s. Note that not all columns are accurately placed. Leader lines point to their exact location.

However, these considerations must not belie the fact that many aspects other than a well's location contribute to its productivity. Apart from different prospecting and drilling techniques, which have been enhanced over the past five decades during which these wells have been created, the reliability of data recording, and a certain amount of luck, several structural and geologic parameters are responsible for the yield of a well. These parameters will be examined in the following section. Yet, it must not be forgotten that they do have a spatial relationship, which might become evident if the density of datapoints on the map were higher. With the present amount of data a direct location-dependency of well productivity cannot be established per se, but only in combination with the following -also location-dependent- structural and geologic entities.

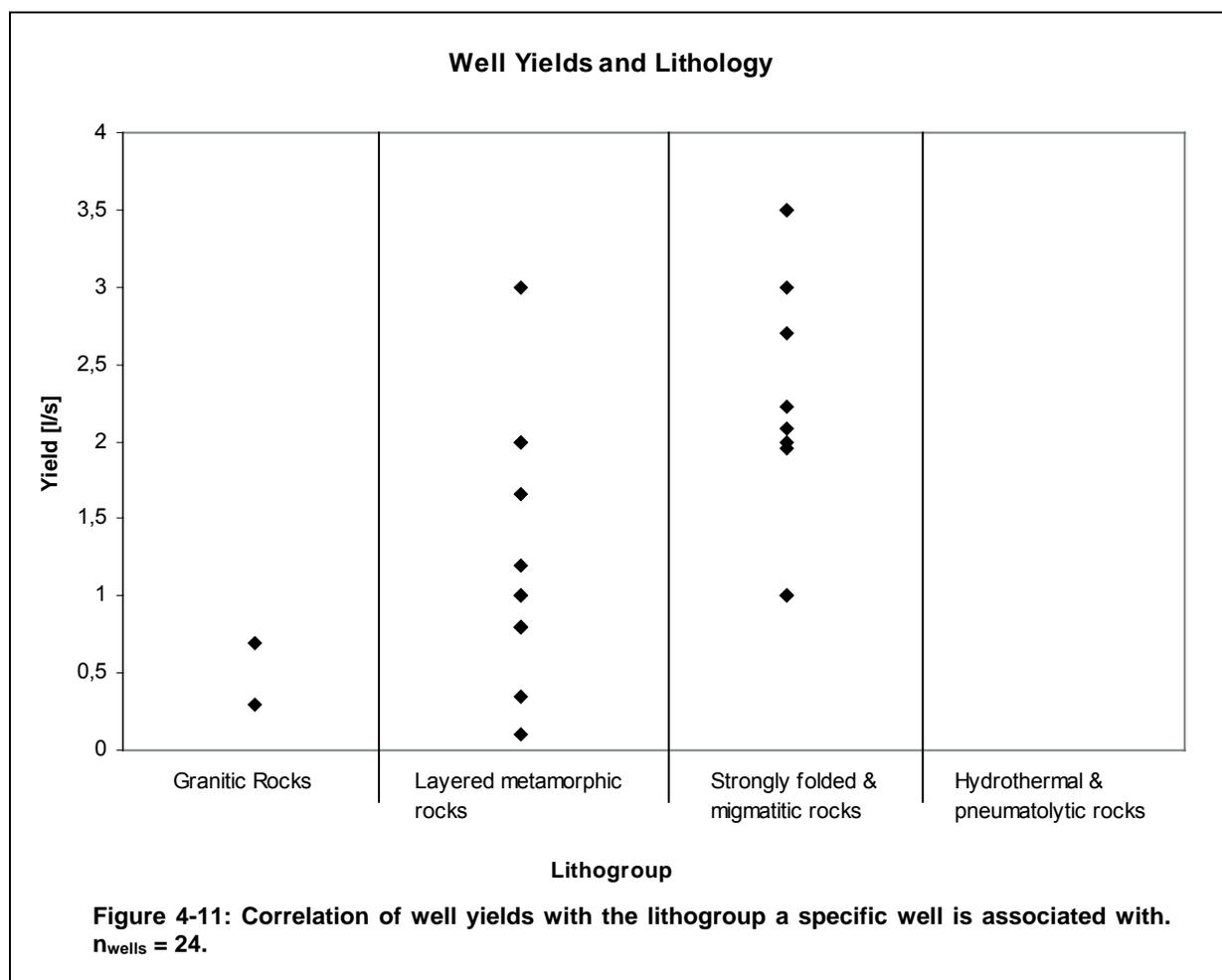
4.2.2 Correlation of well yields with geologic and structural entities

After dealing with the spatial distribution of well yields in the previous section now dependencies between well productivity and various structural and geologic aspects shall be examined. However, caution has to be advised for the interpretation of the following analyses. The productivity of a well depends on the combination of a multitude of parameters, such as the associated lithology, distance to neighboring lineaments, well depth, local variations in the hydraulic conductivity, type and thickness of the overburden and a lot of drilling technique-related aspects, not to speak of the degree of serious effort invested in a particular project by profit-oriented drilling companies. A large part of the influencing factors are unknown at present due to the limitations of the various approaches used. Therefore, the understanding of this hydrogeologic system must stay incomplete until further work adds more pieces of information to it. Thus, even though the following considerations concentrate on one aspect at a time for clarity reasons, the complexity of the system has to be kept in mind.

To begin with, the distribution of yields with respect to the lithologies they occur in will be focused on. As in the analysis of bedrock fractures in section 2 the individual lithologic map units were classified into four lithogroups in order to receive a more uniform coverage of the study area. Furthermore, the creation of lithogroups allows the correlation of rock units across the borders of the various map quadrangles, on which the individual units frequently possess different names. A number of wells are located in areas where surficial deposits such as valley infillings or earth flow sediments were mapped. Since all of those wells reach the bedrock at some point the lithogroup surrounding the respective surficial deposit was attributed in such a case. Figure 4-11 depicts the yields with respect to the lithogroup a specific well is associated with. Only 24 data points could be incorporated here because several sites are located in areas where geologic maps for the establishment of lithogroups were not available. This relatively low number of wells is concentrated in the lithogroups “layered metamorphic rocks” and “strongly folded and migmatitic rocks”, which cover almost two thirds of the study area.

So far, no active water well exists in the hydrothermal and pneumatolytic rocks, which make up only a small portion of the study area’s extent. Similarly, only two wells were drilled in granitic rocks, which comprise approximately 19 per cent of the total study area.

As becomes obvious in fig. 4-11 there is a tendency of higher-yield wells to occur in the strongly folded and migmatitic rocks while the lowest yields exist in the granitic rocks. The layered metamorphic rocks display low to intermediate values. These findings lie in contrast to Stober (1995), who postulates average transmissivities in granites approximately an order of magnitude higher than those in gneisses for the Black Forest/ Germany. However, Karrenberg (1981) lists well yield values from various sampling locations on several continents, which show the opposite in some cases. Conflicting results with respect to well productivity and lithology were also presented by Banks et al. (1992), Banks et al. (1994), Cushman et al. (1953), Daniel (1989), LeGrand (1954), and Williams (2000), mostly for the crystalline basement along the U.S. East coast. Thus, a universally valid classification of igneous and metamorphic rock types regarding their hydraulic properties cannot be established. Rather, the regional or even local conditions of the specific rocks, such as their degree of fracturing and weathering have to be taken into consideration. Nonetheless, the situation in the Bavarian Forest seems to favor metamorphic over igneous rocks in terms of well productivity.



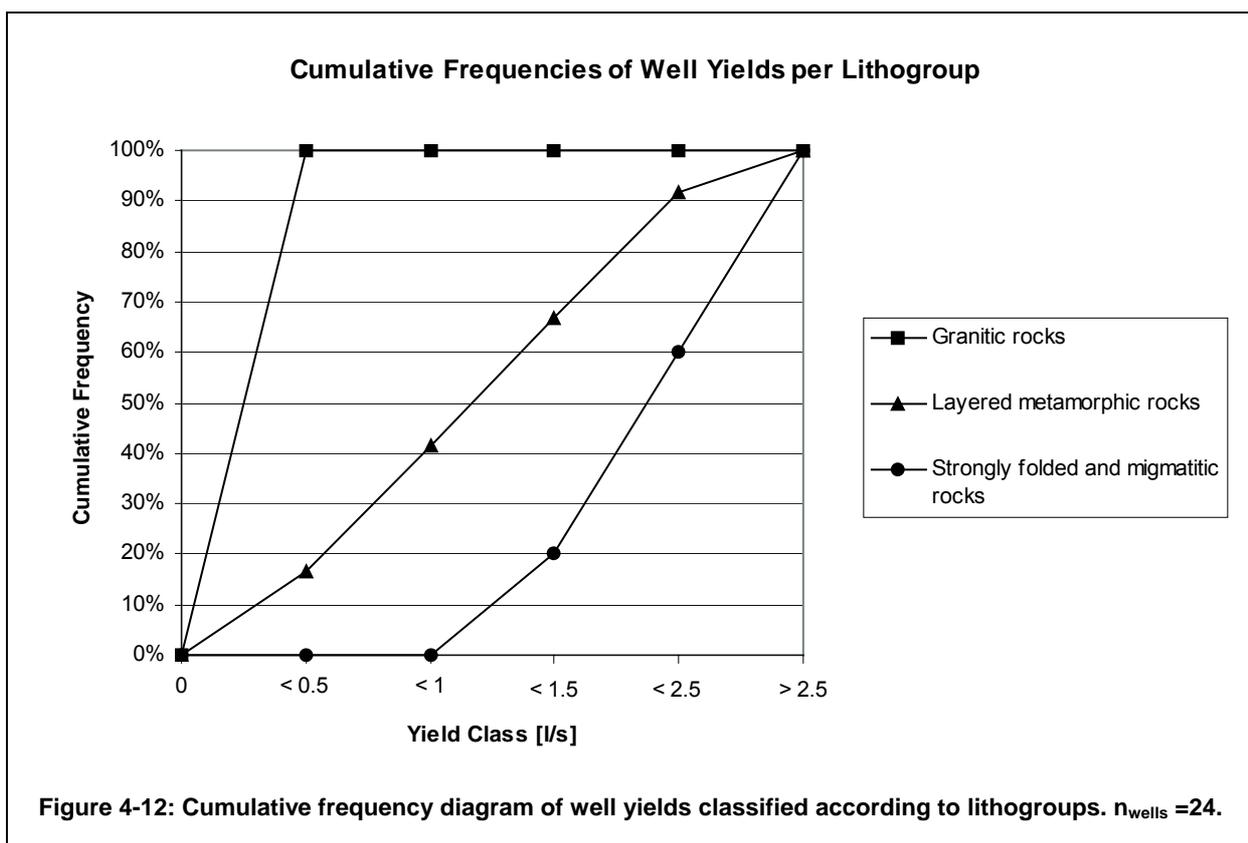


Figure 4-12 depicts the distribution of well yields with respect to the lithogroups they occur in as cumulative frequency diagrams. It shows again that the strongly folded and migmatitic lithologies provide the highest yields and that yields < 1 l/s are commonly not to be expected in this rock type. Approximately 80 per cent of the wells drilled in this lithogroup yield more than 1.5 l/s, 40 % even more than 2.5 l/s. The wells located in layered metamorphic formations appear to be somewhat less productive with more than 40 per cent producing less than 1 l/s and less than 10 per cent yielding more than 2.5 l/s. The granitic rocks represent the least productive lithology, which does not produce wells with yields much higher than 0.5 l/s. The fact that only two public water supplies are known to have been drilled into granitic rocks underlines the unpopularity of this rock type among groundwater prospectors. However, this stands in stark contrast to findings made in section 2 where granites were frequently described as being heavily fractured. Furthermore, several of the fracture sampling sites were located in large granite quarries where groundwater obviously discharging from unroofing joints as well as steeply inclined fractures had to be pumped out to keep the site from drowning (cf. pictures in section 4.3.1). Yet several of these quarries (e.g. the Prünst quarry, 6943-01) are located in valleys suspected to be underlain by large fault systems, which surely possess hydraulic properties different from granites outside the fault zones. Drilling projects into these fault zones are unknown at present, so future wells drilled in the vicinity of these structures might well change the statistics in favor of the granitic lithologies.

The situation in the metamorphic lithologies is complicated by the fact that rock types can be subject to local variations and the metamorphic units appearing on the geological maps are occasionally penetrated by igneous or hydrothermal veins. The comparison of the driller's logs (section 4.1.1.1) with the flow meter measurements (section 4.1.1.3) shows that the points of maximum influx into a well bore penetrating both gneissic and granitic rocks are frequently located at depths where the hole intersects those igneous intrusions. Thus, the image conveyed in figs. 4-11 and 4-12 has to be somewhat modified. While on the scale of geologic maps metamorphic (especially strongly folded and migmatitic) lithologies produce the highest well yields it is frequently the small unmapped intrusions into those units which contribute the largest amounts of water to a well's cumulative yield. This explains why especially the high-grade metamorphic rocks are so productive. In these lithologies partial melting produced a variety of igneous and hydrothermal materials, which again solidified as veins. These relatively thin sheet-like intrusions made up of rocks behave more brittle when subjected to stress than the surrounding metamorphic rocks. Because both rigidity and bed thickness of a rock strongly influence its fracturing behavior (van der Pluijm and Marshak, 1997) these relatively thin veins are more intensely fractured and thus act as highly conductive avenues for groundwater.

Apart from lithologic effects dependencies between well yields and structural entities shall also be highlighted. To this end buffer zones with specific radii around each well location were established in ArcGIS. The zones were given radii of 10 m, 30 m, 50 m, 100 m, 500 m, and 1000 m, respectively. Then, the numbers of both DEM- and photolineaments (cf. section 3 and Zeithöfler (2006b)) intersecting a particular buffer zone were recorded. For the analyses presented here only the distances to the closest lineaments were considered. The correlation between the strikes of these lineaments and potentially water bearing fractures measured in nearby outcrops could only be achieved in the study area *sensu stricto*. Thus, for wells located outside this area no information could be obtained. For well sites inside the study area the fracture correlation to neighboring lineaments depends on the presence of bedrock outcrops in their vicinity. Positive fracture correlation was assumed if an outcrop containing fracture sets striking in the lineament direction is located less than one kilometer from the lineament used for the analysis presented in fig. 4-13. This is the case for the well locations Neusohl, Langdorf, Böbrach, and Geierthal. The visual comparison of stereographic plots of joints sampled in nearby outcrops and the corresponding lineaments showed that in all these sites the lineaments are fracture correlated. While the well sites outside the study area *s. str.* could not be tested for lack of fracture data the good correlation inside the area validates the assumption that the situation in the untested locations is similar.

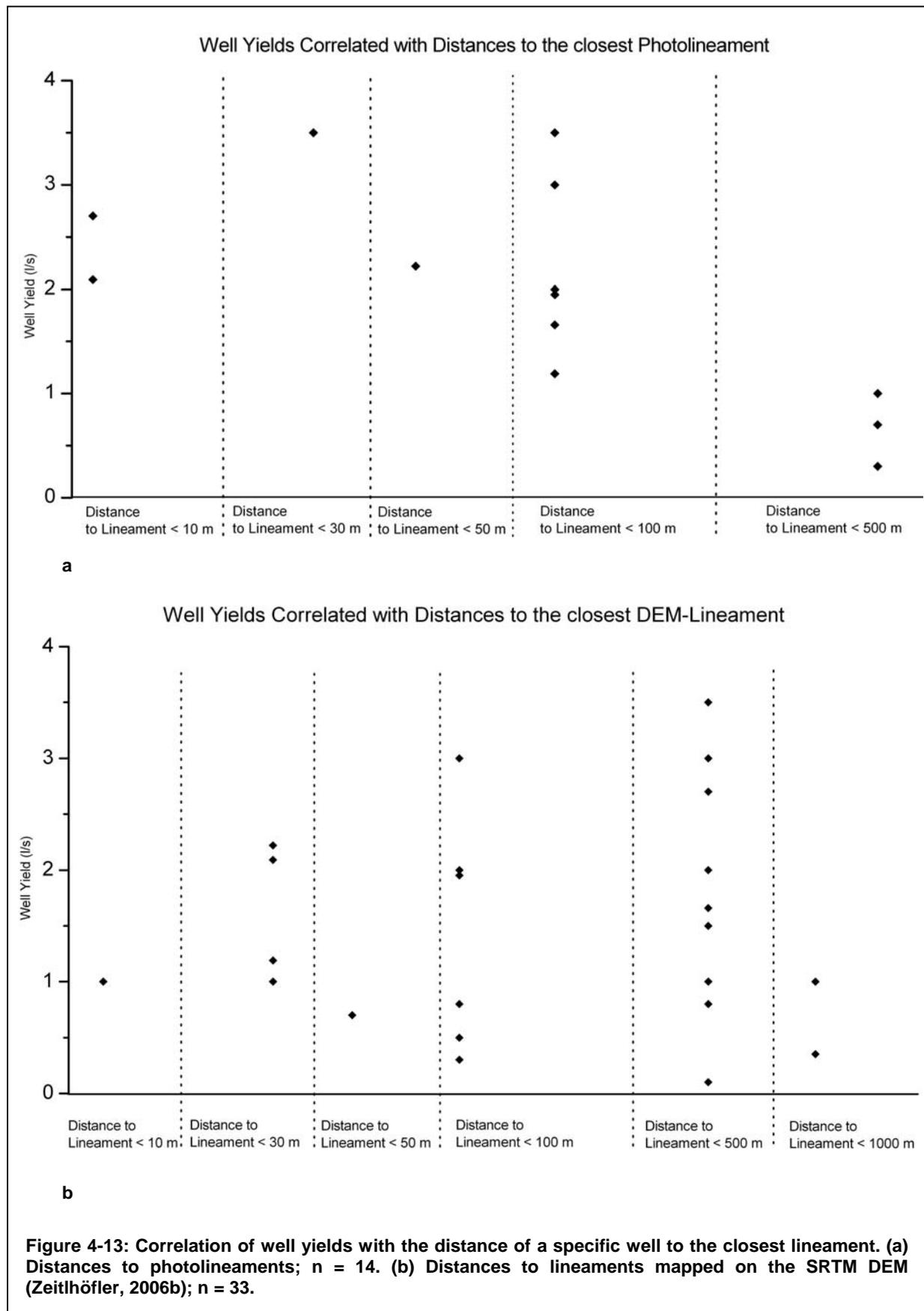


Figure 4-13 compares the yield of a specific well with its distance to the closest mapped lineament. To begin with, it has to be noted that the relatively small number of data points and their high degree of scatter makes it difficult to establish statistically significant trends. Nonetheless, the proximity of wells to lineaments mapped on aerial imagery (fig. 4-13a) seems to have an influence on their productivity. Two wells are essentially located on a photolineament and provide yields above the average and mean values for the wells in this figure (1.9 and 2.0 l/s, respectively). Further high-yield wells can be found at distances of up to 100 m. At greater distances the well productivity drops significantly.

There are several possible reasons to explain the fact that relatively high yields exist at considerable distances to a lineament. First, there is a certain amount of error in the exact placement of a lineament both on an aerial photograph and on the DEM. Second, lineaments are assumed to represent zones of high fracture densities, which can reach significant widths. This effect is not accounted for in the GIS based processing of lineament data. Finally, fault and fracture zones expressed topographically by lineaments are not necessarily vertical. Depending on their inclination wells located at larger distances from their surface traces can intersect them at depth.

The correlation of well yields with DEM lineaments (fig. 4-13b) gives a different impression. A significant drop in productivity does not occur until the <1000 m increment. Up to a distance of 500 m the distribution fans out from the 10 m increment. Thus, the maxima and minima of yield values move further apart with increasing well-lineament distance. This raises the question if the lineaments obtained from the DEM are valid indicators for the productivity of wells. Due to the fact that DEM lineaments possess a significantly lower spatial density compared to the photolineaments and that they rather represent regional structures a possibility exists that small-scale variations in yields of a small number of wells located in a relatively large area do not cause specific trends. If this is the case a more or less random distribution similar to that in fig. 4-13b should be expected, in which increasing the search radius equally raises the chance of encountering low and high yield wells. Thus, at the present density of datapoints on well yields the DEM lineaments cannot be consulted to identify high productivity areas. However, when a more continuous coverage with well data in this area is available a correlation between a well's yield and its proximity to a DEM lineament might become evident.

In summary, it has to be mentioned that the current database allows only very limited statements on the regional hydrogeologic properties of the central Bavarian Forest. Thus, in the following section a number of case studies including qualitative observations in large

bedrock outcrops, the synoptic analysis of a surface geophysical study in association with remote sensing and field data, and the generation of statistical fracture networks and hydrogeologic models in selected fracture sampling stations shall highlight specific aspects of the study area's hydrogeology.

4.3 Case studies

As already mentioned above specific hydrogeologic aspects shall be addressed in the following case studies. All of these studies focus on the nature of fracture networks in the selected sites and their relationship to the local groundwater flow. To this end hydrogeologic properties of fracture sampling stations yielding sufficient information for the creation of fracture and flow models will be analyzed and processed. To refine the models, which are mainly compiled from quantifiable measurements, qualitative observations made in various large bedrock outcrops will be consulted as well.

The last case study will focus on the integration of data obtained from remote sensing, fieldwork, and a surface geophysical survey. Unfortunately, the final step, i.e. the drilling of the geothermal well for the Bad Kötzing spa has not been commenced at the time of completion of this study. Therefore, despite the promising results of the prospection, a positive outcome of the effort cannot yet be reported.

4.3.1 Hydrogeologic properties of selected outcrops

In contrast to the structural geologic analysis in chapter 2, which focused on the tectonic significance of fractures and faults in the study area, the hydrogeologic approach brings parameters such as fracture size, aperture, roughness etc. to closer attention. However, both approaches stand in a relationship to each other, because the type of tectonic deformation commonly has a strong influence on the hydrogeologic properties of a fracture.

To begin with, qualitative observations made in several large bedrock exposures will shortly be reported. However, for lack of televiewer surveys in producing wells the significance of these observations for groundwater exploitation can only be estimated.

The scanline analyses performed on a few selected outcrops are used to generate stochastic fracture networks for the ensuing flow path models in the FracMan/ MAFIC suite. As described in the methodology the scanline approach is thought to provide objective information on fracture parameters, although certain limitations exist in this study area, and

the subjective approach frequently seemed more appropriate. Nonetheless, the scanline data were used for the FracMan/ MAFIC analyses, because they are generally associated with the most complete set of metadata, such as fracture size, aperture, roughness, etc.

4.3.1.1 Qualitative hydrogeologic observations in selected outcrops

Besides the quantitative information available from the analysis of boreholes many observations concerning the presence and the flow of groundwater can be made in large bedrock outcrops. In several cases groundwater emanates from fissures in the rock, whose properties can be evaluated by visual examination. In other cases indirect indicators, such as larger plants, hint at the presence of water in fractures.

In figure 4-14 displaying several outcrops in the Prünst granite quarry (outcrop ID: 6943-01) water emanating from both subhorizontal unroofing joints and steeply inclined fractures is easily recognizable. This phenomenon can be observed over the quarry's entire vertical extent of up to approximately 50 meters. It was mentioned previously that granitic lithologies tend to host mostly low-yield wells in this region, which could be explained pondering the types of fracture networks present in this rock type. Granitic rocks frequently develop a set of unroofing joints parallel to the topographic surface in response to regional uplift. By contrast, foliated metamorphic lithologies in the study area usually reactivate their gently to moderately inclined fractures parallel to their foliation for this process (cf. section 2). Additionally, the granites, being the more competent units with respect to the metamorphic lithologies, do not produce as many fractures with higher inclinations as the foliated rocks, which can accommodate much strain along their metamorphic fabric. However, where granitic intrusions are intersected by major fault zones they are usually associated with dense sets of steeply inclined fractures. With regard to this aspect the Prünst quarry represents a special case in that it is located at the trace of a major N-S trending lineament, which intersects a smaller NE-SW striking lineament in its vicinity. Thus, the density of steeply inclined fractures is considerably higher than that observed in granites further away from large lineaments (e.g. locations 7044-03 or 7043-02, fig. 4-16a). This is important because while most granites are associated with unroofing joints, which potentially bear major amounts of groundwater, steeply inclined fractures intersecting them are crucial to supply them with infiltrating water from the surface (fig. 4-14c). Thus, in locations where significant numbers of steeply inclined fractures are absent a high transmissivity stemming from subhorizontal unroofing joints, along which large apertures were frequently observed, cannot be utilized due to a lack of avenues connecting them to the surface (cf. fig. 4-15).

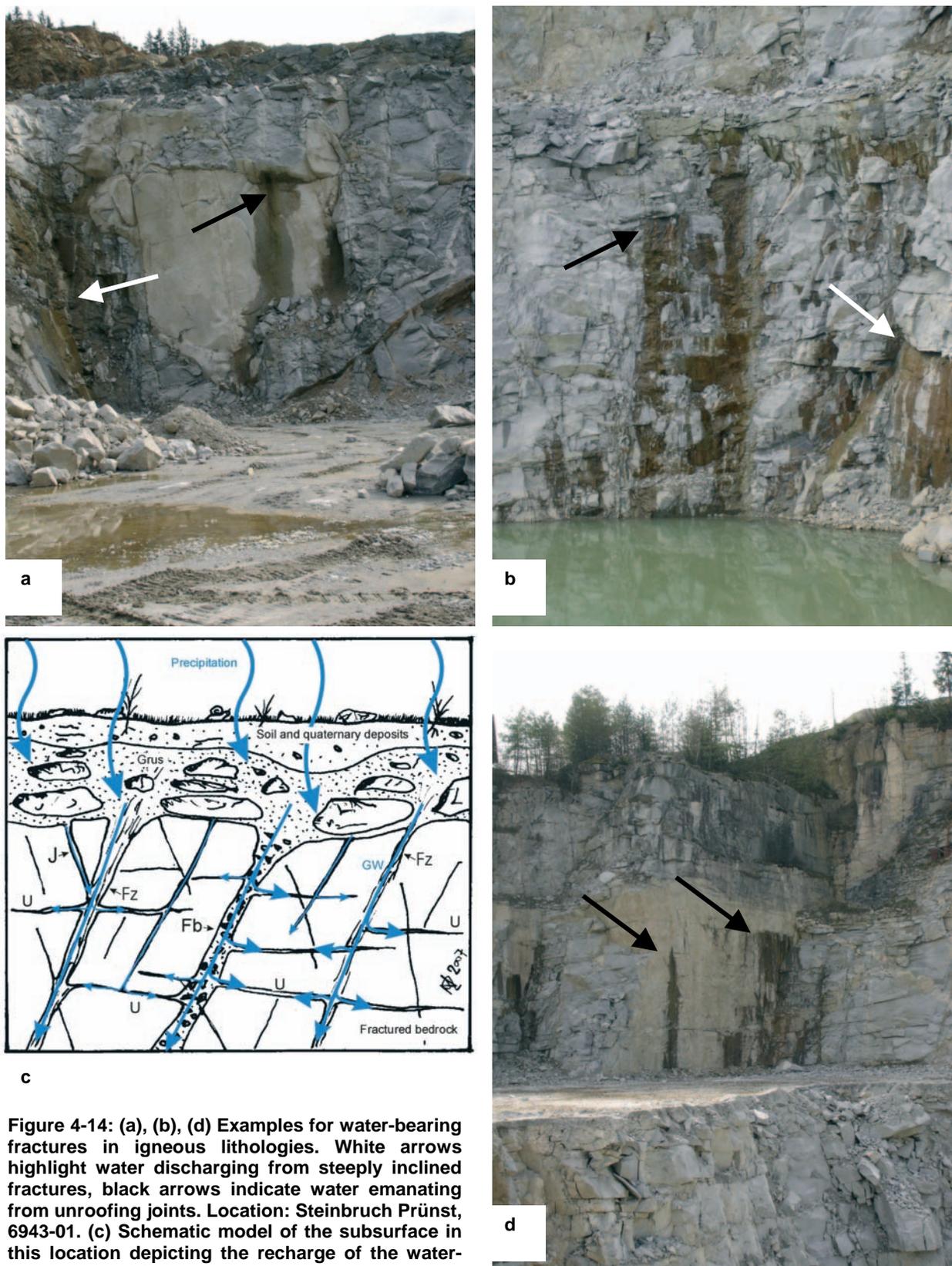


Figure 4-14: (a), (b), (d) Examples for water-bearing fractures in igneous lithologies. White arrows highlight water discharging from steeply inclined fractures, black arrows indicate water emanating from unroofing joints. Location: Steinbruch Prünst, 6943-01. (c) Schematic model of the subsurface in this location depicting the recharge of the water-bearing unroofing joints over steeply inclined fractures. GW: groundwater; U: unroofing joint; J: open extensional fracture; Fb: fault containing breccia ; Fz: zone of high fracture density.

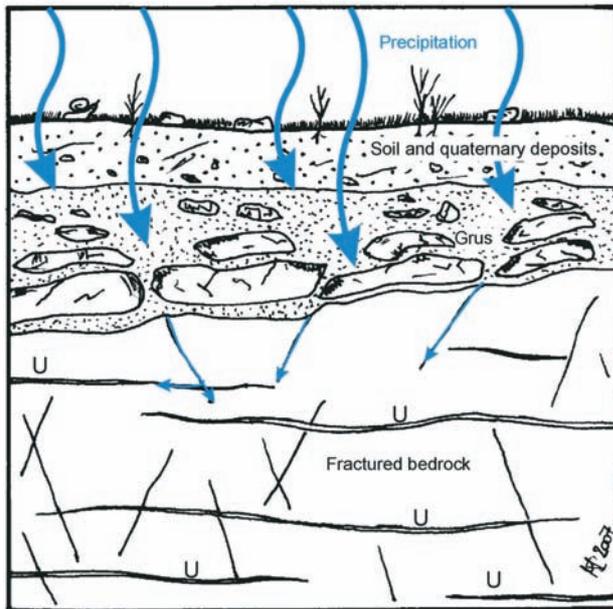


Figure 4-15: Schematic model of the subsurface in granitic lithologies with low densities of steeply inclined fractures, depicting inhibited recharge of unroofing joints. U: unroofing joint.

Examining the water discharge from the unroofing joints in fig. 4-14 more closely shows that only part of a fracture's extent is used for groundwater flow. The high aperture variability of these joints is one possible reason for this behavior, which was also concluded from numerical simulations performed by Parney and Smith (1995). Also, intersections between subhorizontal and steeply inclined fractures were frequently observed to be preferred avenues for flow. This phenomenon is very likely another complicating factor for groundwater prospecting, because even if a relatively dense fracture network is present in a drilling site flow channeling can render parts of the network unused and decrease the chances of intersecting high-flow zones.

Apart from direct observations of groundwater flow in bedrock outcrops, which usually require relatively large and fresh exposures, indirect indicators for water-bearing fractures are ubiquitous occurrences. These indicators range from moist fault infillings (especially coarse-grained gouge) over oxidized patches on fracture planes, which frequently start at intersections with other fractures, to various kinds of vegetation growing out of fissures. Figure 4-16 depicts two sites where it becomes obvious that not only moss and grasses find sufficient moisture in fractures, but that even shrubs and little trees can thrive on the water they draw from bedrock fissures. In fig. 4-16a an unroofing joint is inhabited by a small fir tree while the dog rose bush in fig. 4-16b grows out of a gently to moderately NNE dipping brecciated and densely fractured zone in the rock.

Thus, although the observations presented here cannot be utilized to quantify groundwater flow they prove the general presence of water in bedrock discontinuities and illustrate to a certain extent how flow occurs in the subsurface. The fact that not all fractures in an outcrop were found to transport water has far-reaching implications for the degree of connectivity of a location's fracture network and the transmissivity and aperture of individual fractures within this network, which influences the design of stochastic fracture and flow models.

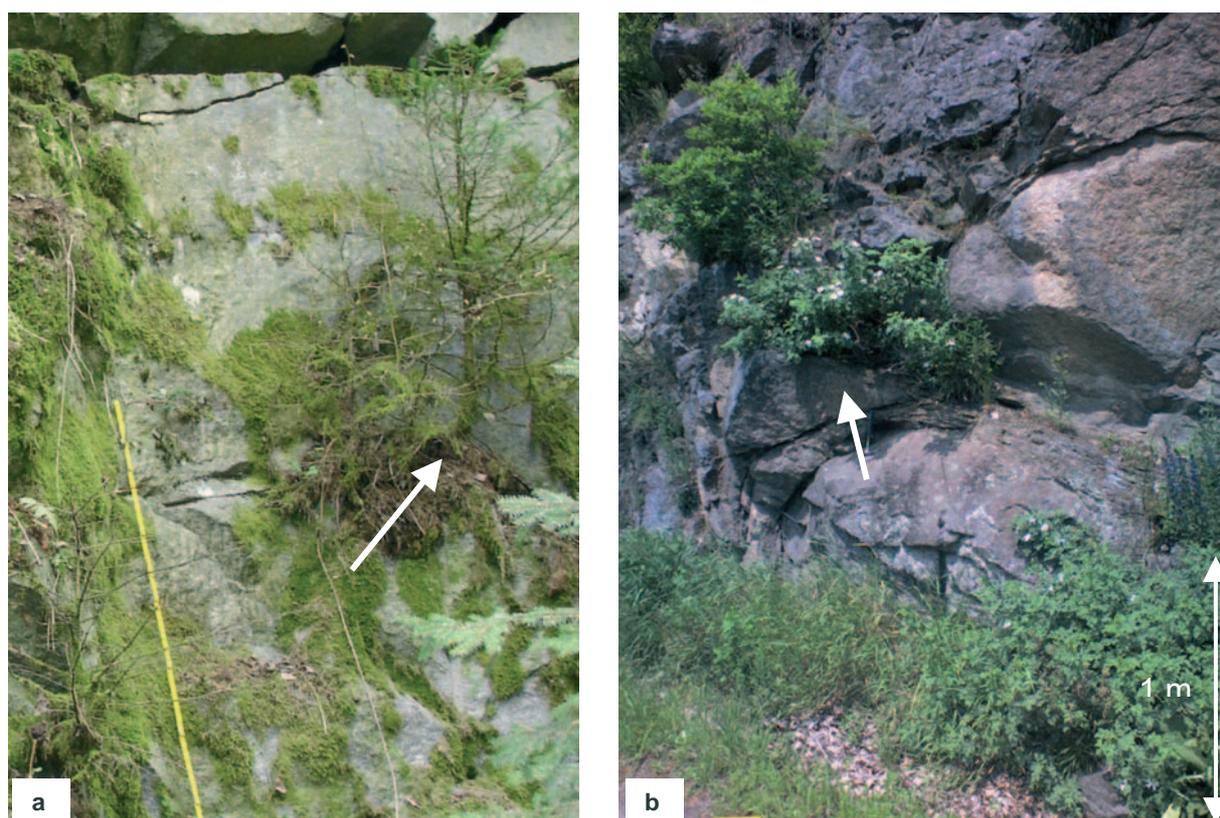


Figure 4-16: Plants as indirect indicators for the presence of groundwater in fractures. (a) Small fir tree (white arrow) growing out of a subhorizontal unroofing joint. Meter stick for scale. Location: Steinbruch Zeitlhof (7043-02). (b) Small dog rose bush and another unknown shrub growing in a densely fractured zone, which dips gently NNE. Location: Rugenmühle (6943-13).

4.3.1.2 Scanline surveys

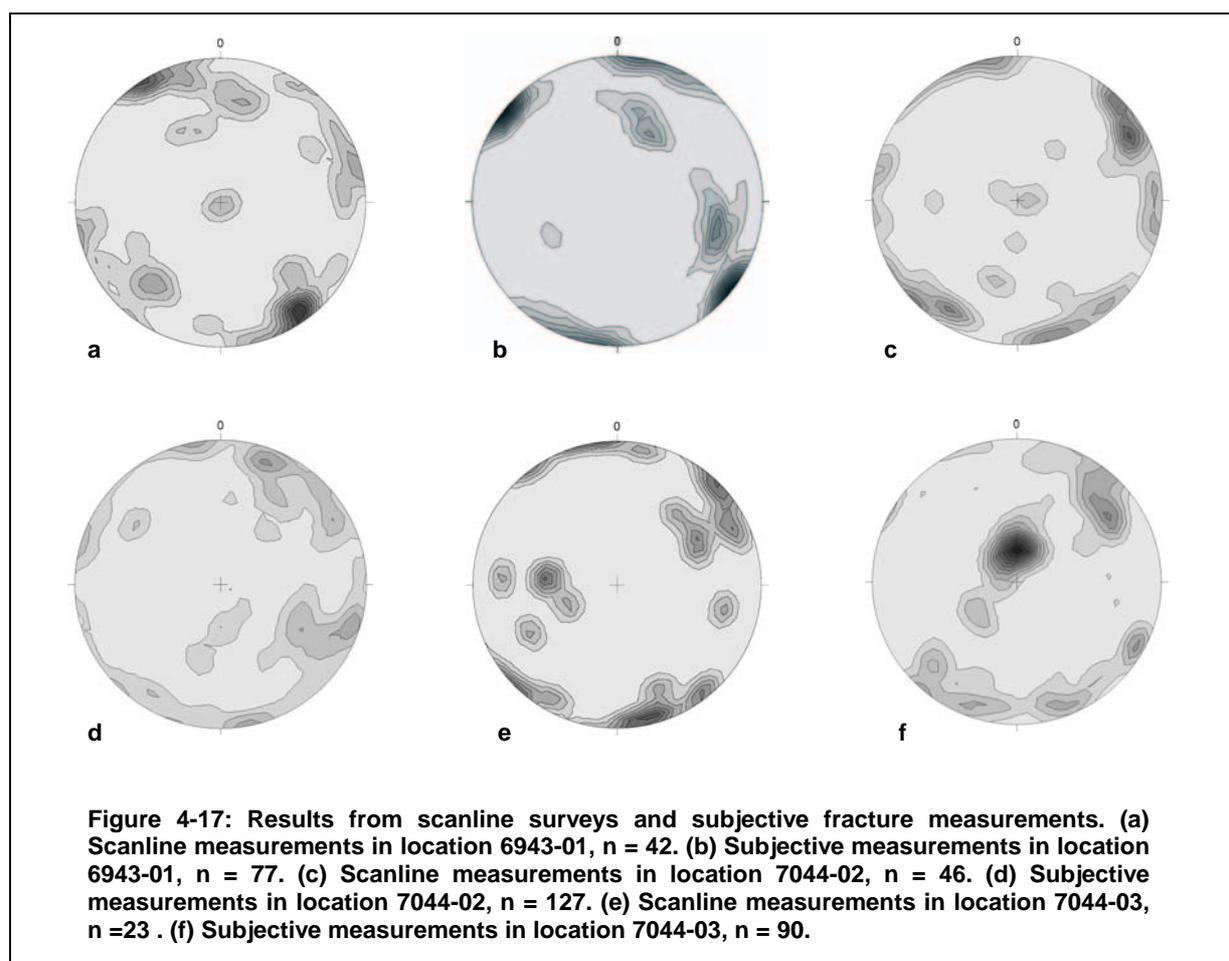
Scanline surveys as described by a variety of authors (Spencer and Kozak, 1974; Walsh and Clark, 2000; Williams, 2000; Winkler, 2003; Witthüser and Himmelsbach, 1998) were conducted on only a small number of bedrock exposures in this study area due to the frequently insufficient quality of the outcrops. The following locations allowed the setup of scanlines with adequate lengths and numbers of measurements:

Outcrop ID	Scanline length [m]	# of measurements	3D control
6943-01	20.0	42	yes
7044-02	19.2	46	no
7044-03	19.6	23	no

Table 4-5: List of scanlines surveys performed in the study area. Column “3D control” indicates sampling sites where orthogonal outcrop walls allowed the verification of the consistency of measurements in three dimensions.

In most other sampling stations the size and geometry of the outcrop, partial coverage with surficial materials, plant overgrowth and difficulties in accessing a continuous stretch of the exposure precluded the sensible design of scanlines. Nonetheless, the

subjective approach yielded similar results in most cases. Subjective data complemented with measurements of fracture spacings of each set encountered also provided a good approximation to the real fracture networks. Direct measurements of fracture spacings are thought to yield an even higher accuracy of the subjective approach with respect to sampling bias in some instances. Figure 4-17 juxtaposes the results of scanline and subjective measurements in the three locations listed in table 4-5.



In general, the fracture orientations determined by the two approaches agree reasonably with minor variations in relative abundances and slight directional deviations. It also has to be kept in mind that the values obtained during the scanline surveys are significantly less numerous, which produces more scattered distributions in the contoured plots and puts more weight on individual fractures. Also, the two approaches were employed in different parts of an outcrop in order to obtain a more extensive coverage. Thus, small-scale variations in relative abundances of differently oriented fracture sets over the extent of the bedrock exposure are reflected in the stereographic plots. Significant undersampling occurs only in sampling station 7044-03 where the scanline survey lacks the subhorizontal to gently S dipping population. This effect is a major drawback of the scanline approach,

because a horizontal scanline intersects more steeply than gently inclined fractures along its trace. Due to frequently very low outcrops and the limited vertical reach of a person measuring the fractures vertical scanlines with reasonable lengths could not be set up. In the subjective measurements of sampling station 6943-01 the subhorizontal fracture set visible in the scanline survey is not absent as the contoured plot suggests. However, the absolute number of fractures is relatively low compared to the steeply inclined ones in this section of the outcrop, which causes them to disappear in the background noise of the plot.

Nonetheless, all scanline surveys were processed with the K-means algorithm due to their almost complete record of fracture metadata. As described in the methodology section this algorithm attributes ID numbers to every fracture based on its orientation and thus allows the calculation of mean values of parameters such as fracture size, aperture, etc. for each fracture cluster. Table 4-6 displays the results of the clustering.

Outcrop ID: 6943-01									
Cluster ID	Strike	Dip	Trace length [m]	Roughness [mean coefficient]	Mean aperture [mm]	avg. X-Type intersections [#m]	avg. Y-Type intersections [#m]	Termination [%]	Mean spacing [m]
1	236	84	2.10	4.75	0.32	0.82	1.20	66	0.41
2	166	88	4.29	4.75	0.50	0.41	1.36	50	1.40
3	281	2	15.00	4.00	1.00	0.41	0.50	n/a	0.28
4	308	59	2.22	4.30	1.08	0.86	0.96	100	1.58
Outcrop ID: 7044-02									
Cluster ID	Strike	Dip	Trace length [m]	Roughness [mean coeff.]	Mean aperture [mm]	avg. X-Type intersections	avg. Y-Type intersections	Termination [%]	Mean spacing [m]
1	210	6	5.94	n/a	1.64	1.81	0.98	67	0.07
2	258	88	1.21	n/a	4.44	1.27	0.89	67	0.57
3	150	78	1.34	n/a	1.06	1.16	0.81	78	0.88
4	231	84	1.00	n/a	1.50	0.33	0.67	100	0.51
Outcrop ID: 7044-03									
Cluster ID	Strike	Dip	Trace length [m]	Roughness [mean coeff.]	Mean aperture [mm]	avg. X-Type intersections	avg. Y-Type intersections	Termination [%]	Mean spacing [m]
1	134	90	2.11	4.70	1.30	0.73	1.03	80	0.80
2	257	84	1.84	5.13	n/a	0.32	0.85	100	1.02
3	4	42	5.44	5.60	0.85	0.27	0.73	100	1.76

Table 4-6: Mean values of fracture orientation and metadata obtained from K-means clustering of scanline measurements in three sampling locations. Column “Roughness” contains the arithmetic mean of roughness coefficients described in the methodology. Columns “avg. X-Type intersections” and “avg. T-type intersections” contain the arithmetic mean of the number of intersections with other fractures per meter trace length. Fractures at X-type intersections cross the fracture trace, fractures at T-type intersections terminate at the fracture. Column “Termination %” contains the percentage of fractures of a specific set terminating at fractures of different sets. Mean spacings are corrected with respect to scanline trend and fracture inclination.

Based on these tabulated values stochastic fracture networks were generated for sampling stations 6943-01 and 7044-02, which, along with subjective data from other locations, will be presented in the following section. Location 7044-03 was omitted due to its

low number of datapoints, which puts enormous weight on outliers in the distribution, thereby distorting the mean values of the fracture metadata. Also, as already mentioned, a significant population was undersampled by the scanline approach in this location.

4.3.1.3 Fracture networks in selected sampling stations

Based on the K-means fracture classification stochastic fracture networks were generated using the FracWorks module of the FraMan/MAFIC modeling suite. This module allows the placement of stochastically distributed fractures in a specified model region. Apart from orientation the various sets of discontinuities can be attributed with several other parameters, for which also stochastic distribution functions were applied. Detailed descriptions of these functions can be found in Dershowitz et al. (1999) and Dershowitz (2002).

The selection of the most appropriate distribution function for fracture orientation was achieved by trial and error until the model log files yielded satisfactory results. The “Enhanced Baecher (BART)” model using the “Bivariate normal distribution” with k_1 and k_2 values of 5 to 10 turned out to come closest to the real distributions of steeply inclined fractures displayed by the stereographic plots of the field data. For gently inclined to subhorizontal fractures the Fisher distribution with relatively high K-values (50 to 200) proved to be the most appropriate in some cases. For fracture size a uniform distribution of values about the mean within the range of one standard deviation was applied. The density of fractures of a specific set was specified in the “ P_{32} ” mode, for which the average area of a fracture per unit volume was applied. The calculation of this parameter is detailed in appendix D. Fracture apertures were entered as the mean values measured in the field distributed uniformly for lack of more detailed information. For the percentage of fractures being connected to discontinuities of other sets (called “termination %” in FracWorks) the percentage of fractures measured in the field, which are visibly connected at one end minimum with respect to the total number of fractures, whose terminations could be observed in a sampling station, was calculated. All other variables in the model were set to default for want of further information.

In the following, several fracture networks generated by FracWorks will be presented and used for the pathway modeling in the ensuing section. Figure 4-18 depicts the network modeled after the scanline survey in location 6943-01. The model region is modeled as a cube with a side length of 20 m. The network consists of a total of 19654 fractures based on the mean values of orientation, size, and spacing determined in the scanline database. The

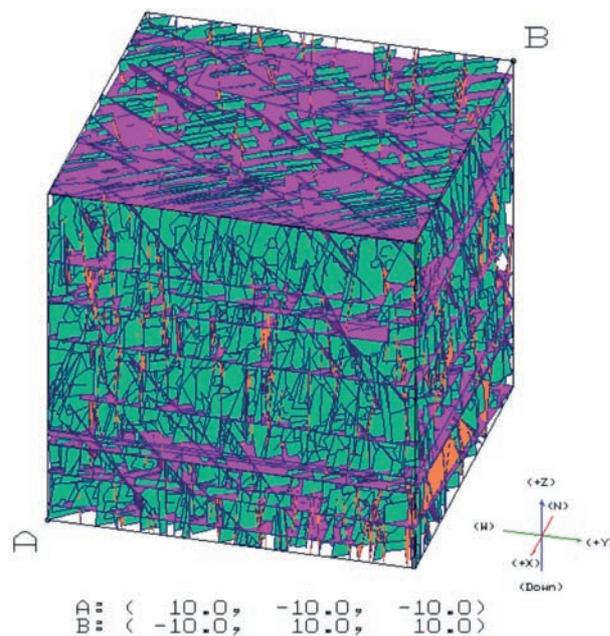


Figure 4-18: FracWorks fracture network model for sampling station 6943-01. Model size: 8000m³, number of fractures: 19654, fracture intensity (P₃₂): 3.759 m²/m³, total fracture porosity: 0.22 %.

resulting mean fracture area per unit volume is 3.759 m²/m³, the total fracture porosity in the model region amounts to 0.22 %, assuming a constant aperture distribution. The fracture network in this model is dominated by set of subvertical fractures striking NE-SW, which is also the direction of a prominent lineament in the location's vicinity. Fractures of this set are relatively small but densely spaced. This dominant set is intersected by extensive subhorizontal unroofing joints. The mean fracture aperture in this set is approximately one order of magnitude higher than in the dominant set, which is assumed to be important for the recharge (see section 4.3.1.1) Two other populations strike NW-SE with moderate

inclinations and NNW-SSE with steep inclinations. The former, although having the lowest intensity and relatively short planes, is associated with the highest mean aperture in this network and thus might play a significant role in the infiltration of precipitation

Cluster ID	Dip Azi./Dip	Orientation Distribution	Intensity [P ₃₂] constant	Size			Aperture mean [m]	Termination %
				Mean [m]	Distribution	Deviation (1 σ)		
1	326-84	Bivariate normal (5/5)	1.92	2.10	Uniform	1.89	3.20e-4	66
2	256-88	Bivariate normal (5/5)	0.56	4.29	Uniform	6.19	5.00e-4	50
3	011-02	Bivariate normal (5/5)	0.79	15.00	Uniform	9.19	1.00e-3	0
4	038-59	Bivariate normal (5/5)	0.50	2.22	Uniform	2.30	1.08e-3	100

Table 4-7: Fracture set parameters employed in the model of sampling station 6943-01.

The results of the scanline survey in sampling station 7044-02 are presented in fig. 4-19. The model region has a side length of 10 meters and contains 14138 individual fractures. The high number of individual fractures necessitated the reduction of the model size due to the limited computing capacity of the computer hardware. The mean fracture area per unit volume amounts to 4.604 m²/m³, resulting in an average secondary porosity of 1.07 %. As in the previous model the NE-SW striking population shows the highest intensities and almost the lowest mean size of individual fractures as well as a comparatively low aperture. A sub-population, generated separately, strikes ENE-WSW with high inclinations. The mean fracture size and intensity is similar to that in the dominant set, but the mean aperture is three times higher. The largest planes exist again in the set of subhorizontal unroofing joints, which, however are significantly smaller than those in fig. 4-18.

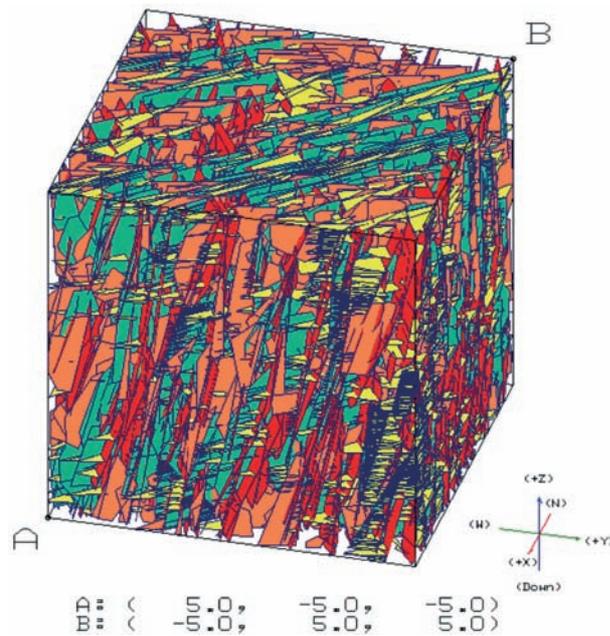


Figure 4-19: FracWorks fracture network model for sampling station 7044-02. Model size: 1000 m³, number of fractures: 14318, fracture intensity (P₃₂): 4.604 m²/m³, total fracture porosity: 1.07 %.

In contrast to sampling station 6943-01 the NW-SE striking fractures are associated with the lowest apertures, but also show a relatively short mean trace length and a low intensity. Mean fracture apertures are relatively high in all sets, ranging from approximately 1 to 4.5 mm, which results in the highest bulk porosity of all the modeled sampling locations.

Fig. 4-20 displays the fracture network modeled for sampling station 6944-18. The fracture intensity is significantly lower than in the previous models.

Cluster ID	Dip Azi./Dip	Orientation Distribution	Intensity [P ₃₂] constant	Size			Aperture mean [m]	Termination %
				Mean [m]	Distribution	Deviation (1 σ)		
1	300-06	Bivariate normal (5/5)	0.79	5.94	Uniform	7.87	1.64e-3	67
2	348-85	Bivariate normal (5/5)	1.38	1.21	Uniform	1.28	4.44e-3	67
3	240-78	Bivariate normal (5/5)	0.89	1.34	Uniform	1.14	1.06e-3	78
4	321-84	Bivariate normal (5/5)	1.54	1.00	Uniform	0.71	1.5e-3	100

Table 4-8: Fracture set parameters employed in the model of sampling station 7044-02.

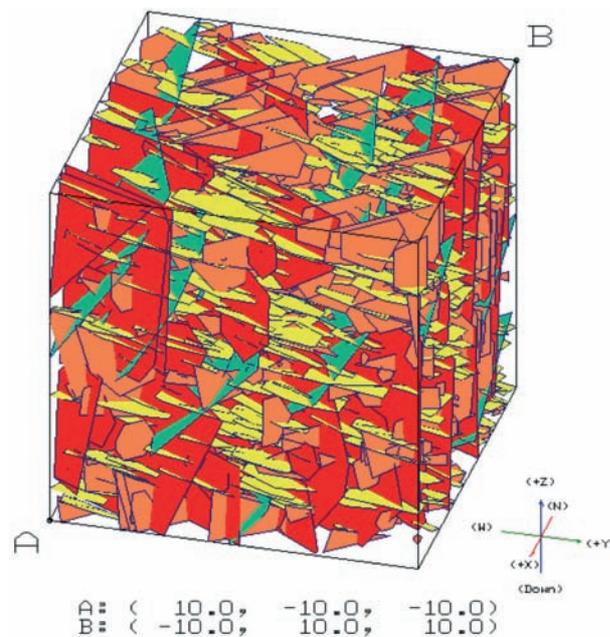


Figure 4-20: FracWorks fracture network model for sampling station 6944-18. Model size: 8000 m³, number of fractures: 1637, fracture intensity (P₃₂): 1.403 m²/m³, total fracture porosity: 0.014 % (based on FracWorks default aperture values).

A bulk porosity could not be calculated, because fracture apertures were not measured in this location due to the bad condition of the bedrock exposure. Nonetheless, the location was included, because a tracer test was conducted on springs in its vicinity by Raum (2002). Thus a comparison between the flow directions indicated by the tracer and the flow paths determined by the numerical modeling can be made, which allows a number of very simplistic estimates about the accuracy of the model.

Cluster ID	Dip Azi./Dip	Orientation Distribution	Intensity [P ₃₂] constant	Size			Aperture mean [m]	Termination %
				Mean [m]	Distribution	Deviation (1 σ)		
1	030-24	Fisher (K = 75)	0.79	1.52	Uniform	7.87	default	0
2	137-86	Bivariate normal (5/5)	0.20	3.79	Uniform	1.28	default	50
3	211-83	Bivariate normal (5/5)	0.26	3.59	Uniform	1.14	default	0
4	253-56	Bivariate normal (5/5)	0.16	3.28	Uniform	0.71	default	50

Table 4-9: Fracture set parameters employed in the model of sampling station 6944-18.

In terms of fracture intensity the distribution is dominated by a set of gently NE dipping fractures, which is oriented parallel to the metamorphic foliation. It is characterized by a comparatively small mean size. However, the size distribution shows a high variability. The remaining fracture populations are attributed with widely similar parameters. Thus, mean intensities and sizes lie within relatively small ranges. Only their orientations differ. Cluster 2 and 3 are both steeply inclined. The former strikes NE-SW, the latter NW-SE. Only the NNW-SSE trending population (Cluster 4) is moderately inclined.

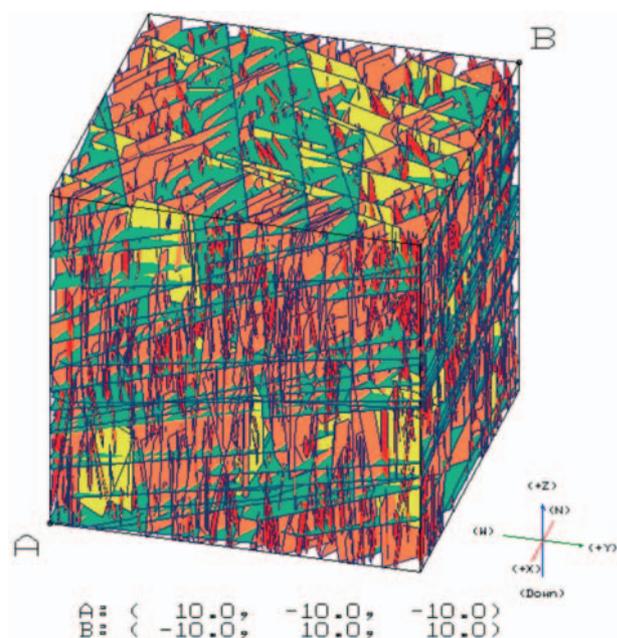


Figure 4-21: FracWorks fracture network model for sampling station 7044-04. Model size: 8000 m³, number of fractures: 5910, fracture intensity (P₃₂): 3.194 m²/m³, total fracture porosity: 0.42 %.

The stochastic fracture network generated for location 7044-04 is displayed in fig. 4-21. Its 5910 individual fractures amount to an average fracture intensity of 3.194 m²/m³ and produce a bulk porosity of 0.42 %. While the number of fractures is significantly lower in this location compared to location 6943-01 its porosity is almost twice as high. The reason for this discrepancy lies in the large number of gently W dipping unroofing joints, which dominate this model both in terms of mean fracture intensity, size, and aperture.

Cluster ID	Dip Azi./Dip	Orientation Distribution	Intensity [P ₃₂] constant	Size			Aperture mean [m]	Termination %
				Mean [m]	Distribution	Deviation (1 σ)		
1	251-18	Bivariate normal (5/5)	1.43	10.02	Uniform	8.76	1.96e-3	0
2	240-90	Bivariate normal (5/5)	0.54	1.87	Uniform	1.84	8.4e-4	87
3	124-90	Bivariate normal (5/5)	0.84	1.97	Uniform	2.05	9.0e-5	75
4	200-90	Bivariate normal (5/5)	0.39	2.64	Uniform	2.41	3.5e-4	50

Table 4-10: Fracture set parameters employed in the model of sampling station 7044-04.

The average sizes, intensities, and apertures of the remaining fracture populations are significantly smaller. All of them are subvertical and strike NE-SW, NW-SE, and WNW-ESE, with decreasing abundance. Their mean apertures are one to two orders of magnitude lower than that of the unroofing joints. Thus, the difficulties in recharging the open subhorizontal fractures via the steeply inclined ones mentioned in section 4.3.1.1 could potentially affect this model.

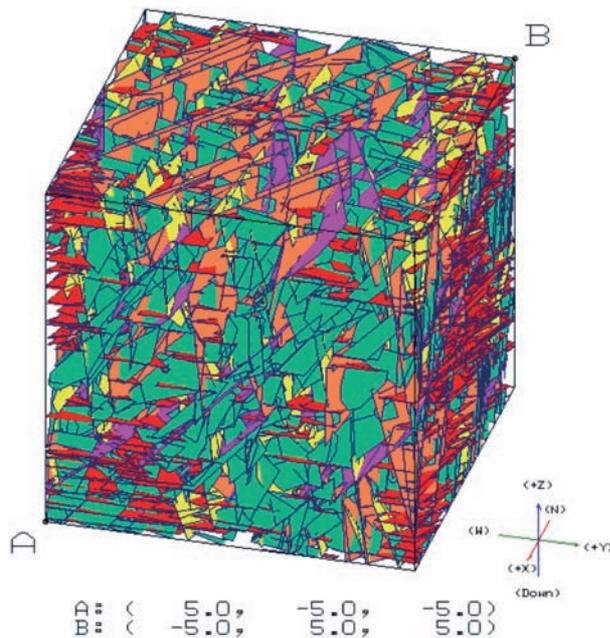


Figure 4-22: FracWorks fracture network model for sampling station 6943-13. Model size: 1000 m³, number of fractures: 8705, fracture intensity (P₃₂): 4.810 m²/m³, total fracture porosity: 0.59 %.

The distribution of fractures in a metamorphic lithology was modeled for location 6943-13. The results are presented in fig. 4-22. In this case the model size had to be reduced again due to the high density of small fractures, which could not be generated for a cube with a side length of 20 m. Thus, the model comprises a volume of 1000 m³. The total number of fractures is 8705, producing an average fracture area of 4.810 m²/m³ per unit volume and a porosity of 0.59 %. The network is majorly dominated by a set of gently N dipping fractures, which in this case were not interpreted as unroofing joints but as discontinuities

parallel to the metamorphic grain, which, however, is only very weakly developed in this location. The fracture size of the population averages at 4.54 m with a mean intensity of 1.43 m²/m³. Its mean aperture is the second highest in the network. Another fracture set possessing large planes strikes NE-SW, but is associated with a comparatively low intensity. WNW-ESE trending fractures show the second highest intensity and relatively large planes, but the lowest mean aperture. The largest mean aperture exists in the moderately WSW dipping population. However, mean size and intensity are relatively low.

Cluster ID	Dip Azi./Dip	Orientation Distribution	Intensity [P ₃₂] constant	Size			Aperture mean [m]	Termination %
				Mean [m]	Distribution	Deviation (1 σ)		
1	198-78	Bivariate normal (5/5)	1.19	1.87	Uniform	1.43	5.0e-4	50
2	000-18	Fisher (K = 200)	1.43	4.54	Uniform	2.85	1.55e-3	50
3	129-84	Bivariate normal (5/5)	0.62	2.63	Uniform	1.94	1.12e-3	50
4	097-78	Bivariate normal (5/5)	0.79	1.22	Uniform	0.75	6.7e-4	50
5	255-48	Bivariate normal (5/5)	0.79	1.58	Uniform	0.85	2.4e-3	50

Table 4-11: Fracture set parameters employed in the model of sampling station 6943-13.

In summary it should be mentioned that the models presented above do not show clear trends in the distribution of bulk fracture porosity with respect to lithology. Both in igneous and metamorphic rocks the models suggest porosities between approximately 0.2 and 1.1 %. The highest and lowest values were modeled for granites and homogenized diatexites (locations 6943-01 and 7044-02), while intermediate porosities exist both in granites (location 7044-04) and gneisses (location 6943-13). All fracture porosities lie in the ranges proposed for crystalline bedrock by Karrenberg (1981) and Hölting and Coldewey (2005), who quote values of less than 2 %, as well as Freeze and Cherry (1979), who suggest values from 0 to 5 % for dense and 0 to 10 % for fractured crystalline rocks.

All outcrops modeled in this section possess both gently and steeply inclined fractures, thus producing quasi-orthogonal fracture networks. Therefore, in theory groundwater flow should be possible in multiple directions, depending on parameters other than fracture orientation. These parameters include size, aperture, intensity, and connectivity of fractures along with the distribution of local hydraulic heads. In the following, these stochastic networks will be utilized in the PAWorks flow modeling.

4.3.1.4 FracMan[®] 3D discrete fracture and flow models of selected locations

In this section, the discrete fracture networks generated in the preceding subchapter will be used to create numerical flow models for the respective fracture sampling locations. To this end, several simplifying assumptions have to be made for the models:

- (1) The flow region is modeled as a cube encompassed completely by the saturated zone.
- (2) The flow region is oriented such that two walls of the cube are oriented perpendicular to the hydraulic gradient.
- (3) Hydraulic gradients are derived from topographic gradients. The magnitude of the hydraulic gradient is chosen to be approximately half of the topographic gradient.
- (4) In order to simulate flow hydraulic heads proportional to the gradient are applied to two side walls of the cube and to its top to simulate infiltration. The remaining two sides and the bottom are determined to be passive no-flow boundaries.
- (5) In several locations wells are inserted in the flow regions. They intersect their entire vertical extents, possess a diameter of 0.3 m, and hydraulic heads equal to two-thirds of their lengths.

A schematic representation of these assumptions is depicted in figure 4-23. The exact model specifications are tabulated in appendix D.

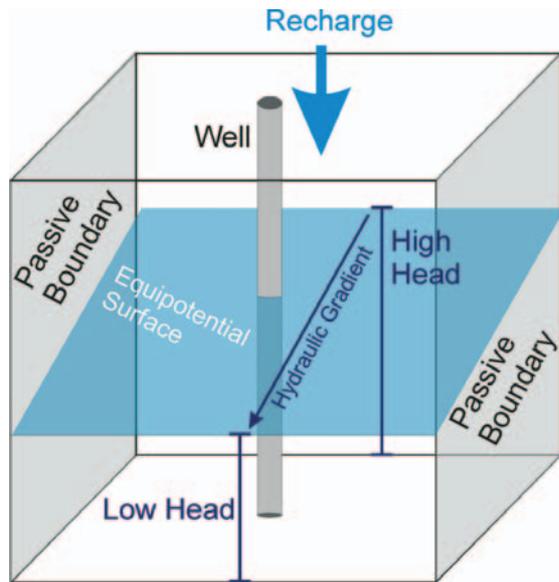


Figure 4-23: Conceptual scheme showing the components of the PAWorks flow model. In the flow region various constant hydraulic heads are applied to the sides of the flow region in order to create a hydraulic gradient similar to the topographic gradient. Three sides of the cube are passive boundaries not influencing the groundwater migration. In the center of the flow region a well penetrates the entire model.

The first flow model generated in PAWorks is that of location 6943-01 (the granite quarry near Patersdorf-Prünst). As can be observed in the photographs displayed in section 4.3.1.1 the fracture density is relatively high and a significant portion of the groundwater flow occurs along subhorizontal unroofing joints. Figure 4-24 highlights this phenomenon. Initially, water infiltrates through steeply inclined fractures until they intersect a major unroofing joint. Along the plane of this joint and along its intersections with steeply inclined fractures gradient-parallel flow occurs until a large subvertical fracture striking NW-SE deflects the path and transports the water out of the model box. Thus, the unroofing joints serve as dominant avenues for groundwater migration in this location. Due to their subhorizontal

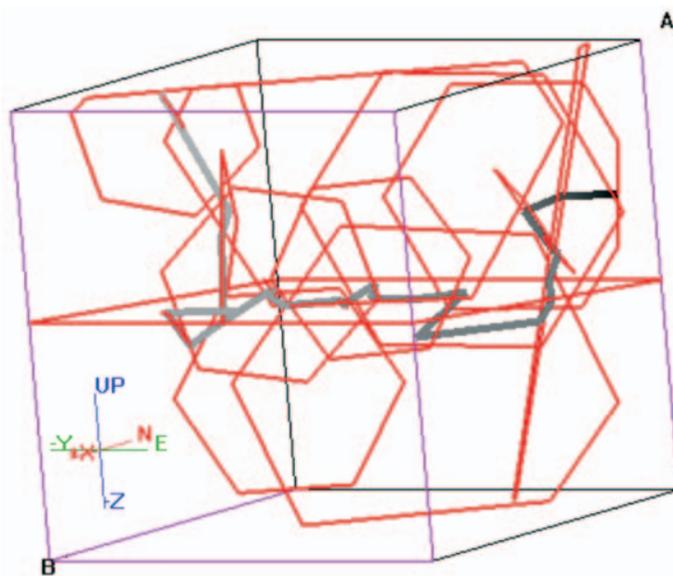


Figure 4-24: PAWorks flow model for one representative path. Size of flow region: 20 x 20 x 20 m. Hydraulic gradient of 0.1 trends S-N. Black/pink box: fracture and flow model region. Red planes: fractures used by flow path. Gray to black line: flow path from high to low hydraulic head, respectively. Location: 6943-01.

character flow anisotropies only have insignificant effects and gradient-parallel flow is possible. Nonetheless, steeply inclined fractures are similarly important, because they allow the infiltrating water to reach the unroofing joints.

The opposite can be observed in the model of sampling station 7044-02 (fig. 4-25, the railroad cut near Schweighof). In this location gently inclined fractures are present, but significantly less numerous than in location 6943-01. Also, fracture sizes in this set are smaller. Only their mean aperture is slightly higher than that of

unroofing joints in location 6943-01. Thus, the decreased connectivity due to smaller sizes and lower numbers seems to be the limiting factor for flow along subhorizontal fractures in this sampling station.

Due to this effect gradient-parallel flow is also inhibited. As a result, the groundwater flow has a strong vertical component due to the utilization of steeply inclined discontinuities. Especially in fig. 4-25b this strong vertical flow becomes evident. There, a horizontal flow component is mainly induced by the presence of an impermeable boundary at the bottom of the model cube, such that the migration is forced sideways. Significant gradient-parallel flow is also precluded by the fact that the dominant fracture population strikes perpendicular to the hydraulic gradient. Thus, only secondary fracture sets allow the flow to follow the gradient. This situation is frequently the case, because dominant steeply inclined fracture sets tend to allow erosion to produce topographic lows subparallel their strikes. Thus, the flanks of these lows are associated with a topographic (and potentially also a hydraulic) gradient oriented at right angles to the trend of the valley, and therefore also to the strike of the dominant fracture set. This effect was discussed in more detail by Zeithöfler (2003).

The insertion of a producing well (fig. 4-25a) does not significantly change the prominent trend. However, most flow paths converge towards the well due to its drawdown, which produces a hydraulic head lower than that of the outflow boundary.

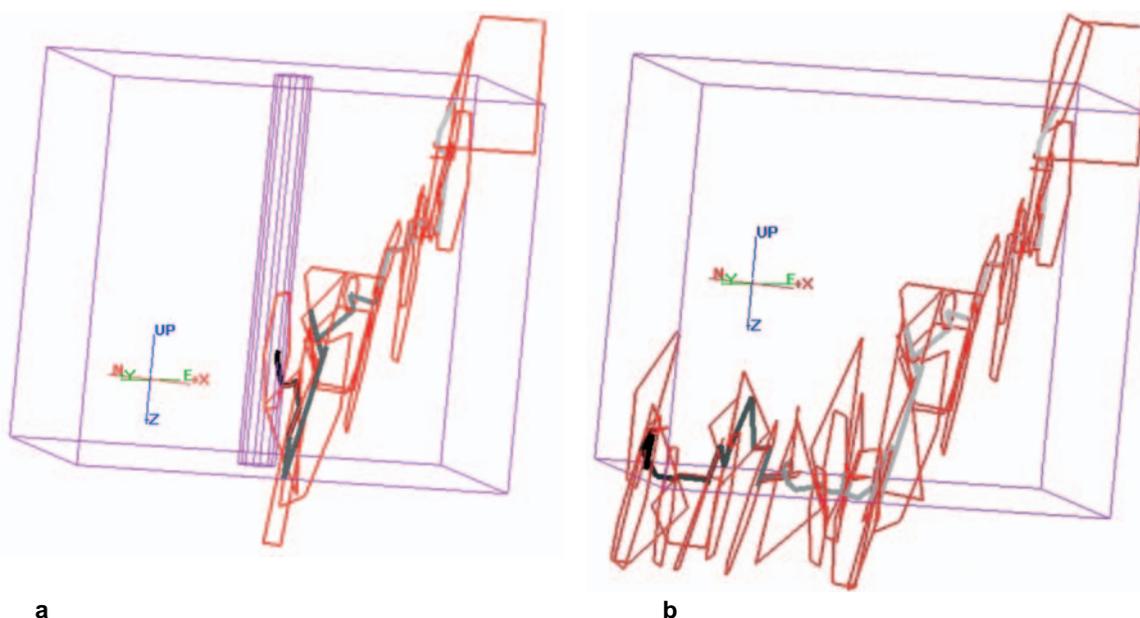


Figure 4-25: PAWorks flow model for one representative path. Size of flow region: 7 x 7 x 7 m. Hydraulic gradient of 0.10 trends SE-NW. Pink box: flow model region. Red planes: fractures used by flow path. Gray to black lines: flow paths from high to low hydraulic head, respectively. (a) Model includes a borehole. Pink tube: simulated well (diameter 0.3, drawdown: $h \cdot 3^{-1}$). (b) Same model without the borehole. Location: 7044-02.

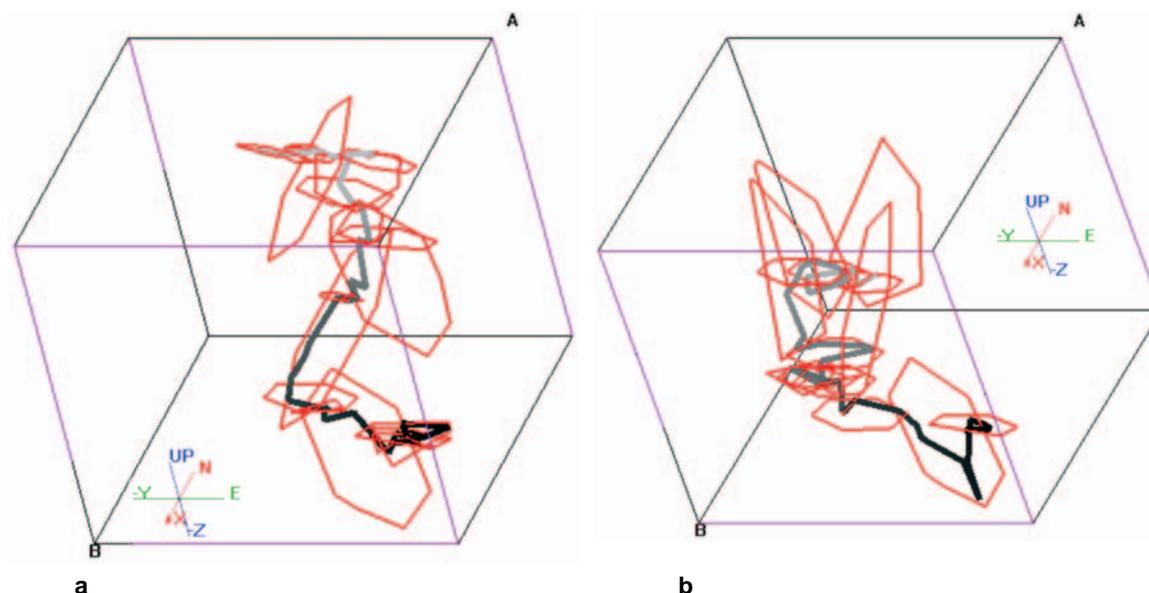


Figure 4-26: PAWorks flow model for one representative path. Size of flow region: 20 x 20 x 20 m. Hydraulic gradient of 0.25 trends N-S. Black/ pink box: fracture and flow model region. Red planes: fractures used by flow path. Gray to black lines: flow paths from high to low hydraulic head, respectively. Location: 6944-18. (a) Flow path with a \pm N-S component. (b) NW-SE oriented flow path.

For sampling station 6944-18 a nearby tracer test performed on springs by Raum (2002) provides the possibility to test the models' predictions. The tracer tests produced two horizontal flow connections, the dominant one trending NW-SE, and the secondary one N(NE)-S(SW). This is exactly what the models presented in fig. 4-26 suggest. Figure 4-26a gives an example for \pm N-S directed gradient-parallel groundwater migration, which becomes deflected towards ESE as it continues down the gradient. Raum (2002) described this connection as relatively weak, which is supported by the modeling. The fracture sampling station is dominated by discontinuities parallel to the NW-SE oriented metamorphic foliation as well as another steeply inclined set with the same strike. Both in the tracer test and the PAWorks model groundwater flow preferentially utilized these avenues (fig. 4-26b). Thus, the migration predominantly proceeds at high angles to the hydraulic gradient. This effect, along with a possible explanation, has already been described for model 7044-02.

Model 7044-04 (granite quarry at the "Teufelstisch" hill) shows again a flow pattern similar to location 6943-01. Infiltration occurs through subvertical fractures while the horizontal flow component is mainly accommodated by the subhorizontal unroofing joints (fig. 4-27). For this simulation the well was not included in the flow solution. Therefore, it did not affect the pathways. Including this well led to effects similar to those in model 7044-02. The slight west-southwesterly inclination (ca. 15°) of the unroofing joints has a noticeable influence on the general flow direction in that they, in combination with the steeply dipping

fractures, deflect the path away from parallelism with the gradient towards SW. Due to the quasi-horizontality (with dips of less than 2°) of the unroofing joints in location 6943-01 this phenomenon does not exist in the Prünst granite quarry. Thus, it becomes obvious that the

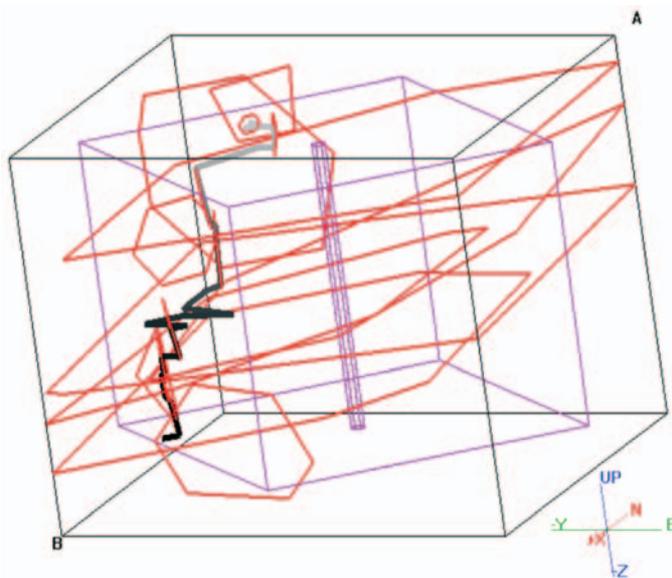


Figure 4-27: PAWorks flow model for one representative path. Size of flow region: 15 x 15 x 15 m. Hydraulic gradient of 0.25 trends NE-SW. Black box: fracture model region. Pink box: flow model region. Pink tube: simulated well (diameter: 0.3m), not included in flow solution. Red planes: fractures used by flow path. Gray to black line: flow path from high to low hydraulic head, respectively. Location: 7044-04.

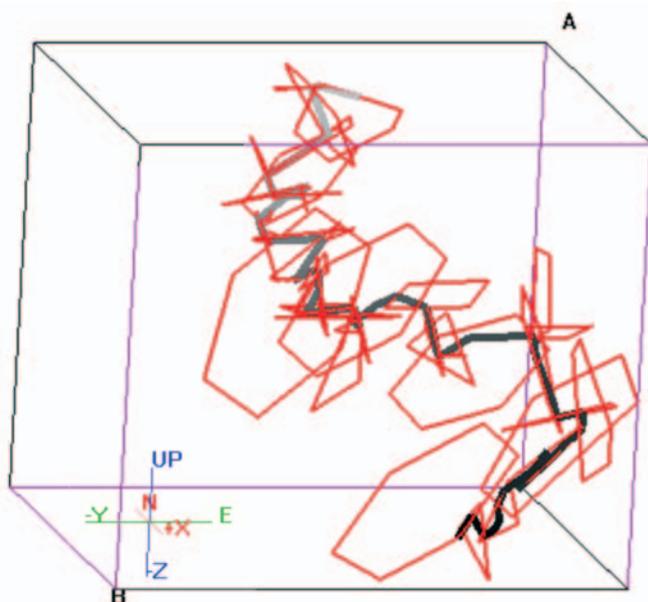


Figure 4-28: PAWorks flow model for one representative path. Size of flow region: 10 x 10 x 10 m. Hydraulic gradient of 0.2 trends N-S. Black/ pink box: fracture and flow model region. Red planes: fractures used by flow path. Gray to black line: flow path from high to low hydraulic head, respectively. Location: 6943-13.

degree of hydraulic anisotropy caused by a fracture's inclination is a continuum from isotropic (along a horizontal fracture) to completely anisotropic (along a vertical fracture).

The final model (location 6943-13) was again created in a metamorphic lithology. There, a pronounced metamorphic foliation is widely absent. Nonetheless, a set of gently N to NNW dipping fractures, approximately subparallel to the regional metamorphic grain, has developed as a secondary population. It is partially utilized by the pathways for the horizontal flow component. Due to the fact that this fracture set dips against the hydraulic gradient flow occasionally occurs up-dip along these fractures. A major portion of the flow, both horizontal and vertical, is accommodated by the dominant subvertical NW-SE and NE-SW striking fractures. Also, the moderately W dipping population serves as avenues, which is possibly due to the comparatively high apertures measured in this fracture set. Because large subhorizontal discontinuities, similar to the unroofing joints in the granitic lithologies, are widely missing, flow is much more restricted to an intricate pattern of intersecting

subvertical fractures, which gives the pathways a very tortuous character, compared to those in the granites.

In conclusion of this subchapter it has to be pointed out that the flow models presented here are in no way designed to provide quantifiable information on the productivity of a well or an aquifer's exact transport characteristics. Both the geologic and hydrologic data available for this region do not warrant such statements. Also, the modeling capabilities of the currently available computer software are still very approximative and it must not be forgotten that all the fracture networks presented above are the result of stochastic generation processes based on the statistical analyses of field measurements. Thus, they represent only one possible layout of fractures in the subsurface of a given location, which is not identical to the actual situation. Examining the response of a well to a real-world fracture network would require the measurement and exact reproduction of every discontinuity present in the volume of interest, which, of course, cannot be realized due to the limitations of sampling techniques and modeling capabilities.

Nonetheless, these models provide interesting insights into the general behavior of specific fracture types in the study area. For instance, unroofing joints in granitic lithologies were identified as prominent avenues for horizontal groundwater flow. However, they remain ineffective without a connection to steeply inclined fractures providing the recharge. Additionally, results from existing studies could be reconstructed by the models, which suggests that both numerical modeling and tracer tests are valid approaches for the solution of flow-related questions in hard rock aquifers and that a connection between fractures measured in bedrock outcrops and groundwater flow in fact exists.

4.3.2 Integration of the results from various prospecting approaches in the Bad Kötzing geothermal drilling project

As the results from the surface geophysical survey have already been presented in section 4.1.2 now the field and remote sensing data will be focused on. Unfortunately, bedrock outcrops are rare in the vicinity of the survey location, so only very few fracture measurements could be taken in the field. These are shown in fig. 4-29. The plot unveils several preferred orientations such as a set of steeply dipping NNW-SSE striking fractures (red planes in fig. 4-29), which are subparallel to both the locally dominant lineament orientation and the general trend of the assumed faults identified in the geoelectric profiles (fig. 4-30). Several other fracture sets exist, among which there are WNW-ESE, ENE-WSW, and NNE-SSW trending ones. Comparing these secondary orientations to the lineament strikes in fig. 4-30 discloses a certain agreement albeit their relative abundances vary somewhat, which, however, is in part due to the scarcity of fracture measurements.

As already mentioned, the plot in fig. 4-30 depicts the orientations of topographic lineaments obtained from a digital elevation model. The database of this lineament analysis, though, is not the same as that used for the analyses in section 3 because its spatial extent did not cover the site of the geoelectric survey. A lineament analysis of the entire Eastern Bavarian basement complex performed by the author for the Bavarian Geological Survey (Zeitlhöfler,

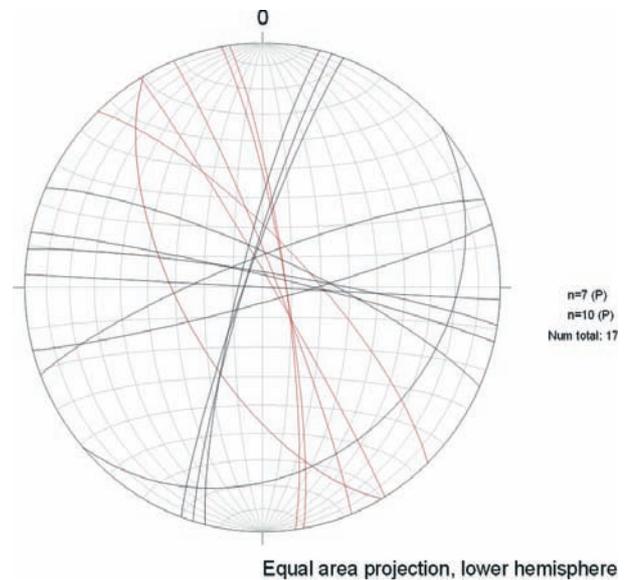


Figure 4-29: Fracture orientations measured in the vicinity of the geophysical survey site near Zeltendorf/ Bad Kötzing. Red planes represent fractures subparallel to the dominant lineament direction as well as the assumed strikes of the faults identified in the geoelectric tomography. $n_{\text{fractures}} = 17$.

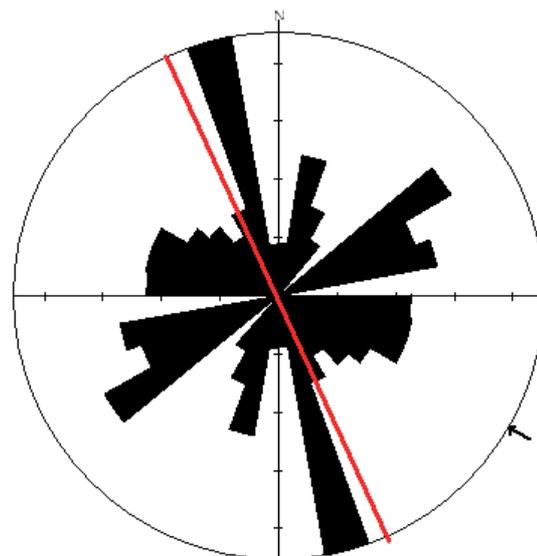


Figure 4-30: DEM lineament orientations obtained from a 5 km radius about the geophysical survey site. Red line: approximate orientations of the assumed faults identified in the geoelectric profiles. Cumulative lineament length: 120.02 km. Scale tick interval is 3.606 km. Data source: Zeitlhöfler (2006b).

2006b) did cover this site and its results were used for this comparison of fracture and lineament orientations. The analysis was based on DEM obtained from NASA's **Shuttle Radar Topography Mission (SRTM)**⁸. The methodical approach was in principle the same as that described for the processing of the ERS-DEM in section 3. The results presented in fig. 4-30 agree extremely well with the findings from the geophysical work, namely that the NNW-SSE direction is the dominant one for structures in this area. Interestingly, the Hercynian NW-SE direction, prominent in most other sampling locations in the study area, is only of minor significance here, although the 5 km buffer zone used for selecting the lineaments in fig. 4-28 covers part of the NW-SE striking Rundinger Zone.



Figure 4-31: Map of the geophysical survey site (same extent as fig. 4-9) depicting the distribution of local lineaments mapped on a DEM. Data source: Zeithöfler (2006b).

Figure 4-31 depicts the location of mapped lineaments in proximity to the geophysical survey site. Due to the relatively coarse resolution of the DEM (ca. 90 m / pixel) and the large scales on which the lineaments were mapped the exact positioning of a lineament in the thalweg of a valley could not always be achieved on a small scale. Thus, the large NNW-SSE trending lineament is placed slightly W of the valley bottom denoted by the little stream. Nonetheless, the orientations stay the same and it becomes obvious that northerly directions

⁸ Further information on the SRTM database is available on the internet at <http://www2.jpl.nasa.gov/srtm/>; SRTM-based DEMs can be downloaded from <http://edc.usgs.gov/srtm/>.

dominate the topographic structure in the immediate vicinity of the Dampfbach valley survey site.

Thus, the three different approaches to identifying local geologic structures show impressive agreement. Unfortunately, the ultimate proof for water to exist in these structures is still not available. At the time of the completion of this dissertation the actual drilling has yet to be conducted, so no further information on the hydrogeologic properties of this fault zone exists at this moment.

4.4 References

- Banks, D., Rohr-Torp, E., and Skarphagen, H., 1994, Groundwater resources in hard rock: experiences from the Hvaler Study, Northeastern Norway, Applied Hydrogeology, Volume 2: Hannover, Germany, Verlag Heinz Heise, p. 33-42.
- Banks, D., Solbjorg, M.L., and Rohr-Torp, E., 1992, Permeability of fracture zones in Precambrian granite.: Quarterly Journal of Engineering Geology, v. 25, p. 377-388.
- Bender, S., 2001, Mixing Processes of Groundwater in the Transitional Zone of Granites and Moldanubian Gneisses, *in* Seiler, K. P., and Wohnlich, S., eds., New Approaches Characterizing Groundwater Flow. - Proceedings of the XXXI IAH-Conference, Munich: Munich, Balkema, p. 903-906.
- Cushman, R.V., Allen, W.B., and H.L. Pree, J., 1953, Geologic factors affecting the yield of rock wells in southern New England.: Journal of the New England Water Works Association, v. 67, p. 77-95.
- Daniel, C.C., 1989, Statistical analysis relating well yield to construction practices and siting of wells in the Piedmont and Blue Ridge provinces of North Carolina., U.S. Geological Survey Water-Supply Paper 2341, U.S. Geological Survey.
- Denzel, S., Behnert, T., Ertel, T., Dinkel, R., and Trost, U., 1995, Handbuch Altlasten und Grundwasserschadensfälle. Methodensammlung: Karlsruhe, Landesanstalt für Umweltschutz Baden-Württemberg, 176 p.
- Dershowitz, W., 2002, FracWorks XP Discrete Feature Simulator. User Documentation Beta Version 0.21: Seattle, Washington, Golder Associates Inc., 81 p.
- Dershowitz, W., Lee, G., Geier, J., Hitchcock, S., LaPointe, P., and Cladouhos, T., 1999, FracWorks/95 Discrete Feature Simulator. User Documentation. Version 1.3.: Seattle, Washington, Golder Associates, Inc.
- Dobner, A., 1983, Hydrogeologische Verhältnisse, *in* Ott, W.-D., ed., Erläuterungen zur Geologischen Karte von Bayern 1:25.000, Blatt Nr. 6943 Viechtach: München, Bayerisches Geologisches Landesamt, p. 50-55.
- Drew, L.J., Karlinger, M.R., Armstrong, T.R., and Moore, R.B., 1999, Relations between Igneous and Metamorphic Rock Fracture Patterns and Groundwater Yield from Variography of Water-Well-Yields - Pinardville Quadrangle, New Hampshire.: Natural Resources Research, v. 8, p. 137-152.
- Freeze, A.R., and Cherry, J.A., 1979, Groundwater: Englewood Cliffs, N.J., Prentice-Hall.
- Höltling, B., and Coldewey, W.G., 2005, Hydrogeologie. Einführung in die Allgemeine und Angewandte Hydrogeologie: München, Spektrum Akademischer Verlag, 326 p.
- Karrenberg, H., 1981, Hydrogeologie der nichtverkarstungsfähigen Festgesteine: Wien, Springer Verlag, 385 p.
- LeGrand, H.E., 1954, Geology and groundwater in the Statesville area, North Carolina.: North Carolina Department of Conservation and Development Bulletin, v. 66, p. 68.

- Parney, R., and Smith, L., 1995, Fluid Velocity and path length in fractured media.: Geophysical Research Letters, v. 22, p. 1437-1440.
- Polivka, J., 1999, Durchführbarkeitsstudie zur Erschließung von Heil- bzw. Thermalwasser im Raum Kötzing: Regensburg, Grundwasserberatung Dipl. Geol. J. Polivka, p. 25.
- Prinz, H., and Strauß, R., 2006, Abriss der Ingenieurgeologie: München, Spektrum Akademischer Verlag, 671 p.
- Propach, G., 1968, Hydrogeologische Verhältnisse, *in* Madel, J., Propach, G., and Reich, H., eds., Erläuterungen zur Geologischen Karte von Bayern 1:25.000, Blatt Nr. 6945 Zwiesel: München, Bayerisches Geologisches Landesamt, p. 77-78.
- Raum, K.-D., 2002, Markierungstechnische, bruchtektonisch-gefügekundliche und fotogeologische Untersuchungen zur Ermittlung der Grundwasserfließverhältnisse in der Verwitterungszone kristalliner Gesteine in Quellgebieten des Oberpfälzer/Bayerischen Waldes (Ost-Bayern/Deutschland) [PhD Dissertation thesis]: Erlangen, Friedrich-Alexander Universität Erlangen-Nürnberg.
- Richert, P., 2002a, Geophysikalische Bohrlochmessungen in der Versuchsbohrung VB 1 Neusohl, Bayern: Niederlindach, German Geo Services, p. 3.
- , 2002b, Geophysikalische Bohrlochmessungen in der Versuchsbohrung VB 2 Neusohl, Bayern: Niederlindach, German Geo Services, p. 3.
- , 2004, Geophysikalische Bohrlochmessungen in der Versuchsbohrung B1 Böbrach, Bayern: Niederlindach, German Geo Services, p. 4.
- , 2005a, Geophysikalische Bohrlochmessungen in der Versuchsbohrung B 1 Wiesenfelden, Bayern: Niederlindach, German Geo Services, p. 1.
- , 2005b, Geophysikalische Bohrlochmessungen in der Versuchsbohrung VB 4 Schweinhütt, Bayern: Niederlindach, German Geo Services, p. 5.
- , 2006, Thermalwasserprospektion Bad Kötzing (Bayerischer Wald). Geophysikalische Untersuchungen (Multielektroden-Geoelektrik): Hessdorf, German Geo Services, p. 13.
- Rohrmüller, J., Mielke, H., and Gebauer, D., 1996, Gesteinsfolge des Grundgebirges nördlich der Donau und im Molasseuntergrund, Erläuterungen zur Geologischen Karte von Bayern 1:500.000: München, Bayerisches Geologisches Landesamt, p. 16-54.
- Spencer, E.W., and Kozak, S.J., 1974, Determination of Regional Fracture Patterns in Precambrian Rocks - a Comparison of Techniques, *in* Hogson, R. A., S.P. Gay, J.Y. Benjamins, ed., First International Conference on New Basement Tectonics: Salt Lake City, Utah, Utah Geological Association.
- Starn, J.J., Stone, J.R., and Mondazzi, R.A., 2002, Characterization of bedrock aquifers in Connecticut: (2) Hydrologic simulation., Geological Society of America Northeastern Section, Annual Meeting: Springfield, Massachusetts, Geological Society of America, p. A-23.
- Stober, I., 1995, Die Wasserführung des kristallinen Grundgebirges: Stuttgart, Ferdinand Enke Verlag, 191 p.

-
- van der Pluijm, B., and Marshak, S., 1997, *Earth Structure: An Introduction to Structural Geology and Tectonics*, WCB/McGraw-Hill, 495 p.
- Walsh, G., J., and Clark, S.F., 2000, Contrasting Methods of Fracture Trend Characterization in Crystalline Metamorphic and Igneous Rocks of the Windham Quadrangle, New Hampshire: *Northeast Geology and Environmental Sciences*, v. 22, p. 109-120.
- Williams, K.W., 2000, Surface and subsurface fracture characterization and the occurrence and characterization of subsurface flow along a cross-strike transect in eastern Massachusetts. [Master's thesis]: Amherst, Massachusetts, University of Massachusetts.
- Winkler, G., 2003, Fracture network analyses for hydraulic modeling. Approaches of fractured aquifers [PhD thesis]: Graz, Austria, Technical University Graz.
- Witthüser, K., and Himmelsbach, T., 1998, Erhebungsmethoden von Kluftparametern für eine stochastische Kluftnetzgenerierung: *Grundwasser*, v. 3, p. 103-109.
- Zeithöfler, M., 2003, Bedrock Structure in Southeastern Connecticut: Hydrologic Implications. [Master's thesis]: Middletown, CT, Wesleyan University.
- , 2006a, Abschlußbericht über die Prospektionsarbeiten zur geplanten Thermalwasserbohrung in Bad Kötzing: Regensburg, p. 15.
- , 2006b, Bericht zur Lineamentanalyse auf Basis von SRTM-Satellitenhöhendaten für die Hydrogeologische Landesaufnahme im EU-Ziel-II-Gebiet im Auftrag des Bayerischen Landesamtes für Umwelt - Geologischer Dienst: München, Bayerisches Landesamt für Umwelt - Geologischer Dienst, p. 51.

5 Discussion and conclusion

In this last section the results of the previous chapters shall briefly be discussed, evaluated and summed up. Furthermore, a general outlook shortly discussing the need for further work in this area and the associated organizational and financial problems will be given.

5.1 Discussion

5.1.1 Results from structural geologic work

In the section on the structural geology of the study area several fracture types have been identified based on genetic aspects and their relationships to the host lithology. These types comprise fractures parallel to the metamorphic foliation, fractures intersecting the metamorphic grain, fractures in unfoliated lithologies, and unroofing joints. Several of these types were additionally classified according to the orientations of various fracture populations. The types were then examined with respect to various physical properties, which will be briefly discussed.

Several orientations are characteristic for specific fracture sets. Discontinuities parallel to the metamorphic foliation commonly dip gently to steeply NNE, while fractures cutting across the grain are generally subvertical and strike in many directions, although NE-SW and NW-SE strikes predominate. As to the genetic aspects of the cross cutting sets two explanations seem viable: Small fractures trending NW-SE frequently connect larger discontinuities parallel to the foliation. Thus, these structures can be interpreted as extensional transform joints ("ramps") accommodating differential shear between two foliation parallel faults. However, many fractures are larger and may form an independent network together with the NE-SW oriented ones. The latter interpretation is supported by the fact that similar fracture patterns were also observed in unfoliated lithologies, where a relationship to fabric-parallel discontinuities cannot exist. However, since the two explanations do not exclude each other possibly both are valid, depending on which individual fracture is observed.

As already mentioned above, similar fracture orientations can be found in the granitic lithologies. There, the steeply inclined NW-SE and NE-SW trending fractures were found to be associated with both plumose structures and slickenlines. Thus, these sets are likely to have originated as more or less orthogonal joint sets, possibly due to regional uplift and interchanging directions of σ_2 and σ_3 , and ensuing reactivation as both dip-slip and strike-slip

faults. Unroofing joints in unfoliated lithologies are generally subhorizontal to gently inclined and commonly follow the curvature of the topographic surface. Orientations in hydrothermal and pneumatolytic rocks differ somewhat from the granitic units in that they expose a generally N-S trending set of steeply inclined fractures instead of the NE-SW striking one. This phenomenon could be observed in all pegmatite and quartz outcrops examined for this study. Although N-S striking fractures do exist in other lithologies they only play a subordinate role there. Thus it seems likely that the stress field producing these discontinuities had a greater effect on the rather thin and sheet-like hydrothermal intrusions than on the surrounding more massive igneous and metamorphic entities.

Regarding planarity and roughness in metamorphic lithologies the fractures parallel to the foliation tend to be rougher and more undulatory than those cutting across the grain. The reason for this is suspected to be related to the observation that the foliation is frequently slightly folded and that foliation planes can be relatively small and discontinuous. Fractures follow these irregularities, which leads to rough and undulatory surfaces. Fractures cutting across the grain are not influenced by preexisting fabrics and therefore penetrate the rock in a rather straight way. In unfoliated lithologies fractures are predominantly planar and mainly associated with smooth to rough surfaces, although a slight proclivity to form rough planes exists. In granitic rocks preexisting planes of weakness usually do not exist in the form of a foliation. If at all, weakness follows individual mineral grain boundaries, which are irregularly oriented in granites. Thus, fracture roughness would be a function of grain size in this case. Plumose structures observed on joints in unfoliated lithologies can increase fracture asperity as well. In contrast, smooth planes may be attributed to smaller grain sizes or secondary smoothing due to shear reactivation of a joint. Unroofing joints are almost exclusively undulatory or curved, and rough. The curvature of unroofing joints is due to the fact that their orientations follow the topographic surface (cf. figure 2-33).

Concerning fracture trace lengths the unroofing joints in igneous rocks were found to produce the largest discontinuities, followed by steeply inclined fractures in the same units. Fractures in metamorphic lithologies are comparatively shorter, although the mean trace lengths of cross cutting fractures in metamorphic and of steeply inclined ones in unfoliated rocks are relatively similar. Fractures parallel to the metamorphic foliation show the shortest average trace lengths. Correlating this parameter with the density of fractures in specific sets an inverse relationship between trace length and density becomes evident. However, densities in foliation-parallel sets are highly heterogeneous, because besides individual discontinuities, for which the inverse relationship holds true, also highly fractured zones exist, which are commonly more widely spaced. As to densities in relation to fracture orientation

contradictory results emerged. The highest densities of fractures intersecting the foliation were found in the NNE-SSW trending sets while the lowest densities are associated with WNW-ESE to E-W striking ones. The opposite is true for steeply inclined fractures in unfoliated rocks. There, WNW-ESE to E-W striking sets are the densest, and the NNE-SSW ones the most widely spaced. One possible explanation for this phenomenon is that in metamorphic rocks much strain could be accommodated by foliation-parallel fractures, so cross cutting fractures with similar strikes (but higher inclinations) did not form as abundantly as in the igneous lithologies, where no foliation exists. The densities of unroofing joints were found to be depth-dependent. Although commonly present over the entire vertical extents of the examined outcrops of igneous rocks, they become less abundant with increasing distance from the topographic surface due to diminished unloading-related strain release at greater depths.

Mean fracture apertures were found to be relatively similar in most populations except in the unroofing joints, which are on average twice as open as the steeply inclined and foliation-parallel fractures. A weak correlation between fracture trace length and aperture could be established in most cases. However, caution has to be advised when considering absolute aperture values. Due to strain release effects in the proximity of a bedrock outcrop's free surface apertures tend to be exaggerated with respect to those further inside the rock mass. Thus, the measured values can only be used to compare the relative openness of the different fracture sets, not to characterize the real porosity of the bulk rock mass.

Fracture mineralizations and infillings exist basically in all fracture sets of the study area. Only unroofing joints are not mineralized, thus suggesting an origin after the hydrothermal activity had ceased in the region. In the other sets usually less than 10 % were found to be associated with mineral precipitates. This indicates that only part of the recent fracture network was present during hydrothermal activity (although most fracture orientations already existed) or that the mineralized fluids did not penetrate the entire network. Another possibility is that post-hydrothermal faulting and weathering obliterated previously existing mineralizations. In any case, most fractures were reopened by later tectonic phases after hydrothermal healing, such that the presence of mineral coatings should not have a significant influence on the fracture networks' permeability. Fracture infillings, such as unconsolidated fault rocks or weathering material, exist in various grain sizes from sandy-clayey gouge and grus to pebble-sized fault breccia. While the former may effectively act as barriers to groundwater flow, depending of on the prevailing grain size fraction, the latter potentially serve as highly transmissive pathways. However, these types of infillings are not restricted to specific fracture sets. Therefore, a general relationship between

fracture orientation and transmissivity cannot be established based on the presence of these materials. Only fractures parallel to the foliation were found to be proportionally less often associated with infillings.

In order to establish relationships between the characteristics and orientations of fractures irrespective of their origin the bulk data set of discontinuities (excluding the unroofing joints) recorded in the study area was sorted with the K-means algorithm. A total of four clusters was identified: Steeply inclined NW-SE striking, steeply inclined NNE-SSW to NE-SW striking, steeply inclined ENE-WSW to E-W striking, and moderately NNE dipping fractures. These clusters are essentially present in the entire study area irrespective of lithology, although with locally varying relative abundances.

Examining the physical properties of fractures based on their affiliation with the respective clusters yielded results of only limited value. Mean fracture roughness and planarity appear to be relatively similar in all steeply inclined sets. They are mainly planar and cover the entire range from smooth to rough surfaces with a slight predominance of rough planes. Only the moderately NNE dipping set, which is partly identical to fractures parallel to the metamorphic grain, but not restricted to metamorphic units, makes a difference. These discontinuities show a clear proclivity to produce rather undulatory and rough planes. Concerning fracture trace lengths no significant distinction could be made. In all clusters fractures shorter than three meters constitute the bulk of the record and generally show an exponentially decreasing abundance with increasing trace length. Fracture apertures range mainly from 0 to 1 mm in all clusters except in the moderately NNE dipping sets, which show a significant portion of the aperture values in the 1 to 5 mm range. A generally satisfactory correlation between fracture trace lengths and apertures was found in all sets. As in the genetic fracture types, mineralizations were found in all clusters in similar quantities (5 to 15 % of the total clusters). Only the moderately NNE dipping fractures exposed a smaller percentage of mineralized planes. Concerning fracture infillings also a relatively uniform distribution was observed.

In summary, the genetic classification proves to be more appropriate in the identification of various fracture properties than the one solely based on regionally dominant fracture orientations, which appears to homogenize the characteristics of otherwise distinct sets. On the other hand, both approaches highlight the different properties of fractures parallel to the metamorphic grain compared to the steeply inclined sets. The generally high roughness and density of the former makes the orientation of the foliation an important factor for the direction of groundwater flow in metamorphic lithologies.

In the following, the brittle tectonic history and characteristics of the fracture systems in the study area shall briefly be discussed. The dominant fault direction in the study area trends NNW-SSE to NNE-SSW, the secondary orientation is NW-SE to WNW-ESE. Concerning the inclinations of faults it is important to mention that almost all but the (W)NW-(E)SE striking ones are close to subvertical. Thus, the latter parallel the foliation in metamorphic lithologies. The subvertical faults in part align with the observed joint systems, so some of them are suspected to represent various phases of reactivation of once extensional features. However, the pronounced (E)NE-(W)SW direction present in the joints is widely absent in the fault data record. Reactivation thus seems restricted to the NNW-SSE to NNE-SSW and (W)NW-(E)SE trending extensional structures.

Kinematic indicators were mainly recorded in the form of slickenlines evidencing both strike- and dip-slip. The paleostress analysis of this dataset yielded two compressive (NE-SW and NNW-SSE directed compression) and two extensional (due to uplift plus NW-SE and NE-SW extension, respectively) stress fields. One new compressional phase was detected in the dataset of conjugate fracture pairs. The compressive subhorizontal stress trends (N)NE-(S)SW, extension is vertical. For one part of the conjugate set the foliation was (re)activated in metamorphic lithologies. Antithetic fractures cut across the grain. Because this type of conjugate relationship was only found in metamorphic lithologies it is assumed that only a very weak compression reactivated preexisting planes of weakness, which do not exist in the more rigid igneous rocks.

Offset features are very rare in the study area and mostly cannot be interpreted without further doubt. Thus, they will not be discussed separately. Fault rocks, such as unconsolidated breccia and gouge exist in all dominant fracture sets of the study area. They are thought to represent geologically rather young products of tectonic deformation, because brecciation and the creation of gouge are restricted to the uppermost crustal levels, which were reached during the later parts of the geologic history due to the regional uplift of the area. The widest breccia and gouge seams were found in moderately inclined fractures of the 80° to 120° strike segments.

The abovementioned findings lead to a brittle tectonic history of the study area, which commenced at the transition from the Paleozoic to the Mesozoic. The detailed succession of events as interpreted from field data and previous works of other authors is presented in section 2.5. As evidenced by the orientations of igneous and hydrothermal dikes (cf. analyses in section 3.3), some of which are filled with Permo-Carboniferous granites and aplites, the layout of the later fracture networks had in part already been established at the

end of the Paleozoic. Additionally, the mainly Variscan metamorphic foliation also served as preexisting planes of weakness for the ensuing brittle deformation. Also the large Hercynian semi-ductile fault complexes, such as the Pfahl or the Rundinger zones, influenced the orientation of a significant part of the fracture network. Throughout the Mesozoic and into the Tertiary alternating jointing and mineralization due to uplift and hydrothermal activity led to a multitude of veinlets and mineralized fractures. During the Tertiary most of the present-day fracture systems formed either due to the reactivation of preexisting joints and faults or due to the reopening of hydrothermally healed discontinuities in response to various tectonic stresses. The compressive regimes are assumed to be related to the far-field effects of processes in the emerging Alpine orogeny while the extensional phases are attributed to regional uplift during periods of diminished push from the Alpine orogenic front. The recent stress regime is believed to have established during the Miocene and consists of both a vertical (uplift-related) and an approximately N-S directed weak compressional component.

5.1.2 Results from remote sensing

Lineament mapping was performed on two different types of datasets, a satellite-based digital elevation model (DEM) and airborne b/w imagery. Despite the different resolutions and scales of observation as well as sampling techniques reasonable agreement between the two lineament analyses exists on a regional scale. While the spatial density of DEM lineaments is significantly lower than that of the photolineaments the DEM yields more pronounced preferred directions, which trend NW-SE, N-S to NNE-SSW, NE-SW, and, very insignificantly, ENE-WSW to E-W. Due to the large number of rather short and locally variable photolineaments the background noise is significantly higher in this dataset and conspicuous peaks emerge only above the scatter in the NW-SE and the N-S to NNE-SSW directions.

In terms of regional density the DEM lineaments show only little spatial variation. Areas of elevated density can be found along the northwestern edge of the study area, as well as parallel to the NW-SE trending Pfahl and Rundinger zones. Higher densities also exist along a N-S striking stretch extending from the northern termination of the Deggendorfer Bucht through the central part of the study area towards its northern corner. Separating the lineaments with regard to their dominant orientations shows that NW-SE striking ones cluster next to the Pfahl and Rundinger zones, while the comparatively shorter N(NE)-S(SW) striking ones are more evenly distributed. The latter only show a lower concentration in the North-central study area where the E(NE)-W(SW) structures

predominate. Comparing the distribution of lineaments to the regional lithologies shows a generally higher density in the igneous and anatectic domains south of the Pfahl zone. Spatially more highly resolved correlations between rock type and lineament density are not obvious.

Because the DEM yielded several distinct lineament directions a tectonic analysis was attempted, which resulted in two possible deformation scenarios. Both include right-lateral strike-slip along the main NW-SE striking structures. Scenario 1 interprets the dominant lineament pattern as a classical Riedel-type shear system, according to which the NW-SE features represent the main slip planes. The lineaments oriented at approximately 10 to 20° clockwise from the main shears were interpreted as synthetic, while the N-S to NNE-SSW ones were deemed antithetic Riedel shear faults. Scenario 2 is a hybrid model including shear and extensional processes. This would account for the rather small angle between the syn- and antithetic Riedel-shears. According to this model the synthetic shears remain the same as in scenario 1, but the N(NE)-S(SW) trending lineaments were interpreted as purely extensional features oriented parallel to a subhorizontal \pm N-S trending σ_1 . However, a major problem exists in scenario 2, because hydrothermal solutions should preferentially intrude the extensional features, which is not the case according to the analyses of quartz mineralizations in section 3.3. These analyses show that mineralization occurred almost exclusively along the NW-SE striking fault systems. The relationship to hydrothermal precipitates, of course, is only significant if the mineralization is assumed to be syntectonic, which is generally the case (cf. citations in section 3.1.1.2). Pertaining to the age of deformation the upper limit is posed by the Permo-Triassic hydrothermal intrusions. Thus, the deformation is attributed to the late Variscan orogeny, because an earlier age seems questionable due to the pervasive Carboniferous high-temperature-low-pressure metamorphism, which overprinted most of the preexisting structures (cf. sections 1.2.1 and 1.2.2).

As already mentioned, the photolineaments are associated with a higher background noise and only two significant preferred directions. The distribution is clearly dominated by NW-SE striking lineaments, the \pm N-S population represents a subordinate peak. With respect to the regional distribution the photolineaments show similarities to those obtained from the DEM. A conspicuously high density exists along the NW edge of the study area in a belt connecting the Pfahl and the Rundinger zones. Also, increased concentrations were found in a zone connecting the southern and the northern corners of the study area. Only the Pfahl and Rundinger zones per se are not as pronounced as in the distribution of DEM lineaments. If separated according to the dominant directions the NW-SE lineaments turn out to be

relatively evenly distributed over the study area. As in the DEM lineaments a slightly higher density could be observed in areas S of the Pfahl zone. The N-S structures also show a relatively uniform distribution except in the vicinity of the Rundinger zone, where a conspicuous low exists. ENE-WSW to E-W striking lineaments, although not present as a distinct peak in the regional distribution, were also mapped separately. These short structures are quite scattered in the study area and only show slightly higher densities in the vicinity of Viechtach, where also DEM lineaments of this orientation cluster.

Groundtruthing and domain overlap analysis generally showed a good regional agreement between the remotely sensed lineaments and in situ sampled fracture systems. Dominant orientations of steeply inclined fractures trend 1° , 35° , 80° , and 120° , which coincide with the peaks in the DEM-, and, to a lesser extent, in the photolineaments. Locally dominant fracture sets could be correlated with neighboring lineaments having similar strikes. The regional rose diagrams of lineament and fracture orientations agree reasonably well with respect to the directional aspect, although the relative abundances in the specific strike segments of fractures and lineaments are different. While the NW-SE direction is dominant in all plots the N-S structures in the lineaments outnumber the NE-SW structures. In the fracture distribution the opposite can be observed. This suggests that NE-SW directed discontinuities were not as active in sculpting the present-day landscape as the other two dominant sets of structures. Regionally continuous fracture domains, i.e. areas where a specific fracture and lineament orientation prevails, could not be defined for the study area, which is most likely due to its limited extent. Research performed by the author on the scale of the entire Eastern Bavarian crystalline basement (cf. citation in section 3.4) produced several domains, in which a certain lineament orientations were dominant.

In the course of the remote sensing and GIS analyses also the orientations of igneous and hydrothermal intrusions were mapped. As in the distributions of lineaments the NW-SE direction dominates this dataset. However, \pm N-S, NE-SW, and E(NE)-W(SW) oriented intrusions were found as well. Thus, the general layout of the recent fracture networks was already established during the Permo-Carboniferous igneous and the ensuing Permo-Triassic hydrothermal activities. Several types of the lithologically distinct intrusions have been radiometrically dated. Based on these ages the structures emerged in the following succession of events: NW-SE structures – ENE-WSW and NE-SW structures – \pm N-S structures. The respectively older structures were frequently also utilized by younger tectonic phases. This is especially true for the NW-SE direction, which is present in almost all but the youngest types of intrusives. The later Permo-Triassic hydrothermal activity suggests an ensuing reactivation of predominantly NW-SE striking faults.

5.1.3 Results from hydrogeologic analyses

The hydrogeologic research carried out for this study includes the analyses of well data, geophysical surveys, qualitative observations in bedrock outcrops, and flow simulation based on numerical discrete fracture models.

For the study area and its immediate vicinity an inventory of a total of 34 bedrock wells with depths ranging from 20 to 77 meters was compiled. Yields lie between 0.1 and more than 7.3 l/s, although several of these values are estimates, and wells producing the highest yields are frequently pumped at much lower rates during long-term operation. The spatial distribution of the datapoints did not warrant a variography exposing areas of homogeneous well yields. However, the correlation of the various well sites with specific parameters highlighted certain trends. The comparison of yield with the lithology in which a well is located showed that in the Bavarian Forest granitic rocks tend to be the least productive units while strongly folded and migmatitic rocks are frequently associated with above-average yields. Layered metamorphic rocks produce intermediate values. However, well yield commonly is a function of several factors, so individual locations may turn out highly variable results. Among these factors is the brittle bedrock structure, which, as already mentioned above, is only to a certain extent dependent on lithology. Thus, a well drilled into a fault zone situated in a granite may eventually be more productive than one located in an undisturbed gneissic lithology. Topographic lineaments were used as proxies for brittle structures in the study area and yields were examined with regard to the distances between wells and neighboring lineaments. While a weak correlation between a well's yield and its distance to the closest lineament could be established for the photolineaments no discernable relationship to the DEM dataset was found. One reason for this might be that photolineaments reflect local fracture systems better due to the higher spatial resolution they provide, which allows a more accurate localization of structures compared to the DEM.

For eleven wells of the bulk inventory more detailed information has been available. This information includes the results of both flowmeter measurements and various borehole geophysical surveys. The most striking outcome of these surveys is the high local variability of well yields as determined by the flowmeter, which suggests a highly heterogeneous aquifer. In this aquifer it is important to intersect discrete highly productive zones in order to obtain significant yields. Depending on the inclination of these zones a vertical borehole is more or less likely to strike them. Since a large part of the fracture sets in the study area, especially at greater depths, are steeply inclined to subvertical the probability of intersecting

them strongly decreases and the variability of well productivity increases even at very small horizontal distances.

With regard to the most productive depth interval of the subsurface it turned out that almost 75 % of the primary influxes into boreholes were situated in the bedrock below the "Zersatz" zone. Significant flow was found down to depths of more than 50 m. However, in most cases a number of influxes, usually distributed over most of a borehole's vertical extent, contribute to the overall yield of a well. Thus, both the overburden and the unweathered bedrock serve as potential sources of groundwater. Because cumulative well yields are generally low in this area even small amounts of discharge into a well represent important portions of the extracted groundwater. Where present, small granite and aplite dikes in metamorphic lithologies serve as preferred avenues for groundwater flow. This is most likely due to a difference in the competence of the two lithologies and the thin, sheet-like character of the intrusions, which may cause a higher degree of fracturing compared to the slightly more ductile host rocks. Also, the contacts between vein and host rock represent planes of weakness potentially followed by fractures, and thus playing a major role in groundwater transport. In contrast, large massive igneous bodies appear to be more rigid with respect to deformation and thus possess less secondary porosity outside large fault zones, which is suggested by the low yields obtained in this lithology. The findings of the flowmeter measurements are generally supported by the results of the borehole geophysical surveys, which are presented in more detail in section 4.1.1.3.

Only one surface geophysical survey is available for the study area's vicinity in the form of a resistivity tomography in a small NNW-SSE trending valley. This survey identified two NNW-SSE striking zones of low electric conductivity, which were interpreted as faults inclined towards each other and situated at the flanks of that valley. The same direction was found both in the data record of a nearby fracture sampling station and the surrounding topographic lineaments. Thus, a relationship between surface and subsurface structures could be established in this location. However, so far no hydrogeologic data exists for this site. Therefore, the hydraulic properties of the identified structures could not be characterized. One problem in the analysis of geoelectric data is that fractured water-bearing and significantly less transmissive clay-filled zones may produce similar resistivity values. Thus, only the geothermal drilling project envisaged for this site will eventually yield unambiguous information on the hydrogeologic potential of these structures.

In addition to quantitative data a number of qualitative observations were made in various fracture sampling stations either in the form of water visibly emanating from specific

discontinuities or from indirect indicators for the presence of groundwater. Especially in the large granite quarry near the village of Prünst several aspects of flow in igneous rocks could be observed. There, a significant portion of the water discharging from fractures comes from subhorizontal unroofing joints. In these joints flow channeling occurs, which leaves part of a discontinuity dry while only small sections are utilized for flow. This observation has far-reaching implications for drilling projects in that the presence of fracture sets does not yet guarantee highly productive wells. If a borehole intersects an unused part of a large discontinuity the well may stay dry. In addition to unroofing joints flow also occurs through steeply inclined fractures, which are necessary for water to infiltrate into deeper parts of the subsurface. If these fractures are absent the subhorizontal ones may not receive sufficient recharge. In metamorphic domains most outcrops are too small and weathered to observe flow directly. In these cases plants growing out of fractures hint at the presence of groundwater. Plant growth was predominantly observed along gently to moderately inclined fractures parallel to the foliation or at intersections of subvertical and gently inclined discontinuities. Thus, it is assumed that a flow system similar to that in granitic rocks exists in the metamorphic lithologies, in which fractures parallel to the foliation in part take over the function of the unroofing joints and accommodate the bulk of horizontal flow while steeply inclined fissures predominantly serve as avenues for infiltrating water. However, due to the fact that foliation-parallel fractures are inclined to a certain degree they may deflect gradient-parallel flow, which should not occur in entirely horizontal fractures, and thus induce anisotropic conditions.

The discrete fracture modeling corroborates many of the abovementioned findings and assumptions. Stochastic fracture networks consisting of four to five individual fracture sets were generated for four sampling stations in various lithologies as cubic model regions with side lengths of 10 to 20 meters. Bulk secondary porosities range from 0.01 to 1.07 per cent. The flow simulations generally support the observations made in the bedrock outcrops.

In models of highly fractured granites water enters the aquifer over steeply inclined fractures and commences horizontal flow subparallel to the hydraulic gradient as soon as it reaches a large unroofing joint. In this joint groundwater migration occurs preferentially along intersections with steeply inclined fractures, such that initial gradient-parallel flow may be deflected and align with the strikes of the high-angle fractures. However, the general flow direction remains approximately parallel to the hydraulic gradient, although significant local deviations are possible. The directions of these deviations depend on the orientations of the prevalent fracture systems in a given location. As determined by fracture measurements and lineament mapping these prevalent directions are NW-SE, \pm N-S, NE-SW and E(NE)-W(SW),

depending on the location within the study area. If large steeply inclined fractures are encountered the flow path may leave the unroofing joint and follow that fracture for some distance until it again reaches a major subhorizontal discontinuity. Thus, although the hydraulic gradient still has a major influence on flow in these lithologies the steeply inclined fractures produce significant hydraulic anisotropies, especially at the scale of the presented fracture networks models.

In fractured diatexites with no discernable metamorphic foliation and only a small number of unroofing joints vertical flow along steeply inclined fractures predominates. This situation complicates the extraction of groundwater with vertical boreholes, which have lower chances of intersecting steeply inclined water-bearing zones. Also, groundwater is expected to migrate relatively rapidly to greater depths until reduced fracture densities and apertures inhibit further downward flow.

In the model region with a gneissic lithology the metamorphic fabric tends to control the horizontal flow component. Infiltration occurs both over steeply inclined fractures intersecting the fabric and discontinuities parallel to it. Since the foliation is commonly gently to moderately inclined in this area gradient-parallel flow, which is only possible in subhorizontal discontinuities, is inhibited, and anisotropic conditions exist. Due to their relatively high surface roughness fractures parallel to the foliation have a lower tendency to close in response to compression and thus are associated with higher average apertures than fractures intersecting the fabric. Therefore, these discontinuities are preferred avenues for groundwater migration, although the cross cutting fractures are involved to a minor extent as well. As a result, enhanced flow in the \pm NW-SE direction of the regional foliation can be expected in the metamorphic domains of the study area. In locations where the fabric is less well-developed or tightly folded a network of short and discontinuous foliation parallel fractures exists. In this case the cross cutting fractures gain importance and the flow path tends to be rather tortuous and less predictable in that it frequently changes its orientation and preferred directions are less well-pronounced.

In summary, the models predict groundwater flow, which is both influenced by hydraulic gradients and the orientations of bedrock fractures. In granitic lithologies subhorizontal unroofing joints are the main avenues for horizontal flow and sources of discharge into boreholes. Due to their subhorizontality a certain degree of gradient-parallel flow is possible, although influenced by the strikes of steeply inclined fracture sets. The availability of water, however, is controlled by the presence and density of steeply inclined fractures, which provide the unroofing joints with infiltrating water. Due to the decreasing

abundance of unroofing joints with increasing depth flow should be concentrated in steeply inclined fractures at greater distances from the topographic surface and thus become increasingly anisotropic. Since steeply inclined discontinuities are less likely to be intersected by vertical boreholes chances of obtaining significant amounts of groundwater from greater depths are limited. In metamorphic lithologies a well-developed foliation controls horizontal flow and also plays an important role for infiltration. Due to the inclinations of these fractures anisotropic flow conditions should be expected over the entire vertical extent of the bedrock aquifer. In less well-foliated rock units fractures intersecting the fabric gain relative importance and flow paths become rather tortuous and less predictable. The relatively low dip angles of fractures parallel to the foliation increase the probability of being intersected by a vertical borehole. This may be one reason for the comparatively higher productivity of bedrock wells in the metamorphic domains of this region.

5.2 Synopsis, conclusion and outlook

From the data presented and discussed in this study it can be concluded that specific sets of brittle tectonic features with characteristic physical properties exist in the central Bavarian Forest. Large-scale members of these sets can frequently be detected by remote sensing techniques and generally align with neighboring smaller structures. The fracture networks present today are the results of a regional tectonic evolution commencing during the late Variscan orogeny. In the initial creation of the present-day petrofabrics ductile and semi-ductile processes, such as the formation of a metamorphic foliation or the mylonitization along regional shear zones, strongly influenced the orientations of later igneous and hydrothermal intrusions as well as prominent fracture populations. The brittle tectonic history of the study area comprises a number of compressional and extensional phases during which preexisting structures were multiply reactivated. This polyphase reactivation complicates the deciphering of the sequence of tectonic events, which in part had to be incorporated from previous research conducted in neighboring areas by various authors. The final layout of the recent fracture networks is attributed to the Eocene and younger deformations when the latest phases of fracturing reopened discontinuities previously healed by hydrothermal activity. Today's dominant fracture systems include a gently to moderately inclined NW-SE striking set parallel to the metamorphic foliation and steeply inclined to subvertical NW-SE striking fractures in unfoliated lithologies. Additionally, unroofing joints are widespread occurrences in igneous rocks. Steeply inclined to subvertical fractures trending \pm N-S, NE-SW, and E(NE)-W(SW) are ubiquitous features with varying abundances in the entire study area.

Similar orientations were found in the analyses of topographic lineaments obtained from aerial imagery and a digital elevation model. While homogeneous domains with characteristic fracture and lineament orientations could not be determined there is good local agreement between the directions of lineaments and prominent fractures in nearby bedrock exposures. The tectonic interpretation of lineaments mapped on the DEM suggests a NW-SE oriented dextral shear system associated with syn- and antithetic Riedel-type shear faults. Because of Permo-Triassic hydrothermal precipitates reported to be present in these shears this type of deformation was attributed to the final stages of the Variscan orogeny.

Hydrogeologically, the subsurface in the central Bavarian Forest can be regarded as a highly heterogeneous aquifer consisting of sometimes extensive weathered blankets and the underlying fractured bedrock. A sharp boundary between these two units does usually not exist. Instead, the degree of decomposition decreases with increasing depth until the unweathered basement is reached, which is commonly the case after less than ten meters, although in some instances the weathered zone may extend over several tens of meters. In the examined wells the unweathered bedrock was found to produce significant portions of the cumulative yields. The highest yields were reported from strongly folded and migmatitic rocks while igneous lithologies turned out to be the least productive. Especially small igneous veins and dikes in the metamorphic host rock were found to serve as avenues for groundwater flow. However, due to the low number of wells this situation may well change after more drilling projects in the various rock types of the study area have been realized. The weak correlation between the yield of a well and its proximity to lineaments obtained from aerial imagery suggests that local-scale structures identified that way can be utilized to raise the probability of drilling productive water supply wells. However, certain scale-related drawbacks exist for the prediction of well productivity with the help of lineaments. Groundwater flow occurs in relatively narrow discrete zones within the bedrock, which need to be intersected by the borehole. Although higher densities of these zones may be expected along topographic lineaments it is still possible that a borehole, frequently being no larger than 0.3 m in diameter, is drilled in between those zones and thus is not connected to water-bearing structures. Thus, every well is drilled into a locally individual set of subsurface structures whose presence, location, orientation, and physical properties cannot be predicted in detail. Therefore, quantitative statements regarding the productivity of a future well cannot be made. Only the chances of success can be raised by a detailed analysis of the surrounding brittle petrofabrics.

This study was not designed to predict well yields at specific sites but to highlight the factors potentially contributing to well productivity in the central Bavarian Forest. Only a

completed borehole can eventually tell if a drilling site was chosen correctly. However, this study's findings can be applied to yet another aspect, which is the design of groundwater protection zones. According to the results presented here flow anisotropies due to specifically oriented fracture sets do not allow the assumption of radial flow towards a well. Although subhorizontal fractures, such as unroofing joints in igneous lithologies, generally enable gradient-parallel flow the presence of steeply inclined discontinuities impose a certain degree of anisotropy, because groundwater migration was found to preferentially occur along intersections of subhorizontal and steeply inclined fractures in this rock type. In metamorphic rocks flow was discovered to take place predominantly along fractures parallel to the foliation. Thus, if a water supply well in a metamorphic unit needs to be protected from contamination the protection zone most likely has to be extended the furthest in the NW-SE direction. Nonetheless, in all cases the locally dominant fracture systems independent of preexisting ductile fabrics, which frequently can be determined from the analyses of remotely sensed datasets, should also be considered in the design of a protection zone.

In summary, a number of reasons why the fractured basement should be given more attention in groundwater prospecting projects shall be mentioned. First, bulk transmissivity values of the "Zersatz" zone and the unweathered fractured bedrock were found to be relatively similar by various workers. On a local scale the transmissivities are highly variable in both media. The analyses of flowmeter measurements showed that the majority of primary zones of discharge into wells are situated below the "Zersatz". Thus, there should be no reason to prefer the overburden except for financial aspects resulting from higher drilling costs for deeper wells. However, the fractured bedrock has a number of advantages over the "Zersatz". Due to the general absence of weathering products at greater depths discontinuities are less likely to be filled with clayey material, which can strongly inhibit flow. Also, less suspension load potentially congesting well screens can be expected from water extracted from bedrock fractures. Water having infiltrated into deeper levels of the aquifer is commonly associated with longer residence times in the subsurface, which allow a more intense removal of anthropogenic contaminants by chemical reactions between groundwater and host rock. Deep-seated reservoirs are also less subject to variations in recharge from precipitation, so dry periods, which are expected to occur more often in the future of this region as a result of global warming, have less effects on the productivities of deeper wells. Nonetheless, the overburden's importance for groundwater storage should not be underestimated. Especially in sandy/ silty grus layers a significant effective porosity may hold larger quantities of groundwater. This water may serve to recharge the underlying fracture networks, through which higher flow velocities transport the water more effectively to a bedrock well than through the grusy matrix, as proposed by various authors (cf. section 1.3).

Finally it shall be mentioned that future work dealing with various aspects of hard rock hydrogeology needs to be carried out in this region in order to obtain a better idea of the fractured bedrock as an aquifer. The different, frequently contradictory, results of research performed in other regions of Germany and the World highlight the limited transferability of findings of regional studies and show the necessity of examining every area of interest individually. The various approaches to deciphering regional hard rock hydrogeology may be applicable in many different geological settings, their outcome, however, is likely to be highly variable. Especially more data from newly constructed water supply wells will show which locations are the most promising with respect to high yields. Unfortunately, the need to be cost-effective leads many communal administrations to save funds on the prospecting and the documentation of their drilling efforts. As a result, little knowledge beyond the production rates of new wells is becoming available, although detailed surveys of boreholes with geophysical methods and televiwers would greatly enhance our understanding of the characteristics of water-bearing zones in the subsurface. Nonetheless, future drilling projects, geophysical surveys, and tectonic studies will continue to yield new and valuable information adding to a more and more comprehensive understanding of the bedrock hydrogeology in the central Bavarian Forest.

6 References

- Ahnert, F., 1999, Einführung in die Geomorphologie: Stuttgart, Ulmer, 440 p.
- Alsleben, S., 2001, Point & Polyline Tools for ArcView 3.x, v. 1.1
- Altamura, R.J., 2003, Tectonics of the Lantern Hill Fault Zone, Southeastern Connecticut: Evidence for the Embryonic Opening of the Atlantic Ocean., in LeTourneau, P. M., Paul E. Olson, ed., The Great Rift Valleys of Pangea in Eastern North America. Volume 1. Tectonics, Structure, and Volcanism., Volume 1: New York, Columbia University Press.
- Altermann, M., and Rabitzsch, K., 1977, Zur Gliederung und Dokumentation der wichtigsten Lockersedimente der Mittelgebirge: Zeitschrift für angewandte Geologie, v. 23, p. 130-139.
- Anbazhagan, S., Aschenbrenner, F., and Knoblich, K., 2001, Comparison of aquifer parameters with lineaments derived from remotely sensed data in Kinzig basin, Germany, in Seiler, K. P., and Wohnlich, S., eds., New approaches characterizing groundwater flow, Volume 2: Lisse, A.A. Balkema Publishers, p. 883-886.
- Anderson, E.M., 1942, The Dynamics of Faulting and Dyke Formation with Applications to Britain: Edinburgh, Oliver and Boyd, 191 p.
- Annau, R., Bender, S., and Wohnlich, S., 1998, Hard rock hydrogeology of the Bohemian Massif. 3rd international workshop. Windischeschenbach, Germany, October 1998: Munich, Ludwig-Maximilians-Universität München, 184 p.
- Bader, K., 1996, Analyse des geologischen Untergrundes mit Hilfe der Geophysik, Erläuterungen zur Geologischen Karte 1:500.000: München, Bayerisches Geologisches Landesamt, p. 280-287.
- Bader, K., and Weinelt, W., 1975, Geologisch-geophysikalische Untersuchungen für die geplante Trinkwassertalsperre Frauenau (Bayerischer Wald): Geologica Bavarica, v. 74, p. 179-192.
- Banks, D., Rohr-Torp, E., and Skarphagen, H., 1994, Groundwater resources in hard rock: experiences from the Hvaler Study, Northeastern Norway, Applied Hydrogeology, Volume 2: Hannover, Germany, Verlag Heinz Heise, p. 33-42.
- Banks, D., Solbjorg, M.L., and Rohr-Torp, E., 1992, Permeability of fracture zones in Precambrian granite.: Quarterly Journal of Engineering Geology, v. 25, p. 377-388.
- Barton, C.A., Zoback, M.D., and Moos, D., 1995, Fluid flow along potentially active faults in crystalline rock.: Geology, v. 23, p. 683-686.

- Barton, C.C., Larsen, E., Page, W.R., and Howard, T.M., 1993, Characterizing fractured rock for fluid-flow, geochemical, and paleostress modeling: Methods and preliminary results from Yucca Mountain, Nevada: Denver, Colorado, United States Geological Survey.
- Barton, N., and Choubey, V., 1977, The shear strength of rock joints in theory and practice: *Rock Mechanics*, v. 10, p. 1-54.
- Bauberger, W., 1969, Geologischer Strukturplan der Oberpfalz: *Geologica Bavarica*, v. 60, p. 45-51.
- Bäumle, R., Hötzl, H., Thüringer, C., and Witthüser, K., 1998, Rock test site for investigations of flow and transport processes in porous fractured media, in Annau, R., Bender, S., and Wohnlich, S., eds., *Hard Rock Hydrogeology of the Bohemian Massif. 3rd International Workshop, Volume 8: Münchner Geologische Hefte, Reihe B: Windischeschenbach, Germany*, p. 111-116.
- Bayerisches Amt für Wasserwirtschaft (ed.), 1998, *Wasserwirtschaftlicher Rahmenplan Naab-Regen*, v. München, 240 p.
- Behr, H.J., Engel, W., and Franke, W., 1980, Guide to excursion, Münchberger Gneismasse und Bayerischer Wald, April 12-15, 1980: Gottingen, Federal Republic of Germany, Geol.-Palaeontol. Inst. Mus., 100 p.
- Bender, S., 2001, Mixing processes of groundwater in the transitional zone of granites and moldanubian gneisses, in Seiler, K. P., and Wohnlich, S., eds., *New approaches characterizing groundwater flow, Volume 2: Lisse, A.A. Balkema Publishers*, p. 903-906.
- Bergerat, F., 1981-1982, Le couloir rhodanien au Paléogène: analyse de la fracturation et interprétation cinématique régionale: *Rev. Géol. dyn. et Géogr. phys.*, v. 23, p. 329-343.
- Bergerat, F., and Geysant, J., 1982, Tectonique cassante et champ de contraintes tertiaire en avant des Alpes orientales: le Jura souabe: *Geologische Rundschau*, v. 71, p. 537-548.
- , 1983, Fracturation tertiaire et evolution des contraintes en Baviere orientale; le Jura franconien et la foret bavaroise (R. F. A.): *Geologische Rundschau*, v. 72, p. 935-953.
- Black, J.H., 1994, Hydrogeology of fractured rocks - a question of uncertainty about geometry: *Applied Hydrogeology*, v. 3, p. 56-70.
- Blum, P., Mackay, R., Riley, M.S., and Knight, J.L., 2007, Hydraulische Modellierung und die Ermittlung des repräsentativen Elementarvolumens (REV) im Kluffgestein: *Grundwasser*, v. 12, p. 48-65.
- Boadu, F.K., 1997, Relating the Hydraulic Properties of a Fractured Rock Mass to Seismic Attributes: Theory and Numerical Experiments.: *Int. J. Rock Mech. Min. Sci.*, v. 34, p. 885-895.

- Bonnet, E., Bour, O., Odling, N.E., Davy, P., Main, I., Cowie, P., and Berkowitz, B., 2001, Scaling of fracture systems in geological media: *Reviews of Geophysics*, v. 39, p. 347-383.
- Bram, K., and Hirschmann, G., 1992, KTB-Report 92-3. Ergebnisse geowissenschaftlicher Umfelduntersuchungen: Hannover, Projektleitung Kontinentales Tiefbohrprogramm der Bundesrepublik Deutschland im Niedersächsischen Landesamt für Bodenforschung, p. 261.
- Breuer, B., 1998, Hydrogeological situation in the weathered zone near the continental deep drilling project (KTB), Upper Palatinate, Germany, in Annau, R., Bender, S., and Wohnlich, S., eds., *Hard Rock Hydrogeology in the Bohemian Massif, Volume 8: Münchner Geologische Hefte, Reihe B*: München, Ludwig-Maximilians-Universität München, p. 19-24.
- Bronstert, A., and Plate, E., 1996, Ein physikalisch begründetes hydrologisches Modell für Hänge und kleine Einzugsgebiete: *Wasserwirtschaft*, v. 86, p. 318-323.
- Bültemann, H.-W., and Hofmann, R., 1986, Die Mineralisation des Bayerischen Pfahls: *Geologisches Jahrbuch, Reihe D*, v. 83, p. 47.
- Cacas, M.C., Ledoux, E., de Marsily, G., Tillie, B., Barbreau, A., Durand, E., Feuga, B., and Peaudecerf, P., 1990, Modeling fracture flow with a stochastic discrete fracture network: Calibration and validation. 1. The flow model: *Water Resources Research*, v. 26, p. 479-489.
- Cetin, B., 1986, Petrographische und gefügekundliche Untersuchungen an duktilen Bewegungszonen des Bayerischen Waldes [PhD thesis]: München, Universität München.
- Cheema, T.J., and Islam, M.R., 1994, Experimental Determination of Hydraulic Anisotropy in Fractured Formations: *Bulletin of the Association of Engineering Geologists*, v. 31, p. 329-341.
- Compton, R.R., 1985, *Geology in the field*: New York, John Wiley & Sons, Inc., 398 p.
- Coyle, D.A., and Wagner, G.A., 1995, Spaltspuren - ein Beitrag zur postvarizischen Tektonik und Abtragung des KTB-Umfelds: *Geowissenschaften*, v. 13, p. 142-146.
- Cushman, R.V., Allen, W.B., and H.L. Pree, J., 1953, Geologic factors affecting the yield of rock wells in southern New England.: *Journal of the New England Water Works Association*, v. 67, p. 77-95.
- Daniel, C.C., 1989, Statistical analysis relating well yield to construction practices and siting of wells in the Piedmont and Blue Ridge provinces of North Carolina., U.S. Geological Survey Water-Supply Paper 2341, U.S. Geological Survey.
- Degnan, J.R., and Clark, S.F., 2002, Fracture-correlated lineaments at Great Bay, Southeastern New Hampshire: *Pembroke, New Hampshire*, U.S. Geological Survey, p. 14.

- Denzel, S., Behnert, T., Ertel, T., Dinkel, R., and Trost, U., 1995, Handbuch Altlasten und Grundwasserschadensfälle. Methodensammlung: Karlsruhe, Landesanstalt für Umweltschutz Baden-Württemberg, 176 p.
- Dershowitz, W., 2002, FracWorks XP Discrete Feature Simulator. User Documentation Beta Version 0.21: Seattle, Washington, Golder Associates Inc., 81 p.
- Dershowitz, W., and Einstein, H.H., 1988, Characterizing rock joint geometry with joint system models: *Rock Mechanics and Rock Engineering*, v. 21, p. 21-51.
- Dershowitz, W., Foxford, T., Sudicky, E., Shuttle, D.A., Eiben, T., and Ahlstrom, E., 2002, PAWorks. Pathway Analysis for Discrete Fracture Networks with LTG Solute Transport. User Documentation. Version 1.64.: Seattle, Washington, Golder Associates, Inc.
- Dershowitz, W., Lee, G., Geier, J., Hitchcock, S., LaPointe, P., and Cladouhos, T., 1999, FracWorks/95 Discrete Feature Simulator. User Documentation. Version 1.3.: Seattle, Washington, Golder Associates, Inc.
- Dershowitz, W., and Miller, I., 1995, Dual porosity fracture flow and transport: *Geophysical Research Letters*, v. 22, p. 1441-1444.
- Desiré-Marchand, J., and Klein, C., 1987, Fichtelgebirge, Böhmerwald, Bayerischer Wald; Contribution a l'étude du problème des Piedmonttreppen, in Bremer, H., and Godard, A., eds., *Geomorphology of European massifs*, Volume 65: *Zeitschrift für Geomorphologie*. Supplementband: Berlin-Stuttgart, Gebrüder Borntraeger, p. 101-138.
- Dobner, A., 1983, Hydrogeologische Verhältnisse, in Ott, W.-D., ed., *Erläuterungen zur Geologischen Karte von Bayern 1:25.000*, Blatt Nr. 6943 Viechtach: München, Bayerisches Geologisches Landesamt, p. 50-55.
- Dorsch, K., Bender, S., and Wohnlich, S., 1998, The Influence of Granitic Intrusions on the Hydrochemistry in Gneiss Areas, in Annau, R., Bender, S. & Wohnlich, S., ed., *Hard Rock Hydrogeology of the Bohemian Massif*, Volume B-8: *Münchner Geologische Hefte*, Reihe B: Munich, Institut für Allgemeine und Angewandte Geologie, Ludwig-Maximilians Universität, München, p. 134-148.
- Drew, L.J., Karlinger, M.R., Armstrong, T.R., and Moore, R.B., 1999, Relations between Igneous and Metamorphic Rock Fracture Patterns and Groundwater Yield from Variography of Water-Well-Yields - Pinardville Quadrangle, New Hampshire.: *Natural Resources Research*, v. 8, p. 137-152.
- Duyster, J., Kontny, A., de Wall, H., and Zulauf, G., 1995, Postvariszische Krustenstapelung am Westrand der Böhmisches Masse: *Geowissenschaften*, v. 13, p. 135-141.
- Einsiedl, F., Maloszewski, P., and Wohnlich, S., 2001, Tracer test in a fractured zone of NAGRA rock laboratory using a new fluorescent dye (PTA), in Seiler, K. P., and Wohnlich, S., eds., *New approaches characterizing groundwater flow*, Volume 1: Lisse, A.A. Balkema Publishers, p. 935-937.
- Eisbacher, G.H., 1991, *Einführung in die Tektonik*: Stuttgart, Enke, 310 p.

- Emery, J.M., and Cook, G.W., 1984, A determination of the nature of recharge to a bedrock fracture system, Eastern Regional Ground Water Conference: Newton, Mass., (USA), The Association, p. 62-77.
- Emmermann, R., and Giese, P., 1989, KTB-Report 89-3. Beiträge zum 2. KTB-Kolloquium, Volume 89-3: Hannover, Projektleitung Kontinentales Tiefbohrprogramm der Bundesrepublik Deutschland im Niedersächsischen Landesamt für Bodenforschung, p. 477.
- ESRI, 2002, ArcGis Spatial Analyst, v. 8.3: Redlands, Ca. (USA)
- Ferrill, D.A., Winterle, J., Wittmeyer, G., Sims, D., Colton, S., and Armstrong., A., 1999, Stressed Rock Strains Groundwater at Yucca Mountain, Nevada.: GSA Today, v. 9, p. 1-8.
- Fischer, G., 1936, Das Dach des Moldanubikums in Schlesien, dem Bayrischen Wald und Mähren: Jahrbuch der Preussischen Geologischen Landesanstalt, v. 56, p. 733-741.
- , 1938, Geologischer Bau und Bodenschätze des Bayerischen Waldes: Jahrbuch der Preussischen Geologischen Landesanstalt, v. 58, p. 855-857.
- , 1959, Der Bau des Vorderen Bayerischen Waldes: Jahresberichte und Mitteilungen des Oberrheinischen Geologischen Vereines, v. 41, p. 1-21.
- , 1965, Über das Moldanubikum in Bayern: Zvástní Otisk Vestníku Ústředního Ústavu Geologického Rocnik, v. 40, p. 221-232.
- , 1967a, Kristallin des Bayerischen Waldes und der Oberpfalz: Fortschritte der Mineralogie, v. 45, p. 8-11.
- , 1967b, Über das Moldanubikum der bayerischen Oberpfalz und des Bayerischen Waldes, Zur Mineralogie und Geologie der Oberpfalz., Volume 16: Der Aufschluss, Sonderheft: Heidelberg, Federal Republic of Germany, Vereinigung der Freunde der Mineralogie und Geologie, p. 27-111.
- Fischer, G., and Troll, G., 1973, Bauplan und Gefügeentwicklung metamorpher und magmatischer Gesteine des Bayerischen Waldes, Petrographische Arbeiten über das Grundgebirge des Bayerischen Waldes., Volume 68: Geologica Bavarica: Munich, Federal Republic of Germany, Bayerisches Geologisches Landesamt, p. 7-44.
- Flurl, M., 1792, Beschreibung der Gebirge von Baiern und der oberen Pfalz: München, 642 p.
- Frank, H., 1996, Geologie Bayerns - ein Überblick, Erläuterungen zur Geologischen Karte von Bayern 1:500.000: München, Bayerisches Geologisches Landesamt, p. 1-15.
- Franke, O.L., Reilly, T.E., Pollock, D.W., and LaBaugh, J.W., 1998, Estimating Areas Contributing Recharge to Wells. Lessons from Previous Studies: Denver, Colorado, U.S. Geological Survey.
- Freeze, A.R., and Cherry, J.A., 1979, Groundwater: Englewood Cliffs, N.J., Prentice-Hall.

- Freudenberger, W., 1996, Tektonik, Deckgebirge nördlich der Donau, in Freudenberger, W., and Schwerd, K., eds., Erläuterungen zur Geologischen Karte von Bayern 1:500.000: München, Bayerisches Geologisches Landesamt, p. 259-265.
- Freudenberger, W., and Schwerd, K., 1996, Erläuterungen zur Geologischen Karte von Bayern 1:500 000: München, Bayerisches Geologisches Landesamt, 329 p.
- Gebauer, D., 1977, Die Entwicklungsgeschichte des Moldanubikums aufgrund radiometrischer Altersbestimmungen, in Bauberger, W., ed., Geologische Karte von Bayern 1:25 000, Erläuterungen zum Blatt Nr. 7046 Spiegelau und zum Blatt Nr. 7047 Finsterau etc: München, Bayerisches Geologisches Landesamt, p. 12-18.
- Geldon, A.L., 2004, Hydraulic tests of Miocene volcanic rocks at Yucca Mountain and Pahute Mesa and Implications for groundwater flow in the Southwest Nevada Volcanic Field, Nevada and California: Boulder, CO, USA, The Geological Society of America, 93 p.
- Gelhar, L., 1993, Stochastic Subsurface Hydrology.: Englewood Cliffs, N.J., Prentice-Hall.
- Geologisches Landesamt Bayern, 1996, Geologische Karte von Bayern 1:500000: München, Bayerisches Geologisches Landesamt.
- Glass, R.J., Nicholl, M.J., and Tidwell, V.C., 1995, Challenging models for flow in unsaturated, fractured rock through exploration of small scale processes.: Geophysical Research Letters, v. 22, p. 1457-1460.
- Gold, D.P., and Parizek, R., 1999, Fracture Trace and Lineament Analysis: Application to Ground Water Resources Characterization and Protection: Westerville, Ohio, National Ground Water Association.
- Gromes, N., 1980, Geologische und mikrothermometrische Untersuchungen zur Mineralisation des Bayerischen Pfahls [Diplom thesis]: Göttingen, University of Göttingen.
- Guimerà, J., Vives, L., and Carrera, J., 1995, A discussion of scale effects on hydraulic conductivity at a granitic site (El Berrocal, Spain): Geophysical Research Letters, v. 22, p. 1449-1452.
- Gümbel, C.W., 1868, Geognostische Beschreibung des Ostbayerischen Grenzgebirges oder des Bayerischen und Oberpfälzer Waldgebirges: Gotha, Justus Perthes, 968 p.
- Gupta, R.P., 2003, Remote Sensing Geology: Berlin, Springer-Verlag, 655 p.
- Gustafson, G., and Krásný, J., 1994, Crystalline rock aquifers: their occurrence, use and importance: Applied Hydrogeology, v. 2/94, p. 64-75.
- Hähne, R., and Franke, V., 1983, Bestimmung anisotroper Gebirgsdurchlässigkeiten in situ im grundwasserfreien Festgestein: Z. angew. Geol., v. 29, p. 219-226.

- Hansen, B.P., Stone, J.R., and John, W.L.J., 1999, Characteristics of Fractures in Crystalline Bedrock Determined by Surface and Borehole Geophysical Surveys, Eastern Surplus Superfund Site, Meddybemps, Maine: Northborough, Massachusetts, U.S. Geological Survey.
- Havlík, M., and Krasny, J., 1998, Transmissivity distribution in southern part of the Bohemian Massif: Regional trends and local anomalies, in Annau, R., Bender, S., and Wohnlich, S., eds., *Hard Rock Hydrogeology of the Bohemian Massif*. 3rd International Workshop, Volume 8: Münchner Geologische Hefte, Reihe B: Windischeschenbach, Germany, p. 11-18.
- Himmelsbach, T., 1993, Untersuchungen zum Wasser- und Stofftransportverhalten von Störungszonen im Grundgebirge (Albtalgranit, Südschwarzwald): Karlsruhe, 14+238 p.
- , 1999, Dipoltests zur Untersuchung des Stofftransportes in Kluffgrundwasserleitern: Steir. Beitr. z. Hydrogeologie, v. 42, p. 131-150.
- Himmelsbach, T., Hötzl, H., and Malozewski, P., 1994, Forced gradient tracer tests in a highly permeable fault zone: Applied Hydrogeology, p. 40-47.
- Hofmann, R., 1962, Die Tektonik des Bayerischen Pfahls: Geologische Rundschau, v. 52, p. 332-346.
- Hölting, B., 1996, Hydrogeologie: Stuttgart, Enke, 441 p.
- Hölting, B., and Coldewey, W.G., 2005, Hydrogeologie. Einführung in die Allgemeine und Angewandte Hydrogeologie: München, Spektrum Akademischer Verlag, 326 p.
- Horn, P., Köhler, H., and Müller-Sohnius, D., 1986, Rb-Sr-Isotopen-Geochemie hydrothermaler Quarze des Bayerischen Pfahls und eines Fluß-Schwespat-Ganges von Nabburg-Wölsendorf: Chemical Geology, v. 58, p. 254-272.
- Ingebritsen, S.E., and Sanford, W.E., 1998, Groundwater in Geologic Processes.: Cambridge, Cambridge University Press, 341 p.
- Jensen, J.R., 2000, Remote sensing of the environment: an earth resource perspective: Upper Saddle River, NJ, Prentice-Hall, Inc., 544 p.
- Jerz, H., 1995, Bayern, in Benda, L., ed., *Das Quartär Deutschlands*: Berlin-Stuttgart, Borntraeger, p. 296-326.
- , 1996, Gesteinsfolge des Quartärs, Erläuterungen zur Geologischen Karte von Bayern 1:500.000: München, Bayerisches Geologisches Landesamt, p. 236-251.
- Kadlubowska, J.Z., and Michler, G., 1989, Paläoökologische Untersuchungen an Sedimentkernen aus dem Rachelsee: Berichte der ANL, v. 13, p. 239-260.
- Karrenberg, H., 1981, Hydrogeologie der nichtverkarstungsfähigen Festgesteine: Wien, Springer Verlag, 385 p.

- Keller, A.A., Roberts, P.V., and Kitanidis, P., K., 1995, Prediction of single phase transport parameters in a variable aperture fracture: *Geophysical Research Letters*, v. 22, p. 1425-1428.
- Kemmis, T., and Kelleher, D., 2002, Improving hydrogeologic analysis of fractured bedrock systems: Sheboygan, Wisconsin (USA), Midwest GeoSciences Group.
- Kim, G.-B., ESRI ArcScript Database, 2004, Lineament Analysis Tool: Redlands, CA (USA)
- Kolditz, O., 1997, *Strömung, Stoff- und Wärmetransport im Kluffgestein*: Berlin-Stuttgart, Borntraeger, 663 p.
- Kossmat, F., 1927, Gliederung des varistischen Gebirgsbaues: *Abh. Sächs. Geol. L.-Anst.*, v. 1, 39 p.
- Krásný, J., 1999, Hard-rock hydrogeology in the Czech Republic: *Hydrogéologie*, v. 2, p. 25-38.
- , 2002, Quantitative hardrock hydrogeology in a regional scale: *Bulletin of the Geological Survey of Norway*, v. 439, p. 7-14.
- Kriegl, C., Vasváry, V., and Goldbrunner, J., 2001, Deep drilling Längenfeld Thermal 2 - first hydrogeological results from a deviated well in metamorphic rocks of the Austroalpine Ötztal-Stubai crystalline complex, Tyrol, in Seiler, K. P., and Wohnlich, S., eds., *New approaches characterizing groundwater flow, Volume 2*: Lisse, A.A. Balkema, p. 995-999.
- Kubiniok, J., 1988, *Kristallinvergrusung an Beispielen aus Südostaustralien und Deutschen Mittelgebirgen*: Köln, 178 p.
- Lachassagne, P., Golaz, C., Thiery, D., Ahmed, C., Maréchal, J., Touchard, F., and Wyns, R., 2001, A methodology for the mathematical modelling of hard-rock aquifers at catchment scale, based on the geological structure and the hydrogeological functioning of the aquifer, in Seiler, K. P., and Wohnlich, S., eds., *New approaches characterizing groundwater flow, Volume 1*: Lisse, A.A. Balkema Publishers, p. 367-370.
- LeGrand, H.E., 1954, *Geology and groundwater in the Statesville area, North Carolina*: North Carolina Department of Conservation and Development Bulletin, v. 66, p. 68.
- Leven, C., McDermott, C.I., Teutsch, G., and Sauter, M., 2001, New methods for the investigation of fractured porous media, in Seiler, K. P., and Wohnlich, S., eds., *New approaches characterizing groundwater flow, Volume 2*: Lisse, A.A. Balkema Publishers, p. 1007-1011.
- List, F.K., and Ott, W.-D., 1982, *Geologische Karte von Bayern 1:25 000. Erläuterungen zum Blatt Nr. 7043 Ruhmannsfelden*: München, Bayerisches Geologisches Landesamt, 55 p.

- Loew, S., 2001, Natural groundwater pathways and models for regional groundwater flow in crystalline rocks, in Seiler, K. P., and Wohnlich, S., eds., *New approaches characterizing groundwater flow*, Volume 2: Lisse, A.A. Balkema Publishers, p. 1013-1318.
- Louis, H., 1984, Zur Reliefentwicklung der Oberpfalz, in Louis, H., ed., *Zur Reliefentwicklung der Oberpfalz*: Berlin-Stuttgart, Borntraeger, p. 1-66.
- Lowrie, W., 1997, *Fundamentals of Geophysics*: Cambridge (UK), Cambridge University Press, 354 p.
- Mabee, S.B., 1999, Factors influencing Well Productivity in Glaciated Metamorphic Rocks.: *Ground Water*, v. 37, p. 88-97.
- Mabee, S.B., Curry, P.J., and Hardcastle, K.C., 2002, Correlation of lineaments to ground water inflows in a bedrock tunnel: *Ground Water*, v. 40, p. 37-43.
- Mabee, S.B., and Hardcastle, K.C., 1997, Analyzing Outcrop-Scale Fracture Features to Supplement Investigations of Bedrock Aquifers: *Hydrogeology Journal*, v. 5, p. 21-36.
- Mabee, S.B., Hardcastle, K.C., and Wise, D.U., 1994, A Method of Collecting and Analyzing Lineaments for Regional-Scale Fractured-Bedrock Aquifer Studies: *Ground Water*, v. 32, p. 884-894.
- MacQueen, J.B., 1967, Some Methods for Classification and Analysis of Multivariate Observations, 5th Berkeley Symposium on Mathematical Statistics and Probability, Volume 1: Berkeley, University of California Press, p. 281-297.
- Madel, J., Propach, G., Reich, H., Brunnacker, K., Vidal, H., Ziehr, H., and Teuscher, E.O., 1968, Erläuterungen zur Geologischen Karte von Bayern 1:25.000, Blatt Nr. 6945 Zwiesel: München, Bayerisches Geologisches Landesamt, 88 p.
- Marshak, S., and Mitra, G., 1988, *Basic Methods of Structural Geology*: Englewood Cliffs, N.J., Prentice-Hall Inc., 446 p.
- Masakova, I., and Kobr, M., 1998, Fracture aquifer well-log analysis for hard rock evaluation, in Annau, R., Bender, S., and Wohnlich, S., eds., *Hard Rock Hydrogeology of the Bohemian Massif*. 3rd International Workshop: Münchner Geologische Hefte, Reihe B: Windischeschenbach, Germany, p. 157-164.
- Masch, L., and Cetin, B., 1991, Deformationsmechanismen in ausgewählten Hochtemperatur-Mylonitzonen im Moldanubikum des Bayerischen Waldes: *Geologica Bavarica*, v. 96, p. 7-27.
- Mauldon, M., Dunne, W.M., and Rohrbaugh, M.B., Jr., 2001, Circular scanlines and circular windows: new tools for characterizing the geometry of fracture traces: *Journal of Structural Geology*, v. 23, p. 247-258.
- Melvin, R.L., Stone, J.R., Craft, P.A., Lane, J.W.J., and Davies, B.S.r., 1995, *Geohydrology of the Durham Center Area, Durham Connecticut*: Hartford, CT, U.S. Geological Survey.

- Mira, F., and Chambel, A., 2001, Productivity of hard rock aquifers in Alentejo region, South Portugal, in Seiler, K. P., and Wohnlich, S., eds., *New approaches characterizing flow*, Volume 2: Lisse, A.A. Balkema, p. 1035-1039.
- Neuendorf, K.K.E., Mehl, J.P., Jr., and Jackson, J.A., 2005, *Glossary of Geology*: Alexandria, Va., USA, American Geological Institute, 779 p.
- Nieto-Samaniego, A.F., Alaniz-Alvarez, S.A., Tolson, G., Oleschko, K., Korvin, G., Xu, S.S., and Pérez-Venzor, J.A., 2005, Spatial distribution, scaling and self-similar behavior of fracture arrays in the Los Planes Fault, Baja California Sur, Mexico: *Pure and Applied Geophysics*, v. 162, p. 805-826.
- Olsson, O., Black, J.H., Gale, J.E., and Holmes, D.C., 1988, *Site Characterization and Validation*: Stockholm, Sweden, Swedish Geological Company.
- Ott, W.-D., 1983, *Geologische Karte von Bayern 1: 25 000. Erläuterungen zum Blatt Nr. 6943 Viechtach*: München, Bayerisches Geologisches Landesamt, 71 p.
- Papadopoulos, I.S., 1967, Nonsteady flow to a well in an infinite anisotropic aquifer., *Hydrology of fractured rocks.*, Volume 1: Dubrovnic, Yugoslavia, Int. Ass. Sci. Hydrol., p. 21-31.
- Parney, R., and Smith, L., 1995, Fluid Velocity and path length in fractured media.: *Geophysical Research Letters*, v. 22, p. 1437-1440.
- Peterek, A., 2001, Zur geomorphologischen und morphotektonischen Entwicklung des Fichtelgebirges und seines unmittelbaren Raumes: *Geol. Bl. NO-Bayern*, v. 51, p. 37-106.
- Peterek, A., Schröder, B., and Nollau, G., 1996, Neogene Tektonik und Reliefentwicklung des nördlichen KTB-Umfeldes (Fichtelgebirge und Steinwald): *Geologica Bavarica*, v. 101, p. 7-25.
- Peterhoff, F., 1986, *Morphologische Untersuchungen zur Talgeschichte des mittleren Regens [PhD thesis]*: Regensburg, Universität Regensburg.
- Pfaffl, F., 1968, Über Andalusit von der Blötz im Bayerischen Wald: *Der Aufschluß, Sonderheft*, v. 19, p. 237-239.
- , 1969, Allanit (Orthit) von Tittling (Bayerischer Wald): *Der Aufschluß, Sonderheft*, v. 20, p. 26-28.
- , 1971, Schriftgranit aus dem Bayerischen Wald: *Der Aufschluß, Sonderheft*, v. 22, p. 83-84.
- , 1972a, Die Rauchquarze von Saldenburg im Bayerischen Wald: *Der Aufschluß, Sonderheft*, v. 23, p. 386-388.
- , 1972b, Kluftminerale aus Bischofsmais im Bayerischen Wald: *Der Aufschluß, Sonderheft*, v. 23, p. 338-339.

-
- , 1972c, Verbreitung und Mineralführung der Pegmatite bei Bodenmais: Geologische Blätter für Nordost-Bayern und Angrenzende Gebiete, v. 22, p. 43-55.
 - , 1973a, Die Pegmatit- und Kontaktlagerstaette Stanzen bei Eck im Bayerischen Wald: Der Aufschluss, Sonderheft, v. 24, p. 236-240.
 - , 1973b, Faserkiesel aus dem Bayerischen Wald (Beitrag zur Morphologie des ostbayerischen Moldanubikums): Geologische Blaetter fuer Nordost-Bayern und Angrenzende Gebiete, v. 23, p. 123-128.
 - , 1973c, Neuer Meta-Autunit-Fund vom Huehnerkobel: Der Aufschluss, Sonderheft, v. 24, p. 372.
 - , 1979a, Die Mineralien des Hühnerkobel-Pegmatits bei Zwiesel (Bayerischer Wald): Der Aufschluss, v. 30, p. 93-99.
 - , 1979b, Kluftmineralien aus dem Bayerischen Wald: Lapis (Muenchen), v. 4, p. 28-29.
 - , 1980, Erstmaller Fund von "Wüfelquarzen" im Kristallin des Bayerischen Waldes: Geologische Blätter für Nordost-Bayern und Angrenzende Gebiete, v. 30, p. 43-47.
 - , 1981a, Die Mineralien des Bayerischen Waldes: Grafenau, Morsak, 100 p.
 - , 1981b, Pseudokubische Quarzkristalle ("Wüfelquarze") aus dem Kristallin des Bayerischen Waldes, in Anonymous, ed., Referate der Vorträge auf der 59. Jahrestagung der Deutschen Mineralogischen Gesellschaft und der Tagung der Österreichischen Mineralogischen Gesellschaft, Volume 59; 1: Fortschritte der Mineralogie, Beiheft: Stuttgart, E. Schweizerbart'sche Verlagsbuchhandlung, p. 154.
 - , 1985a, Beryllvorkommen im Bayerischen Wald: Der Bayerische Wald, v. 8, p. 115-117.
 - , 1985b, Vivianit vom Silberberg bei Bodenmais (Bayerischer Wald): Der Bayerische Wald, v. 10, p. 182-183.
 - , 1985c, Zur Geologie der Lößvorkommen im Bayerischen Wald; Teil 1: Der Bayerische Wald, v. 8, p. 120-130.
 - , 1985d, Zur Geologie der Lößvorkommen im Bayerischen Wald; Teil 2: Der Bayerische Wald, v. 9, p. 134-155.
 - , 1986, Glazialmorphologische Untersuchungen an den Lachen im Arbergebiet, Bayerischer Wald: Geologische Blaetter fuer Nordost-Bayern und Angrenzende Gebiete, v. 36, p. 269-278.
 - , 1988a, Die Mineralien der Kalksilikatfelse und Pegmatite von Lichtenthal bei Zwiesel/ Bayerischer Wald: Geologische Blaetter fuer Nordost-Bayern und Angrenzende Gebiete, v. 38, p. 93-96.
 - , 1988b, Die Titanmineralparagenese von Steinerleinbach bei Waldkirchen (Bayerischer Wald): Geologische Blaetter fuer Nordost-Bayern und Angrenzende Gebiete, v. 38, p. 97-106.

-
- , 1988c, Glazialmorphologische Untersuchungen am Bachel-Nordkar und am Großen Arbersee im Bayerischen Wald: Geologische Blätter für Nordost-Bayern und Angrenzende Gebiete, v. 38, p. 7-26.
- , 1989, Der Bayerische Wald im Tertiär und Quartär: Geologische Blätter für Nordost-Bayern und Angrenzende Gebiete, v. 39, p. 1-38.
- , 1990a, Der Mineralien der Sulfiderz-Lagerstätte Silberberg bei Bodenmais, Bayerischer Wald: Mineralien-Welt, v. 1, p. 49-55.
- , 1990b, Zur Geologie und Mineralogie des Blattes Bodenmais 1:25000 (Nr. 6944) im Bayerischen Wald: Geologische Blätter für Nordost-Bayern und Angrenzende Gebiete, v. 40, p. 123-172.
- , 1991, Die Kluftmineralien vom Granitsteinbruch am Teufelstisch, Bischofsmais (Bayrischer Wald): Mineralien-Welt, v. 2, p. 42-44.
- , 1992, Zur Geologie und Mineralogie des Blattes Kötzing 1:25000 (Nr. 6843) im Bayerischen Wald: Geologische Blätter für Nordost-Bayern und Angrenzende Gebiete, v. 42, p. 167-204.
- , 1993, Kritische Anmerkungen zum Toteishügel-Problem im Bayerischen Wald: Geologische Blätter für Nordost-Bayern und Angrenzende Gebiete, v. 43, p. 341-348.
- , 1994, Idiomorphe Quarzkristalle in Porphyren des Hauzenberger Granitmassivs (Südlicher Bayerischer Wald): Geologische Blätter für Nordost-Bayern und Angrenzende Gebiete, v. 44, p. 109-112.
- , 1995, Zur Geologie und Mineralogie des Blattes Lam 1:25.000 (Nr. 6844) im Bayerischen Wald: Geologische Blätter für Nordost-Bayern und Angrenzende Gebiete, v. 45, p. 103-151.
- Pfaffl, F., and Niggemann, M., 1967, Tracht und Habitus von Turmalinkristallen aus einigen Pegmatiten des Bayrischen Waldes: Der Aufschluss, v. 18, p. 171-178.
- , 1976, Rechts- und Links-Quarze aus einer Granitkluft bei Bischofsmais im Bayerischen Wald: Der Aufschluss, v. 27, p. 161-162.
- Pfaffl, F., Puhm, G., and Puhm, H., 1976, Über Mineralisationen in den Gneisen bei Hochbruck und Schönberg im Bayerischen Wald: Der Aufschluß, v. 27, p. 347-351.
- Pfaffl, F., and Troll, G., 1981, Zur Geschichte der geologischen und mineralogischen Erforschung des Bayerischen Waldes, in Troll, G., ed., Mineralvorkommen im oestlichen Bayerischen Wald; Bildung, Inhalt und Bergbaugeschichte, Volume 31: Der Aufschluss, Sonderheft: Heidelberg, Federal Republic of Germany, Vereinigung der Freunde der Mineralogie und Geologie, p. 9-13.
- Pfaffl, F.A., 1982, Erstfund im Bayerischen Wald; Würfelquarz vom Teufelstisch: Mineralien Magazine, v. 6, p. 456-459.

- Piscopo, V., 2001, Fracturing degree of outcropping rocks compared to pumping test results in two aquifers of Southern Italy, in Seiler, K. P., and Wohnlich, S., eds., *New approaches characterizing groundwater flow*, Volume 2: Lisse, A.A. Balkema Publishers, p. 1041-1046.
- Polivka, J., 1999, Durchführbarkeitsstudie zur Erschließung von Heil- bzw. Thermalwasser im Raum Kötzing: Regensburg, Grundwasserberatung Dipl. Geol. J. Polivka, p. 25.
- Power, W.L., and Durham, W.B., 1997, Topography of natural and artificial fractures in granitic rocks: Implications for studies of rock friction and fluid migration: *Int. J. Rock Mech. Min. Sci.*, v. 34, p. 979-989.
- Priehäuser, G., 1930, Die Eiszeit im Bayerischen Wald: *Abh. geol. Landesunters. Bayer. Oberbergamt*, v. 2, p. 46.
- , 1937a, Ablagerungen unter Gletscher- und Firneis und Fliesserdebildungen im Bayr. Wald.
- , 1937b, Fossile Roterde im Bayrischen Wald, vorläufige Mitteilung.
- , 1938, Eiszeitliche Toteisbildungen im Bayerischen Wald: *Zs. Gletscherkunde*, v. 26, p. 97-111.
- , 1951, Der Nachweis der Eiszeitwirkungen im Bayer. Wald mit Hilfe von Schuttausbildungen: *Geologische Blätter für Nordost-Bayern und angrenzende Gebiete*, v. 1, p. 81-91.
- , 1952a, Roterdevorkommen im Bayerischen Wald: *Geologische Blätter für Nordost-Bayern und angrenzende Gebiete*, v. 2, p. 81-89.
- , 1952b, Über die natürliche Speicherung von Wasser im Bayerischen Wald: *Landw. Jb. f. Bayern*, v. 29, p. 449-484.
- , 1955, Störungen im Zersatz kristalliner Gesteine unter eiszeitlichen Schuttdecken im Bayerischen Wald: *Geologische Blätter für Nordost-Bayern und angrenzende Gebiete*, v. 5, p. 97-109.
- , 1956, Der Klimaablauf der Späteiszeit im Bayerischen Wald: *Geologische Blätter für Nordost-Bayern und angrenzende Gebiete*, v. 6, p. 55-66.
- , 1958, Über den Aufbau und die Oberflächenformen der Ablagerungen aus dem Firneis der letzten Kaltzeit (Endwürm) im Bayerischen Wald: *Geologische Blätter für Nordost-Bayern und angrenzende Gebiete*, v. 8, p. 152-157.
- , 1961, Felsfreistellungen, Blockmeere, Blockströme und Blockstreuungen im Bayer. Wald: *Geologische Blätter für Nordost-Bayern und angrenzende Gebiete*, v. 11, p. 123-132.
- , 1963a, Altpleistozäne Eiszeitspuren im Bayerischen Wald: *Geologische Blätter für Nordost-Bayern und angrenzende Gebiete*, v. 13, p. 163-177.

-
- , 1963b, Über die Sicherung des Landschaftswasserhaushaltes im Bayerischen Wald: Landw. Jb. f. Bayern, v. 40, p. 334-353.
- , 1966, Beitrag zur Frage der Entstehung von Lockerbraunerde im Bayerischen Wald auf pleistozäner Bodenunterlage: Geologische Blätter für Nordost-Bayern und angrenzende Gebiete, v. 16, p. 183-191.
- , 1968, Über die Verwitterung kristalliner Gesteine zu Zersatz von der Oberfläche aus; Beispiele aus dem Bayerischen Wald: Geologische Blätter für Nordost-Bayern und angrenzende Gebiete, v. 18, p. 162-172.
- , 1971, Über Trinkwasservorräte im Zersatz kristalliner Gesteine im Bayerischen Wald: Geologische Blätter fuer Nordost-Bayern und angrenzende Gebiete, v. 21, p. 127-135.
- Prinz, H., and Strauß, R., 2006, Abriss der Ingenieurgeologie: München, Spektrum Akademischer Verlag, 671 p.
- Probst, M., Schöpfer, C., and Zipfel, K., 2001, Analysing regional groundwater flow in fractured aquifers using a conceptual model, in Seiler, K. P., and Wohnlich, S., eds., New approaches characterizing groundwater flow, Volume 2: Lisse, A.A. Balkema, p. 1047-1049.
- Propach, G., 1968, Hydrogeologische Verhältnisse, in Madel, J., Propach, G., and Reich, H., eds., Erläuterungen zur Geologischen Karte von Bayern 1:25.000, Blatt Nr. 6945 Zwiesel: München, Bayerisches Geologisches Landesamt, p. 77-78.
- Raab, T., 1999, Würmzeitliche Vergletscherung des Bayerischen Waldes im Arbergebiet: Regensburg, Institut für Geographie an der Universität Regensburg, 327 p.
- Raum, K.-D., 2002, Markierungstechnische, bruchtektonisch-gefügekundliche und fotogeologische Untersuchungen zur Ermittlung der Grundwasserfließverhältnisse in der Verwitterungszone kristalliner Gesteine in Quellgebieten des Oberpfälzer/Bayerischen Waldes (Ost-Bayern/Deutschland) [PhD thesis]: Erlangen, Friedrich-Alexander Universität Erlangen-Nürnberg, 239 p.
- Reinecker, J., Heidbach, O., Tingay, M., Connolly, P., and Müller, B., 2004, The 2004 release of the World Stress Map, The World Stress Map Project, Retrieved: 23.06.2004 from <http://www-wsm.physik.uni-karlsruhe.de/>
- Richert, P., 2002a, Geophysikalische Bohrlochmessungen in der Versuchsbohrung VB 1 Neusohl, Bayern: Niederlindach, German Geo Services, p. 3.
- , 2002b, Geophysikalische Bohrlochmessungen in der Versuchsbohrung VB 2 Neusohl, Bayern: Niederlindach, German Geo Services, p. 3.
- , 2004, Geophysikalische Bohrlochmessungen in der Versuchsbohrung B1 Böbrach, Bayern: Niederlindach, German Geo Services, p. 4.
- , 2005a, Geophysikalische Bohrlochmessungen in der Versuchsbohrung B 1 Wiesenfelden, Bayern: Niederlindach, German Geo Services, 1 p.

-
- , 2005b, Geophysikalische Bohrlochmessungen in der Versuchsbohrung VB 4 Schweinhütt, Bayern: Niederlindach, German Geo Services, 5 p.
- , 2006, Thermalwasserprospektion Bad Kötzing (Bayerischer Wald). Geophysikalische Untersuchungen (Multielektroden-Geoelektrik): Hessdorf, German Geo Services, 13 p.
- Rohrmüller, J., Mielke, H., and Gebauer, D., 1996a, Gesteinsfolge des Grundgebirges nördlich der Donau und im Molasseuntergrund, Erläuterungen zur Geologischen Karte von Bayern 1:500.000: München, Bayerisches Geologisches Landesamt, p. 16-54.
- , 1996b, Tektonik, Grundgebirge, Erläuterungen zur Geologischen Karte von Bayern 1:500.000: München, Bayerisches Geologisches Landesamt, p. 252-259.
- Saker, R., and Jordan, H., 1977, Zu hydrologischen Eigenschaften der Verwitterungszonen erzgebirgischer Gneise: *Z. angew. Geol.*, v. 23, p. 606-611.
- Schild, M., Braun, R., Siegesmund, S., and Vollbrecht, A., 2001, Modellierung lokaler hydraulischer Wegsamkeiten und ihre Bedeutung für die Endlagerung in Kristallingesteinen: *Zeitschrift der Deutschen Geologischen Gesellschaft*, v. 152, p. 577-591.
- Seiler, K.P., and Müller, K., 1995, Grundwasserneubildung und Grundwasserumsatzräume im Kristallin des Bayerischen Waldes: *Deutsche Gewässerkundliche Mitteilungen*, v. 39, H. 6, p. 194-199.
- Seiler, K.P., and Wohnlich, S., 2001a, New approaches characterizing groundwater flow, *Proceedings of the XXXI International Association of Hydrogeologists Congress, Volume 1: Munich*, A.A. Balkema Publishers, Lisse, p. 1-688.
- , 2001b, New approaches characterizing groundwater flow, *Proceedings of the XXXI International Association of Hydrogeologists Congress, Volume 2: Munich*, A.A. Balkema Publishers, Lisse, p. 691-1328.
- Sibson, R.H., McMoore, J., and Rankin, R.H., 1975, Seismic pumping - a hydrothermal fluid transport mechanism: *Journal of the Geologic Society of London*, v. 131, p. 653-659.
- Simpson, C., and Schmid, S.M., 1983, An evaluation of criteria to deduce the sense of movement in sheared rocks: *Geological Society of America Bulletin*, v. 94, p. 1281-1288.
- Skernjaa, L., and Jørgensen, N.O., 1994, Evaluation of local fracture systems by azimuthal resistivity surveys: Examples from South Norway: *Applied Hydrogeology*, v. 2, p. 19-26.
- Snoke, A.W., Tullis, J., and Todd, V.R., 1998, *Fault-related rocks: a photographic atlas*: Princeton, New Jersey, Princeton University Press, p. 617.

- Spencer, E.W., and Kozak, S.J., 1974, Determination of Regional Fracture Patterns in Precambrian Rocks - a Comparison of Techniques, in Hogson, R. A., S.P. Gay, J.Y. Benjamins, ed., First International Conference on New Basement Tectonics: Salt Lake City, Utah, Utah Geological Association.
- Sprenger, W., Bittersohl, J., Willy, H., Aschauer, K., Schöttl, C., and Irmgard, H., 2005, Grund- und Bodenwasser, Wasserwirtschaftlicher Bericht - Niedrigwasserperiode 2003, Volume 2/05: Informationsberichte des Bayerischen Landesamtes für Wasserwirtschaft: München, Bayerisches Landesamt für Wasserwirtschaft, p. 27-70.
- Starn, J.J., Stone, J.R., and Mondazzi, R.A., 2002, Characterization of bedrock aquifers in Connecticut: (2) Hydrologic simulation., Geological Society of America Northeastern Section, Annual Meeting: Springfield, Massachusetts, Geological Society of America, p. A-23.
- Stásko, S., and Tarka, R., 2001, Ground water flow in fractured hard rock based on field data from the Sudety Mts., SW Poland, in Seiler, K. P., and Wohnlich, S., eds., New approaches characterizing groundwater flow, Volume 2: Lisse, A.A. Balkema, p. 1069-1072.
- Stein, E., 1988, Die strukturgeologische Entwicklung im Übergangsbereich Saxothuringikum/Moldanubikum in NE-Bayern, in Schwerd, K., ed., Strukturgeologie, Lagerstätten-Typisierung und Metallogene im Übergangsbereich Saxothuringikum-Moldanubikum in Nordostbayern, Volume 92: *Geologica Bavarica*: München, Bayerisches Geologisches Landesamt, 150 p.
- Steiner, L., 1969, Scherflächenpaare in Oberbau und Unterbau: *Geotekt. Forsch.*, v. 33, p. 62.
- Stettner, G., 1992, Geologie im Umfeld der Kontinentalen Tiefbohrung Oberpfalz - Einführung und Exkursionen: München, Bayerisches Geologisches Landesamt, 240 p.
- , 1996, Zu den geotektonischen Beziehungen von Saxothuringikum, Moldanubikum und Bohemikum im Umfeld der Tiefbohrung Oberpfalz: *Geologica Bavarica*, v. 101, p. 181-209.
- Stettner, G., Rohrmüller, J., and Hirschmann, G., 1997, Bayerischer Wald / Oberpfälzer Wald (14), Stratigraphie von Deutschland II: Ordovizium, Kambrium, Vendium, Riphäikum, Teil I: Thüringen, Sachsen, Ostbayern: Courier Forschungsinstitut Senckenberg 200, Frankfurt am Main, Senckenbergische Naturforschende Gesellschaft, p. 373-399.
- Stibitz, M., 1998, Investigation of groundwater potential in the crystalline of the Bohemian Massif in Austria. - Methodical framework, in Annau, R., Bender, S., and Wohnlich, S., eds., *Hard Rock Hydrogeology of the Bohemian Massif*. 3rd International Workshop, Volume 8: *Münchener Geologische Hefte*, Reihe B: Windischeschenbach, Germany, p. 123-128.
- Stober, I., 1986, Strömungsverhalten in Festgesteinsaquiferen mit Hilfe von Pump- und Injektionsversuchen: *Geologisches Jahrbuch*, v. C 42, 204 p.

-
- , 1995, Die Wasserführung des kristallinen Grundgebirges: Stuttgart, Ferdinand Enke Verlag, 191 p.
- , 2007a, Fortbildungsveranstaltung Hydrogeologie der Festgesteine: Freiburg, FH-DGG.
- , 2007b, Hydrologie der Festgesteine. Einführung, Allgemeines, in Stober, I., ed., Fortbildungsveranstaltung Hydrogeologie der Festgesteine: Freiburg.
- Stone, J.R., 2002, Characterization of bedrock aquifers in Connecticut: (1) Geologic mapping and analysis., Geological Society of America Northeastern Section, Annual Meeting: Springfield, Massachusetts, Geological Society of America, p. A-23.
- Suess, F.E., 1903, Bau und Bild der Böhmisches Masse, Bau und Bild Österreichs, Volume L: Wien, p. 1-322.
- Tait, J.A., Bachtatse, V., Soffel, H.C., and Franke, W., 1996, Paleomagnetic constraints on the evolution of the European Variscan Foldbelt: *Geologica Bavarica*, v. 101, p. 221-232.
- Terzaghi, R.D., 1965, Sources of error in joint surveys: *Géotechnique*, v. 15, p. 287-304.
- Thums, S., 1993, Niederschlags- und Abflussauswertung der 10jährigen Meßreihe 1980-1989 für das Einzugsgebiet der Großen Ohe im Nationalpark Bayerischer Wald in Anlehnung an die Auswerteempfehlung des Deutschen IHP/OHP - Nationalkomitees, 196 p.
- Thüringer, C., Bäuml, R., and Hötzl, H., 2001, Evaluation of hydraulic parameters in fissured rocks by gas tracing, in Seiler, K. P., and Wohnlich, S., eds., *New Approaches Characterizing Groundwater Flow*, Volume 2: Lisse, A.A. Balkema Publishers, p. 1073-1077.
- Toynton, R., 1983, The relation between fracture patterns and hydraulic anisotropy in the Norfolk Chalk, England.: *The Quarterly Journal of Engineering Geology*, v. 16, p. 169-185.
- Tröger, U., Düssel, M., Moeck, I., and Schandelmeier, H., 2001, A new approach to the reconnaissance of groundwater flow in hard rocks: Hydrotectonic, in Seiler, K. P., and Wohnlich, S., eds., *New approaches characterizing groundwater flow*, Volume 2: Lisse, A.A. Balkema Publishers, p. 1079-1083.
- Troll, G., 1964, Geologische Übersichtskarte des Bayerischen Waldes: München, Bayerisches Geologisches Landesamt.
- , 1967a, Bau und Bildungsgeschichte des Bayerischen Waldes, in Troll, G., ed., *Führer zu geologisch-petrographischen Exkursionen im Bayerischen Wald. Teil I: Aufschlüsse im Mittel- und Ostteil*, Volume 58: *Geologica Bavarica*: München, Bayerisches Geologisches Landesamt, p. 15-21.
- , 1967b, Die blastokataklastischen Kristallingesteine der Stallwanger Furche, Bayerischer Wald, in Troll, G., ed., *Führer zu geologisch-petrographischen Exkursionen im Bayerischen Wald. Teil I: Aufschlüsse im Mittel- und Ostteil*, Volume 58: München, Bayerisches Geologisches Landesamt, p. 22-33.

-
- , 1967c, Führer zu geologisch-petrographischen Exkursionen im Bayerischen Wald; Teil I, Aufschlüsse im Mittel- und Ostteil: München, Bayerisches Geologisches Landesamt, 188 p.
- , 1968, Führer zu geologisch-petrographischen Exkursionen im Bayerischen Wald; Teil II, Aufschlüsse im Westteil: Regensburger Wald: München, Bayerisches Geologisches Landesamt, 188 p.
- , 1974, Igneous and metamorphic rocks in the southern Bavarian Forest, Excursion Guidebook; Excursion B 8., Volume 52; 1: Fortschritte der Mineralogie: Stuttgart, Federal Republic of Germany, Deutsche Mineralogische Gesellschaft, p. 167-194.
- Unger, H.J., 1996, Tektonik, Molassebecken, in Freudenberger, W., and Schwerd, K., eds., Erläuterungen zur Geologischen Karte von Bayern 1:500.000: München, Bayerisches Geologisches Landesamt, p. 265-266.
- van der Pluijm, B., and Marshak, S., 1997, Earth Structure: An Introduction to Structural Geology and Tectonics, WCB/McGraw-Hill, 495 p.
- Van der Voo, R., 1983, A plate-tectonics model for the Paleozoic assembly of Pangea based on paleomagnetic data., in R.D Hatcher, H. W., I. Zietz, ed., Contributions to the Tectonics and Geophysics of Mountain Chains: Boulder, Colorado, Geological Society of America, p. 19-23.
- , 1988, Paleozoic paleogeography of North America, Gondwana, and intervening displaced terranes: Comparisons of paleomagnetism with paleoclimatology and biogeographical patterns: Geological Society of America Bulletin, v. 100, p. 311-324.
- Vejnar, Z., 1965, Bemerkungen zur lithostratigraphischen Beziehung zwischen dem mittelböhmischen Algonkium und dem Moldanubikum: N. Jb. Geol. Paläont. Mh., p. 102-111.
- Vesely, M., and Mls, J., 1998, Groundwater flow in a long fracture with variable aperture, in Annau, R., Bender, S., and Wohnlich, S., eds., Hard Rock Hydrogeology of the Bohemian Massif. 3rd International Workshop, Volume 8: Münchner Geologische Hefte, Reihe B: Windischeschenbach, Germany, Ludwig-Maximilians-Universität München, p. 129-134.
- Völkel, J., 1995, Periglaziale Deckschichten und Böden im Bayerischen Wald und seinen Randgebieten: Z. Geomorphol., v. Suppl. Bd. N.F. 96, p. 1-301.
- Walsh, G., J., and Clark, S.F., 2000, Contrasting Methods of Fracture Trend Characterization in Crystalline Metamorphic and Igneous Rocks of the Windham Quadrangle, New Hampshire: Northeast Geology and Environmental Sciences, v. 22, p. 109-120.
- Wang, M., Kulatilake, P.H.S.W., Panda, B.B., and Rucker, M.L., 2001, Groundwater resources evaluation case study via discrete fracture flow modeling: Engineering Geology, v. 62, p. 267-291.

- Weise, S.M., Bräuer, K., Strauch, G., Kämpf, H., Koch, U., and Tesar, J., 1998, Seismically induced release of deep-seated fluids as tracer of fast transport up to surface in fractured rocks of the Bohemian Massif, in Annau, R., Bender, S., and Wohnlich, S., eds., *Hard Rock Hydrogeology of the Bohemian Massif. 3rd International Workshop, Volume 8: Münchner Geologische Hefte, Reihe B: Windischeschenbach, Germany*, p. 183-184.
- Weiss, E.G., 1989, Über die Notwendigkeit einer Korrektur bei kluftstatistischen Aufnahmen, die Berechnung des mittleren Kluftabstandes und die Darstellung des Zerklüftungsgrades: *Z. dt. geol. Ges.*, v. 140, p. 193-200.
- Wikipedia-contributors, 2005, K-means algorithm, Wikipedia, The Free Encyclopedia, October 9, 2005, Retrieved: December 12, 2005 from http://en.wikipedia.org/w/index.php?title=K-means_algorithm&oldid=25103743
- Williams, K.W., 2000, Surface and subsurface fracture characterization and the occurrence and characterization of subsurface flow along a cross-strike transect in eastern Massachusetts. [Master's thesis]: Amherst, Massachusetts, University of Massachusetts.
- Winkler, G., 2003, Fracture network analyses for hydraulic modeling. Approaches of fractured aquifers [PhD thesis]: Graz, Austria, Technical University Graz.
- Witthüser, K., and Himmelsbach, T., 1998, Erhebungsmethoden von Kluftparametern für eine stochastische Kluftnetzgenerierung: *Grundwasser*, v. 3, p. 103-109.
- Zeithöfler, M., 2003, Bedrock Structure in Southeastern Connecticut: Hydrologic Implications. [Master's thesis]: Middletown, CT, Wesleyan University.
- , 2006a, Abschlußbericht über die Prospektionsarbeiten zur geplanten Thermalwasserbohrung in Bad Kötzing: Regensburg, 15 p.
- , 2006b, Bericht zur Lineamentanalyse auf Basis von SRTM-Satellitenhöhendaten für die Hydrogeologische Landesaufnahme im EU-Ziel-II-Gebiet im Auftrag des Bayerischen Landesamtes für Umwelt - Geologischer Dienst des LfU Bayern: München, Bayerisches Landesamt für Umwelt - Geologischer Dienst, 51 p.
- Zeithöfler, M., and Raum, K.D., 2005, Relationships between brittle tectonic structure and groundwater migration patterns in fractured rock aquifers of the Central Bavarian Forest, SE Germany, in Freiwald, A., Röhling, H.-G., and Löffler, S.-B., eds., *GeoErlangen 2005. System Earth - Biosphere Coupling. Regional Geology of Central Europe - International Conference and Annual Meeting Geologische Vereinigung (GV), Deutsche Gesellschaft für Geowissenschaften (DGG)*, Volume 39: Schriftenreihe der Deutschen Gesellschaft für Geowissenschaften: Erlangen, Deutsche Gesellschaft für Geowissenschaften, p. 423-424.
- Zhang, X., and Sanderson, D.J., 1999, Scale up of two-dimensional conductivity tensor for heterogeneous fracture networks: *Engineering Geology*, v. 53, p. 83-99.

Appendix A – Outcrop Descriptions

Steinbruch Prünst, Outcrop ID: 6943-01

Rock Types: Granit (GK25): Whitish, medium-grained granite (non-foliated) interspersed with dark gray, sometimes foliated rock (Quarz-Glimmer-Diorit, GK25).

Outcrop: GK: 457270E 542964N; UTM: 353175E 5429383N
Sohle 1, Start at quarry entrance road (NE corner of quarry). Outcrop is about 10-20 high (reaches land surface). Generally dense fracturing grading upwards into weathering (grus) and soil zone. Fractures measured along NNE facing wall, ca. 90 paces WNW-ESE.

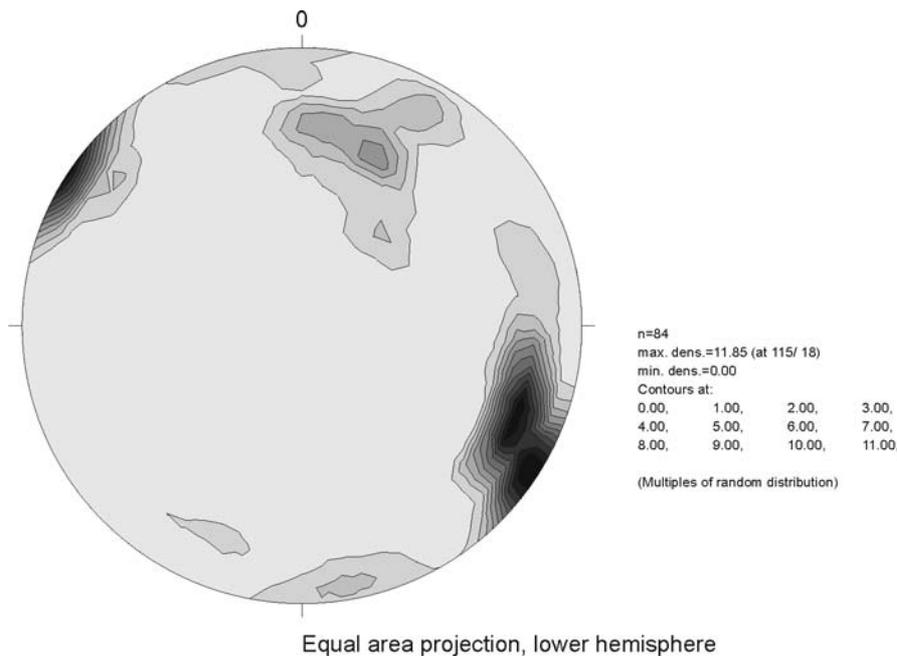


Figure A-1: Contoured poles to all fractures in outcrop (file: So1_co.jpg).

Mean Trend	Mean Plunge	Angle long axis (°)	Angle short axis (°)	Mrd max.	Comment
115	18	14	7	11,85	
123	5	14	10	11,7	
25	36	57	48	4,5	
172	7	38	29	2,4	

Fractures do not seem to be influenced by rock fabrics. Even in the foliated parts of the “Quarz-Glimmer-Diorit” foliation-parallel fracturing is practically non-existent. The dominant fracture system trends NNE-SSW with generally steep dips. Minor systems dip moderately SSW and steeply NNW. Oxidation occurs mostly on NNE-SSW fractures. Epidote and chlorite also occur predominantly on NNE-SSW fractures, as well as on some moderately dipping SSW (not chlorite, instead one NNE-) dipping fractures.

Few kinematic indicators were found exclusively on NNE-SSW trending fractures, suggesting two types of motion:

Oblique reverse ($103\sigma_1/55$; $322\sigma_3/29$) and oblique dextral ($61\sigma_1/29$; $329\sigma_3/4$).

Brecciated and gougy zones occur in all sets, thus suggesting that virtually all fractures originated, or were reactivated as shear fractures.

Other interesting features:

- Aplitic vein (170v50) more strongly fractured than surrounding granite.
- Large fault zone (ca. 200f70), traceable over ca. 7m and connected to land surface, exposes a 10-20cm wide zone of accessory fractures, breccia and gouge. Zone fans out towards land surface. Accessory fractures could represent synthetic shears (suggesting normal motion). Zone is very wet and acts as conduit for ground water infiltration. Similar fault zone also exists about 10m ESE of the previous one. Containing moss, gouge and breccia it intersects the land surface about 8, above Sohle1, but is less wet than the fault 10m WNW. Also, accessory fractures do not show angular relationships with fractures in main fault zone.
- Existing foliations (maybe ca. 120-50 in the Quarz-Glimmer-Diorit) are cut by fractures at very acute angles, i.e. rock fabrics do not seem to influence fracture orientations in this rock type.
- One ca. 20cm wide strongly gougy and brecciated zone (ca. 90f90) cuts and offsets another brecciated zone (ca. 140f30). S-block down. No magnitude of displacement recorded.
- Generally, fractures connected to the land surface seem to contain various amounts of water. Both fractures of N-S and E-W trending sets are wet.
- A feature requiring a lot of imagination, but still worth mentioning: A large fault (ca. 200f70) with water seeping out is connected to the land surface and fans out upwards. It cuts and maybe offsets a ca. 30cm wide brecciated zone (90f63) 30cm in reverse direction.
- General note: Many fractures both in the granite and in the “Quarz-Glimmer-Diorit” show undulatory, conchoidal fracturing. Origin? Maybe not tectonic features, but due to blasting?

Steinbruch Prünst, Outcrop ID: 6943-01

Rock Types: Granit (GK25): Whitish, medium-grained granite (non-foliated) interspersed with dark gray, sometimes foliated rock (Quarz-Glimmer-Diorit, GK25).

Outcrop: GK: 457270E 542964N; UTM: 353175E 5429383N
Sohle 2, Start ca. 20m SE of the entrance road (SE corner of quarry). Outcrop wall faces about N and is ca. 8m high (upper end is Sohle 1). Fractures measured along an E-W section ca. 65 paces wide.

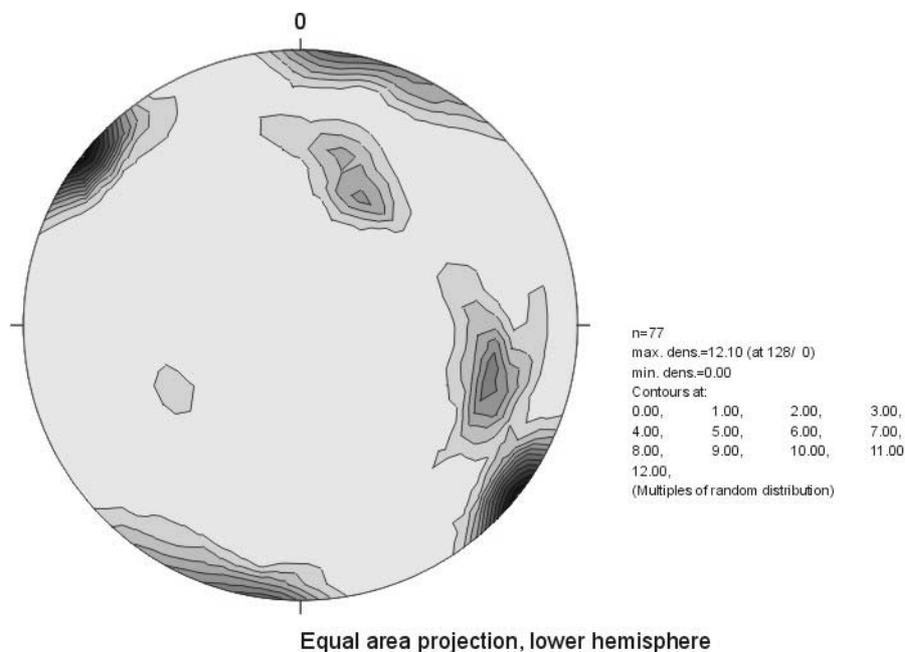


Figure A-2: Contoured poles to all fractures in outcrop (file: So2_co.jpg).

Mean Trend	Mean Plunge	Angle long axis (°)	Angle short axis (°)	Mrd max.	Comment
128	0	29	28	12,1	
8	1	57	25	6,5	
107	29	37	22	5,8	
26	47	51	26	4,4	

The outcrop consists of two distinct lithologic units (granite and “Quarz-Glimmer-Diorit”) separated by a brecciated zone (91f58, gouge, moss, wet). The zone also cuts a quartz vein (194v63) showing a slight drag in reverse direction. However, the degree of brecciation of the vein compared to the brecciated zone suggests a post-brecciation intrusion and some reactivation (reverse motion, $181\sigma_128$; $1\sigma_362$) along the brecciated zone, which slightly offset and dragged the quartz vein. Thus, the juxtaposition of the granite and quartz-glimmer-diorit units (if it occurred by faulting and major displacement) had to be pre-emplacment of the vein. In turn, another part of the same E-W trending brecciated zone (90f58) is cut and slightly offset (ca. 5cm reverse) by a fault of the NNE-SSW set (200f55). The resulting stress field is $290\sigma_125$; $110\sigma_365$. A moderately W dipping aplite vein (185v57, ca. 20cm wide) is apparently right-laterally offset by a fracture of the moderately S dipping set (orientation not measured, 90f50 chosen for reference). The resulting stress configuration is $294\sigma_119$; $37\sigma_334$.

These cross cutting relationships lead to the following possible sequence of events:

- 1) Shear and brecciation along the moderately dipping E-W set (e.g. 91f58).
- 2) Intrusion of roughly trending N-S quartz and aplite veins (e.g. 185v57).
- 3) Formation of moderately WNW inclined fractures (possibly related to the quartz and aplite veins). Reverse offsets of brecciated E-W zones along these faults due to a gently inclined WNW-ESE compression. Steps 2) and 3) could be coeval.
- 4) Reactivation of the E-W brecciated zones leading to small dextral offsets along the quartz and aplite veins due to a gently inclined WNW-ESE compression.

A second scenario would be:

- 1) Intrusion of the granite into the quartz-glimmer-diorit.
- 2) Faulting and emplacement of the quartz and aplite veins.
- 3) Faulting and formation of the E-W trending breccia zones with almost no displacement.
- 4) Formation of the NNE-SSW faults cutting and reversely offsetting the E-W brecciated faults.

However, the relatively clear-cut and strongly mineralized N-Sish trending fractures suggest an origin (maybe as joints) in an extensional regime (maybe an E-W σ_3). This would also suggest a formation at shallow crustal levels and therefore a relatively young age.

Mineralizations of epidote, chlorite and quartz, as well as oxidation occur in all fracture sets except in the moderately SE dipping ones, which, however, could be due to sampling problems.

Steinbruch Prünst, Outcrop ID: 6943-01

Rock Types: Granit (GK25): Whitish, medium-grained granite (non-foliated) interspersed with dark gray, sometimes foliated rock (Quarz-Glimmer-Diorit, GK25).

Outcrop: GK: 457270E 542964N; UTM: 353175E 5429383N
Sohle 3, SE corner, below shredder (massive E-W wall). Outcrop wall faces about NNE and is ca. 15-20m high (upper end is Sohle 2). Fractures measured along an ENE-WSW section ca. 75 paces wide.

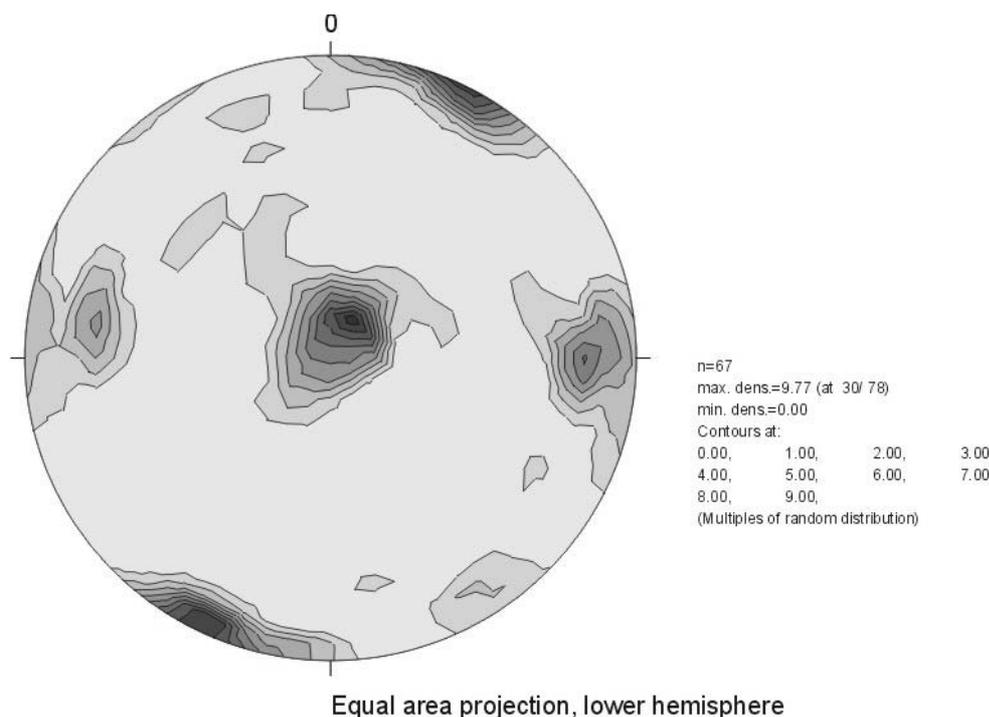


Figure A-3: Contoured poles to all fractures in outcrop (file: So3_co.jpg).

Mean Trend	Mean Plunge	Angle long axis (°)	Angle short axis (°)	Mrd max.	Comment
30	78	42	30	9,77	
205	4	51	32	8,9	
90	18	25	22	6,2	
279	24	20	17	4,4	

This outcrop is entirely located within the granite. The first 20 paces from the WNW end consist of a massive wall, ca. 25-30m high, ending at the rock shredder. Except for some roughly E-W trending, gently to moderately dipping fractures (maybe unroofing joints) there is little fracturing. However, the E-W fractures show apertures of 1-2mm (sometimes with water seeping out) with their density increasing towards the topographic surface. Also, very few fractures (spaced at about 3m and traceable over ca. 5-10m) of the moderately WNW dipping set (ca. 200f60) are visible. The large wall itself (ca. 295f85) is oxidized in places where water is running down. In other places patches of quartz, epidote and chlorite are exposed. Otherwise the wall is grusy and weathered. Mineral lineations suggest some vertical (in one case oblique) motion (maybe reverse shear sense) along the large wall. A quartz/aplite vein (165v35, ca. 2-3cm wide) is reversely offset by about 4cm by a fracture (325f20), suggesting compression in a roughly NW-SE direction.

Patches of quartz and epidote (belong to large E-W wall) apparently cover part of the quartz vein and the offset, indicating that quartz vein (165v35) and reverse fault (325f20) are older than the large E-W wall and its mineralizations.

A fracture set not found in the other outcrops dips moderately ESE. These fractures are only present at the ESE end of the large E-W wall and are traceable over 2-4m. The planes are rough and undulatory. Brecciation, accessory fractures and apertures of up to 5mm are present as well.

A fracture (201f85) strongly mineralized with quartz and epidote shows three generations of CPOs. The oldest lineation is subvertical (-75) and clearly indicated reverse motion. A younger set of lineations is gently inclined (-25) and suggests sinistral motion. A third CPO (+15) is very faint. Shear sense could not be determined.

One fracture (55f34) is associated with short accessory fractures (85f20), indicating Riedel relationships. In this case (55f34) represents the P-shear, and (85f20) the synthetic R-shears, thereby suggesting reverse shear sense due to a roughly NW-SE oriented compression. Similar relationships were found along a fracture (85f15), which however would indicate a more N-S oriented compression.

A population of subhorizontal fractures is only present on Sohle 3. They are generally 2-4mm open, partly wet and grusy and are most likely unroofing joints. Spacings in this set are 0.2-0.5m.

Fractures of the N-S to NE-SW sets as well as the WNW-ESE set often occur in relatively dense zones (spaced at ca. 8-10cm). At some intersections between dense zones water is dripping down.

Steinbruch Prünst, Outcrop ID: 6943-01

Rock Types: First half of transect: Quarz-Glimmer-Diorit (GK25), in places foliated (ca. 125-25); second half: Granit (GK25): Whitish, medium-grained granite (non-foliated). The granite exists as veins in the Quarz-Glimmer-Diorit and is thus younger.

Outcrop: GK: 457270E 542964N; UTM: 353175E 5429383N
Sohle 1, Start at the end of NW-SE trending transect of Sohle 1 (13.04.04). This transect trends SSW => NNE. Outcrop is mostly about 10-20 high, in places up to 25-30m (reaches land surface or a small "Zwischensohle"). Generally dense fracturing grading upwards into weathering (grus) and soil zone. Fractures measured along WNW facing wall, ca. 200 paces SSW=>NNE. Part of the outcrop is covered by debris fans. Length of the useable outcrop transect: ca. 120 paces.

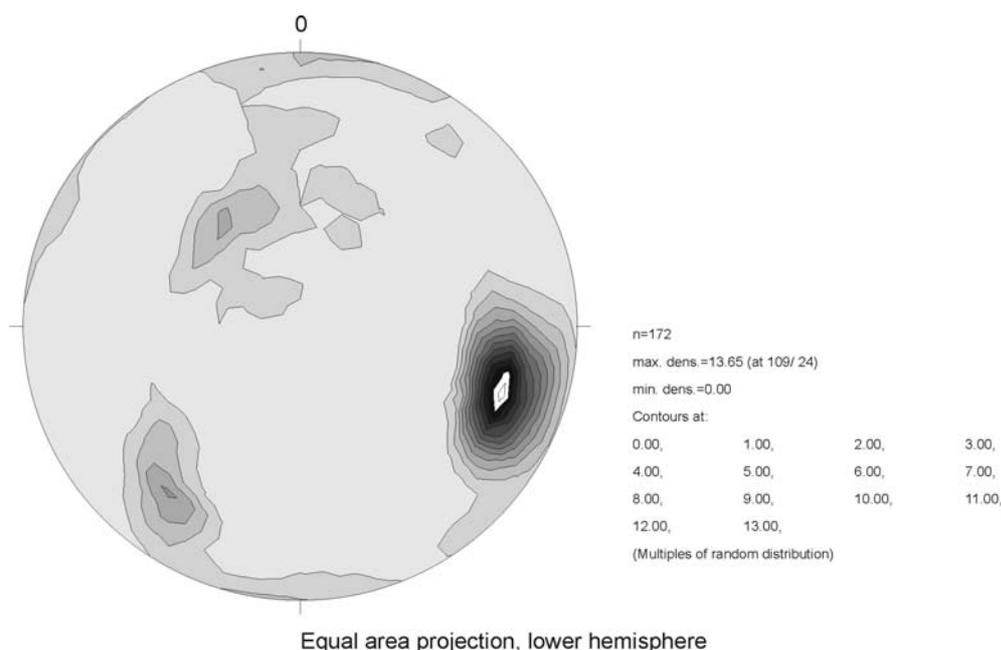


Figure A-4: Contoured poles to all fractures in outcrop (file: So1_co1.jpg).

Mean Trend	Mean Plunge	Angle long axis (°)	Angle short axis (°)	Mrd max.	Comment
109	24	76	48	13,65	
218	24	39	14	4,2	
321	54	67	26	3,1	
8	1	15	4	2,2	

Fractures do not seem to be influenced by rock fabrics. Even in the foliated parts of the “Quarz-Glimmer-Diorit” foliation-parallel fracturing is –with a few exceptions- practically non-existent. The by far dominant fracture system trends NNE-SSW with generally steep dips (Mrd max. is about 3 times as high as the second most important set). Minor systems dip steeply NE, gently to moderately SE and subvertically S. Biased sampling has to be corrected for by comparing this data with the NW-SE transect (13.04.04).

Planes of the steeply dipping NNE-SSW trending fractures are mostly clear-cut, plane and smooth (except for some ridges => Riedel shears?), and are abundantly mineralized. Some fractures of this set cut the whole outcrop and represent zones of dense fracturing and brecciation. They are most likely major faults and frequently serve as subvertical conduits for ground water (some densely fractured zones contain moss and plants, are very wet or even have water pouring out of them). East-Westerly trending fractures are frequently rough, undulatory and generally show less strongly mineralized planes (although minerals are present). Subhorizontal fractures possess varying strikes and are frequently associated with brecciated zones.

Oxidation as well as epidote, chlorite, manganese (if that's what it is) and quartz occur mostly on NNE-SSW fractures, also on steeply NE and SW dipping fractures. However, sampling could be biased by the fact that gently dipping (e.g. gently SE dipping set) fractures were usually only exposed as traces or covered with sandy/dirty stuff.

Two types of mineral lineations were found. The apparently older one plunges gently positively and negatively, almost exclusively on NNE-SSW striking fracture planes. Most of the lineations suggest dextral motion, few indicate sinistral motion. This implies either a subhorizontal ENE-WSW or a NNW-SSE directed compression, respectively. Similarly, small ridges on a steeply WNW dipping plane also suggest sinistral motion. The apparently younger set of lineations plunges generally dip-parallel to planes of the NNE-SSW trending set. They mainly suggest reverse motion, thus implying a moderately W plunging σ_1 and a moderately ESE plunging σ_3 .

Cross-cutting relationships indicate the following sequence of fracture formation:

- 1) East-Westerly trending fractures (oldest)
- 2) NNE-SSW trending fractures
- 3) Subhorizontal fractures (youngest)

The contact between Quarz-Glimmer-Diorit and Granite consists of a ca. 5m wide highly fractured and brecciated zone, suggesting that the juxtaposition of the two units was accomplished by fault motion. Fracture planes in this contact zone are mostly small and discontinuous, but are well connected. The zone transports water downwards. The granite side of the contact looks less severely fractured than the Quarz-Glimmer-Diorit side. In the granite the fractures look more chaotic, rougher and more conchoidal.

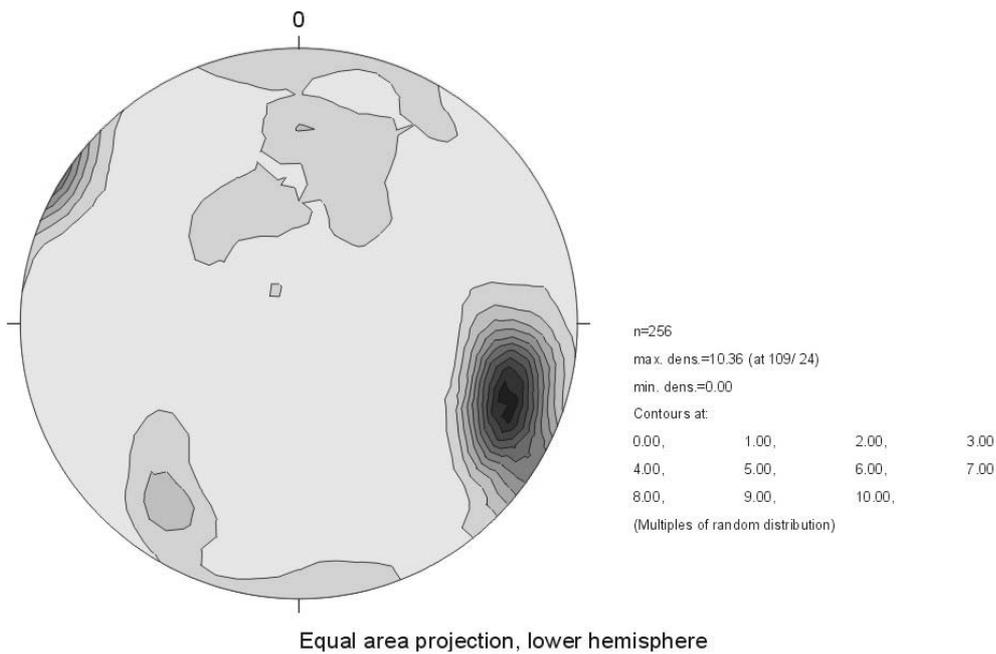


Figure A-5: Contoured poles to all fractures on Sohle 1 (combined with profile of 13.04.04) (file: So1_co2.jpg).

Mean Trend	Mean Plunge	Angle long axis (°)	Angle short axis (°)	Mrd max.	Comment
109	24	67	57	10,36	
216	20	69	22	2,8	
1	29	48	28	2,1	
336	55	33	18	1,9	

Figure A-5 shows the combined measurements of the NW-SE and the NNE-SSW transects, thus giving a 3D representation of the fracture orientations on Sohle 1.

Bodenmais Riesloch, Outcrop ID: 6944-01

Rock Types: Cordierit-Sillimanit-Gneis, “Arbergneis” (GK25), looks more like folded migmatite, though. All surfaces are heavily weathered; the entire outcrop is covered with lichen.

Outcrop: GK: 4582123E 543926N
The outcrop is located at the Riesloch hiking trail (“Bequemer Weg), about 180m NNE from the fork in the trail. Exposure faces W, is 8-10m high, 35 paces N-S and 10 paces E-W (on a steep hill).

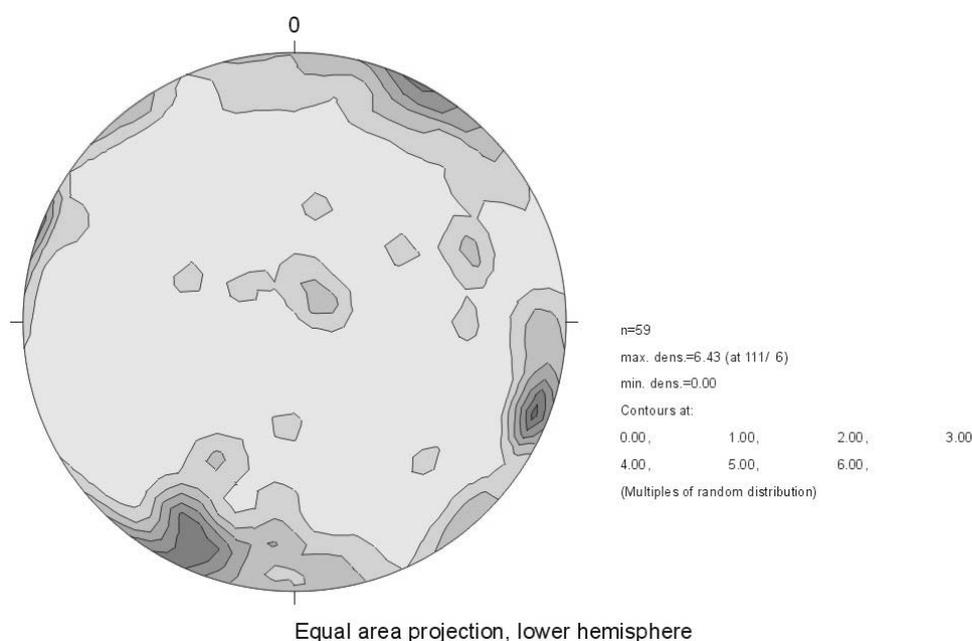


Figure A-6: Contoured poles to all fractures in outcrop (file: 6944-01.jpg).

Mean Trend	Mean Plunge	Angle long axis (°)	Angle short axis (°)	Mrd max.	Comment
111	6	35	19	6,43	Set is parallel to valley
203	11	66	44	5,7	Foliation parallel
320	0	18	12	2,8	
60	79	37	16	2,6	

There are two dominant sets of fractures in this location. Two fold axes were measured (305b20 and 294b13), and one was determined from foliation planes (330b04). Due to the waviness of the in places strongly folded foliation (generally oriented WNW-ESE, subvertical) fractures are often only subparallel to it and frequently cut across. However, they were still called foliation parallel fractures. Planes in this set are mostly rough and undulatory and occur in all sizes (they can be up to 4x4m), frequently in dense zones. In the field some fractures of the steeply dipping WNW-ESE set (then defined as the dominant set) were identified as cross-cutting fractures with large planes, breccia (sometimes boulder-sized) and accessory fractures.

The dominant set on the Schmid plot consists of steeply dipping NNE-SSW fractures. In the field they were described as frequently small, undulatory and discontinuous. They parallel the local topography (Riesloch gorge). Few unroofing joints were found, if at all in the upper part of the outcrop. There they had extensive planes with large openings. Mineralizations were sparse (probably removed by weathering). If present they consisted of hematite and patchy quartz. Lineations were not found.

Some fractures showed unusually large openings (>5cm, sometimes real „caves“). This leads to the suspicion that even large blocks of the outcrop may have slightly shifted (downslope creep?).

Bodenmais Riesloch, Outcrop ID: 6944-02

Rock Types: Cordierit-Sillimanit-Gneis, “Arbergneis” (GK25), looks more like folded migmatite, though. All surfaces are heavily weathered. The rock is strongly foliated, quartz is weathered out.

Outcrop: GK: 458173E 543943N
The outcrop is located at the NE end of the rocky ridge above the “Bequemer Weg”, ca. 60 vertical meters above the trail. The exposure faces NW, reaches ca. 55 paces NE-SW and is about 20m high.

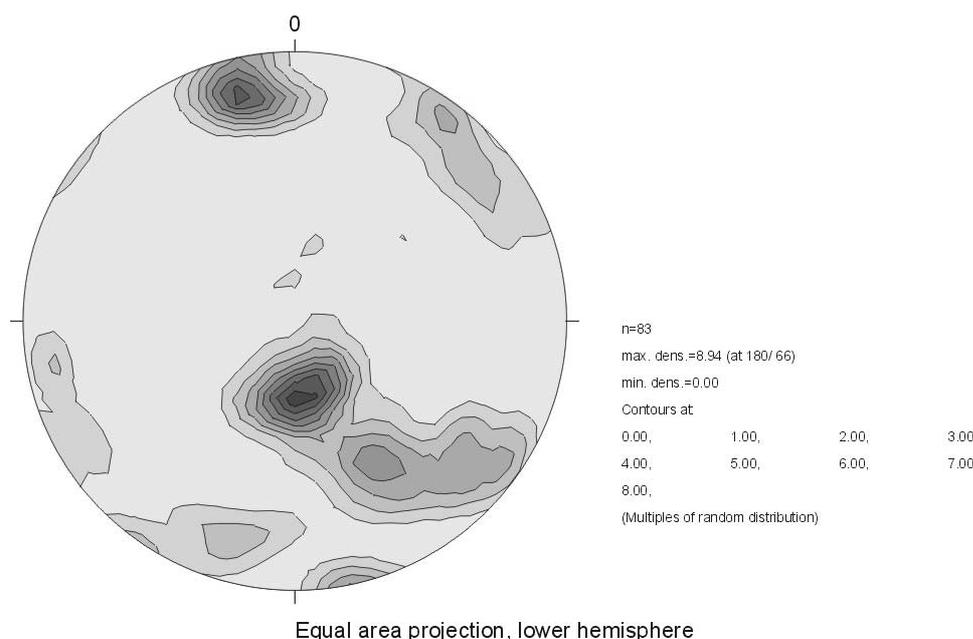


Figure A-7: Contoured poles to all fractures in outcrop (file: 6944-02.jpg).

Mean Trend	Mean Plunge	Angle long axis (°)	Angle short axis (°)	Mrd max.	Comment
180	66	31	28	8,94	Foliation parallel set dominant, controls valley in this location
346	15	40	36	7,1	Parallel to valley in this location
150	41	55	15	4,8	
39	6	35	15	3,2	
196	18	18	10	2,7	

The two dominant fracture sets strike parallel to the local topography (the ENE-WSW trending Riesloch gorge). At the ENE end of the outcrop foliation parallel fractures are not as abundant as other fracture sets (mostly occur in dense sets with spacings of 1-5cm where the foliation is not that tightly folded). Planes in this part are small and discontinuous. However, at the WSW end (rocks are very wet) foliation shows the highest degree of fracturing of all sets (spacings of up to 1-2cm), thus making it the overall dominant set in the outcrop (see fig. A-7). In this ca. 7m wide part of the outcrop the foliation shows relatively little folding and gentle dips. In this part the set looks like a shear zone.

The steeply dipping, ENE-WSW striking set forms the face of the outcrop. It consists of large, rough and undulatory fractures, often traceable over several meters. Most other cross-cutting sets occur in zones of dense fracturing, thus suggesting an origin as shear fractures. Large discrete fractures often possess wide apertures (frequently on the order of several cm). Similar to outcrop 6944-01 this suggests that the blocks might have shifted. Unroofing joints were not found. However, gently dipping foliation parallel fractures might have accommodated this strain.

Mineralizations (except for oxidation) are sparse on fracture planes. They were probably taken off by weathering, since some planes still show some patches of quartz. On surface (74f70) showed subvertical lineations (-60)

Steinbruch Zeitlhof, Outcrop ID: 7043-02

Rock Types: Whitish, medium-grained granite (non-foliated) with abundant biotite (flakes up to 3mm in diameter) and little kspar.

Outcrop: GK: 456917E 542757N
 Outcrop consists of two walls. One faces SSE and is ca. 25m wide and 8m high. The other one faces NW and is 20m wide and ca. 6m high.

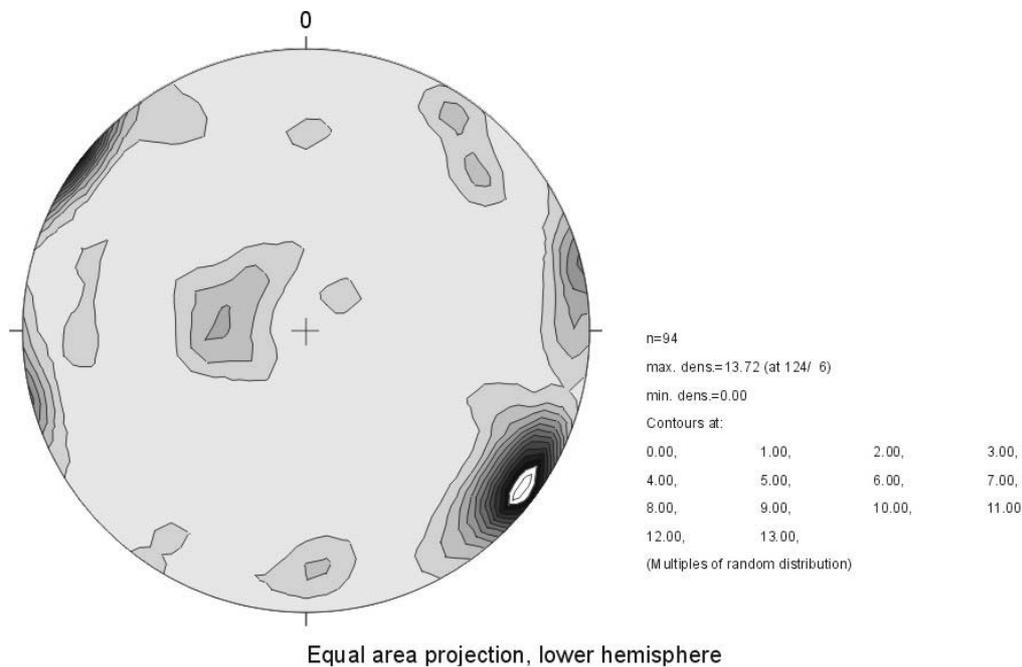


Figure A-8: Contoured poles to all fractures in outcrop (file: 7043-02.jpg).

Mean Trend	Mean Plunge	Angle long axis (°)	Angle short axis (°)	Mrd max.	Comment
124	6	36	34	13,72	
76	1	31	18	5,3	
270	67	47	38	3,2	
45	17	33	16	2,4	
179	17	24	19	2,1	

Due to the lack of a foliation in the granite there is no foliation-parallel set of fractures. The dominant system trends NNE-SSW to NE-SW and dips steeply in both directions. Fractures of this set usually possess planes traceable over several meters, are clear-cut and smooth and were most likely active during strike-slip faulting, since many planes contain subhorizontally plunging slickenlines and mineralizations. Mineralizations on planes consist mostly of quartz and maybe chlorite. A few planes contain thick quartz covers (former veins), which are fractured as well. Fractures in these veins dip at right angles to the dip of the main fracture plane and strike at angles of 60-70° with the acute bisector dip-parallel to the main fracture plane (thus forming an X-pattern on the vein). Some planes are oxidized.

A secondary set trends slightly W of N and also dips subvertically. Some fractures also show subhorizontal mineralizations and slickenlines. Mineralizations on planes consist of quartz and maybe chlorite (and hematite).

Unroofing joints dip gently ESE, parallel to the local topography. Fractures of this set are spaced 1-2 m (higher density towards the top of the outcrop) and generally have apertures of 1-2 mm, sometimes up to 1 cm. Planes are usually traceable over several meters. Some unroofing joints are associated with densely fractured/brecciated zones, thus suggesting shear.

Stress configurations calculated from slickensided fractures suggest a subhorizontal NNE-SSW compression ($09\sigma_1 02$; $104\sigma_3 04$).

Bodenmais, Riesloch, Outcrop ID: 6944-03a

Rock Type: “Arber-Gneis” (Cordierit-Sillimanit); heller, mittelkörniger Gneis mit deutlichem Lagenbau (GK25). Field observations: Migmatite, in places tightly folded. Up to 20cm (but generally 1-3cm) wide concordant quartz veins and Augen. Rocks heavily overgrown with moss, grass & lichen. Whole outcrop is wet; all faces are strongly weathered.

Outcrop: GK: 458170E 543953N; UTM: 362251E 5438926N
Outcrop is located at the bridge over the waterfall (S-bank of stream). Ca. 15 paces ENE-WSW & 6m high. Wall faces NNW. The whole outcrop is wet.

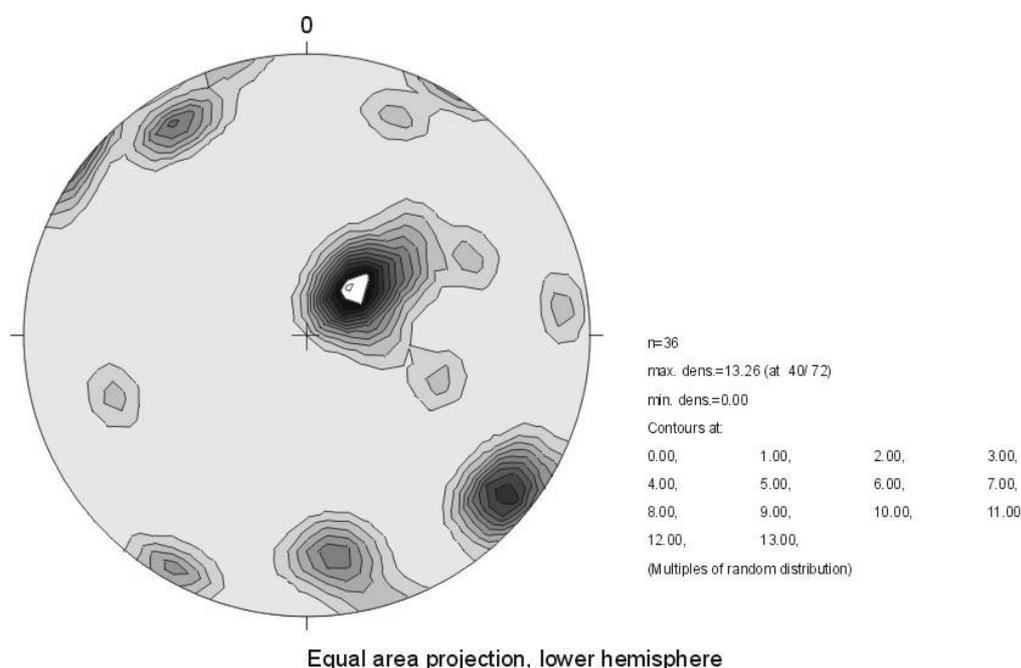


Figure A-9: Contoured poles to all fractures in outcrop (file: 6944-03a.jpg).

Mean Trend	Mean Plunge	Angle long axis (°)	Angle short axis (°)	Mrd max.	Comment
40	72	64	38	13,26	Some fractures foliation parallel
129	10	32	32	9,6	
328	12	22	16	6,3	
175	24	22	18	5,7	
210	6	17	16	4,6	

In this outcrop the gently SW dipping fracture set seems to be the dominant one. In places it is parallel to the foliation, which, however, is folded and interspersed with quartz veins and large porphyroblasts. Thus, fractures from this population also cut across the grain. Most planes (especially where they parallel the foliation) are short, and wavy and are concentrated at the ENE end of the outcrop. There they form fine foliation parallel laminae (ca. 1-2mm), probably enhanced by differential weathering. These dense zones are easily eroded and therefore form large, open (cave-like) “fractures”.

The subvertical NE-SW trending fractures are also fairly common. The generally very smooth planes in this set are among the largest in the outcrop. Another distinct population trends ENE-WSW and dips both NNW and SSE. N-S trending fractures are rather sparse. However, some densely spaced/brecciated zones suggest that this set originated from shearing.

Bodenmais, Riesloch, Outcrop ID: 6944-03b

Rock Type: Grobkörniger Granit mit großen Kalifeldspateinsprenglingen (GK25). Field observations: same rock type as in 6944-03a (Migmatite, see above).

Outcrop: GK: 458173E 543953N; UTM: 362251E 5438905N
The outcrop is located in the stream bed at the waterfall, ca. 30m above the bridge (6944-03a). Measurements taken over an interval of ca. 20m upstream.

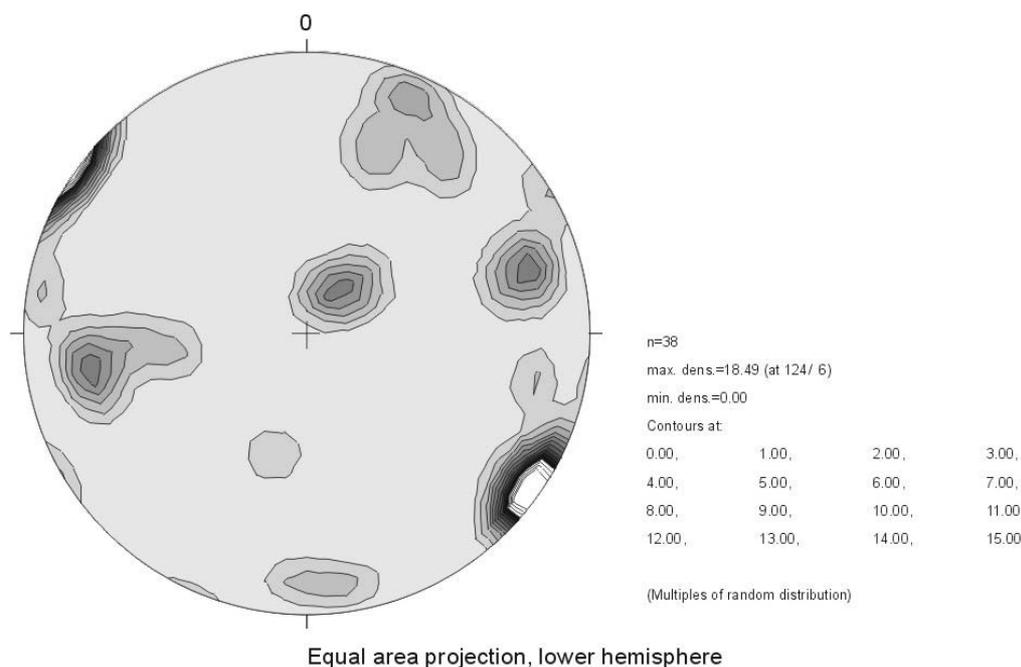


Figure A-10: Contoured poles to all fractures in outcrop (file: 6944-03b.jpg).

Mean Trend	Mean Plunge	Angle long axis (°)	Angle short axis (°)	Mrd max.	Comment
124	6	30	30	18,49	
75	19	25	20	5,9	
262	25	41	21	5,8	
41	72	32	23	5,7	Unroofing joints
23	12	44	33	3,8	Partly foliation parallel
179	12	25	18	2,8	

The dominant fracture set in this outcrop trends about NE-SW and dips subvertically. This population parallels local topographic features (i.e. the Riesloch gorge). Fracture planes are very clear-cut and smooth and occur in locally dense sets (spacings of 5-10cm).

A secondary set, which is absent in outcrop 6944-03a trends slightly W of N and dips moderately to steeply in both directions. The appearance of this set with increasing proximity to the bend of the Riesloch gorge towards north-southerly directions suggest a fracture control of the local geomorphology.

Other sets of minor importance dip gently SW (most likely unroofing joints) and steeply SSW and N. Foliation parallel fractures are difficult to identify, but they seem to trend WNW-ESE and dip gently NNE (only one plane measured) and steeply SSW (locally). From these measurements a fold axis (291b6) was calculated. In places the formation of the stream bed (steps in the waterfall) seems to have been influenced by the foliation.

Steinbruch Prünst, Sohle 3, Outcrop ID: 6943-01

Rock Type: Granite

Outcrop: GK: 457270E 542964N; UTM: 353175E 5429383N
The transect is located on Sohle 3 and reaches about 110 paces SW=>NE. About 58 paces of it consist of debris fans or lose pieces of wall. The outcrop is bounded by Sohle 2 (ca. 15m above ground).

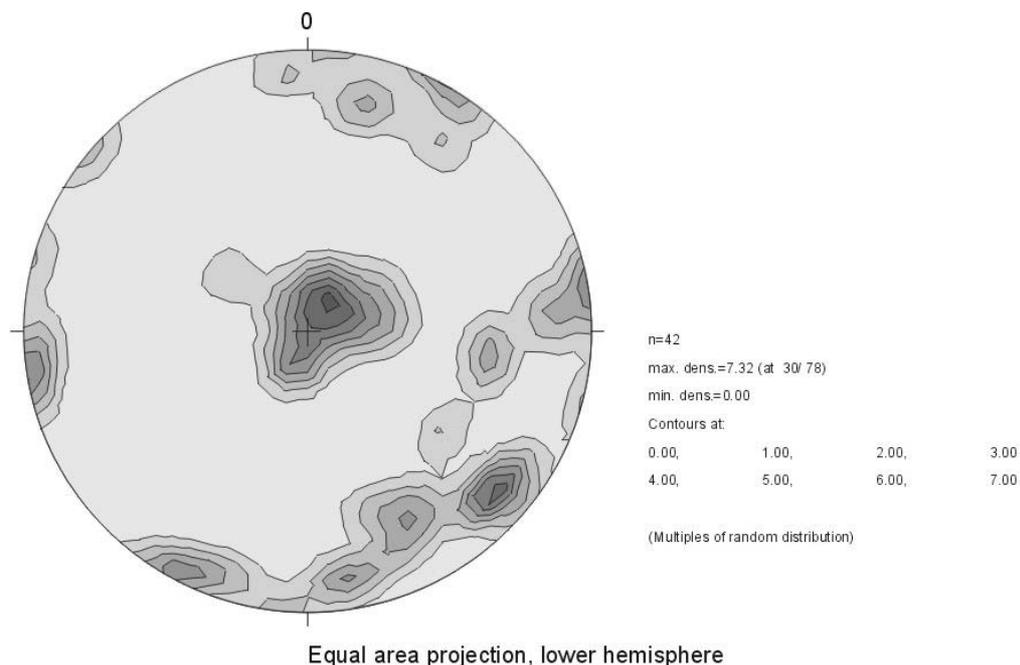


Figure A-11: Contoured poles to all fractures in transect (file: 200504co.jpg).

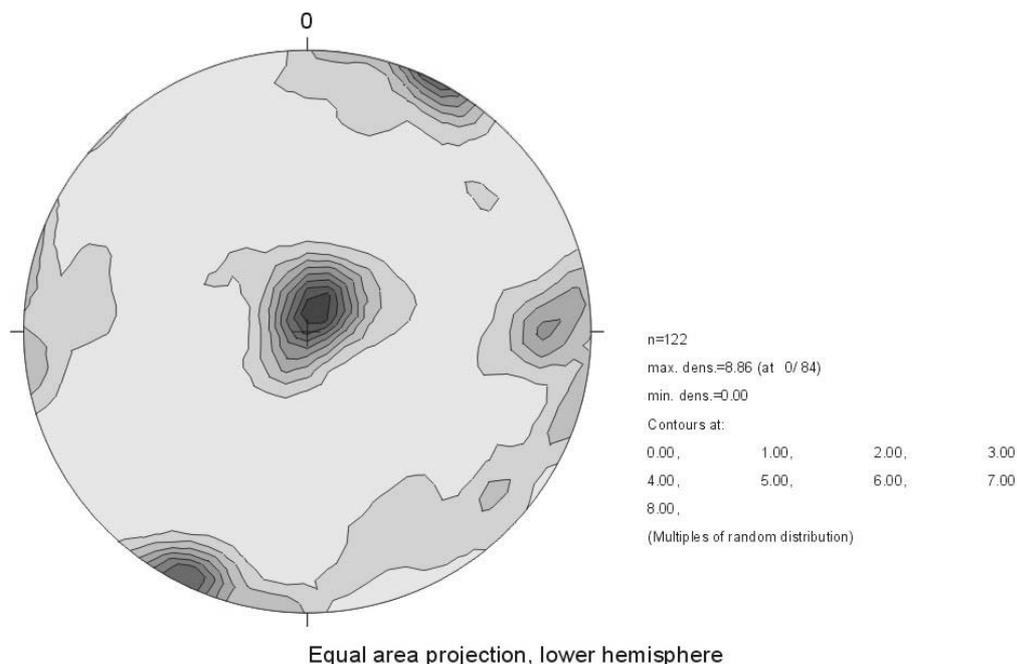


Figure A-12: Contoured poles to all fractures on Sohle 3 (file: allso3co.jpg).

Mean Trend	Mean Plunge	Angle long axis (°)	Angle short axis (°)	Mrd max.	Comment
0	84	59	47	8,86	Unroofing joints
206	0	38	27	6,9	
90	19	23	12	4,4	

The dominant fractures in this section of the quarry are the subhorizontal unroofing joints. Some fractures of this set occur in densely spaced zones and frequently possess apertures of 1-2mm. Also, some brecciation seems to have occurred, thus suggesting deformation by shear. However, especially the steeply dipping, N-S and NE-SW trending fractures form large (several meters in diameter), smooth and often mineralized (epidote, K-feldspar, chlorite, quartz) and oxidized planes. One fracture (220f75) shows clear plumose structures, suggesting an origin as tensile joint. E-W trending fractures possess mostly rough and wavy planes.

Fractures of all populations contain moss, grass, and are wet (locally, water is trickling out of fractures). Large parts of the outcrop look loose and might have shifted due to blasting and gravitational loosening. Thus, fracture apertures might not reflect real values. The low number of measurements along this transect produce a somewhat chaotic distribution in fig. A-11. Combined with other data from Sohle 3 (fig. A-12) the picture becomes clearer.

Bodenmais, Silberberg, Outcrop ID: 6944-04

Rock Type: Metatektischer Granat-Cordierit-Sillimanit-Gneis ohne Plagioklas, bzw. Plagioklasarm (gcgn2, GK25). Field: Highly deformed, folded rock with schistose look. All faces are heavily mineralized and rusty.

Outcrop: GK: 458230E 543608N; UTM: 363012E 5435438N
The outcrop is located at the entrance of the “Wolfgangstollen”. It reaches ca. 17 paces WNW-ESE (facing SSW) and is about 6m high.

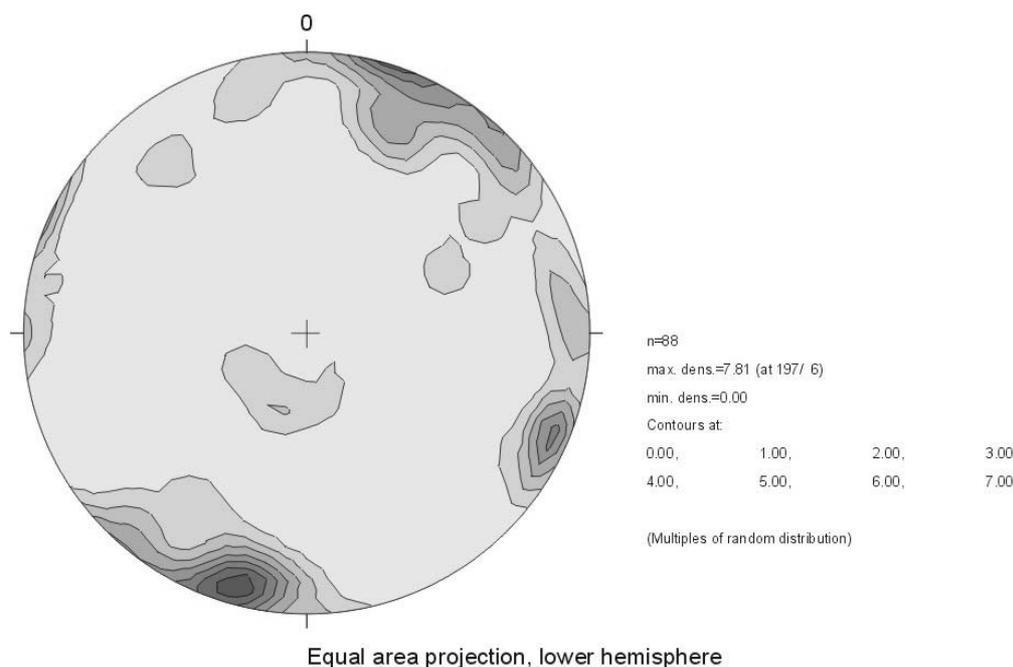


Figure A-13: Contoured poles to all fractures in outcrop (file: 6944-04.jpg).

Mean Trend	Mean Plunge	Angle long axis (°)	Angle short axis (°)	Mrd max.	Comment
197	6	80	69	7,81	Parallel to topography, face of outcrop
112	6	24	20	5,4	
90	5	20	14	2,8	
200	66	35	17	2,1	Foliation parallel

The dominant fracture set (dipping steeply both NNE and SSW) in this outcrop parallels the local topography (WNW-ESE trending valley) and forms the face of the outcrop. It possesses the largest planes (up to a few meters in diameter), although smaller ones are also common. Planes are mostly straight, smooth, and rusty and contain mineralizations of quartz and some blackish mineral (Manganese?). Apertures are generally <1mm although weathering widened them at the exposure.

Another important set of fractures trends in northerly directions (there might be two subpopulations trending N-S and NNE-SSW) and dips subvertically. Planes in this set are also smooth and can also reach several meters in size, only less frequently than the WNW-ESE ones. Apertures are generally <1mm and mineralizations are similar to the ones of the WSW-ESE set. At the top of the outcrop there is a zone of smooth, straight NNE-SSW trending fractures (ca. 25/2m), suggesting that this sets can be locally very dense and might be the dominant one in places.

Further up towards the summit very large planes of both the WNW-ESE and the NNE-SSW set were found (locally only moderately rather than steeply dipping). Unfractured areas (up to several m wide) are interspersed with highly fractured zones. Here, fractures look gravitationally widened and

the fracture geometry suggests normal motion along both sets. Unfortunately, the rocks in this part of the mountain are partially magnetized (Fe-ores, lightning strike?) and Brunton measurements could not be taken.

Foliation parallel fractures are rare in this outcrop and only present where the grain is fairly planar. Where fractures exist they dip gently NNE. In other places the foliation shows tight intrafolial folding and even looks crenulated, thus suggesting at least two hi-P/T° metamorphic events.

Brittle kinematic indicators were found both on WNW-ESE and N-S trending planes in the form of faint slickenlines and mineral lineations with mainly subvertical and subhorizontal rakes, although moderately plunging ones were also observed. The subvertically plunging lineations (all on NNW-SSE trending planes) suggest normal motion (96σ₁68; 235σ₃18), while the subhorizontal ones indicate dextral displacement (132σ₁30; 42σ₃4).

Some ductile and semi-ductile kinematic indicators, including δ- and σ-type rotated porphyroblasts as well as small folds, were found. They suggest an easterly verging transport direction.

Bodenmais, Hochfall, Outcrop ID: 6944-05

Rock Type: Metatektische Granat-Cordierit-Sillimanit-Gneis. Dunkler Lagengneis mit hellen, linsig ausgebildeten Quarz-Feldspat-Aggregaten (gcgn1, Gk25).

Outcrop: GK: 457943E 543924N; UTM: 360274E 5438714N (6944-05a)
 GK: 457943E 543929N; UTM: 360276E 5438761N (6944-05b)

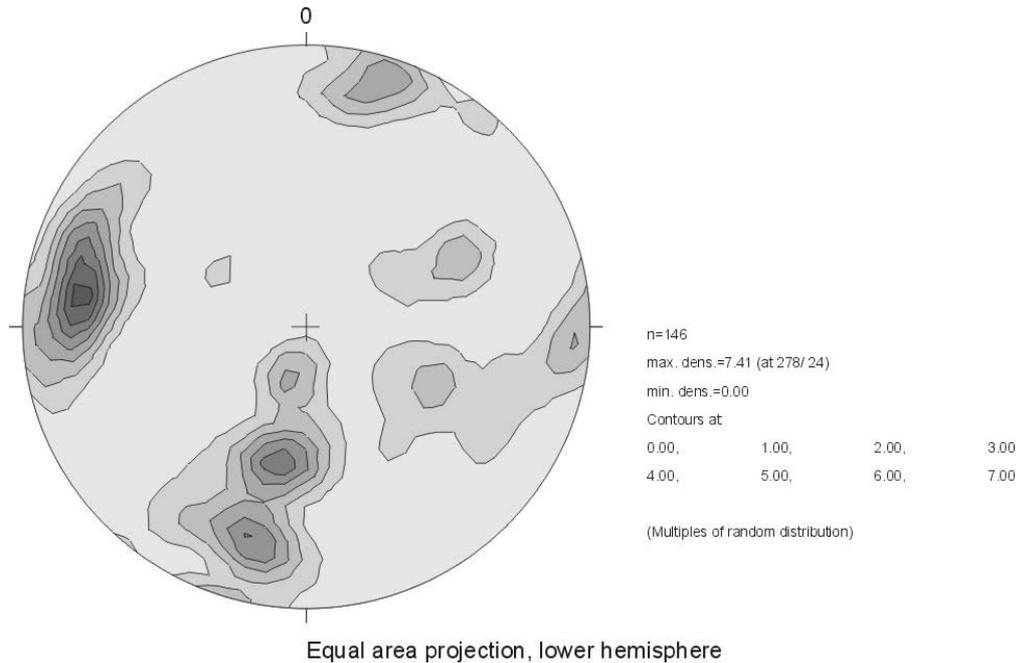


Figure A-14: Contoured poles to all fractures in outcrop (file: 6944-05.jpg).

Mean Trend	Mean Plunge	Angle long axis (°)	Angle short axis (°)	Mrd max.	Comment
278	24	50	48	7,41	Foliation (folded) parallel and cross fractures
189	48	113	42	5,8	
68	41	39	19	2,9	
113	49	13	11	2,7	

The dominant fracture system in this outcrop is valley-parallel and trends N-S to NNE-SSW dipping subvertically. They possess the largest planes (several meters in diameter) and smooth surfaces. Apertures are highly variable and range from virtually non-existent to <1cm.

Foliation is folded in relatively large (meter-scale) as well as tight intrafolial folds (b-axis determined from foliation-planes: 289b7). It strikes WNW-ESE and dips gently to steeply NNE and steeply SSW (NNE-SSW trending belt of poles in fig. A-14). Foliation is more intensely fractured in places where it is not tightly folded; in larger folds fractures occasionally curve with the foliation. In places where the foliation dips about 55° a separate set of cross fractures –strike-parallel to the grain and dipping 70° - 90° - form. A minor set dips moderately SW to WSW.

Kinematic indicators were not found. There is possibly a normal offset (about 1m) of a fractured zone along a steeply ESE (10f70) dipping fracture. The evidence is very vague, though.

General observations:

- Quartz veins and porphyroblasts are more highly fractured than the surrounding gneisses.
- Rocks seem to be more highly and chaotically fractured (by different sets) near mesoscopic folds. Fractures are mostly short, but well connected.
- Fracture apertures are highly variable in all sets.
- In places of dense fracturing spacings decrease in all sets and become similar.

**Bodenmais, Road Bodenmais-Langdorf (St. 2132), ca. 150m SE of Rotary to Böbrach
Outcrop ID: 6944-06**

Rock Type: Metatektischer bis anatektischer Cordierit-Sillimanit-Gneis (cngn, GK25). Strongly folded and foliated migmatitic gneiss.

Outcrop: GK: 457951E 543670N; UTM: 360241E 5436176N
The outcrop is located at a road cut along ST 2132. It extends about 65 paces NW-SE (facing NE) and is ca. 7m high. All faces are heavily weathered and overgrown with lichen.

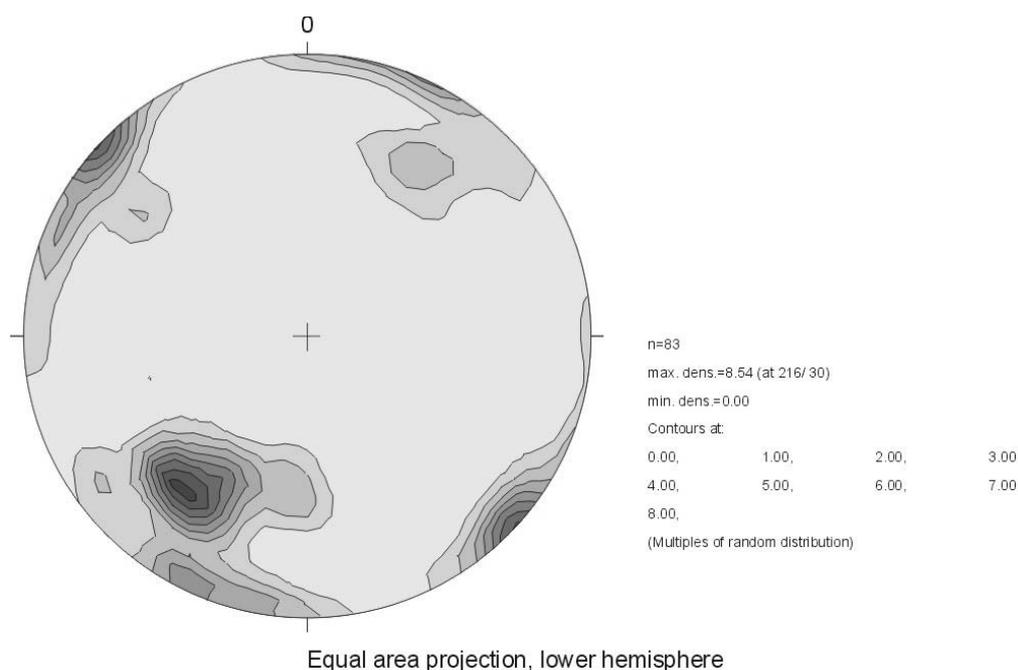


Figure A-15: Contoured poles to all fractures in outcrop (file: 6944-06.jpg).

Mean Trend	Mean Plunge	Angle long axis (°)	Angle short axis (°)	Mrd max.	Comment
216	30	30	29	8,54	Partly foliation parallel
312	1	71	51	7,1	
207	6	29	13	4,5	
30	30	15	12	2,9	

The dominant fracture sets trend NW-SE and NE-SW. The NW-SE fractures (form the face of the outcrop) possess dips of 40°-90°. The NE-SW fractures mainly dip steeply. The foliation dips moderately NE and foliation parallel fractures are part of the NW-SE set (where the foliation is visible and non-folded).

Both major sets possess large planes (up to several meters in diameter), although the NW-SE fractures have somewhat larger planes. Fractures in these populations have both smooth and rough planes (the smoothest ones belong to the NE-SW set) and frequently occur in swarms. Some planes possess quartz and hematite mineralizations. Some brecciated zones are also oriented in the dominant directions. One moderately SE dipping fracture seems to have brecciated a plane of the NE-SW set and thus might have been active after the NE-SW fracturing event.

Minor populations trend NW-SE and dip moderately SW or are subvertical. They could also be part of the major sets. Some of the large planes (especially NE dipping ones) are associated with wedge-shaped zones of dense fracturing (R-shears?), which would suggest normal motion (subvertical σ_1 and NW-SE extension). However, the data is very vague.

Unroofing joints are very rare. Apertures are highly variable in all sets (range from closed to 1cm open).

Bodenmais, Road Bodenmais-Langdorf (St. 2132), ca. 500m SE of Exit to Böhmhof Outcrop ID: 6944-07

Rock Type: Metatektischer bis anatektischer Cordierit-Sillimanit-Gneis (cngn, GK25). Strongly folded and foliated migmatitic gneiss.

Outcrop: GK: 458154E 543463N; UTM: 362196E 5434024N
The outcrop is located at a road cut along ST 2132. It extends about 155 paces NNW-SSE (facing ENE) and is ca. 15-20m high. All faces are heavily weathered and overgrown with lichen (although less than 6944-06). Most planes are oxidized.

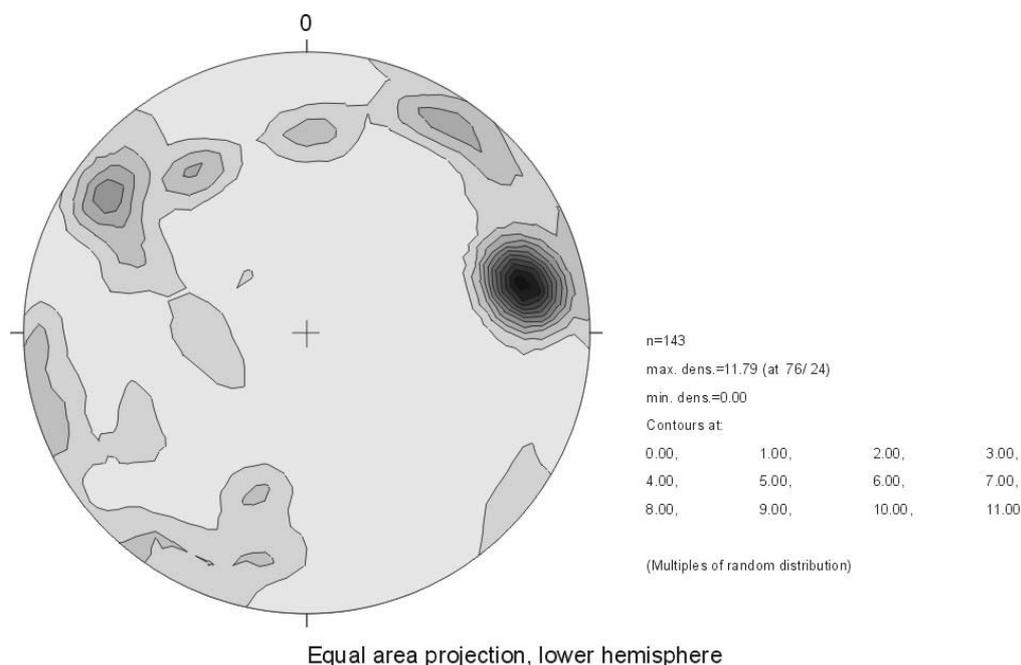


Figure A-16: Contoured poles to all fractures in outcrop (file: 6944-07.jpg).

Mean Trend	Mean Plunge	Angle long axis (°)	Angle short axis (°)	Mrd max.	Comment
76	24	30	25	11,79	Partly foliation parallel
305	17	38	21	4,7	
32	13	31	25	3,8	
324	31	15	12	3,3	

The dominant population trends NNW-SSE with subvertical dips and consists of large faults. Those faults are clear-cut. Brecciation exists, but it is hard to attribute to a specific population. Large fault surfaces are frequently mineralized with quartz, epidote, chlorite (the usual hydrothermal mix). Many planes in this set are slickensided or show mineral lineations.

At least three generations of linear features were detected. Two sets of lineations plunge gently both positively and negatively, one set plunges subvertically and is thought to be the youngest (although this is vague). One population of subhorizontally plunging kinematic indicators on the NNW-SSE faults suggests sinistral motion. Combined with the dextral motion detected on a steeply NNE dipping fracture this would indicate a subhorizontal NW-SE compression ($139\sigma_1$, $47\sigma_3$, 14). One moderately SSW dipping fracture ($166f69$) is left-laterally offset (ca. 8cm) by a moderately NE dipping fracture ($330f69$), which is consistent with the mineral lineations. Minor concentrations dip steeply SE and SW as well as S.

Generally, the foliation dips moderately to steeply NNE and SSW. Individual planes can have different orientations. It is fractured where it is developed and straight. Generally, foliation parallel fractures are of minor importance. Low angle fractures could be interpreted as unroofing joints, but they are highly variable in size, spacing and orientation. Apertures are highly variable in all sets and are most likely influenced by gravity.

Teisnach, Marienthal, RR-Tracks ca. 150m N of Fahrrad Röhl, Outcrop ID: 6943-02

Rock Type: Körnelgneis (bgn, GK25). Granitic-looking gneiss with quartz-feldspar porphyroblasts (about 1mm in diameter) and up to 3cm large euhedral K-feldspar crystals.

Outcrop: GK: 457280E 543430N; UTM: 353456E 5434042N
The outcrop extends ca. 45 paces N-S (facing E) and is 7-8m high. Most planes are overgrown with moss & lichen.

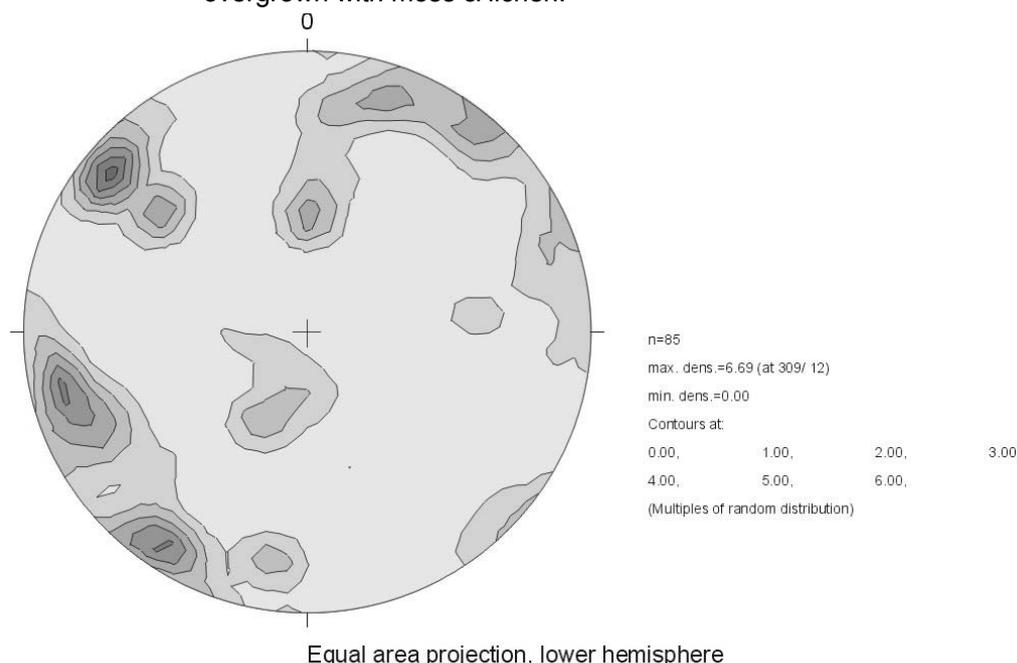


Figure A-17: Contoured poles to all fractures in outcrop (file: 6943-02.jpg).

Mean Trend	Mean Plunge	Angle long axis (°)	Angle short axis (°)	Mrd max.	Comment
309	12	56	32	6,69	Partly foliation parallel
256	12	34	34	5,2	
214	7	29	24	5,1	
0	19	13	8	3,6	
18	14	13	8	3,5	
204	59	38	33	2,8	

There are several major fracture sets in this outcrop. The largest planes (faults) dip steeply SE and ENE, thus suggesting that two major fault zones intersect at this location. Fracture sizes can be up to 5-6m in diameter and planes are mostly straight and relatively smooth. Due to their geometry and one slickensided plane (+70) the NNW-SSE trending fractures seem to be normal faults and are spaced at about 5m.

The large faults are associated with wedge-shaped (pinching out with depth) accessory fractures. One SE-dipping (37f71) is cut and brecciated by a steeply NE-dipping (330f75) fracture, which indicates that motion along the NE-dipping fractures is younger than the one along SE-dipping planes.

The foliation – where it is visible – dips gently in northerly directions. Fractures parallel to it are of minor importance. Due to its gentle dip the foliation might have been reactivated during the unroofing process.

Viechtach, Pfahlriegel, Outcrop ID: 6943-03

Rock Type: Quartz (95-98% SiO₂)

Outcrop: GK: 456311E 453855N; UTM: 343939E 5438669N
The outcrop is a prominent Ridge along the B85, ca. 200 NW of the Riedbach Bridge. It extends ca. 280m NW-SE and is up to 10 high. Fractures were measured at the SW facing side.

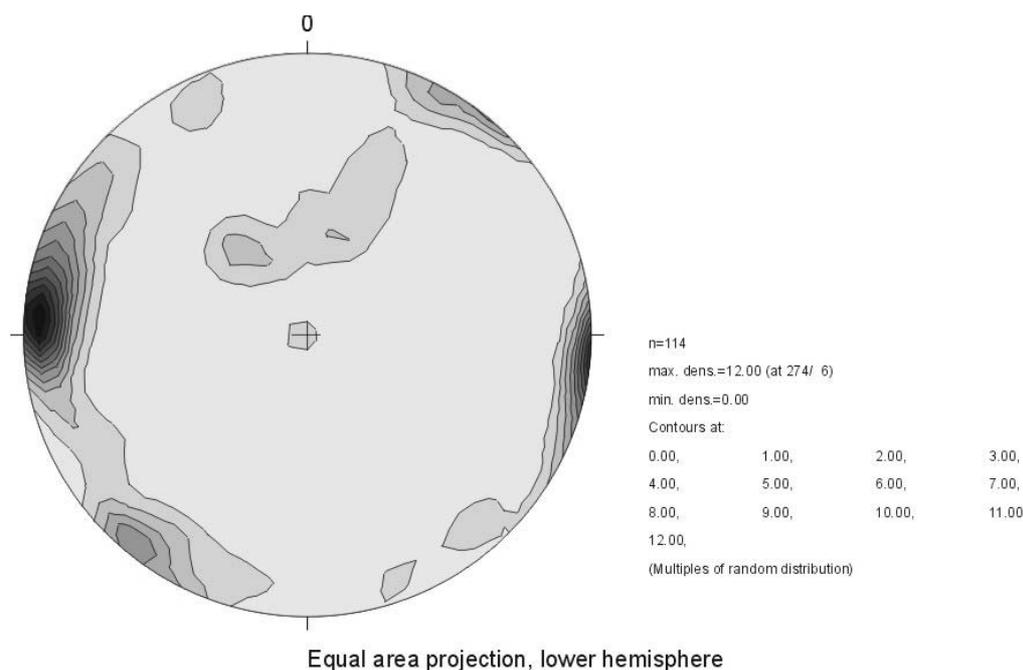


Figure A-18: Contoured poles to all fractures in outcrop (file: 6943-03.jpg).

Mean Trend	Mean Plunge	Angle long axis (°)	Angle short axis (°)	Mrd max.	Comment
274	6	62	32	12,00	
219	5	31	24	5,00	
323	61	64	22	2,6	
336	12	18	12	1,5	
323	89	8	8	1,4	

The dominant fracture set in this outcrop trends roughly N-S and possesses steep dips. Spacings in this population are about 5-10cm and plane sizes are highly variable (cm to m scale). Most kinematic indicators were found in this set. Two types of slickenlines were found. The most prominent one consists of subhorizontally plunging lineations suggesting a sinistral sense of motion. The resulting stress field is a NNW-SSE compression ($154\sigma_1$, $248\sigma_3$). The other set of slickenlines plunges moderately (about +60). The sense of motion could not be determined for these lineations.

The secondary set trends parallel to the Pfahl ridge (NW-SE) and also dips steeply. Spacings in this population are slightly larger (ca. 10-50cm) than those in the N-S set. Plane sizes are also highly variable. Kinematic indicators were not found in this fracture family.

A set of large subhorizontal fractures was detected. They are several meters in diameter and possess relatively large apertures (up to 1cm). Spacings are large (m scale) and irregular. Some planes are associated with brecciated zones, thus suggesting shear along those fractures, making an origin as unroofing joints uncertain.

The very high degree of fracturing in all sets produces a very well connected fracture network.

Other general observations:

- Some quartz veins trend parallel to the N-S fractures and are fractured at the contacts. The veins also contain breccia of wall rock. This leads to the following sequence of events:
 - 1) Formation of N-S trending fractures by shearing motion (creation of fault breccia)
 - 2) Silicification of the fractures by a hydrothermal event.
 - 3) Second fracturing event.
- One fracture plane of the N-S set (359f82) was cut by a WNW-ESE fracture (110f68), suggesting that the last motion event occurred along the WNW-ESE set.
- Some fracture planes contain euhedral quartz crystals, suggesting that the last silicification event occurred in an extensional regime without shear. However, on one plane slickenlines were found which seem to lie on top of the crystals.
- Most planes are relatively smooth and straight except the shallowly dipping ones.
- Some moderately SE dipping fractures (e.g. 53f38) seem to be associated with R-shears suggesting normal motion. Indicators are very vague, though.

Arnetsried, Quarzbruch Waschinger Outcrop ID: 7044-01

Rock Type: Quartz (95-98% SiO₂)

Outcrop: GK: 457740E 542857N; UTM: 357824E 5428130N

The outcrop is a NW-SW trending quartz quarry, extending about 975m in that direction and up to 50m deep. Many planes are covered with a sandy/grusy weathering material, so kinematic indicators and other small-scale features are obscured.

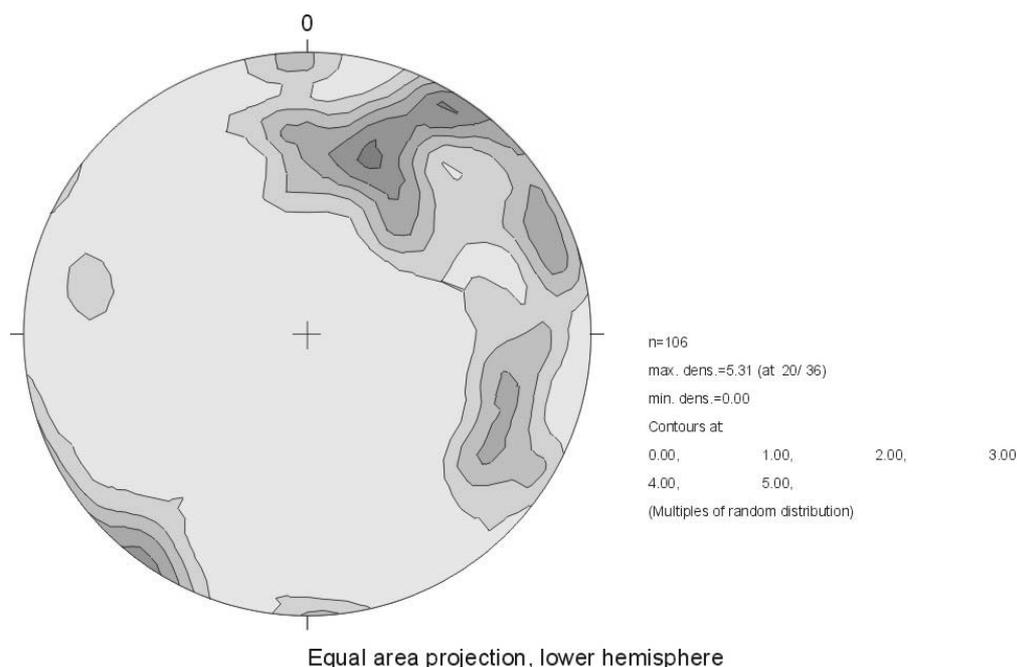


Figure A-19: Contoured poles to all fractures in outcrop (file: 7044-01.jpg).

Mean Trend	Mean Plunge	Angle long axis (°)	Angle short axis (°)	Mrd max.	Comment
20	36			5,31	
32	7			5,1	
67	12	20	10	3,7	
120	25	42	28	3,3	
358	2	8	7	2,3	
283	23	15	15	1,9	

The dominant fracture sets (largest planes and highest densities) in this location trend NW-SE and NNE-SSW. The NW-SE trending population displays a wide variety of dips. Most are steep, but there is also a moderately SW dipping group. The strikes and dips of the NNE-SSW fractures are somewhat more constrained. They mostly dip steeply WNW and look like faults with dip-parallel displacement. They occur in densely populated zones spaced at about 3 meters.

The few mineral lineations discovered on the grus-covered fracture planes were mostly found on NW-SE trending planes. They are usually very faint and transport directions are not obvious. Rakes range from subhorizontal to subvertical. The lineations are not sufficient to deduce paleo-stress fields.

Mineralizations on fracture planes are generally absent, except for some Fe-oxide stains. Generally, the whole outcrop is highly broken up and fractures of all sets are irregularly, but densely spaced. Fracture sizes range from cm to m in traces and diameters.

Gr. Arbersee, Geigenbachfall, Outcrop ID: 6844-01

Rock Type: Strongly folded (recumbent) gneiss/migmatite

Outcrop: GK: 458403E 544107N; UTM: 364937E 5440335N
The outcrop extends about 20 paces ENE-WSW, facing SSW and is ca. 4m high. The whole outcrop is wet and covered with lichen & moss.

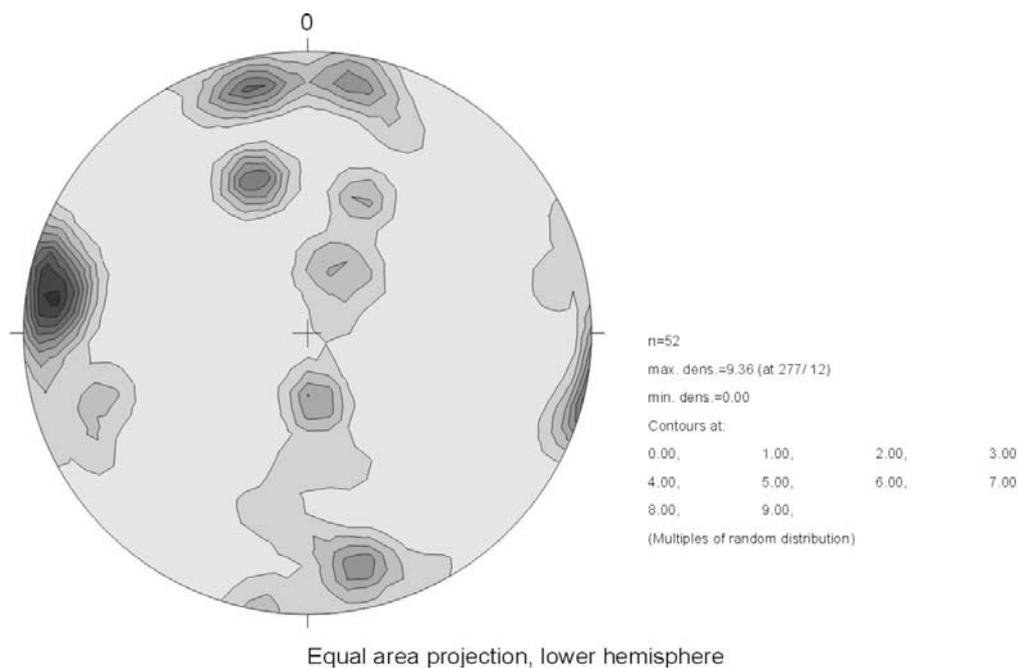


Figure A-20: Contoured poles to all fractures in outcrop (file: 6844-01.jpg).

Mean Trend	Mean Plunge	Angle long axis (°)	Angle short axis (°)	Mrd max.	Comment
277	12	38	31	9,36	
346	12	22	12	5,9	
339	43	23	23	5,6	
167	18	23	22	4,2	
NNE-SSW trending belt of poles					Foliation parallel fractures

The dominant fracture set in the stereo plot dips steeply both WNW and ESE, although the steep E-Wish trending fractures were identified as the dominant system in the field. Planes of the E-W set form the face of the outcrop and thus might be undersampled. Fracture spacings in both populations range from 0.5 to 1m, while the steep E-W striking fractures possess the largest planes in the outcrop. Many fractures of the NNE-SSW set end at foliation parallel fractures (T- intersections). Planes of this population are generally smooth.

The foliation in this set is strongly folded (recumbent folds, no vergence detectable). Thus, foliation parallel fracturing is highly irregular and, compared to cross fractures, of minor importance. However, some limbs of larger folds contain meter-sized foliation parallel fractures. Generally, most foliation parallel fractures are several cm long and irregularly spaced. Three fold axes were measured, all plunging gently W (272b12, 275b8, 280b7). The fold axis determined from foliation planes is oriented 276b6).

No kinematic indicators or offsets were encountered.

Bodenmais, Schönebene/Brandtnerriegel, Outcrop ID: 6944-08

Rock Type: gcgn2 (Map). Well-foliated migmatite.

Outcrop: GK: 458336E 543579N; UTM: 364057E 5435106N
The outcrop consists of several 10-20m wide and up to 25m high blocks. The examined part extends about 20 paces ENE-WSW, facing SSE and is about 6m high. Many faces are strongly weathered and covered with moss & lichen.

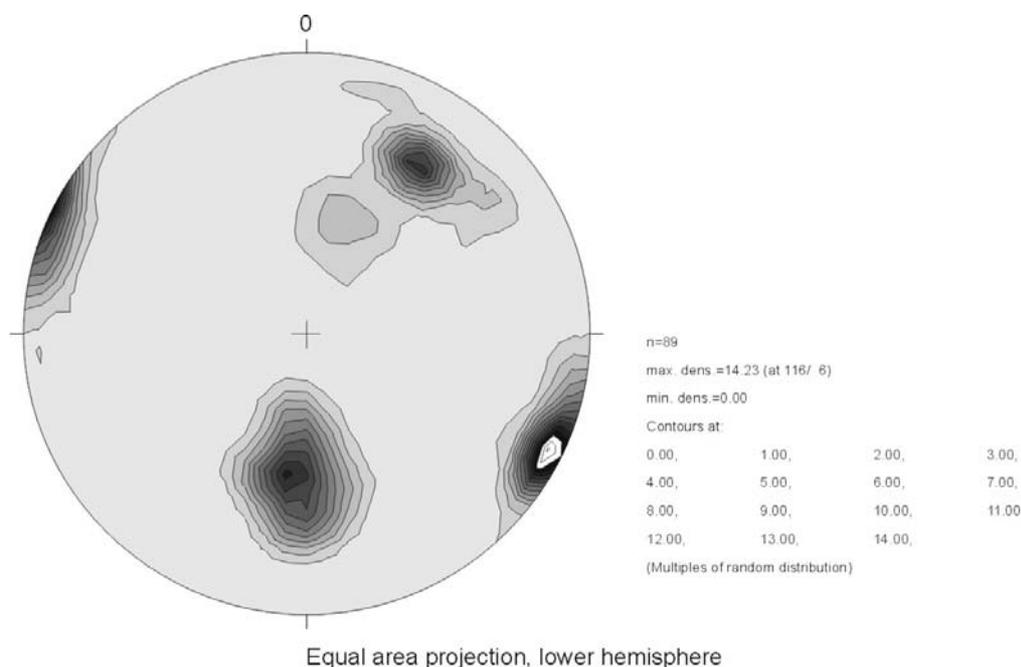


Figure A-21: Contoured poles to all fractures in outcrop (file: 6944-08.jpg).

Mean Trend	Mean Plunge	Angle long axis (°)	Angle short axis (°)	Mrd max.	Comment
116	6	47	38	14,23	Foliation parallel fractures
186	49	59	38	10,4	
33	30	33	25	9,3	
27	55	16	12	2,4	

The dominant fracture set in this location trends NNE-SSW and dips steeply. It forms the face of the outcrop and fracture planes possess sizes of up to several meters in diameter (largest plane found is 4x6m). Also, cm-scale fractures, usually spaced at 5-20cm were found in this population. Spacings of meter-sized fractures could not be determined.

The foliation in this outcrop is well-developed and only slightly folded. Thus, foliation parallel fractures represent the second most important set in this location. Large foliation parallel discontinuities occur as single fracture planes or as 20-50cm wide highly fractured/brecciated zones, both spaced at 2-3 meters. Centimeter-scale fractures are highly irregular –due to the small-scale folding- in their orientations and spacings. Some of the smaller fractures could be in a Riedel-relationship to the larger planes or in an en echelon array. However, sense of motion could not be determined.

The third population dips moderately to steeply SSW. Fractures in this set occur as meter-sized planes, spaced at 4-5m or as zones of densely-spaced cm-scale fractures.

A minor set dips gently to moderately S to SSW. It could be in a conjugate relationship with the fractured foliation. This would indicate a thrusting event with a NNE-SSW directed σ_1 and a subvertical σ_3 .

In the center of the outcrop there is a ca. 3x5m large section of very compact rock with little fracturing. Fracture apertures are highly variable in all populations, ranging from essentially closed to ca. 5cm in brecciated zones. The largest apertures seem to exist in the foliation parallel set. No offsets or kinematic indicators were found throughout the exposure.

Quarzbruch Hennenkobel, Outcrop ID: 6945-01

Rock Type: Granite and Pegmatite (GK 25: Pegmatit)

Outcrop: GK: 458558E 543558N; UTM: 366272E 5434807N
The outcrop extends ca. 37 paces NE-SW and is about 7-8m high. Most planes are strongly weathered and covered with lichen.

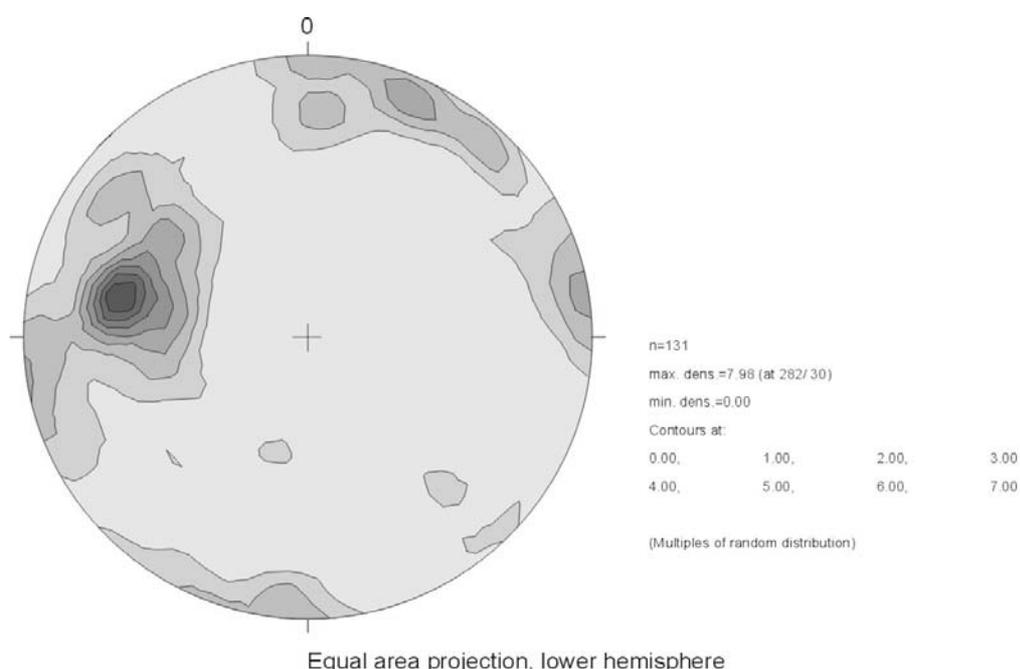


Figure A-22: Contoured poles to all fractures in outcrop (file: 6945-01.jpg).

Mean Trend	Mean Plunge	Angle long axis (°)	Angle short axis (°)	Mrd max.	Comment
282	30	36	32	7,98	
23	11	66	33	3,7	
81	5	10	7	3,2	

This outcrop is located within a clearly brittle NNE-SSW trending fault zone. Indicators are a NNE-SSW trending topographic lineament and a number of slickensided/polished slip planes interspersed with compacted breccia sheets, similar to the ones encountered at faults in Delphi and Kostalexis (Greece). The majority of the lineations on the slip planes are subvertical and formed most likely due to normal motion during uplift and WNW-ESE extension. Another set of slickenlines was detected within the compacted breccia sheets and is thus assumed to be younger than the subvertical one. It suggests dextral strike-slip displacement due to an ENE-WSW directed compression.

The dominant fracture population trends NNE-SSW and dips steeply ESE. It also possesses the largest planes (several fractures are a few meters in diameter), which are frequently polished and/or slickensided. Mineralizations on the slickensides consist mainly of hematite and the typical hydrothermal chlorite-epidote-mix. A few large planes are covered with abundant cm-sized flakes of muscovite. Major fractures of this set are spaced at 25 to 50cm. Some fractures in this population were found in a rock assumed to be granitic rather than pegmatitic and possess curvy planes looking like real granitic exfoliation (Half-Dome type). These fractures are oriented subparallel to the

topographic surface. However, they are also parallel to the NNE-SSW faults and could be related to them.

A secondary concentration of subvertical NNW-SSE trending fractures exists on the stereo plot. Since kinematic indicators were not found it is not clear if it is an individual population or a subconcentration of the NNE-SSW set.

The set trending in East-Westerly directions has more variable orientations with a dominant WNW-ESE strike. All fractures of this family dip steeply both in southerly and northerly directions. Slickenlines or polished planes were not detected. Most planes in this set are 0.5-1m in diameter and fractures are generally closed, except in zones of dense fracturing/brecciation.

Generally, the highest fracture densities were found in sections of the outcrop where the rocks consist of almost pure quartz. The lowest fracture densities exist in the compacted breccia sheets. Fracture size was determined to be inversely proportional to fracture density.

Schareben, Hochstein, Outcrop ID: 6844-02

Rock Type: Mesoscopically well-foliated rock with salt-and-pepper structure (Mylonite?). Handsample looked as if it had an S-C fabric. Contains some broken-up quartz-porphyroblasts. Foliation strikes WNW-ESE – parallel to the Rundinger Zone- and is folded.

Outcrop: GK: 457774E 544349N; UTM: 358753E 5443019N
 The outcrop consists of several exposures within a 100m radius around the summit of the Hochstein (1134m). All planes are strongly weathered and covered with moss and lichen.
 Outcrop 6844-02a: The outcrop is located ca. 100m WSW of the summit. It extends about 20 paces NW-SE and is ca. 2m high. It faces SW. (Time: 11:50-2:30)
 Outcrop 6844-02b: The exposure lies directly below the summit cross. It reaches about 40m WNW-ESE and is ca. 15-20m high, facing SSE. (Time: 2:30-15:30)

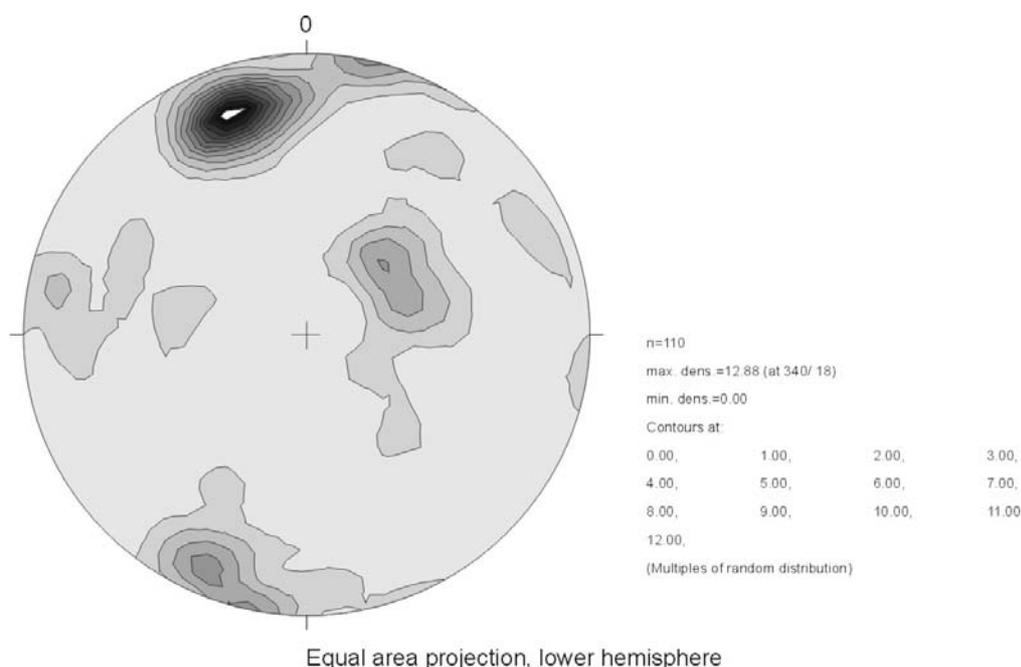


Figure A-23: Contoured poles to all fractures in outcrop (file: 6844-02a.jpg).

Mean Trend	Mean Plunge	Angle long axis (°)	Angle short axis (°)	Mrd max.	Comment
340	18	36	31	12,88	Foliation parallel
203	12	35	29	4,7	
48	60	74	38	4,2	
284	12	44	28	2,4	

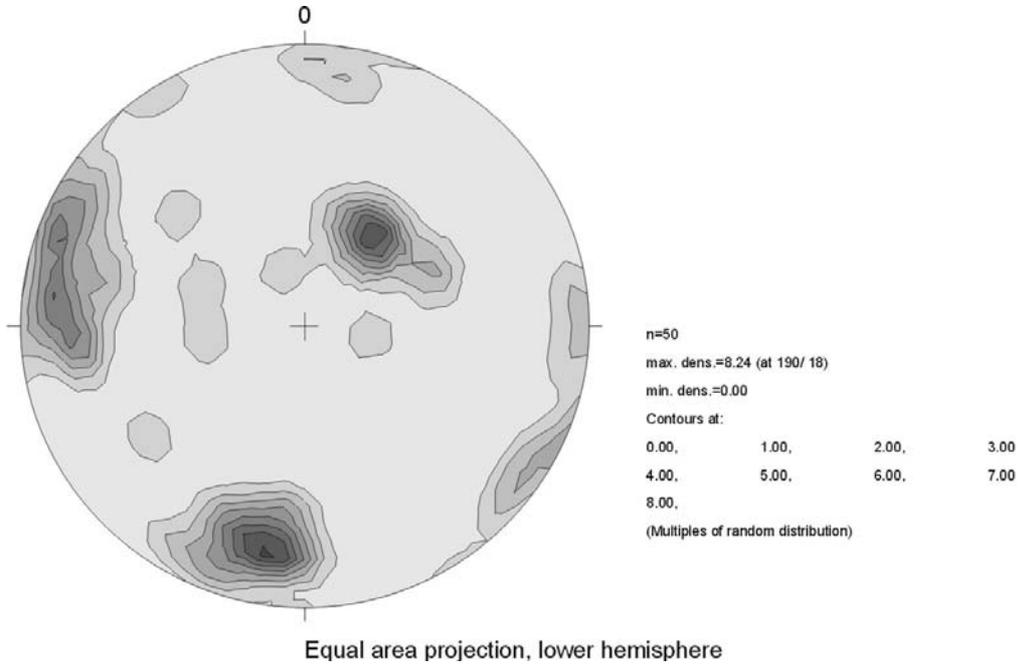


Figure A-24: Contoured poles to all fractures in outcrop (file: 6844-02b.jpg).

Mean Trend	Mean Plunge	Angle long axis (°)	Angle short axis (°)	Mrd max.	Comment
190	18	38	32	8,24	Foliation parallel
36	58	48	32	7,7	
277	12	55	53	6,1	

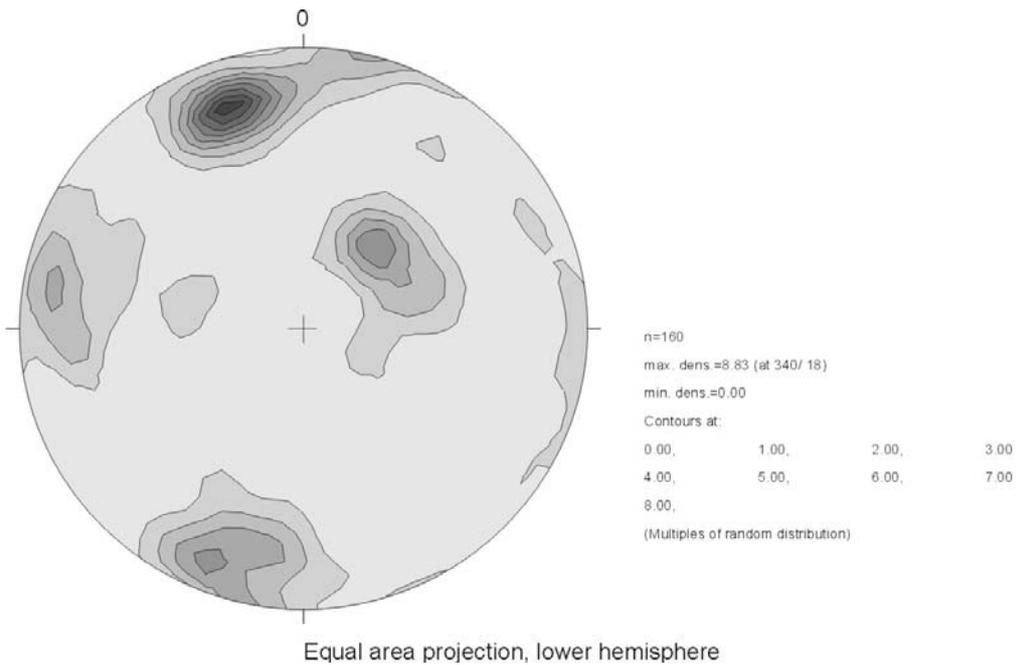


Figure A-25: Contoured poles to all fractures in outcrop (file: 6844-02.jpg).

Mean Trend	Mean Plunge	Angle long axis (°)	Angle short axis (°)	Mrd max.	Comment
340	18	31	28	8,83	Foliation parallel
42	59	54	30	4,9	
203	11	28	27	4,4	
279	11	51	48	3,4	

6844-02a: The dominant fracture population trends ENE-WSW with steep SSE dips. This set has the most consistent orientations. Most planes are straight and relatively smooth. They often occur in swarms of several fractures spaced at about 10-20cm and are traceable over up 1 meter. A secondary population in this concentration trends WNW-ESE and dips steeply NNE. It is parallel to the foliation, which is often hard to identify. In places where the foliation is well visible these fractures are relatively abundant, 10-50cm long and spaced at 0,3-0,5m.

The gently to moderately SW dipping sets could be related to unroofing. However, some of these planes are heavily fractured or brecciated suggesting that there was at least one phase of shearing motion along them. These subhorizontal fractures are usually 0,5-1m long and spaced at about 10-20cm. Compared to 6844-02b the steeply E to ESE dipping is only of minor importance.

Many planes are opened up by weathering, which does not allow any statements on fracture apertures and introduces noise into orientation measurements. One fold axis (284b24) was measured. No offsets or kinematic indicators were found.

6844-02b: In addition to the observations made in 6844-02a the following are of special interest:

- The gently to moderately SW dipping fractures are spaced at about 40cm
- The steeply ESE dipping fractures are spaced at 20-40cm.
- The foliation parallel fractures are highly variable in size and density.
- Compared to 6844-02a the location possesses a relatively strong subvertical NNE-SSW trending fracture population. This could identify a fault zone going through this part of the outcrop. However, no offsets or kinematic indicators were found.

Regen between Schönau & Gumpenried, ca. 500 SSE of Wurz, Outcrop ID: 6943-04

Rock Type: Körnelgneis (bgn, GK25); Gneiss with large K-feldspar phenocrysts oriented along their c-axis (foliation parallel?).

Outcrop: GK: 457114E 543752N; UTM: 351921E 5437326N
The outcrop extends about 40 paces WNW-ESE and is 6-8m high. Almost all planes are covered with dirt, lichen, and moss and are strongly weathered.

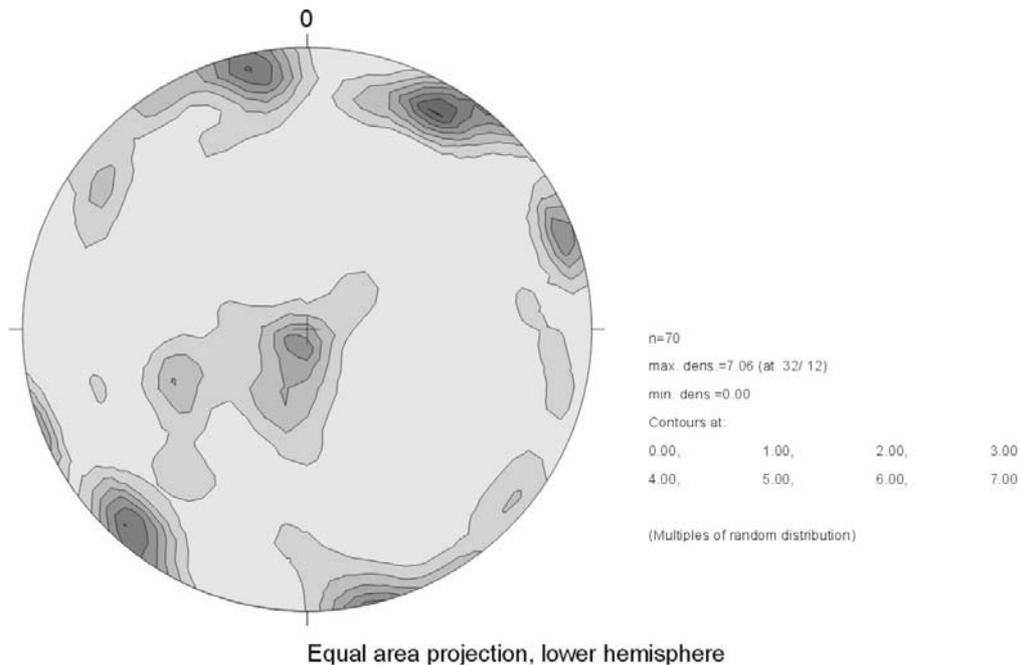


Figure A-26: Contoured poles to all fractures in outcrop (file: 6943-04.jpg).

Mean Trend	Mean Plunge	Angle long axis (°)	Angle short axis (°)	Mrd max.	Comment
32	12	60	27	7,06	
347	5	70	41	6,1	
69	5	26	24	4,9	
188	84	35	19	4,6	Foliation parallel?

The dominant fracture population in this outcrop trends WNW-ESE with subvertical dips. Fractures in this set form the face of the outcrop and possess the largest planes (up to several meters in diameter). Planes are relatively smooth and are believed to have formed by shearing motion. Spacings of meter-sized fractures in this set are 1-2m. In the field the ENE-WSW trending set was thought to belong to the same population, but turns out to be a separate concentration on the stereoplot. Planes in this population are also generally meter-sized. Other physical parameters were not recorded for this set.

Fractures of the steeply dipping NNW-SSE trending family frequently occur in zones with spacings of 10-15cm. Fractures in these zones possess trace lengths of several meters. Apertures are generally low, although some fractures were up to 5cm opened by weathering.

The gently to moderately NNE dipping set seems parallel to the orientation of the c-axis of the K-feldspar crystals, and was therefore determined to be parallel to the foliation. However, other considerations are an origin as thrust faults or unroofing joints. Shear displacement must have occurred along these fractures, since many of them exist as zones of dense fracturing/brecciation (up to 50cm wide). Single fractures are common as well. Both kinds are usually traceable over several meters, some fractures/zones cut the entire outcrop. Spacings of major discontinuities in this set are variable and range from 0,4 to 1m. Due to its gentle dip the population is most likely undersampled.

One low angle fracture (16f4, Freiburger) exposes an apparent 7cm reverse offset of a subvertical one (354f85, Freiburger), which is cut by a subvertical NNW-SSE trending fracture (248f85, Freiburger). This gives the following possible sequence of events: 1) motion along 354f85 2) motion along 248f85 3) reverse motion along 16f4 (all values are Freiburger measurements). The last phase of displacement in this sequence would have been thrust faulting due to a north-southerly compression. This assumption is also supported by the presence of breccia along gently NNE dipping fractures.

One large plane (traceable <7m) cuts the entire outcrop and seems to be associated with R-shears suggesting normal motion due to an east-westish crustal extension.

Regen between Schönau & Gumpenried, ca. 400 SE of Wurz, Outcrop ID: 6943-05

Rock Type: Körnelgneis (bgn, GK25), similar to 6943-04

Outcrop: GK: 457114E 543779N; UTM: 351934E 5437586N

The outcrop extends about 120 paces in WNW-ESE direction. The exposure is separated into 2 blocks (53 and 40 paces wide) separated by a ca. 27 paces wide zone of unconsolidated material/soil). The outcrop is 4-8m high. Most planes are covered with moss and lichen. Fractures were measured in the WNW (53 paces wide) block.

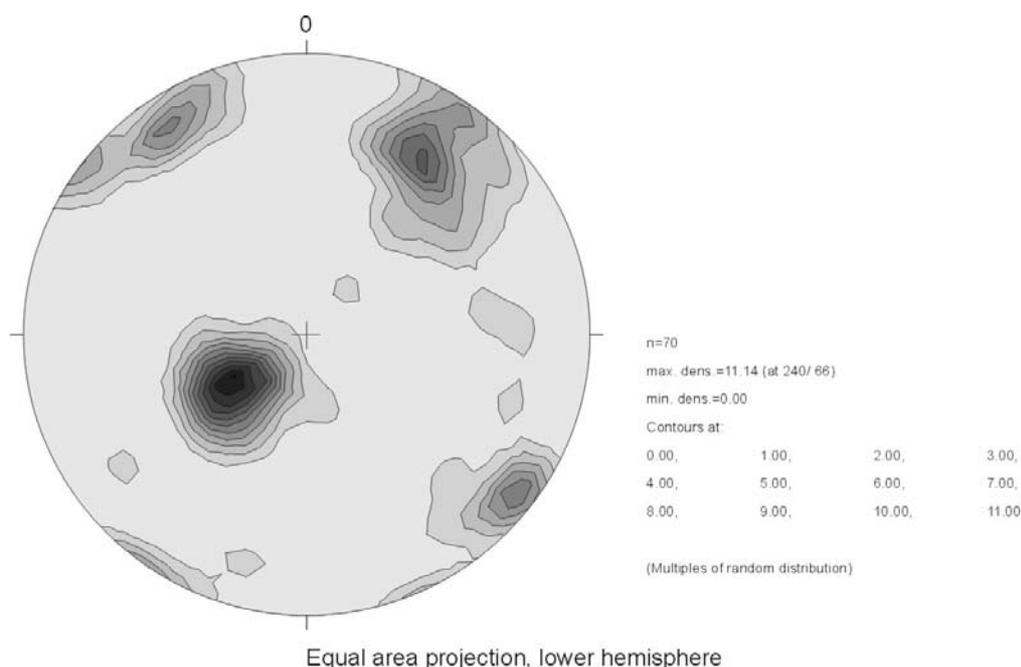


Figure A-27: Contoured poles to all fractures in outcrop (file: 6943-05.jpg).

Mean Trend	Mean Plunge	Angle long axis (°)	Angle short axis (°)	Mrd max.	Comment
240	66	51	45	11,14	Foliation parallel
33	26	68	44	7,2	
128	7	23	21	5,8	
327	12	24	15	5,5	

Both the foliation parallel and the steeply SSW to SW dipping fractures are the dominant sets. Foliation parallel fractures are generally traceable over more than 1m (up to several meters, cutting the entire outcrop). They are densely spaced (ca. 5-10cm), but mainly closed. Foliation parallel fractures with larger apertures (>1cm) and planes (>2m in diameter) occur every 2m. Breccia along foliation parallel planes suggest shear motion.

The moderately to steeply dipping WNW-ESE trending fractures frequently possess rough and wavy planes. Spacings and apertures could not be determined for this population.

Several large subvertical NE-SW trending fractures were found especially in the WNW block of the outcrop. They are several meters in diameter and spaced at 2-3m. They frequently possess large apertures or occur as swarms/brecciated zones. Single planes are straight, clear-cut and relatively smooth. Some accessory fractures in the planes could be interpreted as synthetic Riedel shears suggesting normal motion. One large NE-SW fracture (308f84, Freiburger) is apparently offset by foliation parallel fractures, suggesting sinistral strike-slip along the fractured foliation. The cumulative left-lateral displacement along four foliation parallel fractures is about 40cm. However, the

entire outcrop might have shifted due to gravitational creep. Thus, this strike-slip could have been the result of this creep, although the shear sense is roughly normal to the gravitational potential.

No slickensides or mineral lineations were found in this location.

Regen, Railroad tracks ca. 400m NE of Schnitzmühle, Outcrop ID: 6943-06

Rock Type: Pergneis (gnp, GK25); Weakly foliated granitic gneiss with round plagioclase crystals 1-2mm in diameter

Outcrop: GK: 456723E 543750N; UTM: 348014E 543745N
The exposure extends about 85 paces WNW-ESE (in a curve of the railroad tracks) and is ca. 6m high. Most planes are covered with moss and lichen.

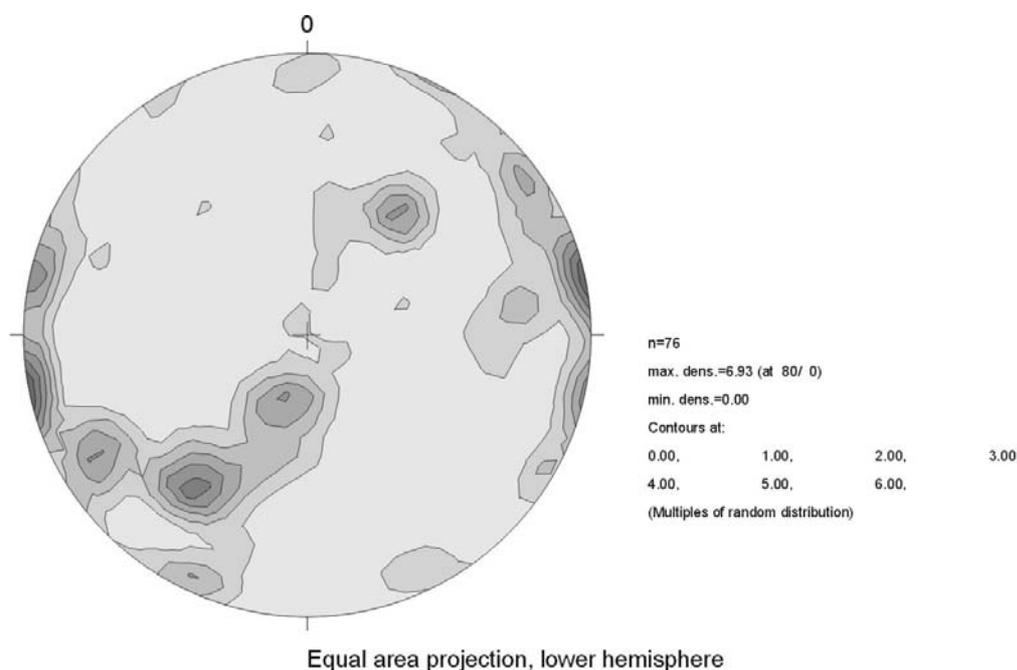


Figure A-28: Contoured poles to all fractures in outcrop (file: 6943-06.jpg).

Mean Trend	Mean Plunge	Angle long axis (°)	Angle short axis (°)	Mrd max.	Comment
80	0	20	12	6,93	
216	31	26	16	5,4	
281	1	14	12	4,4	
36	47	46	21	4,1	
240	14	15	11	4,1	
199	70	17	12	4,1	
205	6	13	10	3,1	

The dominant fracture system in this location trends in north-southerly directions with steep to subvertical dips. However, this population becomes only dominant about 35 paces WNW from the ESE end of the outcrop. Fractures are mostly closed or possess low apertures and are smooth (even look polished). Many fractures are traceable over several meters (some cut the entire outcrop). They usually occur in swarms in which they are spaced about 0,5-1m.

Steep to subvertical fractures form the face of the outcrop and are the second most important set in the exposure. At the ESE end of it, where N-S fractures are virtually absent they are the

dominant population. Planes usually are meter-sized. Spacings and apertures could not be determined.

Two concentrations of low angle fractures are present in this location. One dips gently NNE, the other dips moderately SW, intersecting each other. They are traceable over tens of meters and frequently brecciated, thus suggesting a shearing event along these planes. Some gently NE dipping planes might be parallel to the weak foliation. Spacings of major fractures or brecciated zones are about 1m.

One fracture (22f47, Freiburger) was interpreted as a major fault with about 50cm of weathered gouge and breccia. Another one (20f23, Freiburger) also shows an about 10cm wide zone of breccia. Other kinematic indicators were not found in this location.

Altneußberg, Burgruine, Outcrop ID: 6943-07

Rock Type: Körnelgneis (bgn, GK25). Weakly foliated granitic gneiss with up to 3cm long K-feldspar crystals, frequently oriented along their c-axes.

Outcrop: GK: 457072 E 543638 N
The outcrop consists of several small exposures around the castle area. They will be described individually.

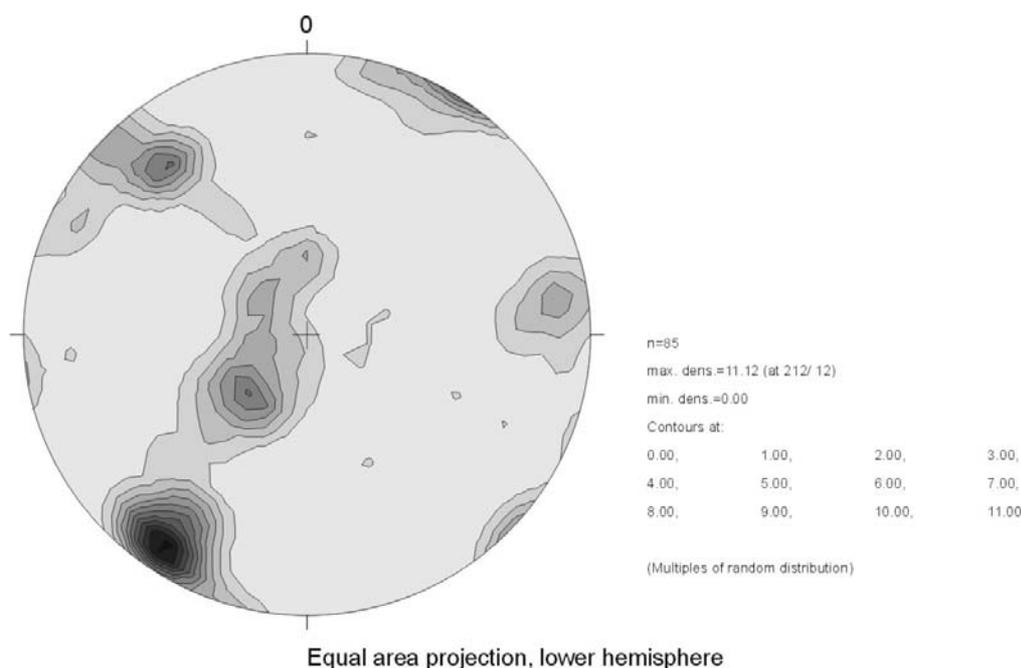


Figure A-29: Contoured poles to all fractures in outcrop (file: 6943-07.jpg).

Mean Trend	Mean Plunge	Angle long axis (°)	Angle short axis (°)	Mrd max.	Comment
212	13	39	38	11,12	Maybe foliation parallel
225	66	66	28	6,2	
322	24	60	25	6,2	
83	12	39	27	3,7	

6943-07a: The exposure is located at the E wall of the castle. It extends about 20 paces NNW-SSE, facing E and is about 1m high. All fracture planes are weathered and covered with moss and lichen. In the field the foliation parallel fractures were determined to be the dominant set.

Fractures possess the largest planes (1-4m in diameter) and apertures (some are 1-2mm open) and are spaced at about 5-10cm. Their orientations are irregular, thus intersecting each other. Due to their gentle dips they are most likely undersampled. Thus, the steeply dipping, WNW-ESE trending set is dominant in the stereoplot.

Fractures in this WNW-ESE population possess meter-sized, smooth planes. They occur in swarms in which they are spaced at 10-50cm. Fractures are generally closed to <1mm open. Minor fractures in large planes seem to be arranged in a synthetic Riedel array, thus suggesting sinistral strike-slip due to NW-SE compression.

Few subvertical fractures with large planes trend NE-SW. Another minor concentration consists of subvertical, N-S trending fractures.

No slickenlines or mineral lineations were found.

6943-07b: The outcrop is located at the S-wall of the castle. It extends 17 paces WNW-ESE, facing SSE and is ca. 7m high. In this location the foliation is hard to identify. It is more or less subhorizontal and mainly represented by oriented K-feldspar crystals (parallel to their c-axis). Subhorizontal fractures are the dominant system in this location. They occur as 10-30cm wide brecciated zones or single planes ranging from centimeters to meters in size. Planes are generally traceable over several meters and opened up (which could have been caused surficially by weathering). Spacings of smaller (generally <1m trace) fractures are 25-50cm in the lower part of the outcrop and 5-10cm in the top 3m of the exposure. Large planes (several meters trace) and brecciated zones are spaced at about 1-2m.

Other fracture populations WNW-ESE and NE-SW. they are irregularly spaced and possess generally straight planes. Several foliation parallel fractures are offset (10cm, normal displacement) along a steeply SE dipping fracture (144f66, Freiburger). However, others show no offset along the same plane. One fracture (37f80, Freiburger) shows small steps in its plane, which were interpreted as R-shears suggesting sinistral strike-slip due to E-W compression. One steeply SSW dipping fracture (207f74, Freiburger) forms the face of the exposure. Patches of polished quartz-feldspar mineralizations were found on its plane.

6943-07c: The exposure is located at the W wall of the castle. It extends about 23 paces NNE-SSW, facing E, and is up to 5m high. Gently NNE dipping fractures (most likely parallel to the foliation) are the dominant system. Fractures frequently occur as ca. 10cm wide zones of breccia or densely spaced fractures (<1cm spaced) suggesting an origin as shear zone. The zones are spaced at about 0,5-1m and are traceable over several meters. Minor fractures of this population are <1m long and are spaced on a dm scale.

The face of the outcrop (ca. 20x5m) was identified as outcrop-scale fault (partly silicified, 1-2mm thick qtz-fsp coating), trending NE-SW with a steep SE dip.

Moderately to steeply W dipping fractures occur as discrete, straight planes spaced at about 1-1,5m. Steeply SSW dipping fractures were determined to be the least important in this location. They occur as discrete fractures, some slightly brecciated, and are very irregularly spaced (>2m). Moderately to steeply NE dipping fractures are partially silicified. Where they are gaping <1cm long euhedral quartz crystals are visible, thus suggesting the absence of shear after the silicification event. However, some fractures in this set show brecciation, which either happened before the silicification, of shear reactivated this set only partially. Major fractures in this set are spaced at 1-1,5m. Many cut the entire exposure and contain moss and grass. Minor fractures (<1m trace length) have spacings of about 0,5m and are up to 1mm open.

Böbrach/Haidenberg (ca. 1km SW of Bärenloch, right bank of Regen), Outcrop ID: 6944-09

Rock Type: Perliger Cordierit-Sillimanit Gneis (cgnp, GK25). Foliated gneiss. Layers of biotite interspersed with qtz-fsp layers

Outcrop: GK: 457489 E 543339 N; UTM: 355512 E 5433040 N
The outcrop consists of several small exposures along a freshly-cut dirt road. They will be described individually.

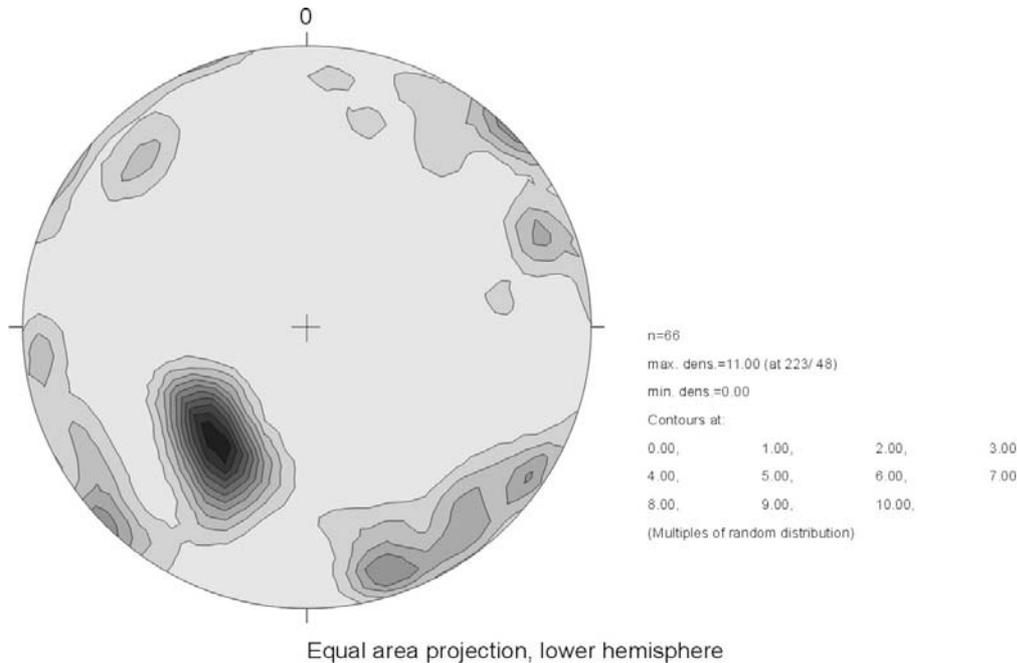


Figure A-30: Contoured poles to all fractures in outcrop (file: 6944-09.jpg).

Mean Trend	Mean Plunge	Angle long axis (°)	Angle short axis (°)	Mrd max.	Comment
223	48	45	30	11,00	Foliation parallel
162	11	66	36	4,8	
226	1	34	19	4,5	
263	6	17	16	3,8	
316	19	24	20	2,9	

6944-09a: The exposure extends about 5m E-W and is ca. 3m high, facing S. Most planes look fresh with no or insignificant moss/lichen overgrowth. However, many planes are covered with sand and dirt. Most foliation parallel fractures are strongly oxidized.

The dominant population consists of fractures parallel to the moderately NNE dipping foliation. Individual planes are generally rough and wavy and are highly irregular (cm to m-sized) in their sizes. Spacings of smaller fractures range from 1-5cm. Irregularly spaced brecciated/densely fractured zones exist as well, thus suggesting shear along the foliation.

The second most important set trends ENE-WSW (parallel to the river valley). In the field they were determined to be right-lateral strike-slip faults (see below). They possess relatively large (up to 1m trace length) and strongly slickensided, sometimes oxidized planes. Spacings are irregular but were estimated to average around 0,5m.

N-Sish trending fractures are insignificant in this exposure. Trace lengths are <0,5m and apertures are 1-2mm (probably induced by slight gravitational shifting of the entire outcrop).

6944-09b: The exposure is located about 20 paces WSW of 6944-09a. It is ca. 4m wide and 2m high, facing SSE. Most planes are oxidized.

In this exposure foliation parallel fractures were found to be relatively unimportant. Clear fractures are spaced at 10-50cm and are usually not brecciated. Trace lengths are <40cm. In the field subvertical NE-SW and NW-SE trending fractures were determined to be dominant in this location. They are closed or possess very low apertures. Trace lengths are up to 1m. Planes are straight and smooth; many of the NW-SE set are subvertically and subhorizontally slickensided (see below). Spacings in this set average around 0,5m.

6944-09c: This exposure is located about 55 paces ESE of 6944-09b, is discontinuous (ca. 10m wide) and 1-1,5m high. It faces SSE.

In this location foliation parallel fractures are the most abundant set, although their planes are generally short, rough (ca. 10cm trace length) and discontinuous. Spacings are locally 3-5cm. Many planes are oxidized. The central part of this outcrop is very compact, so fractures parallel to the foliation exist mainly at the edges of the exposure. One foliation parallel fracture is enveloped by an abrupt and significant reduction in grain size (from ca. 1mm to ca. 150µm) thus suggesting a cataclastic deformational mechanism acting on the foliation prior to purely brittle deformation.

Cross cutting fractures in this exposure trend NW-SE and NE-SW with subvertical dips. Due to the small size of the outcrop fracture sizes, spacings and apertures could not be described with confidence. Most fractures in these populations are straight and relatively smooth with frequently oxidized planes.

Several interesting kinematic indicators were detected in the form of slickenlines. They occur in two populations (subhorizontal and subvertical) on NE-SW and NW-SE trending fractures. Subvertical slickenlines were found only on one fracture (84f85 (-82), Freiburger), together with subhorizontal ones. However, neither their shear sense nor their age relative to the subhorizontal lineations could be determined.

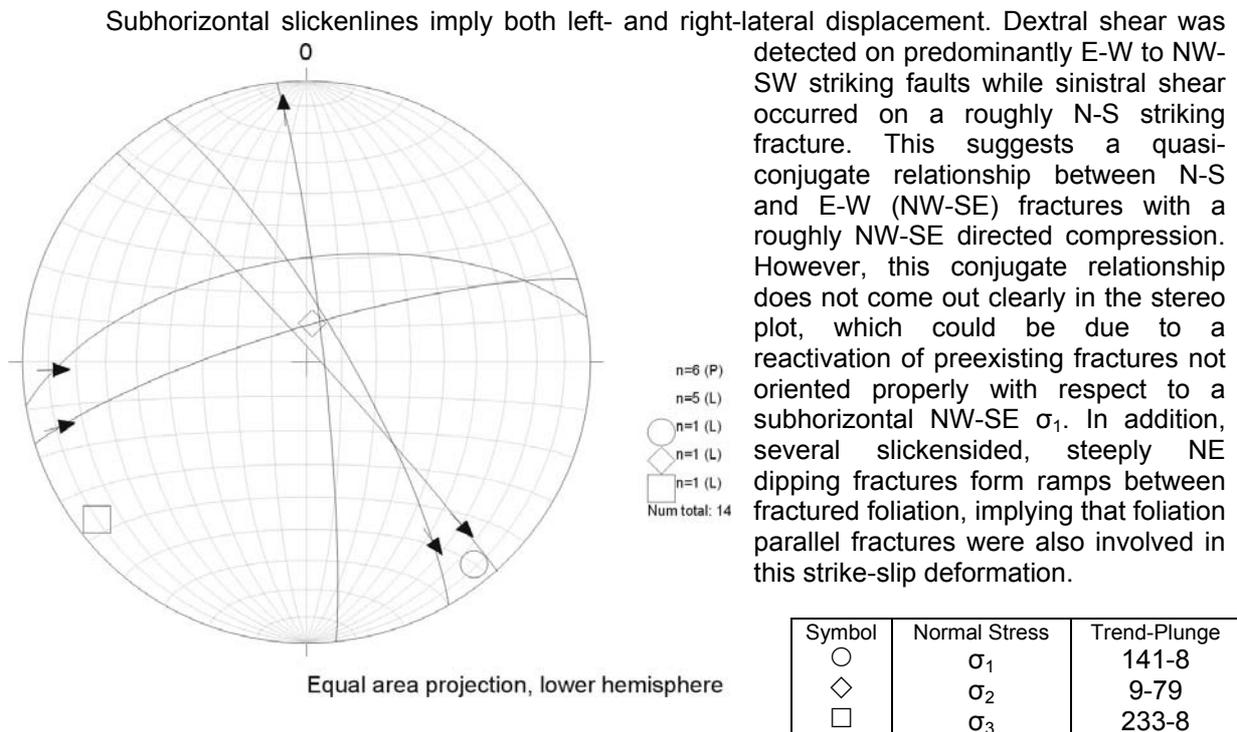


Figure A-31: Slickensided planes (where shear sense was obvious) in location 6944-09.

Böbrach, Hubertushof, Outcrop ID: 6944-10

Rock Type: Pegmatite vein in gneissic rock (granite in GK25)

Outcrop: GK: 457647 E 543672 N; UTM: 357213 E 5436308 N
The outcrop is located in an old pegmatite (quartz) quarry and extends 23 paces NE-SW, of which 10 paces are in man-made cave. Inside the cave the exposure is 6-7m high, outside ca. 3m. Most planes inside the cave are wet. Outside most planes are oxidized and covered with moss and lichen.

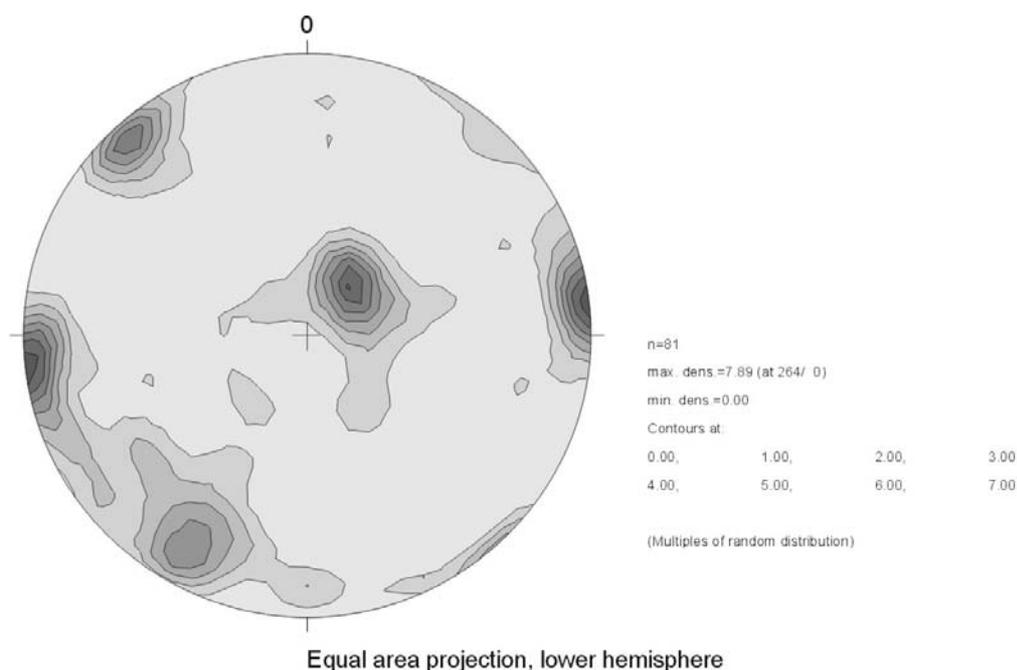


Figure A-32: Contoured poles to all fractures in outcrop (file: 6944-10.jpg).

Mean Trend	Mean Plunge	Angle long axis (°)	Angle short axis (°)	Mrd max.	Comment
264	0	47	30	7,89	
40	72	59	69	7,1	
317	6	35	29	5,9	
208	14	42	34	4,9	

Although the subvertical N-S trending population is dominant in the stereo plot the low angle fractures (mrd max. at 40-72) were determined to be dominant in the field, since they possessed the largest planes (traceable over several meters), high densities and breccia zones (spaced at ca. 1 m).

The N-S trending fractures frequently occur in swarms and are irregularly spaced. Some planes in this population are associated with Riedel shears suggesting high angle normal motion. Smaller fractures (which also occur as subvertical NW-SE fractures) possess relatively smooth and straight planes. They are closed or have very low apertures. The two populations (trending N-S and NW-SE) could be in a conjugate relationship, suggesting subhorizontal NNW-SSE compression and ENE-WSW extension.

The subvertical NE-SW trending set is parallel to the pegmatite-gneiss contact (the country rock was mapped as granite, but was identified as gneissic rock in the field). Fractures in this concentration are few, but relatively large (traceable over several meters).

No offsets or kinematic indicators were found in this location.

Bodenmais, Silberberg, Parking lot, Outcrop ID: 6944-11

Rock Type: Foliated migmatitic gneiss, hydrothermally altered; GK25: Körnelgneiss (bgn)

Outcrop: GK: 458181 E 543652 N; UTM: 362539 E 5435895 N
The outcrop extends 27 paces N-S, facing W and is ca. 5m high. Almost all planes are rusty.

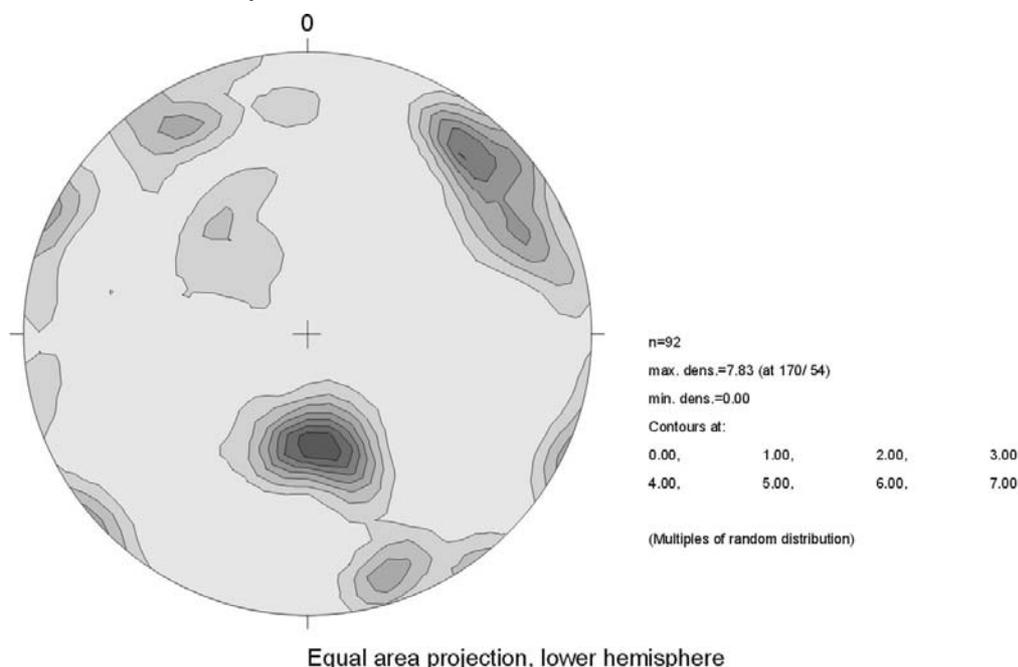


Figure A-33: Contoured poles to all fractures in outcrop (file: 6944-11.jpg).

Mean Trend	Mean Plunge	Angle long axis (°)	Angle short axis (°)	Mrd max.	Comment
170	54	40	28	7,83	Foliation parallel
41	18	61	40	6,0	
161	12	20	17	3,8	
330	18	26	18	3,4	
295	1	36	22	3,4	
322	48	42	32	2,3	

In terms of abundance the dominant fracture set in this location is parallel to the gneissic foliation. Planes in this population are relatively small, possibly due to small-scale folding. Some larger discontinuities exist as brecciated/gougy zones, suggesting motion along foliation parallel fractures. They possibly form a conjugate set with the gently to moderately SSE dipping fractures, thus suggesting NNW-SSE directed compression. Spacings of foliation parallel fractures are very irregular. Small fractures are spaced on a cm-scale, larger ones at 0,5-1m.

Subvertical NW-SE striking fractures have the largest planes in the outcrop (several meters in diameter) and are spaced at about 0,5m. Patches of rusty ore (limonite?) were found predominantly on the NW-SE striking fractures. Planes in this set are mainly smooth and straight.

The subvertical NNE-SSW to NE-SW trending fractures possess sometimes rough, and slightly smaller planes than the NW-SE ones. These fractures occur in irregularly spaced swarms (spacings in the swarms are about 10cm).

The gently to moderately SE dipping fractures frequently occur in brecciated zones. Spacings could not be determined. They are assumed to be in a conjugate relationship with foliation parallel fractures. In one gougy/brecciated zone small accessory fractures are oriented at an acute angle to the main fracture plane and were interpreted as R-shears indicating reverse/thrusting motion.

No offsets or slickenlines were found in this location.

Liebestal, N-outcrop, Outcrop ID: 6943-08

Rock Type: Granitic rock with mostly felsic/white minerals and flakes of biotite (GK25: Kristallgranit) in contact with Körnelgneis (bgn). The granite is interspersed with lenses of Körnelgneis, thus suggesting that country rock was incorporated in the granite body or that the granite intruded in lenses parallel to the gneissic foliation.

Outcrop: GK: 456685 E 543667 N; UTM: 347599 E 5436632 N
The outcrop extends 31 paces NW-SE and is ca. 5m high, facing SW. Most planes are covered with moss and lichen.

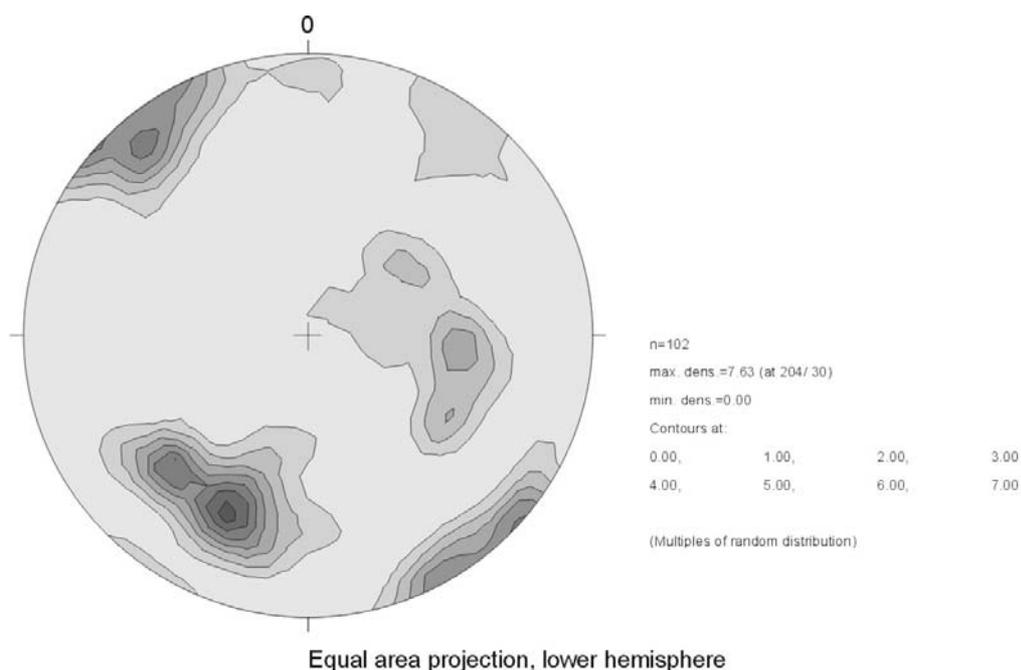


Figure A-34: Contoured poles to all fractures in outcrop (file: 6943-08.jpg).

Mean Trend	Mean Plunge	Angle long axis (°)	Angle short axis (°)	Mrd max.	Comment
204	30	65	52	7,63	Parallel to fabric in the granite?
319	11	51	47	5,5	
95	46	64	30	3,7	

The dominant fracture system in this location is difficult to determine, since fracture spacings are highly irregular in all sets. In the field, gently to moderately dipping fractures in general were determined to be dominant. In the stereo plot the highest density occurs in the gently to moderately NNE dipping fractures. Planes in this set –generally rough and undulatory- can reach trace lengths of >1m and spacings of 0,5-1m. These fractures are also suspected to have formed along a preexisting fabric in the granite (the gneissic foliation in the country rock dips more gently than the granitic fabric), which consists of oriented axes of feldspar crystals. Contacts between gneiss and granite were measured as 17-66 and 22-63 (Freiberger measurement). Thus, the fabrics are unrelated and cannot be attributed to on single tectonic event.

The subvertical NE-SW striking fractures show the second highest density in the stereo plot. They possess very smooth, sometimes polished and oxidized, planes with trace lengths of >1m. Spacings of larger (>1m) planes are about 1-2m and sometimes occur as swarms. Smaller fractures are irregularly spaced (maybe on a dm scale?). One fracture in this population (138f77, Freiberger) contains faint oblique slickenlines (+55) and steps at right angles to the lineations in the plane. In the field the steps could not be characterized with certainty. They are either R-shears, which would

suggest oblique reverse (NW-SE compression), or terminations of slickenlines, suggesting normal motion (uplift and NW-SE extension).

Subvertical fractures of other sets (e.g. NW-SE striking) are mostly rough and undulatory with irregular spacings (fractures >1m spaced at >1m). Larger fractures can reach trace lengths of >1-2m.

Gently to moderately fractures are frequently densely fractured and brecciated. Conjugate relationships between cross-cutting and fabric parallel fractures are possible. This would suggest subhorizontal compression in a roughly NE-SW direction. One moderately dipping densely fractured zone (276f47) cuts across the granite-gneiss contact and causes no visible offset.

Liebestal, near N-end of clearing, Outcrop ID: 6943-09

Rock Type: Körnelgneis (GK25: bgn)

Outcrop: GK: 456699 E 543663 N; UTM: 347749 E 5436603 N
The outcrop extends ca. 80 paces NNW-SSE and is up to 6m high, facing WNW. Measurements were taken within 20 paces of SSE end (least weathered part). Most planes are weathered and covered with moss and lichen.

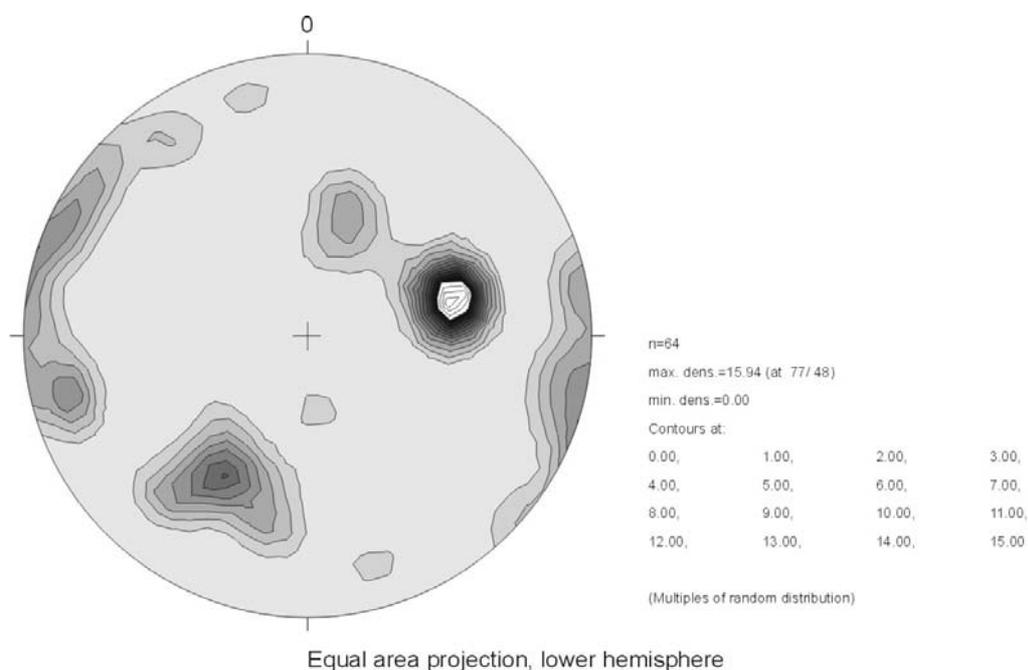


Figure A-35: Contoured poles to all fractures in outcrop (file: 6943-09.jpg).

Mean Trend	Mean Plunge	Angle long axis (°)	Angle short axis (°)	Mrd max.	Comment
77	48	30	30	15,94	
210	42	44	37	7,2	
255	12	83	38	4,7	

The dominant fracture systems trend WNW-ESE to NNW-SSE. Spacings of major fractures (>1m trace) can be as close as 10cm. Many fractures in this set are closed, but some occur in densely spaced/brecciated zones. Some very large, rough, and undulatory (>4m trace) fractures with NW-SE strikes are slightly open and brecciated. In the field they were interpreted as valley parallel faults, although no other kinematic indicators were not found.

Subvertical fractures in this location almost continuously trend NNW-SSE to NE-SW. They mostly occur in swarms in which fractures are spaced at 10-20cm. Spacings between swarms are highly irregular (can be up to 4m). Planes of individual fractures are mostly smooth and look polished. Trace lengths of individual fractures are about 1m. Small breccia zones sometimes occur within densely fractured swarms. Few of the swarms cut the entire outcrop, are brecciated, and contain moss and plants.

Foliation is assumed to dip moderately NNE, although only few foliation parallel fractures were found. No kinematic indicators were detected in this location.

Böbrach, Bodenmaiser Straße, E-End of village, Outcrop ID: 6944-12

Rock Type: Gneissic rock with feldspar porphyroblasts several centimeters in diameter. The rock possesses a well-developed foliation. No folding is visible. The entire rock is sprinkled ca. 2mm feldspar „pearls“. The outcrop is mapped (GK25) as „metatektischer bis anatektischer Cordierit-Sillimanit Gneis (cgj)“, but macroscopically fits better the description of the adjacent unit („perliger Cordierit-Sillimanit Gneis, cgnp).

Outcrop: GK: 457606 E 543600 N; UTM: 356780 E 5435608 N
The outcrop extends about 31 paces NW-SE, facing SW. It is ca. 2m high. Most planes are covered with moss and lichen. Many planes are rusty, most likely from surficial runoff.

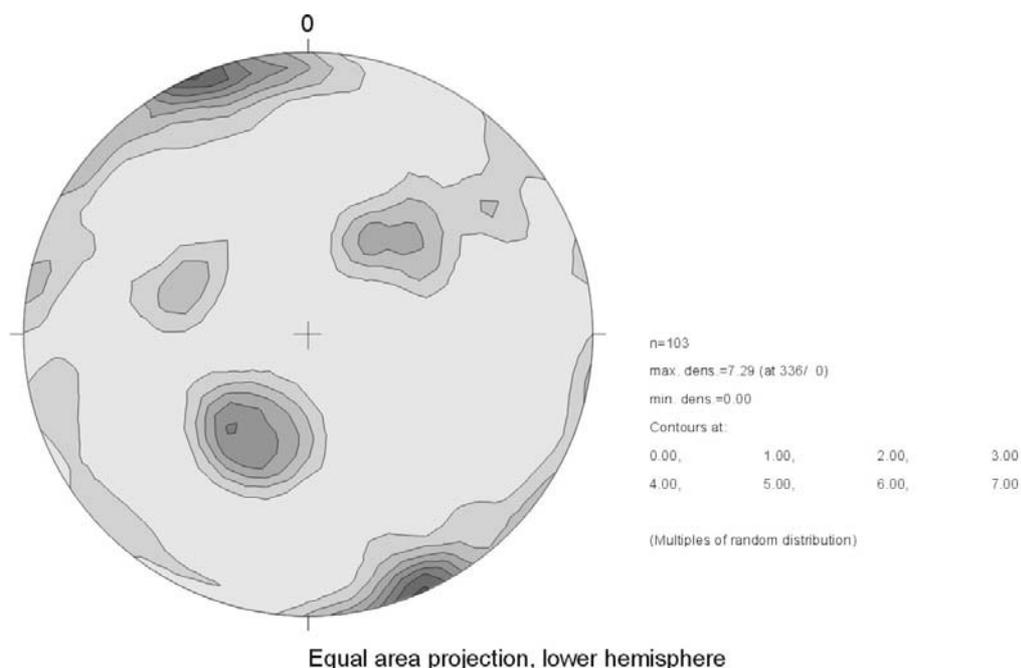


Figure A-36: Contoured poles to all fractures in outcrop (file: 6944-12.jpg).

Mean Trend	Mean Plunge	Angle long axis (°)	Angle short axis (°)	Mrd max.	Comment
336	0	65	35	7,29	Foliation parallel
219	55	41	37	5,1	
40	55	28	17	3,6	
291	53	31	20	2,8	
281	3	10	7	2,2	

In the field, the dominant system was determined to be parallel to the foliation, although the stereo plot identifies the subvertical ENE-WSW striking population as the most abundant. Foliation

parallel fractures are spaced at 5-10cm (fractures with trace lengths <40cm) and at 0,4-0,5m for fractures with trace lengths >40cm. They often occur as densely fractured/brecciated zones or as single fractures with surficial apertures of about 1mm. Foliation parallel planes are mainly rough and bumpy. Few smooth ones exist.

Subvertical fractures trend predominantly ENE-WSW, although many fractures also strike more in north-southerly directions. These fractures are irregularly spaced (usually >1m) and often occur in swarms, in which fractures are spaced at 10-30cm. Planes are relatively rough and many trace <1m; few cut the entire outcrop (>2m trace length). The larger fractures are frequently gaping and associated with brecciated zones, gouge, soil, and moss. Some more moderately inclined fractures of this set (dipping 60°-70°) connect foliation parallel fractures. Some swarms of moderately ESE dipping fractures cut the entire outcrop. The swarms are spaced at 3-4m. Some are brecciated, others have single, smooth planes.

In the field, the set of gently to moderately SSW dipping fractures was assumed to be conjugate to foliation parallel fractures. Planes trace several meters and are spaced at 0,5-1m. Some slickensided planes were found. One subvertical NNE-SSW striking fracture contains two sets of lineation. Dip-parallel (+89) lineations lie on top of gently raking (+10) ones. They suggest reverse motion due to moderately inclined WNW-ESE compression (could be uplift-related) and right-lateral strike slip due to subhorizontal NE-SW compression, respectively. Another dip-parallel lineation (-80) was found on a moderately ESE dipping (117f36, Freiberger) fracture. Sense of motion could not be determined.

Another interesting feature was found in the form of an abrupt grain-size reduction (from ca. 1mm to 250-350µm) along a foliation-parallel fracture (43-36, Freiberger). The zone of reduced grain-size is about 2cm wide and exposes a salt'n pepper structure. It was interpreted of a mylonitized zone, which was later preferentially fractured as a preexisting zone of weakness.

Viechtach, Liebestal, near bridge, Outcrop ID: 6943-10

Rock Type: Körnelgneis (bgn, GK25). C-axes of K-feldspar crystals seem parallel to the foliation. Some concordant bands of (foliated?) granite.

Outcrop: GK: 46716 E 543623 N; UTM: 347896 E 5436188 N
The outcrop extends about 57 paces N-S and is up to 4m high. Many planes are covered with moss and lichen.

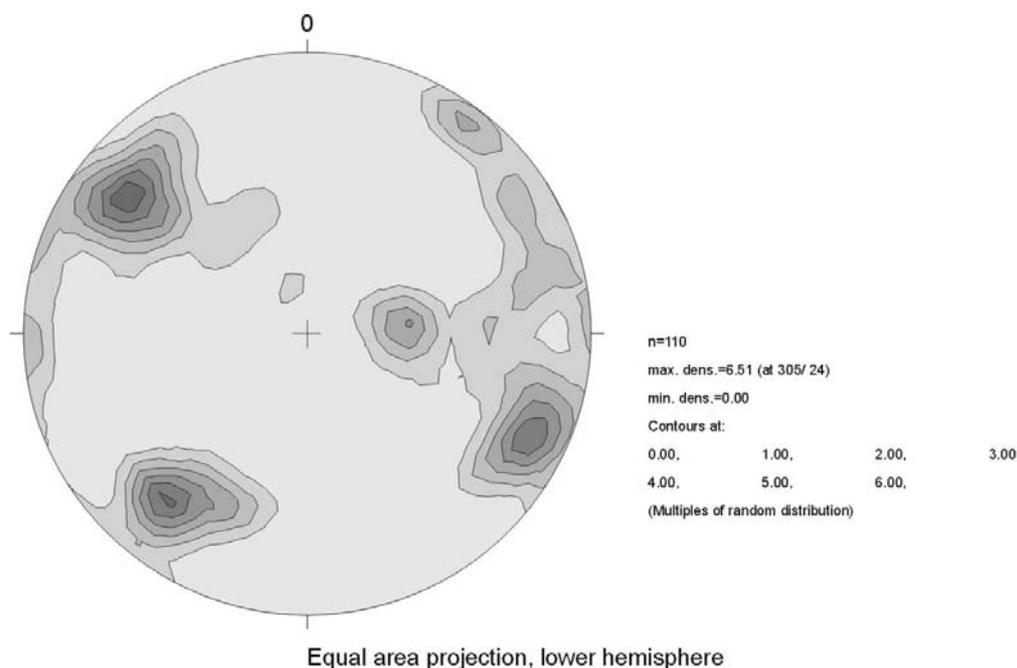


Figure A-37: Contoured poles to all fractures in outcrop (file: 6943-10a.jpg).

Mean Trend	Mean Plunge	Angle long axis (°)	Angle short axis (°)	Mrd max.	Comment
305	24	39	33	6,51	Foliation parallel
218	24	33	33	6,3	
115	13	25	23	5,8	
85	61	20	17	4,2	Unroofing Joints?
38	7	17	14	3,2	

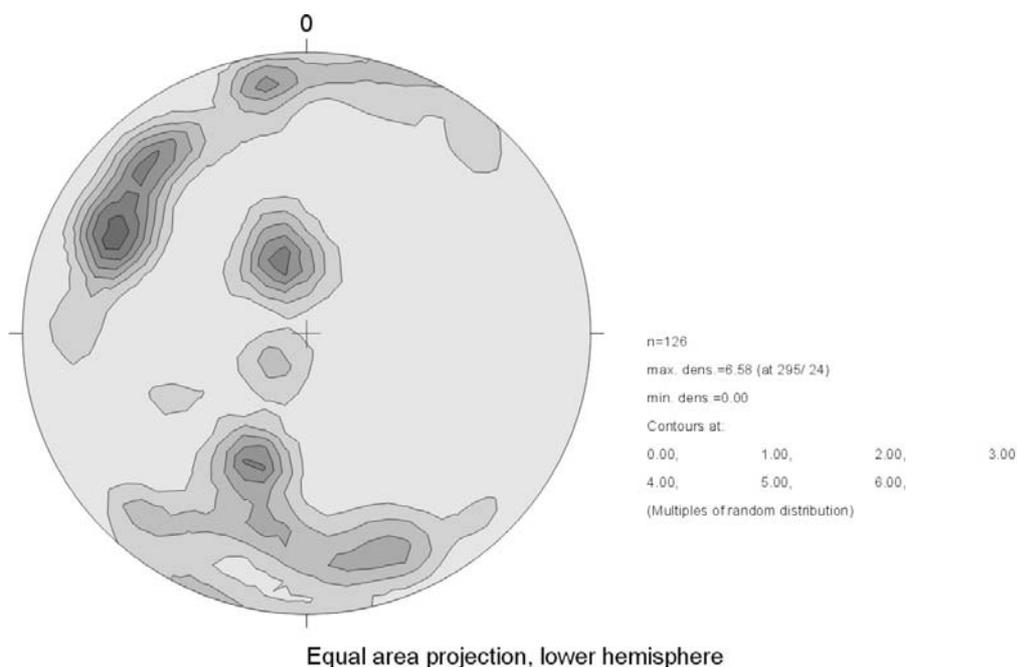


Figure A-38: Contoured poles to all fractures in outcrop (file: 6943-10b.jpg).

Mean Trend	Mean Plunge	Angle long axis (°)	Angle short axis (°)	Mrd max.	Comment
295	24	49	29	6,58	Unroofing joints? Foliation parallel?
344	66	69	33	5,5	
202	48	36	15	5,1	
351	12	13	13	4,6	
165	18	19	10	3,6	

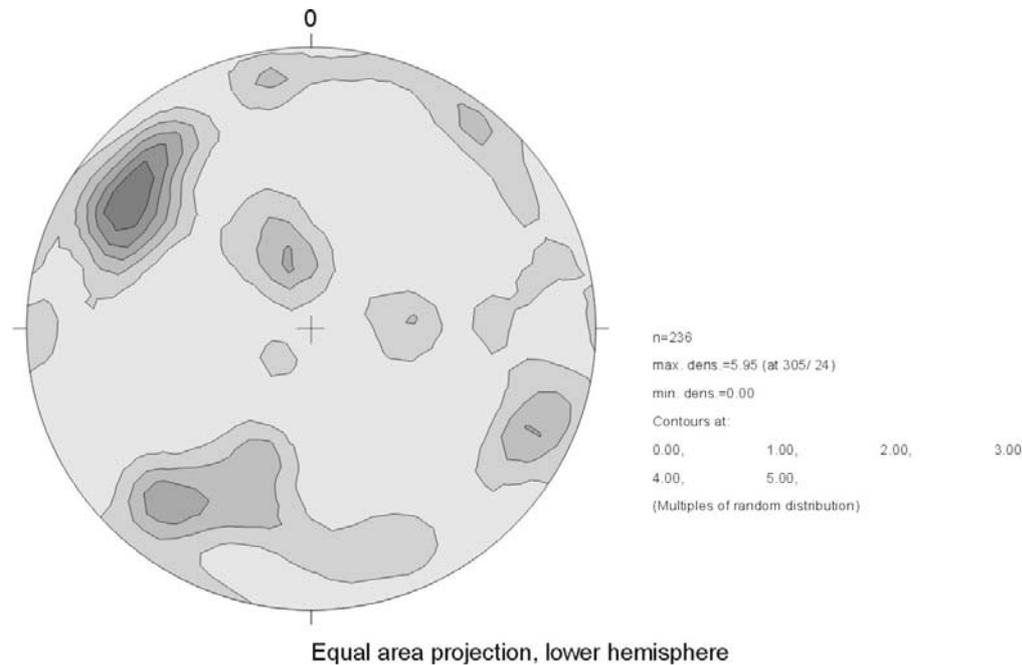


Figure A-39: Contoured poles to all fractures in outcrop (file: 6943-10.jpg).

Mean Trend	Mean Plunge	Angle long axis (°)	Angle short axis (°)	Mrd max.	Comment
305	24	41	33	5,95	
219	23	44	20	3,8	Partly foliation parallel
339	71	35	25	3,1	Unroofing joints?
115	14	20	19	3,0	

In this location two dominant fracture systems were found. One is oriented parallel to the local trend of the Aitnach valley, the other one trends parallel to the nearby Pfahl-fault zone and the associated (mylonitic?) foliation (the western end of the outcrop touches the mapped (GK25) extent of the mylonite unit). The cumulative plot of outcrops 6943-10a and -b clearly shows the predominance of the NNE-SSW striking fracture population. For 6943-10a this set was described as meter-sized planes, spaced at 0,5 to 1m. The fractures are mostly straight and only occasionally associated with breccia. In 6943-10b fracture sizes for this set were also estimated to be on the order of several meters, but the spacings were found to be irregular. This is possibly a sampling problem, since the outcrop trends mostly parallel to the NNW-SSE population.

In 6943-10a the foliation – mainly expressed through aligned c-axes of K-feldspar crystals – is more consistently oriented than in –10b, which might be due to the proximity of the exposure's W end to the Pfahl mylonite. Also, it generally dips more steeply. In –10a the foliation, though the second densest population possesses only short, rough, discontinuous and irregularly spaced fractures. The reason for that might be that the foliation is only locally –and frequently as aligned crystals – well-developed. Another important population in –10a is a set of gently W dipping fractures. Some are brecciated and/or gapping and are traceable over several meters. Spacings of major planes in this concentration are 1-1,5m. One larger brecciated/gougy ESE dipping fault (133f66) was found. In the field it was interpreted as a normal fault conjugate to the WNW dipping fractures, which was later reactivated by dextral strike-slip.

In 6943-10b the eastern and western parts of the outcrop –separated by soil, plants and debris- have slightly different properties (the exposure curves from SSE to SSW). In the E the dominant set was determined to be a family of NE-SW striking fractures with steep dips. They form the

face of the outcrop. Planes in this set trace over several meters, are mainly straight and smooth-looking. Spacings of major fractures are on the order of 0,5-1m. The second dominant set in this part of the exposure trends WNW-ESE. Planes are slightly smaller than the NE-SW ones and spaced irregularly (>1m). Foliation parallel fractures were identified as a separate population (in addition to the WNW-ESE trending fractures), although they also dip moderately to steeply in northerly directions. Planes are mostly short and discontinuous. Some occur in several meters tracing densely fractured/brecciated zones. These zones are spaced at approximately 2-3m.

In the western part of the exposure a set of subhorizontal (gently S dipping) fractures was determined to be dominant. Their attitude follows the orientation of the topography (they even curve with the topographic surface). Thus, they were identified as unroofing joints in the field. Spacings of meter-sized fractures in this population are frequently on the order of 0,3-0,7m. Their density increases towards the top of the outcrop. Some fractures are gaping up to 0,5cm. Moderately to steeply NNE dipping –most likely foliation parallel- fractures were determined to be the 2nd most important set. They frequently trace over more than 1m. Major fractures are spaced at about 0,5-1m. Another significant set trends dips also NNW, but more steeply than the foliation. Planes in this population often trace more than 2m and possess quartz lineations and slickenlines. Spacings of major fractures are 1-1,5m.

Plots of kinematic indicators are presented in figs. A-40 to A-43.

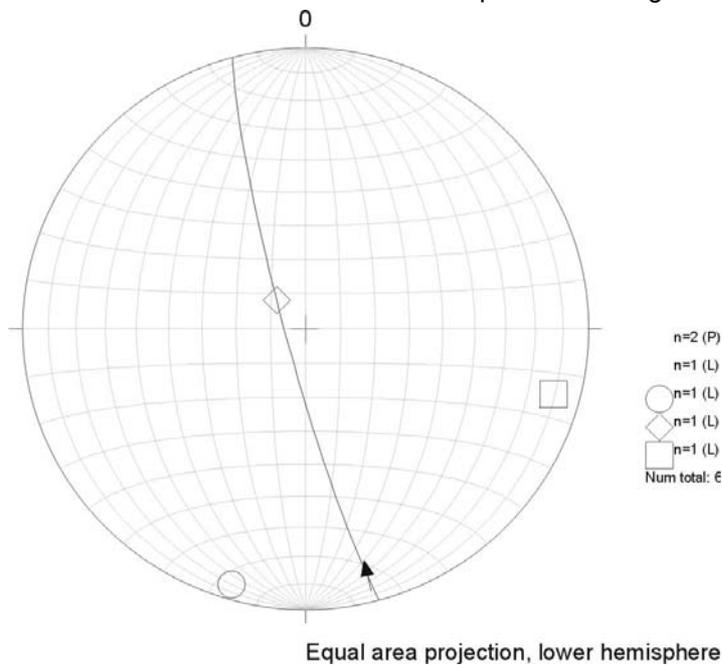


Figure A-40: Slickensided plane suggesting dextral displacement (6943-10, file: 694310de.jpg).

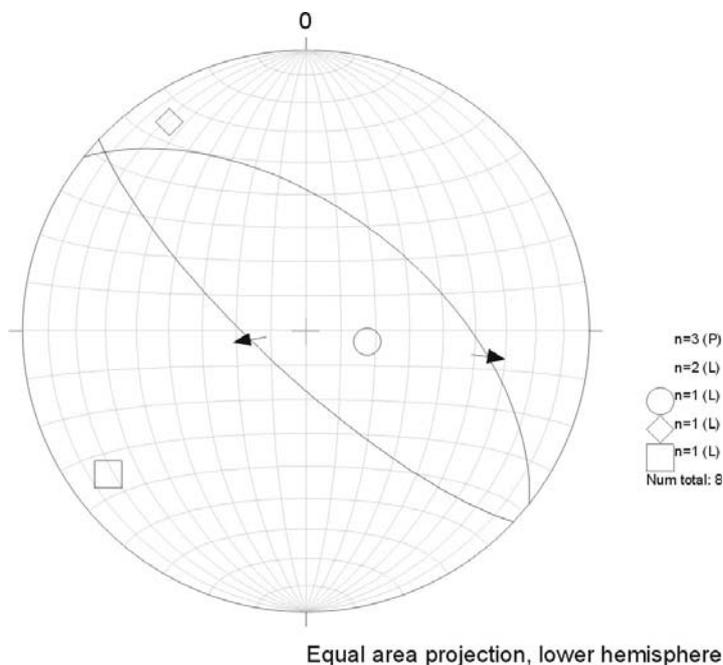


Figure A-41: Slickensided planes suggesting (oblique) normal motion (6943-10b, file: 694310no.jpg).

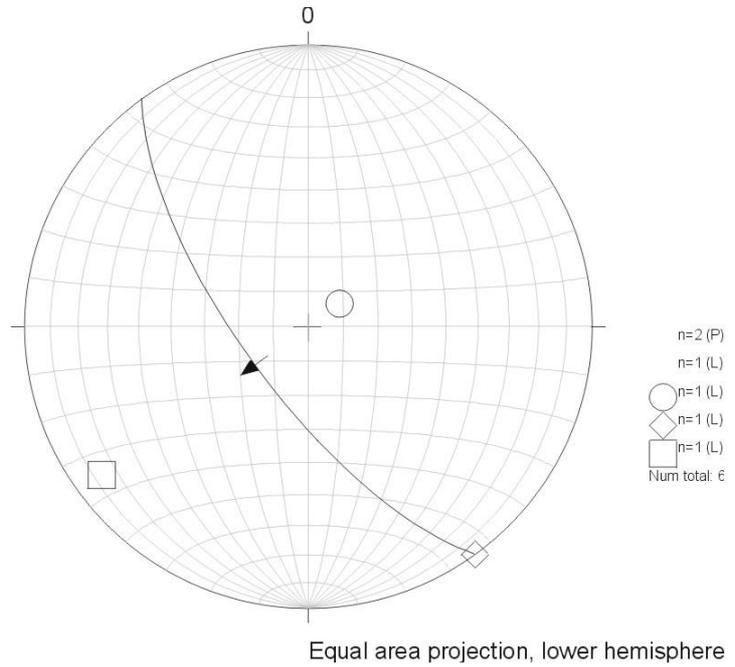


Figure A-42: Fracture offsetting 2 small NNE-SSW striking fractures ca. 15cm normal (6943-10, file: 694310of.jpg).

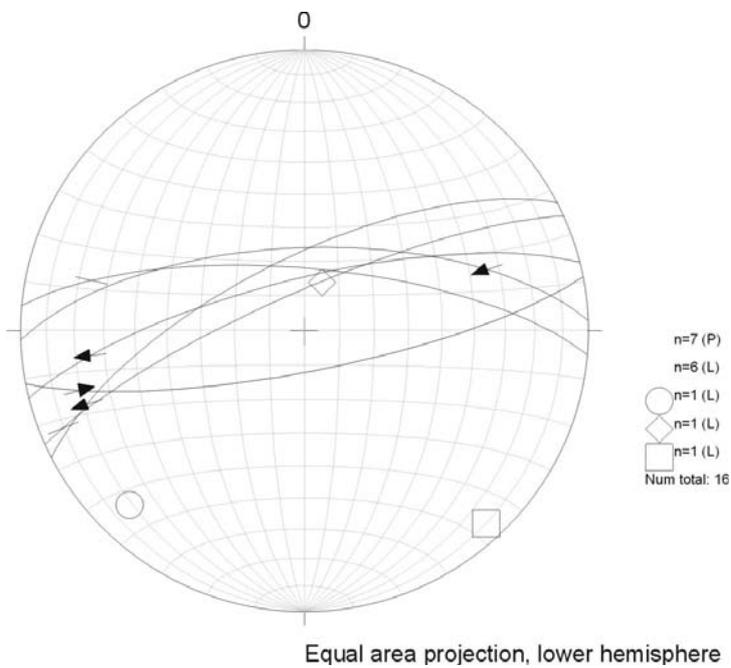


Figure A-43: Slickensided planes suggesting sinistral displacement (6943-10b, file: 694310si.jpg).

Unterried/Haberbühl Quarry, Outcrop ID: 6944-13

Rock Type: Mylonite (GK 25), Unfoliated Cataclasite (Field)

Outcrop: GK: 458654 E 543942 N; UTM: 357395 E 5439000 N
The outcrop extends about 70 paces NW-SE and is ca. 8m high. The main fault plane dips NE. Only ca. 10m at the SE end of the main fault plane were accessible, due to a quarry lake.

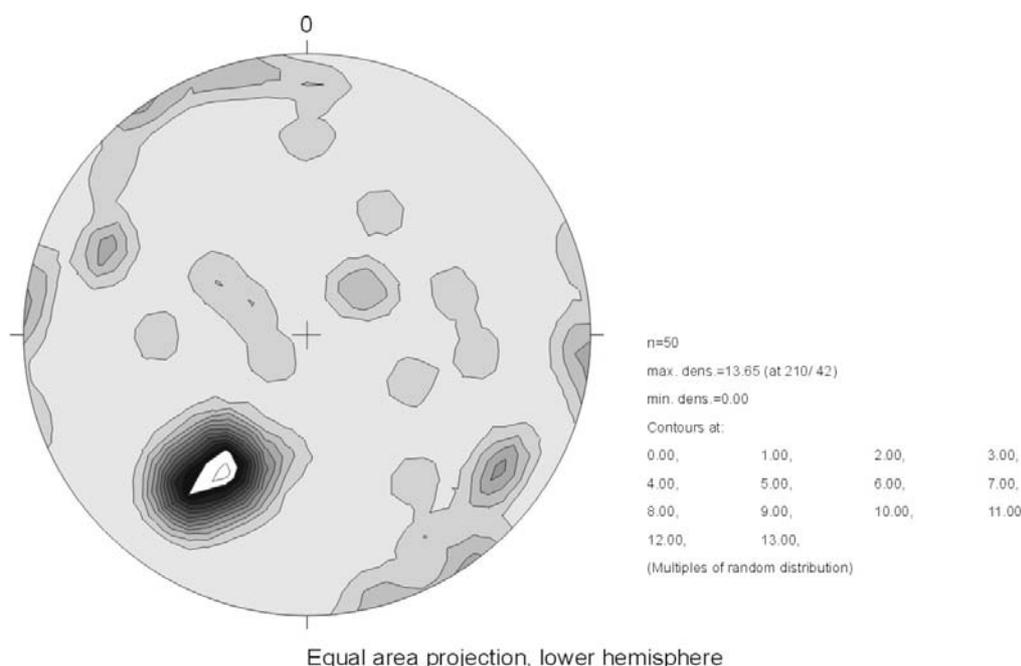


Figure A-44: Contoured poles to all fractures in outcrop (file: 6944-13.jpg).

Mean Trend	Mean Plunge	Angle long axis (°)	Angle short axis (°)	Mrd max.	Comment
210	42	55	39	13,65	Parallel to an old, mylonitic foliation?
125	17	19	17	4,5	
295	24	15	13	3,8	
94	1	16	15	3,3	

The outcrop lies within a large fault zone (Rundinger Zone) containing a wide range of deformational features such as cataclasites, slickensides and both compact and loose fault breccia. Since cataclasites are presumed to originate at shallower levels (10-15km) than mylonites (>15km) the deformational event producing this type of rock did most likely not coincide with the Pfahl-mylonitization, i.e. is probably younger. It is still possible that the Rundinger Zone was active before cataclasis, however, the last stage obliterated traces of the (paleozoic mylonitic?) protolith.

The major brittle fault plane dips moderately NE and so do most other foliation-parallel fractures, making this set the dominant one in this location. These fractures are several meters in size (the main fault can be traced along the entire NW-SE extent of the outcrop). Spacings are on the order of 0,5m. Many planes in this population are covered with a thin layer of glassy black material, which was determined to be graphite in the field. Two samples (UR_01 and UR_02) were taken of these mineralizations and analyzed by X-ray diffraction. The dominant reflection peaks in both samples coincide with the peak of a highly oriented pyrolytic graphite (HOPG) calibration curve, which proves it to be graphite mixed with other mineral constituents. This black mineral was found along with other hydrothermal minerals such as quartz and epidote on these planes. Other fracture sets have more variable orientations.

Minor populations trend NNE-SSW to NE-SW, dipping steeply both ways as well as NW-SE with gentle SW dips. These fractures are mostly irregularly spaced (usually at several meters), although some densely spaced zones exist. The fractures striking in northeast-southwesterly directions can frequently be traced over several meters and were determined to be the second most important set. The set of moderately SW dipping fractures forms a relatively large angle with the main fracture system. However, a conjugate relationship is still possible, since similar pairs of fracture populations were found elsewhere. In those places they were often associated with breccia zones, thus suggesting a geologically young NNE-SSW directed thrusting event.

Two generations of slickenlines were found, predominantly on NE dipping fractures (fig. A-44). The majority of them trends subparallel to the fracture dip, mainly suggesting normal motion (fig. A-45). Paleostress analysis suggests uplift and ENE-WSW extension ($12\sigma_180$; $212\sigma_310$). NW-SE striking faults also expose a set of subhorizontal slickenlines, mostly indicating left-lateral displacement along with right-lateral motion on NNE-SSW striking planes. This gives a –not very clear- conjugate relationship due to ENE-WSW compression ($73\sigma_17$; $159\sigma_37$; fig. A-46).

Age relationships between the slickensides are not entirely clear, but in most places it seems as if the subvertical ones predate the subhorizontal ones. Loose breccia along the large NW-SE fault planes are associated with the latest tectonic event. The following rough sequence of events can be deduced from the above findings:

- [(1) Paleozoic faulting and mylonitization (formation of the Rundinger Zone) contemporaneously with the Pfahl fault zone. No clear evidence for this tectonic phase in this location.]
- (2) Faulting and formation of the unfoliated cataclasite at shallower crustal levels.
- (3) Faulting of the cataclasite due to regional uplift and NE-SW directed crustal extension. Both slickensides and fault geometry (ca. 60° dips) support this phase as the first stage of real brittle deformation.
- (4) Strike-slip reactivation of preexisting faults and the formation of the subhorizontal slickenlines as a result of subhorizontal ENE-WSW compression.
- (5) Faulting and the formation of the compact breccia sheets on top of a relatively unfractured cataclasite (found at the NW entrance of the quarry).
- (6) Faulting and the formation of loose breccia zones perhaps due to a NNE-SSW directed thrusting event (for explanation see text above).

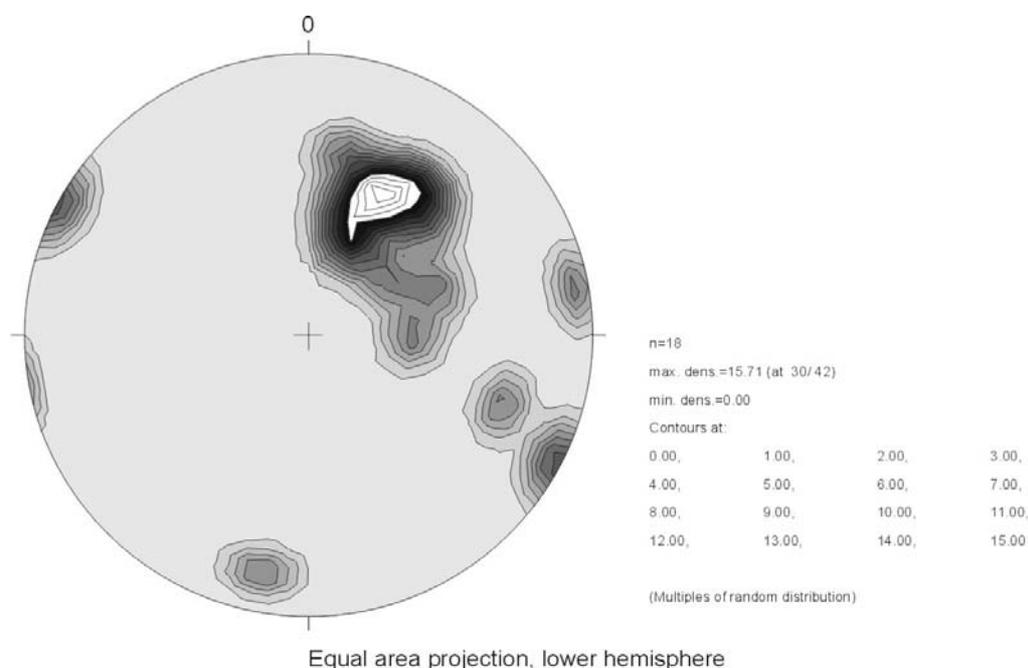


Figure A-45: All lineations/slickensides found on fracture planes in 6944-13 (file: 694413li.jpg).

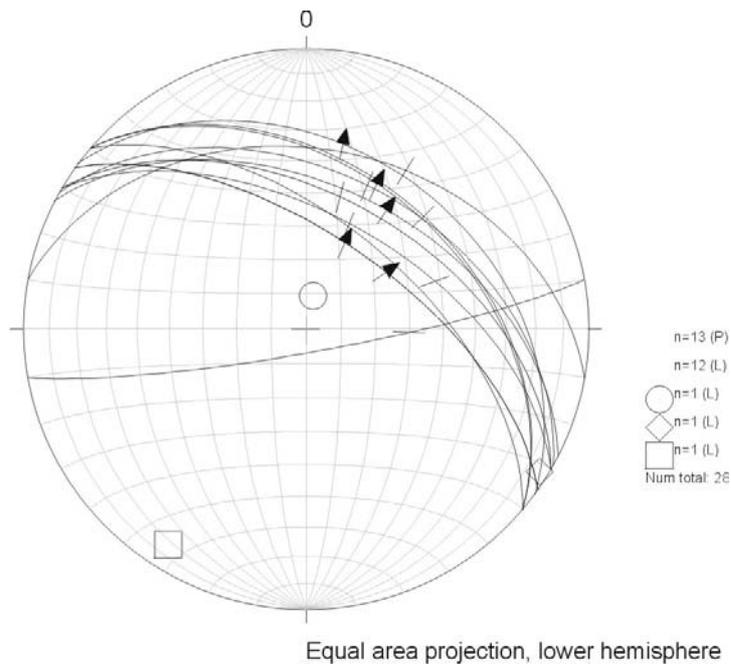


Figure A-46: All slickensided surfaces in 6944-13 suggesting dip-slip (normal) displacement (file: 694413no.jpg).

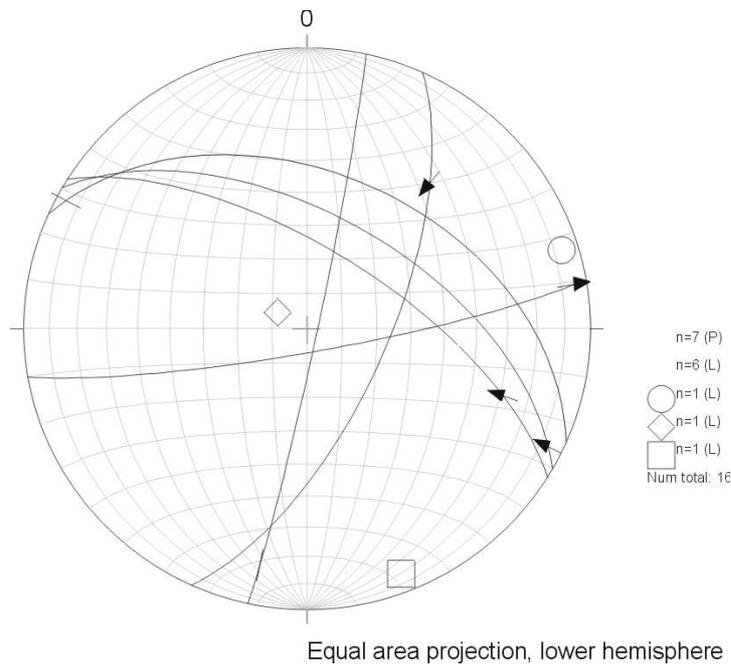


Figure A-47: All slickensided planes in 6944-13 suggesting strike-slip displacement (file: 694413ss.jpg).

Mühlriegelkamm, ca. 100m W of Ödriegel (1166m), Outcrop ID: 6844-03

Rock Type: Layered Gneiss with concordant quartz streaks/lenses, in places granitic-looking, slight folding

Outcrop: GK: 457489 E 544731 N; UTM: 356059 E 5446956 N
The outcrop is accessible from four sides. The W facing (extending ca. 21 paces N-S) and N facing (extending ca. 13 paces E-W) walls were surveyed. Many planes are heavily weathered and/or covered with moss and lichen.

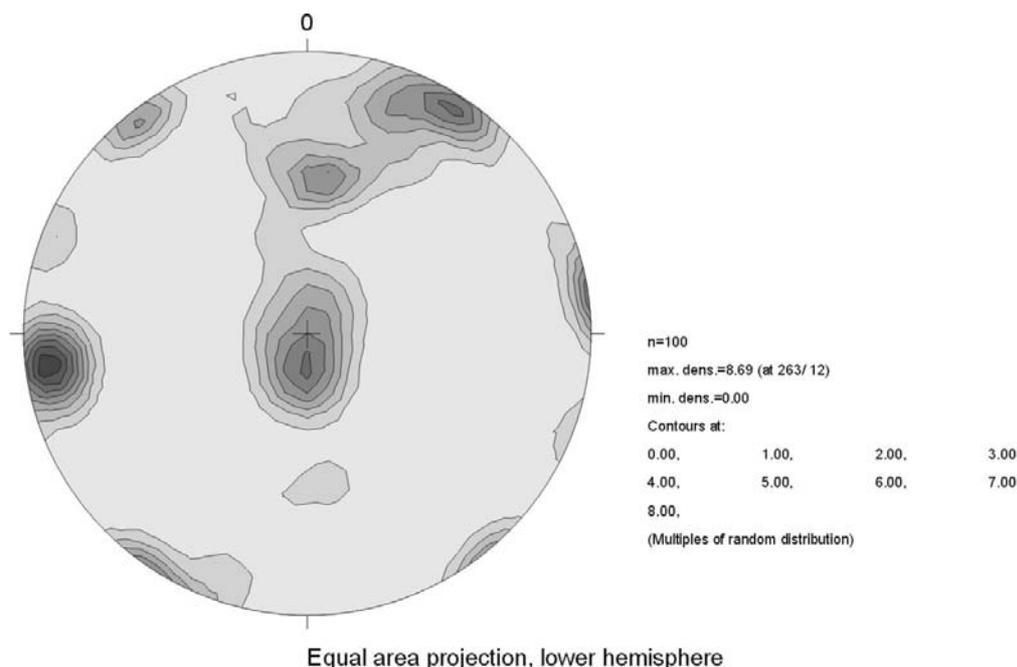


Figure A-48: Contoured poles to all fractures in outcrop (file: 6844-03.jpg).

Mean Trend	Mean Plunge	Angle long axis (°)	Angle short axis (°)	Mrd max.	Comment
263	12	38	28	8,69	Foliation parallel Conjugate to foliation parallel fractures?
34	6	31	17	6,5	
180	78	43	26	6,3	
7	42	18	12	5	
322	6	23	22	4,2	

The dominant fracture system in this location trends approximately N-S and dips subvertically. In addition to their highest abundance of all sets they also possess the largest planes (frequently traceable over several meters). Many fractures in this population have straight and clear-cut - sometimes even smooth planes with little brecciation along them. Spacings of major fractures are about 1m.

The second most important fracture family is also subvertical and strikes WNW-ESE. Planes of this set are also traceable over several meters and often form highly fractured/brecciated zones. Some are straight, others are curvy and rough. Large, straight fractures are frequently gaping and/or associated with a ca. 5cm wide breccia seam. Spacings in this set are very irregular and range from 2 to 3m. Towards the top of the exposure some 2-3m long E-Wish trending fractures are spaced at one meter.

Some 1-2m wide highly broken-up zones exist, where fractures are small and irregularly oriented and thus highly connected. Interesting feature for hydrologic considerations...

The gently N dipping foliation parallel fractures are generally densely spaced, but often short and closed with blind endings. Due to their subhorizontality the planes possess variable strikes. Some large (traceable over several meters) highly fractured/brecciated zones were found, especially along concordant quartz veins and lenses. There, the quartz is highly fractured. Spacings of foliation parallel breccia zones are 1-1,5m. Some of these zones have water seeping out of them.

A minor population of moderately S dipping fractures was interpreted as fractures forming a conjugate angle with the foliation due to a N-S compressive thrusting event.

Several marker horizons such as concordant quartz veins were examined. However, no offsets, even along outcrop-sized fractures were detected.

Mühlriegelkamm, ca. 140m W of Ödriegel (1166m) (“3 Säulen”), Outcrop ID: 6844-04

Rock Type: Layered Gneiss with concordant quartz streaks/lenses, in places granitic-looking. The foliation is only slightly intrafolially folded, for the most part is relatively straight. Some foliation parallel fractures possess (most likely only surficial) exsolution cavities. These could be differentially weathered and broken-out quartz augen.

Outcrop: GK: 457483 E 544317 N; UTM: 356002 E 5445962 N
The outcrop is accessible from four sides. The SSW facing (extending ca. 47 paces ENE-WSW) and E facing (extending ca. 18 paces N-S) walls were surveyed. Many planes are heavily weathered and/or covered with moss and lichen.

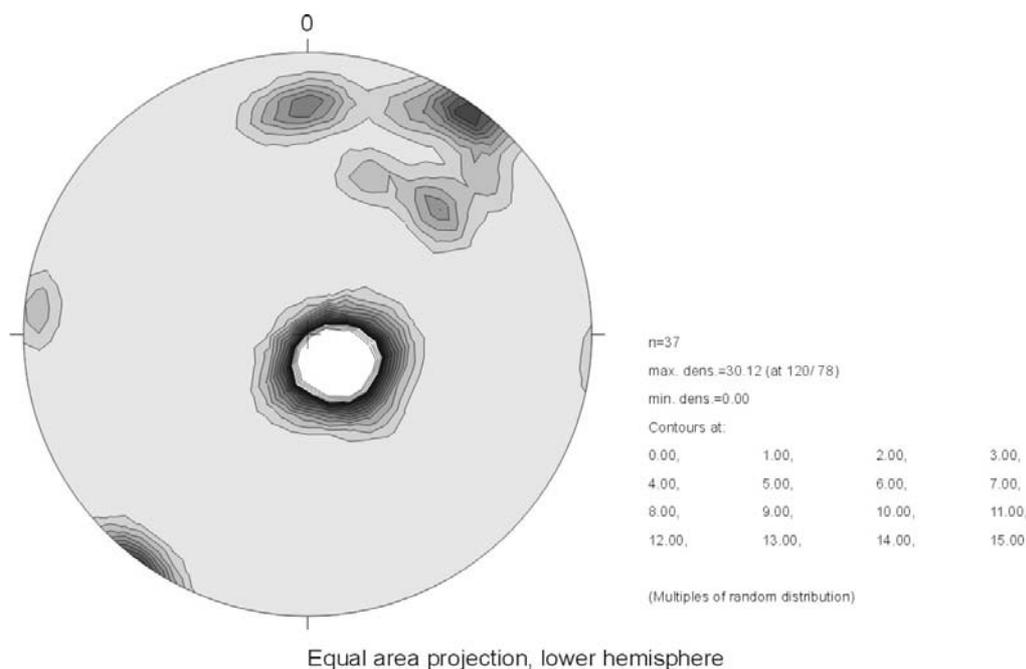


Figure A-49: Contoured poles to all fractures in outcrop (file: 6844-04.jpg).

Mean Trend	Mean Plunge	Angle long axis (°)	Angle short axis (°)	Mrd max.	Comment
120	78	51	43	30,12	Foliation parallel
36	4	22	20	8,5	
0	21	23	17	5,5	
274	6	18	17	2,9	

In this location more work needs to be done (time was running out). A curious feature is the “vanishing” foliation in the western-most column of the 3 “Säulen”. Towards (at about the same level as the other two columns) the top it is well-developed and even visible from the ground. Below a relatively prominent boundary zone it cannot be identified (in part because all planes are heavily weathered and covered with moss and lichen). If present, it is very chaotically oriented. One explanation could be that the top block was thrust over an unfoliated (higher-grade?) one along a thrust fault subparallel to the foliation.

Due to the low number of measurements it cannot be used for structural analysis at this time. More work needs to be done (if not, add the data to 6844-03)!

Viechtach, Liebestal, near bridge (Alte B85), Outcrop ID: 6943-10b

Rock Type: Körnelgneis (bgn, GK25). C-axes of K-feldspar crystals seem parallel to the foliation. Some concordant bands of (foliated?) granite.

Outcrop: GK: 46716 E 543623 N; UTM: 347896 E 5436188 N
The outcrop is located at the W end of the bridge. From there it extends about 140 paces in East-Westerly directions, facing southerly. The exposure is ca. 6m high. Most planes are covered with moss and lichen.

Data and descriptions are included in Field Report KW39 (Outcrop 6943-10).

Patersdorf, B85, Am Hamischbühl, Outcrop ID: 6943-11

Rock Type: Mittelkörniger Granit, Gm (GK 25), Granite (Field)

Outcrop: GK: 457227 E 543110 N; UTM: 352801 E 5430860 N
The outcrop extends about 95 paces E-W, but not continuously (interspersed with zones of soil), facing S. It is up to 4m high. Many planes are weathered, some are oxidized.

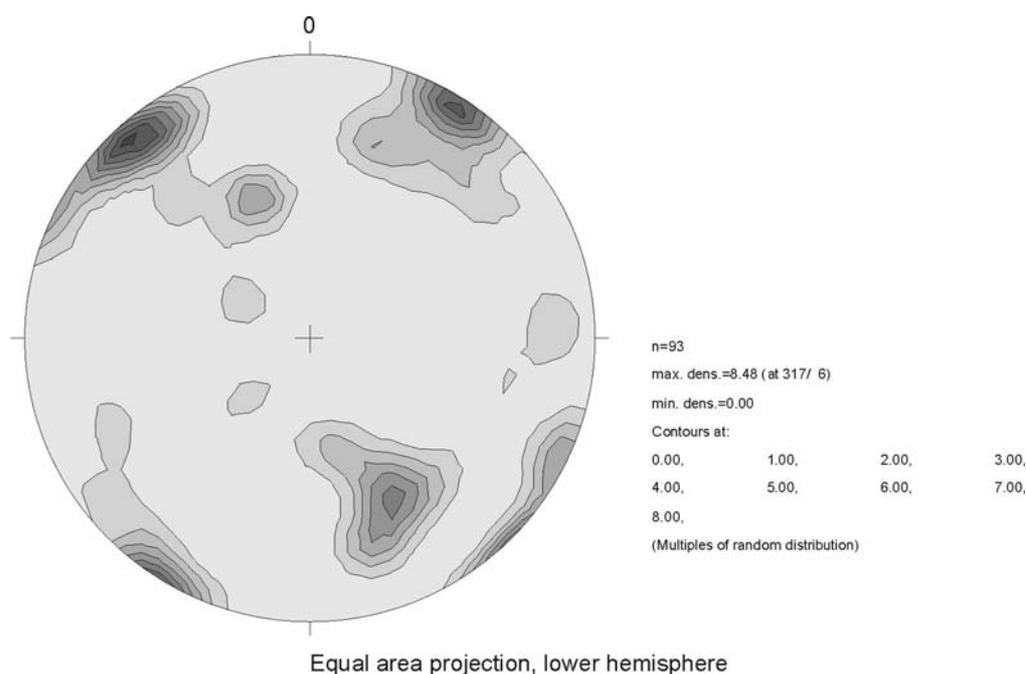


Figure A-50: Contoured poles to all fractures in outcrop (file: 6943-11.jpg).

Mean Trend	Mean Plunge	Angle long axis (°)	Angle short axis (°)	Mrd max.	Comment
317	6	46	23	8,48	
34	6	49	31	7,2	
154	37	48	41	5,6	
339	48	17	14	3,8	

By visual inspection of the outcrop in the field, the dominant fracture set in terms of abundance was determined to be the steeply dipping, NE-SW trending one; in terms of size the steeply dipping, WNW-ESE trending one is dominant. The following fracture parameters were calculated from spacing and aperture measurements for the three most important populations:

Set (strike)	Mean Fracture Spacing	Mean Fracture Aperture
NE-SW, steeply dipping	32,8 cm	0,9 mm
WNW-ESE, steeply dipping	44,1 cm	1,8 mm
NE-SW, moderately NW dipping	44,8 cm	1,6 mm

The roughest planes both the steeply dipping WNW-ESE trending and the moderately NW dipping, NE-SW trending sets. Only few steeply dipping, NE-SW trending fractures possess rough surfaces. Most of them are relatively smooth. In terms of curviness the steeply dipping, NE-SW trending population tends to possess the straightest planes. More undulatory planes were found in the steeply dipping, WNW-ESE trending as well as in the moderately NW dipping sets, although a number of moderately NW dipping planes are rather straight. Brecciation was detected on only very few planes (n=5). These belong either to the steeply dipping WNW-ESE trending, or to the moderately NW dipping populations.

Only two slickensided surfaces were found, one of which gave a faint indication of the shear sense (198f73, -9, dextral). The other one (34f82, -10, ?) did not yield a shear sense. The resulting stress field is a subhorizontal NW-SE compression ($316\sigma_1$; 16 ; $48\sigma_3$ 10).

Two planes with accessory fractures interpreted as synthetic Riedel shears exist. One (291f88) suggests sinistral strike-slip (NE-SW compression; $51\sigma_1$; 1 ; $141\sigma_3$ 2), the other one (210f79) suggests oblique reverse motion due to an inclined ENE-WSW compression ($240\sigma_1$ 42; $14\sigma_3$ 37).

Railroad cut between Schweighof & Rohrbach, Outcrop ID: 7044-02

Rock Type: Field: High grade Anatexite, locally foliated

Outcrop: GK: 457924 E 542488 N; UTM: 359514 E 5424379 N
 The outcrop extends about 350 NE-SW to ENE-WSW and consists of two walls on both sides of the railroad. Fractures were measured on the SE facing fall only. It is up to 6m high. Many planes are weathered and covered with moss and lichen.
 A 20m scanline was installed in addition to subjective measurements.

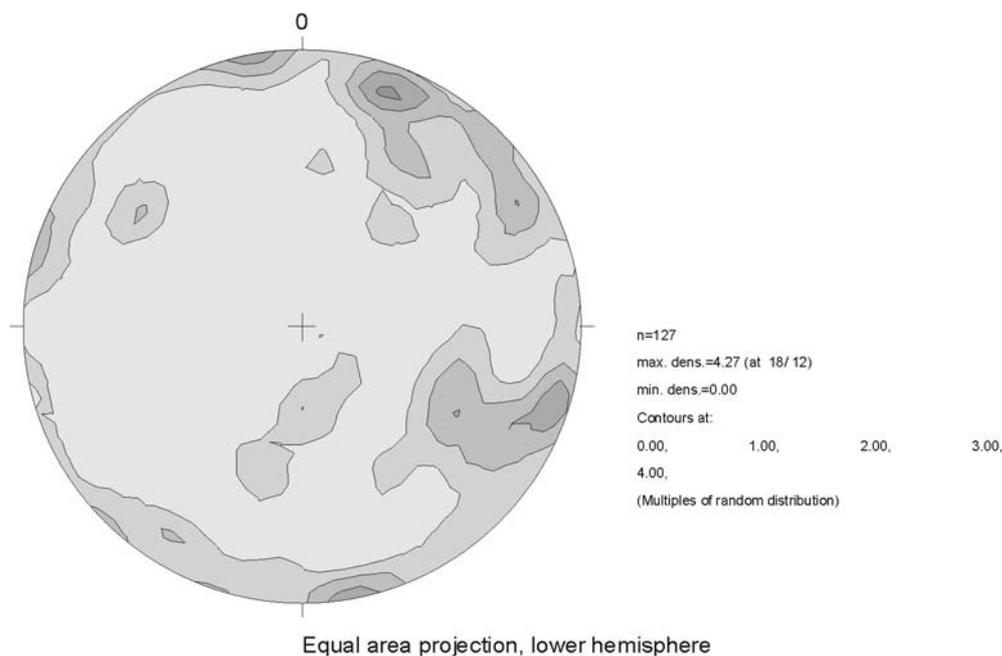


Figure A-51: Contoured poles to all fractures in outcrop (file: 7044-02.jpg).

Mean Trend	Mean Plunge	Angle long axis (°)	Angle short axis (°)	Mrd max.	Comment
18	12	53	17	4,27	Partly foliation parallel
108	6	51	29	3,9	
169	1	20	15	3,6	
305	30	18	17	2,2	
179	66	52	16	2,0	

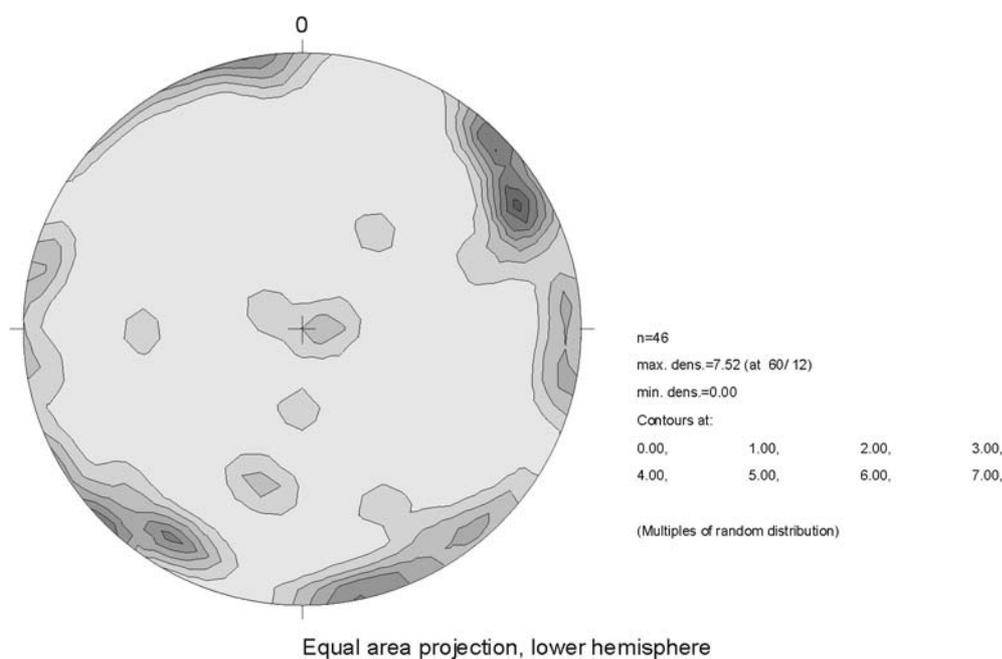


Figure A-52: Contoured poles to all fractures in outcrop (file: 7044-02scanline.jpg). Plot contains all fracture orientations measured in a 20m scanline.

Mean Trend	Mean Plunge	Angle long axis (°)	Angle short axis (°)	Mrd max.	Comment
60	12	41	25	7,52	
138	1	64	45	5,1	
86	5	31	15	3,4	
194	42	21	16	2,5	
96	84	33	17	2,3	

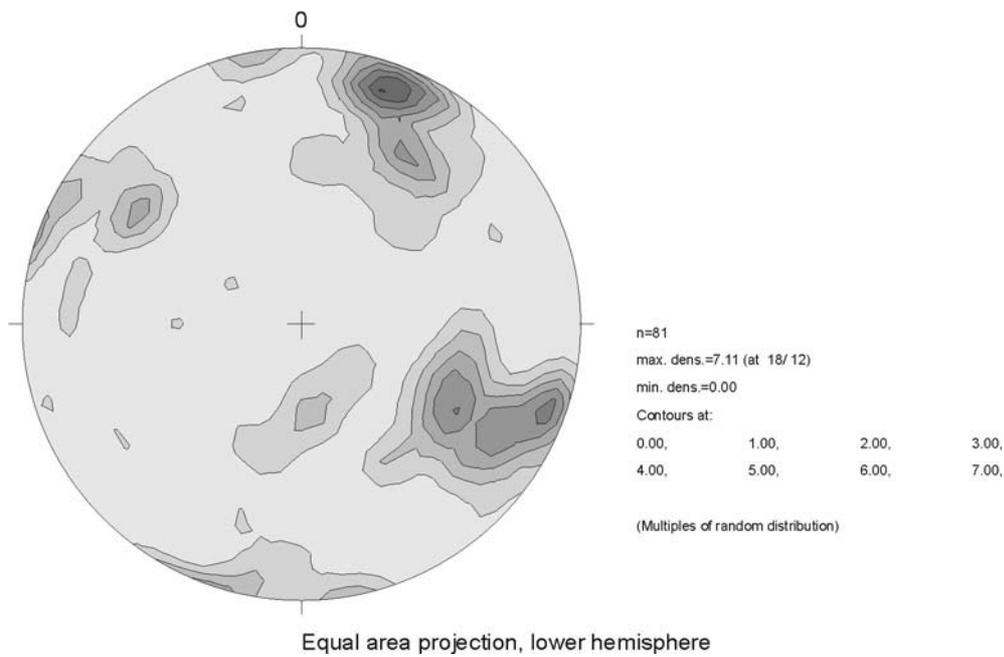


Figure A-53: Contoured poles to all fractures in outcrop (file: 7044-02subjective.jpg). Plot contains all fracture orientations measured with the subjective approach.

Mean Trend	Mean Plunge	Angle long axis (°)	Angle short axis (°)	Mrd max.	Comment
18	12	35	27	7,11	Partly foliation parallel
109	6	27	12	5,3	
120	37	16	12	5,1	
305	31	16	13	3,7	
180	62	48	19	2,3	

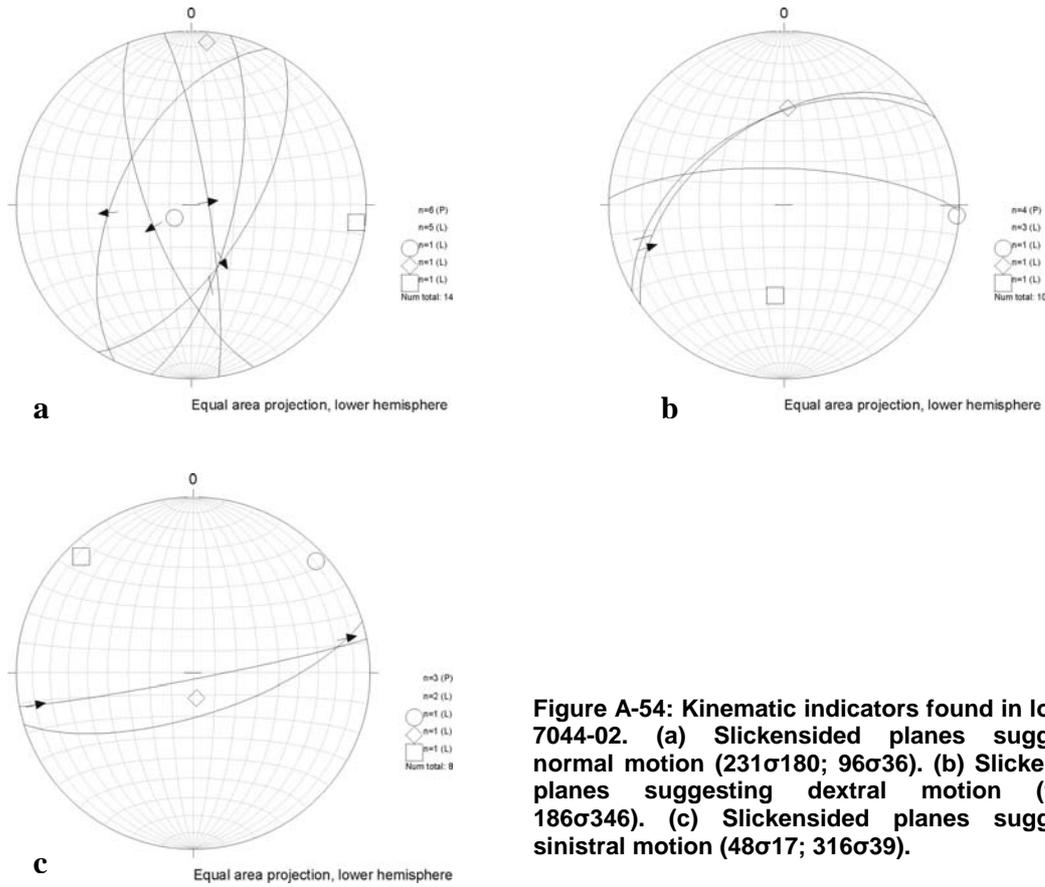


Figure A-54: Kinematic indicators found in location 7044-02. (a) Slickensided planes suggesting normal motion (231σ180; 96σ36). (b) Slickensided planes suggesting dextral motion (94σ11; 186σ346). (c) Slickensided planes suggesting sinistral motion (48σ17; 316σ39).

Fracture Density in Outcrop 7044-02

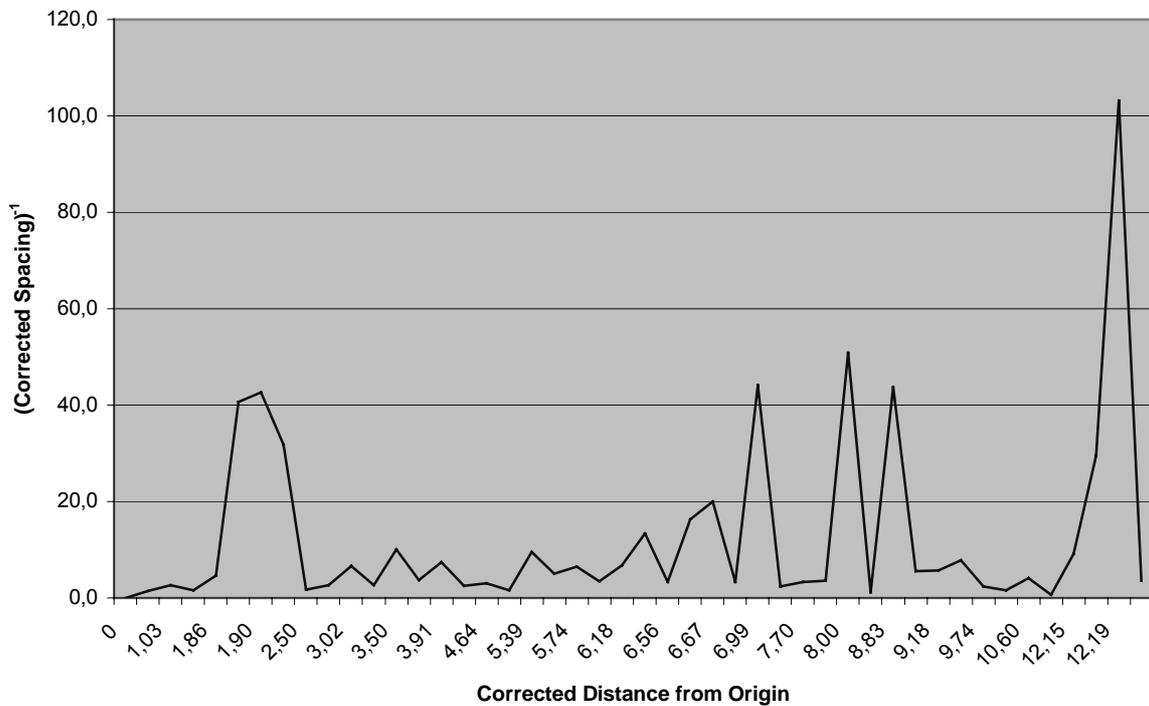


Figure A-55: Fracture densities measured in location 7044-02. Values are directionally corrected with respect to the scanline trend.

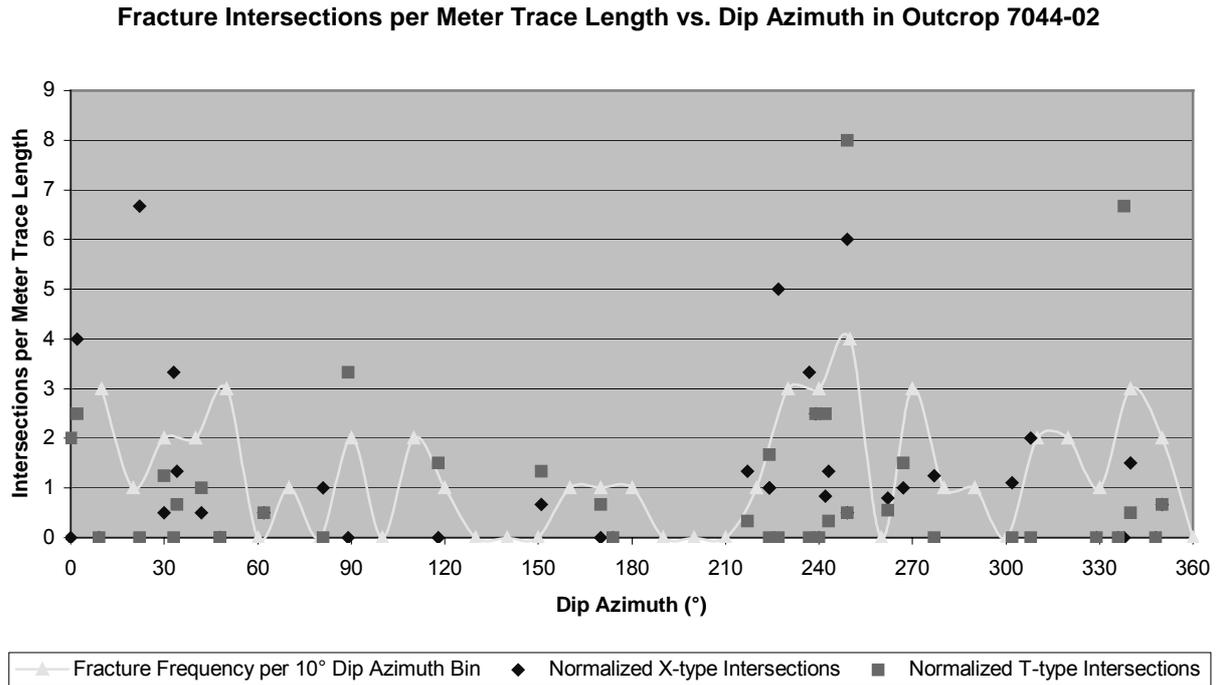


Figure A-56: Numbers and types of intersections per fracture and dip azimuth along the 20m scanline.

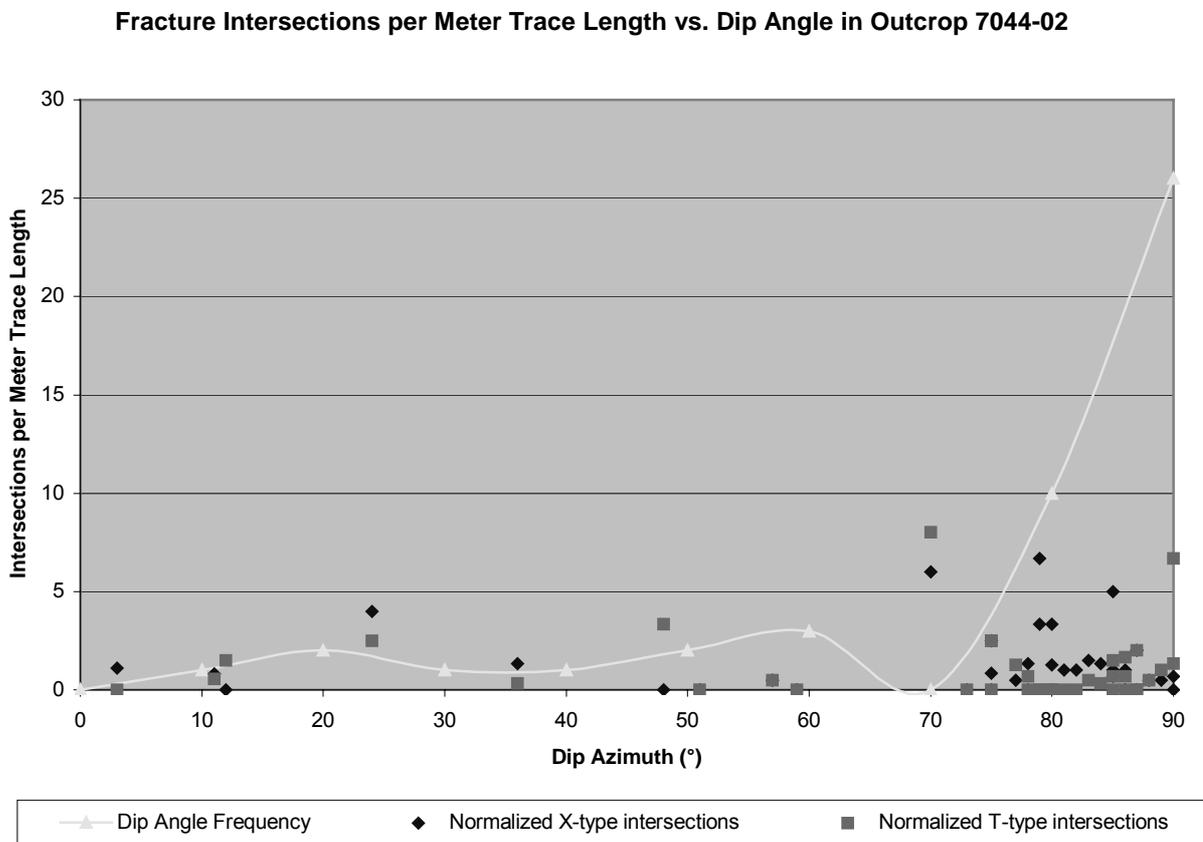


Figure A-57: Numbers and types of intersections per fracture and dip angle along the 20m scanline.

In this location both subjective and scanline-measurements were taken. Figure A-52 shows a plot of the scanline data; figure A-53 represents data collected subjectively. Despite the usually good agreement of data obtained in the two different ways there are considerable differences in the two plots. The highest concentrations of poles lie approximately 40° apart and other concentrations do not match perfectly either. An explanation for this discrepancy might be that the sampling locations of the two data sets were not the same within the outcrop. The scanline data was collected in the southern part of the exposure, where it trends NE-SW, while the subjective data was obtained in the northern part, where the outcrop trends rather ENE-WSW. Another explanation for the discrepancy might be the difference in sample size (n=46 vs. n=81), which can skew the concentrations, and the undersampling of scanline-parallel fractures. Comparing individual fracture planes in the Schmidt nets shows that the subjective data set contains all the orientations plotted in the scanline data set, but in different proportions. In contrast, several orientations are missing in the scanline data. Thus, in this case the subjective data can possibly be more trusted, since it contains also the outcrop-(sub)parallel fractures, which often are an important set.

The following remarks all relate to the cumulative plot in figure A-51. The dominant fracture set in the plot trends WNW-ESE. This was confirmed by observations in the field, where both the largest planes and highest densities were attributed to this set. The foliation in this outcrop also trends WNW-ESE, dipping steeply SSW (which is opposite to the regional dip direction). However, the foliation is only locally and weakly developed. Thus, the WNW-ESE trending set cannot really be called foliation-parallel.

Another important set of fractures trends NNE-SSW, dipping predominantly steeply WNW. This population seems to consist of two subgroups, one dipping steeply (<80°), and the other one dipping moderately (50°-60°). The moderately WNW dipping group could be in a conjugate relationship to the moderately to steeply ESE dipping one, thus indicating uplift and a subhorizontal WNW-ESE trending σ_3 . This stress field could also be obtained from slickensided planes (figure A-54a). Fractures in this set are often large brecciated faults, often associated with weathered zones of compacted fault rocks. Zones of dense fracturing also occur frequently in this set.

Several gently dipping fractures, mostly with northerly dips, were initially interpreted as unroofing joints, due to their frequent following of the topographic surface. However, several are associated with brecciation and could also be thrust or low angle normal faults. Fractures in this set are generally spaced at 0.5 to 1.5m, can often be traced over several tens of meters, and possess relatively large apertures. Some contain moss, plants, or even little trees.

Another population, which is relatively prominent in the scanline data set, but less important in the subjective data, trends ENE-WSW to E-W, dipping steeply in both directions. Although it was determined to be of minor importance it contains several slickensided planes suggesting strike-slip displacement. However, the sense of motion was interpreted as both dextral (figure A-54b) and sinistral (figure A-54c), either due to a misinterpretation of some slickenlines, or due to two different phases of motion, and thus to different stress fields.

The fracture density diagram in figure A-55 shows the reciprocal of the corrected fracture spacings along the outcrop. Zones of high density alternate with zones of lower density. Since this plot shows fracture spacings of all orientations along the scanline it gives a good impression of the bulk fracture porosity in the outcrop. For the detailed examination of the fracturing behavior of individual fracture sets the data has to be separated and spacings of the specific sets have to be plotted.

Figure A-56 gives an impression of the abundance of fracture intersections per meter trace length with regard to the fracture dip azimuth they occur with. However, the only recognizable pattern shows that the more fractures of a specific orientation are present the higher the number of fracture intersections gets. In general, the number of X-type intersections seems to be slightly higher than the number of T-type intersections, but there are no directional preferences recognizable. Figure A-57 relates the number of fracture intersections per meter trace length to the dip of the fractures they were encountered in. Here, there is a slight trend from a low intersection count at low dip angles to a high intersection count at high angles. However, if the absolute numbers of intersections per fracture (non-normalized to length) the trend reverses, and the highest intersection counts occur among the low angle fractures. This is in part due to sampling bias, since the outcrop's horizontal extent is much larger than its vertical extent. On the other hand, gently dipping fractures can frequently be traced over tens of meters and therefore contain a high number of intersections.

Gumpenried, Outcrop ID: 6944-14

Rock Type: GK25: Perliger Cordierit-Sillimanit Gneis (cgnp); Field: Biotite-rich (granitic) gneiss; relatively fine-grained

Outcrop: GK: 457324 E 543773 N; UTM: 354033 E 5437445 N
 The outcrop is located at the N-bank of the river Regen, near the dam of the power station. It extends ca. 135 paces NW-SE, but is not continuous (interspersed with soil and vegetation sections). The exposure is up to 5m high. Most planes are covered with lichen and moss, and are partially weathered.

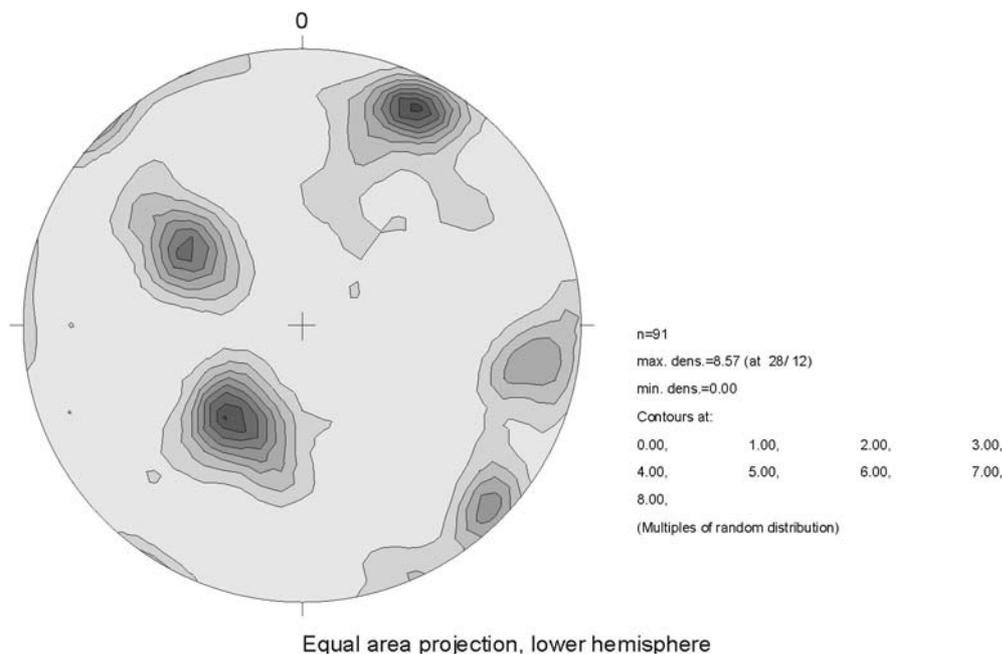


Figure A-58: Contoured poles to all fractures in outcrop (file: 6944-14.jpg).

Mean Trend	Mean Plunge	Angle long axis (°)	Angle short axis (°)	Mrd max.	Comment
28	12	62	37	8,57	Foliation parallel
220	55	48	40	8,1	
300	49	53	31	6,4	
133	6	24	21	4,6	
100	17	29	27	4,0	

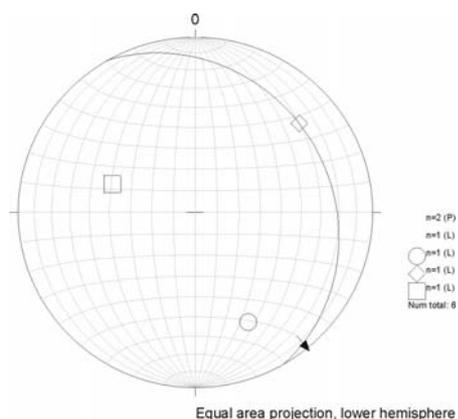


Figure A-59: Kinematic indicators found in location 6944-14. Slickensided plane suggesting oblique-dextral strike-slip motion (155σ₁31; 289σ₃49).

The dominant fracture set in this location trends NW-SE, dipping steeply SW; subparallel to local trend of the river valley. The largest planes frequently measure several meters in diameter. The highest densities are also suspected in this set. Most of the large planes are very straight and relatively smooth, only occasionally associated with brecciation and/or zones of accessory fractures. Some fractures of this set also dip moderately to gently in southwesterly directions and were assumed to be conjugate thrust faults related to foliation parallel faults, thus suggesting a NE-SW compression and a subvertical σ_3 .

In the field, the secondary set trends NNE-SSW, mostly dipping steeply WNW, although the plot in fig. A-58 suggests otherwise. Planes are also straight and frequently smooth, but on average smaller than the NW-SE trending ones. They often terminate at foliation parallel or other low angle fractures. In some cases they occur as densely spaced zones (dm-spacing), often associated with brecciation.

Foliation parallel fractures dip gently to moderately NE. In the field, it was observed that they occur not so much as individual fractures, but rather as densely spaced/brecciated zones (zone of brecciation frequently 20-30cm wide). They are laterally very extensive (often trace over more than 10m) and locally have water seeping out. These zones were interpreted as foliation parallel (thrust?) faults, possibly in conjugate relationship with the gently to moderately SW dipping planes. The gently to moderately SE dipping fractures were not specifically described in the field. However, some of these fractures seem to be in a Riedel-type relationship, suggesting NW-SE directed thrusting. The evidence is not unambiguous, though. Figure A-59 shows the only slickensided surface in the data set. Its interpretation suggests right-lateral strike-slip displacement along a foliation parallel fracture due to a subhorizontal NW-SE trending σ_1 . Other kinematic indicators, such as offsets, were not found in this location.

Blossersberg, ca. 400m SSW of Hartbühl, Outcrop ID: 6943-12

Rock Type: Mittelkörniger Granit, Gm (ca. 120m long & 30m wide, NW-SE striking lense); Körnelgneis, bgn (GK 25); Unfoliated, granitic-looking anatexite with large qtz/fsp porphyroblasts; strongly weathered, granite at the NE end of the outcrop (Field)

Outcrop: GK: 456634 E 543947 N; UTM: 347208 E 5439458 N
The outcrop extends 32 paces NE-SW, facing NW. It is up to 3 meters high and exposes many fresh-looking planes. Other planes are covered with lichen and moss or are oxidized. Brecciated zones are frequently heavily weathered.

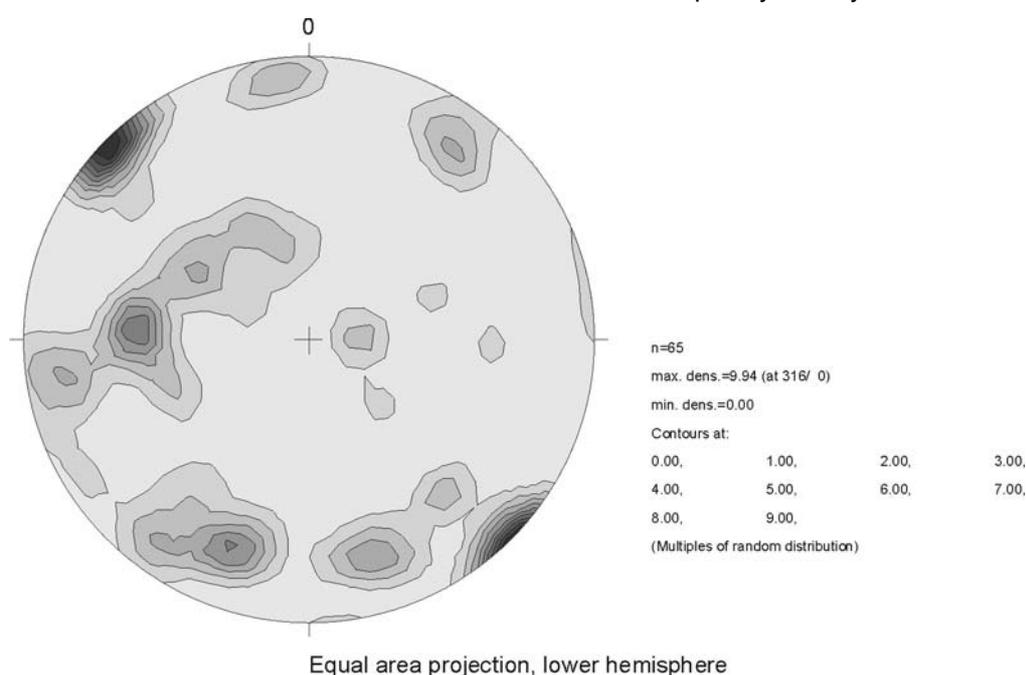


Figure A-60: Contoured poles to all fractures in outcrop (file: 6943-12.jpg).

Mean Trend	Mean Plunge	Angle long axis (°)	Angle short axis (°)	Mrd max.	Comment
316	0	26	24	9,94	Mean spacing: 38,3 cm Mean spacing: 45,4 cm Mean spacing: 28,2 cm (only in the granitic part of the outcrop)
274	38	77	31	5,6	
201	23	35	21	5,1	
164	21	19	17	3,7	Mean spacing: 59,7 cm Mean spacing: 52,9 cm
35	18	17	16	3,3	
356	7	21	20	3,0	
91	76	18	15	2,4	

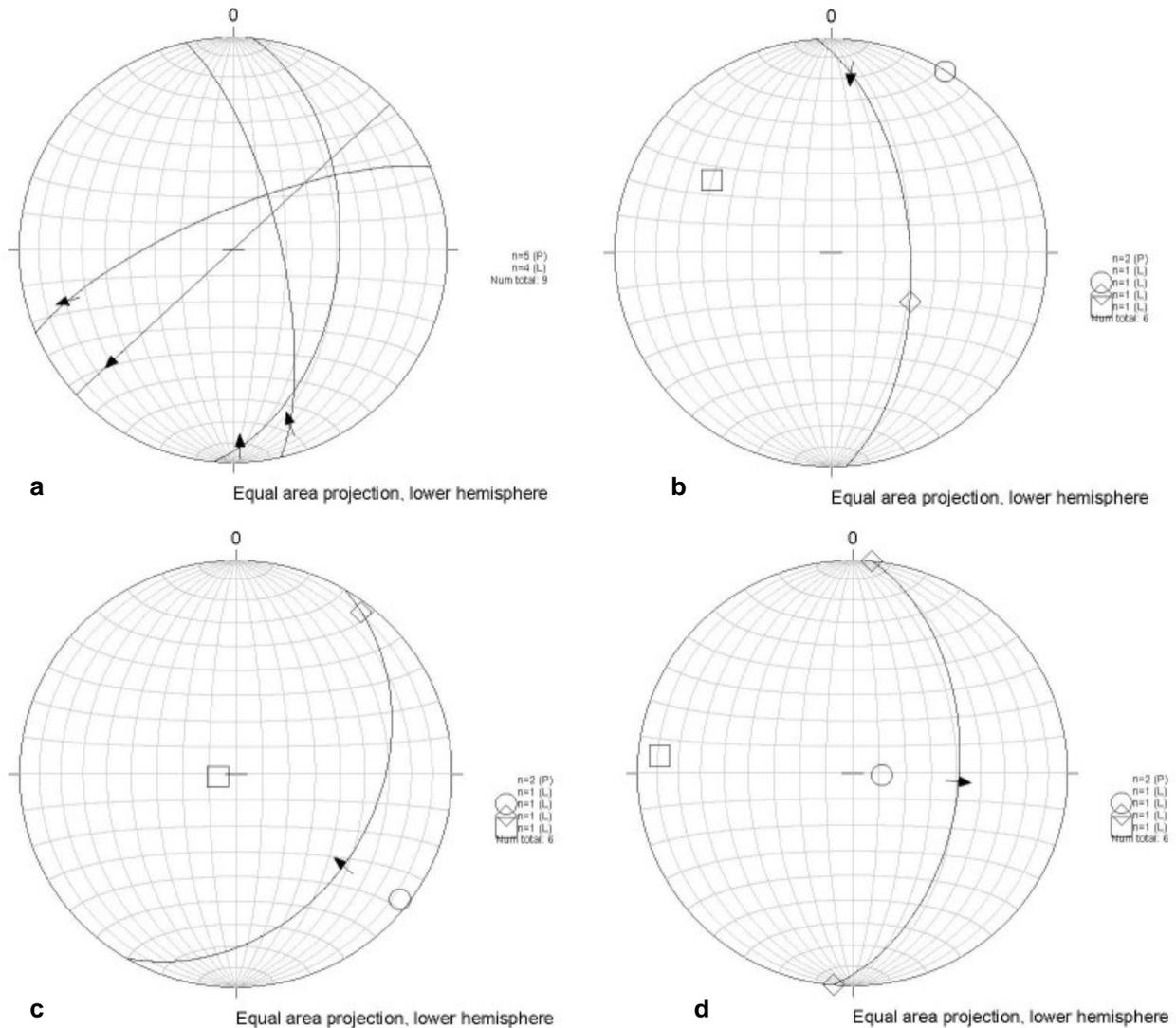


Figure A-61: Kinematic indicators found in location 6943-12. If sensible results could be expected stress configurations were added to the plots. (a) Slickensided planes suggesting sinistral strike-slip motion. (b) Slickensided planes suggesting dextral strike-slip motion (32σ₁0; 302σ₃36). (c) Slickensided planes suggesting reverse motion (128σ₁4; 259σ₃83). (d) Fracture offsetting a gently dipping densely fractured/brecciated zone suggesting normal motion (95σ₁79; 275σ₃11).

The most striking observation in this outcrop is that the granitic NE part of the exposure is more strongly fractured than its SW part. In both parts the steeply dipping, NE-SW striking set of fractures is dominant both in fracture size and abundant. It represents the face of the outcrop and also trends subparallel to local photo- and DEM-lineaments. Fracture apertures in this set are generally low (<1mm).

Other important fractures trend in north-southerly directions, dipping moderately to steeply E. Fracture planes are smaller than in the NE-SW set, but traces still can reach several meters. Apertures are also low (<1mm). A few N-S fractures possess gentle dips. These can be traced over several meters and possess apertures of up to 2mm. Rough planes and breccia/accessory fractures are also characteristic for this small, gently dipping population.

An especially prominent fracture set in the granitic part of the outcrop trends NW-SE, dipping steeply both NE and SW. The mainly straight and smooth planes rarely trace more than 1,5m and apertures are also generally low (<1mm). Other fracture sets are of minor importance. Fracture spacings are listed in mean fracture orientations table. Generally, steeply dipping fractures are mostly straight and relatively smooth, gently dipping fractures are frequently rough and sometimes undulatory.

Some kinematic indicators were encountered. Slickenlines on steeply dipping fractures suggest both left- and right-lateral strike-slip displacement (figures A-61a and b). Sinistral strike-slip was detected both on N-S and NE-SW striking fractures. Although the fracture strikes differ considerably it is possible that the displacement occurred during one single event, provided it reactivated existing fractures. A N-S to NNW-SSE directed compressive stress field can then be assumed. Right-lateral strike-slip was found on one N-S trending fracture. This had to have occurred during a different stress field (NNE-SSW to NE-SW compression), since other N-S fractures expose indicators for sinistral strike-slip. Unfortunately, none of the fractures show evidence for both sinistral and dextral displacement, so relative ages of deformation events could not be established. Also, the slickensides are often relatively poorly developed. Errors in the interpretations of the motion directions are therefore possible (especially since there is only one fracture suggesting dextral strike-slip).

However, one fracture clearly shows slickenlines indicating reverse motion along a gently SE dipping fracture due to a NW-SE directed compressive stress regime (figure A-61c). Another fracture offsets a gently S dipping zone of dense fracturing/brecciation (fault?) about 0,3m downdip, thus suggesting uplift and E-W extension.

Viechtach – Rugenmühle, Outcrop ID: 6943-13

Rock Type: Körnelgneis, bgn (GK25); Granitic gneiss with large sub- to euhedral partially oriented K-feldspar crystals, no clear foliation; several aplite dikes/veins (maybe slightly foliated)

Outcrop: GK: 456482 E 543988 N; UTM: 345705 E 5439922 N
The outcrop extends about 98 paces E-W, facing South, and is between 5 and 10 meters high. Most planes are oxidized, many are covered with lichen. The top part of the outcrop is grusy and strongly weathered, grading into the topsoil.

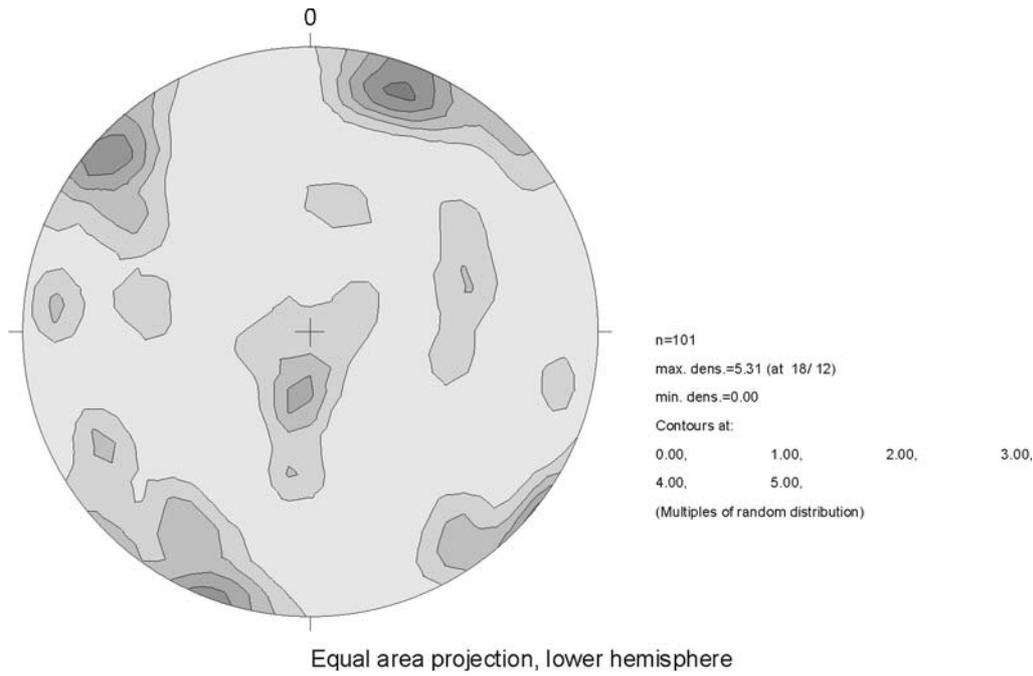


Figure A-62: Contoured poles to all fractures in outcrop (file: 6943-13.jpg).

Mean Trend	Mean Plunge	Angle long axis (°)	Angle short axis (°)	Mrd max.	Comment
18	12	59	57	5,31	
311	5	66	41	4,9	
186	71	57	22	3,2	
277	12	20	16	2,3	
73	43	50	19	2,1	

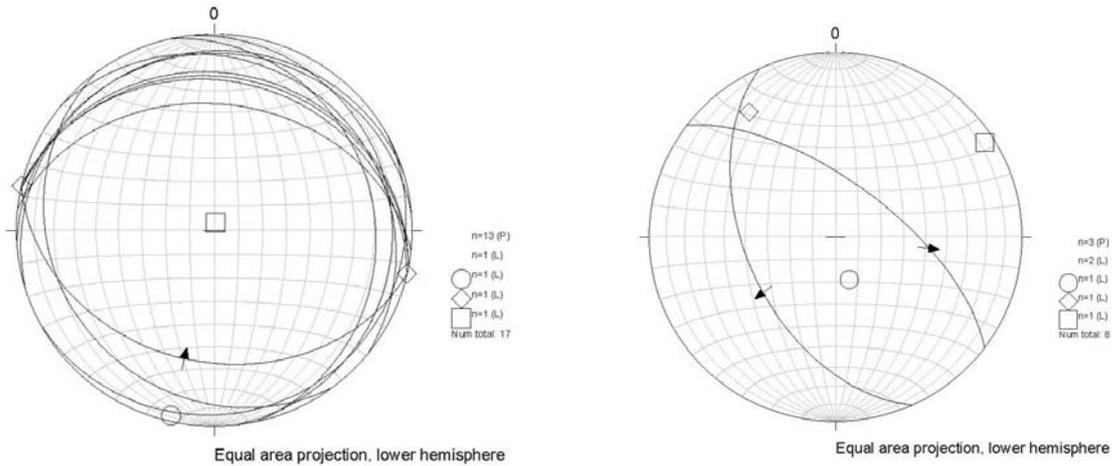


Figure A-63: (a) Conjugate low angle faults. Arrow depicts offset direction of aplite dikes. (b) Quasi-conjugate set of slickensided normal faults. Paleostress symbols on both images: $\circ = \sigma_1$, $\diamond = \sigma_2$, $\square = \sigma_3$.

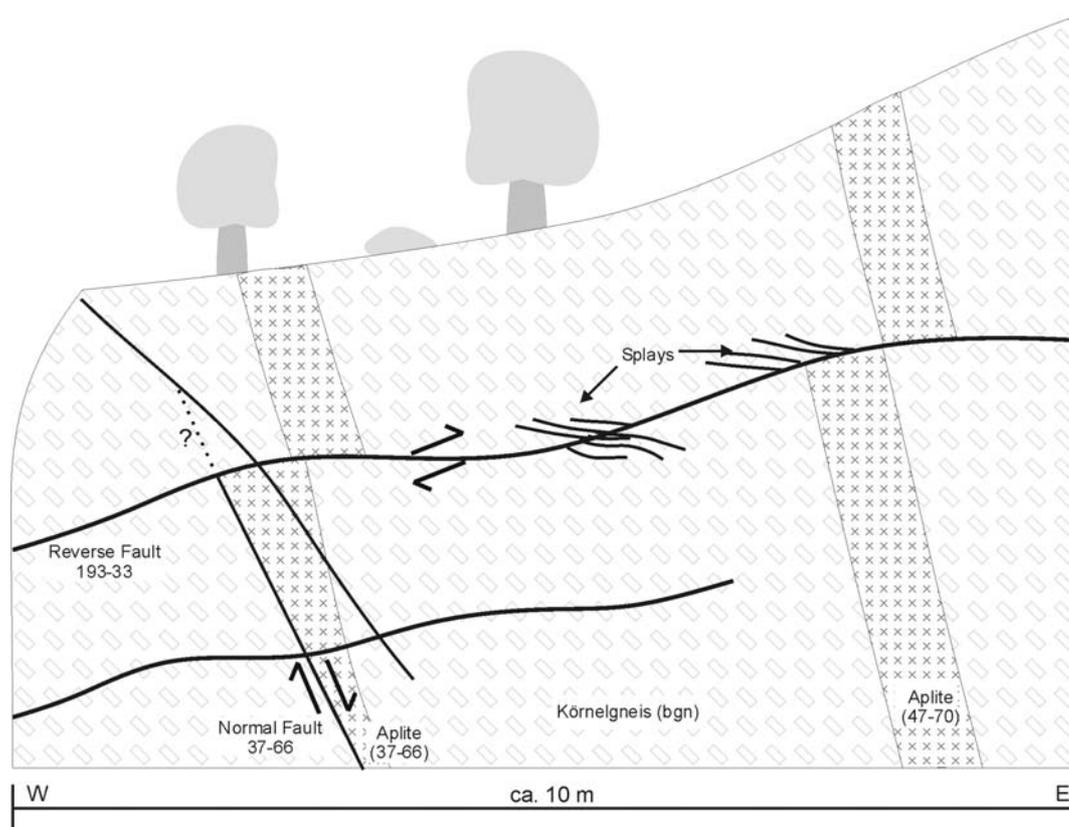


Figure A-64: Partial cross-section of outcrop 6943-13. The large reverse fault (193-33) cuts and offsets two aplite dikes about 50cm reversely. Fault splays, interpreted as synthetic Riedel-shears in the field, also indicate updip motion. Note that the direction of displacement along this fault is not parallel to this section but trends at an angle to it. The slickensided fracture parallel to the contact of the left aplite dike was interpreted as normal fault. It is not clear whether the continues upwards and merges with the fracture cutting across the dike or whether it is cut and offset by the upper thrust fault.



Figure A-65: Offset aplite dike in outcrop 6943-13. Thin red lines: contact to aplite dike (dashed where contact is suspected); bold red line: trace of thrust fault.

The dominant fracture set in this location trends at an acute angle to the face of the outcrop WNW-ESE with steep dips. Fractures in this population are frequently meter-sized (average trace length: 2m), straight, relatively rough and not brecciated. Fracture apertures range between 0 and 1 mm, averaging at 0,5mm; the average fracture spacing is 0,66m. The subvertical NE-SW striking set of fractures is the second most dominant population. Although the average fracture trace length (3,2m, ranging from 1 to 8 m) is larger than that of the WNW-ESE set its spacings (1,27m) are considerably lower. Fracture apertures range from 0,5-2,6mm, averaging at 1,1mm. Fracture planes are relatively smooth to rough and are only occasionally brecciated.

A set of subhorizontal fractures shows a slight tendency to dip in northnortheasterly directions, although SSE dips occur as well. A certain degree of sampling bias due to the vertical extent of the exposure and the limited access to the topmost fractures has to be taken into consideration. Thus, it is possible that it actually represents the dominant set in this

location. Average spacings of 0,55m and 0,94m for fractures and major brecciated/densely fractured zones, respectively are lower than in the sets described above. Fracture apertures range from 1,5-3mm, averaging at 2,1mm; the average trace length is 4,4m (ranging from 1,5 to 10m). Fracture planes are generally rough to very rough, are highly undulatory, and are associated with 5 to 30cm wide brecciated/densely fractured zones. These zones frequently contain moss and plants and moisture. In one zone flowing water was observed. Thus, this set is possibly the most significant with respect to groundwater flow.

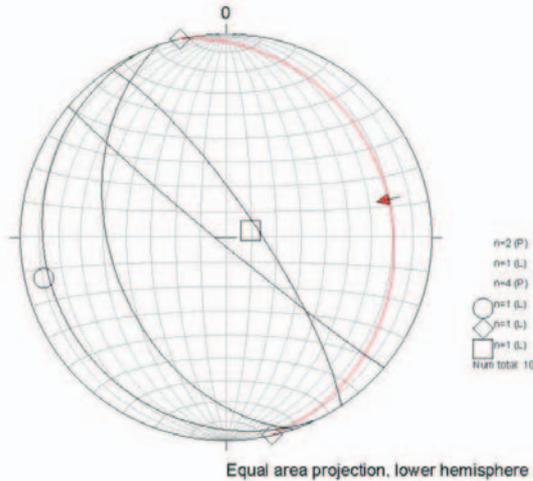


Figure A-66: Brecciated zone (red plane) and associated horsetails (black planes). Red arrow indicates transport direction.

○= σ_1 ◇= σ_2 □= σ_3 .



Figure A-67: Low angle fracture cutting (but not offsetting) a densely fractured/ brecciated zone, thus suggesting two phases of low angle fracturing.

Other sets of steeply dipping fractures generally possess the characteristics of the subvertical WNW-ESE and NE-SW fractures, but are less abundant. The moderately WSW dipping concentration (73f43 in fig. A-62) is a series of contacts and faults in aplite veins and dikes. These dikes, although only local features are heavily fractured and represent irregularly spaced, narrow zones of highly increased permeability. Polished and slickensided planes in the aplite dikes suggest an activation during (normal?) faulting.

A classification of fracture apertures according to fracture dip yields interesting results. Thus, the average aperture for fractures dipping less than 50° is 1,6mm, while the average aperture for fractures dipping more than 50° is 0,9mm.

Figures A-63 to A-67 show various tectonic aspects of the outcrop. Fig. A-63a depicts a conjugate set of low angle thrust faults. Almost all planes are brecciated. Fault splays, interpreted as synthetic Riedel-shears, suggest reverse motion due to a subhorizontal NNE-SSW compression. This transport direction is corroborated by the offset of two aplite dikes (fig. A-64, A-65). Normal motion was detected on slickensided faults following aplite veins. In these veins brecciated zones alternate with polished and slickensided planes. Slickenlines suggest slightly oblique normal displacement as does the angular relationship between the two planes (fig. A-63b). The paleostress configuration suggests NE-SW extension. In case σ_1 and σ_2 are of similar magnitude a transtensional regime seems possible, which would explain both the obliquity of some of the slickenlines and the subhorizontal lineations suggesting right-lateral strike-slip found in other locations (e.g. 6843-01).

Age relationships between the normal faulting and the thrusting events are difficult to establish. As indicated in figure A-64 a contact-parallel normal fault formed at some time in the deformational history of the outcrop. Due to the heavy overgrowth and weathering in parts of the exposure it is not entirely obvious whether or not the normal fault has been offset by the thrusting event. Also, there seems to be no fault at the left side of the hanging part of the aplite dike. Thus, it is possible that either normal faulting occurred after the thrusting and the normal fault extends into the Körnelgneis as indicated by the dotted line in fig. A-64 or that the fault is not contact-parallel (due to the condition of the outcrop this interpretation is possible, see fig. A-65, dashed line) and has in fact been offset by the thrusting. So far, the latter scenario seems more appealing, since the formation of slickenlines is generally attributed to a relatively lower crustal regime compared to the formation of loose fault breccia, and might therefore be relatively older as well.

Splays at the upper end of a densely fractured/brecciated zone (77f20) were interpreted as horsetails suggesting thrusting motion due to ENE-WSW compression (fig. A-66). Since the orientation of this fracture is completely different from the orientations of the other thrusts (fig. A-63a) a different phase of low angle faulting has to be assumed. Another piece of evidence for multiphase low angle faulting exists in the form of a low angle fracture (310f41) cutting, but not offsetting a low angle breccia zone. This fracture is not brecciated, but consists of one single plane (fig. A-67). An age relationship for this set of fractures could not be determined.

One relatively large, moderately NW dipping fracture (310f41) was found to cut one of the undulatory low-angle breccia zones and thus indicates a post-brecciation fracturing event. Thus, the formation of this fracture set might represent the youngest stage of deformation in this outcrop.

Pirka, Gasthof Müller, Outcrop ID: 6843-01

Rock Type: Mid- to fine-grained granite with two types of mica

Outcrop: GK: 456478 E 544117 N; UTM: 345717 E 5441218 N
 The outcrop extends about 42 paces NW-SE, facing SW, and is approximately 3 meters high. Most planes are oxidized or covered with black-grayish minerals. Due to the outcrops proximity to a road some of the dark crust could also be the product of exhaust emissions. Dendritic manganese oxide mineralizations exist where fracture planes intersect. The top part of the outcrop is grusy and strongly weathered, grading into the topsoil.

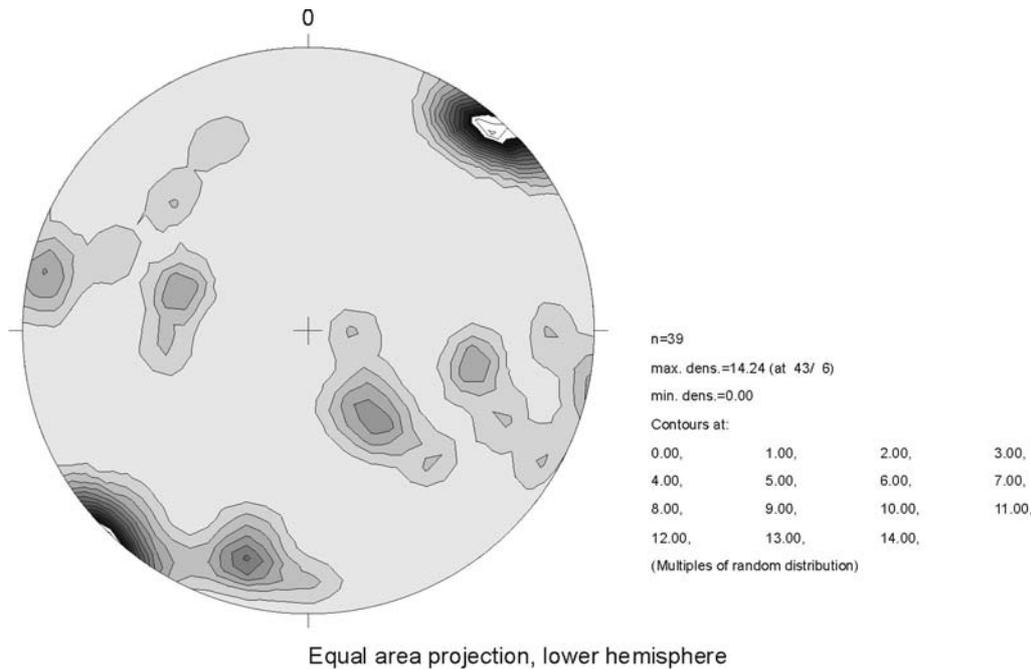
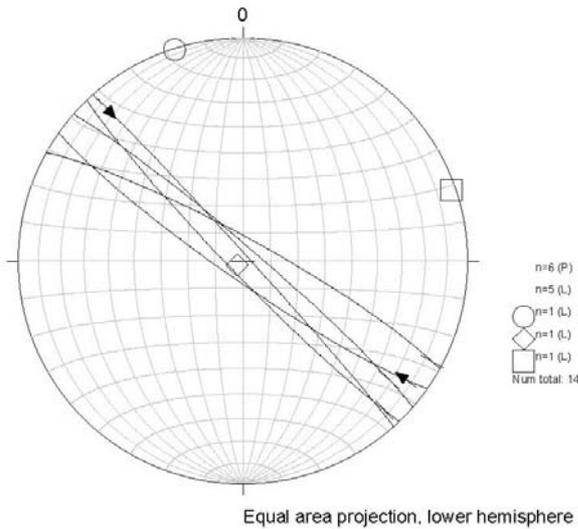


Figure A-68: Contoured poles to all fractures in outcrop (file: 6843-01.jpg).

Mean Trend	Mean Plunge	Angle long axis (°)	Angle short axis (°)	Mrd max.	Comment
43	6	32	31	14,24	
195	18	18	16	6,3	
145	60	57	25	4,7	
283	6	19	15	4,1	
104	41	15	13	3,9	
290	55	34	28	3,7	

The dominant fracture set in this location strikes NW-SE with subvertical dips. Both the largest planes (average trace length is 1,5 meters) and the densest fracture spacings (0.5-1 m) were found in this population. However, due to the low height of the outcrop the size of steeply dipping fractures is generally undersampled. Dendritic manganese oxide mineralizations (figure A-70) are a common occurrence on planes of this fracture set, especially at intersections with fractures of other sets. This implies that manganese-rich fluids were not restricted to the dominant fracture set, but flowed freely throughout the entire fracture network. Many of these fractures contain patches of silicified and slickensided slip planes, all suggesting right-lateral displacement (fig. A-69) due to subhorizontal NNW-SSE compression. Other fractures of this set show plumose and hackly structures thus indicating an origin as extensional joints. Thus, the following sequence of events was envisioned in the field:



- (1) NE-SW extension and formation of joints
- (2) Intrusion of hydrothermal solutions and silicification of joints
- (3) NNW-SSE compression and reactivation of joints as dextral strike-slip faults

Phases (2) and (3) could have occurred contemporaneously.

Figure A-69: Slickensided fractures suggesting dextral strike-slip displacement.

Paleostress configuration: ○= σ_1 ◇= σ_2 □= σ_3 .

Fractures belonging to other populations are relatively scarce and scattered. A subconcentration of the dominant one trends WNW-ESW with steep dips. They could be interpreted as synthetic Riedel-shears related to the steeply dipping, NW-SE striking fracture set. However, this would imply a sinistral strike-slip regime rather than the dextral one implied by the slickensided quartz mineralizations.



A concentration of gently to moderately NW dipping fractures was found. These fractures are frequently associated with zones of densely spaced accessory fractures and breccia. The mean trace length of these zones is 2,9m, the mean aperture is 6,5mm. Due to the low height of the exposure a bias in the estimation of trace lengths is possible (i.e. trace lengths of steeply dipping fractures are underestimated relative to gently dipping ones). Other fracture populations consist of only a few individual fractures and are therefore hard to characterize.

Generally it was found that fracture apertures do not correlate well with fracture strike but with dip. Thus, the mean aperture for fractures dipping $>50^\circ$ is 0,9mm, for fractures dipping $<50^\circ$ 4,25mm. Note that apertures only sampled in N-S to NE-SW striking fractures (i.e. the ones cutting the face of the outcrop) and that the sample size is very small (n = 6).

Figure A-70: Dendritic manganese oxide mineralizations at fracture intersections.

Kötzting, Dampfbachtal, Outcrop ID: DB-01

Rock Type: Relatively fine-grained irregularly foliated para(?)gneiss

Outcrop: GK: 456129 E 545231 N; UTM: 342677 E 5452488 N
The outcrop consists of two faces at right angles to each other. One side extends about 6m in a North-Southerly direction, facing E, the other one reaches approximately 5m E-W, facing S. The exposure is ca. 5m high. All planes are strongly weathered and covered with lichen.

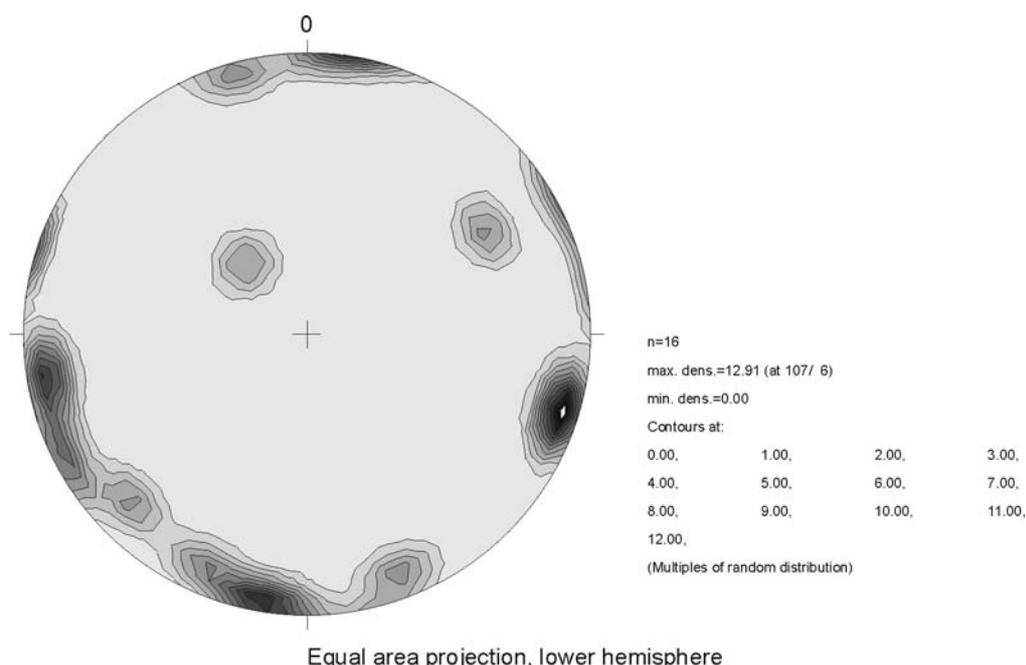


Figure A-71: Contoured poles to all fractures in outcrop (file: DB-01.jpg).

Mean Trend	Mean Plunge	Angle long axis (°)	Angle short axis (°)	Mrd max.	Comment
107	6	25	25	12,91	Other “sets” consist of only 2 to 3 fractures

The dominant fracture set in this location strikes NNE-SSW and dips subvertically. Planes in this population form one face of the exposure and usually measure several meters (average about 2m). Fracture spacings average at approximately 1m with generally massive and unfractured rock in between. Some of the large fractures are associated with brecciated zones, and planes are commonly very rough. One major fracture of this set exposed shiny blackish (polished) patches of an old surface (now mostly weathered away), so fault motion is likely along the NNE-SSE set..

The second dominant set, striking WNW-ESE with subvertical dips, forms the other face of the outcrop. Fractures are similar to the NNE-SSW in size, but are not as abundant. Brecciation also occurs along in this set. Planes are generally rough to very rough. No polished patches were found on planes of this set.

A population of low-angle fractures were also encountered, but only few could be measured due to the geometry of the exposure. They usually trace more than 2m, are spaced at 0,7-1m, brecciated, and frequently contain plants.

Gaisruck (Tiefenried), Outcrop ID: 7044-03

Rock Type: Granit mit Einlagerungen von dunklem Diatexit; Quarz-Glimmer-Diorit (GK25); granite?, probably medium to fine-grained highly homogenized diatexitite (higher biotite content than normal granite)

Outcrop: GK: 457749 E 542533 N; UTM: 357791 E 5424890 N
The outcrop extends discontinuously about 75 meters E-W, facing S, and is up to 10m high. Most planes are covered with lichen.

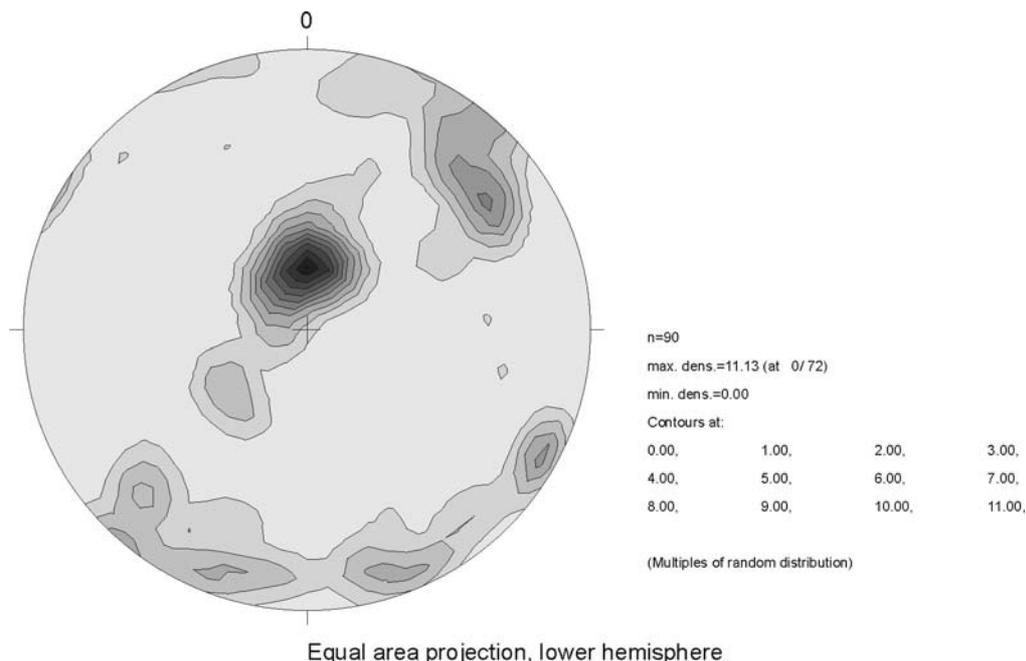
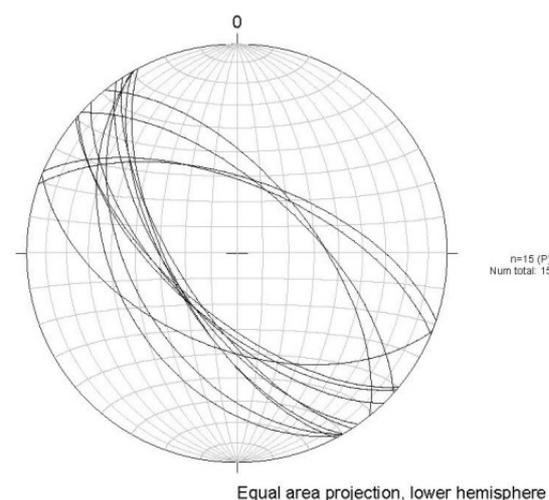


Figure A-72: Contoured poles to all fractures in outcrop (file: 7044-03.jpg).

Mean Trend	Mean Plunge	Angle long axis (°)	Angle short axis (°)	Mrd max.	Comment
0	72	42	31	11,13	Unroofing joints
55	23	36	19	5,3	
120	6	17	14	4,4	
159	6	26	14	3,4	



In this location unroofing joints are the dominant fracture system both with respect to fracture size (average trace length is 8,55m) and spacing (average fracture spacing is 34,7cm). To a certain degree a depth-dependence of fracture spacings was noted, i.e. the fracture density decreased with increasing distance from the topographic surface. However, superimposed clustering effects were found as well, i.e. depth-independent zones of higher and lower densities.

Other fracture sets do not form distinct concentrations. Nonetheless there are a moderately to steeply dipping, NW-SE striking, a subvertical NNE-SSW striking, and a subvertical East-Westerly

Figure A-73: Conjugate set of fractures in location 7044-03 (conjugate angle: 57°).

population. However, their concentrations show only one quarter to one half of the mrd values of the dominant set (see table below fig. A-72).

The fractures trending in East-Westerly directions commonly possess curved and very rough/bumpy planes. Their average trace length is 1,6 m, and their spacings average at 40,5 cm. T-type connections to other fractures, especially unroofing joints, are very common in this set. Thus, they could represent a set of young transform fractures accommodating differential slip along unroofing joints. This could even be the result of present-day gravitational sliding of single unroofing slabs. Due to these considerations they were suspected to be the effects of the quarrying (they strike parallel to the face of the quarry) without any tectonic significance.

In contrast to the E-W fractures the NW-SE trending set are relatively large (average trace length is 3,68 m) and locally densely spaced (average spacing is 75 cm, ranging from 30 cm to more than 1 m). Since the fractures of this population dip both steeply to moderately NE and SW they form a conjugate set (conjugate angle 57°) implying a subvertical σ_1 and NE-SW extension.

The subvertical NNE-SSW striking fracture set is of only minor importance. The average trace length is 0,84 m, the average fracture spacing is 168,8 cm.

Only few kinematic indicators were found, none of which gave unequivocal transport directions.

Wurzer Spitze, Outcrop ID: 6843-02

Rock Type: Partially layered, medium-grained gneiss, some banding (light-dark); Perlgneis? intruded by aplite veins

Outcrop: GK: 456715 E 544409 N; UTM: 348195 E 5444039 N
The outcrop extends ca. 10m NNE-SSW, facing ESE. It is 2.5-3m high. Almost all planes are covered with moss and lichen, and are heavily weathered.

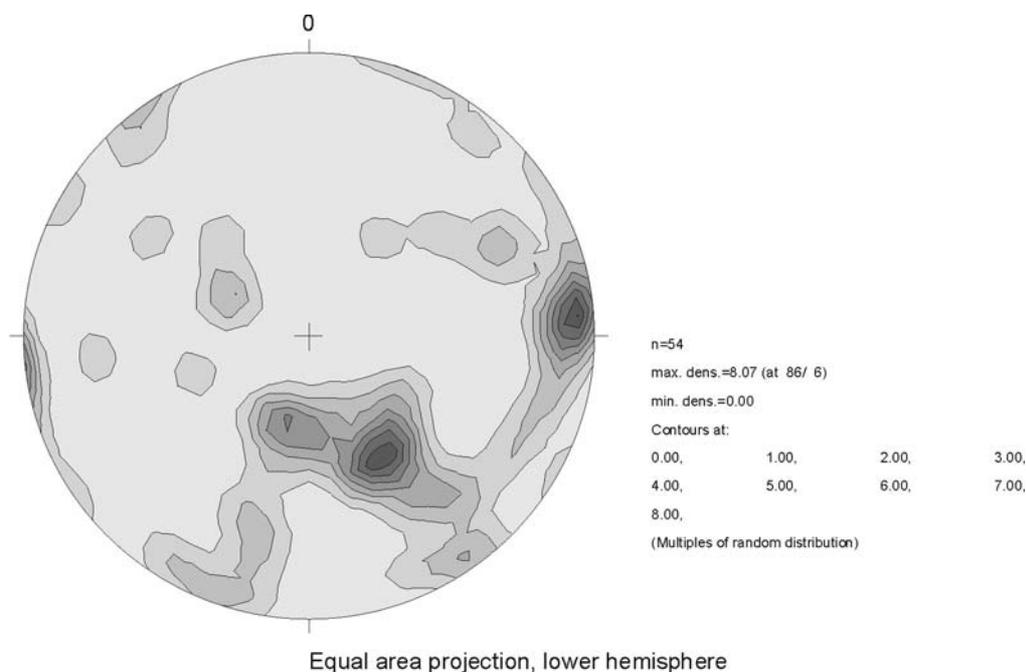


Figure A-74: Contoured poles to all fractures in outcrop (file: 6843-02.jpg).

Mean Trend	Mean Plunge	Angle long axis (°)	Angle short axis (°)	Mrd max.	Comment
86	6	26	21	8,07	Foliation parallel
146	48	63	28	8,0	
300	66	32	18	3,0	

There are two dominant fracture sets in this outcrop. One trends N-S dipping subvertically, the other one dips gently in north-northwesterly directions and is oriented parallel to the gneissic foliation. Both of these populations are partially intruded by aplite veins, thus indicating a late-paleozoic formation age with later brittle reactivation evidenced by fractures with similar orientations in the aplite. Several planes of the N-S striking population are relatively smooth, although rough ones exist as well. Trace lengths are highly variable ranging from 0,5 to >3m. Fracture spacings were also highly variable and could not be determined. Some densely spaced zones (spacings of about 2cm) of smaller fractures were found.

Fractures parallel to the foliation are among the largest in the outcrop. Trace lengths are variable, ranging from 0,5 to >3m, although planes generally tend to be larger than those of the N-S set. However, due to the gentle dip of the foliation parallel fractures and the low height of the exposure the trace length estimation is likely to be biased towards higher values for the fractured foliation. Spacings of fractures traceable over several meters are approximately 2m on average. Densely spaced zones (ca. 5cm spacings) of smaller fractures occur occasionally. Planes in this population are rough to very rough and sometimes are associated with breccia.

A minor concentration dips gently SSE, thus forming a 60° angle with the fractured foliation. Brecciation was observed on one such plane. Planes tend to be rough. Other physical properties were not recorded. Other fractures are highly variable in their orientations and physical properties. They commonly trace <1m.

Generally, it was observed that the aplite veins were more densely fractured than the surrounding gneiss, although these fractures –probably due to the limited extent of the veins – are shorter. Since a foliation is absent in the aplite the subvertical N-S trending fractures are predominant. Fracture planes in the aplite are smoother than in the gneiss.

A large number of fracture in this location are gaping and show highly rounded and weathered edges where they intersect the outcrop surface. Thus, sensible aperture measurements could not be taken. Although it is assumed that the rocks are still in situ slight gravitational motion as well as unloading are believed to be responsible for these excessive apertures. Fracture orientations are expected to be widely accurate.

No kinematic indicators were observed in this location.

Frath, Sender, Outcrop ID: 6944-15

Rock Type: Metatektischer bis anatektischer Cordierit-Sillimanit-Gneis (cgnj; GK 25); medium (to locally fine)-grained gneiss with a locally well-developed foliation; in other places the rock is rather massive or the foliation is heavily undulatory.

Outcrop: GK: 457483 E 543970 N; UTM: 355694 E 5439348 N
The outcrop is a discontinuous, NW-SE striking ridge, a section of which was measured. It extends about 19 paces NW-SE, faces SW, and is ca. 2.5m high. Most planes are strongly weathered and covered with moss and lichen. It is questionable if parts of the outcrop are still exactly in place.

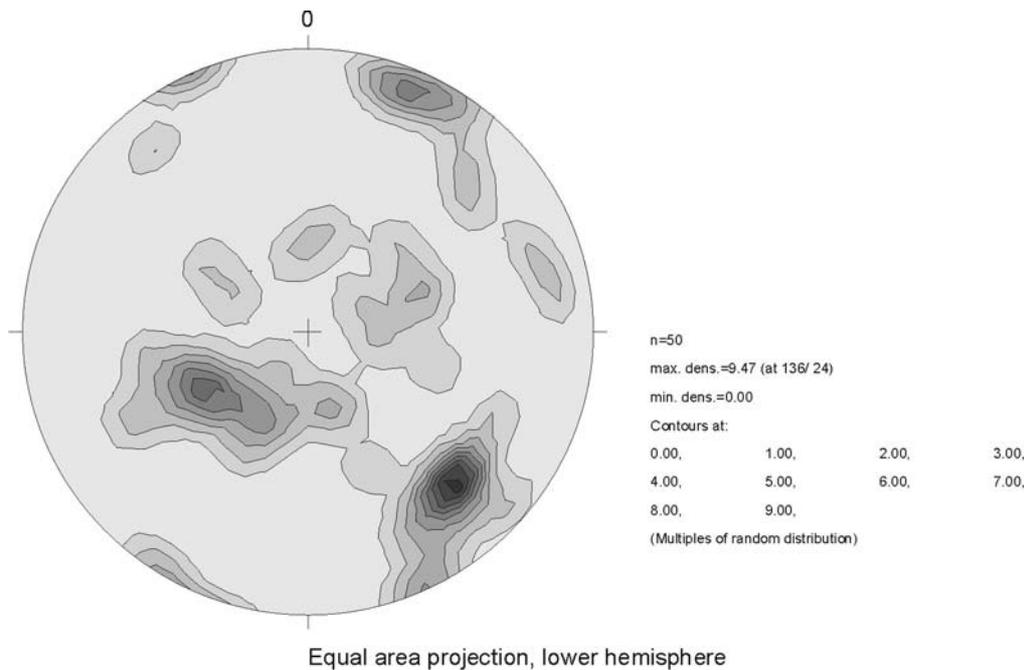


Figure A-75: Contoured poles to all fractures in outcrop (file: 6944-15.jpg).

Mean Trend	Mean Plunge	Angle long axis (°)	Angle short axis (°)	Mrd max.	Comment
136	24	24	22	9,47	
240	54	68	23	6,8	Foliation parallel
335	0	12	5	4,1	
70	54	49	35	3,4	Foliation parallel

Due to the bad condition of this outcrop little can be said about its tectonic structures. The fractures parallel to the foliation are highly irregular, are usually short and discontinuous, and do not show a characteristic spacing. Other fractures do not expose regular features as well. Almost all planes in this location are rough to very rough.

The steeply dipping, NW-SE striking set as well as the more gently dipping specimen seem to possess the largest planes (sampling bias for low angle fractures due to the low outcrop height is possible). The steeply dipping, NE-SW striking fractures seem to be the most abundant (see fig. A-75, again: possible oversampling due to outcrop geometry). They frequently connect low angle fractures and are thus of a rather limited length (0,5-1m). No kinematic indicators were found in this exposure.

Steinbruch am Eck, Outcrop ID: 6843-03

Rock Type: Granat-Cordierit-Sillimanit-Gneis (Troll, 1967); relatively massive medium-grained gneiss, locally well foliated (migmatitic) and folded; two fold generations: b_1 (older): subhorizontal NE-SW trending; b_2 : moderately WNW plunging, WNW-ESE trending. b_2 refolds b_1 . In other places the foliation looks fairly straight, especially where concordant aplite veins intruded with sharp contacts.

Outcrop: GK: 457278 E 544472 N; UTM: 353852 E 5446940 N
The exposure extends 28 meters WNW-ESE, facing SSW, and is up to about 10m high. Many planes look relatively fresh (the location was quarried from 1957-1960, Troll (1967)), although some moss and lichen are present.

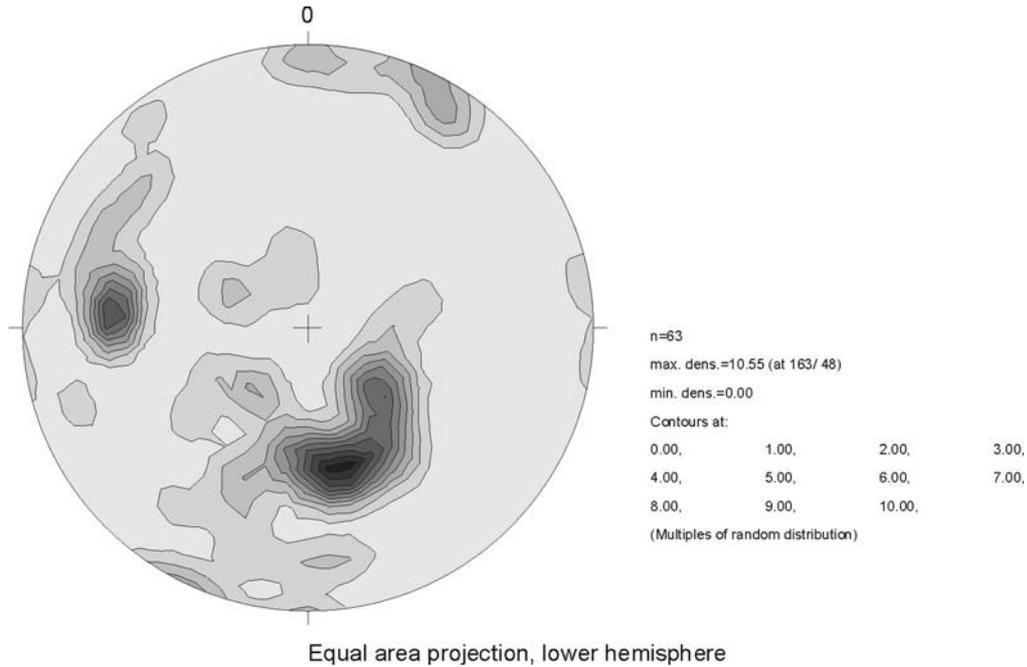


Figure A-76: Contoured poles to all fractures in outcrop (file: 6843-03.jpg).

Mean Trend	Mean Plunge	Angle long axis (°)	Angle short axis (°)	Mrd max.	Comment
163	48	56	31	10,55	Mostly foliation parallel
275	29	55	31	7,7	
32	13	24	15	3,7	
299	65	35	19	2,4	

The most striking observation in this location is that large parts of the outcrop are very massive and virtually unfractured. These unfractured parts seem to coincide with either unfoliated or heavily folded section of the exposure. Generally, foliation parallel fractures seem to be dominant though highly irregularly spaced (from <0.5 to >2 meters). Trace lengths are also highly inconsistent in this set. They range from <1 to >10 meters. Fracture apertures seem to depend on the fracture trace lengths, such that longer fractures are more open than shorter ones. Some large foliation parallel fractures are brecciated and thus suggest low angle thrust or normal motion.

Cross fractures are highly irregular in terms of length, spacing etc. Sometimes two to three short (<1m trace length) fractures are relatively closely spaced (30-40cm), but the average spacing seems more like >1-2m, sometimes even more. Only few cross fractures trace more than one meter, most lengths lie between 0,5 and 1m. A dominant fracture population could not be determined in the field. From the plot above the foliation parallel set seems to be the most abundant.

Few kinematic indicators were found in the form of slickensided fracture planes. Only one slickenside could be attributed with a shear sense, which suggests right-lateral displacement and thus a NNW-SSE oriented compressive regime. The fractures dip moderately to steeply NE to ENE and are in part foliation parallel.

Viechtach, Alterberg (Radweg), Outcrop ID: 6943-14

Rock Type: Körnelgneis (bgn; GK 25); gneissic rock, partially foliated with large plagioclase phenocrysts, in between layers of fine-grained rock; granite dike

Outcrop: GK: 456541 E 543896 N; UTM: 346252 E 5438980 N
The outcrop extends about 71 meters NE-SW, facing SE. It is up to ca. 20m high. Most planes are heavily weathered and covered with lichen.

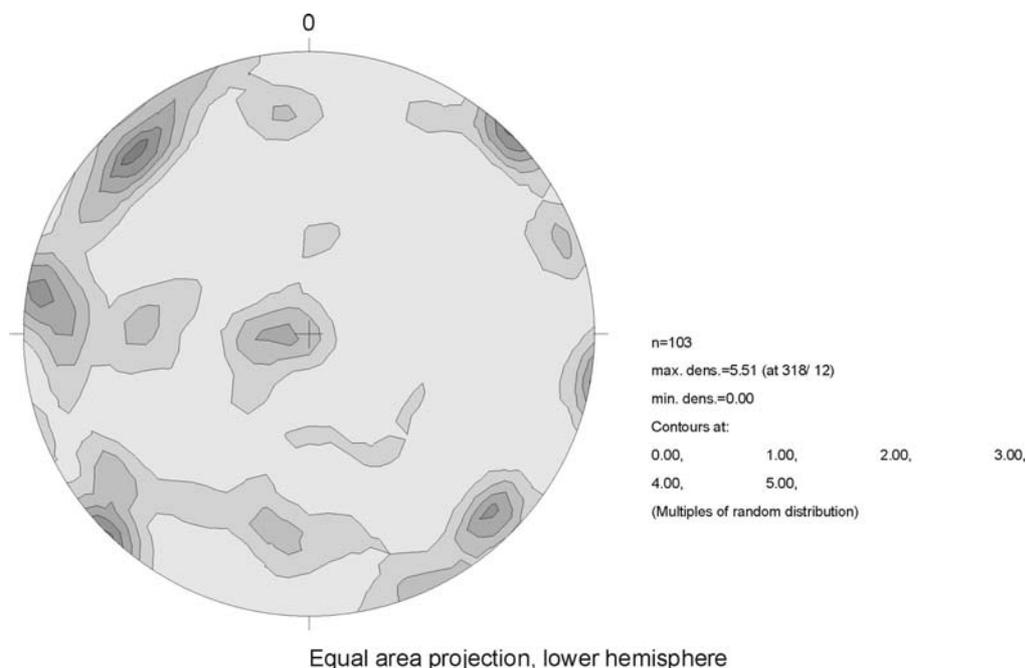


Figure A-77: Contoured poles to all fractures in outcrop (file: 6943-14.jpg).

Mean Trend	Mean Plunge	Angle long axis (°)	Angle short axis (°)	Mrd max.	Comment
318	12	33	17	5,41	
225	1	34	17	5,1	
279	5	35	16	4,5	
134	11	17	18	4,3	
269	79	41	29	3,3	
187	30	15	9	2,5	

The dominant fracture system in this outcrop is subvertical and trends NE-SW, subparallel to the face of the exposure. Several large planes are slickensided and suggest subhorizontal sinistral strike-slip motion due to a subhorizontal NNE-SSW directed compression ($194\sigma_1$; 34 ; $293\sigma_3$; 16). Fracture sizes range from 0,8-5 meters. Spacings were determined to be about 2 meters and larger. Planes are mostly rough, although some (relatively) smooth ones also occur, especially in the granitic dike.

The subvertical NW-SE trending system is the second most important one. Locally, its fractures have the highest density, especially at the SE end of the outcrop (0,5-1m), whereas in other places the density is significantly lower and highly irregular. In general, it decreases towards NE. The average fracture size is ca. 2,2m, values range from 0,7 to 7 meters. The average aperture is 0,3mm, being <1mm in all cases; many fractures are completely closed. Planes are generally relatively smooth to relatively rough. A number of fractures terminate at low-angle (unroofing) joints, although some also cut across, in which case no offsets were observed. Two large fractures (4 and 5m trace length) are associated with a 5cm wide densely fractured zone or 8cm of breccia/gouge, respectively.

Low angle fractures are the third dominant system. They possess the largest planes (in part due to sampling bias from the outcrop geometry), ranging from 0,7 to >21 meters averaging around 7 meters. Planes are generally relatively rough to very rough. Apertures are relatively high with an average of 1,7mm, ranging from 0,5 to 5mm. Spacings are relatively irregular and range from 1 to 3 meters. Many of the low angle fractures are either wet or even show water dripping out of them. The set can be subdivided into two groups. One group is composed of clear-cut fractures, which are thought to be unroofing joints, which have not undergone shear deformation. The other group is associated with up to 80cm wide zones of breccia, gouge and densely spaced small fractures. Thus, the second group is interpreted as low-angle (thrust?) faults, or reactivated unroofing joints.

Mineralizations of fracture planes were not observed, possibly due to the cover of lichen and weathered material.

Regen, Schönecker Riegel, Outcrop ID: 6944-16

Rock Type: Metatektischer bis anatektischer Cordierit-Sillimanit Gneis (cgnj; GK 25). Foliated gneiss with strongly developed melano- and leucosome zonation; at least two folding phases.

Outcrop: GK: 548309 E 543057 N; UTM: 363591 E 5429909 N
 The outcrop extends 49 meters WNW-ESE (110°), facing SSW. It is about 6m high. Most planes are heavily weathered and covered with moss and lichen.

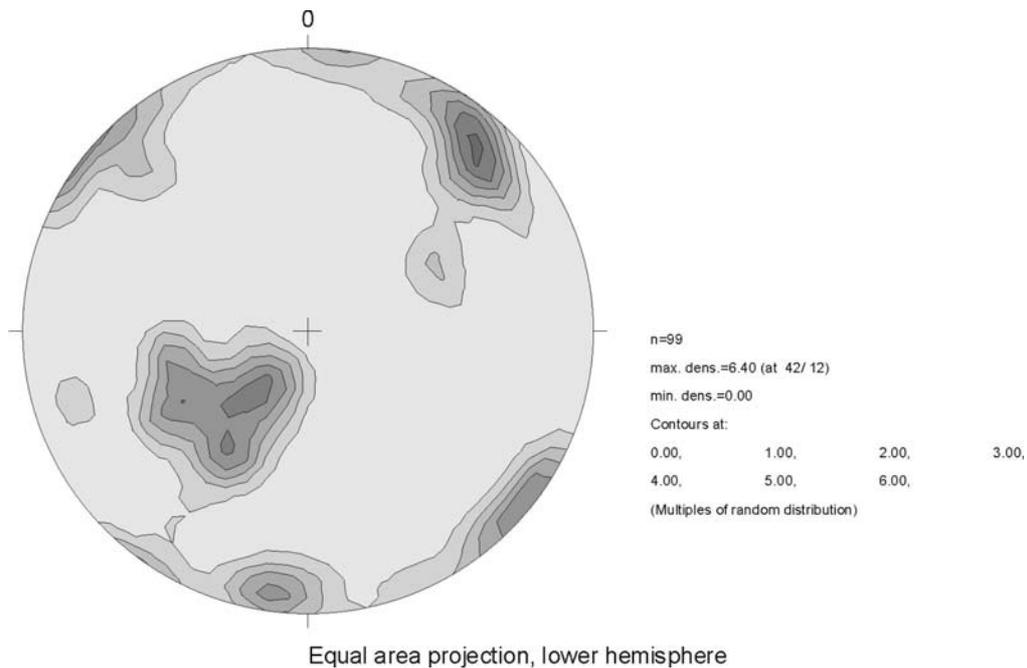


Figure A-78: Contoured poles to all fractures in outcrop (file: 6944-16.jpg).

Mean Trend	Mean Plunge	Angle long axis (°)	Angle short axis (°)	Mrd max.	Comment
42	12	38	33	6,12	Foliation parallel
225	67	54	51	5,4	
128	6	32	31	4,6	
188	5	23	21	4,3	

In the field, the most abundant fracture set was determined to be the one parallel to the foliation. In the plot above it is only the second most abundant. Foliation parallel fracture planes are smooth to very rough, depending on the grain-size and the degree of folding of the rock section they

cut. Thus, fractures in fine-grained sections and sections with no folding are straight and smooth, fractures in coarse grained and tightly folded sections are rough and undulatory. The fracture density is higher in sections where the foliation is unfolded and straight. For the entire outcrop the fracture density is highly irregular ranging from a few centimeters to over one meter. Trace lengths range from 0,5 to 1,5 meters, averaging at 1,05m.

According to the plot in fig. A-78 the most abundant set dips steeply SW. It consists of large planes (the largest in this location), many of them several meters in diameter. The fractures form the face of the outcrop. Most planes are straight and relatively rough to very rough, although a few relatively smooth ones exist as well. In the field the small population of moderately SE dipping fractures bulging out from the main concentration was interpreted as a set conjugate to the foliation parallel fractures. The measured angle between the maxima in the plot lies at 64°. This would suggest a subvertical σ_1 and NE-SW extension.

In the field, the NE-SW trending population was determined to be the second most important set. The plot shows otherwise. The planes are comparatively short, ranging from 0,2 to 3 meters in length (average: 1,43m) and predominantly relatively smooth, although some rough ones exist as well. The population of subvertical WNW-ESE trending fractures is of only minor importance. Fractures in this set trace between 0,2 and 1,7 meters with an average trace length of 0,75m. Planes are generally relatively rough to very rough.

No kinematic indicators were found in this location.

Quarzbruch Zuckenried, Outcrop ID: 6944-17

Rock Type: Pfahlquarz

Outcrop: GK: 457450 E 543037 N; UTM: 345998 E 5430048 N
The outcrop extends 45 meters WNW-ESE (120°), facing NNE. It is ca. 7m high. Some planes are covered with lichen; many are covered with silt and/or sand.

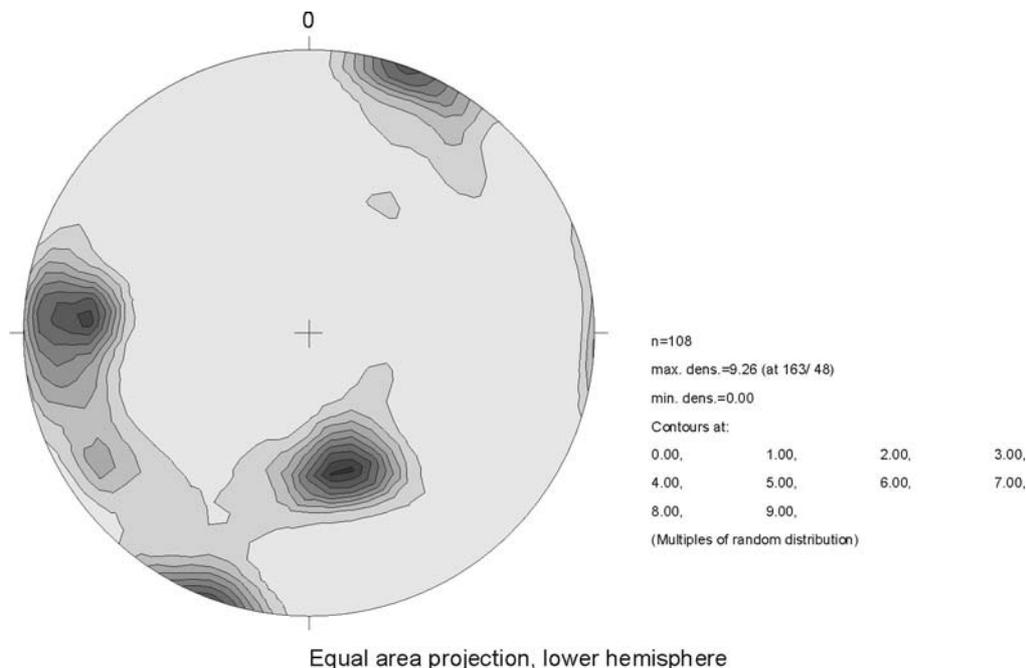


Figure A-79: Contoured poles to all fractures in outcrop (file: 6944-17.jpg).

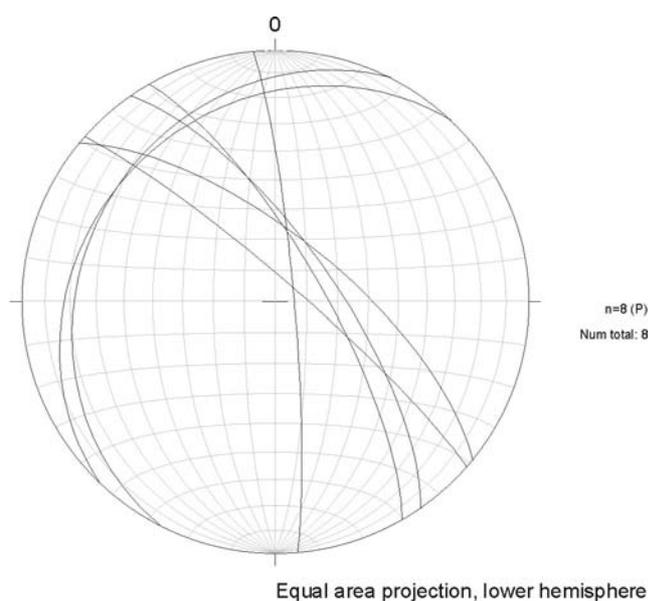
Mean Trend	Mean Plunge	Angle long axis (°)	Angle short axis (°)	Mrd max.	Comment
163	48	38	31	9,26	
274	23	58	33	8,4	
20	1	31	24	7,5	

The Pfahlquarz outcrops are the most densely fractured ones in the entire study area. Many fractures are filled with sand/silt-sized material. The majority of those fractures is very short (<40cm trace length). These fractures usually possess highly variable orientations and were therefore not measured. However, the larger ones are much more consistent in their orientations as fig. A-79 shows. Also, a correlation between fracture size and spacing was observed. Thus, the larger a fracture is the larger is also the distance between fractures of this size.

In this location there are three fracture populations of almost equal importance. According to fig. A-79 the dominant set dips moderately to gently in northerly directions. Several of those fractures are associated with breccia. In one case the breccia are imbricated in a way which suggests thrust motion. A tiny set of moderately SSW dipping fractures could be conjugate to these thrust faults. The resulting stress field would be a subhorizontal N-S to NNE-SSW directed compression. Trace lengths in northerly dipping set range from 0,4 to 5,5 meters (average 1,7m). The planes are smooth to very rough. The average fracture spacing is 0,27m, ranging from 0,13 to 0,75m

The two steeply dipping populations are similarly abundant, only their trace lengths are somewhat shorter (possibly in part due to a sampling bias from the outcrop geometry). For the WNW-ESE striking set the average length is 0,87m, ranging from 0,4 to 3 meters. Fracture planes are relatively rough to very rough, and the spacing averages at 0,19m, ranging from 0,09 to 0,3m. For the N-S striking set the average trace length is 1,67m, the shortest being 0,25m and the largest being 7m. The set also possesses the highest density with an average spacing of 0,18m and a range of 0,07 to 0,4 meters. Planes are relatively smooth to very rough. Thus, this set is, in contrast to fig. A-79, the dominant one. However, the orientations are more widely scattered, so the contour plot does not show it as such a high concentration.

Several quartz veins were observed, i.e. reactivated silicified fractures. The veins are oriented similar to the now open fractures (fig. A-80), which suggests that these fracture systems originated at a time during which hydrothermal fluid still circulated in the rocks. Today's open fractures are thus reactivated features.



No kinematic indicators were found in this location.

Figure A-80: Fractured quartz veins in location 6944-17.

Steinbruch Teufelstisch, Bischofsmais, Outcrop ID: 7044-04

Rock Type: Mittelkörniger Granit (Gm, GK 25); Granite

Outcrop: GK: 457796 E 542227 N; UTM: 358237 E 5421367 N
The outcrop extends about 160 meters NNW-SSE (350°), and ca. 13 meters ENE-WSW. The main wall faces WNW. Many planes are fresh, only some are covered with moss and lichen. Many are surficially mineralized by manganese oxides.

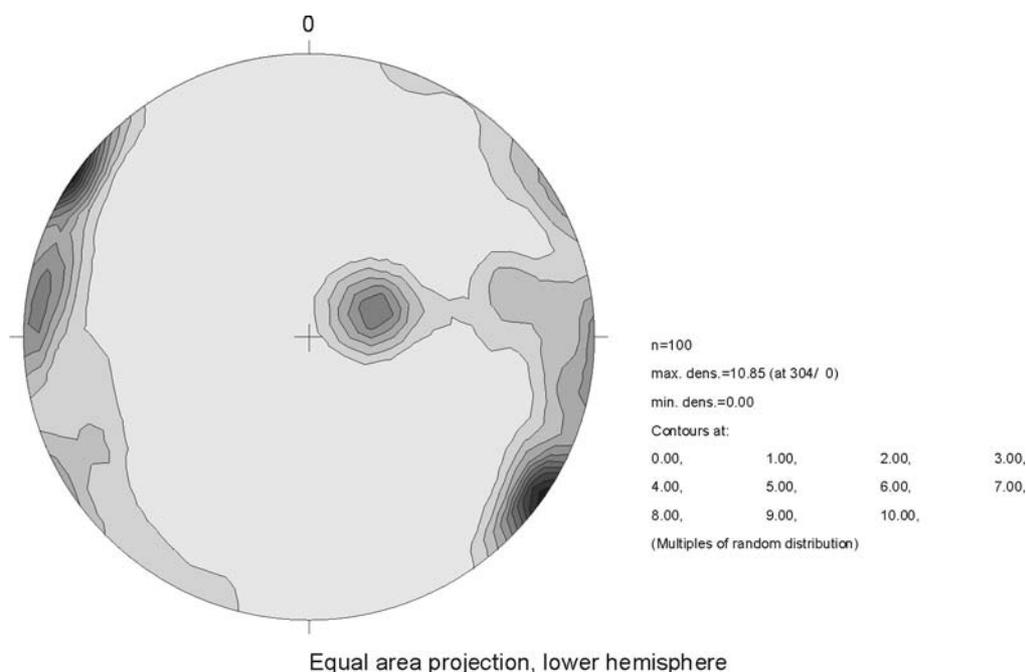


Figure A-81: Contoured poles to all fractures in outcrop (file: 7044-04.jpg).

Mean Trend	Mean Plunge	Angle long axis (°)	Angle short axis (°)	Mrd max.	Comment
304	0	29	22	10,85	Unroofing joints
278	6	25	17	5,6	
70	72	26	23	5,5	
61	1	25	23	3,5	

According to fig. A-81 the dominant fracture system in this location trends NE-SW although its average fracture spacing of 0,93 m (minimum: 0,13 m; maximum: 7 m) ranks only second lowest. This is due to a sampling bias, since the fractures were measured along the longest part of the outcrop wall. Fractures are frequently mineralized with hydrothermal minerals. Trace lengths average at 1,57 m, ranging from 0,2 to 4 m. The average aperture is 0,2 mm, ranging from closed to 0,7 mm. Planes are mostly straight and smooth to relatively smooth, although rough ones were also observed. Some fractures connect unroofing joints. One plane exposes plumose structures, thus suggesting an origin as extensional joint and a possible reactivation by shear.

Several planes of this set are slickensided they were interpreted both as normal and reverse faults (due to the high angle a clear identification was not always possible). Normal motion suggests WNW-ESE extension ($68\sigma_1$; $284\sigma_3$), reverse motion suggests a similar extensional direction, however with a less steeply inclined σ_1 ($302\sigma_1$; $108\sigma_3$). Slickensides indicating both dextral and sinistral strike-slip displacement were also found, although they are more abundant in other sets (see fig. A-82).

The dominant system with respect to fracture spacing and plane size is represented by the unroofing joints. Fracture spacings average at 0,55 m (minimum: 0,12 m; maximum: 1,4 m), while a

general increase of spacings away from the topographic surface was observed. Trace lengths frequently exceed the lateral extent of the outcrop. The average measured trace length lies at 12,47 m (minimum: 3 m; maximum: >40 m). The fractures possess the largest apertures in the database (average: 2,21 mm; min: 0,5 mm, max: 12 mm). Almost all planes are very rough. Several fractures are wet or expose dripping water.

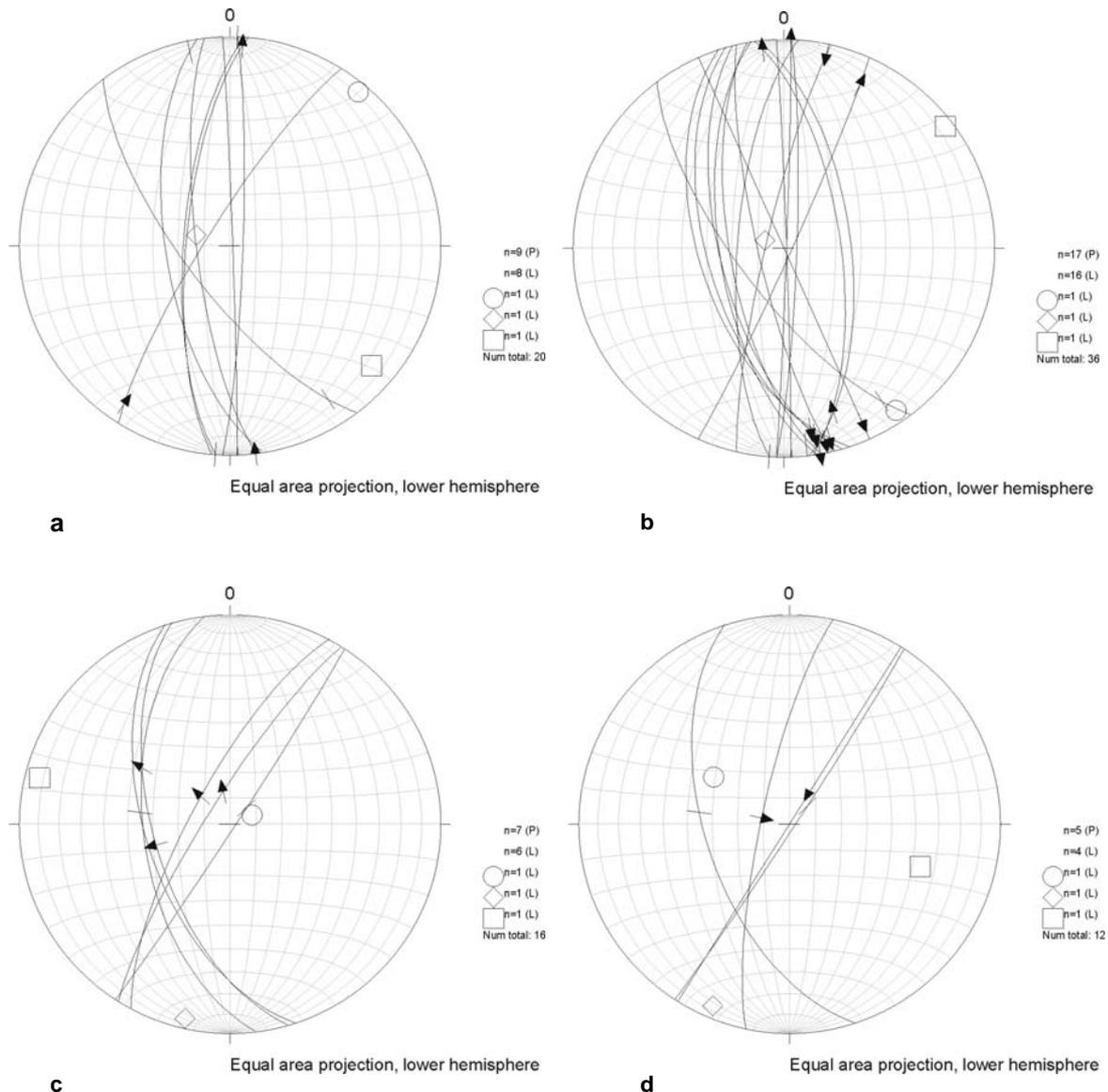


Figure A-82: Slickensided fractures in location 7044-04. (a) Dextral strike-slip (b) Sinistral strike-slip (c) Normal motion (d) Reverse motion. ○ = Paleostress σ_1 ◇ = Paleostress σ_2 □ = Paleostress.

N(NW)-S(SE) striking fractures represent a relatively strong population in fig. A-81, although their average spacing of 1,45 m (min: 0,35 m, max: 3,95 m) is the largest measured in this outcrop. Due to the exposure's small ENE-WSW extent, which cannot attenuate a large lateral variability as well as the NNW-SSE direction, a sampling bias is likely. Trace lengths average at 2,27 m (min: 0,2 m; max: >10 m), the mean aperture lies at 0,5 mm, ranging from closed to 1,4 mm). Planes are on average straight and relatively rough, although roughness varies from smooth to rough. Many of the planes are slickensided (fig. A-82), a number of them are covered with hydrothermal mineralizations such as quartz/feldspar, chlorite and epidote. Plumose structures on some planes suggest an origin of this set as extensional joints and a later reactivation by shear.

A general observation is that the fracture densities in all sets seem to decrease with increasing depth below the topographic surface, which, however, could also be due to the outcrop geometry.

Böbrach, Wolfgangskapelle, Outcrop ID: 6944-18

Rock Type: Metatektischer bis anatektischer Cordierit-Sillimanit-Gneis (cgnj, GK 25); Well-foliated gneiss, some folding.

Outcrop: GK: 457569 E 543694 N; UTM: 356558 E 5436109 N
 The outcrop extends about 38 meters NW-SE (300°) and ca. 10 meters NE-SW. It is about 10 meters high. The rocks are heavily weathered; most planes are covered with moss and lichen. Parts of the outcrop are covered with soil and debris.

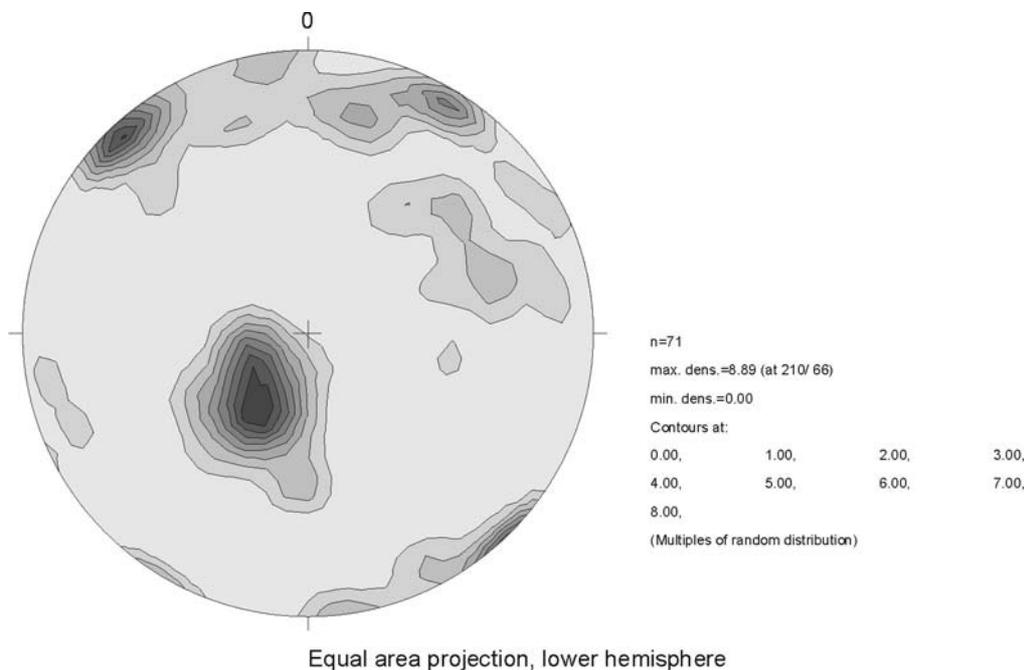


Figure A-83: Contoured poles to all fractures in outcrop (file: 6944-18.jpg).

Mean Trend	Mean Plunge	Angle long axis (°)	Angle short axis (°)	Mrd max.	Comment
210	66	62	50	8,89	Foliation parallel
317	6	27	27	8,2	
30	7	39	16	5,3	
73	36	44	36	2,7	

In terms of abundance the dominant fracture set in this location is parallel to the gneissic foliation, which, however, is highly variable and dependent on rock properties. Foliation parallel fractures occur (a) as 1 to >3 meters tracing undulatory fractures spaced at 0,1 to 1m in sections of the outcrop where the foliation is well-developed an unfolded or (b) as intricate patterns of highly undulatory/curved fractures with trace lengths <0,1m, which form a highly connected network (fig. A-84). The second variety seems to be concentrated in sections of the outcrop where the foliation weakly developed, partly destroyed, or tightly folded. Large parts of the outcrop show almost no foliation parallel fractures. There the spacings of small, unconnected fractures usually exceed 5 meters. For the entire exposure the average trace length is 1,52m. ranging from 0,38 to 3,75m (n.b.: the short, undulatory fractures forming the highly connected networks could not be measured). All planes of this set are relatively to very rough.

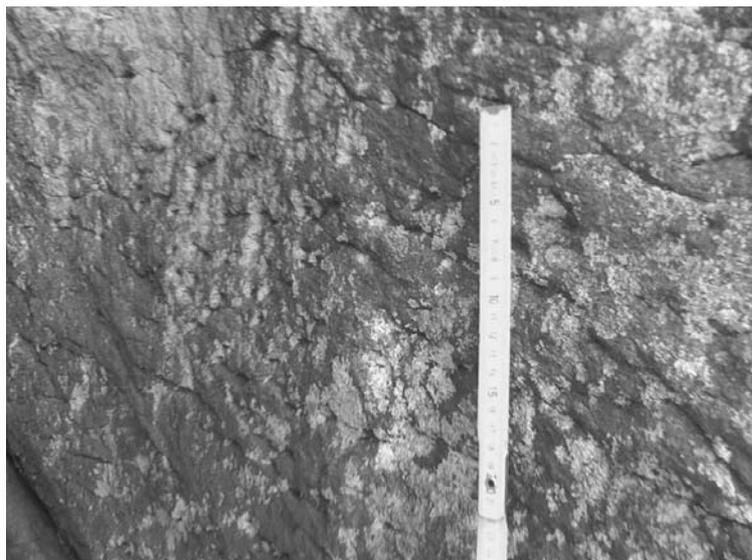


Figure A-84: Short, irregular fractures parallel to the foliation.

In the field the steep NE-SW and WNW-ESE striking fracture sets were determined to be the dominant ones. The former consists of large, straight, and relatively smooth planes with an average trace length of 3,17m (min: 0,4m; max: >10m). Fractures frequently occur in densely spaced zones (spacings of 10-15cm), which in turn occur every 3-5m. The latter is made up of very large, relatively rough and straight planes tracing on average 3,49m (min: 0,55m; max: >10m). They form the face of the outcrop. On fractures of both sets patches of quartzofeldspathic as well as ore mineralizations occur. Due to the outcrop geometry fractures of the NE-SW set are most likely undersampled with respect to fracture size while the WNW-ESE

fractures are probably undersampled with respect to their abundance.

A minor fracture population dips moderately SW. It was not described in the field. The mainly straight and relatively rough fractures possess an average trace length of 3,3 meters with a range of 1,2 to 8m. A conjugate relationship to the foliation parallel fractures is possible. This would suggest normal motion along those two sets due to \pm NE-SW extension.

Generally, weathering and gravitative processes most likely have increased fracture roughness and aperture.

Kaitersberg/Kötztinger Hütte, Outcrop ID: 6843-04

Rock Type: Massive, granitic? gneiss; foliation (where present) seems relatively straight; most planes mineralized with quartz/feldspar (former veins) and leached-out ores.

Outcrop: GK: 456890 E 544896 N; UTM: 350255 E 5448380 N
The outcrop extends about 24 paces NW-SE (ca. 300°) and 19 paces NE-SW (ca. 40°). The walls face SW and SE, respectively. The exposure is up to 5 meters high. All planes are covered with moss and lichen, and are strongly weathered.

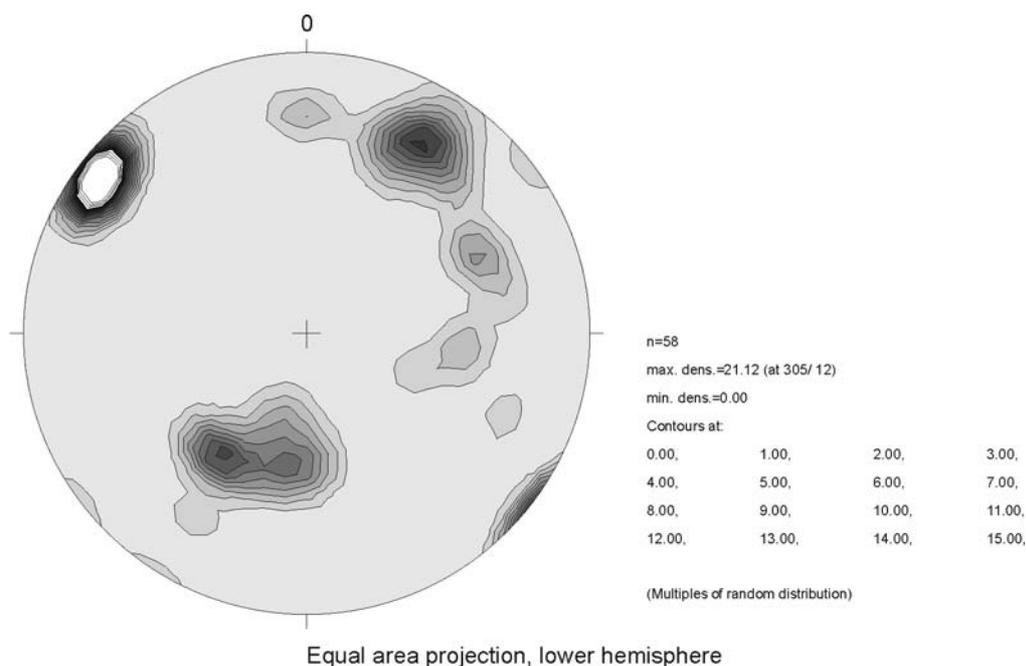


Figure A-85: Contoured poles to all fractures in outcrop (file: 6843-04.jpg).

Mean Trend	Mean Plunge	Angle long axis (°)	Angle short axis (°)	Mrd max.	Comment
305	12	35	33	21,12	Foliation parallel
32	29	38	32	9,2	
214	47	53	48	8,6	
66	34	21	15	4,2	

The dominant fracture system in this location is the subvertical NE-SW trending one. Besides its high density (average fracture spacing: 0,24m, min: 0,03m, max: 0,68m, median: 0,17m) it, also possesses the largest planes in the outcrop (average trace length: 1,86m, min: 0,25m, max: >4,5m, median: 1,03m). However, planes in this set are generally straight, smooth, and thus closed. Also, they are frequently mineralized with polished-looking quartz/feldspar as well as leached-out ore coatings. It is only in this set that slickenlines subparallel to the dip azimuth exist. The suggest normal motion due to uplift and NW-SW extension (266 σ_1 66; 136 σ_3 17).

The population of northwest-southeasterly striking fractures consists of one highly concentrated main group (center: 32-29; fig. A-85) and two subgroups. Fractures in this set are characterized by relatively short (mean trace length: 0,61m, min: 0,2m, max: 2,1m, median: 0,5m), and on average relatively rough and undulatory planes. With a mean spacing of 0,43m (min: 0,13m, max: 1,03m; median: 0,37m) the fracture density is the lowest in this location. Some planes are mineralized with leached-out ores. A conjugate relationship between the main group and the foliation-parallel fractures is possible (conjugate angle of ca. 68°). This would suggest normal motion due to uplift and NE-SW extension.

The foliation parallel fractures are very irregularly distributed, often end blindly in the rock and are relatively short (average trace length: 0,66m, min: 0,4m, max: 1,1m, median: 0,66m). The fracture spacing averages at 0,1m (min: 0,04m, 0,22m, median: 0,1m). However, as in many other locations in the gneissic area there are regions with a network of very undulatory and short, but highly connected foliation parallel fractures in the outcrop, especially close to the free surfaces of the exposure. In general, the relatively gently dipping foliation parallel fractures seem to be more abundant close to these free surfaces and could therefore be features caused by strain-release mechanisms. Two slickensided planes were found in this population. Both rake subhorizontally and suggest (dextral) strike-slip motion due to NW-SE compression (129 σ_1 10; 230 σ_3 45).

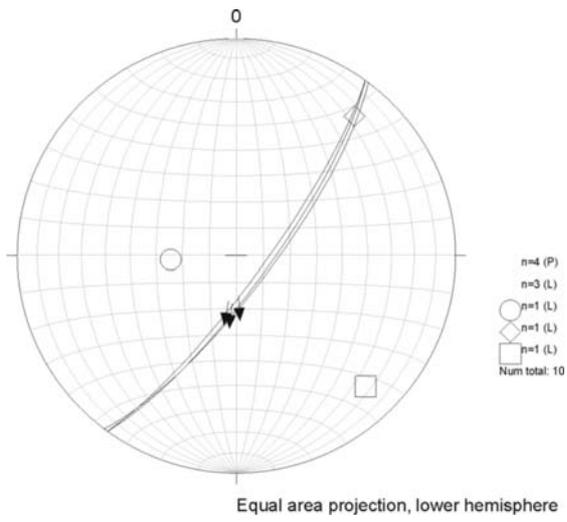


Figure A-86: Slickensided fractures suggesting normal motion.

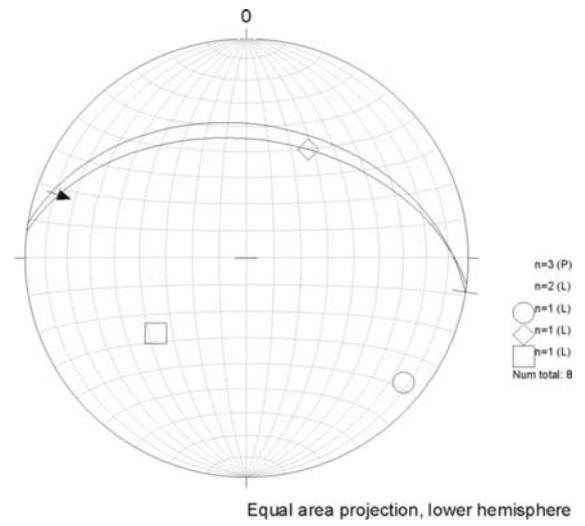


Figure A-87: Slickensided planes suggesting (dextral) strike-slip.

Appendix B – Lithologic descriptions of drillers' logs

The following descriptions of well cuttings were compiled by members of the SVB Prösl geotechnical consulting company (Velden/Vils, Germany) and translated by the author.

Neusohl Br. IV (VB 1)

-	0.20 m	Clay, brown
-	1.00 m	Silt, sandy, gray-brown
-	2.00 m	Silt, sandy, gray
-	10.00 m	Silt, sandy, clayey, gray with reddish spots
-	11.00 m	Silt, sandy, gray-black-reddish
-	12.00 m	Silt, sandy, gray-white
-	13.00 m	Silt, sandy, gray-black with white inclusions
-	15.00 m	Silt, sandy, brown
-	16.00 m	Grus and sand, brown
-	47.00 m	Sequence of heavily weathered fractured gneiss and silty/grusy/clayey sand, reddish gray-brown
-	56.00 m	Weathered gneiss, decreasing intensity of weathering with increasing depth

Neusohl Br. V (VB 2)

-	3.00 m	Silt, sandy, gray, small pebbles
-	5.00 m	Silt, very sandy, grusy, gray
-	7.00 m	Silty, grusy sand, red-brown to gray
-	10.00 m	Silt, sandy, gray-brown
-	13.00 m	Sand, silty, grusy, mainly brownish, also gray-white
-	15.00 m	Silt, sandy, grusy, red-brown
-	16.00 m	Residual boulders, sandy, gray-black-brown
-	19.00 m	Silt, sandy, grusy, gray-white-reddish
-	43.00 m	intensely weathered gneiss, gray-white-brown
-	56.00 m	Weathered gneiss, decreasing intensity of weathering with increasing depth

Schweinhütt, Br. 1 (VB 4)

-	3.00 m	Pebbles in a sandy clay matrix
-	10.00 m	Tightly packed sand, very grusy, silty, brownish
-	11.00 m	Weathered gneiss large fractures, brownish
-	56.00 m	weathered gneiss, locally fractured, decreasing intensity of weathering with increasing depth, from approximately 52 m downwards no signs of significant loosening by fractures or weathering

Böbrach, Br. 1 (B 1)

-	9.00 m	Sand, weakly grusy, silty, light brown
-	16.00 m	Sand, silty, weakly clayey, light brown
-	22.00 m	Sand, grusy, brown
-	25.00 m	Sand, silty, dark brown
-	31.00 m	Sand, silty, grusy, brown with small fragments of gneiss, gray
-	33.00 m	Sand (predominantly fine), silty, dark gray-brown
-	34.00 m	Sand, very grusy, gneiss fragments up to 1 cm long, dark gray-brown
-	38.00 m	Sand, grus, dark gray-brown
-	40.00 m	Sand, small fragments of gneiss, dark brown-gray
-	47.00 m	Fragments of gneiss with fractures, gray up to 5 cm long
-	50. m	Fragments of gneiss with occasional fractures up to 2 cm long, fragments become smaller with increasing depth

Böbrach, Br. 2

-	8.00 m	Sand, grusy, silty, brown
-	12.00 m	Fragments of partially weathered, intensely fractured gneiss, sand, grus, gray-brown
-	17.00 m	Fragments of partially weathered, intensely fractured gneiss, brown-gray, minor amounts of sand, grus, indication of shear zone, coated fractures
-	22.00 m	Gneiss, locally weathered and fractured
-	24.00 m	Gneiss, locally weathered and intensely fractured
-	38.00 m	Gneiss, locally weathered and fractured
-	40.00 m	Gneiss, predominantly fresh, decreasing intensity of weathering with increasing depth

Wiesenfelden Br, 2 (B 1)

- 4.00 m grusy-sandy clay with pebbles, beige
- 12.00 m Gneiss, very grusy/sandy weathered, brownish
- 15.00 m Gneiss, very grusy/sandy weathered, locally intensely fractured, gray-brown
- 24.00 m Biotite-rich gneiss, locally intensely fractured, few signs for weathering, mainly dark gray, to a lesser degree brownish
- 39.00 m Biotite-rich gneiss, locally fractured, black-gray, in places light gray
- 43.00 m Aplitic vein light gray to grayish white
- 55.00 m Biotite-rich gneiss, locally weakly fractured, black-gray

Kirchdorf im Wald Br. 1 (VB 1)

- 7.00 m Sand, silty, beige-brown (quaternary cover and intensely weathered, loosened gneiss)
- 18.00 m Sand, silty, grusy, brown, (intensely weathered, loosened gneiss)
- 50.00 m Gneiss, slightly weathered in the upper part, decreasing intensity of weathering with increasing depth locally fractured, decreasing intensity of fracturing with increasing depth

Kirchdorf im Wald Br. 2 (VB 6)

- 6.00 m Sand, slightly silty and grusy, gray-brown (quaternary cover and intensely weathered, loosened gneiss)
- 7.00 m Gneiss, slightly weathered, intensely fractured
- 10.00 m Gneiss, intensely weathered, locally slightly weathered and intensely fractured
- 20.00 m Gneiss, slightly weathered to weathered, mainly intensely fractured
- 50.00 m Gneiss, locally slightly weathered and fractured, otherwise fresh

Kirchdorf im Wald Br. 3 (VB 3)

- 4.00 m Rocks, clay
- 11.50 m Gneiss with narrow granite veinlets, intensely weathered, brown
- 51.30 m Gneiss, brown and gray, locally intensely fractured, decreasing intensity of fracturing and weathering with increasing depth

Kirchdorf im Wald Br. 4 (VB 4)

- 0.30 m Anthropogenic sediment
- 0.50 m Organic soil, black
- 20.10 m Fine to medium-grained sand, grus, residual boulders, brown
- 26.00 m Gneiss, weathered, weakly fractured, brown-black
- 35.70 m Gneiss, weathered, locally intensely fractured
- 51.40 m Granite, partially unfractured, partially intensely fractured, decreasing intensity of fracturing with increasing depth, gray

Kirchdorf im Wald Br. 5 (VB 5)

- 3.00 m Clay, sandy, some pebbles, brown
- 7.00 m Gneiss, intensely weathered, brown-black
- 15.00 m Gneiss, intensely weathered, sandy, gray-brown
- 20.00 m Granite, gray, intensely fractured
- 28.00 m Granite, weathered, brown-gray, locally intensely fractured
- 30.00 m Granite, weathered, gray-black, intensely weathered
- 41.00 m Granite, partially unfractured, partially intensely fractured, gray
- 45.00 m Granite, partially unfractured, partially intensely fractured, gray and slightly brownish
- 47.00 m Granite, unfractured, gray, unweathered
- 49.00 m Granite, slightly weathered, gray-brown, locally slightly fractured

Bayerisch Eisenstein TBr. Grafhüttenbach

- 2.00 m Fragments of gneiss and concrete, clay
- 9.00 m Weathered fragments of gneiss, brownish, sandy/ silty grus, concrete fragments at ca. 5.50 m
- 12.00 m brownish fragments of weathered gneiss, sandy/ silty grus, to a lesser extent brownish weathered gneiss fragments
- 65.00 m dark gray fragments of gneiss plus gravel pack and fragments of PVC casing

Appendix C - K-means analysis of fracture data

1 Conceptual model

The K-means algorithm is commonly used for the analysis of neural networks, multivariate statistical problems in the biosciences, or the processing and data reduction of digital imagery. In the characterization of fractured rock aquifers it is a useful tool for the classification of fracture populations based on their attitudes in three dimensions and the sorting and/or filtering of metadata, such as fracture roughness coefficient, aperture, trace length, etc. in relation to the mean orientations of the specified clusters.

“The K-means algorithm is an algorithm to cluster objects based on attributes into k partitions. It is a variant of the expectation-maximization algorithm in which the goal is to determine the k means of data generated from gaussian distributions. It assumes that the object attributes form a vector space. The objective it tries to achieve is to minimize total intra-cluster variance, or, the function

$$V = \sum_{i=1}^k \sum_{j \in S_i} |x_j - \mu_i|^2 \quad \text{eq. C-1}$$

where there are k clusters S_i , $i = 1, 2, \dots, k$ and μ_i is the centroid or mean point of all the points $x_j \in S_i$ ” (Wikipedia-contributors, 2005).

For the purpose of analyzing fracture data it can be utilized to group fracture families with respect to their mean orientations via a specific cluster ID number. Once the individual fractures have been grouped and attributed to a certain cluster they can be further processed within each particular cluster with regard to their associated metadata, a feature most commonly available stereographic plotting programs do not offer.

The number of clusters to which individual fractures are attributed is estimated by the visual examination of contoured stereographic plots of the bulk dataset. Then the K-means procedure categorizes the fracture planes F_l ($l = 1, \dots, N$) according to the “similarities” of their normal poles \vec{n}_l . The input data comprise the dip azimuth α_l (DIP_AZI in the program) and dip δ_l (DIP) of the recorded fractures. They are related to the intersections $\vec{\xi}_k$ of their polar coordinates $(\varphi_l, \mathcal{G}_l)$ with a unit sphere the following:

$$\mathcal{G}_l = \delta_l$$

$$\varphi_l = \begin{cases} \alpha_l - 180 & \text{if } \alpha_l - 180^\circ \geq 0 \\ \alpha_l + 180^\circ & \text{else} \end{cases} \quad \text{eq. C-2}$$

The convention to project the poles of fracture planes only in the lower hemisphere of the unit sphere poses additional problems. This approach leads to the effect that normally continuous pole clusters with inclinations close to horizontal are separated and placed at opposite sides along the rim of the hemisphere. Thus, the algorithm has to account for this separation and merge the separated clusters.

2 Algorithm

Clustering of low-dimensional data with a predefined number of clusters can be achieved utilizing the K-means algorithm (MacQueen, 1967). The algorithm is based on the following postulates:

Datapoints \vec{x}_j and the number K of the required cluster centroids $\vec{\mu}_k$ are given. The K-means approach determines the centroids with the objective of minimizing the intra-cluster variance. Thus, the task to be solved by the approach can be formulated the following:

Determine

$$\min_{\vec{\mu}_j} \sum_{i=1}^K \sum_{x_i \in S_j} |\vec{x}_i - \vec{\mu}_j|^2 \quad \text{eq. C-3}$$

where $\vec{\mu}_j$ are the sought-after centroids of clusters S_j .

The standard approach to the solution of this problem is the following:

- Step 1** Initialize all $\vec{\mu}_j$ at random.
- Step 2** Attribute all points \vec{x}_j to that cluster j whose centroid vector $\vec{\mu}_j$ is associated with the minimal distance $|\vec{x}_i - \vec{\mu}_j|^2$
- Step 3** Move all centroid vectors $\vec{\mu}_j$ individually such that $\sum_{x_i \in S_j} |\vec{x}_i - \vec{\mu}_j|^2$
- Step 4** As long as at least one centroid vector changes its position significantly repeat from step 2.

Several variations of this approach exist, one of which is the so-called online-procedure. It modifies the approach the following:

- Step 1** Initialize all $\vec{\mu}_j$ at random.

- Step 2** Select one datapoint \vec{x}_j (e.g. at random)
- Step 3** Move that centroid vector $\vec{\mu}_j$, which lies closest to point \vec{x}_j selected in step 2, such that $|\vec{x}_i - \vec{\mu}_j|^2$ is reduced. Reductions by 1% are common.
- Step 4** Repeat from step 2 until the appropriate abort criterion is reached.

3 Adjustments of the online procedure to the data clustering

The online K-means algorithm has to be adjusted to the clustering of the data collected in this study.

3.1 Metrics

First of all, metrics appropriate for the problem has to be defined in lieu of the standard measure of distance $\Delta_{std}(\vec{x}_i, \vec{x}_j) = |\vec{x}_j - \vec{x}_i|$ (i.e. the Euclidean distance). For the new measure of distance in this approach the distance between two points along the surface of a unit sphere ($r := 1$) is used:

$$\Delta(\vec{x}_i, \vec{x}_j) := \arccos[\sin \vartheta_i \sin \vartheta_j \cos(\varphi_i - \varphi_j) + \cos \vartheta_i \cos \vartheta_j] \quad \text{eq. C-4}$$

3.2 Derivation

As is generally known the shortest distance between two points \vec{x}_1, \vec{x}_2 along the surface of a sphere of radius r is always part of a great circle. Let β be the angle between the two points. Then, their distance along the surface of the sphere is:

$$\Delta(\vec{x}_1, \vec{x}_2) = r \cdot \beta \quad \text{eq. C-5}$$

Angle β can be expressed by the ordinary scalar product:

$$|\vec{x}_1 \circ \vec{x}_2| = |\vec{x}_1| \cdot |\vec{x}_2| \cdot \cos \beta \quad \text{eq. C-6}$$

$$\Rightarrow \beta = \arccos \frac{|\vec{x}_1 \circ \vec{x}_2|}{|\vec{x}_1| \cdot |\vec{x}_2|} \quad \text{eq. C-7}$$

Using the common convention of polar coordinates:

$$\vec{x}_i = \begin{pmatrix} r_i \sin \vartheta_i \cos \varphi_i \\ r_i \sin \vartheta_i \sin \varphi_i \\ r_i \cos \vartheta_i \end{pmatrix} \quad \text{eq. C-8}$$

leads to

$$\begin{aligned} \beta &= \arccos \left(\frac{r_1 r_2 \sin \vartheta_1 \sin \vartheta_2 (\cos \varphi_1 \cos \varphi_2 + \sin \varphi_1 \sin \varphi_2) + r_1 r_2 \cos \vartheta_1 \cos \vartheta_2}{r_1 \cdot r_2} \right) \\ &= \arccos (\sin \vartheta_1 \sin \vartheta_2 \cos(\varphi_1 - \varphi_2) + \cos \vartheta_1 \cos \vartheta_2) \end{aligned} \quad \text{eq. C-9}$$

3.3 Further problem-specific modifications

3.3.1 Vector doubling

In order to account for the cluster separation inherent to the exclusive projection of datapoints into the lower hemisphere (i.e. the projection convention used in structural geology, cf. fig. C-1) the datapoints \vec{x}_j of N intersections $\vec{\xi}_l$ with the unit sphere are determined the following:

$$\begin{aligned} \vec{x}_{2l-1} &= \vec{\xi}_l \\ \vec{x}_{2l} &= -\vec{\xi}_l \end{aligned} \quad \text{eq. C-10}$$

Thus, the dataset contains for every polar vector also its opposite vector derived from point inflection. This is necessary for the distance calculation, which can only be achieved on the full sphere, but not on a hemisphere.

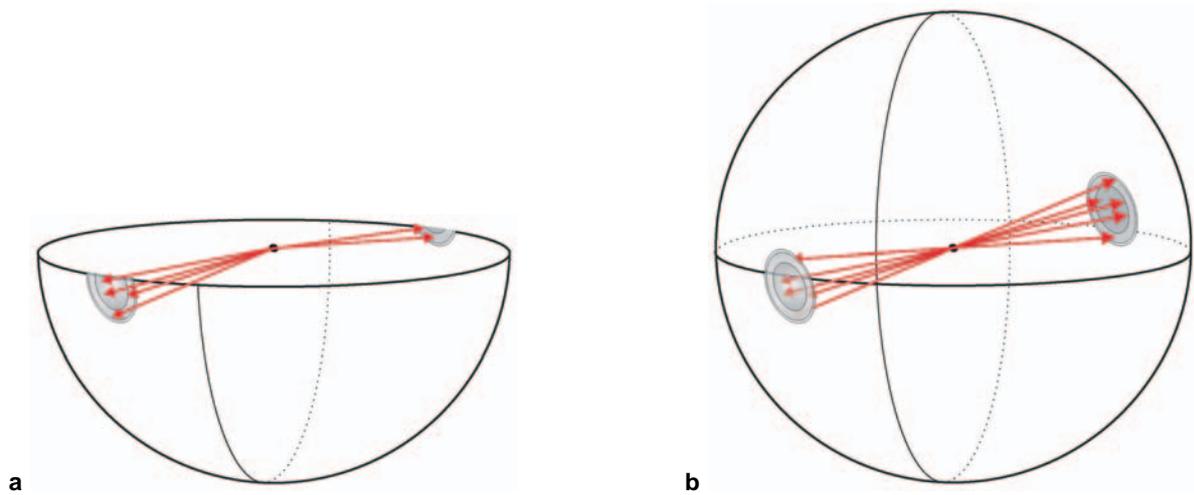


Figure C-1: Conceptual model of the vector doubling procedure. (a) Projection of poles (red arrows) only in the lower hemisphere. Clusters are separated and datapoints cannot be attributed correctly to a centroid. (b) Vector doubling: Every fracture pole is point inflected through the center of a unit sphere. Two identical clusters are created to which the poles can be attributed. At the end of the clustering the centroids and datapoints in the upper hemisphere are discarded and the information on their affiliations is transferred to their counterparts in the lower hemisphere.

3.3.2 Centroid doubling

While K centroids are required to be found in the original dataset the online K-means procedure requires the identification of $2K$ clusters due to the vector doubling described in section 3.3.1. Additionally, it is requested for all centroids of the problem that the expression

$$\vec{\mu}_j = -\vec{\mu}_{j+1} \text{ for } j = 1, \dots, 2K - 1 \text{ and } j \text{ is odd-numbered} \quad \text{eq. C-11}$$

is valid.

3.3.3 Interpretation

When the online K-means algorithm has sufficiently merged clusters and centroids by the specified number of iterations the clusters can ultimately be attributed to the original datapoints $\vec{\xi}_i$.

4 Program procedure

The abovementioned K-means algorithm has been implemented as a Microsoft Excel VBA macro. The initial *.xls file contains three worksheets called “Table 1”, “Table 2”, and “Parameters. Sheet “Table 1” can be used to import ASCII files of fracture data. The only prerequisite for the data format is the presence of fracture orientation information as dip azimuth and dip in two separate columns. These two columns are copied and pasted in sheet “Table 2” below the headings “DIP_AZI” and “DIP”, respectively. The two polar plots in this sheet depict the approximate locations of the fracture poles projected both in the upper and lower hemispheres.

Then, several settings can be made on the sheet “Parameters”. Besides several color schemes as well as sizes and positions for the polar plots the algorithm parameters can be set. The following fields control the analysis procedure:

Field	Function
KMeans-Percentage	Determines the magnitude of convergence between centroid and datapoints per iteration in per cent (default value is 1).
Number of Iterations	Specifies the number of iterations to be passed before the output of the results. As a rule of thumb, 1000 iterations per input datapoint is recommended, although large datasets containing several hundreds of points do not allow such high numbers. In these cases the number of iterations has to be significantly reduced in order to obtain reasonable computing times and to prevent program crash. In practice, nonetheless, clustering large datasets with lower numbers of iterations commonly yielded adequate results.
Show Updates	Specifies if the results of the analysis should be displayed on the polar plots. 0 = no; 1 = yes. N.b.: Setting the option to 1 sometimes causes long computing times, especially with large datasets.
Number of Clusters to find	Specifies the expected number of clusters in a dataset. This number is determined by the visual examination of the data on a contoured stereographic plot. Here, the reliability of the results depends on the experience of the analyzing geologist – and sometimes on his imagination.

After setting the analysis parameters the range in table 2 containing the dataset and the headings “DIP_AZI”, “DIP”, and “CLUSTER_ID” have to be selected. The macro is started (Menu “Tools → Macro → Macros → doKmeansWithPoles”). After the abort criterion has been reached numbers will appear in the column headed by “CLUSTER_ID”. These numbers represent the clusters to which the individual datapoints were attributed. This

column can be copied and pasted back to the original dataset in sheet “Table 1” and used to sort the data accordingly. Figures C-1 and C-2 depict screen shots of a sample analysis.

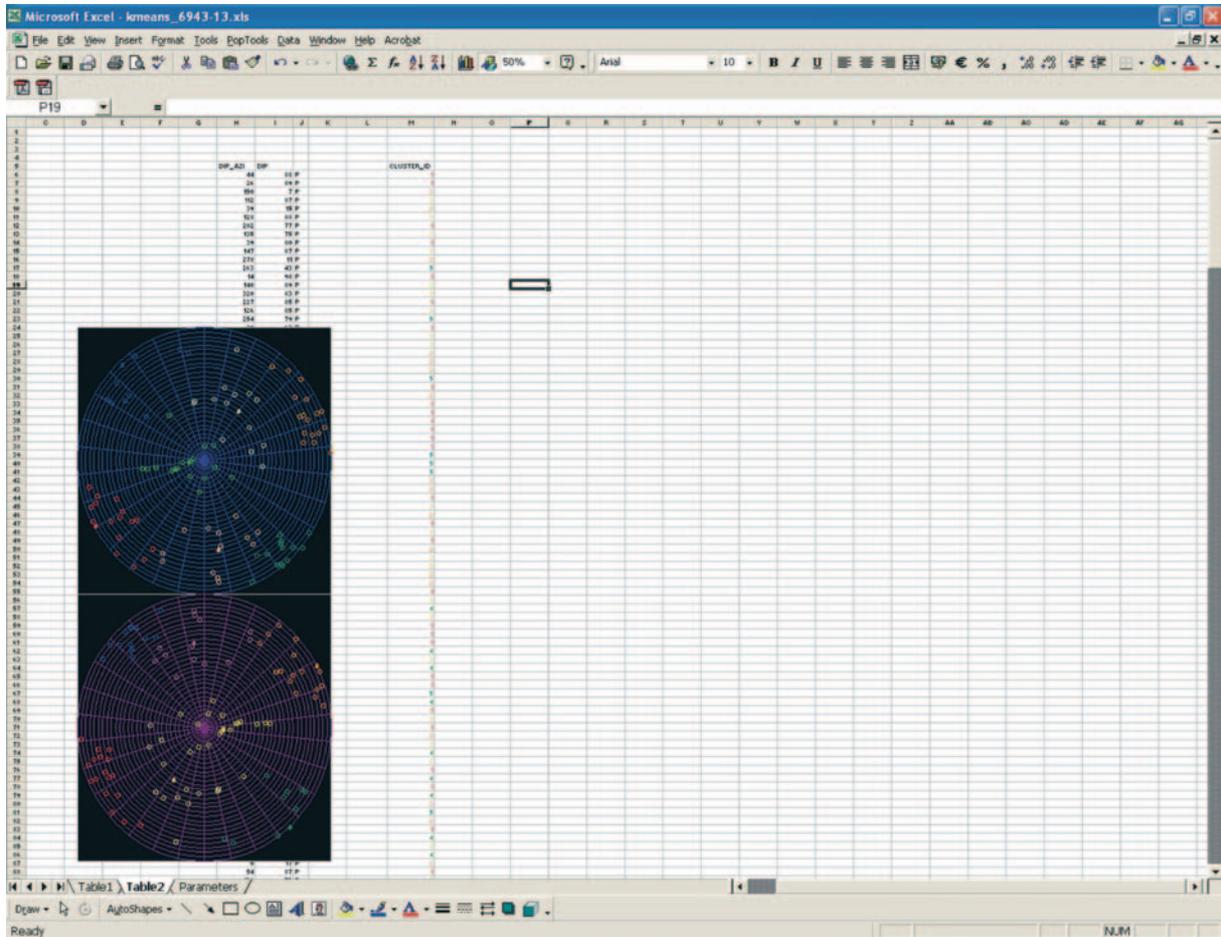


Figure C-2: Screenshot of the MS Excel VBA macro on worksheet "Table 2".

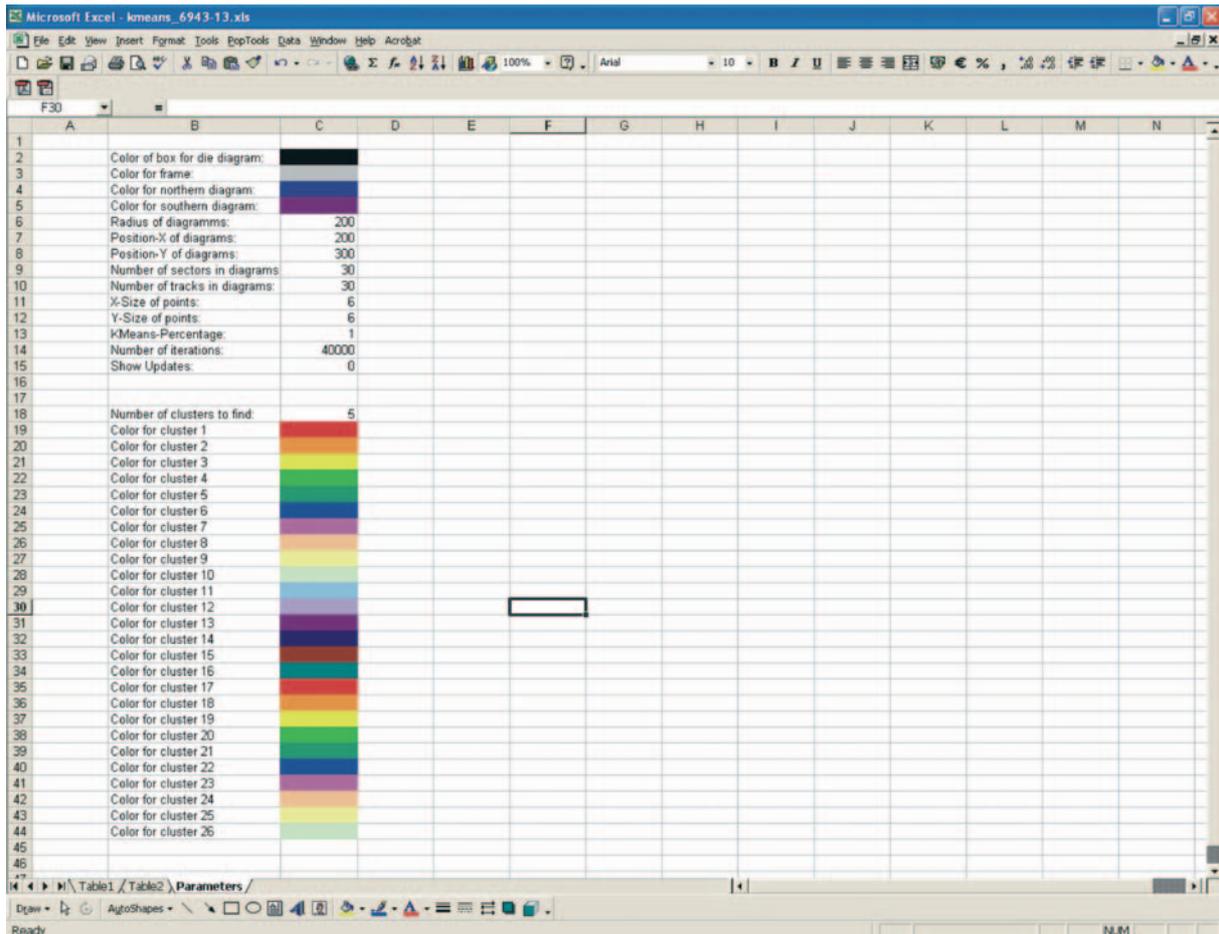


Figure C-3: Screenshot of the MS Excel VBA macro on worksheet "Parameters".

5 References

MacQueen, J.B., 1967, Some Methods for Classification and Analysis of Multivariate Observations, 5th Berkeley Symposium on Mathematical Statistics and Probability, Volume 1: Berkeley, University of California Press, p. 281-297.

Wikipedia-contributors, 2005, K-means algorithm, Wikipedia, The Free Encyclopedia, October 9, 2005, Retrieved: December 12, 2005 from http://en.wikipedia.org/w/index.php?title=K-means_algorithm&oldid=25103743

Appendix D – FracMan/ MAFIC discrete fracture and flow modeling

1 Introduction

For the discrete fracture and flow modeling in this study the FracMan/ MAFIC model suite developed by Golder Associates Inc. (Seattle/ Washington, USA) was used. Both the software versions FracWorks/95, v. 1.4 and FracWorks XP Beta Version 0.21 as well as PAWorks, v. 1.64 were made available free of charge by the developing company.

FracMan/ MAFIC is a suite of individual software components contributing to the overall modeling process. Fig. D-1 gives a conceptual overview of the interactions of these components. The following text will mainly focus on the FracWorks and the PAWorks modules, which are the user interfaces in which the model design is established.

The MeshMaker, EdMesh, and MAFIC modules are utilized by these two interfaces. Figure D-2 details the PAWorks module and depicts the functions of subordinate components.

The modeling procedure starts with the generation of a fracture network in FracWorks. To this end, mean values of various fracture-related parameters, such as orientation, size, intensity, termination, and aperture are entered

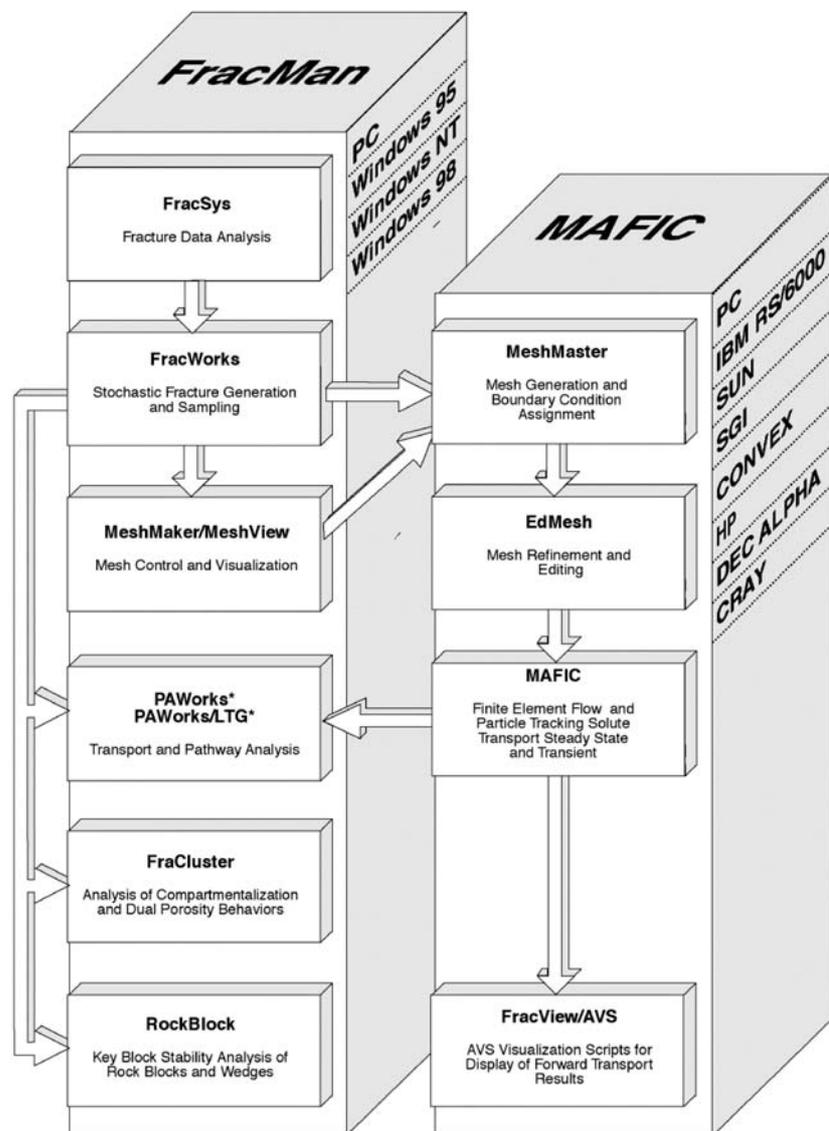


Figure D-1: Conceptual overview of the software components of the FracMan/ MAFIC suite. Source: Dershowitz et al. (1999).

in the software for each individual fracture cluster previously generated with the K-means analysis. Then, FracWorks creates a stochastic fracture network based on these mean values and the specified distribution functions in a pre-defined cubic model region. The distribution functions selected in this study will be detailed in the following section.

After the completion of the fracture network generation the resulting fracture file is imported into the PAWorks module, in which the exploration and search parameters are specified (details in section 2.2 of this appendix).

Conceptually, FracMan/ MAFIC allows the generation of a 3D stochastic fracture network by utilizing the MeshMaker module, from which a network of two-dimensional flow pipes connected with one-dimensional nodes is constructed (fig. D-3) in PAWorks. For this system of pipes and nodes the MAFIC finite element solver can calculate a head field, i.e. the values of the hydraulic potential at each of the nodes based on the applied boundary conditions. The distribution of the head values thus produces gradients, which are followed by the virtual groundwater flow.

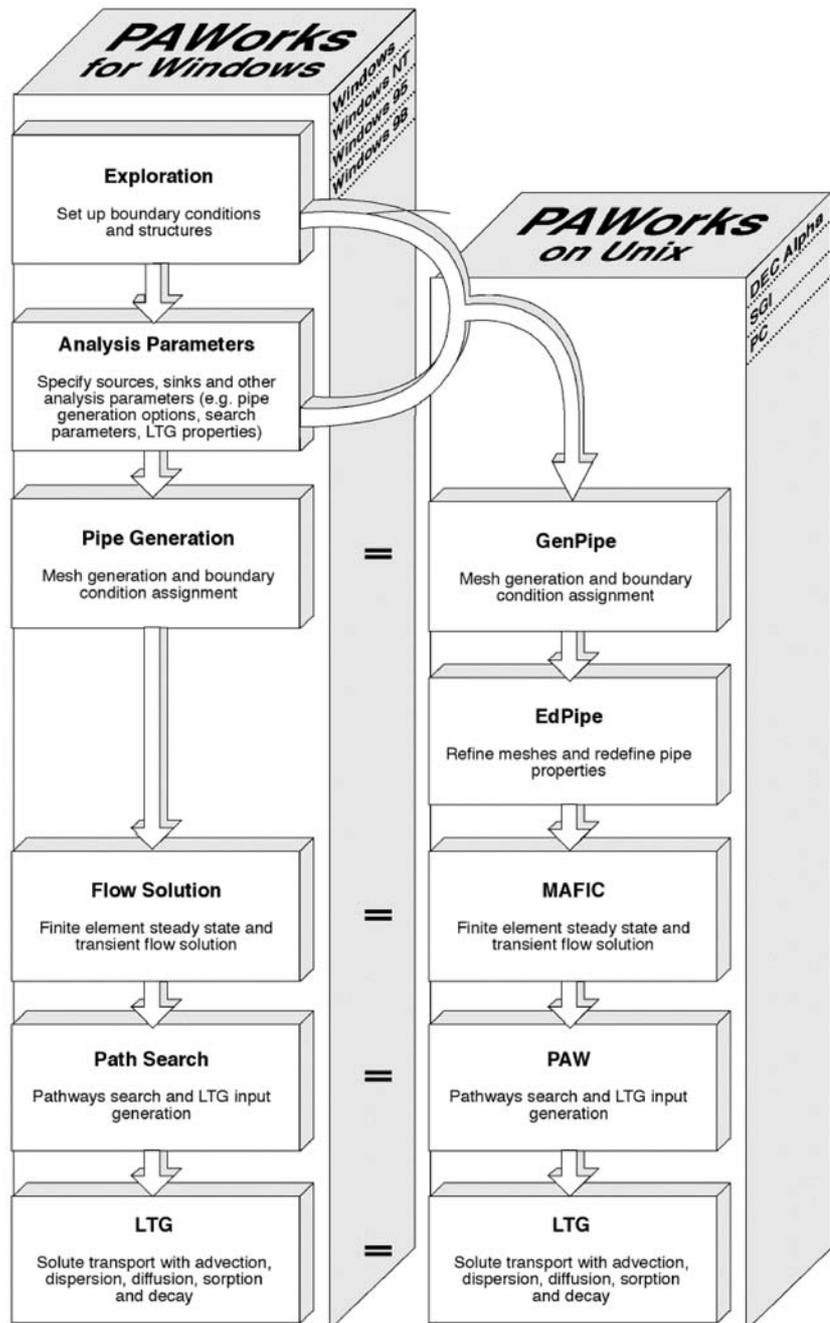


Figure D-2: Conceptual overview of the software components of the PAWorks module. Source: Dershowitz et al. (2002).

Before going into further detail in the following sections it has to be pointed out that this software suite is not designed to provide unambiguous quantitative results, but to conceptualize groundwater flow in an approximative way. In doing so the model results can only be as good as the data input and the boundary conditions applied. Herein lies the general dilemma of hydrogeologic modeling. The assumed boundary conditions have to be very simplistic for various reasons. For one, several hydraulic parameters of a real-world flow region making up the boundary conditions, such as continuous head distributions, are only partially known due to the limitations of the sampling techniques and the measuring equipment. On the other hand, the computing capabilities of presently available computer hardware are not yet sufficient to include all aspects over significantly large sampling regions.

Another problem is posed by the fact that fractures are very inhomogeneous entities whose properties can only be recorded along two-dimensional outcrop walls. Hydraulically significant parameters such as size, roughness, aperture, intensity, and type of termination inside the rock mass can only be estimated based on the fractures' surface expression.

Having mentioned the basic procedures and limitations of the FracMan/ MAFIC software its application to cases in the study area will be described in the following sections with respect to the specific model generation and application of boundary conditions.

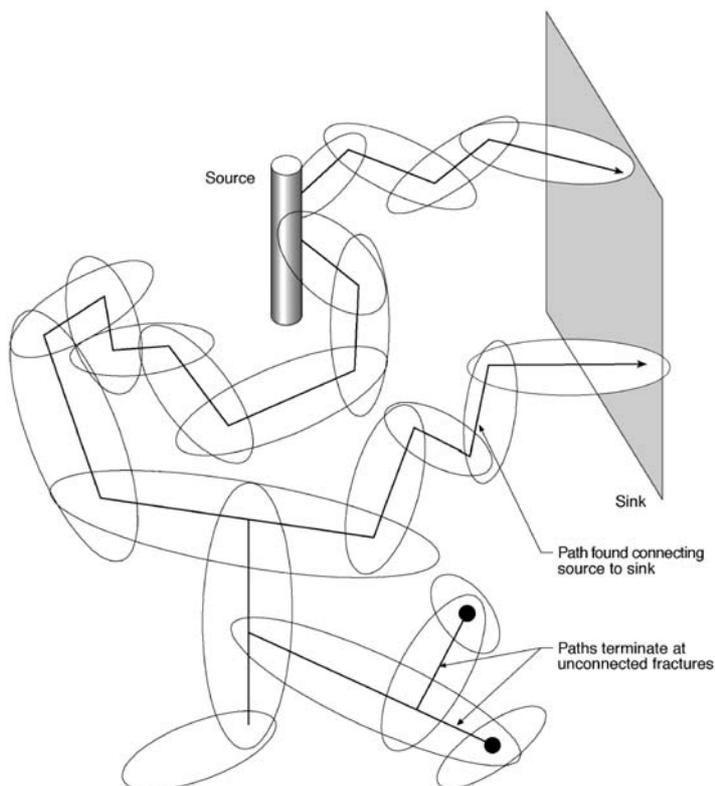


Figure D-3: Flow pathway concept in PAWorks. Ellipses depict modeled fractures, lines represent the calculated pipes connected by nodes at the ends of their segments
Source: Dershowitz et al. (2002).

2 Model generation and basic assumptions

The stochastic fracture models for the analysis in section 4.3 were created based on field measurements obtained both with the subjective and scanline approach. For the scanline data cubic model regions with side lengths equal to the length of the respective scanline were generated. In locations where subjective measurements were taken it was attempted to create a cubic region approximating the size of the respective outcrop. On some occasions, however, the model size exceeded the computing capabilities of the computer hardware. This problem occurred in locations where relatively small fractures occurred in high densities. In these cases the size of the model was reduced to the point at which a stable processing of the data was possible.

After its generation in the FracWorks module a stochastic fracture network was imported into the PAWorks module, in which a system of potential flow paths (“pipe network”) was created. For these flow paths a MAFIC flow solution was calculated and hydraulic heads were attributed to the zero-dimensional nodes. Based on these calculations groundwater flow was simulated and visualized.

In the following the parameters and boundary conditions applied in the creation of the FracMan models will be described in more detail.

2.1 Parameters and boundary conditions in FracWorks

For the generation of stochastic fracture networks a number of parameters had to be specified. These parameters include fracture orientation, size, shape, intensity, termination, and aperture. Their specifications will be detailed in the following. Other parameters, such as fracture transmissivity, storativity, etc., could not be entered due to the lack of the respective data, and therefore were set to default values.

Fracture orientations

Mean values of fracture clusters determined from pole distributions on stereographic plots of a given sampling station were used for the generation of stochastic fracture sets. In a trial-and-error approach to model the distributions in FracWorks a Bivariate Normal Distribution with K1 and K2 values of 5 to 10 proved to resemble best the real-world situation. Equation D-1 shows how this algorithm calculates the orientation (Φ , θ) of a fracture:

$$f(\phi, \theta) = \frac{1}{2\pi\phi_\sigma\theta_\sigma\sqrt{1-\rho^2}} \exp\left\{-\frac{1}{2(1-\rho^2)} \left[\left(\frac{\phi-\bar{\phi}}{\phi_\sigma} \right)^2 - 2\rho \frac{(\phi-\bar{\phi})(\theta-\bar{\theta})}{\theta_\sigma\phi_\sigma} + \left(\frac{\theta-\bar{\theta}}{\theta_\sigma} \right)^2 \right] \right\}$$

eq. D-1

where $(\Phi_\sigma, \theta_\sigma)$ are the standard deviations of dip and dip azimuth and ρ is the correlation coefficient (Dershowitz, 2002).

For subhorizontal to gently inclined discontinuities the Bivariate Normal Distribution produced somewhat distorted populations. Thus, a univariate Fisher Distribution (eq.D-2) was employed for this type of fractures, which yielded more appropriate results.

$$f(\varphi', \theta') = \frac{\kappa \sin \varphi' e^{\kappa \cos \varphi'}}{2\pi(e^\kappa - 1)} \quad 0 \leq \theta' \leq 2\pi$$

eq. D-2

where κ is the distribution parameter specified by the user. (φ', θ') is the variation about a fracture set's mean direction (φ, θ) , i.e. dip and dip azimuth, respectively). κ is determined the following:

$$\kappa \approx \frac{N_F}{N_F - |R|}$$

eq. D-3

where $|R|$ is the magnitude of the vector sum of the unit vectors for orientation and N_F is the number of fractures (Dershowitz, 2002). κ values of 50 to 200 proved to yield the best results.

Fracture sizes

For this parameter the mean sizes of the specific fracture populations as well as their standard deviations were calculated. For the stochastic generation of values a uniform distribution was selected and a size variation of one standard deviation about the mean was specified.

Fracture shapes

For lack of detailed information of fracture shape (in most locations only two-dimensional trace lengths could be measured) the default setting presented by the software was accepted. This setting models fractures as equidistant six-sided polygons with diameters equivalent to the specified trace lengths.

Fracture intensities

Fracture intensity, i.e. the degree of fracturing of a volume of rock, was specified in the P₃₂ mode, which determines this parameter as the mean area of a given fracture set within a unit volume. Based on fracture size and spacing the mean area of a fracture per unit volume is calculated the following:

The minimum cuboid volume v enclosing a circular fracture with radius r and area a is defined by its diameter ($2r$) and its spacing d :

$$a = r^2 \pi \quad \text{eq. D-4}$$

$$v = d \cdot (2r)^2 \quad \text{eq. D-3}$$

Thus, the fracture area per volume is

$$\frac{a}{v} = \frac{r^2 \pi}{d \cdot (2r)^2} \quad \text{eq. D-5}$$

This value has to be normalized with respect to the unit volume v_u (i.e. area a_u per v_u):

$$\frac{a_u}{v_u} = \frac{v_u}{v} \cdot a \quad \text{eq. D-6}$$

Example: A fracture set is associated with the following mean values: fracture diameter: 0.8m; spacing: 1.4m. Applying the abovementioned equations yields an average area of 0.561 m²/m³.

Fracture terminations

For the fracture network generation with the Enhanced Baecher Distribution the percentage of fractures terminating at other fractures they intersect had to be entered in the model. In the scanline surveys this parameter was recorded quantitatively as number of “t-type terminations” at either one end of the fracture or both. To calculate the termination percentage the portion of fractures associated with at least one t-type termination with respect to the remaining fractures whose ends were exposed in the outcrop was used.

Fracture apertures

For each fracture set simulated in FracWorks its mean aperture value determined by the field measurements was used. Since aperture variations over the vertical extent of bedrock exposures were not observed in the respective sampling stations the mean aperture was assumed to be more or less constant for the depth interval of the model. Thus, the depth-correlation function was not activated.

Hydraulic properties

As already mentioned no information could be obtained for parameters such as fracture transmissivity and storativity. Therefore, default values were used for the modeling. However, since quantitative simulations of transport and well yield characteristics were not the purpose of the modeling the lack of data on hydraulic properties has no significant effect on the outcome.

2.2 Parameters and boundary conditions in PAWorks

As already mentioned in section 4.3.1.4 the following general assumptions were made for the generation of the flow models:

- (1) The flow region is modeled as a cube located completely in the saturated zone.
- (2) The flow region is oriented such that two walls of the cube are oriented perpendicular to the hydraulic gradient.
- (3) Hydraulic gradients are derived from topographic gradients. The magnitude of the hydraulic gradient is chosen to be approximately half of the topographic gradient.

- (4) In order to simulate flow hydraulic heads proportional to the gradient are applied to two side walls of the cube and to its top to simulate infiltration. The remaining two sides and the bottom are determined to be passive no-flow boundaries.
- (5) In several locations wells are inserted in the flow regions. They intersect their entire vertical extents, possess a diameter of 0.3 m, and hydraulic heads equal to two-thirds of their lengths.

3 Model protocols

For each of the models presented in section 4.3.1.4 a protocol of the generation process is presented here. These protocols include both the specifications of the stochastic fracture networks (FracWorks) and of the flow model (PAWorks). Parameters not listed in the protocols were set to default.

FracMan Specs									
Model ID		Location							
7044-04		Steinbruch Teufelstisch, Bischofsmais							
Fracture Set File	*.fab File		Model Region		Comments				
	7044-04a.fab		Type	Size [m]	Topographic gradient: 0.5 (N-S)				
			Box	20 x 20 x 20					
Fracture Set File	Orientation		Intensity		Size			Properties (Constant Values)	
	Dip Azi./Dip	Distribution	Type	Value	Mean	Distribution	Deviation [± 1σ]	Transmissivity	Aperture
x04set1a.set	251-18	Bivar. norm. (5/5)	P ₃₂ , const.	1.43	10.02	Uniform	8.76	default	1.96e-3
x04set2a.set	240-90	Bivar. norm. (5/5)	P ₃₂ , const.	0.54	1.87	Uniform	1.84	default	8.4e-4
x04set3a.set	214-90	Bivar. norm. (5/5)	P ₃₂ , const.	0.84	1.97	Uniform	2.05	default	9.0e-5
x04set4a.set	200-90	Bivar. norm. (5/5)	P ₃₂ , const.	0.39	2.64	Uniform	2.41	default	3.5e-4

PAWorks Specs									
Model ID		Location							
7044-04a		Steinbruch Teufelstisch, Bischofsmais							
Files		Sampling Structures							
*.sab File	*.fab File	Flow Region		Name	Boundary Conditions		Length [m]	Borehole Head [m]	Diameter [m]
7044-04a.sab	7044-04a.fab	Type	Size [m]	NoFlow	Type	Head/Flux	15	6	0.3
		Box	15 x 15 x 15	Head5	Const. Flux	0			
				Head10	Const. Head	5			
					Const. Head	10			
Flow Region Boundaries		Analysis Parameters							
Box Wall	Head [m]	Head Calculation:		Boundary Specification		Search Parameters			
NE	10	Mafic Pipe Network		Source	Head10	Weight Generation:		None	
SE	NoFlow	Weighted		Sink	Head5	Maximum Paths:		500	
SW	5	Box region				Maximum branches/			
NW	NoFlow	Borehole				source:		100	
Top	10	Representative Path							
Bottom	NoFlow	Generation based on:							
		Sink Location							

FracMan Specs											
Model ID	6944-18		Location							Böbrach, Wolfgangskapelle	
Fracture Set File	*.fab File	Model Region		Comments							
		Type	Size [m]	Topographic gradient: 0.5 (N-S)							
		Orientation		Intensity		Size		Properties (Constant Values)			
		Dip Azi./Dip	Distribution	Type	Value	Mean	Distribution	Deviation [± 1σ]	Transmissivity	Aperture	
x18set1a.set		030-24	Fisher (K = 75)	P ₃₂ , const.	0.79	1.52	Uniform	0.98	default	default	
x18set2a.set	6944-18a.fab	137-86	Bivar. norm. (5/5)	P ₃₂ , const.	0.20	2.79	Uniform	3.40	default	default	
x18set3a.set		211-83	Bivar. norm. (5/5)	P ₃₂ , const.	0.26	3.59	Uniform	2.70	default	default	
x18set4a.set		253-56	Bivar. norm. (5/5)	P ₃₂ , const.	0.16	3.28	Uniform	3.22	default	default	

PAWorks Specs											
Model ID	6944-18a		Location							Böbrach, Wolfgangskapelle	
Files		Sampling Structures									
*.sab File	*.fab File	Flow Region		Name	Boundary Conditions		Head/Flux	Length [m]	Borehole Head [m]	Diameter [m]	
6944-18a.sab	6944-18a.fab	Type	Size [m]	NoFlow	Const. Flux	Head/Flux					
		Box	20 x 20 x 20	Head5	Const. Head	5					
				Head0	Const. Head	0					
Flow Region Boundaries		Analysis Parameters									
Box Wall	Head [m]	Head Calculation:		Boundary Specification		Search Parameters					
N	5	Mafic Pipe Network		Source	Sourcegroup	Weight Generation:	None				
S	NoFlow	Aperture Calculation: Weighted		Sink	Sinkgroup	Maximum Paths:	1000				
E	0	Outer Flow Boundary: Box region				Maximum branches/					
W	NoFlow	Inner Flow Boundary: none				source:	100				
Top	5	Representative Path									
Bottom	NoFlow	Generation based on: Source Location									

FracMan Specs											
Model ID	7044-02b		Location							Schweighof	
Fracture Set File	*.fab File	Model Region		Comments							
		Type	Size [m]	Topographic gradient: 0.16 (SE-NW)							
		Orientation		Intensity		Size		Properties (Constant Values)			
		Dip Azi./Dip	Distribution	Type	Value	Mean	Distribution	Deviation [± 1σ]	Transmissivity	Aperture	
x02set1b.set		300-06	Bivar. norm. (5/5)	P ₃₂ , const.	0.79	5.94	Uniform	7.87	default	1.64e-3	
x02set2b.set		348-85	Bivar. norm. (5/5)	P ₃₂ , const.	1.38	1.21	Uniform	1.28	default	4.44e-3	
x02set3b.set		240-78	Bivar. norm. (5/5)	P ₃₂ , const.	0.89	1.34	Uniform	1.14	default	1.06e-3	
x02set4b.set		321-84	Bivar. norm. (5/5)	P ₃₂ , const.	1.54	1.00	Uniform	0.71	default	1.50e-3	

PAWorks Specs											
Model ID	7044-02bNEW		Location							Schweighof	
Files		Sampling Structures									
*.sab File	*.fab File	Flow Region		Name	Boundary Conditions		Head/Flux	Length [m]	Borehole Head [m]	Diameter [m]	
7044-02bNEW.sab	7044-02b.fab	Type	Size [m]	NoFlow	Const. Flux	Head/Flux					
		Box	7 x 7 x 7	Head7	Const. Head	7		7	4.9	0.3	
				Head6.3	Const. Head	6.3					
				Well4.9	Const. Head	4.9					
Flow Region Boundaries		Analysis Parameters									
Box Wall	Head [m]	Head Calculation:		Boundary Specification		Search Parameters					
NE	No Flow	Mafic Pipe Network		Source	Sourcegroup	Weight Generation:	None				
SE	7	Aperture Calculation: Weighted		Sink	Well	Maximum Paths:	1000				
SW	No Flow	Outer Flow Boundary: Box region				Maximum branches/					
NW	6.3	Inner Flow Boundary: Borehole				source:	10				
Top	7	Representative Path									
Bottom	NoFlow	Generation based on: Sink Location									

FracMan Specs

Model ID 7044-02b		Location Schweighof								
* .fab File 7044-02b.fab		Model Region Type Box		Size [m] 10 x 10 x 10		Comments Topographic gradient: 0.16 (SE-NW)				
Fracture Set File	Orientation Dip Azi./Dip		Distribution		Intensity Type Value		Size Mean Distribution Deviation [± 1σ]		Properties (Constant Values) Transmissivity Aperture	
x02set1b.set	300-06		Bivar. norm. (5/5)		P _{2c} . const. 0.79		5.94 Uniform 7.87		default 1.64e-3	
x02set2b.set	348-85		Bivar. norm. (5/5)		P _{2c} . const. 1.38		1.21 Uniform 1.28		default 4.44e-3	
x02set3b.set	240-78		Bivar. norm. (5/5)		P _{2c} . const. 0.89		1.34 Uniform 1.14		default 1.06e-3	
x02set4b.set	321-84		Bivar. norm. (5/5)		P _{2c} . const. 1.54		1.00 Uniform 0.71		default 1.50e-3	

PAWorks Specs

Model ID 7044-02bNEW_NoWell		Location Schweighof									
Files * .sab File 7044-02bNEWNoWell.sab		* .fab File 7044-02b.fab		Sampling Structures							
		Flow Region Type Size [m]		Name		Boundary Conditions Type		Head/Flux	Length [m]	Borehole Head [m]	Diameter [m]
		Box 7 x 7 x 7		NoFlow Head7 Head6.3 Well4.9		Const. Flux Const. Head Const. Head Const. Head		0 7 6.3 4.9			
Flow Region Boundaries Box Wall NE SE SW NW Top Bottom		Head [m] No Flow 7 No Flow 6.3 7 NoFlow		Analysis Parameters				Boundary Specification		Search Parameters	
				Head Calculation: Mafic Pipe Network Aperture Calculation: Weighted Outer Flow Boundary: Box region Inner Flow Boundary: Borehole Representative Path Generation based on: Travel Time				Source Sink Sourcegroup Sinkgroup		Weight Generation: None Maximum Paths: 1000 Maximum branches/ source: 10	

FracMan Specs

Model ID 6943-13b		Location Rugenmühle								
* .fab File 6943-13b.fab		Model Region Type Box		Size [m] 10 x 10 x 10		Comments Topographic gradient: 0.4 (N-S)				
Fracture Set File	Orientation Dip Azi./Dip		Distribution		Intensity Type Value		Size Mean Distribution Deviation [± 1σ]		Properties (Constant Values) Transmissivity Aperture	
x13set1b.set	198-78		Bivar. norm. (5/5)		P _{2c} . const. 1.19		1.87 Uniform 1.433		default 5.0e-4	
x13set2b.set	000-18		Fisher (K = 200)		P _{2c} . const. 1.43		4.54 Uniform 2.848		default 1.55e-3	
x13set3b.set	129-84		Bivar. norm. (5/5)		P _{2c} . const. 0.62		2.63 Uniform 1.935		default 6.0e-4	
x13set4b.set	097-78		Bivar. norm. (5/5)		P _{2c} . const. 0.79		1.22 Uniform 0.748		default 6.7e-4	
x13set5b.set	255-48		Bivar. norm. (5/5)		P _{2c} . const. 0.79		1.58 Uniform 0.853		default 2.4e-3	

PAWorks Specs

Model ID 6943-13b		Location Rugenmühle									
Files * .sab File 6943-13b.sab		* .fab File 6943-13b.fab		Sampling Structures							
		Flow Region Type Size [m]		Name		Boundary Conditions Type		Head/Flux	Length [m]	Borehole Head [m]	Diameter [m]
		Box 10 x 10 x 10		NoFlow Head2 Head0		Const. Flux Const. Head Const. Head		0 2 0			
Flow Region Boundaries Box Wall N E S W Top Bottom		Head [m] 2 No Flow 0 No Flow 2 NoFlow		Analysis Parameters				Boundary Specification		Search Parameters	
				Head Calculation: Mafic Pipe Network Aperture Calculation: Weighted Outer Flow Boundary: Box region Inner Flow Boundary: Representative Path Generation based on: Source Location				Source Sink Source group Sink Group		Weight Generation: None Maximum Paths: 100 Maximum branches/ source: 100	

FracMan Specs

Model ID 6943-01b		Location Steinbruch Prünst							
*.fab File 6943-01b.fab		Model Region		Comments					
		Type Box	Size [m] 20 x 20 x 20	Topographic gradient: 0.2 (S-N)					
Fracture Set File	Orientation	Dip Azi./Dip	Distribution	Intensity	Mean	Size	Deviation	Properties (Constant Values)	
				Type	Value	Distribution	[± 1σ]	Transmissivity	Aperture
x01set1b.set	326-84	Bivar. norm. (5/5)	P ₃₂ .const	1.92	2.10	Uniform	1.89	default	3.20e-4
x01set2b.set	256-88	Bivar. norm. (5/5)	P ₃₂ .const	0.56	4.29	Uniform	6.19	default	5.00e-4
x01set3b.set	011-02	Bivar. norm. (5/5)	P ₃₂ .const	0.79	15.00	Uniform	9.19	default	1.00e-3
x01set4b.set	038-59	Bivar. norm. (5/5)	P ₃₂ .const	0.50	2.22	Uniform	2.30	default	1.08e-3

PAWorks Specs

Model ID 6943-01b		Location Steinbruch Prünst							
Files		Sampling Structures							
*.sab File 6943-01b.sab	*.fab File 6943-01b.fab	Flow Region		Name	Boundary Conditions		Length [m]	Borehole Head [m]	Diameter [m]
		Type	Size [m]	NoFlow	Type	Head/Flux			
		Box	20 x 20 x 20	Head2	Const. Head	2			
				Head0	Const. Head	0			
Flow Region Boundaries		Analysis Parameters							
Box Wall	Head [m]	Head Calculation:		Boundary Specification		Search Parameters			
N	0	Mafic Pipe Network		Source	Source group	Weight Generation: None			
E	No Flow	Weighted		Sink	Sink Group	Maximum Paths: 1000			
S	2	Outer Flow Boundary:		Maximum branches/ source: 100					
W	No Flow	Box region							
Top	2	Inner Flow Boundary:							
Bottom	NoFlow	Representative Path							
		Generation based on:							
		Source Location							

4 References

Dershowitz, W., 2002, FracWorks XP Discrete Feature Simulator. User Documentation Beta Version 0.21: Seattle, Washington, Golder Associates Inc., 81 p.

Dershowitz, W., Foxford, T., Sudicky, E., Shuttle, D.A., Eiben, T., and Ahlstrom, E., 2002, PAWorks. Pathway Analysis for Discrete Fracture Networks with LTG Solute Transport. User Documentation. Version 1.64.: Seattle, Washington, Golder Associates, Inc.

Dershowitz, W., Lee, G., Geier, J., Hitchcock, S., LaPointe, P., and Cladouhos, T., 1999, FracWorks/95 Discrete Feature Simulator. User Documentation. Version 1.3.: Seattle, Washington, Golder Associates, Inc.

Appendix E – Geophysical logs

In the following the geophysical logs examined in sections 4.1.1.2 and 4.1.1.3 will be displayed. The logs include survey stations

Böbrach B 1

Neusohl VB 1

Neusohl VB 2

Schweinhütt VB 4

Wiesenfelden B 1

Bayerisch Eisenstein

Kirchdorf VB 1

Kirchdorf VB 3

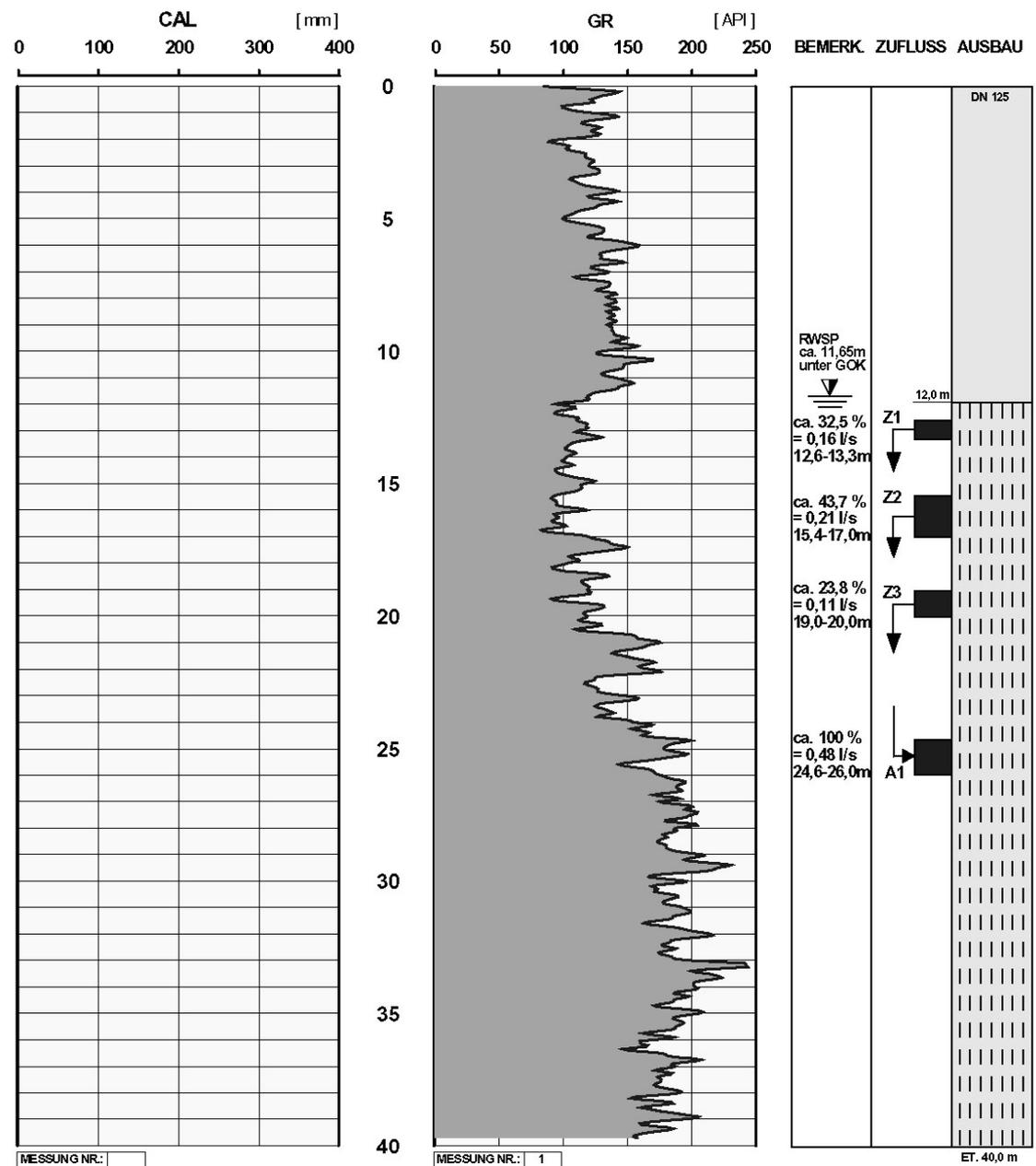
Kirchdorf VB 4

Kirchdorf VB 5

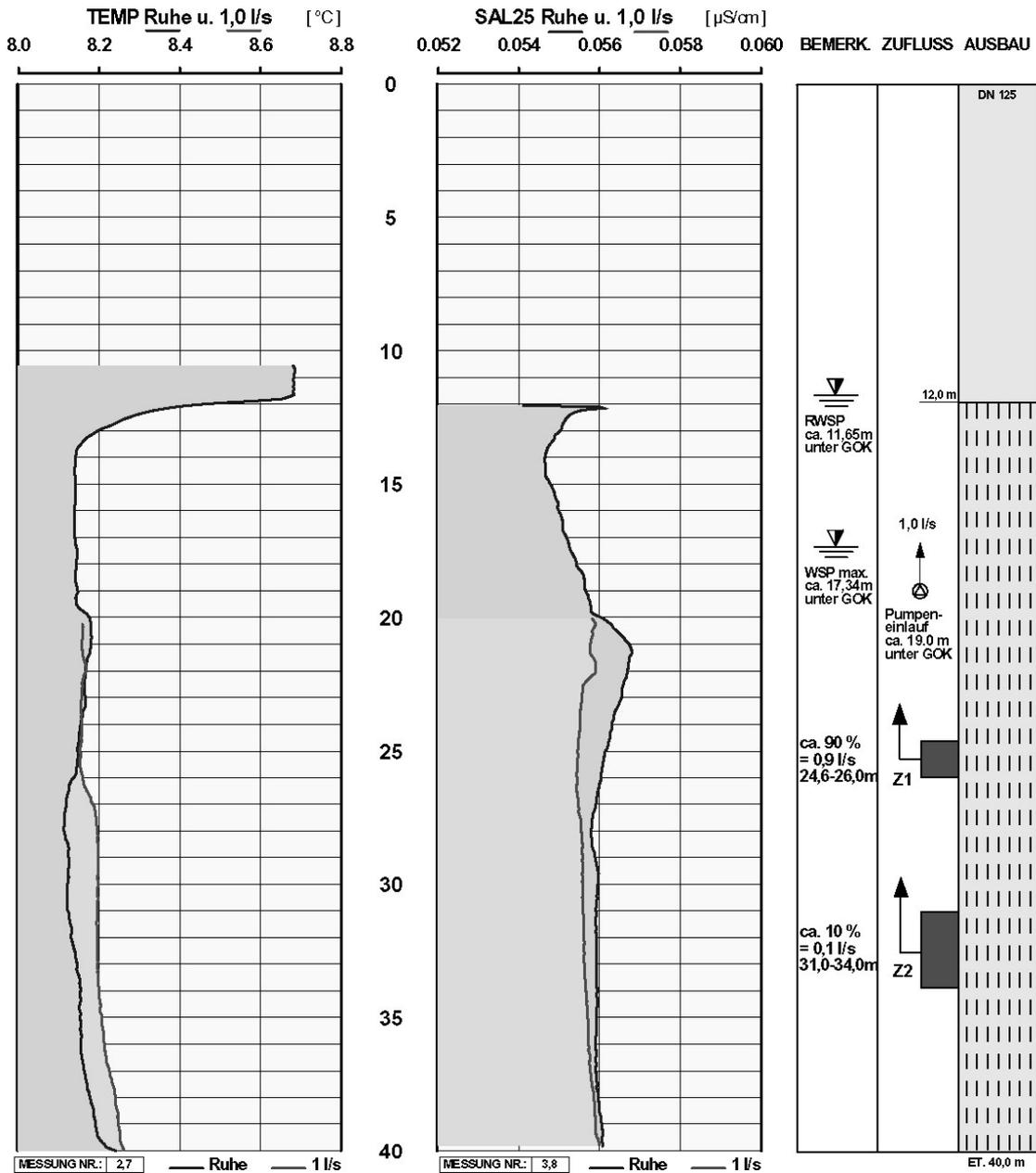
Kirchdorf VB 6

The logs were provided by German Geo Services and Fontus Logging Services.

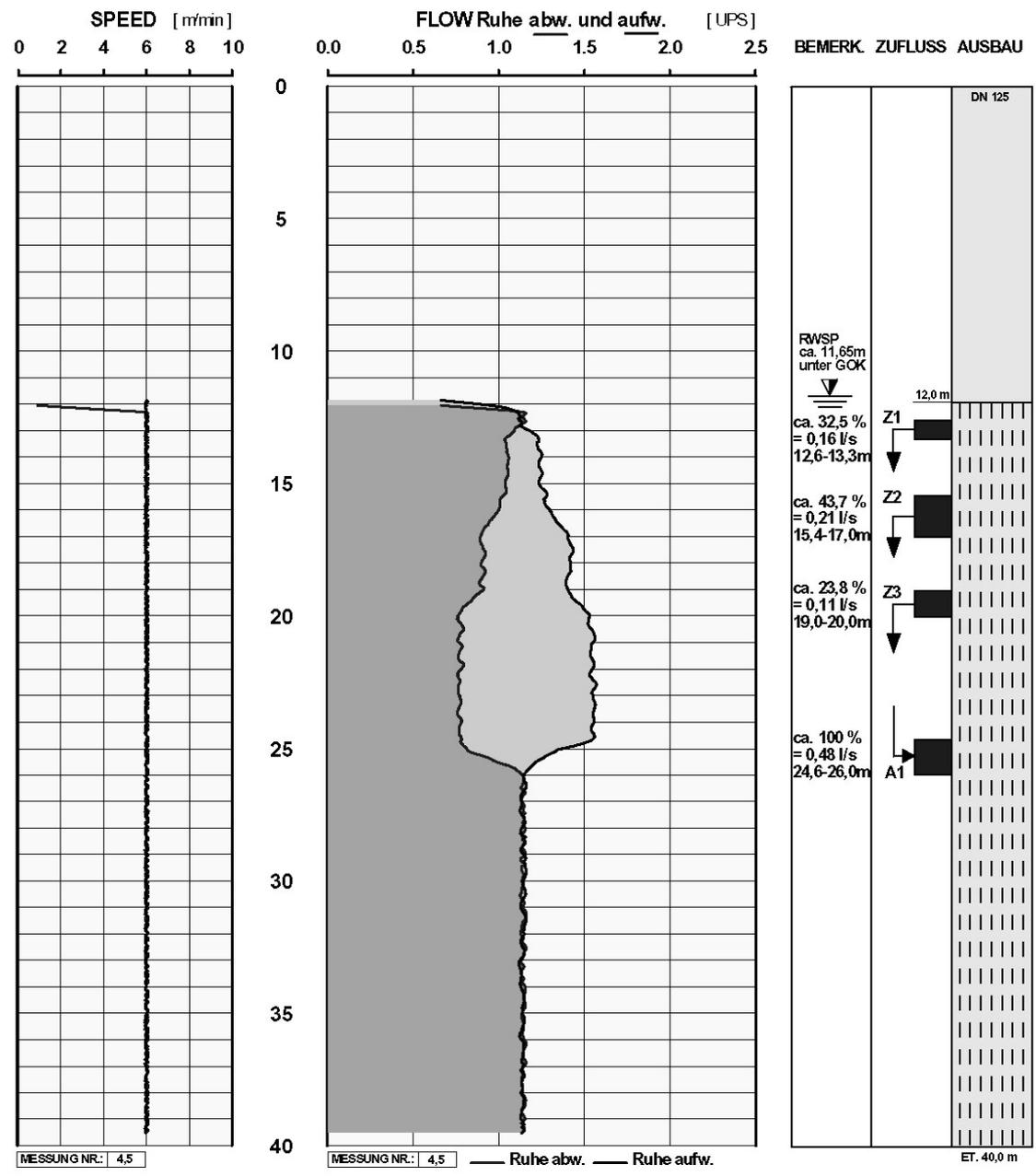
GERMAN GEO SERVICES <small>DANNBERGER WEG 12 91093 NIEDERLINDACH TEL. 09135-722542</small> BOHRLOCHVERMESSUNG		Gamma Ray Log (GR)	
AUFTRAGGEBER : <u>TAFELMEIER Bohr GmbH</u>	BOHRUNG-NR. : <u>B 1</u>		
PROJEKT : <u>WV Böbrach</u>	DATUM : <u>04.10.2004</u>		
ORT : <u>Böbrach</u>	MESSAUFTRAG : <u>B04100401</u>		
BUNDESLAND : <u>Bayern</u>	MESSWAGEN : <u>N-PR-787</u>		



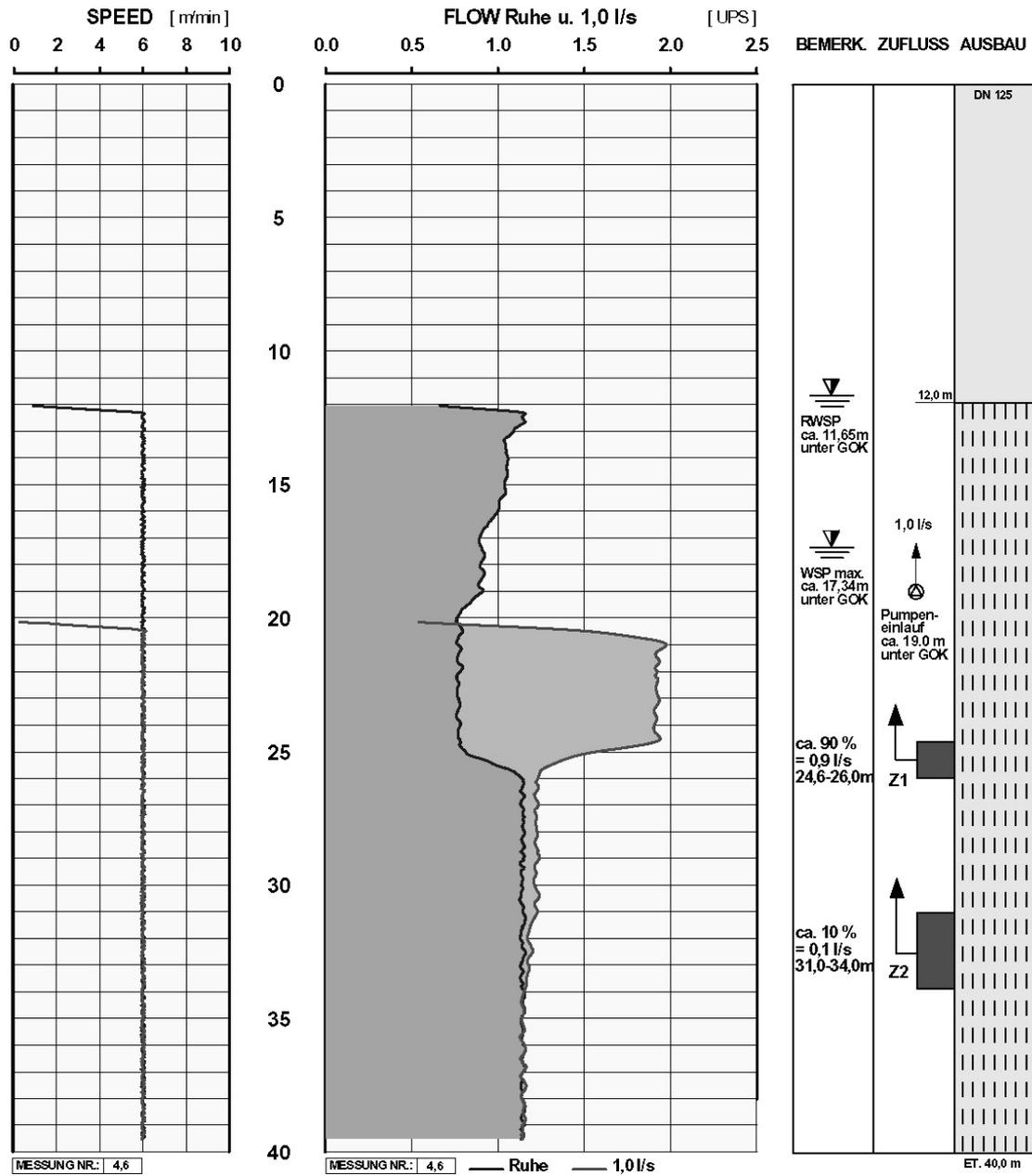
<p>GERMAN GEO SERVICES DANNBERGER WEG 12 91093 NIEDERLINDACH TEL. 09135722542 BOHRLOCHVERMESSUNG</p>	<p>Temperatur Log (TEMP) Salinometer Log (SAL) Ruhe und Produktion 1,0 l/s</p>
<p>AUFTRAGGEBER : <u>TAFELMEIER Bohr GmbH</u></p> <p>PROJEKT : <u>WV Böbrach</u></p> <p>ORT : <u>Böbrach</u></p> <p>BUNDESLAND : <u>Bayern</u></p>	<p>BOHRUNG-NR. : <u>B 1</u></p> <p>DATUM : <u>04.10.2004</u></p> <p>MESSAUFTRAG : <u>B04100401</u></p> <p>MESSWAGEN : <u>N-PR-787</u></p>



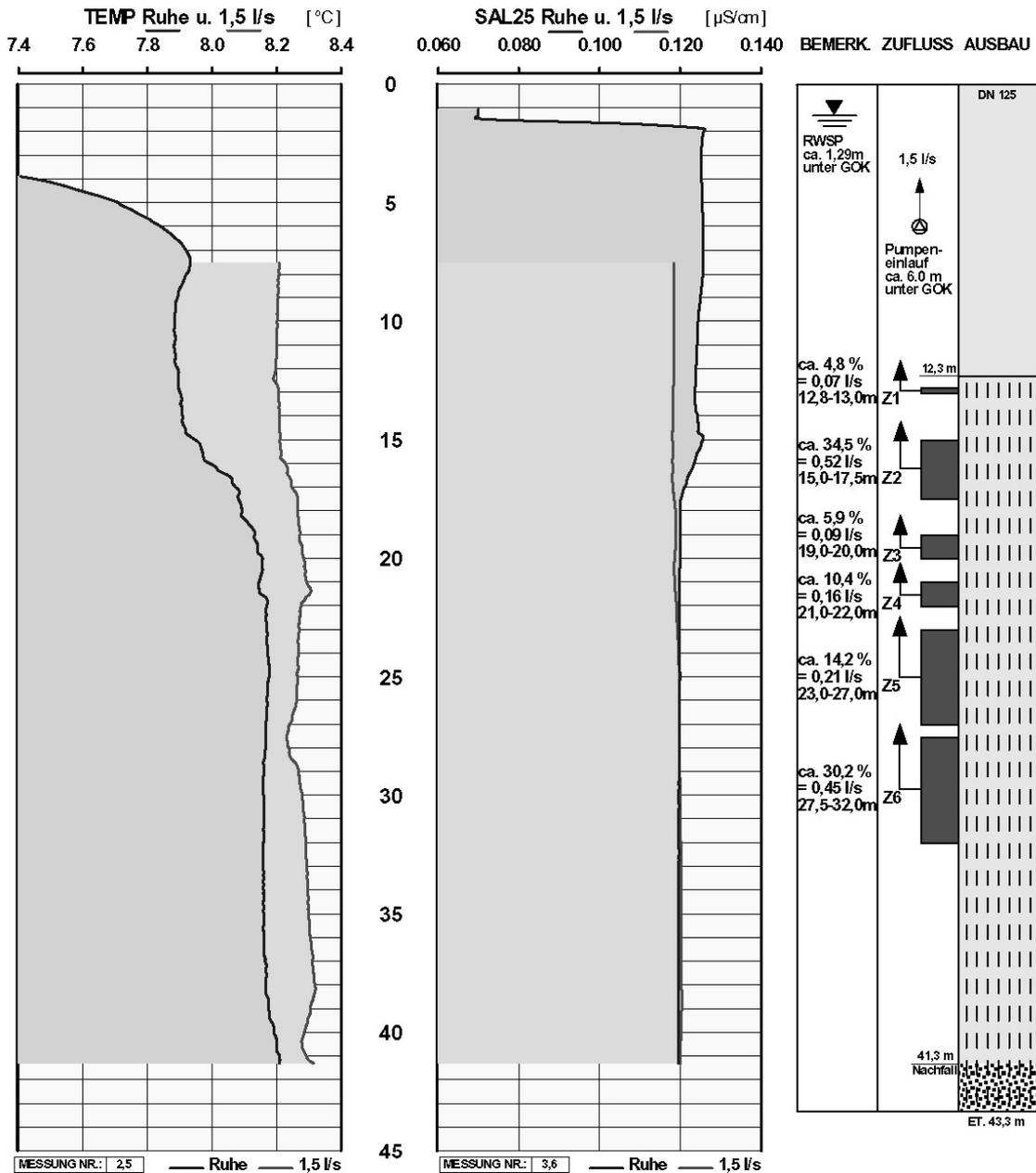
GERMAN GEO SERVICES <small>DANNBERGER WEG 12 91093 NIEDERLINDACH TEL. 09135-722542</small> BOHRLOCHVERMESSUNG	Flowmeter Log (FLOW) <i>Ruhezustand, Messrichtungen ab- und aufwärts</i>
AUFTRAGGEBER : <u>TAFELMEIER Bohr GmbH</u>	BOHRUNG-NR. : <u>B 1</u>
PROJEKT : <u>WV Böbrach</u>	DATUM : <u>04.10.2004</u>
ORT : <u>Böbrach</u>	MESSAUFTRAG : <u>B04100401</u>
BUNDESLAND : <u>Bayern</u>	MESSWAGEN : <u>N-PR-787</u>



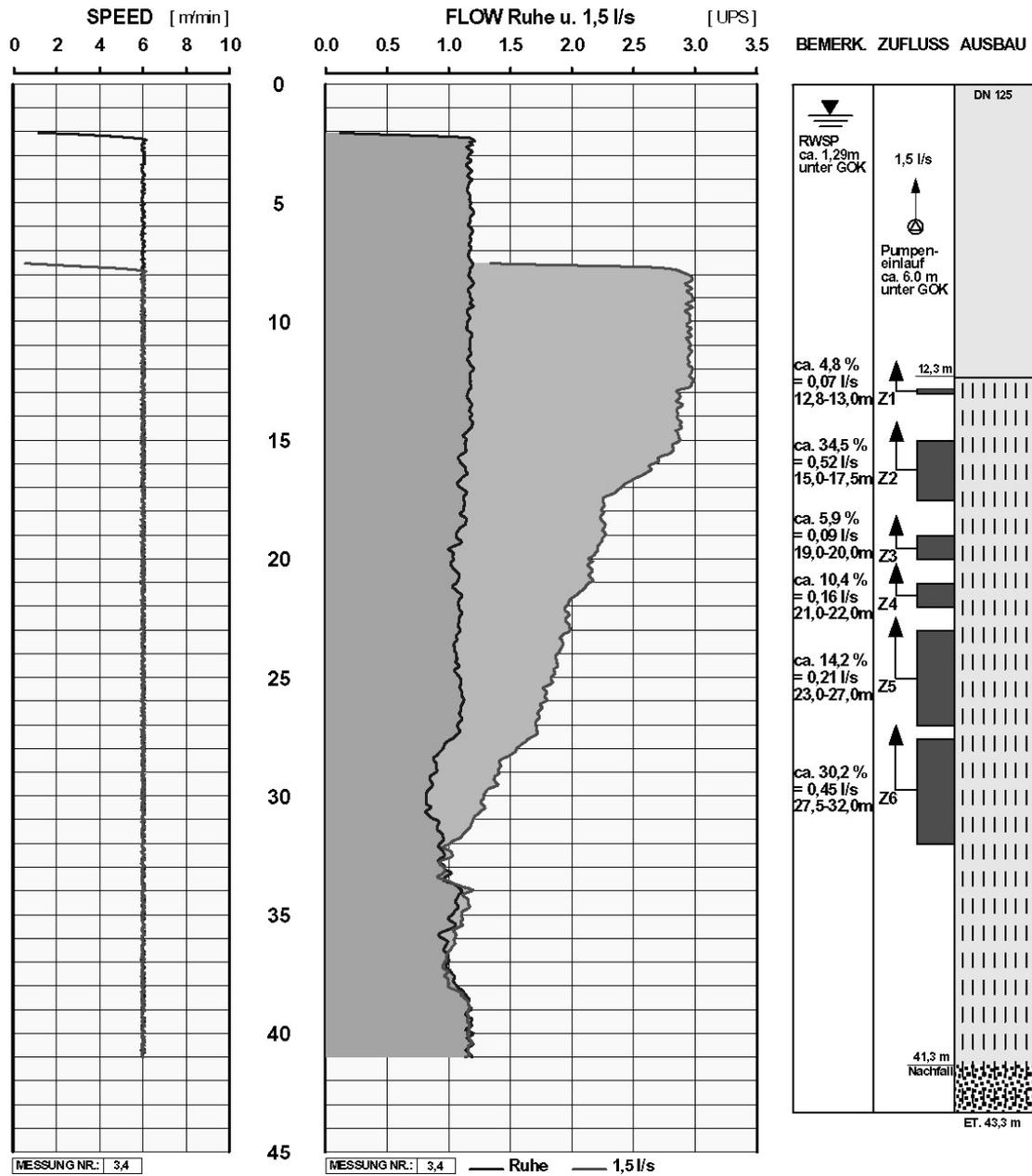
GERMAN GEO SERVICES <small>DANNBERGER WEG 12 91093 NIEDERLINDACH TEL. 09135-722542</small> BOHRLOCHVERMESSUNG	Flowmeter Log (FLOW) <i>Ruhe und Produktion 1,0 l/s</i>
AUFTRAGGEBER : <u>TAFELMEIER Bohr GmbH</u>	BOHRUNG-NR. : <u>B 1</u>
PROJEKT : <u>WV Böbrach</u>	DATUM : <u>04.10.2004</u>
ORT : <u>Böbrach</u>	MESSAUFTRAG : <u>B04100401</u>
BUNDESLAND : <u>Bayern</u>	MESSWAGEN : <u>N-PR-787</u>



GERMAN GEO SERVICES DANNBERGER WEG 12 91093 NIEDERLINDACH TEL. 09135722542 BOHRLOCHVERMESSUNG		Temperatur Log (TEMP) Salinometer Log (SAL) Ruhe und Produktion 1,5 l/s	
AUFTRAGGEBER :	TAFELMEIER Bohr GmbH	BOHRUNG-NR. :	VB 1
PROJEKT :	Stadtwerke Regen	DATUM :	19.12.2002
ORT :	Neusohl	MESSAUFTRAG :	B02121901
BUNDESLAND :	Bayern	MESSWAGEN :	N-PR-787

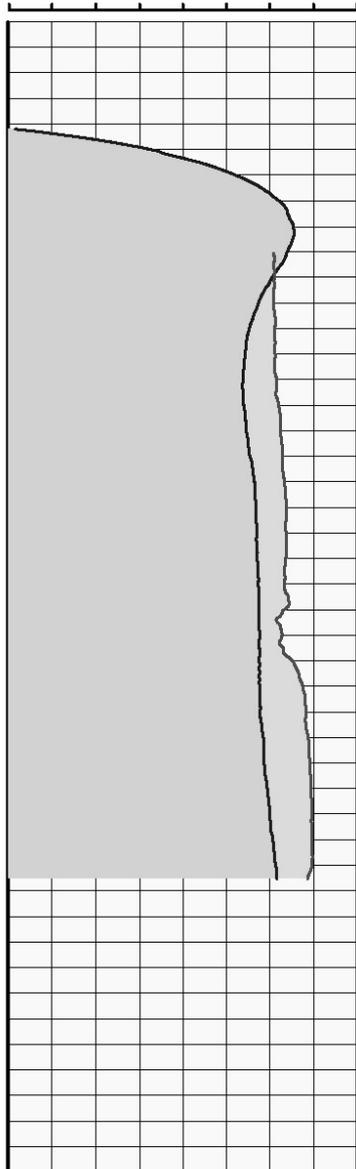


GERMAN GEO SERVICES DANNBERGER WEG 12 91093 NIEDERLINDACH TEL. 09135-722542 BOHRLOCHVERMESSUNG	Flowmeter Log (FLOW) Ruhe und Produktion 1,5 l/s
AUFTRAGGEBER : <u>TAFELMEIER Bohr GmbH</u>	BOHRUNG-NR. : <u>VB 1</u>
PROJEKT : <u>Stadtwerke Regen</u>	DATUM : <u>19.12.2002</u>
ORT : <u>Neusohl</u>	MESSAUFTRAG : <u>B02121901</u>
BUNDESLAND : <u>Bayern</u>	MESSWAGEN : <u>N-PR-787</u>



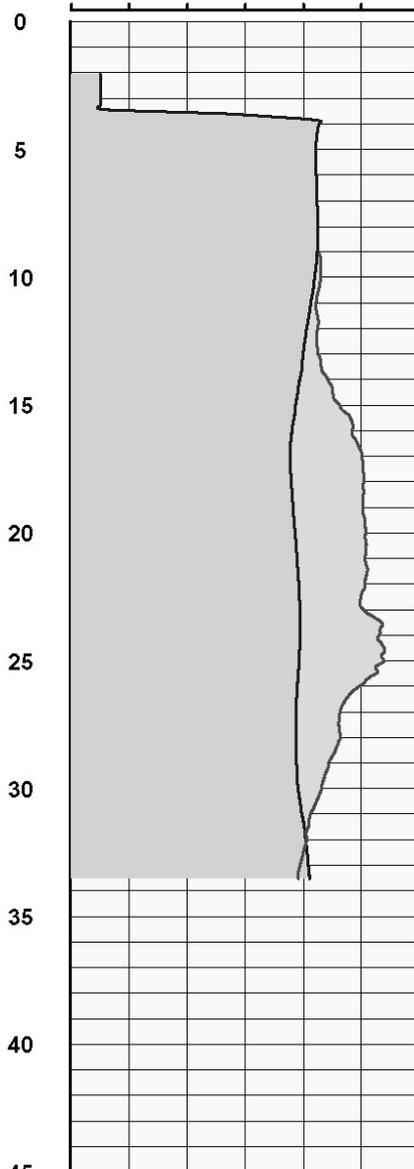
GERMAN GEO SERVICES DANNBERGER WEG 12 91093 NIEDERLINDACH TEL. 09135722542 BOHRLOCHVERMESSUNG		Temperatur Log (TEMP) Salinometer Log (SAL) Ruhe und Produktion 1,5 l/s	
AUFTRAGGEBER :	TAFELMEIER Bohr GmbH	BOHRUNG-NR. :	VB 2
PROJEKT :	Stadtwerke Regen	DATUM :	19.12.2002
ORT :	Neusohl	MESSAUFTRAG :	B02121902
BUNDESLAND :	Bayern	MESSWAGEN :	N-PR-787

TEMP Ruhe u. 1,5 l/s [°C]
7.4 7.6 7.8 8.0 8.2 8.4 8.6 8.8 9.0



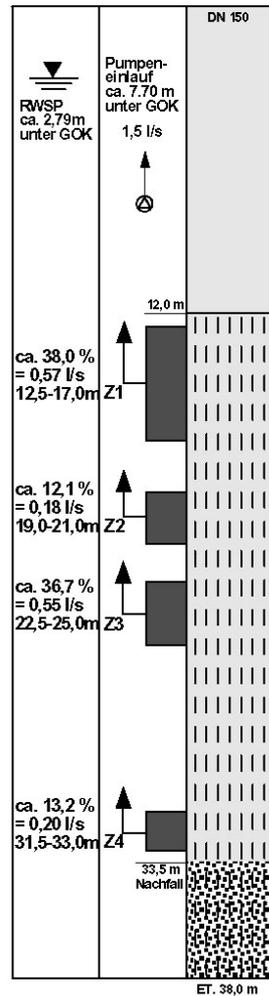
MESSUNG NR.: 25 Ruhe 1,5 l/s

SAL25 Ruhe u. 1,5 l/s [µS/cm]
0.060 0.080 0.100 0.120 0.140 0.160 0.180

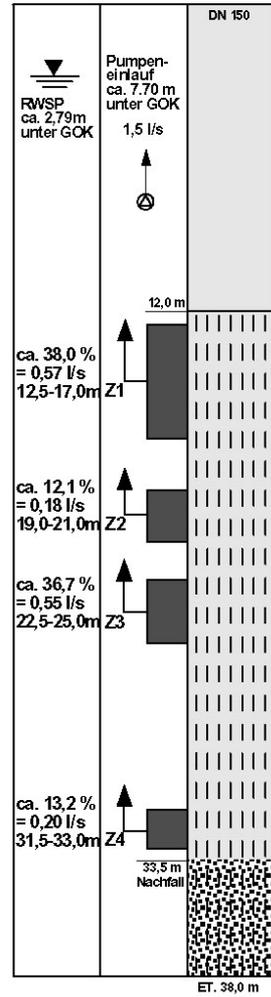
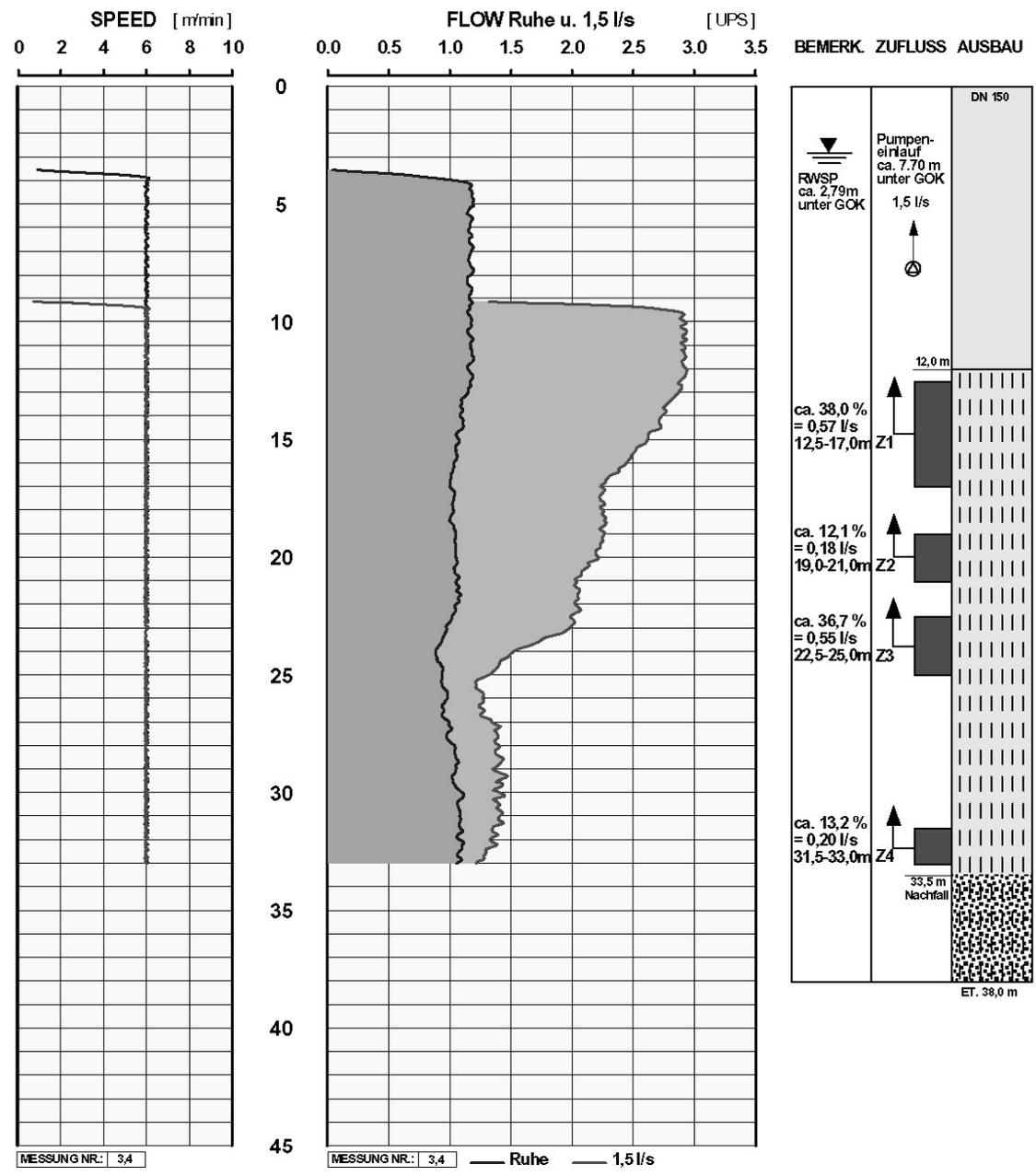


MESSUNG NR.: 3,6 Ruhe 1,5 l/s

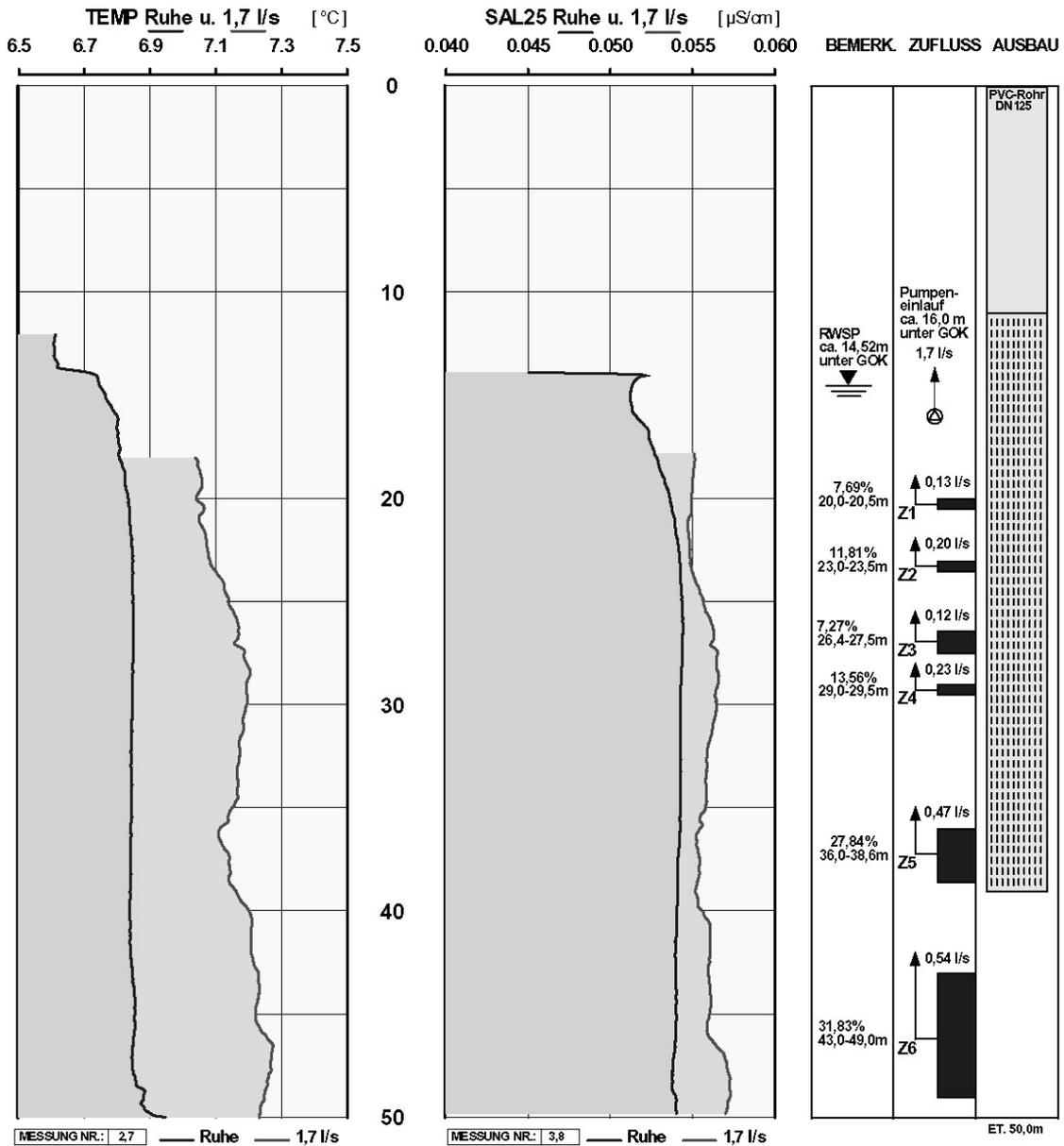
BERMERK. ZUFLUSS AUSBAU



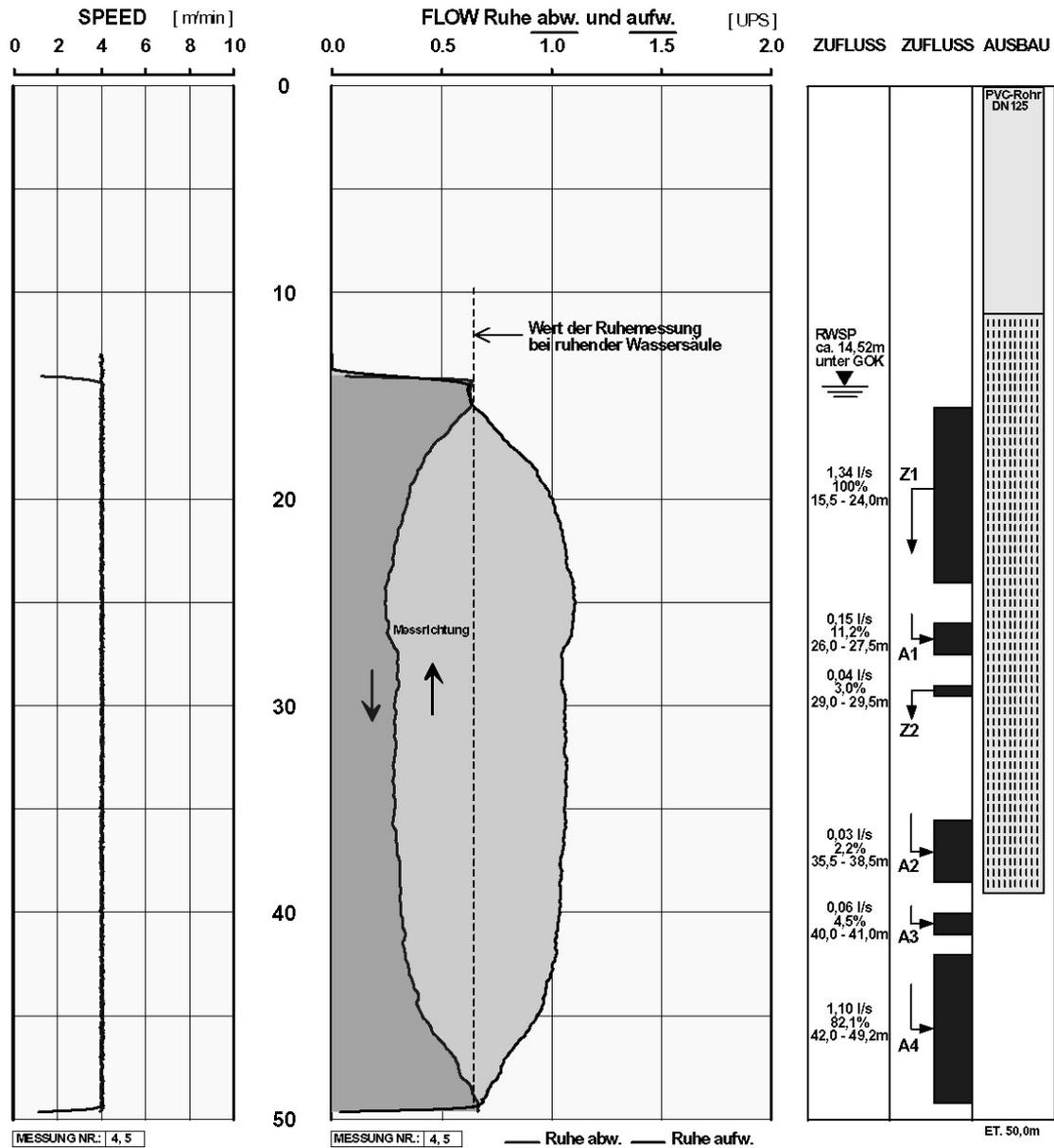
<p>GERMAN GEO SERVICES DANNBERGER WEG 12 91093 NIEDERLINDACH TEL. 09135-722542 BOHRLOCHVERMESSUNG</p>	<p>Flowmeter Log (FLOW) Ruhe und Produktion 1,5 l/s</p>
<p>AUFTRAGGEBER : <u>TAFELMEIER Bohr GmbH</u></p> <p>PROJEKT : <u>Stadtwerke Regen</u></p> <p>ORT : <u>Neusohl</u></p> <p>BUNDESLAND : <u>Bayern</u></p>	<p>BOHRUNG-NR. : <u>VB 2</u></p> <p>DATUM : <u>19.12.2002</u></p> <p>MESSAUFTRAG : <u>B02121902</u></p> <p>MESSWAGEN : <u>N-PR-787</u></p>



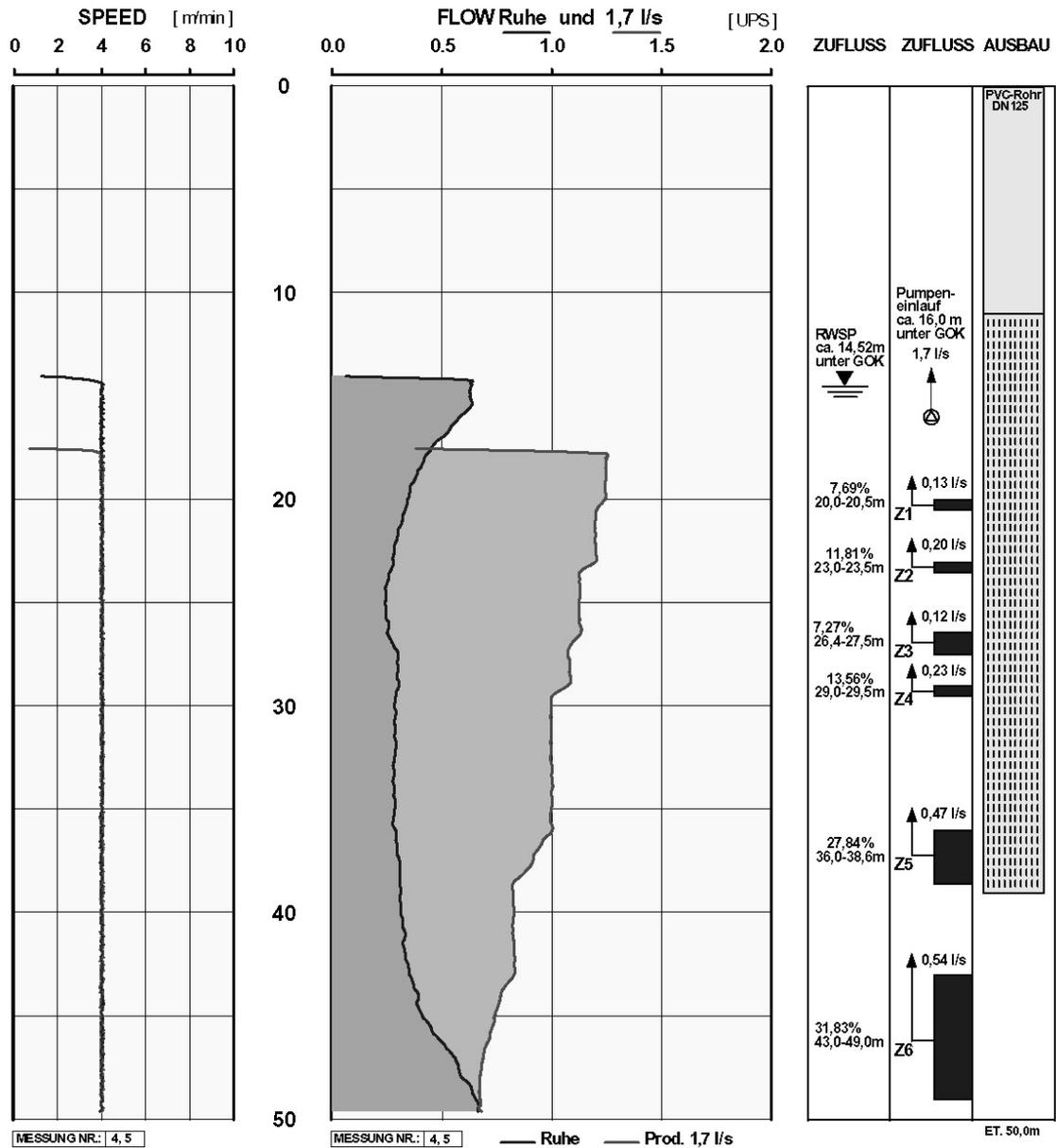
GERMAN GEO SERVICES DANNBERGER WEG 12 91093 NIEDERLINDACH TEL. 09135722542 BOHRLOCHVERMESSUNG		Temperatur Log (TEMP) Salinometer Log (SAL) Ruhe und Produktion 1,7 l/s	
AUFTRAGGEBER :	Tafelmeier Tiefbrunnen-Bau GmbH	BOHRUNG-NR. :	VB 4
PROJEKT :	Satdtwerke Regen - WG Schweinhütt	DATUM :	09.11.2005
ORT :	Schweinhütt	MESSAUFTRAG :	B05110901
BUNDESLAND :	Bayern	MESSWAGEN :	N-PR - 787



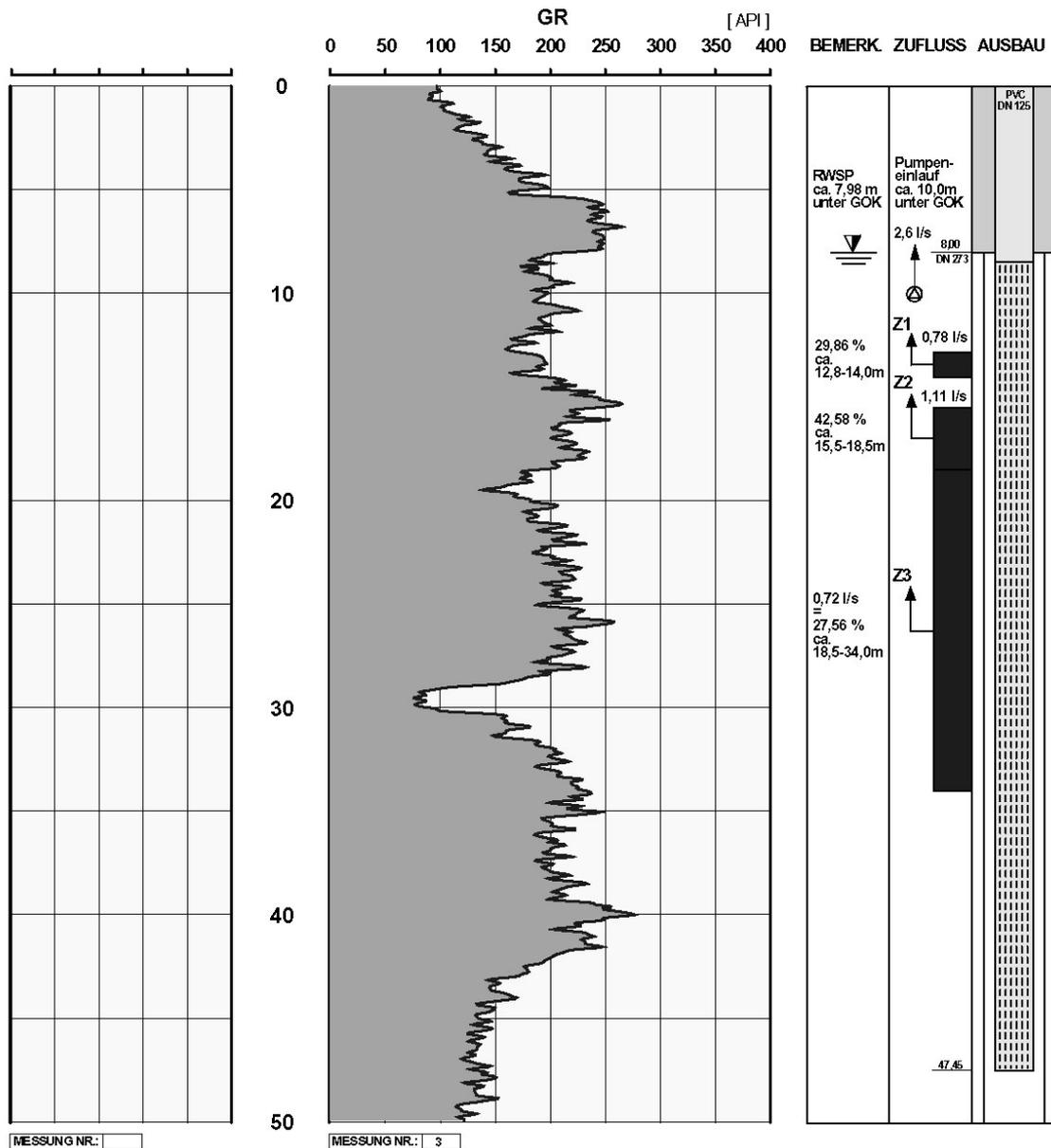
GERMAN GEO SERVICES DANNBERGER WEG 12 91093 NIEDERLINDACH TEL. 09135-722542 BOHRLOCHVERMESSUNG	Flowmeter Log (FLOW) <i>Ruhezustand, Messrichtungen ab- und aufwärts</i>
AUFTRAGGEBER : <u>Tafelmeier Tiefbrunnen-Bau GmbH</u>	BOHRUNG-NR. : <u>VB 4</u>
PROJEKT : <u>Stadtwerke Regen - WG Schweinhütt</u>	DATUM : <u>09.11.2005</u>
ORT : <u>Schweinhütt</u>	MESSAUFTRAG : <u>B050110901</u>
BUNDESLAND : <u>Bayern</u>	MESSWAGEN : <u>N-PR-787</u>



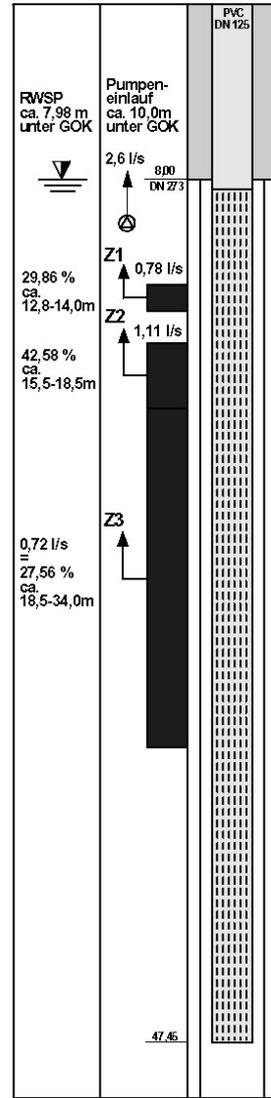
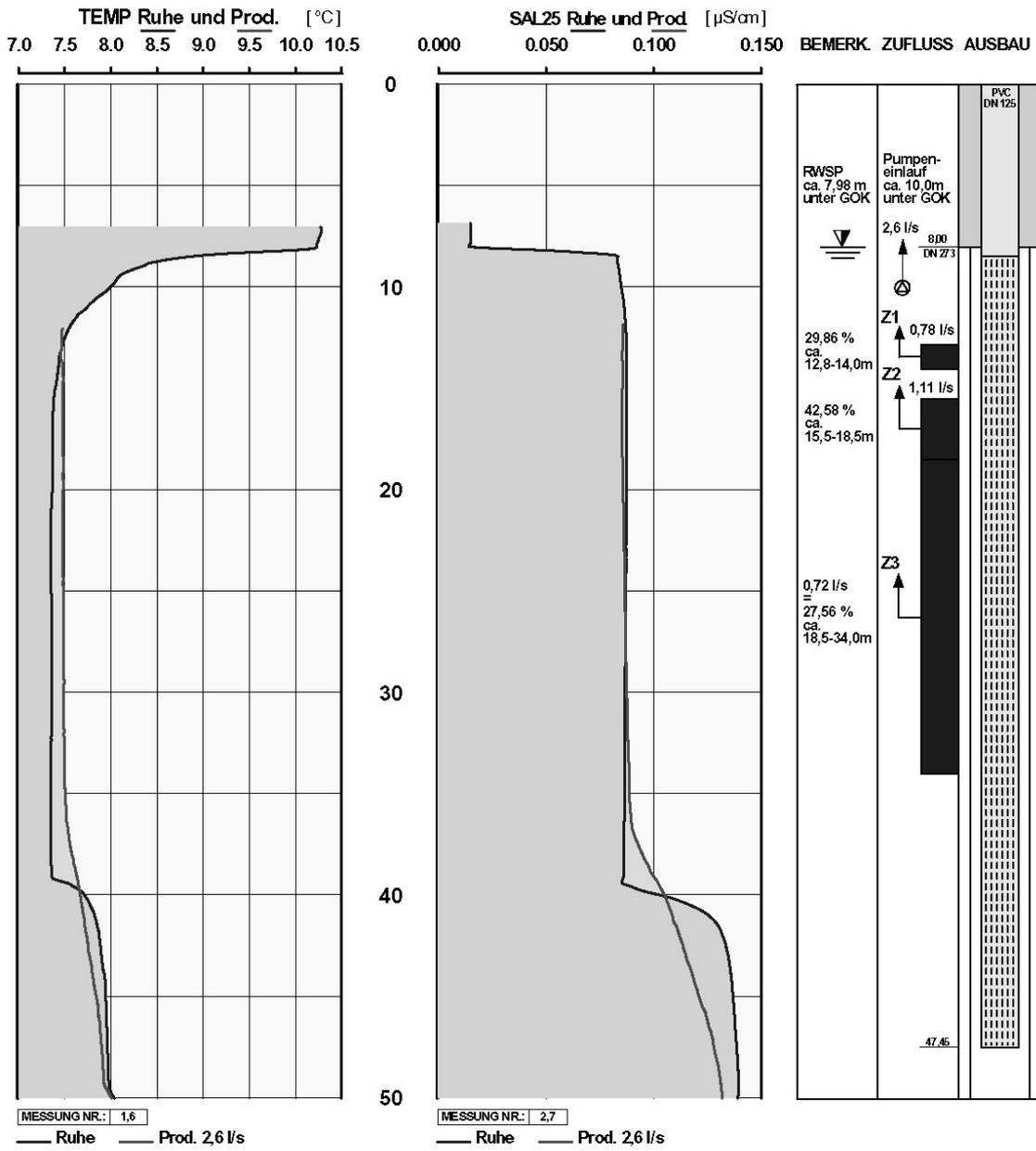
GERMAN GEO SERVICES <small>DANNBERGER WEG 12 91093 NIEDERLINDACH TEL. 09135-722542</small> BOHRLOCHVERMESSUNG	Flowmeter Log (FLOW) <i>Ruhe und Produktion 1,7 l/s</i>
AUFTRAGGEBER : <u>Tafelmeier Tiefbrunnen-Bau GmbH</u>	BOHRUNG-NR. : <u>VB 4</u>
PROJEKT : <u>Stadtwerke Regen - WG Schweinhütt</u>	DATUM : <u>09.11.2005</u>
ORT : <u>Schweinhütt</u>	MESSAUFTRAG : <u>B050110901</u>
BUNDESLAND : <u>Bayern</u>	MESSWAGEN : <u>N-PR-787</u>



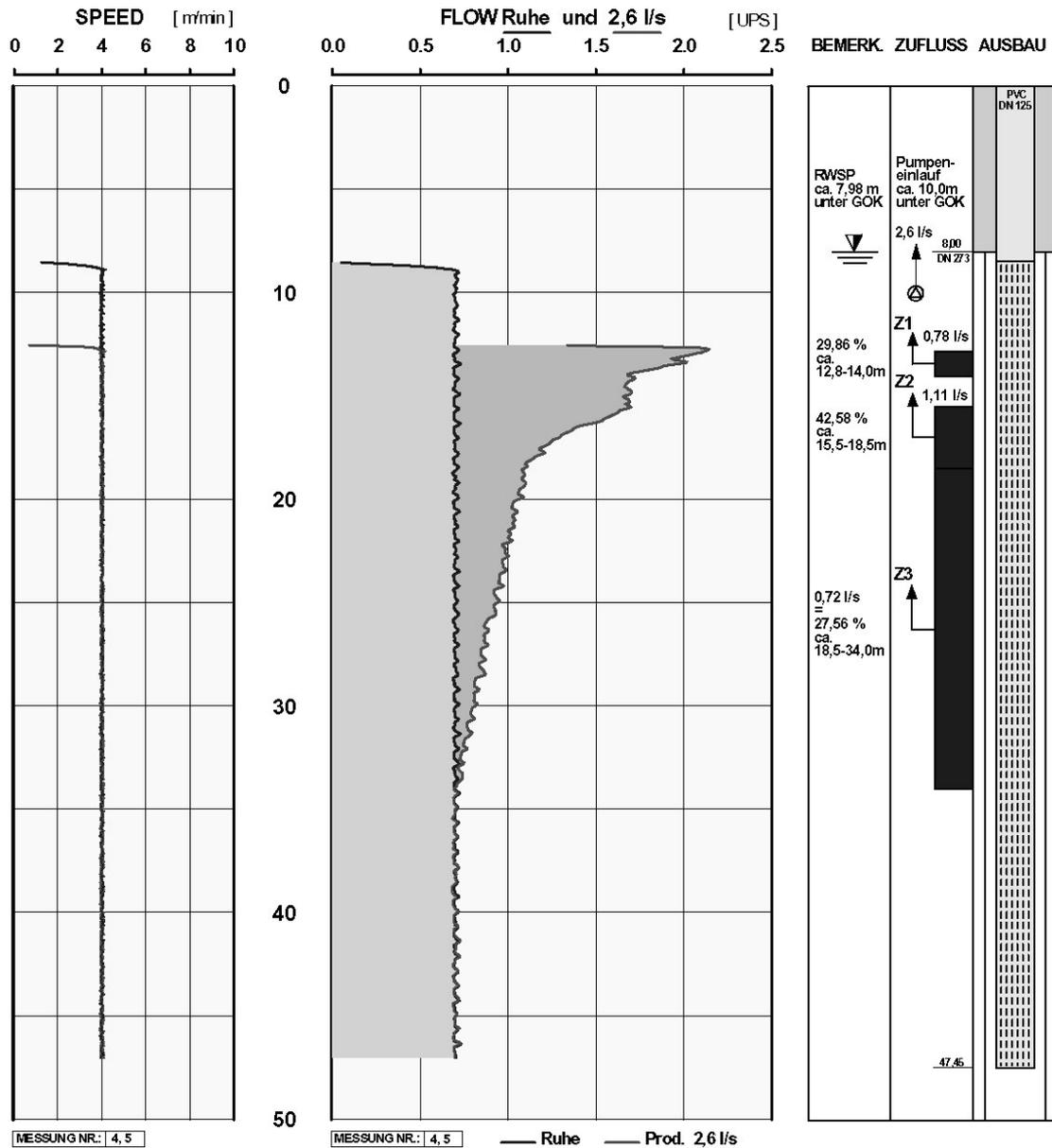
GERMAN GEO SERVICES <small>DANNBERGER WEG 12 91093 NIEDERLINDACH TEL. 09135-722542</small> BOHRLOCHVERMESSUNG		Gamma Ray Log (GR)	
AUFTRAGGEBER :	TAFELMEIER Tiefbrunnenbau GmbH	BOHRUNG-NR. :	B 1
PROJEKT :	Wasserversorgung	DATUM :	04.07.2005
ORT :	Wiesenfelden	MESSAUFTRAG :	B05070402
BUNDESLAND :	Bayern	MESSWAGEN :	ERH - PR - 300



GERMAN GEO SERVICES DANNBERGER WEG 12 91093 NIEDERLINDACH TEL. 09135-722542 BOHRLOCHVERMESSUNG		Temperatur Log (TEMP) Salinometer Log (SAL25°C) Ruhe und Produktion 2,6 l/s	
AUFTRAGGEBER :	TAFELMEIER Tiefbrunnenbau GmbH	BOHRUNG-NR. :	B 1
PROJEKT :	Wasserversorgung	DATUM :	04.07.2005
ORT :	Wiesenfelden	MESSAUFTRAG :	B05070402
BUNDESLAND :	Bayern	MESSWAGEN :	ERH-PR-300



GERMAN GEO SERVICES DANNBERGER WEG 12 91093 NIEDERLINDACH TEL. 09135-722542 BOHRLOCHVERMESSUNG	Flowmeter Log (FLOW) <i>Ruhe und Produktion 2,6 l/s</i>
AUFTRAGGEBER : <u>TAFELMEIER Tiefbrunnenbau GmbH</u>	BOHRUNG-NR. : <u>B 1</u>
PROJEKT : <u>Wasserversorgung</u>	DATUM : <u>04.07.2005</u>
ORT : <u>Wiesenfelden</u>	MESSAUFTRAG : <u>B05070402</u>
BUNDESLAND : <u>Bayern</u>	MESSWAGEN : <u>ERH-PR-300</u>



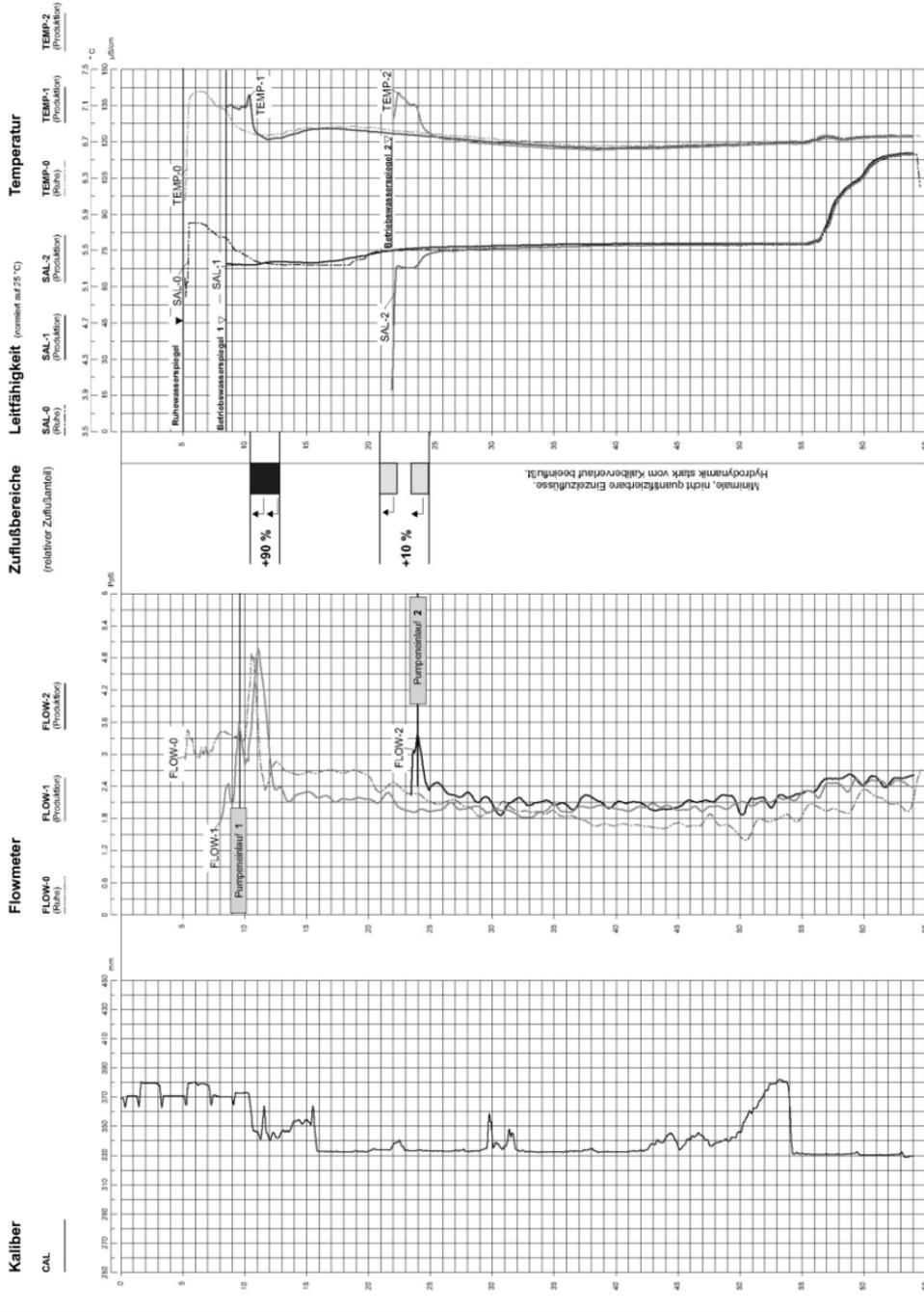
Tiefbrunnen Grafhüttenbach

Bayerisch Eisenstein
 Teufenmaßstab: 1 : 250
 Ausführung / Interpretation: W. Beck
 Bearbeitung / Datenprocessing: M. Fedirsei

Geophysikalische Bohrlochmessungen

Datum: 05.12.2003
 Bohrer: E-M Bohr-GmbH
 Bohrtiefe: 65,00 m
 Bohr-Ø: 311 mm
 Sperrroh-Ø: 368 / 521 mm
 Leistung: 1,5 l/s
 Meßflutpunkt: GOK

gbs-Bohrlochgeophysik
 Wallenrodstr. 3
 91126 Schwabach
 Tel. 09122 / 83 29 260
 Fax 09122 / 83 29 270
 Beck & Seitz Partnerschaft e-mail: g-b-s@t-online.de



Geophysikalische Bohrlochmessungen

VB 1 Habichtstein

WV Gem. Kirchdorf im Wald

Datum: 24.06.2004

Auftraggeber: Sib.Dr. Pröhl

gbs-Bohrlochgeophysik



Wallenrodstr. 3
91126 Schwabach
Tel. 091/22/83 26 260
Fax 091/22/83 26 261
Beck & Seitz Partner GmbH
E-Mail: gbs@gbs-geophysik.de

Bohr-Ø: 203/152/115 mm

Bohrtiefe: 50,0 m

Wallerodstr. 3
91126 Schwabach
Tel. 091/22/83 26 260
Fax 091/22/83 26 261
Beck & Seitz Partner GmbH
E-Mail: gbs@gbs-geophysik.de

Teufenmaßstab: 1 : 200

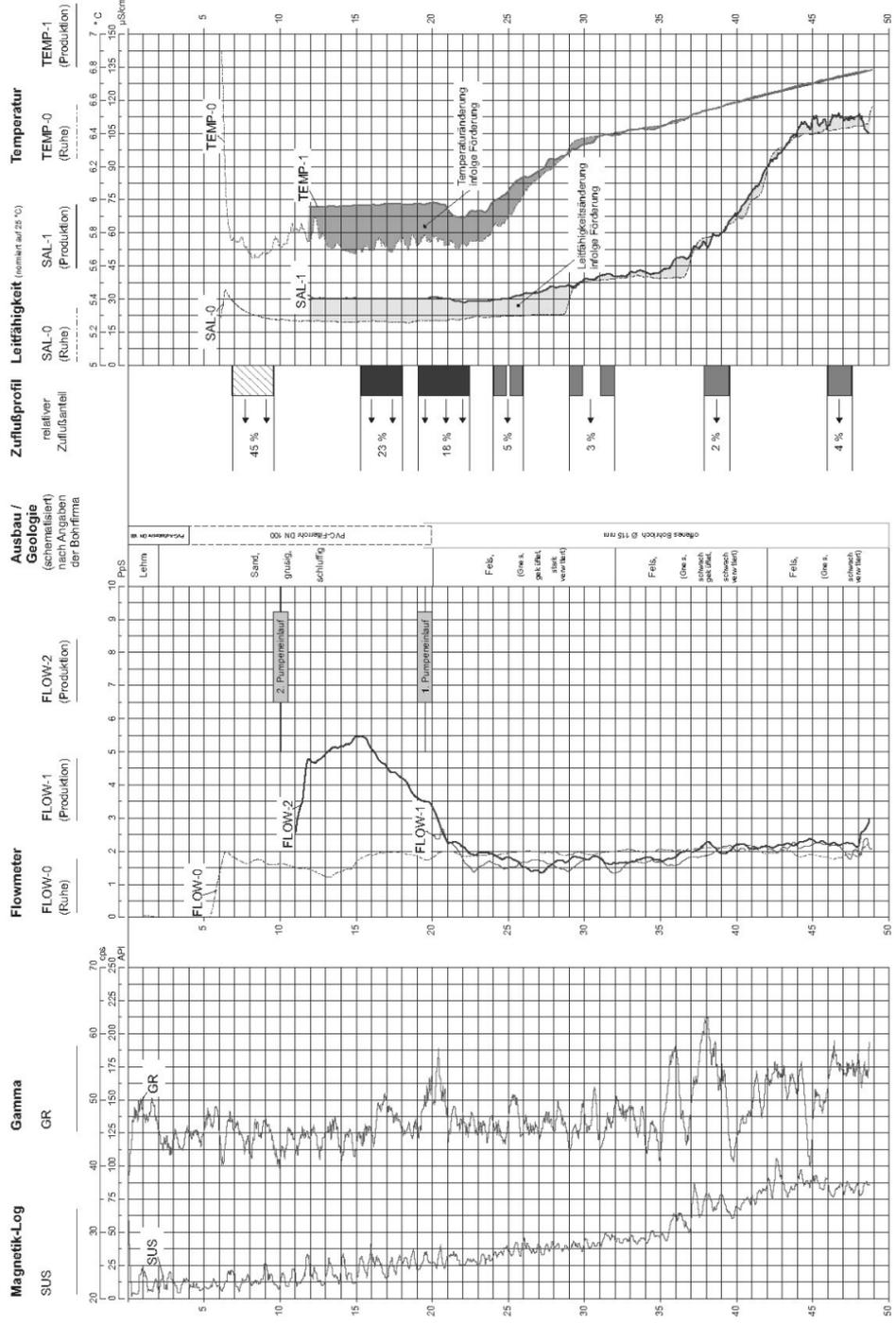
Pumpenablauf: 19,5 / 10,0 m

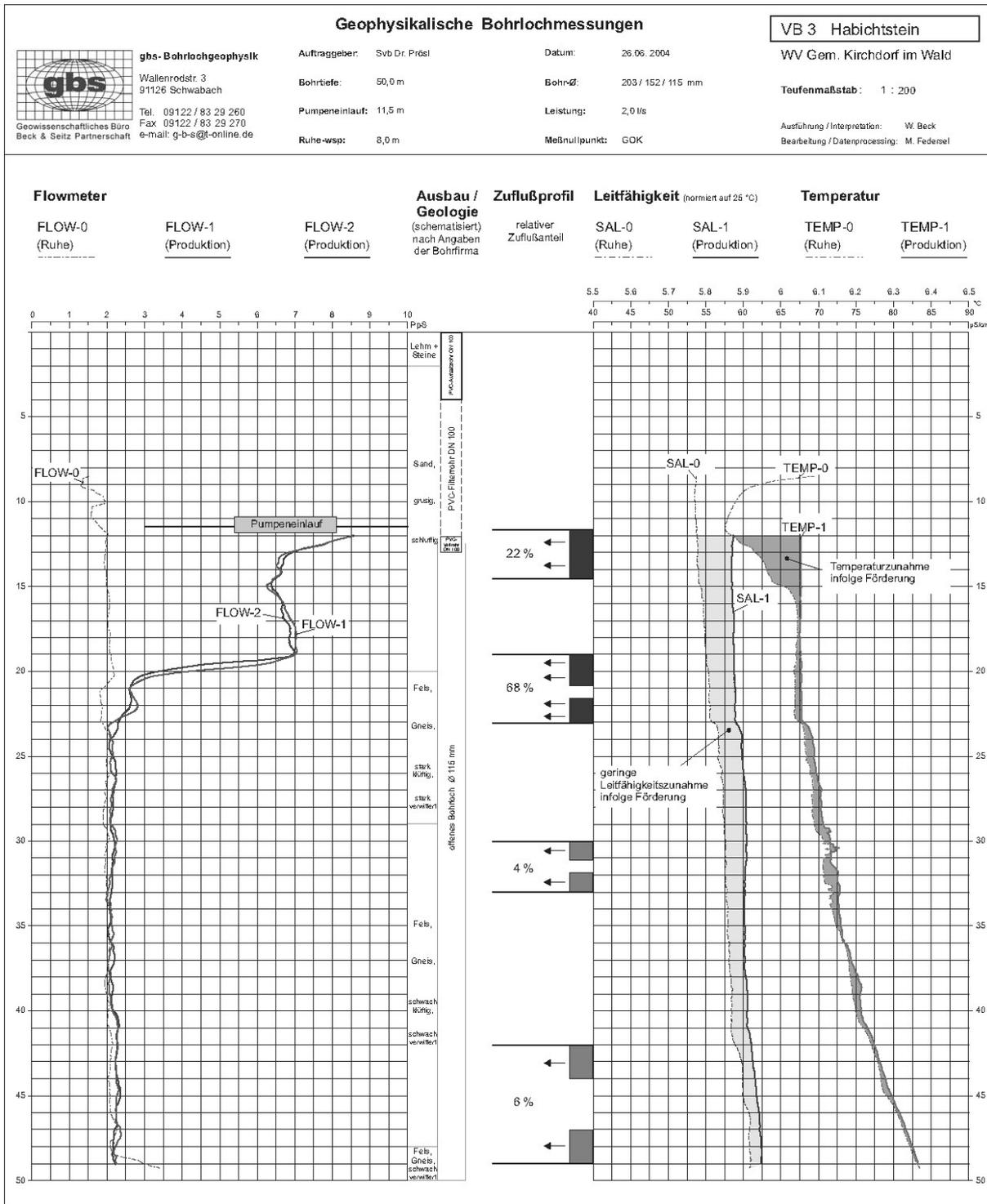
Leistung: 2,0 l/s

Bohrtiefe: 50,0 m

Ausführung / Interpretation: W. Beck
Bearbeitung / Datenprocessing: M. Federsal

Meßwippenpunkt: GOK







gbs-Bohrlochgeophysik
 Wallenrodstr. 3
 91126 Schwabach
 Tel. 09122 / 83 29 260
 Fax 09122 / 83 29 270
 e-mail: g-b-s@t-online.de

Geophysikalische Bohrlochmessungen

Auftraggeber: Svb Dr. Prösl
Datum: 26.06.2004
Bohrtiefe: 50,0 m
Bohr-Ø: 203 / 152 / 115 mm
Pumpeneinlauf: 11,5 m
Leistung: 2,0 l/s
Ruhe-wsp: 5,0 m
Meßnullpunkt: GOK

VB 4 Habichtstein

WV Gem. Kirchdorf im Wald

Teufenmaßstab: 1 : 200

Ausführung / Interpretation: W. Beck
Bearbeitung / Datenprocessing: M. Federeel

Flowmeter

FLOW-0
(Ruhe)

FLOW-1
(Produktion)

FLOW-2
(Produktion)

Ausbau / Geologie

(schematisiert nach Angaben der Bohrfirma)

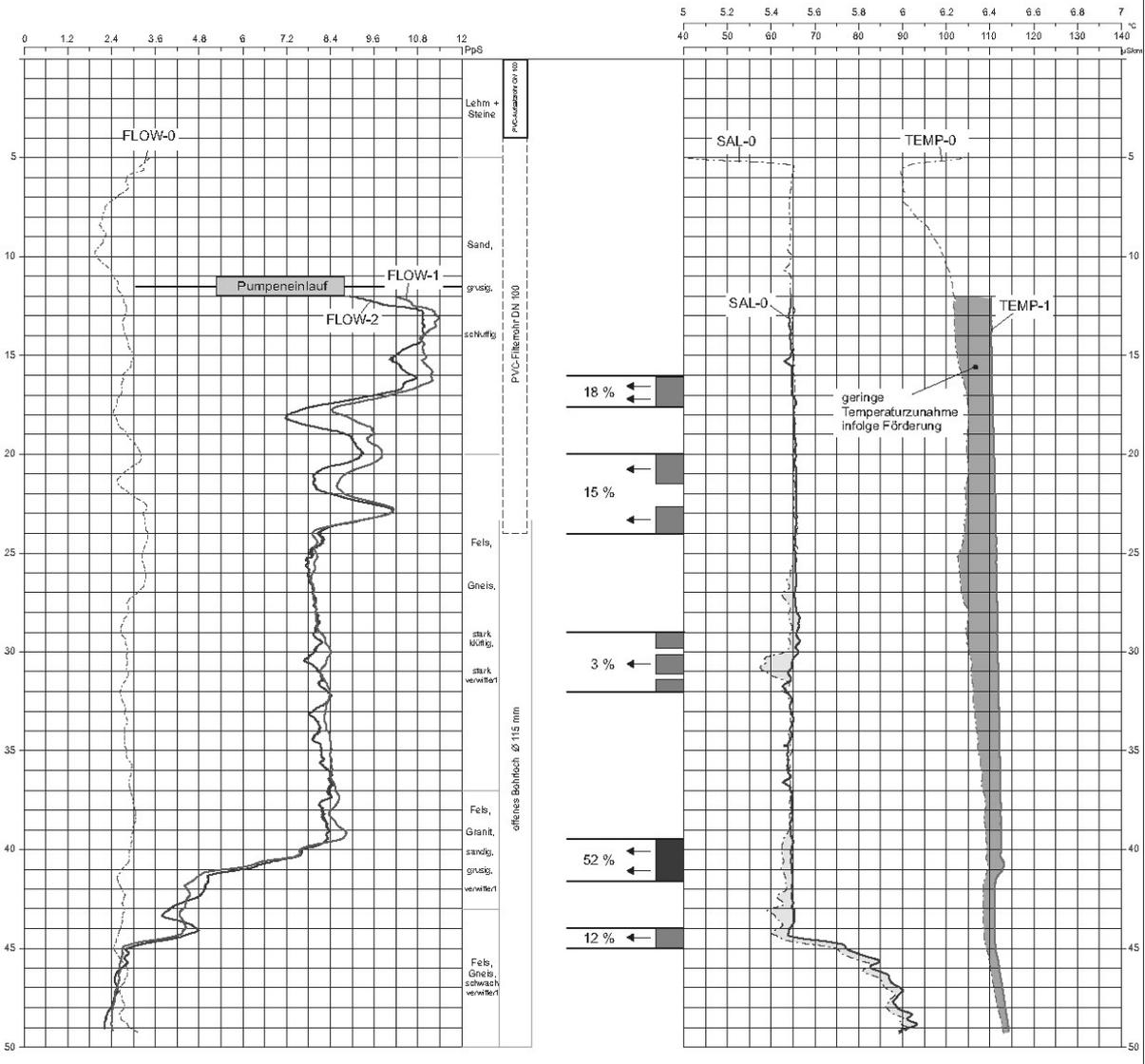
Zuflußprofil
relativer Zuflußanteil

Leitfähigkeit (normiert auf 25 °C)
SAL-0 (Ruhe) **SAL-1** (Produktion)

Temperatur

TEMP-0 (Ruhe)

TEMP-1 (Produktion)





gbs-Bohrlochgeophysik
 Wallenrodstr. 3
 91126 Schwabach
 Tel. 09122 / 83 29 260
 Fax 09122 / 83 29 270
 e-mail: g-b-s@t-online.de

Geophysikalische Bohrlochmessungen

Auftraggeber: Svb Dr. Prösel
Datum: 25.06.2004
Bohrtiefe: 50,0 m
Bohr-Ø: 203 / 152 / 115 mm
Pumpeneinlauf: 14,0 m
Leistung: 2,0 l/s
Ruhe-wsp: 8,3 m
Meßnullpunkt: GOK

VB 5 Habichtstein
WV Gem. Kirchdorf im Wald
Teufenmaßstab: 1 : 200
Ausführung / Interpretation: W. Beck
Bearbeitung / Datenprocessing: M. Federael

Flowmeter

FLOW-0 (Ruhe)
FLOW-1 (Produktion)
FLOW-2 (Produktion)

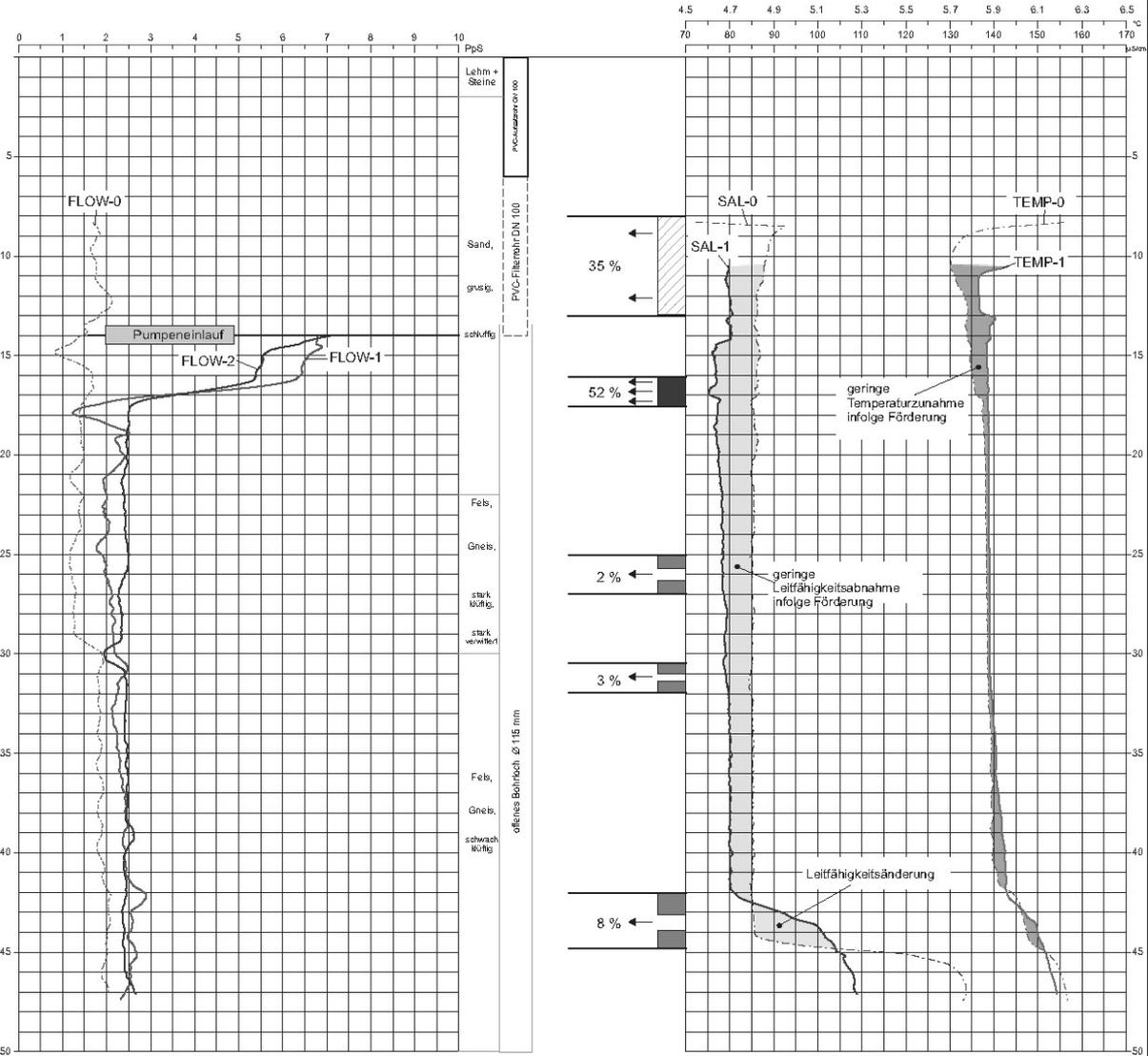
Ausbau / Geologie
 (schematisiert nach Angaben der Bohrfirma)

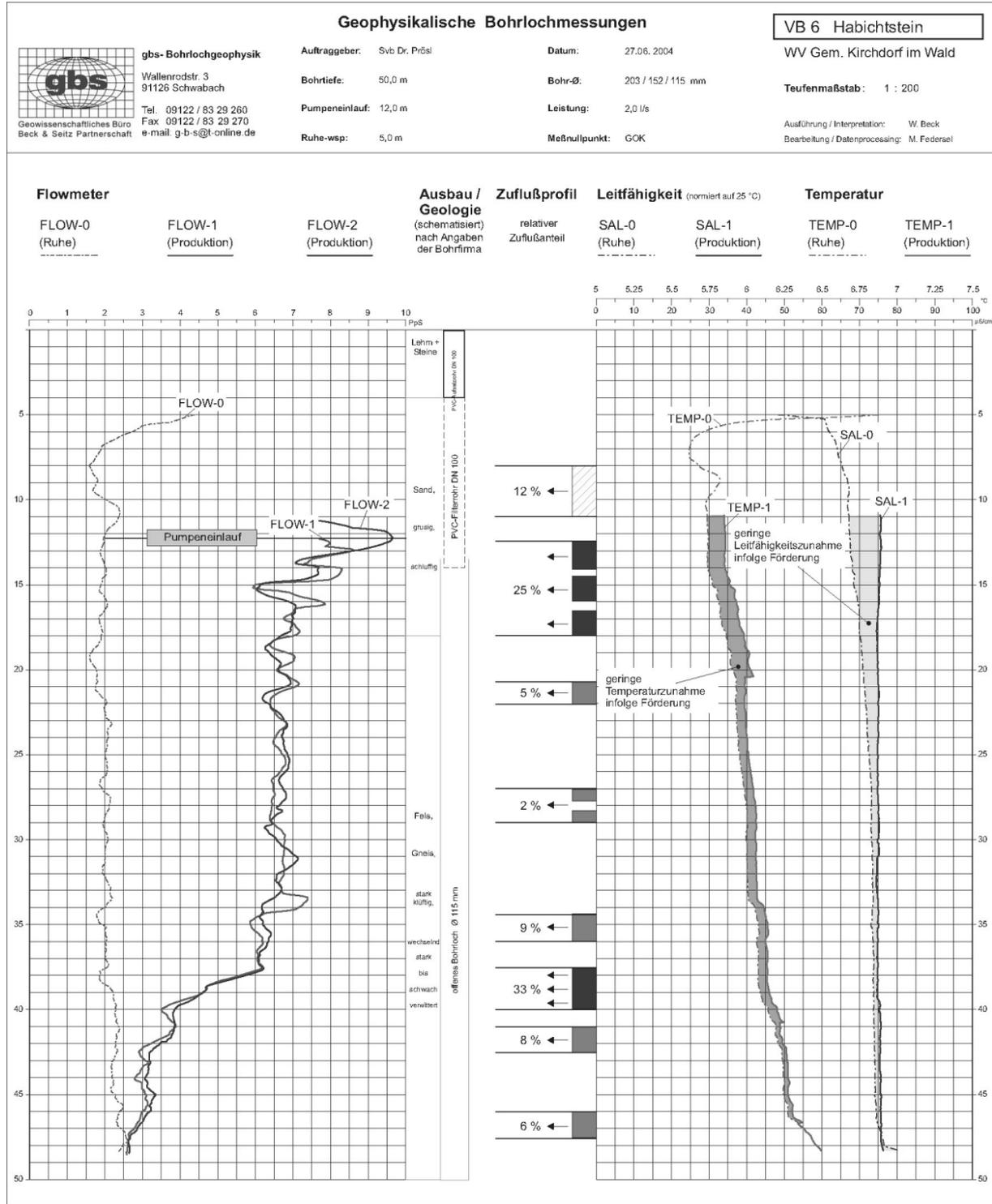
Zuflußprofil
 relativer Zuflußanteil

Leitfähigkeit (normiert auf 25 °C)
SAL-0 (Ruhe)
SAL-1 (Produktion)

Temperatur

TEMP-0 (Ruhe)
TEMP-1 (Produktion)





Appendix E – Geophysical logs

In the following the geophysical logs examined in sections 4.1.1.2 and 4.1.1.3 will be displayed. The logs include survey stations

Böbrach B 1

Neusohl VB 1

Neusohl VB 2

Schweinhütt VB 4

Wiesenfelden B 1

Bayerisch Eisenstein

Kirchdorf VB 1

Kirchdorf VB 3

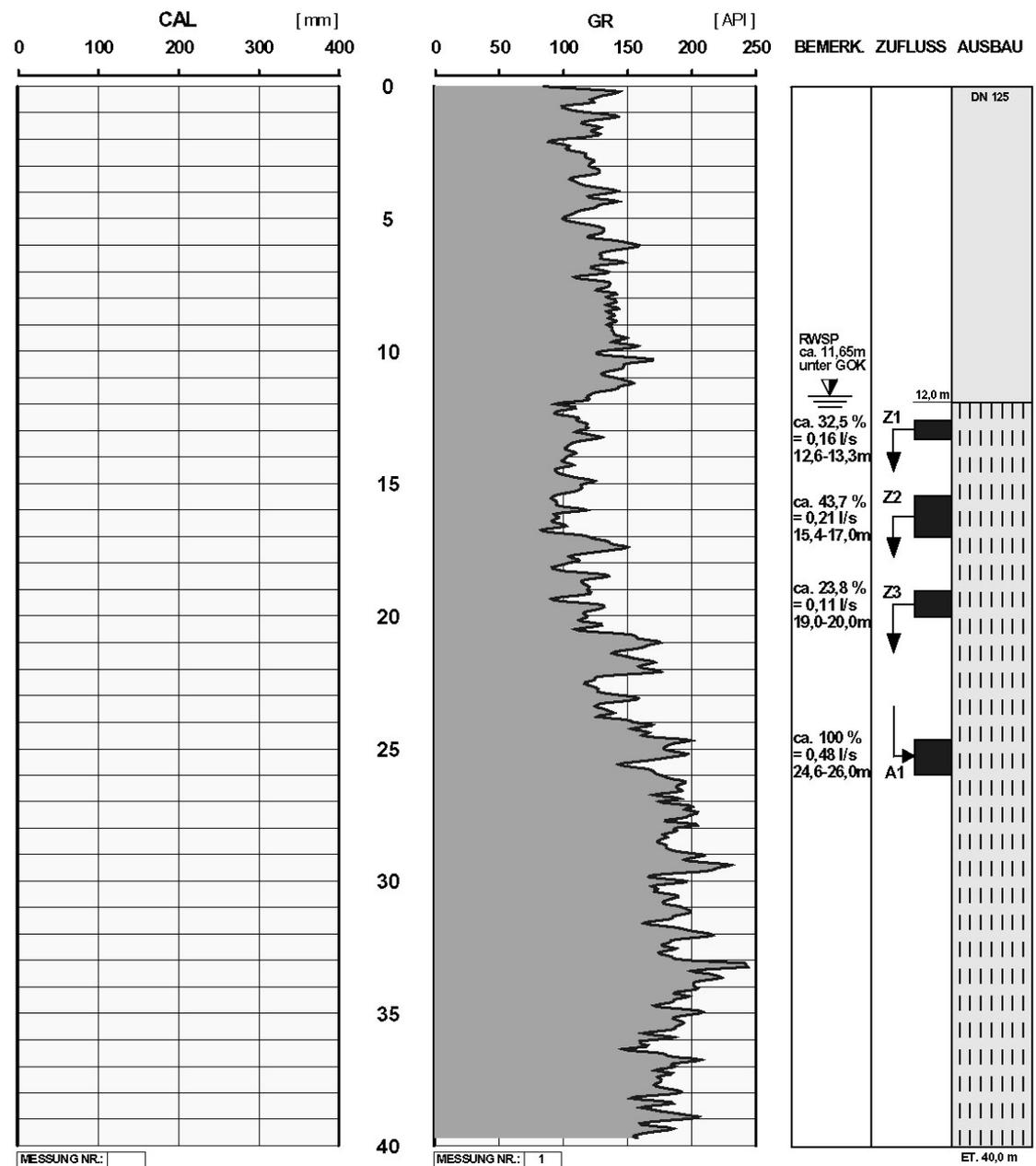
Kirchdorf VB 4

Kirchdorf VB 5

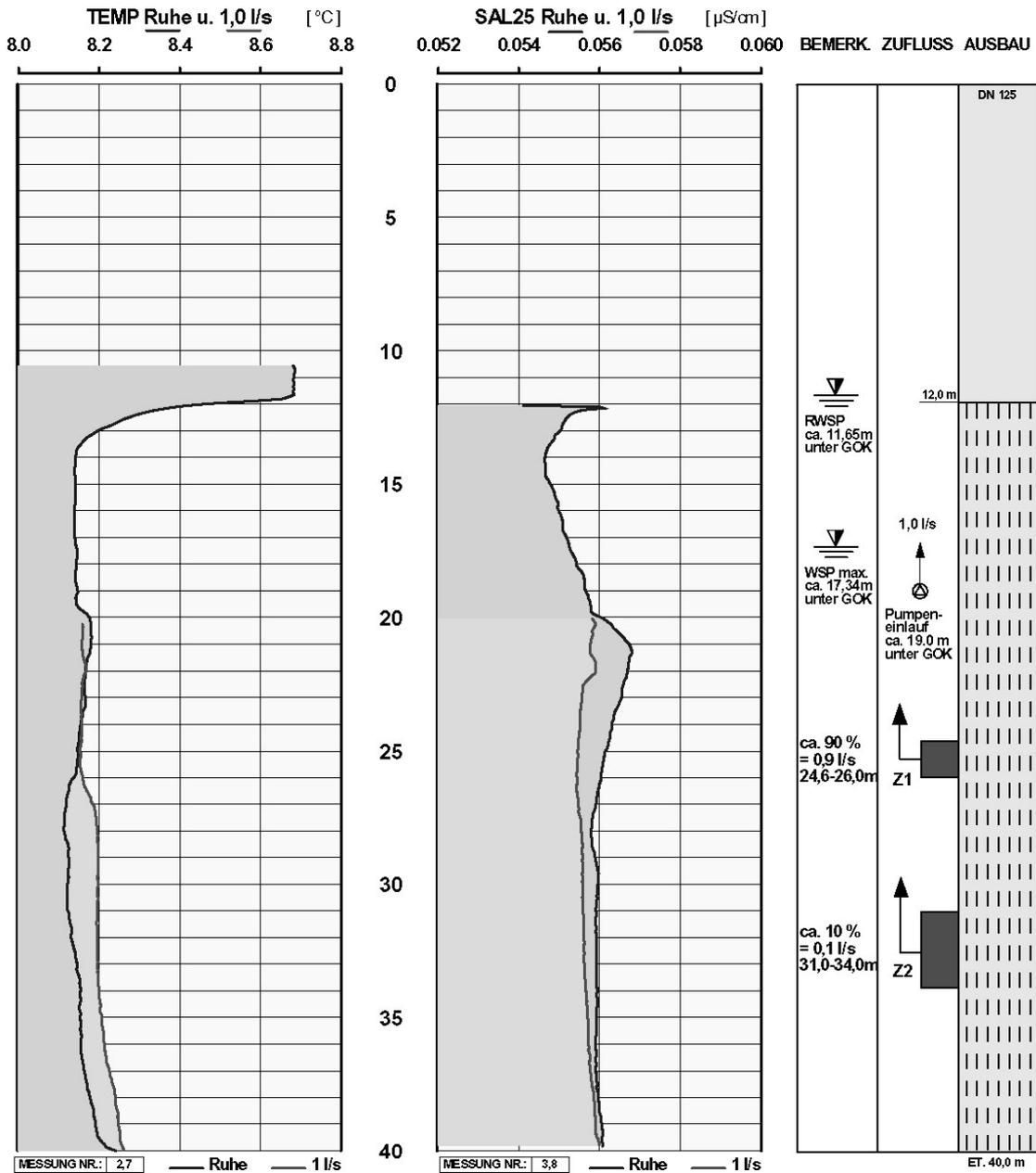
Kirchdorf VB 6

The logs were provided by German Geo Services and Fontus Logging Services.

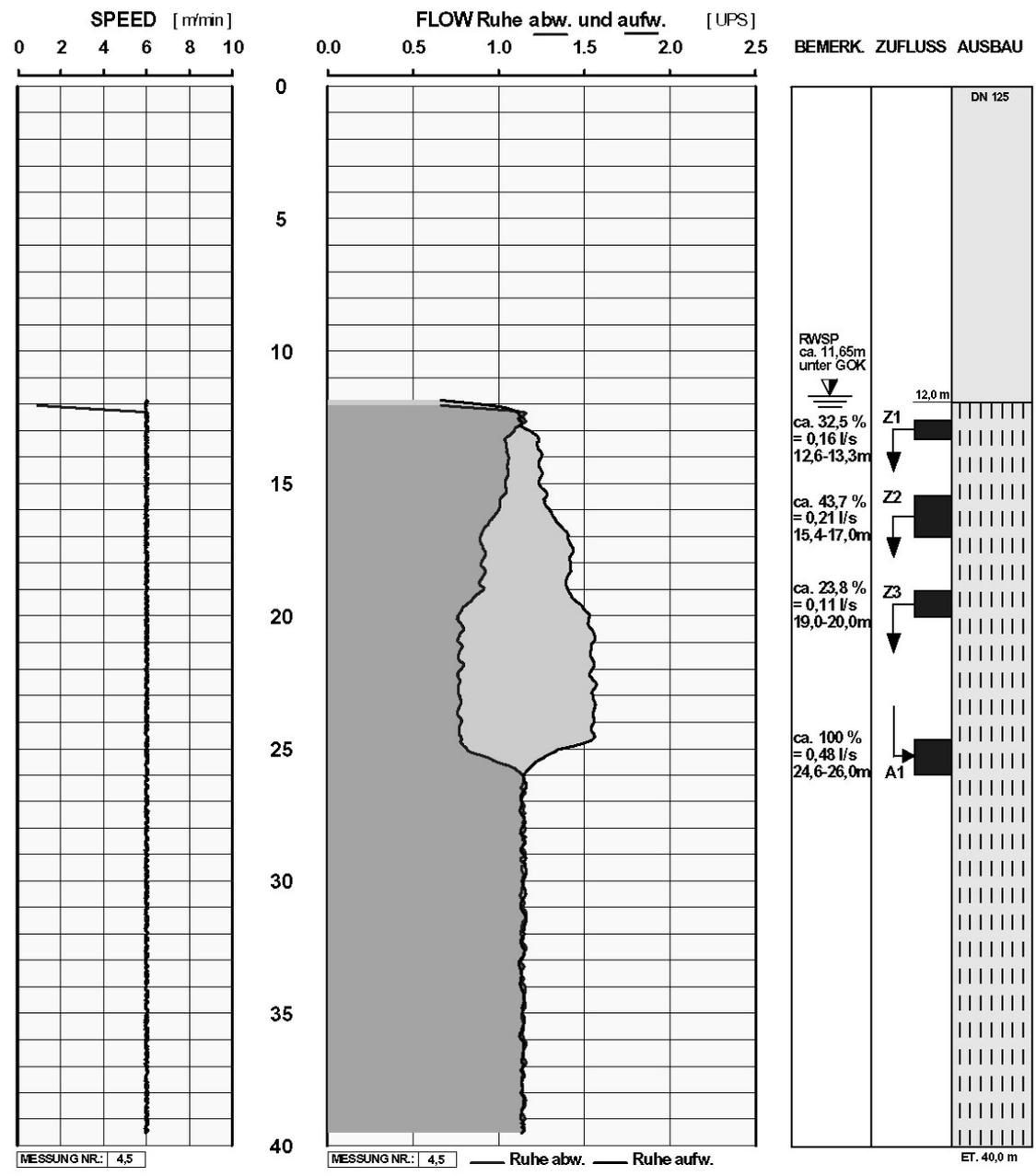
GERMAN GEO SERVICES <small>DANNBERGER WEG 12 91093 NIEDERLINDACH TEL. 09135-722542</small> BOHRLOCHVERMESSUNG		Gamma Ray Log (GR)	
AUFTRAGGEBER : <u>TAFELMEIER Bohr GmbH</u>	BOHRUNG-NR. : <u>B 1</u>		
PROJEKT : <u>WV Böbrach</u>	DATUM : <u>04.10.2004</u>		
ORT : <u>Böbrach</u>	MESSAUFTRAG : <u>B04100401</u>		
BUNDESLAND : <u>Bayern</u>	MESSWAGEN : <u>N-PR-787</u>		



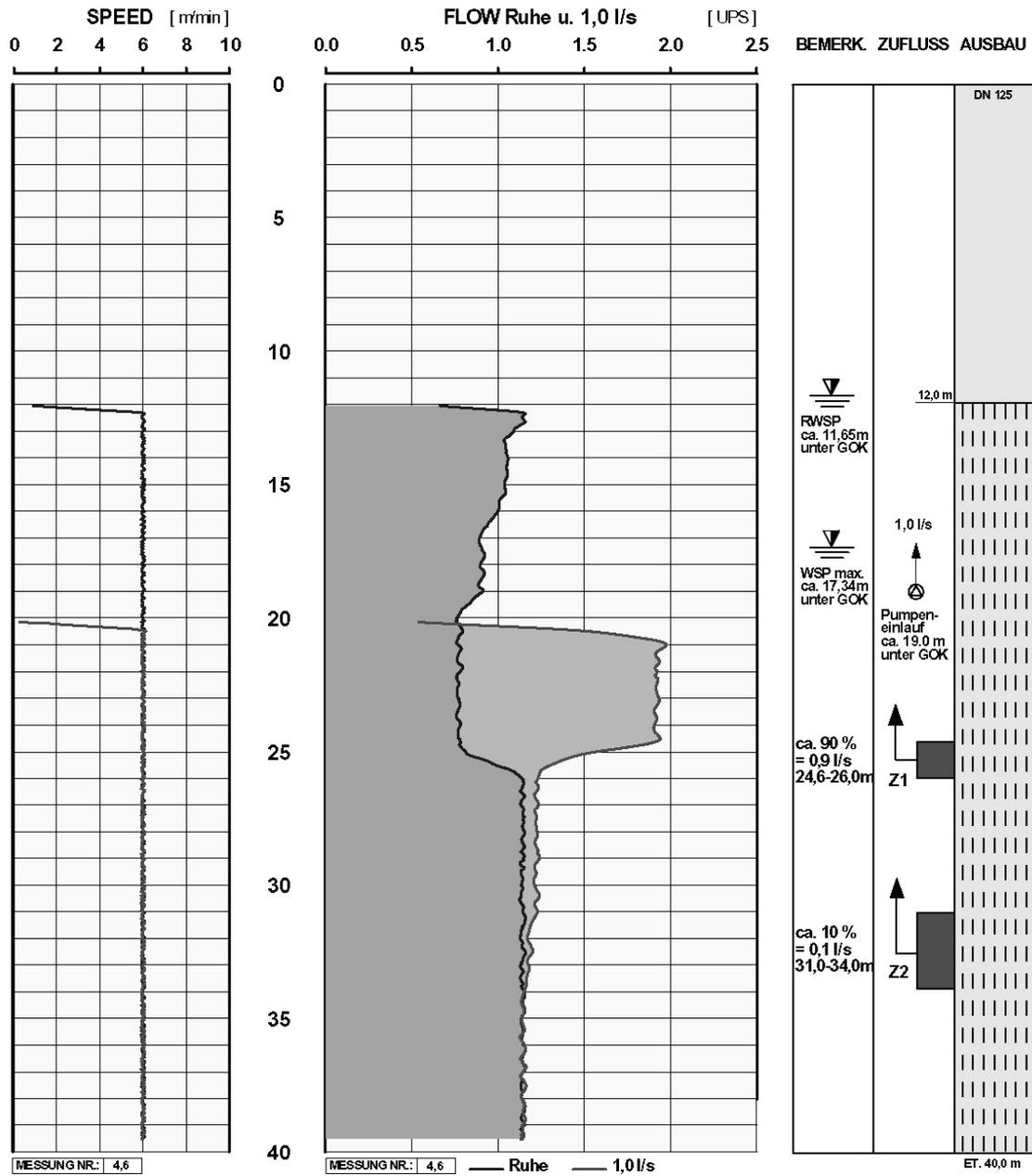
GERMAN GEO SERVICES DANNBERGER WEG 12 91093 NIEDERLINDACH TEL. 09135722542 BOHRLOCHVERMESSUNG		Temperatur Log (TEMP) Salinometer Log (SAL) Ruhe und Produktion 1,0 l/s	
AUFTRAGGEBER :	TAFELMEIER Bohr GmbH	BOHRUNG-NR. :	B 1
PROJEKT :	WV Böbrach	DATUM :	04.10.2004
ORT :	Böbrach	MESSAUFTRAG :	B04100401
BUNDESLAND :	Bayern	MESSWAGEN :	N-PR-787



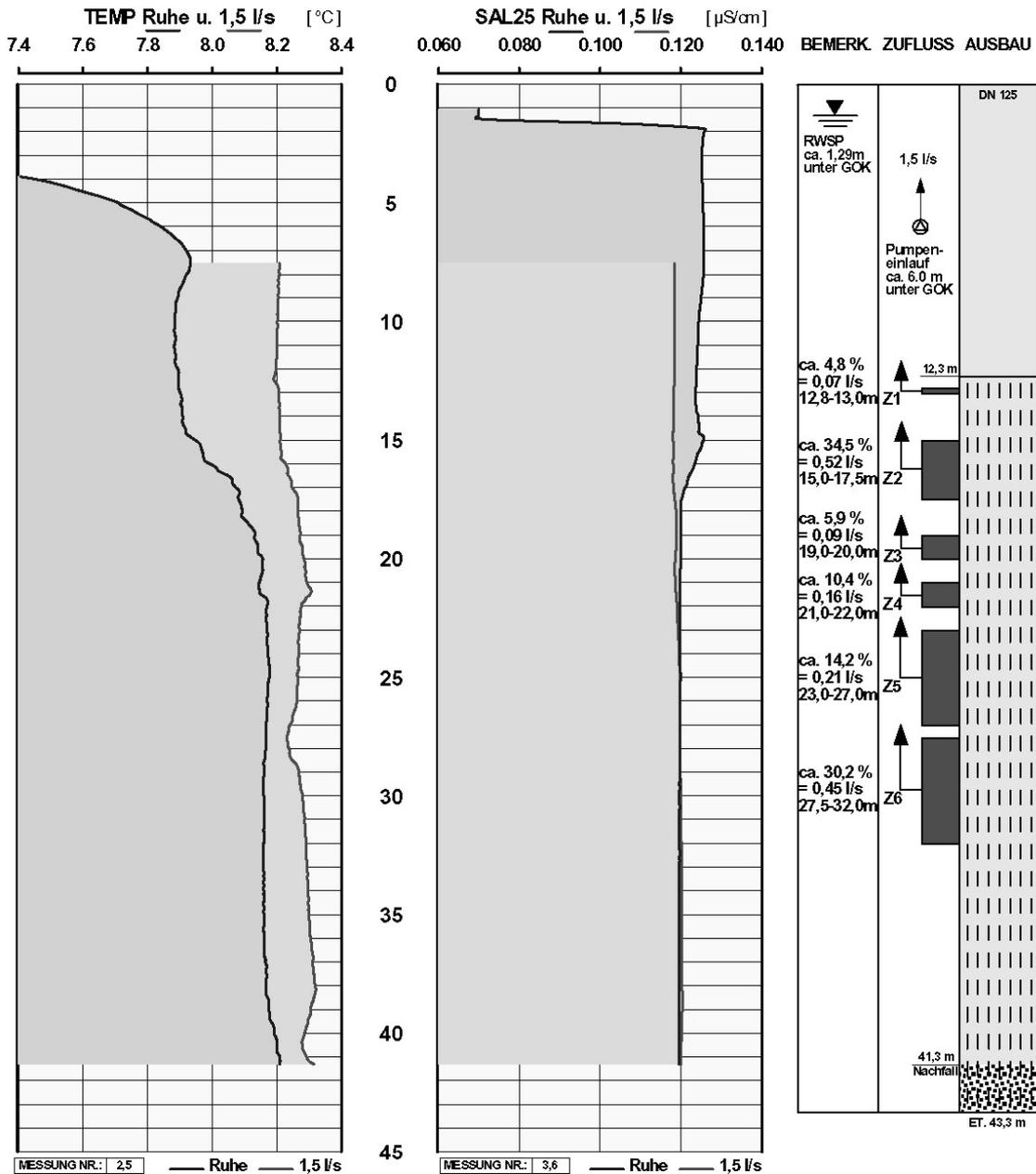
GERMAN GEO SERVICES <small>DANNBERGER WEG 12 91093 NIEDERLINDACH TEL. 09135-722542</small> BOHRLOCHVERMESSUNG	Flowmeter Log (FLOW) <i>Ruhezustand, Messrichtungen ab- und aufwärts</i>
AUFTRAGGEBER : <u>TAFELMEIER Bohr GmbH</u>	BOHRUNG-NR. : <u>B 1</u>
PROJEKT : <u>WV Böbrach</u>	DATUM : <u>04.10.2004</u>
ORT : <u>Böbrach</u>	MESSAUFTRAG : <u>B04100401</u>
BUNDESLAND : <u>Bayern</u>	MESSWAGEN : <u>N-PR-787</u>



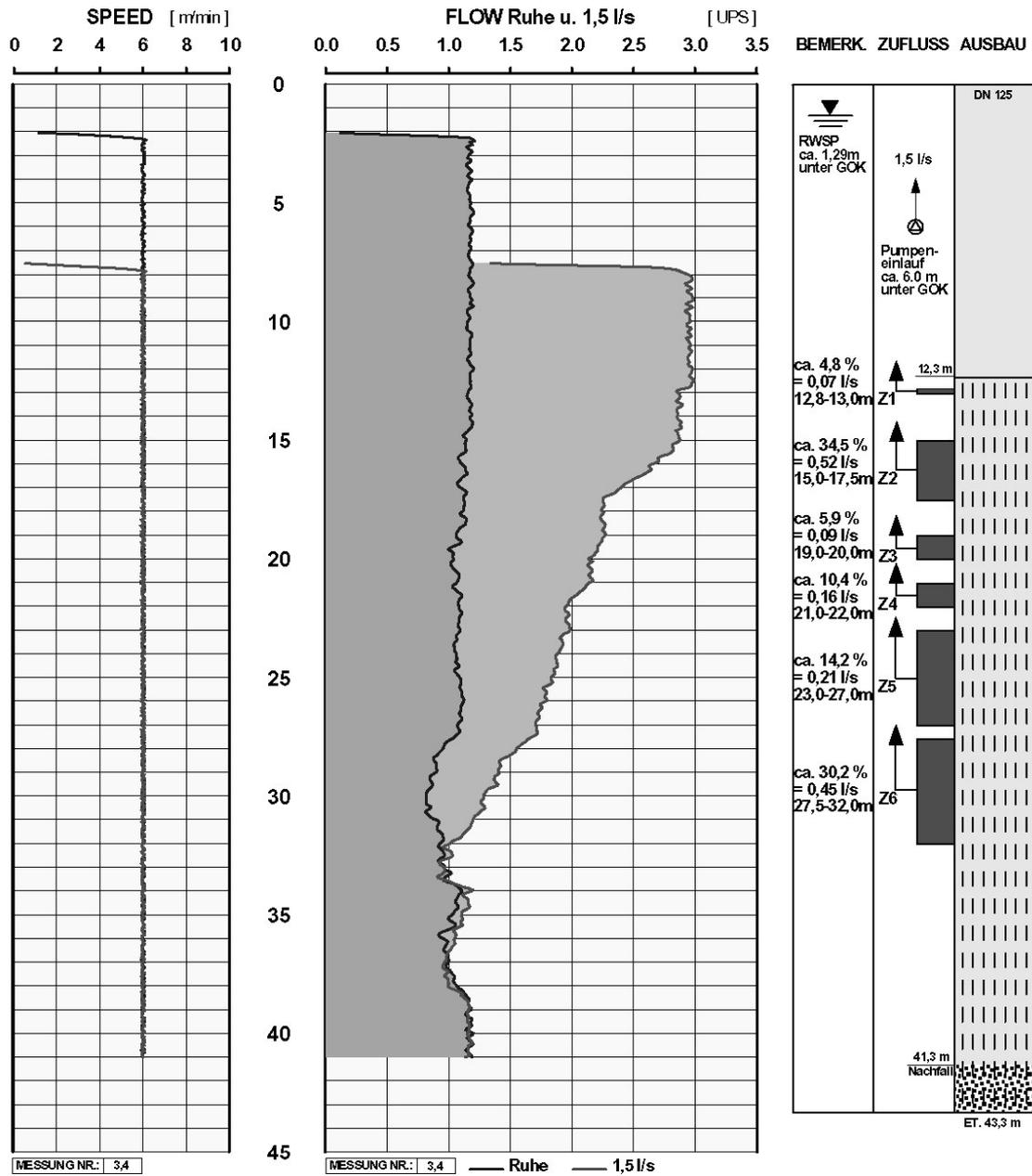
GERMAN GEO SERVICES DANNBERGER WEG 12 91093 NIEDERLINDACH TEL. 09135-722542 BOHRLOCHVERMESSUNG	Flowmeter Log (FLOW) Ruhe und Produktion 1,0 l/s
AUFTRAGGEBER : <u>TAFELMEIER Bohr GmbH</u>	BOHRUNG-NR. : <u>B 1</u>
PROJEKT : <u>WV Böbrach</u>	DATUM : <u>04.10.2004</u>
ORT : <u>Böbrach</u>	MESSAUFTRAG : <u>B04100401</u>
BUNDESLAND : <u>Bayern</u>	MESSWAGEN : <u>N-PR-787</u>



GERMAN GEO SERVICES DANNBERGER WEG 12 91093 NIEDERLINDACH TEL. 09135722542 BOHRLOCHVERMESSUNG		Temperatur Log (TEMP) Salinometer Log (SAL) Ruhe und Produktion 1,5 l/s	
AUFTRAGGEBER :	TAFELMEIER Bohr GmbH	BOHRUNG-NR. :	VB 1
PROJEKT :	Stadtwerke Regen	DATUM :	19.12.2002
ORT :	Neusohl	MESSAUFTRAG :	B02121901
BUNDESLAND :	Bayern	MESSWAGEN :	N-PR-787

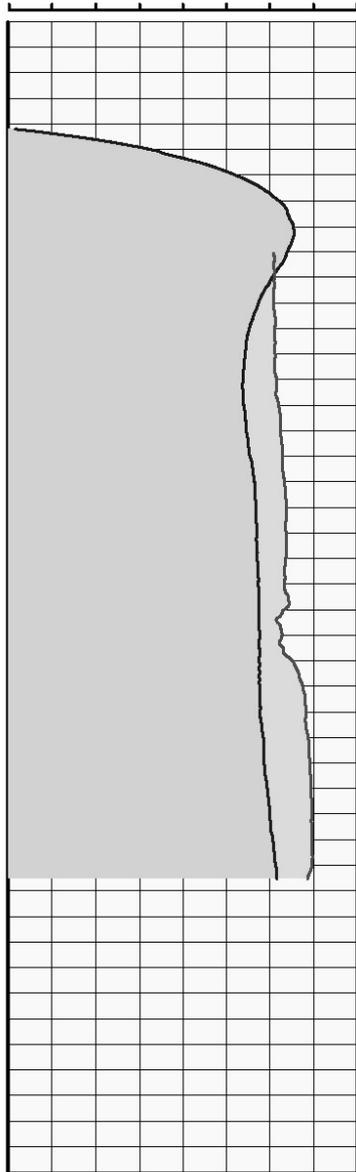


GERMAN GEO SERVICES DANNBERGER WEG 12 91093 NIEDERLINDACH TEL. 09135-722542 BOHRLOCHVERMESSUNG	Flowmeter Log (FLOW) <i>Ruhe und Produktion 1,5 l/s</i>
AUFTRAGGEBER : <u>TAFELMEIER Bohr GmbH</u>	BOHRUNG-NR. : <u>VB 1</u>
PROJEKT : <u>Stadtwerke Regen</u>	DATUM : <u>19.12.2002</u>
ORT : <u>Neusohl</u>	MESSAUFTRAG : <u>B02121901</u>
BUNDESLAND : <u>Bayern</u>	MESSWAGEN : <u>N-PR-787</u>



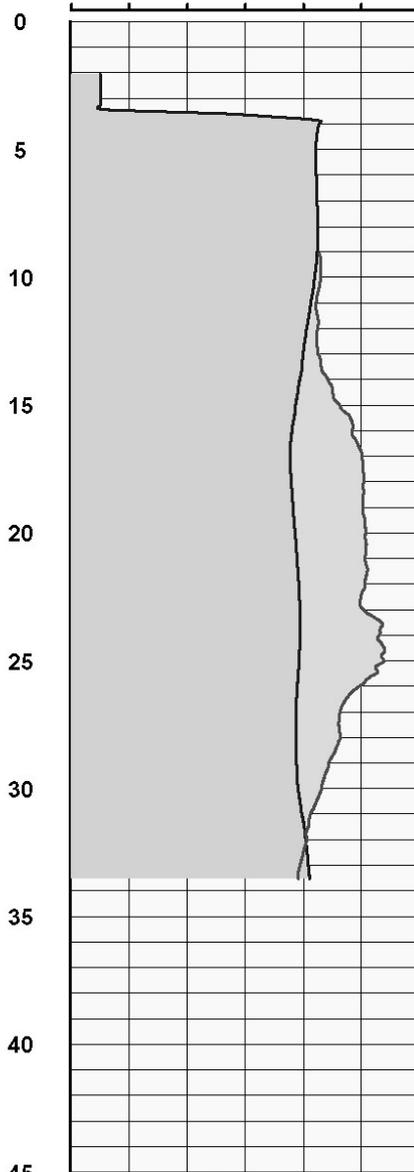
GERMAN GEO SERVICES DANNBERGER WEG 12 91093 NIEDERLINDACH TEL. 09135722542 BOHRLOCHVERMESSUNG		Temperatur Log (TEMP) Salinometer Log (SAL) Ruhe und Produktion 1,5 l/s	
AUFTRAGGEBER :	TAFELMEIER Bohr GmbH	BOHRUNG-NR. :	VB 2
PROJEKT :	Stadtwerke Regen	DATUM :	19.12.2002
ORT :	Neusohl	MESSAUFTRAG :	B02121902
BUNDESLAND :	Bayern	MESSWAGEN :	N-PR-787

TEMP Ruhe u. 1,5 l/s [°C]
7.4 7.6 7.8 8.0 8.2 8.4 8.6 8.8 9.0



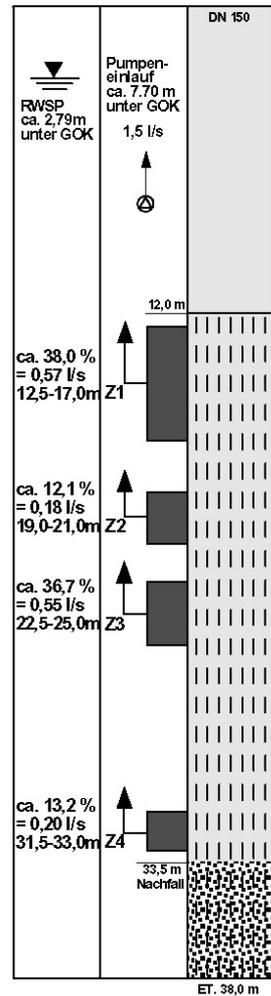
MESSUNG NR.: 25 Ruhe 1,5 l/s

SAL25 Ruhe u. 1,5 l/s [µS/cm]
0.060 0.080 0.100 0.120 0.140 0.160 0.180

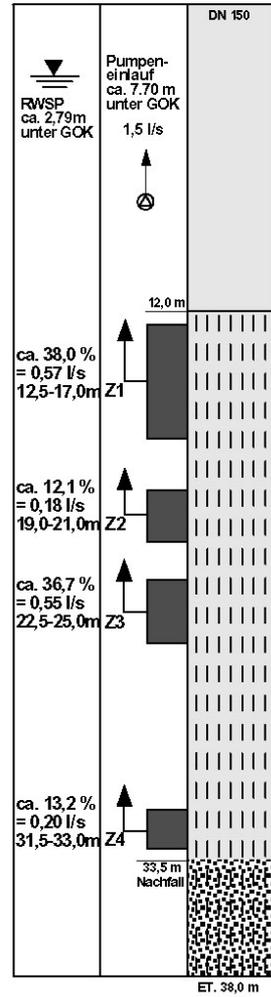
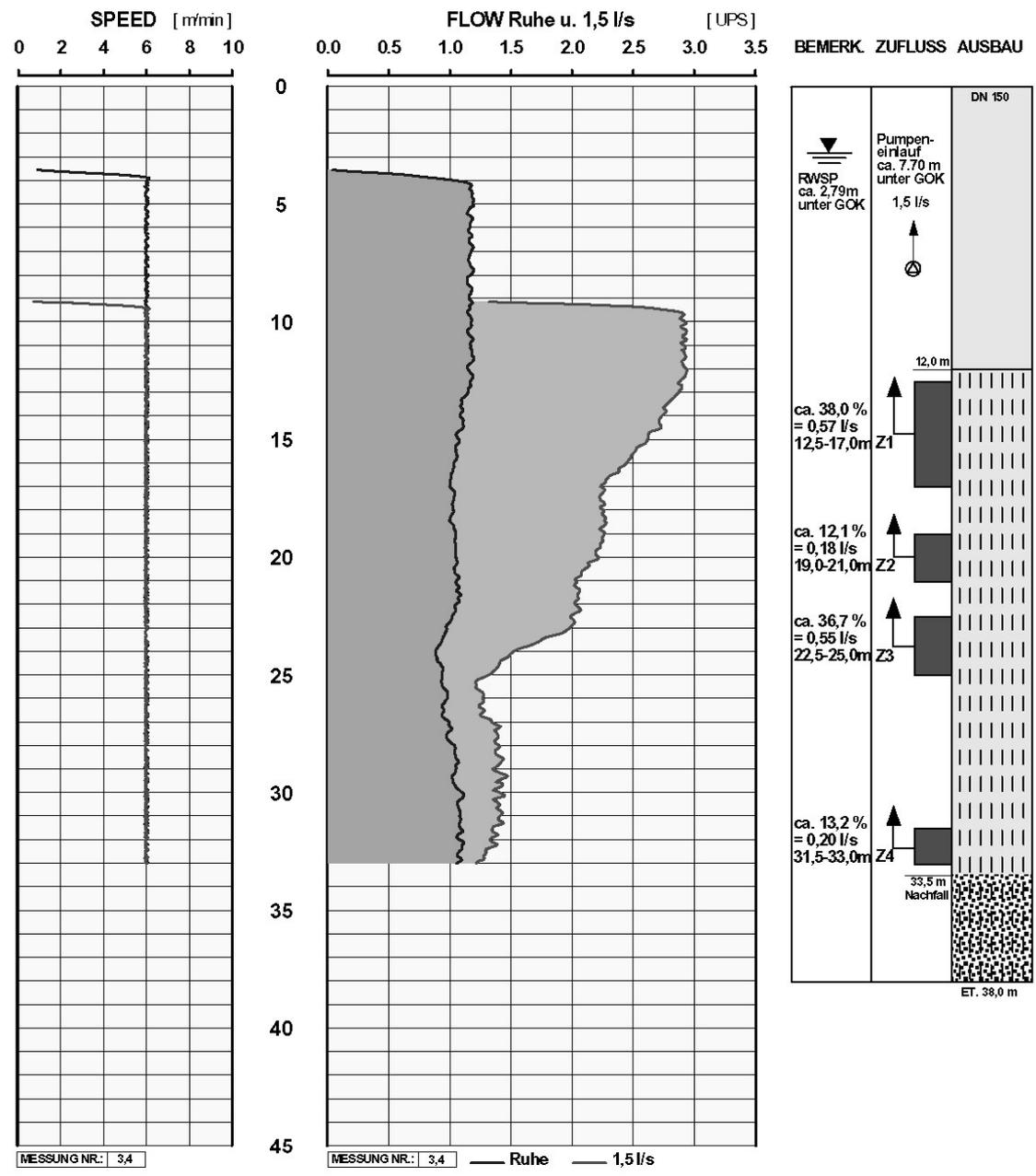


MESSUNG NR.: 3,6 Ruhe 1,5 l/s

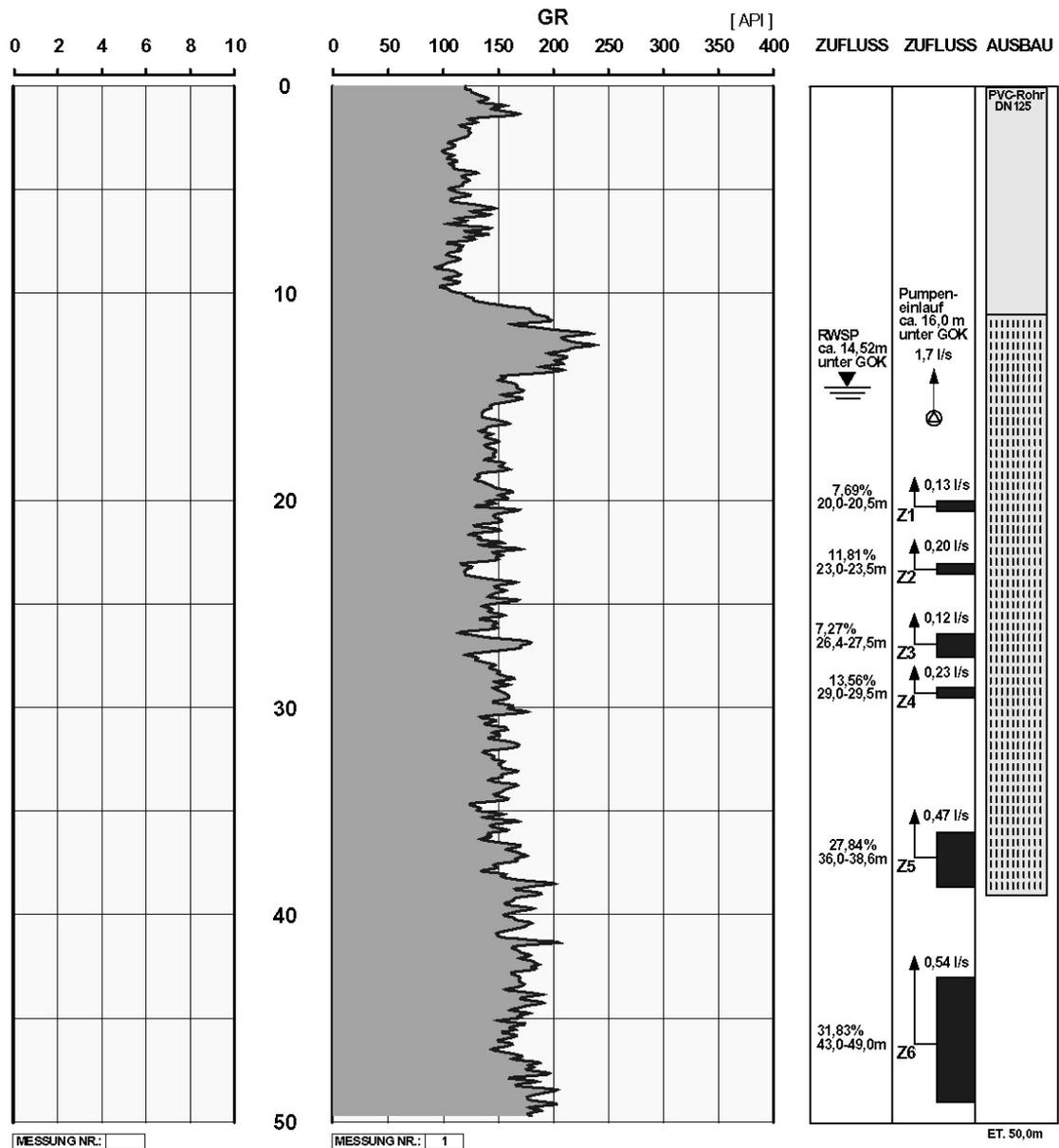
BERMERK. ZUFLUSS AUSBAU



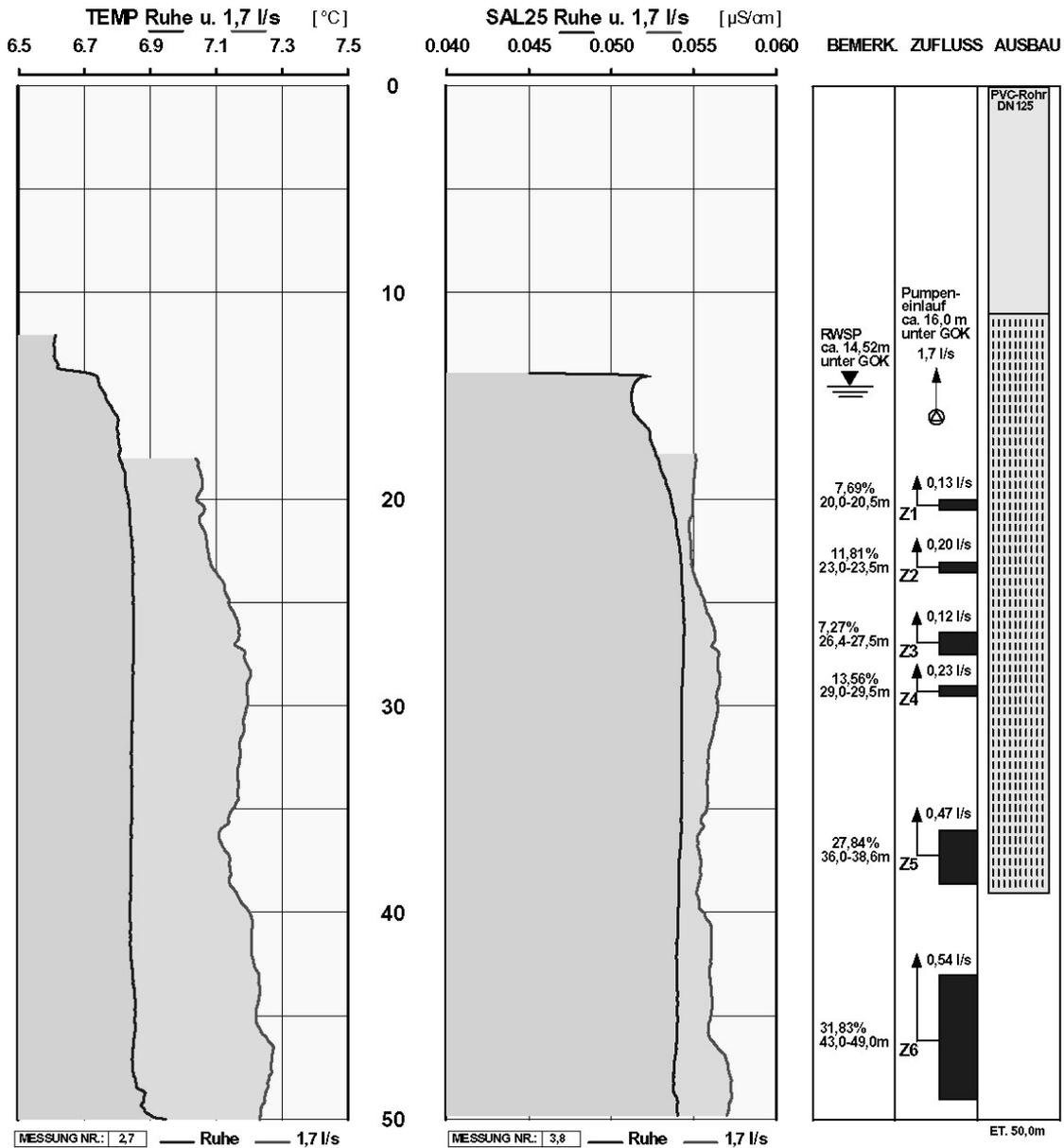
<p>GERMAN GEO SERVICES DANNBERGER WEG 12 91093 NIEDERLINDACH TEL. 09135-722542 BOHRLOCHVERMESSUNG</p>	<p>Flowmeter Log (FLOW) Ruhe und Produktion 1,5 l/s</p>
AUFTRAGGEBER : <u>TAFELMEIER Bohr GmbH</u>	BOHRUNG-NR. : <u>VB 2</u>
PROJEKT : <u>Stadtwerke Regen</u>	DATUM : <u>19.12.2002</u>
ORT : <u>Neusohl</u>	MESSAUFTRAG : <u>B02121902</u>
BUNDESLAND : <u>Bayern</u>	MESSWAGEN : <u>N-PR-787</u>



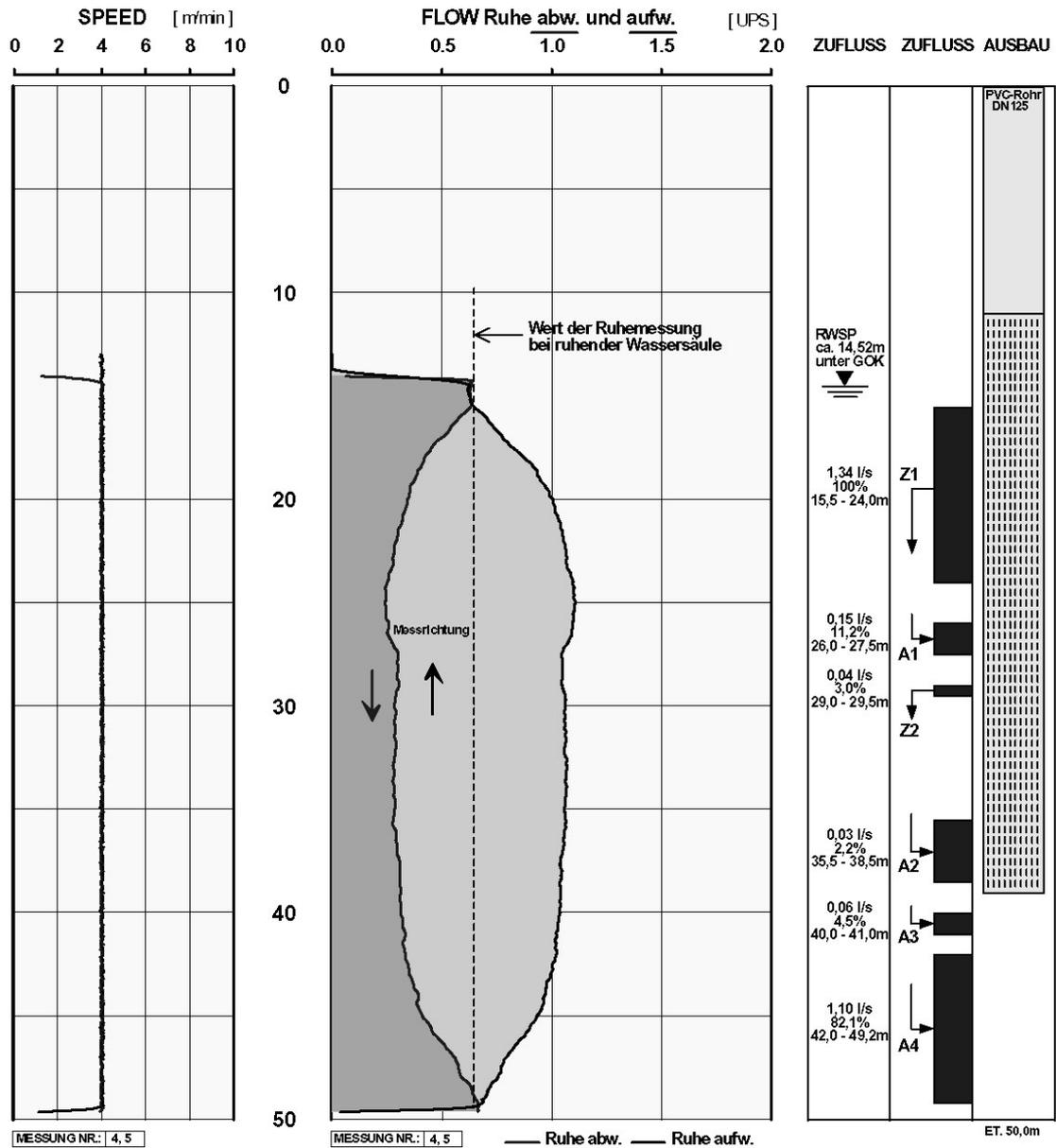
GERMAN GEO SERVICES DANNBERGER WEG 12 91093 NIEDERLINDACH TEL. 09135-722542 BOHRLOCHVERMESSUNG		Gamma Ray Log (GR)	
AUFTRAGGEBER :	Tafelmeier Tiefbrunnen-Bau GmbH	BOHRUNG-NR. :	VB 4
PROJEKT :	Satdtwerke Regen - WG Schweinhütt	DATUM :	09.11.2005
ORT :	Schweinhütt	MESSAUFTRAG :	B05110901
BUNDESLAND :	Bayern	MESSWAGEN :	N-PR-787



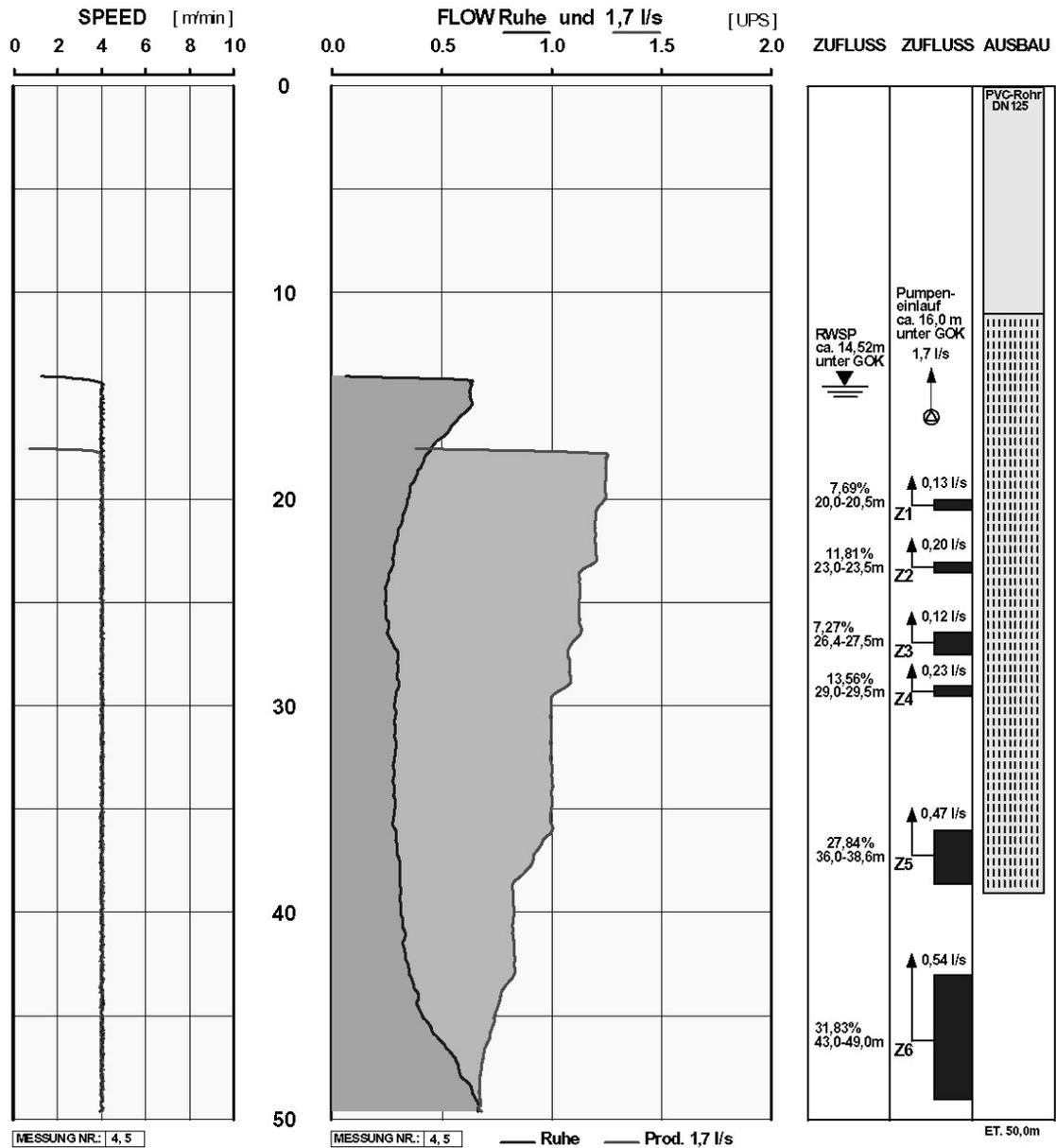
GERMAN GEO SERVICES DANNBERGER WEG 12 91093 NIEDERLINDACH TEL. 09135722542 BOHRLOCHVERMESSUNG		Temperatur Log (TEMP) Salinometer Log (SAL) Ruhe und Produktion 1,7 l/s	
AUFTRAGGEBER :	Tafelmeier Tiefbrunnen-Bau GmbH	BOHRUNG-NR. :	VB 4
PROJEKT :	Satdtwerke Regen - WG Schweinhütt	DATUM :	09.11.2005
ORT :	Schweinhütt	MESSAUFTRAG :	B05110901
BUNDESLAND :	Bayern	MESSWAGEN :	N-PR - 787



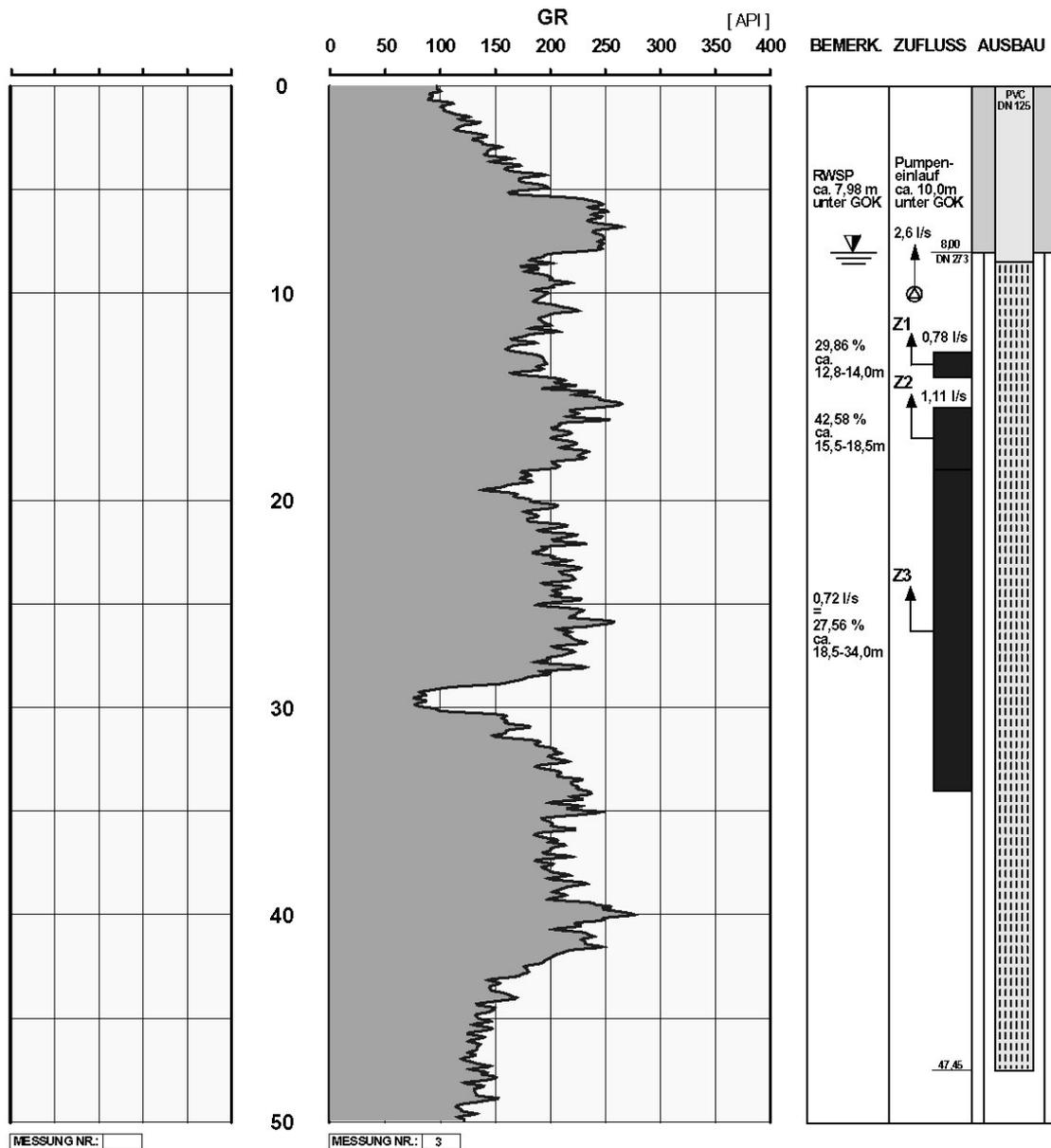
GERMAN GEO SERVICES <small>DANNBERGER WEG 12 91093 NIEDERLINDACH TEL. 09135-722542</small> BOHRLOCHVERMESSUNG	Flowmeter Log (FLOW) <i>Ruhezustand, Messrichtungen ab- und aufwärts</i>
AUFTRAGGEBER : <u>Tafelmeier Tiefbrunnen-Bau GmbH</u>	BOHRUNG-NR. : <u>VB 4</u>
PROJEKT : <u>Stadtwerke Regen - WG Schweinhütt</u>	DATUM : <u>09.11.2005</u>
ORT : <u>Schweinhütt</u>	MESSAUFTRAG : <u>B050110901</u>
BUNDESLAND : <u>Bayern</u>	MESSWAGEN : <u>N-PR-787</u>



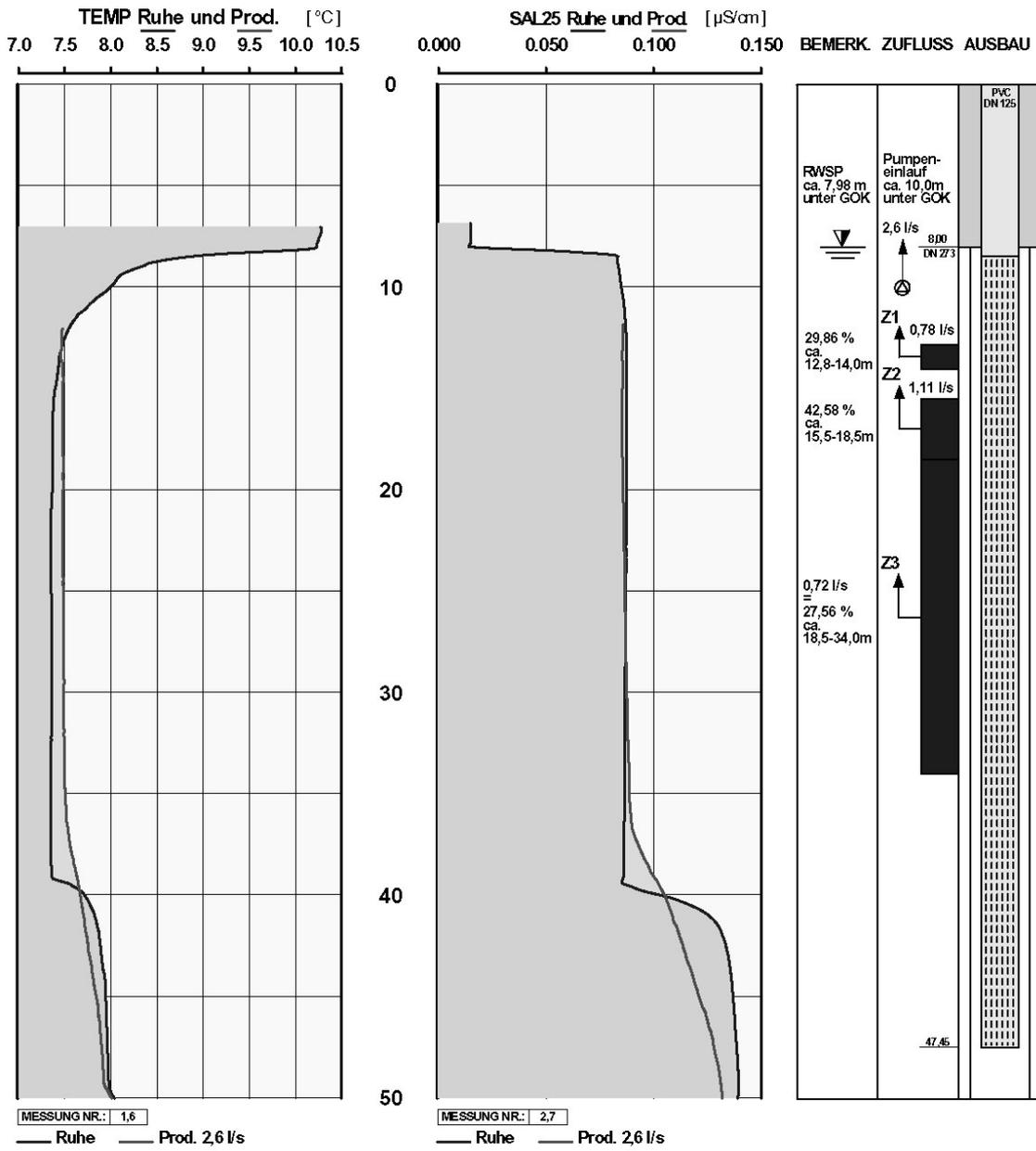
GERMAN GEO SERVICES DANNBERGER WEG 12 91093 NIEDERLINDACH TEL. 09135-722542 BOHRLOCHVERMESSUNG	Flowmeter Log (FLOW) <i>Ruhe und Produktion 1,7 l/s</i>
AUFTRAGGEBER : <u>Tafelmeier Tiefbrunnen-Bau GmbH</u>	BOHRUNG-NR. : <u>VB 4</u>
PROJEKT : <u>Stadtwerke Regen - WG Schweinhütt</u>	DATUM : <u>09.11.2005</u>
ORT : <u>Schweinhütt</u>	MESSAUFTRAG : <u>B050110901</u>
BUNDESLAND : <u>Bayern</u>	MESSWAGEN : <u>N-PR-787</u>



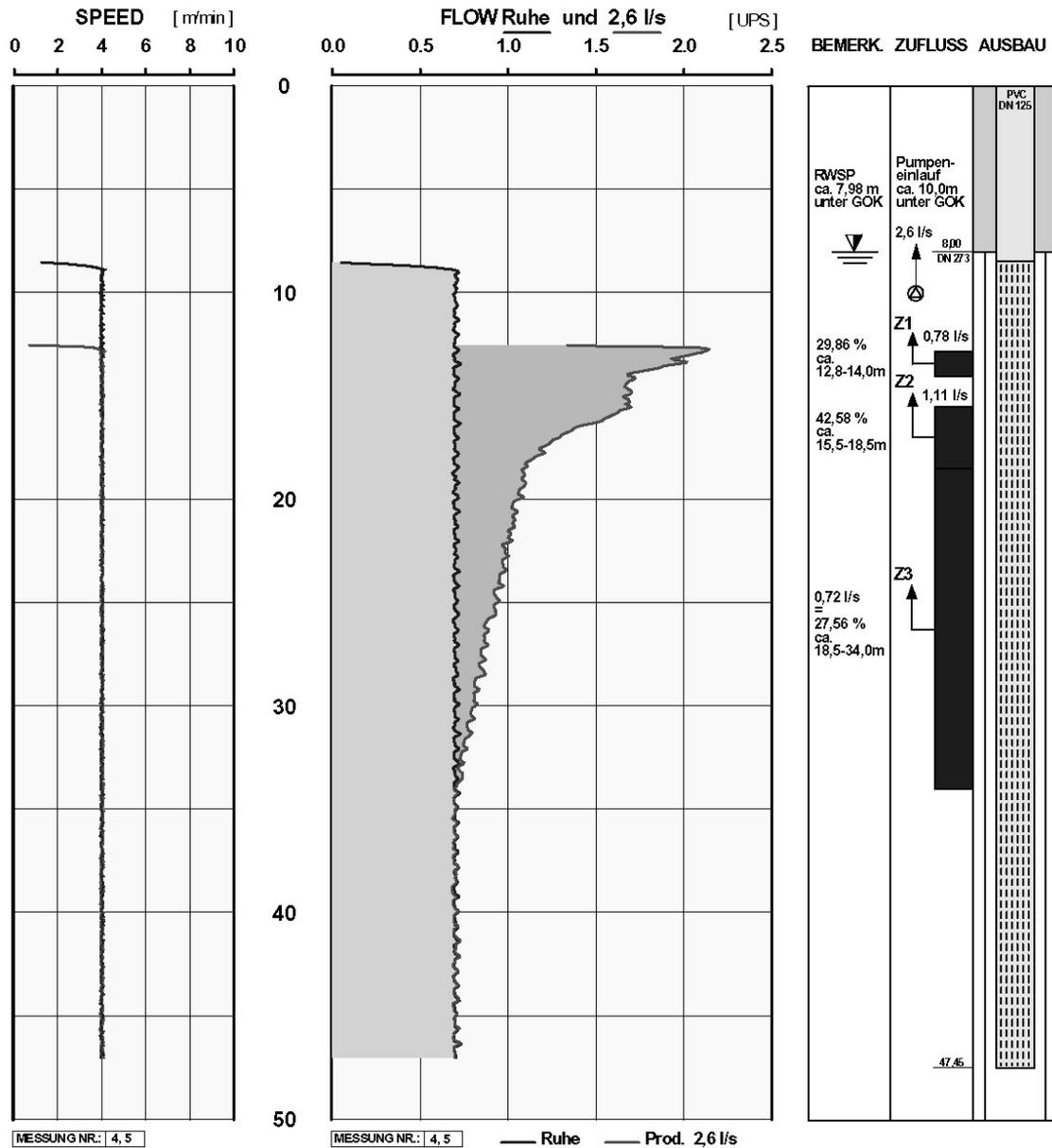
GERMAN GEO SERVICES <small>DANNBERGER WEG 12 91093 NIEDERLINDACH TEL. 09135-722542</small> BOHRLOCHVERMESSUNG		Gamma Ray Log (GR)	
AUFTRAGGEBER :	TAFELMEIER Tiefbrunnenbau GmbH	BOHRUNG-NR. :	B 1
PROJEKT :	Wasserversorgung	DATUM :	04.07.2005
ORT :	Wiesenfelden	MESSAUFTRAG :	B05070402
BUNDESLAND :	Bayern	MESSWAGEN :	ERH - PR - 300



GERMAN GEO SERVICES <small>DANNBERGER WEG 12 91093 NIEDERLINDACH TEL. 09135-722542</small> BOHRLOCHVERMESSUNG		Temperatur Log (TEMP) Salinometer Log (SAL25°C) <i>Ruhe und Produktion 2,6 l/s</i>	
AUFTRAGGEBER :	TAFELMEIER Tiefbrunnenbau GmbH	BOHRUNG-NR. :	B 1
PROJEKT :	Wasserversorgung	DATUM :	04.07.2005
ORT :	Wiesenfelden	MESSAUFTRAG :	B05070402
BUNDESLAND :	Bayern	MESSWAGEN :	ERH-PR-300



GERMAN GEO SERVICES DANNBERGER WEG 12 91093 NIEDERLINDACH TEL. 09135-722542 BOHRLOCHVERMESSUNG	Flowmeter Log (FLOW) <i>Ruhe und Produktion 2,6 l/s</i>
AUFTRAGGEBER : <u>TAFELMEIER Tiefbrunnenbau GmbH</u>	BOHRUNG-NR. : <u>B 1</u>
PROJEKT : <u>Wasserversorgung</u>	DATUM : <u>04.07.2005</u>
ORT : <u>Wiesenfelden</u>	MESSAUFTRAG : <u>B05070402</u>
BUNDESLAND : <u>Bayern</u>	MESSWAGEN : <u>ERH-PR-300</u>



Tiefbrunnen Grafhüttenbach

Bayerisch Eisenstein
 Teufenmaßstab: 1 : 250
 Ausführung / Interpretation: W. Beck
 Bearbeitung / Datenprocessing: M. Fedirsei

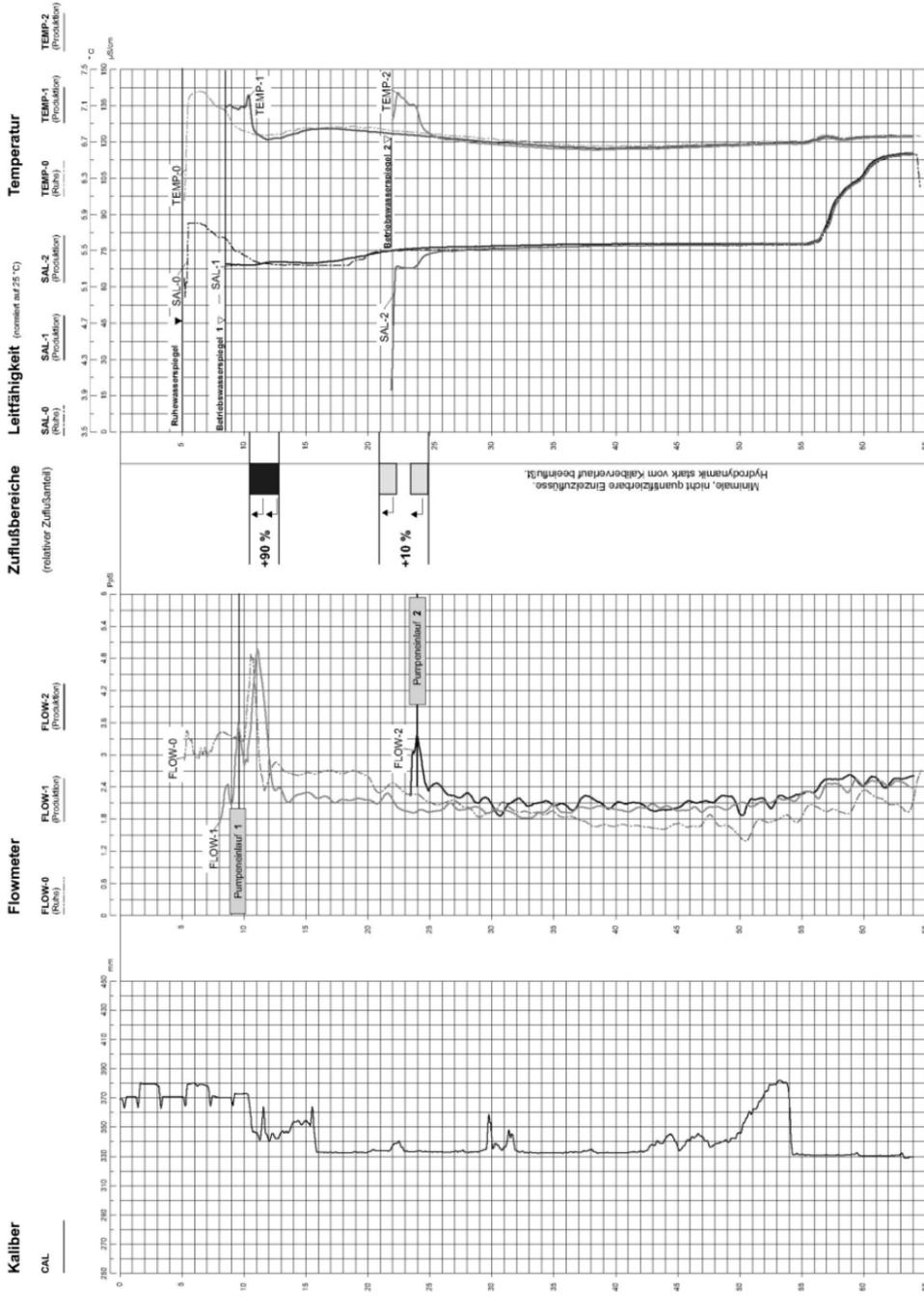
Geophysikalische Bohrlochmessungen

Datum: 05.12.2003
 Bohr-Ø: 311 mm
 Sperrroh-Ø: 368 / 521 mm
 Leistung: 1,5 l/s
 Meßflutpunkt: GOK

gbs-Bohrlochgeophysik
 Wallenrodstr. 3
 91126 Schwabach
 Tel. 09122 / 83 29 260
 Fax 09122 / 83 29 270
 Beck & Seitz Partnerschaft e-mail: g-b-s@t-online.de



Auftraggeber: E-M Bohr-GmbH
 Bohrtiefe: 65,00 m
 Sperrhohtiefe: 7,2 / 10,5 m
 Pumpeneinlauf: 10,40 / 24,0 m
 Ruhe-wsp: 5,0 m



Geophysikalische Bohrlochmessungen

VB 1 Habichtstein

WV Gem. Kirchdorf im Wald

Datum: 24.06.2004

Auftraggeber: Sib.Dr. Präbel

gbs-Bohrlochgeophysik



Wallenrodstr. 3
91126 Schwabach
Tel. 091/22/83 26 260
Fax 091/22/83 26 261
Beck & Senz Partner GmbH
E-Mail: gbs@gbs-geophysik.de

Bohr-Ø: 203/152/115 mm

Bohrtiefe: 50,0 m

Wallerodstr. 3
91126 Schwabach

Leistung: 2,0 l/s

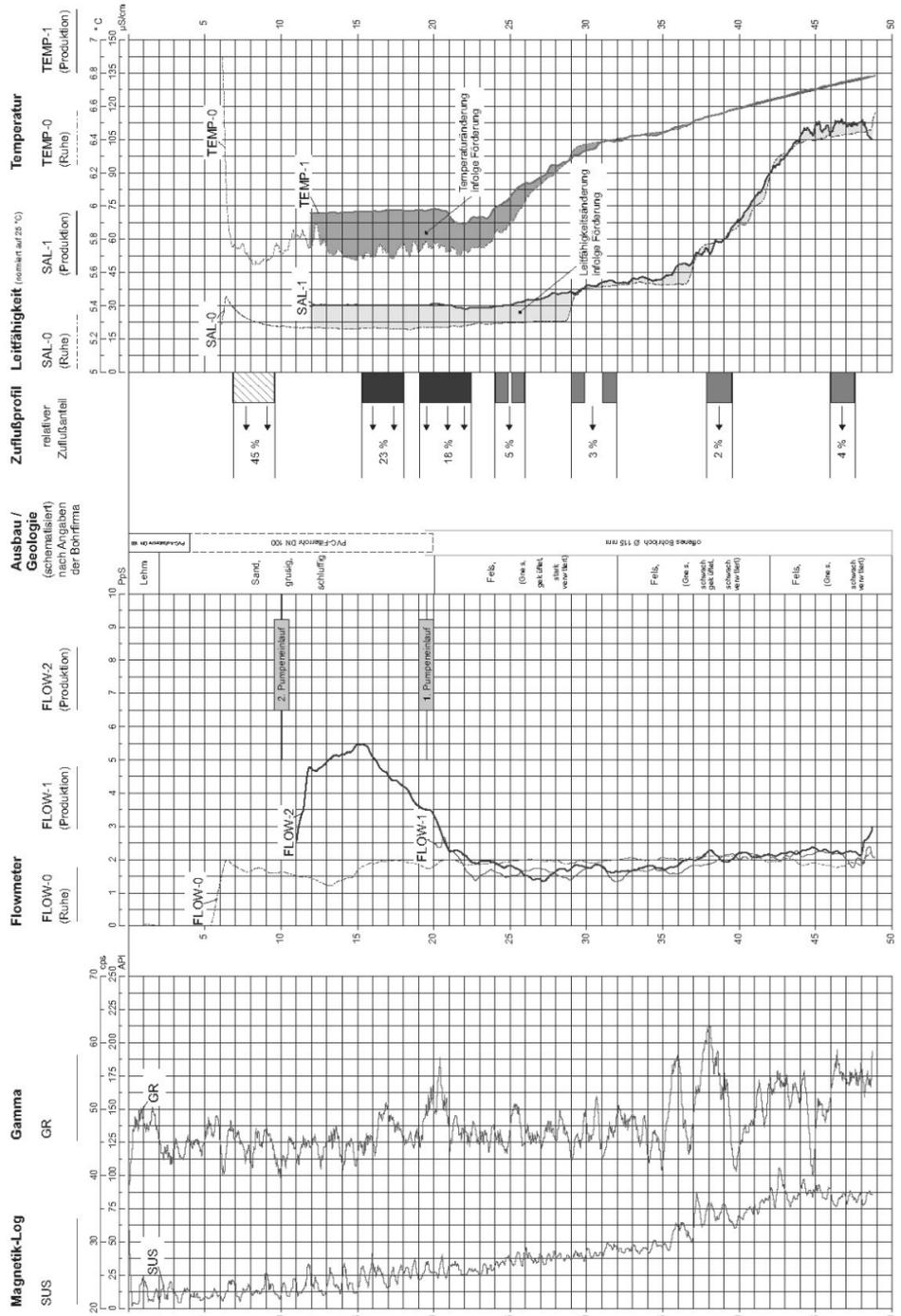
Pumpenhub: 19,5/10,0 m

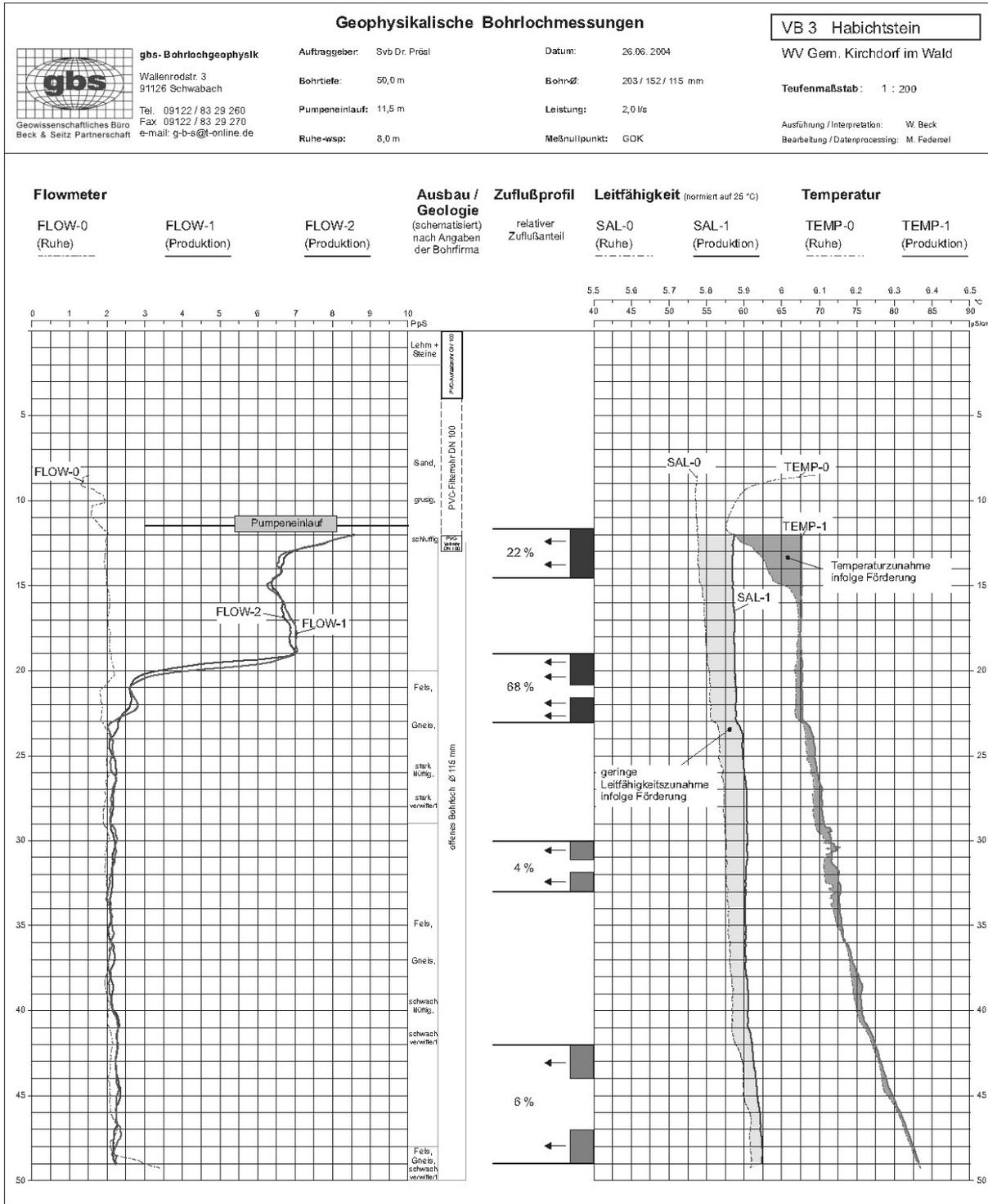
Bohr-Ø: 203/152/115 mm

Meßwippen: COK

Ruhe-wsp: 6,1 m

Bohr-Ø: 203/152/115 mm







gbs-Bohrlochgeophysik
 Wallenrodstr. 3
 91126 Schwabach
 Tel. 09122 / 83 29 260
 Fax 09122 / 83 29 270
 e-mail: g-b-s@t-online.de

Geophysikalische Bohrlochmessungen

Auftraggeber: Svb Dr. Prosl
Datum: 26.06.2004
Bohrtiefe: 50,0 m
Bohr-Ø: 203 / 152 / 115 mm
Pumpeneinlauf: 11,5 m
Leistung: 2,0 l/s
Ruhe-wsp: 5,0 m
Meßnullpunkt: GOK

VB 4 Habichtstein

WV Gem. Kirchdorf im Wald

Teufenmaßstab: 1 : 200

Ausführung / Interpretation: W. Beck
Bearbeitung / Datenprocessing: M. Federeel

Flowmeter

FLOW-0
(Ruhe)

FLOW-1
(Produktion)

FLOW-2
(Produktion)

Ausbau / Geologie

(schematisiert nach Angaben der Bohrfirma)

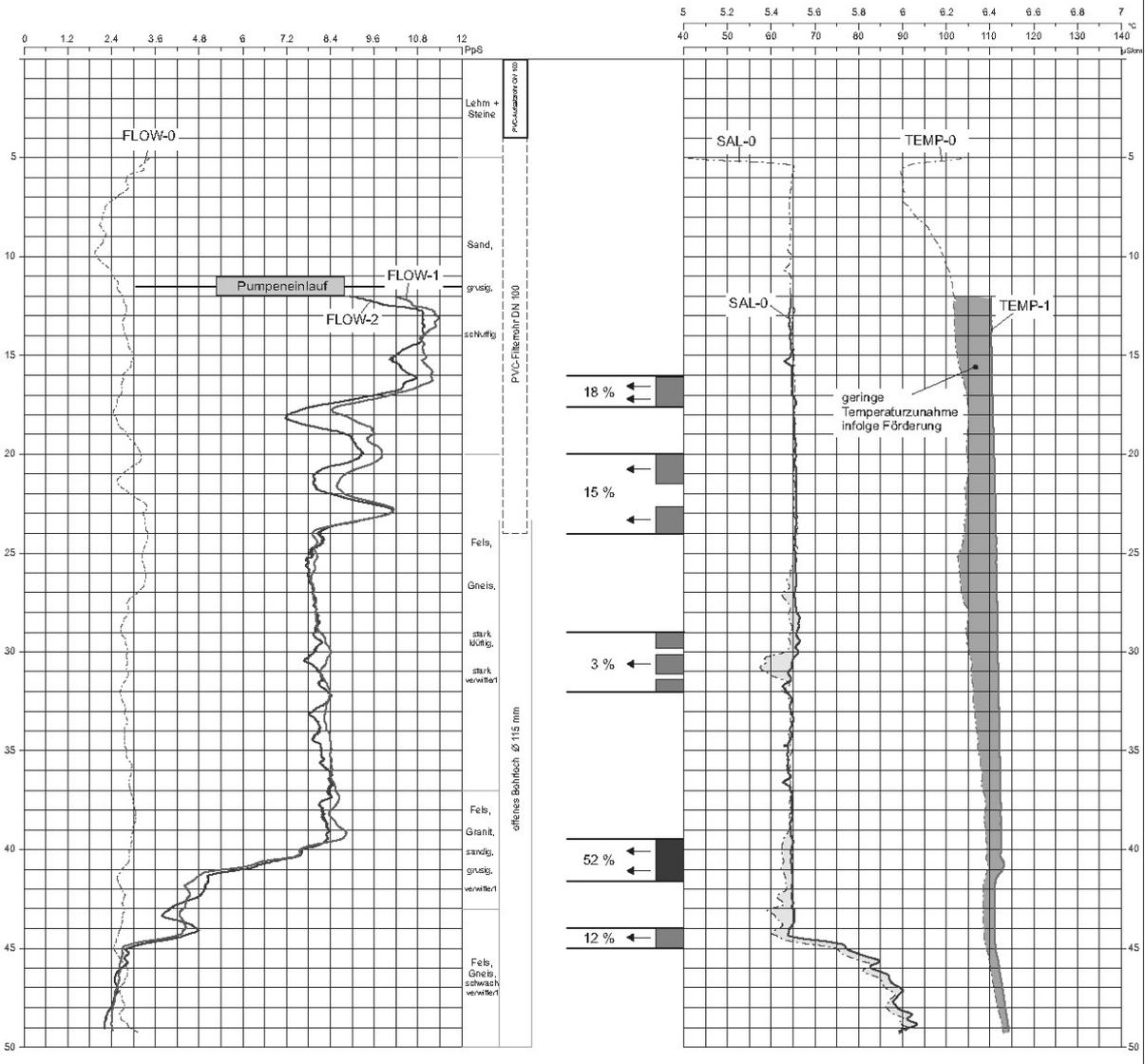
Zuflußprofil
relativer Zuflußanteil

Leitfähigkeit (normiert auf 25 °C)
SAL-0 (Ruhe) **SAL-1** (Produktion)

Temperatur

TEMP-0 (Ruhe)

TEMP-1 (Produktion)





gbs-Bohrlochgeophysik
 Wallenrodstr. 3
 91126 Schwabach
 Tel. 09122 / 83 29 260
 Fax 09122 / 83 29 270
 e-mail: g-b-s@t-online.de

Geophysikalische Bohrlochmessungen

Auftraggeber: Svb Dr. Prösel
Datum: 25.06.2004
Bohrtiefe: 50,0 m
Bohr-Ø: 203 / 152 / 115 mm
Pumpeneinlauf: 14,0 m
Leistung: 2,0 l/s
Ruhe-wsp: 8,3 m
Meßnullpunkt: GOK

VB 5 Habichtstein
WV Gem. Kirchdorf im Wald
Teufenmaßstab: 1 : 200
Ausführung / Interpretation: W. Beck
Bearbeitung / Datenprocessing: M. Federael

Flowmeter

FLOW-0 (Ruhe)
FLOW-1 (Produktion)
FLOW-2 (Produktion)

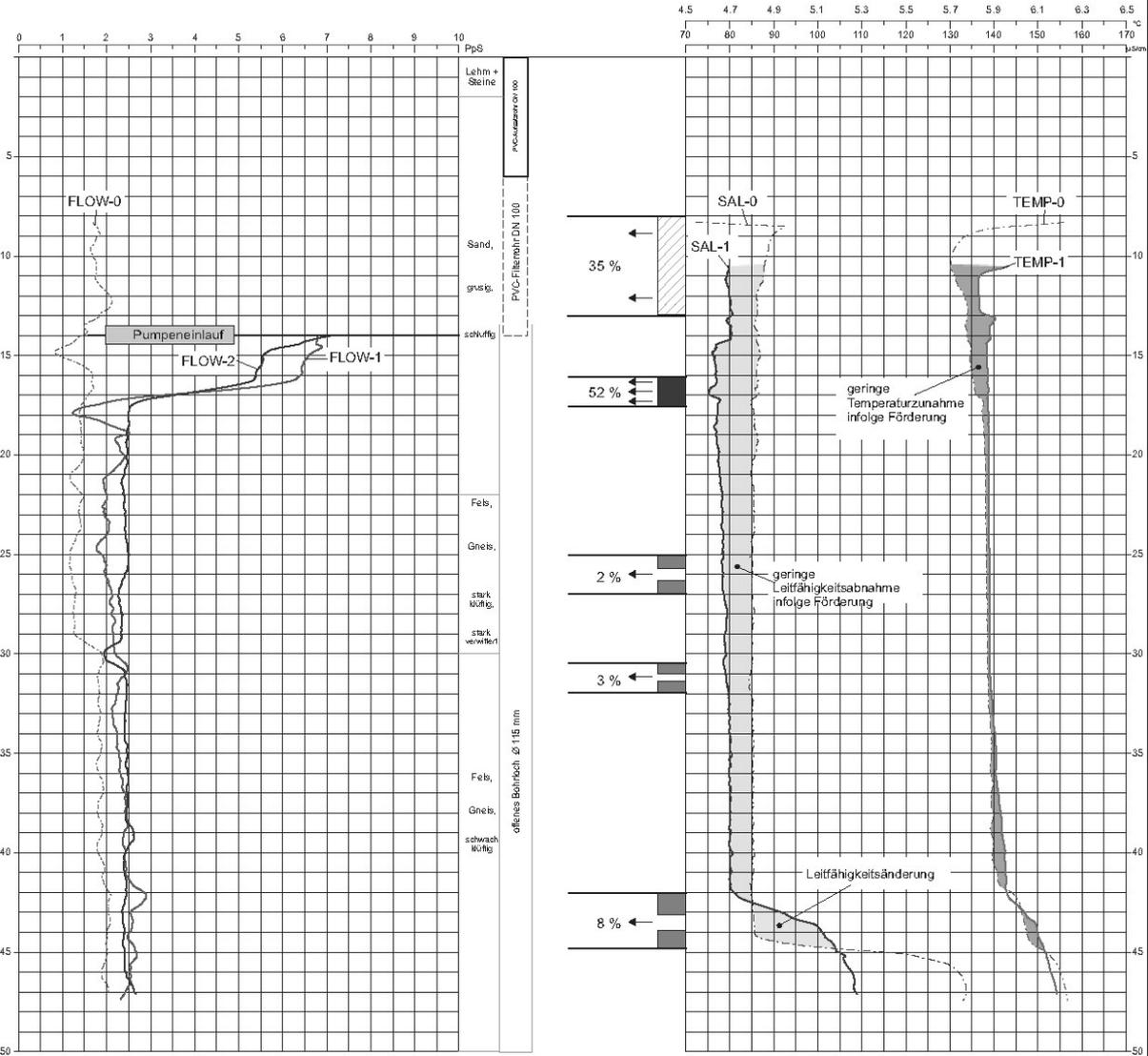
Ausbau / Geologie
 (schematisiert nach Angaben der Bohrfirma)

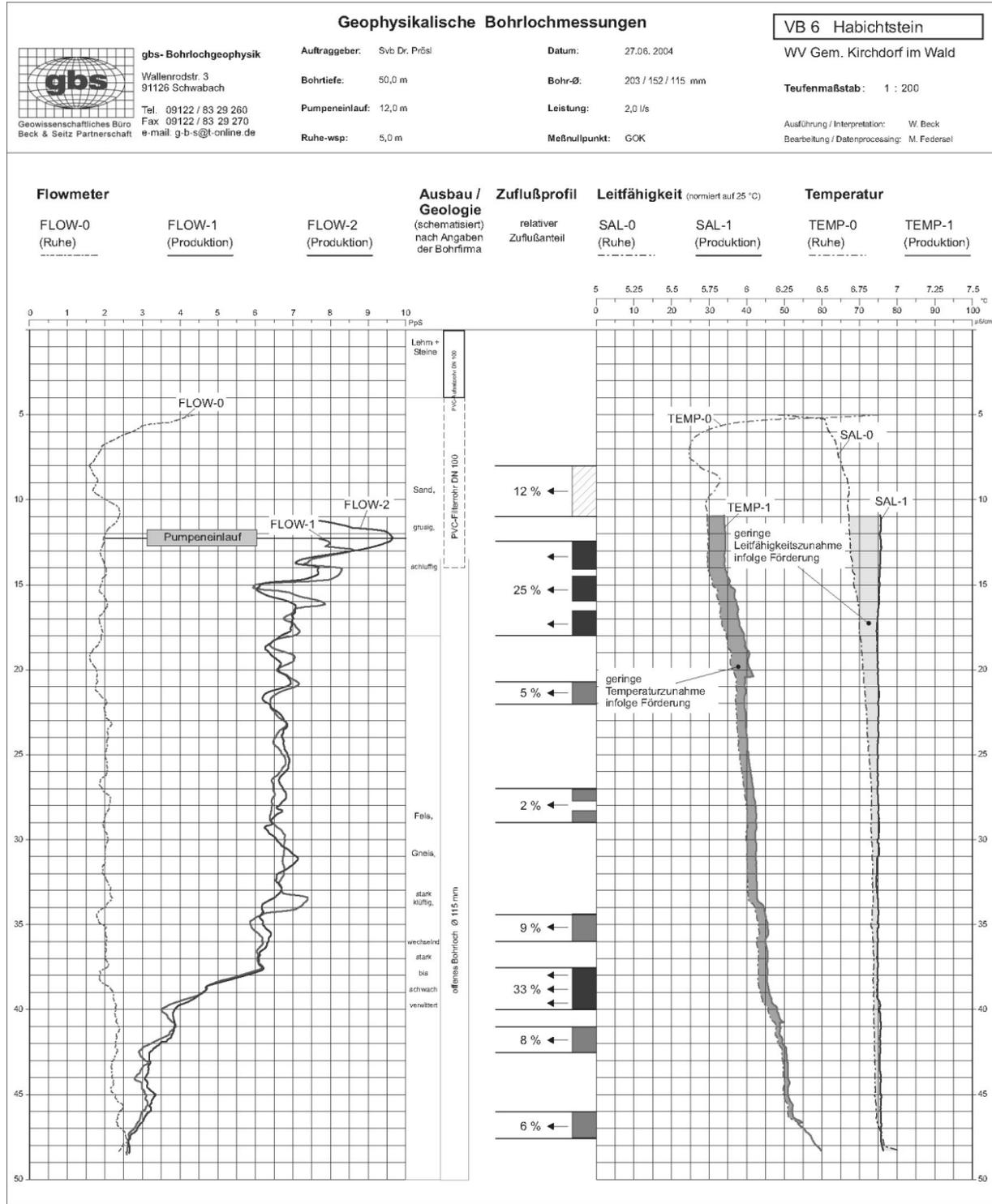
Zuflußprofil
 relativer Zuflußanteil

Leitfähigkeit (normiert auf 25 °C)
SAL-0 (Ruhe)
SAL-1 (Produktion)

Temperatur

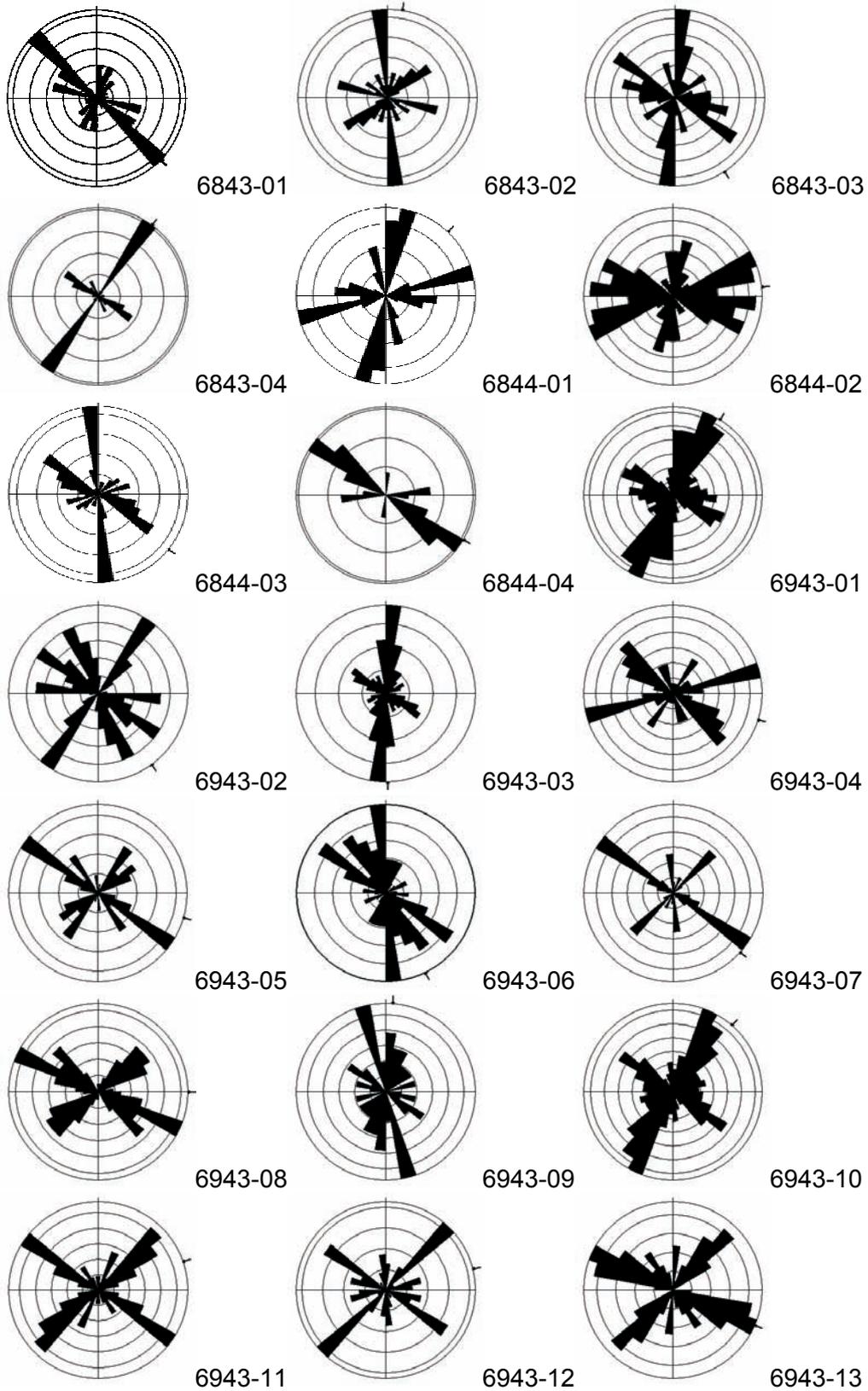
TEMP-0 (Ruhe)
TEMP-1 (Produktion)



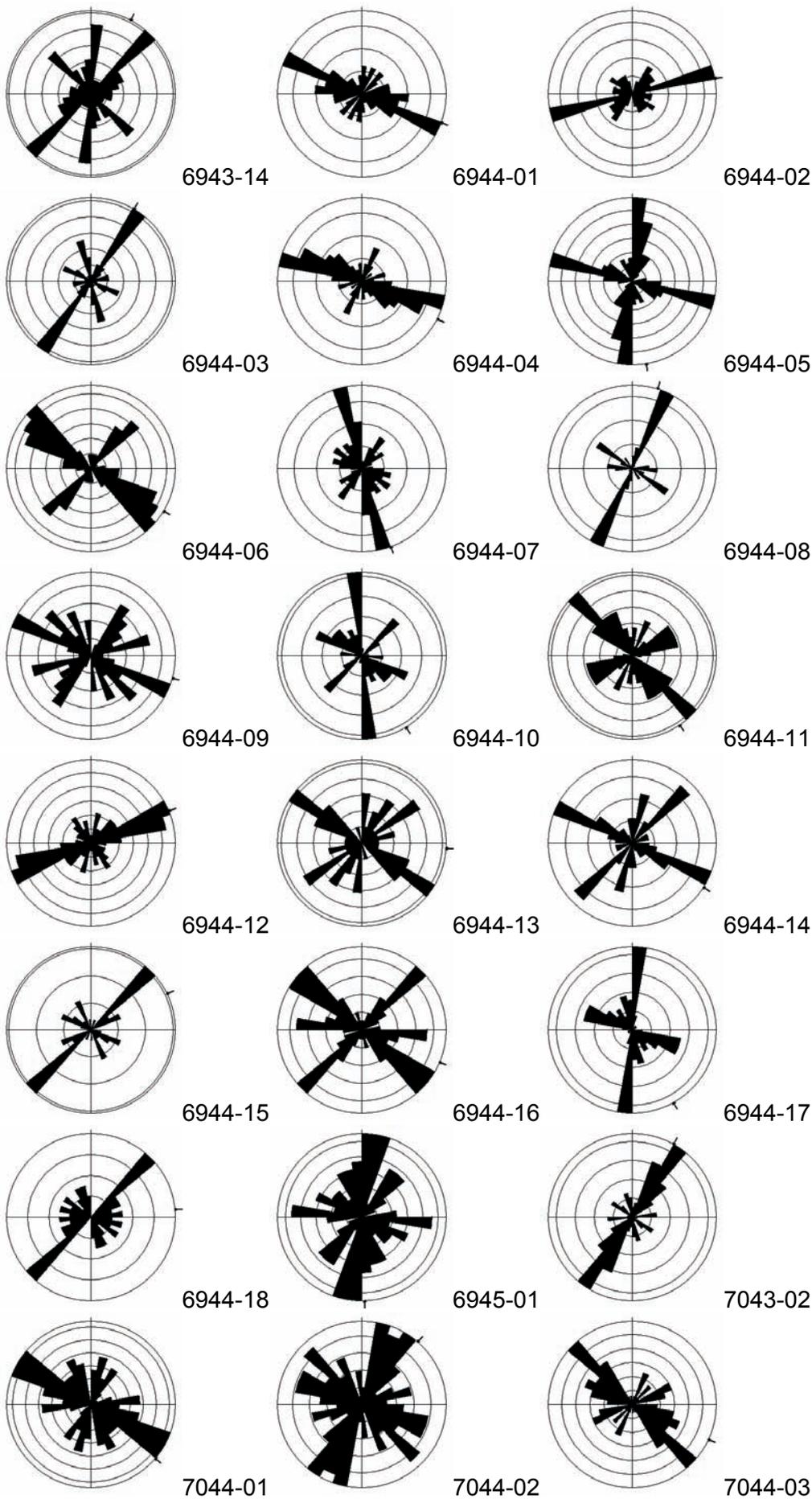


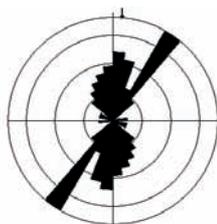
Appendix F – Cumulative stereographic plots and rose diagrams

1 Rose diagrams of steeply inclined fractures¹



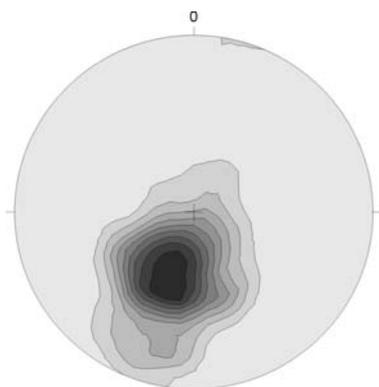
¹ Numbers to the right of the respective rose diagrams denote the sampling station ID number. Petal length is proportional to the relative abundances of fractures per 10° strike segment.



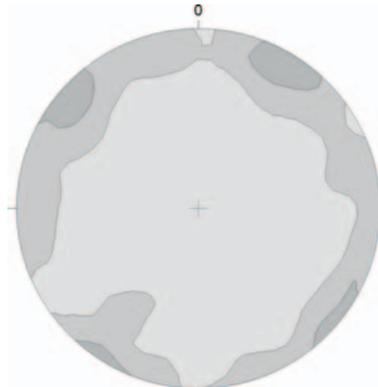


7044-04

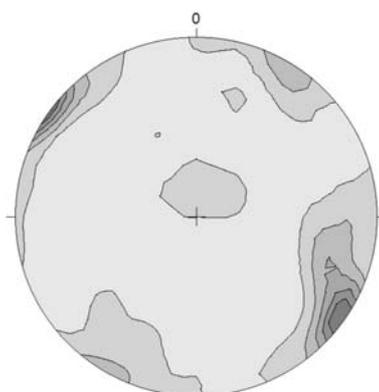
2 Miscellaneous cumulative stereographic plots



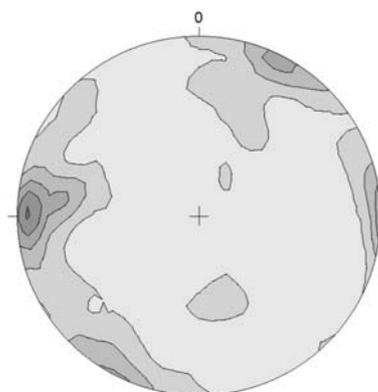
All fractures parallel to the meta-
morphitic foliation. n = 574.



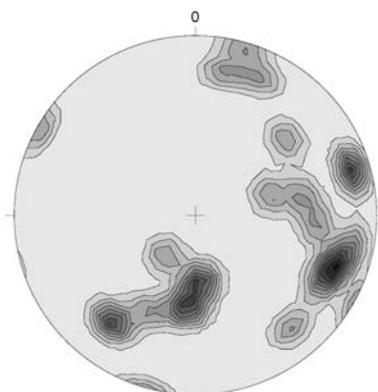
All fractures intersecting
the metamorphic foliation. n = 2332.



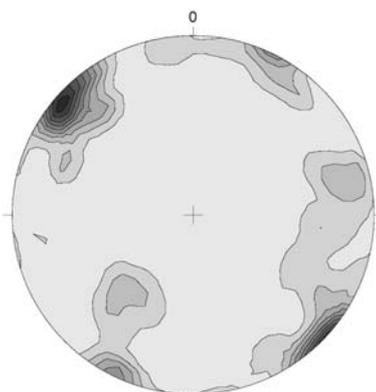
All fractures in granitic lithologies.
n = 1054.



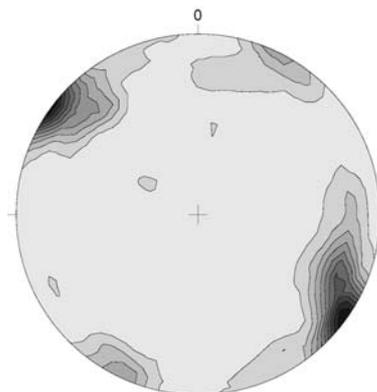
All fractures in hydrothermal
lithologies. n = 537.



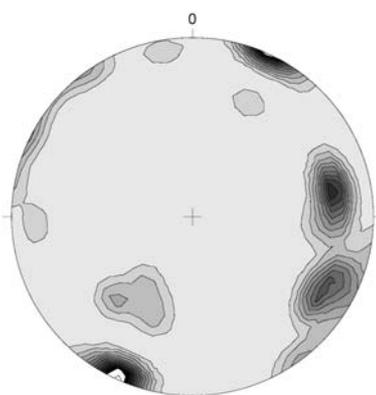
Orientations of all aplite dikes
and veins measured in the study area. n = 23.



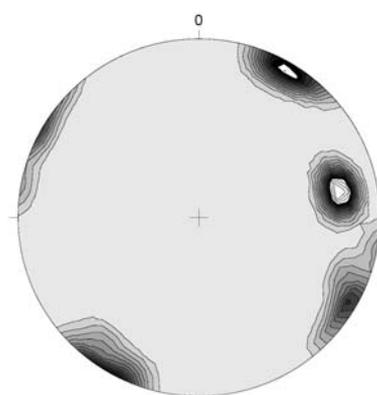
Fractures containing quartz mineralizations. n = 98



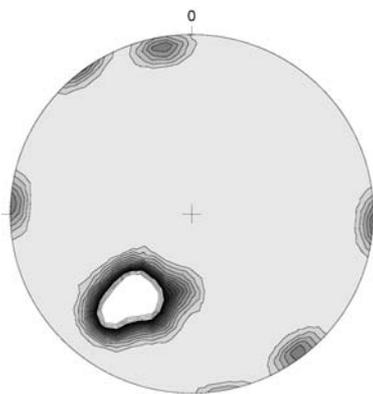
Fractures containing hematite mineralizations. n = 112.



Fractures containing epidote mineralizations. n = 42.



Fractures containing chlorite mineralizations. n = 23.



Fractures containing graphite mineralizations. n = 16.

Appendix H – Maps

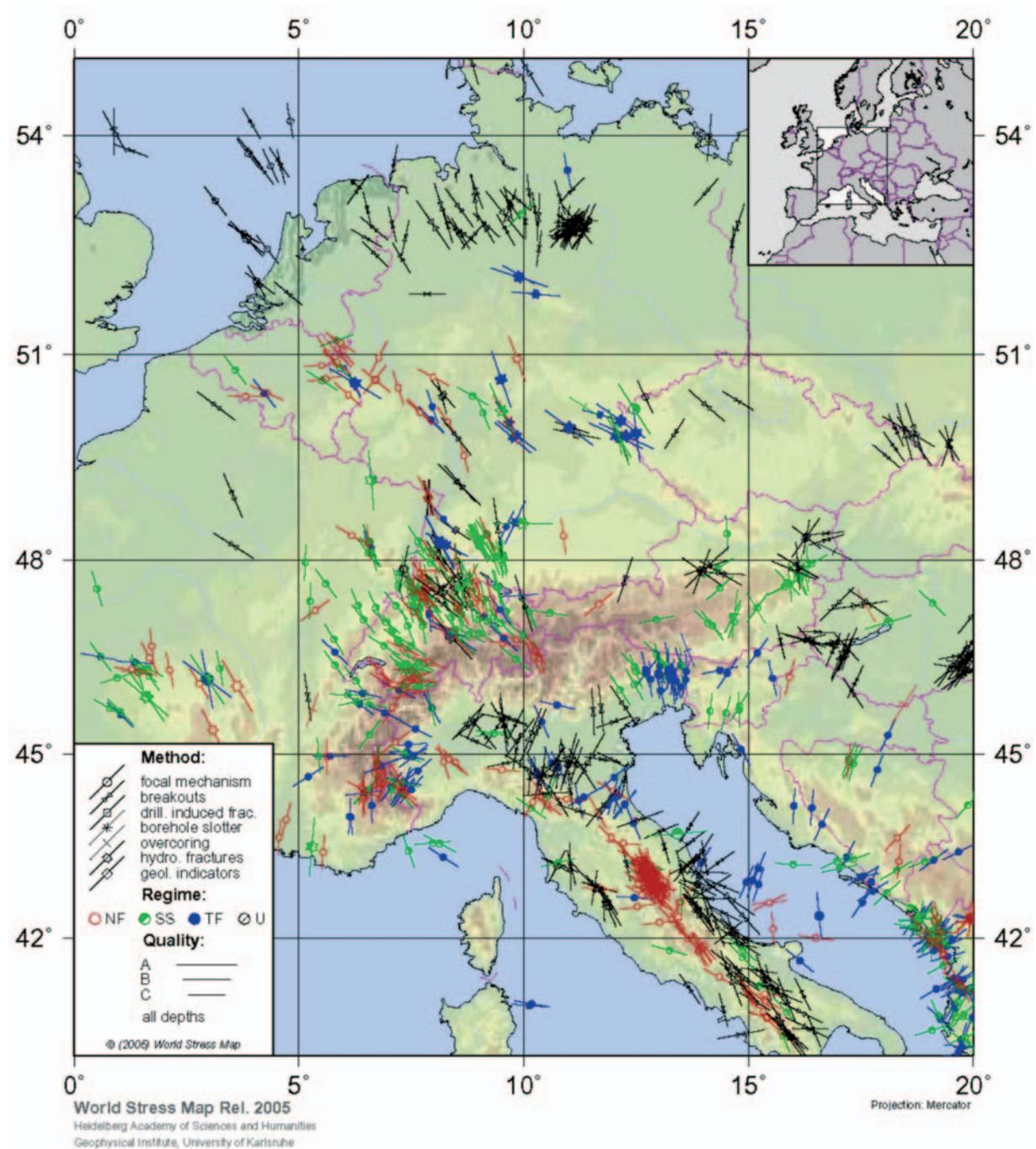


Figure H-1: World Stress Map 2005 of Germany. Symbols point in the direction of the maximum compressive stress. Source: Reinecker et al. (2005).

Appendix I – Attribution of regionally important rock types to lithogroups

This list of rock types was compiled from units of the 1:25,000 geologic maps published by the Bavarian State Geological Survey. The same units can have different map signatures and names on different quadrangles and thus are listed separately. The attribution to specific lithogroups reflects tectonic rather than petrographic aspects, because for this study the rocks' behavior with respect to brittle deformation is of interest. Individual lithologic units were classified based on field observations or unit descriptions obtained from map legends and reports.

Map Signature	Short Legend text	Lithogroup
,L	Lamprophyr	Granitic rocks
,Qt	Quarzit	Granitic rocks
Dr	Diorit	Granitic rocks
G	Massiv- und Ganggranit	Granitic rocks
G	Feinkörniger Granit	Granitic rocks
Ga	Paragranodiorit	Granitic rocks
Ga	Kollnburger Granodiorit, homogenisierter Diatexit	Granitic rocks
Ga/K	Paragranodiorit mit Kalifeldspat-Blastese	Granitic rocks
Ga+Pa	Kollnburger Granodiorit, homogenisierter Diatexit	Granitic rocks
Gb	Gabbro	Granitic rocks
gbgn	Granat-Biotit-Plagioklas-Gneis, Orthogneis	Granitic rocks
Gfl	Mittelkörniger Granit, geflasert	Granitic rocks
Gk	Grobkörniger, porphyrischer Granit	Granitic rocks
Gk+pgn	Grobkörniger, porphyrischer Granit	Granitic rocks
Gm	Mittelkörniger Granit	Granitic rocks
Gm+Pa	Mittelkörniger Granit	Granitic rocks
Gm+qDr	Mittelkörniger Granit	Granitic rocks
Pa	Dunkler Diatexit ("Palit")	Granitic rocks
qDr	Quarz-Glimmer-Diorit	Granitic rocks
qDr+Ga	Quarz-Glimmer-Diorit	Granitic rocks
qDr+Gm	Quarz-Glimmer-Diorit	Granitic rocks
A-Gr	Aplitgranit	Granitic rocks
Gk	Grobkörniger, porphyrischer Granit	Granitic rocks
Gr	Granit (ohne Zuordnung)	Granitic rocks
Gr,2Gl	kleinkörniger Zweigl.-Granit	Granitic rocks
Gr-My	Granit (mylonitischer Signatur)	Granitic rocks
Ksf +Gr	Kalksilikatfels und Granit	Granitic rocks
mGr,2Gl	mittelkörn. 2-GlimmerGranit	Granitic rocks
Qzt	Quarzit	Granitic rocks
BW,lkGrf	Mylonitisierter Granit (+my)	Granitic rocks
BW,Grfm	Granit, fein- bis mittelkörnig	Granitic rocks
BW,bGr	Biotit-Granit, mittel- bis grobkörnig	Granitic rocks
am	Amphibolit	Layered metamorphic rocks
am	Amphibolit, Biotit-Amphibolit	Layered metamorphic rocks
bpgn	Biotit-Plagioklas-Mylonitgneis	Layered metamorphic rocks
cgn	Cordierit-Sillimanit-Gneis	Layered metamorphic rocks
cgn-b	Granat-Cordierit-Sillimanit-Gneis	Layered metamorphic rocks
cgnp	Cordierit-Sillimanit-Gneis (mit Tendenzen zu Perlgneis)	Layered metamorphic rocks

cg-n-u	Cordierit-Sillimanit-Gneis, undeutlich geschiefert	Layered metamorphic rocks
gcgn1	Metatektischer Granat-Cordierit-Sillimanit-Gneis	Layered metamorphic rocks
gcgn2	Metatektischer Granat-Cordierit-Sillimanit-Gneis	Layered metamorphic rocks
gn	Granat-Cordierit-Sillimanit-Gneis mit Scheuereck	Layered metamorphic rocks
gnp	Perlgneis	Layered metamorphic rocks
gnL	Leptynitischer Gneis	Layered metamorphic rocks
gnp/c	Cordieritführender Perlgneis	Layered metamorphic rocks
gnz	Lagengneis (Zeilengneis)	Layered metamorphic rocks
my	Mylonit	Layered metamorphic rocks
myu	Ultramylonit	Layered metamorphic rocks
pgn	Biotit-Plagioklas-Gneis	Layered metamorphic rocks
qbg-n	Quarz-Biotit-Plagioklas-Gneis	Layered metamorphic rocks
cg-n,m	metatekt. Gneis, Cordiorit, Sillimanit, Granat	Layered metamorphic rocks
Gl-gn	Glimmergneise	Layered metamorphic rocks
Gn-My	Gneis tektonisiert (mylonitisch-kataklastisch)	Layered metamorphic rocks
My-+Granit	Mylonit mit Granitgängen	Layered metamorphic rocks
Qz-Gl-Schiefer	Quarzglimmerschiefer	Layered metamorphic rocks
M,csGn*mx	Metatektischer Cordierit-Sillimanit-Kalifeldspat	Layered metamorphic rocks
M,Gn*dx	Diatektischer Cordierit-Kalifeldspat-Gneis	Layered metamorphic rocks
M,Gno	Granodioritischer leukokrater Gneis (Orthogneis)	Layered metamorphic rocks
öG	Ödwieser Granit	Strongly folded and migmatitic rocks
amj	Hornblende-Anatexit	Strongly folded and migmatitic rocks
bgn	Körnelgneis	Strongly folded and migmatitic rocks
bgn	Heller Diatexit, z.T. homogenisiert ("Körnelgneis")	Strongly folded and migmatitic rocks
cg-nj	Metatektischer bis anatektischer Cordierit-Sillimanit-Gneis	Strongly folded and migmatitic rocks
pgnj	Palit	Strongly folded and migmatitic rocks
M,Dx+Gr	Diatektischer Cordierit-Kalifeldspat-Gneis	Strongly folded and migmatitic rocks
M,lkDx	Heller homogenisierter Diatexit	Strongly folded and migmatitic rocks
M,kfDx,h	Dunkler homogenisierter Diatexit	Strongly folded and migmatitic rocks
M,KS	Kalsilikatfels, Silikatmarmor, kontaktmetamo	Strongly folded and migmatitic rocks
A	Aplit	Hydrothermal and pneumatolytic rocks
Pe	Pegmatitgang	Hydrothermal and pneumatolytic rocks
Q	Quarzgang	Hydrothermal and pneumatolytic rocks
.qz*g	Quarzgang	Hydrothermal and pneumatolytic rocks
BW,Pe	Pegmatit	Hydrothermal and pneumatolytic rocks

Lebenslauf

Persönliche Angaben:

Name: Matthias Zeitlhöfler
Geburtstag: 17.08.1977
Geburtsort: Regen/ Bayer. Wald
Eltern: Walter Zeitlhöfler, Justizamtmann
Ursula Zeitlhöfler, geb. Mühlbauer, verstorben
Familienstand: verheiratet

Schulbildung und berufliche Laufbahn:

September 1983	Einschulung in die Staatliche Grundschule Viechtach/Bayer. Wald
September 1986	Übertritt an die Vorschule der Regensburger Domspatzen in Pielenhofen bei Regensburg
September 1987	Übertritt an das Musikgymnasium der Regensburger Domspatzen, Regensburg
Mai 1996	Abitur am Musikgymnasium der Regensburger Domspatzen
Oktober 1996	Zivildienst beim Diakonischen Werk Regensburg
November 1997	Studium an der Universität Regensburg, Lehramt Gymnasium Erdkunde/Englisch
November 1999	Zwischenprüfung im Fach Englisch
Mai 2000	Zwischenprüfung im Fach Erdkunde
August 2000	Auslandsjahr in den USA an der Wesleyan University, Middletown, CT
Frühjahr 2001	Erfolgreiche Bewerbung für das Master's Program am Department of Earth & Environmental Sciences der Wesleyan University
Sommer 2001 bis Frühjahr 2003	Arbeit an der Master's Thesis (Titel: „Bedrock Structure in Southeastern Connecticut: Hydrologic Implications“) in Zusammenarbeit mit dem U.S. Geological Survey und dem Connecticut Department of Environmental Protection
Mai 2003	Master's Degree in Earth Sciences an der Wesleyan University
November 2003	Beginn des Promotionsstudiums an der Ludwig-Maximilians-Universität München; Stipendiat der Bayerischen Begabtenförderung bis Januar 2006
Februar bis Mai 2006	Mitarbeit an der Hydrogeologischen Landesaufnahme Bayerns im EU-Ziel-2-Gebiet beim Geologischen Dienst des Bayerischen Landesamtes für Umweltschutz
Juni 2006 bis März 2007	Wissenschaftlicher Mitarbeiter am Department für Geowissenschaften an der Ludwig-Maximilians-Universität München
seit Mai 2007	Mitarbeiter am Bayerischen Landesamt für Umwelt, Hof - Referat 104, Fachbereich Hydrogeologie

